Advances in High Energy Physics

New Physics Landmarks: Dark Matter and Neutrino Masses

Lead Guest Editor: Farinaldo Queiroz
Guest Editors: Jose W. F. Valle, Yann Mambrini, and Giorgio Arcadi

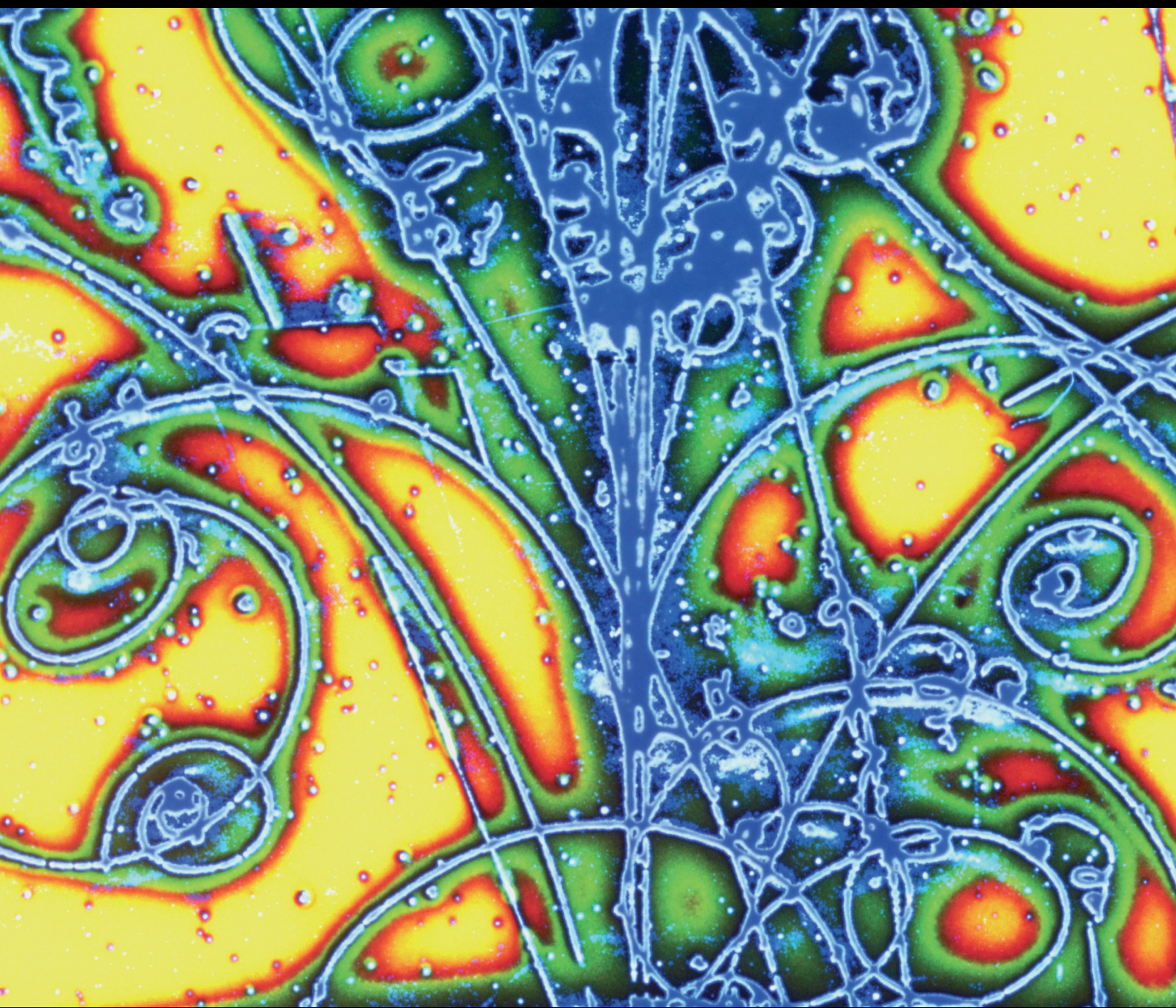

New Physics Landmarks: Dark Matter and Neutrino Masses

Advances in High Energy Physics

New Physics Landmarks: Dark Matter and Neutrino Masses

Lead Guest Editor: Farinaldo Queiroz
Guest Editors: Jose W. F. Valle, Yann Mambrini, and Giorgio Arcadi

Editorial Board

Contents

Hindawi
Advances in High Energy Physics
Volume 2018, Article ID 2652536, 2 pages
https://doi.org/10.1155/2018/2652536

Editorial

New Physics Landmarks: Dark Matter and Neutrino Masses

Farinaldo S. Queiroz,[1] **José W. F. Valle**,[2] **Yann Mambrini**,[3] **and Giorgio Arcadi**[4]

[1] *International Institute of Physics, Universidade Federal do Rio Grande do Norte, Campus Universitario, Lagoa Nova, 59078-970 Natal, RN, Brazil*
[2] *AHEP Group, Instituto de Física Corpuscular CSIC/Universitat de Valencia Edificio de Institutos de Paterna, C/Catedratico José Beltran 2, 46980 Paterna, Valencia, Spain*
[3] *Laboratoire de Physique Théorique (UMR8627), CNRS, Univ. Paris-Sud, Université Paris-Saclay, 91405 Orsay, France*
[4] *Max-Planck-Institut für Kernphysik, Saupfercheckweg 1, 69117 Heidelberg, Germany*

Correspondence should be addressed to Farinaldo S. Queiroz; farinaldo.queiroz@iip.ufrn.br

Received 22 October 2018; Accepted 25 October 2018; Published 17 December 2018

The Standard Model has endured several decades and represents the most accurate description of nature we have. Despite the fact that it represents most probably the best description for the electroweak and strong interactions in nature, we have at least two conclusive evidences that the Standard Model is not complete: (i) through the observation of neutrino oscillations we have established nonzero neutrino masses; (ii) a collection of cosmological and galactic observations requires the presence of nonbaryonic dark matter in our universe. The absence of explanations of these two facts within the Standard Model strongly motivates the quest for theory extensions.

Hence, it is paramount to explore new physics directions where these observables and their phenomenological implications are addressed in order to pave the road towards a new Standard Model accounting for all the observed phenomena in nature.

This special issue presents a collection of reviews of some of the most accredited extensions of the Standard Model explaining the origin of neutrino masses and/or the dark matter component of the Universe, as well as original works.

The special feature includes works trying to give an unified description for neutrinos masses in the context of the SU(5) symmetry ("Neutrino Mass, Coupling Unification, Verifiable Proton Decay, Vacuum Stability, and WIMP Dark Matter in SU(5)", by B. Sahoo et al.) as well as those trying to connect neutrino masses to some flavor groups such as (27) ("Fermion Masses and Mixings in a 3-3-1 Model with $Delta(27)$ Family Symmetry and Inverse Seesaw Mechanism", by A. C. Hernández et al.). In these frameworks, the neutrino mass matrix can get complicated and it is mandatory to investigate its phenomenological impact. The study along this line has been presented by the manuscript "Investigating the Hybrid Textures of Neutrino Mass Matrix for Near Maximal Atmospheric Neutrino Mixing", by M. Singh, which investigated the impact of hybrid textures on the neutrino mass matrix for near maximal atmospheric neutrino mixing. The mixings and oscillations in the neutrino sector were scrutinized in long-baseline experiments by P. Pasquini in "Long-Baseline Oscillation Experiments as a Tool to Probe High Energy Flavor Symmetry Models".

Still, in the context of neutrino mass mechanisms, one popular method to explain neutrino masses is via the addition of Majorana neutrinos which gives rise to neutrinoless double beta decay. The implications have been studied in a model with the SU(3)xSU(3)xU(1) gauge group ("Lower Mass Bound on the W' Mass via Neutrinoless Double Beta Decay in a 3-3-1 Model", by A. C. O. Santos and P. Vasconcelos). These works altogether encompass several aspects of neutrino physics going from theory to experimental signatures.

As far as dark matter is concerned, one paper nicely tied neutrino masses to dark matter ("Neutrino Mass and the Higgs Portal Dark Matter in the ESSFSM", by N. Khan), while another focused on having a viable dark matter candidate

in a popular model where baryon and lepton numbers are promoted to gauge symmetries ("Z' Portal Dark Matter in the Minimal B – L Model", by S. Okada). Implications to some recent flavour anomalies are connected to dark matter which is detailed in the work entitled "Anomalies in $b \longrightarrow s$ Transitions and Dark Matter", by A. Vicente. A broader perspective of such dark matter models was detailed in the paper by E. Morgante in "Simplified Dark Matter Models". We also have papers discussing dark matter in the context of well-motivated supersymmetric models "The Discreet Charm of Higgsino Dark Matter: A Pocket Review", by K. Kowalska and E. M. Sessolo, and cosmic-ray physics "Impact of Cosmic-Ray Physics on Dark Matter Indirect Searches", by D. Gaggero and M. Valli.

In summary, this special issue contains important works that will allow the reader to be up to date with neutrino and dark matter physics that goes from a more theoretical perspective to an experimental one.

Conflicts of Interest

The authors declare that they have no conflicts of interest.

Farinaldo S. Queiroz
José W. F. Valle
Yann Mambrini
Giorgio Arcadi

Hindawi
Advances in High Energy Physics
Volume 2018, Article ID 5012043, 13 pages
https://doi.org/10.1155/2018/5012043

Review Article

Simplified Dark Matter Models

Enrico Morgante

Deutsches Elektronen-Synchrotron DESY, Notkestraße 85, 22607 Hamburg, Germany

Correspondence should be addressed to Enrico Morgante; enrico.morgante@desy.de

Received 30 March 2018; Accepted 16 May 2018; Published 17 December 2018

Academic Editor: Farinaldo Queiroz

I review the construction of simplified models for dark matter searches. After discussing the philosophy and some simple examples, I turn the attention to the aspect of the theoretical consistency and to the implications of the necessary extensions of these models.

1. Introduction

Producing and studying the properties of the dark matter (DM) particles at the LHC are an extremely exciting possibility that would open the door to a new understanding of the interplay between astrophysics, cosmology, and particle physics. Essentially all the naturalness-inspired scenarios can accommodate the presence of a good dark matter candidate: a neutral and very long-lived particle that was copiously produced in the early universe and then lost thermal contact with the SM (if it ever occurred) leaving a relic density $\Omega_{\mathrm{DM}} \sim 0.26$ of cold particles. The fact that such a stable weakly interacting massive particle with a mass around the weak scale has automatically a relic abundance close to the measured one is a remarkable property which is often dubbed *WIMP miracle*. The LHC is a perfectly suited machine to look for this kind of particles, and current bounds from ATLAS and CMS complement those from direct and indirect searches.

A key task in these studies is that of choosing a theoretical framework to compare with data and compare the results of different experiments. Given the plethora of particle physics models beyond the SM providing a WIMP candidate, it is highly desirable to study the signatures of this DM candidate in a model-independent way. In the early stages of the LHC, this was achieved by means of the effective field theory approach (EFT). In this framework, the Standard Model (SM) is complemented by a set of non-renormalizable operators that parametrize the interaction of the DM particle with SM fields in terms of one effective scale Λ and of the DM mass m_χ [1]. The EFT approach has proven to be very useful in the analysis of LHC Run I data [1–15], because of the great advantage of giving bounds that are as model-independent as possible: for a given choice of the spin of the DM particle, the number of operators that can couple it to the SM and may give interesting signatures at the LHC is limited, for a fixed mass dimension. Since direct and indirect detection of WIMPs, as well as WIMP production at the LHC, all require an interaction of the WIMPs with the SM particles, and such an interaction may be generated by the same operator, the EFT approach has the additional advantage of facilitating the analysis of the correlations between the various kinds of experiments.

The important drawback of the EFT description is its intrinsic energy limitation. At energies larger than some cutoff Λ, the contribution of higher dimension operators to the computation of scattering amplitudes becomes comparable to the lower ones, signalling the breakdown of perturbativity. More in particular, if the EFT is seen as the low energy limit of a theory with a mediator of mass M which is above the energy scale probed by the experiment, the cutoff is obtained as $\Lambda^2 \sim M^2/g^2$, where g is some combination of the coupling constants, and the theory is valid up to a momentum exchange $p^2 \lesssim M^2 \sim \Lambda^2$, where we have assumed $g \sim 1$. In direct and indirect detection this constraint is typically satisfied thanks to the low velocity of the incoming particle. On the other hand, the momentum exchanged in the partonic interactions at the LHC is of order few TeV, larger than the values of Λ that can be excluded within the EFT framework, making the naïve EFT bounds unreliable

except for values of the couplings close to the perturbative bound $g \lesssim 4\pi$ [16–18]. In principle this does not mean that the EFT approach is not useful. Recasting procedures can be adopted to rederive bounds considering only a fraction of the events in the simulation that correspond to those which fulfil the requirement on the momentum [17, 19]. Clearly, the new bounds would be much weaker, but their simplicity still suggests that they should not be disregarded.

Partly in response to the problems of EFTs, and partly inspired by their rich phenomenological implications, in more recent years the LHC community has turned its attention to the tool-kit of simplified models. Such models are characterized by the most important state mediating the interaction of the DM particle with the SM, as well as the DM particle itself (see, for example, [14, 20–24] for early proposals). Including the effect of the mediator's propagator allows avoiding the energy limitation of the EFT, and simplified models are able to describe correctly the full kinematics of DM production at the LHC, at the price of a moderately increased number of parameters. As we are going to discuss below, the introduction of simplified models opens a new set of possibilities compared to the simpler EFT approach, while opening at the same time a set of new questions.

This paper is structured as follows. In Section 2, we are first going to describe the construction of DM simplified models from a bottom-up approach, providing some examples in Section 3. Then, in Section 4, we will point out the theoretical issues of such a construction, introducing a second generation of simplified models that have gained a lot of attention in recent times. Section 5 will contain our conclusions.

Thorough discussions about simplified DM models may be found in [25–30]. The second-generation models of Section 4 are discussed in [31, 32]. The discussion in this paper will be partly based on [33].

2. Philosophy of Simplified DM Models

As in the case of the EFT, the idea behind simplified models is to provide a good representation of possibly all realistic WIMP scenarios within the energy reach of the LHC, restricting to the smallest possible set of benchmark models, each with the minimal number of free parameters. Simplified models should be complete enough to give an accurate description of the physics at the scale probed by colliders, but at the same time they must have a limited number of new states and parameters.

The starting point is always the SM Lagrangian, complemented with a DM particle and a mediator that couples to it, through renormalizable operators, to quarks and gluons, which is necessary for the production of these states at a hadron collider. A coupling to other SM particles can be included as well and will add interesting experimental signatures to the model. In general, some simplifying assumptions can be made: for example, one can take all couplings to be equal, or the couplings to third generation's quarks to be dominant. Interactions that violate the accidental global symmetries of the SM must be handled with great care. Indeed, constraints on processes that violate these symmetries are typically very strong and may overcome those coming from DM searches or even rule out all of the interesting parameter space of the simplified model. For this reason, CP, lepton number, and baryon number conservation is typically assumed, together with minimal flavour violation (MFV). (Constraints on BSM models from CP and flavour violating observables are very strong, and the energy scale at which new physics may show up must be larger than tens of TeV in the best case, if the flavour structure of the model is generic. Minimal Flavour Violation is a way to reconcile these constraints with possible new physics at the TeV scale [34]. The basic idea is that the structure of flavour changing interactions must reproduce that of the SM. The SM is invariant under the flavour group $\mathcal{G}_F = \mathrm{SU}(3)_q \times \mathrm{SU}(3)_u \times \mathrm{SU}(3)_d$, except a small breaking associated with the Yukawa matrices Y_u and Y_d. The invariance is restored if these matrices are regarded as "spurions" with transformation law $Y_u \sim (3, \overline{3}, 1)$ and $Y_d \sim (3, 1, \overline{3})$. Imposing MFV amounts to requiring that new physics is invariant under $\mathcal{G}_F$.) Even with this assumption, there are cases in which constraints from flavour physics may be stronger than those coming from mono-X searches [35] (see also [36] for a discussion of a non-minimally flavour violating dark sector).

Most simplified models of interest may be understood as the limit of a more general new physics scenario, where all new states but a few are integrated out because they have a mass larger than the energy scale reachable at the LHC or because they have no role in DM interactions with the SM. Similarly, in the limit where the mass of the mediator is very large, the EFT framework may be recovered by integrating out the mediator. On the contrary, there are new physics models which cannot be recast in terms of vanilla simplified models, typically because more than just one operator is active at the same time, possibly interfering with each other. The situation is summarized in Figure 1.

Even if this may sound obvious, we should stress that the correspondence between simplified models and EFT is not one to one. Simplified models that involve mediators of different spin nature may give rise to the same effective operator after a Fierz rotation, as pointed out in [19] with the example of a Majorana DM particle embedded in a Z' model or a SUSY-inspired model with coloured scalar mediators in the t-channel.

Even when a simple correspondence between the EFT and the simplified model is assumed, limits on the EFT cannot be readily translated onto the simplified model because of the possible resonant enhancement (that would make the limit stronger) or the typically softer missing energy spectrum (that would weaken the limit) [37]. Moreover, the different missing energy spectrum may require *ad hoc* optimization strategy by the experimental searches, and considering mediators of different mass requires different optimization for each case. Finally, models with a heavy mediator that would correspond to the EFT limit tend to predict a too large relic DM density (assuming no deviation from the standard cosmological history and no states other than the SM ones to annihilate into) and are therefore less appealing as a model of DM [38].

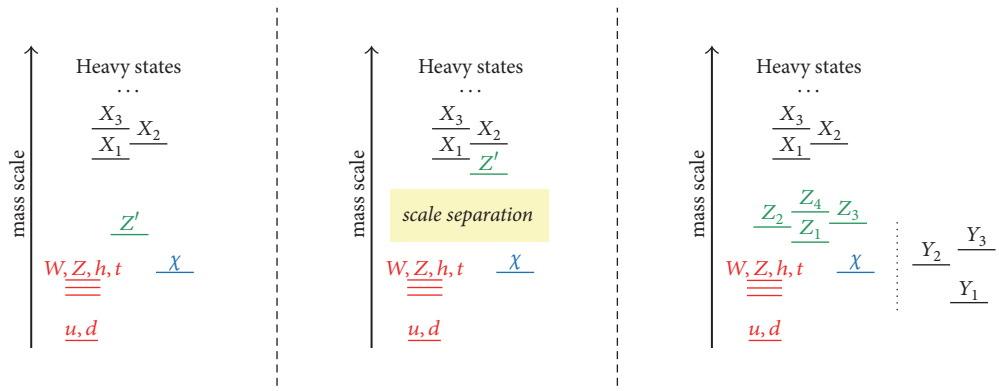

Figure 1: *Left:* a simplified model viewed as a sector of a more general new physics scenario. The SM is complemented by the DM particle χ and a mediator Z'. Other heavy states $X_1, X_2, X_3, \ldots$ may be integrated out because they are very heavy. *Centre:* in the case in which the mediator Z' itself has a very large mass, it may be integrated out as well and the interaction is mediated by effective operators. *Right:* in a generic setup the DM-SM interaction is mediated by a number of operators, possibly interfering with each other. Moreover, additional states $Y_1, Y_2, Y_3, \ldots$ that do not couple directly to DM may be present. Those states can constitute a new handle on the dark sector, other than DM. The 'less simplified' models described in Section 4 fall in this category.

From the point of view of LHC searches, the enlarged physical spectrum and parameter space of simplified models with respect to the EFT represents a challenge, and a greater variety of search channels is involved. While within the EFT approach the mono-X searches hold the stage, simplified models of DM can be constrained also with multi-jet + MET searches, with di-jet and di-leptons resonance searches and many others, depending on the degree of sophistication and on the ingredients of the model. Interestingly, many of these searches do not involve the DM particle, but only the mediator, and constraints are often stronger than the mono-X ones. On the other hand, the EFT is still a useful tool when dealing with strongly coupled theories, where a description in terms of a perturbative simplified model is not viable [39, 40].

3. First Generation of Simplified Models

3.1. s-Channel Mediators. We are now going to list a few examples of the simplified models of relevance for LHC searches, starting with those that include a fermionic DM χ (which for now we assume to be a Dirac spinor, but this is not necessary) and a mediator exchanged in the s-channel. The models under consideration are the following:

$$\mathcal{L}_V \supset \frac{1}{2}m_V^2 V_\mu V^\mu - m_\chi \bar{\chi}\chi - g_\chi V_\mu \bar{\chi}\gamma^\mu \chi - g_q^{ij} V_\mu \bar{q}_i \gamma^\mu q_j, \quad (1)$$

$$\mathcal{L}_A \supset \frac{1}{2}m_A^2 A_\mu A^\mu - m_\chi \bar{\chi}\chi - g_\chi A_\mu \bar{\chi}\gamma^\mu\gamma_5\chi - g_q^{ij} A_\mu \bar{q}_i \gamma^\mu \gamma_5 q_j, \quad (2)$$

for a spin-1 mediator and

$$\mathcal{L}_S \supset -\frac{1}{2}m_S^2 S^2 - m_\chi \bar{\chi}\chi - y_\chi S\bar{\chi}\chi - y_q^{ij} S\bar{q}_i q_j + \text{h.c.}, \quad (3)$$

$$\mathcal{L}_P \supset -\frac{1}{2}m_P^2 P^2 - m_\chi \bar{\chi}\chi - iy_\chi P\bar{\chi}\gamma_5\chi - iy_q^{ij} P\bar{q}_i\gamma_5 q_j + \text{h.c.}. \quad (4)$$

for a spin-0 mediator, where V, A, S, P stand for a vector, axial-vector, scalar, or a pseudoscalar mediator, respectively, $q = u, d$ and $i, j = 1, 2, 3$ are flavour indices. In the heavy m_{med} limit, the mediators can be integrated out, recovering the effective operators:

$$\begin{aligned} \text{D1: } & \frac{m_q}{\Lambda^3}\bar{\chi}\chi\ \bar{q}q \\ \text{D4: } & \frac{m_q}{\Lambda^3}\bar{\chi}\gamma^5\chi\ \bar{q}\gamma^5 q \\ \text{D5: } & \frac{1}{\Lambda^2}\bar{\chi}\gamma_\mu\chi\ \bar{q}\gamma_\mu q \\ \text{D8: } & \frac{1}{\Lambda^2}\bar{\chi}\gamma_\mu\gamma^5\chi\ \bar{q}\gamma_\mu\gamma^5 q \end{aligned} \quad (5)$$

where the nomenclature was first adopted in [1].

Let us briefly point out, and we will come back to this in Section 4, that the scalar and pseudo-scalar models of (3), (4) are not gauge invariant. This may lead to spurious results in processes where a W/Z boson is emitted. Moreover, in the axial-vector model perturbative unitarity is violated in a large portion of parameter space. We will return to these issues in Section 4.

Consistently with the MFV hypothesis, we force the couplings to be diagonal: $g_q^{ij} = g_q^i \delta^{ij}$. Moreover, we assume them to be flavour-blind in the (axial-)vector case and proportional to the SM Yukawa in the (pseudo)scalar ones:

$$\begin{aligned} & g_d^i = g_u^i \equiv g_q, \\ & y_q^{ij} \equiv y\frac{m_i}{v}\delta^{ij} \\ & \qquad \text{for } i = 1, 2, 3. \end{aligned} \quad (6)$$

In this way the spin-0 models have an enhanced coupling to the third generation's quarks, which makes the phenomenology quite different from the spin-1 models, both because of

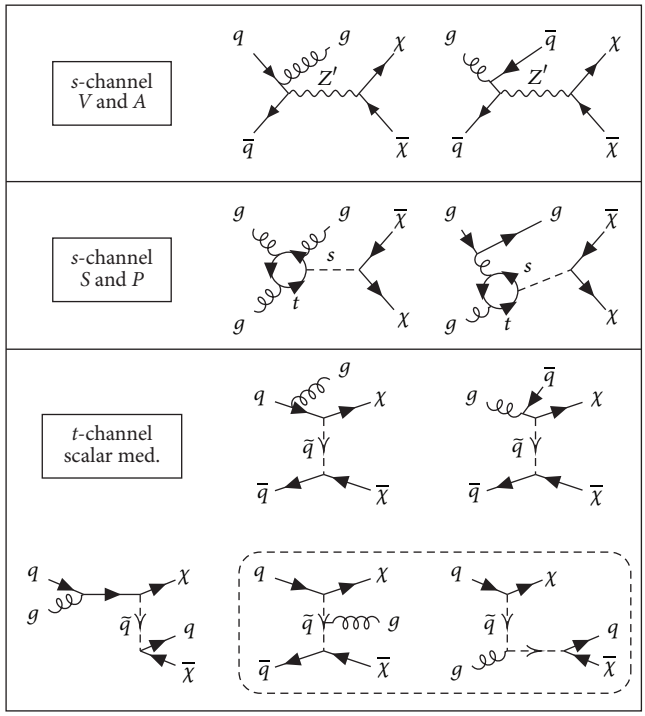

Figure 2: Feynman diagrams for the production of a DM pair in association with a quark or a gluon, leading to a mono-jet signature. Additional diagrams obtained by exchanging a fermion and a anti-fermion, as well as the ones obtained by permuting the gluon vertices in the loop in the (pseudo)scalar case, are neglected. The diagrams enclosed in the dashed box in the t-channel model are suppressed in the EFT limit.

the different production mechanism (gluon fusion with a top loop instead of $q\bar{q}$ annihilation) and because of the possibility of constraining such models with searches in b/t channels. As an example, Figure 2 shows the Feynman diagrams involved in the calculation of the mono-jet cross section.

In addition to the parameters of the Lagrangian, in the calculation of scattering amplitudes one must also include the decay width Γ of the mediator, which can be thought as a free parameter that encodes the unknown decay probability to other particles belonging to the dark sector. In this case, in the computation of the cross sections the couplings constants factor out and they affect only the normalization of the cross section through their product $g_q g_\chi$, while the spectra depend only on the masses m_{med}, m_χ. The problem with this approach is that, typically for large values of m_{med}, the benchmark value of Γ becomes smaller than the sum of the partial widths for decays into DM and quarks, which makes the choice unphysical [38]. To avoid the problem it is usually assumed that the mediator can not decay into particles other than the SM ones and, depending on its mass, the DM, and the width is computed accordingly as

$$\Gamma = \Gamma_\chi + \sum_f \Gamma_f + \Gamma_{gg} \tag{7}$$

This is usually referred to as the "minimal width assumption". Even if this choice eliminates one parameter, its drawback is that now the cross sections depend nontrivially on the couplings:

$$\sigma \propto \frac{g_\chi^2 g_q^2}{\left(s - m_{\text{med}}^2\right)^2 + m_{\text{med}}^2 \Gamma^2} \tag{8}$$

where Γ at the denominator depends on g_χ, g_q. Nevertheless, in most cases the dependence on the couplings is less important than the one on the masses, and so it is a good choice to fix the couplings and let the mass vary, thus presenting results as exclusion plots in the plane m_χ versus m_{med}. Following the recommendations of the LHC Dark Matter Working Group, useful benchmarks for the vector (V) and axial-vector (A) models are as follows [41, 42]:

$$\begin{aligned} V&: \begin{cases} g_\chi = 1, & g_q = 0.25, \quad g_\ell = 0 \\ g_\chi = 1, & g_q = 0.1, \quad g_\ell = 0.01 \end{cases} \\ A&: \begin{cases} g_\chi = 1, & g_q = 0.25, \quad g_\ell = 0 \\ g_\chi = 1, & g_q = 0.1, \quad g_\ell = 0.1 \end{cases} \end{aligned} \tag{9}$$

The exclusion lines that LHC draws have typically a simple structure. In MET+X searches in which DM is pair produced from the mediator and recoils against a SM particle (a photon, a hadronic jet or other) that is necessary to tag the event, the best sensitivity is obtained for $m_{\text{med}} > 2m_\chi$, where DM can be produced on resonance and the cross section is consequently enhanced. On the other hand, for $m_{\text{med}} < 2m_\chi$, the cross section is suppressed. (In the mono-jet channel, for $m_{\text{med}} \lesssim 2m_\chi$, the LHC at 14 TeV with 300 fb^{-1} is sensitive to $\mathcal{O}(1)$ couplings only for $m_\chi \lesssim \mathcal{O}(100\ \text{GeV})$, while for $\text{m}_\chi \sim 1$ TeV it is sensitive only to couplings of order $g_\chi \cdot g_q \gtrsim 10$ [25]) Finally, for large m_{med} the EFT limit is recovered, but then again the constraining power is suppressed by the large m_{med}^4. Mono-jet limits in this region extend up to around 1.5 – 2 TeV, depending on the search, on the choice of vector or axial-vector mediator and to the values of the couplings (see, e.g., Figures 3 and 4 of [43] for the dependence of the m_{med} limit on the values g_q, g_χ). This gives rise to a typical triangular shape in the exclusion plots sketched in Figure 3 (see, e.g., [44] for a very recent example of such an exclusion plot in the mono-Z/W channel).

Sometimes, it proves very useful to show the constraints on s-channel simplified models in the plane $m_{\text{med}} - \Lambda$ for fixed m_χ, where $\Lambda = m_{\text{med}}/\sqrt{g_q g_\chi}$ is defined as the contact interaction scale. In this plane, the bounds have the typical shape shown in the right panel of Figure 3. For light mediator (Region I), DM production proceeds off-shell, and the cross section is suppressed (compared to the corresponding EFT result) by (m_{med}^4/s^2), where $\sqrt{s}$ can be estimated as $\min(\text{MET}^2, m_\chi^2)$. In Region II, the mediator is produced on-shell, and the cross section is enhanced. In this region the limit depends on the choice of the width Λ, as the cross section scales as $g_\chi^2 g_q^2/(m_{\text{med}}^2 \Gamma^2)$. Finally, in Region III, the EFT limit is recovered.

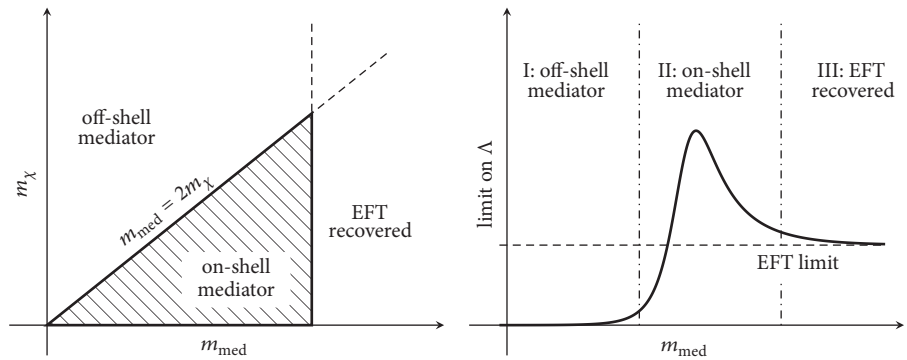

FIGURE 3: *Left:* sketch of the limits obtained from mono-X analysis in the $m_{\text{med}} - m_\chi$ plane (*left*, adapted from [32]) and in the $m_{\text{med}} - \Lambda$ plane (*right*, adapted from [37]).

Missing transverse energy searches are not the only handle that we have on simplified models. Searches for the mediator, for example, in the resonant di-jet channel, can lead to more stringent bounds in m_{med} for the same value of the coupling to quarks g_q.

Constraints on *s*-channel simplified models have been obtained by numerous groups, with a particular attention to the case of a (axial-)vector mediator, due to the problematic nature of the (pseudo)scalar models of (3), (4) (see the discussion in Section 4). Mono-jet constraints were discussed in [45–50]. A thorough comparison of mono-jet searches to di-jet searches, direct detection limits, dark matter overproduction in the early universe, and constraints from perturbative unitarity is performed in [43, 51–54]. In [55, 56] the problem of deriving limits for arbitrary values of the coupling constants starting from the benchmark ones is addressed. The case for a light DM (thus evading constraints from direct searches) is analysed in [22, 57, 58].

A very interesting phenomenology arises in the case where the couplings to third-generation quarks is larger than the couplings to the first two, as it is the case in the spin-0 models with MFV introduced above. Strong constraints on these models come from searches for one or two b-tagged jet + MET and $t\bar{t}$ + MET (see [59] for an early proposal within the EFT framework and [28, 48, 60–64] for a discussion in terms of simplified models). Summarizing, for light DM (m_χ = 1 GeV) current bounds obtained in the $t\bar{t}$ + MET channel can exclude couplings $g \gtrsim 1$ up to $m_{\text{med}} \lesssim 100$ GeV [63, 64], while this value can decrease to ≈ 0.5 at the end of the planned LHC runs [62]. These values are similar in magnitude to the ones obtained by a mono-jet analysis (see, e.g., [61]), which are much weaker than in the (axial-)vector case due to the assumed SM-Yukawa-like structure, which suppresses the coupling to light quarks. Still, LHC searches can provide the most stringent limit in some region of parameter space, complementing those coming from direct detection and from the relic abundance constraint and proving once more the importance of the complementarity of different probes [61].

3.2. t-Channel Mediators. Another interesting possibility is that of a coloured fermionic mediator with an interaction vertex between quarks and the WIMP resulting in a t-channel exchange, as with squark in supersymmetric models:

$$\mathscr{L} = \mathscr{L}_{\text{SM}} + \sum_i \left(g_L^i \overline{Q}_L^i \widetilde{Q}_L^i + g_u^i \overline{u}_R^i \widetilde{u}_R^i + g_d^i \overline{d}_R^i \widetilde{d}_R^i \right) \chi + \text{mass terms} + c.c., \tag{10}$$

where Q_L^i, u_R^i, d_R^i are the usual SM quarks, $\widetilde{Q}_L^i, \widetilde{u}_R^i, \widetilde{d}_R^i$ correspond to the respective scalar mediator (the squarks), and i represents a flavour index. Unlike the usual case in supersymmetry, here the WIMP χ can be taken to be either Dirac or Majorana fermion. This model is extensively analysed in [65–72]. While in the model above the flavour index is carried by the mediators, it could be the case that this index is assigned to the DM itself. This is the so-called "flavoured DM" scenario [73, 74]

As it can be easily understood, also in the case of t-channel mediators the phenomenology depends on the relative values of the couplings and of the masses involved. The minimal flavour violation hypothesis forces the couplings g^i and the masses of the scalars m_i to be equal. This assumption can be relaxed for the third generation. Particularly interesting is the case in which the coupling to the third generation is enhanced, and strong constraints come from searches for b, t quarks in the final state [25, 74–81]. A distinct phenomenology arises in the case of small couplings, in which the relic density is obtained by a out-of-equilibrium freeze-out mechanism and exotic collider signatures such as disappearing tracks and displaced vertices [80, 81].

Two interesting features of this model are worth listing that makes it qualitatively different from its low energy EFT limit. Firstly, being the squarks coloured, gluons may be emitted not only as initial state radiation but also from the mediator itself. This process is suppressed in the EFT limit by two powers of M_{med}, and this makes a large qualitative difference in the kinematic distribution within the simplified model and the corresponding operator. Secondly, when the mediator is light enough, its pair production becomes kinematically accessible, and an event like $p\ p \longrightarrow \tilde{q}\ \tilde{q} \longrightarrow q\chi\ q\chi$ leads to a di-jet + MET signature (or in general jets + MET, when additional jet radiation is taken into account).

Interestingly, this signature with two high-p_T jets leads to constraints stronger then the mono-jet one on a large portion of parameter space, except for the compressed region $|m_{med} - m_\chi| \ll m_{med}$ [70].

An interesting phenomenology arises in the case in which the t-channel mediators couple DM to both quarks and leptons, as in [82, 83]. Radiative corrections in this model strongly alter the spectrum of the Drell-Yan process $q\bar{q} \longrightarrow \ell^+\ell^-$. With this signal, one can probe "compressed regions" that are difficult to probe in direct searches for mediators like jets + MET searches. Moreover, these features can be used to make qualitative statements about dark matter's self-conjugation, mass, spin, and chirality of interactions.

3.3. Other Models. In addition to the models listed above, many interesting ones may be constructed that cannot be addressed here. Those include spin-2 mediators [84], t-channel fermionic mediators, fermiophobic scalar mediators [85], gluphylic mediator models [86–88], models with SM portals (Higgs or Z) [89], models of scalar DM [90], vector DM [91, 92], Higgs portal models with DM of diverse spin number [93–95], and others. A recent and comprehensive review is given in [30]. Interesting cosmological features of a model in which DM couples predominantly to the top quark are explored in [96]. In this case, it is possible to obtain the correct abundance with annihilations of DM particles to heavier states, at the tail of the velocity distribution.

4. Less Simplified Models

4.1. A Critical Look. The simplified models that we discussed so far can be viewed as an improvement of effective operators, where the effective scale Λ^4 is replaced with a propagator's denominator $(p^2 - M^2)^2 + \Gamma^2 M^2$ in order to avoid energy limitations and exploit resonant enhancement in the production cross section. This is one step above in a bottom-up approach. Nevertheless, the models described above suffer from other limitations and are not fully self consistent, as we are going to illustrate in a moment.

The reason why the theoretical consistency of the simplified models is important is twofold. On the one hand, violation of perturbative unitarity can lead to spuriously large predictions (e.g., in the process of W emission), leading to artificially strong bounds on the parameter space of the model. On the other hand, thinking of a full UV completion from which simplified models may descend, theoretical consistency is a necessary requirement at the level of the full theory. One could argue that this may not be the case for the simplified model, since other fields belonging to the full theory may restore the desired consistency. While this is generically true, these additional fields may add interesting ingredients to the phenomenology of the model, as they may produce new final states at the LHC and modify the annihilation cross section that enters the relic abundance calculation and the indirect detection fluxes, and their inclusion is therefore mandatory.

4.1.1. Gauge Non-Invariance of the (Pseudo-)Scalar Model. The scalar and pseudo-scalar models of (3), (4) are manifestly not gauge invariant. The problem comes with the Yukawas of the scalar mediator: assuming the DM is a singlet under the SM group, the invariance of the term $S\overline{\chi}\chi$ forces S to be a singlet as well, while for the Yukawas with the SM quarks $S\bar{q}q$ and $P\bar{q}\gamma_5 q$ the mediator should transform as a doublet. Clearly such a model can exist only as a consequence of EW symmetry breaking, and the DM-SM interaction has to be suppressed at low energy by some power of v_{EW}/m_{med} [97, 98]. Clearly, a UV completion of the model is necessary.

As we will detail below, this issue can be fixed if the mediator is assumed to couple at tree level *only* to the DM and to the Higgs through the gauge invariant portal terms $S|H|^2$, $S^2|H|^2$, etc. that gives rise to a non-zero mixing angle after EW symmetry breaking [98–101]. This construction can be replicated for a pseudo-scalar, with the advantage of avoiding strong direct detection bounds, but at the price of introducing a new source of CP violation [102–104].

In [98], the model of (3) in compared to three possible consistent variations of it: first, the one in which the coupling of the scalar mediator to SM quarks is suppressed by v_{EW}/m_{med}; second, the model in which the mediator is replaced with the Higgs itself and the coupling to the DM particle is suppressed by the same factor; finally, the Higgs portal model including the $S - h$ mixing mentioned above. Naively, one could think that the S-mediator and the h mediator models can provide good approximations of the Higgs portal model. This is true only for large S mass ($m_S \gtrsim 1$ TeV for $m_\chi = 50$ GeV, or $m_S \gtrsim 5$ TeV for $m_\chi = 400$ GeV), in which case the Higgs portal resembles the model with the Higgs as a mediator, because the heavy scalar S can be integrated out. On the other hand, for lower masses the behaviour of the Higgs portal model descends from the interplay of the two mediating particles h and S, and the limits can be both stronger or weaker than the ones obtained in the two single-mediator models. In the case $m_\chi > m_h/2$, where the mixing angle is not constrained by the Higgs-to-invisibles branching ratio, the DM production cross section is dominated by S exchange, and in the heavy S limit a bound $M_\star \gtrsim 20$ GeV can be imposed, where

$$\frac{1}{M_\star^3} \approx \frac{\lambda \sin\alpha \cos\alpha}{v_H m_h^2}, \tag{11}$$

α being the mixing angle and λ the coupling of the scalar S to the DM particle [98].

A model of this kind naturally replicates the SM Yukawa-like structure of (3), (4) and displays promising experimental signatures (mono-jet, heavy quarks, mono-V, see [32] and references therein). Nevertheless, the mixing angle ϵ is strongly constrained by Higgs physics measurements (in particular the decay rate into invisible particles and the Higgs signal strength that are respectively enhanced and reduced by a non-zero mixing angle), and it does not add anything new to the LHC models' toolbox. An interesting option is to extend it to a two Higgs doublets model (2HDM) with the addition of a singlet scalar, evading all such constraints [101, 105].

4.1.2. Gauge Non-Invariance and Violation of Perturbative Unitarity. The vector and axial-vector simplified models of

(1), (2) are not in general invariant under the full SM gauge group $\mathrm{SU}(3)_c \times \mathrm{SU}(2)_L \times \mathrm{U}(1)_Y$ but only under the unbroken subgroup $\mathrm{SU}(3)_c \times \mathrm{U}(1)_{\mathrm{e.m.}}$. In particular, if the couplings to up and down quarks are different the mediator does not couple to the left handed quark doublet but to its two components separately, thus breaking gauge invariance. Similarly, the t-channel model of (10) is not gauge invariant unless the scalar mediator $\widetilde{Q}_L^i$ is charged and transforms as $(\mathbf{2}, -1/2)$ under $\mathrm{SU}(2)_L \times \mathrm{U}(1)_Y$. Violation of the electroweak gauge symmetry can lead to spuriously enhanced cross section for DM production with the initial state radiation of a W boson [97, 106]. This problem does not only affect the mono-W searches: W can indeed decay hadronically, enhancing the signal in the mono-jet search. For example, in the case of a vector mediator with opposite sign couplings to up and down quarks, this process dominates the mono-jet cross section for $\not{E}_T > 400$ GeV [107]. Similar issues should be present when considering Z or γ emission. In passing, this example shows that constraints descending from the internal consistency of the model cannot be neglected even when restricting to a particular MET search such as the mono-jet one that at first sight looks safe. Referring to the case of a vector mediator, different couplings of the up and down quarks can be made compatible with perturbative unitarity if an appropriate vertex WWZ' is added (where Z' is the new vector mediator), in similarity to what happens for the Z boson in the SM. In the t-channel model, instead, perturbative unitarity is restored if W emission from the charged mediator's line is included in the calculation.

4.1.3. Violation of Perturbative Unitarity with a s-Channel Axial-Vector Mediator. In the axial-vector model (2) the coupling to the longitudinal mode of the mediator is enhanced for heavy fermions by the ratio m_f/m_A. In particular, considering the elastic scattering of fermions (both SM fermions or DM) the perturbative unitarity bound on this model reads $m_f \lesssim m_{Z'}/(\sqrt{2} g_f^A)$ [108], where f may stand for both a SM fermion or the DM particle. Even if such a bound is satisfied, perturbative unitarity is still violated in the process of 2 fermions annihilation into $Z'Z'$, which is important for the calculation of the relic density and for indirect detection. In order to restore unitarity some additional ingredient has to be invoked. In particular, what violates unitarity is the longitudinal mode of the Z' boson; therefore the addition to the model of a scalar particle, invariant under the SM gauge group, that give rise to its mass via Higgs mechanism serves the purpose. In this case, the condition on the mass of the Z' would be the following [108]:

$$\sqrt{\pi} \frac{m_{Z'}}{g_{\mathrm{DM}}^A} \geq \max\left[m_s, \sqrt{2} m_{\mathrm{DM}}\right], \tag{12}$$

where m_s is the mass of the new scalar. At this point, it is clear that such an issue is not present in the vector model, because the mass of the mediator in that case can be obtained via a Stueckelberg mechanism without the need of additional particles (see [109] for further discussion).

4.1.4. Invariance of the SM Yukawas. Again referring to the axial-vector model of (2), if this is thought as a gauge extension of the SM, then the SM fermions must be charged under the new gauge symmetry (we restrict for simplicity to a $\mathrm{U}(1)'$ theory, often referred to as a "Z' model"). Therefore, the Yukawa terms $H\overline{Q}_L d_R$ are gauge invariant only if the Higgs is charged as well, with $q_H = q_{qL} - q_{uR} = q_{dR} - q_{qL} = q_{eR} - q_{\ell L}$ (which is zero only if the SM fermions are vector-like under the new symmetry, as in the $B - L$ case) [108]. From this relation one sees that leptons have to be charged in this model, thus resulting in strong constraints from di-lepton searches. Another important consequence is that, after electroweak-symmetry breaking, the SM Z and the Z' have a non-zero mixing angle, and a tree level hZZ' vertex appears, with important phenomenological consequences and a complicate interplay between the two effects [110, 111].

4.1.5. Cancellation of Gauge Anomalies. If the interaction of DM with SM fermions is due to an extended gauge symmetry, in order for the theory to be consistent at the quantum level the charge assignment under the new gauge group cannot be generic. If all the fermions of the dark sector are uncharged under $\mathrm{SU}(3)_c \times \mathrm{SU}(2)_L \times \mathrm{U}(1)_Y$, then the SM ones must have charges chosen in such a way to cancel the mixed anomalies of the dark gauge group with the SM. It can be shown that for a $\mathrm{U}(1)'$ theory this forces the charges to be a linear combination of the SM hypercharge Y and of $B - L$ [112]. This implies that the mediator must couple to leptons, leading to tight constraints from resonance searches in the di-lepton channel (see, e.g., [110]).

Alternatively, additional heavy fermions, charged under the SM, may be added to the model. The mass of these fermions cannot be arbitrarily large: in order to cancel the anomalies, they must be chiral at least under the dark gauge group, and their mass is given by the vev of the dark Higgs. Fortunately, imposing the invariance of the SM Yukawa terms as discussed above in Section 4.1.4, it turns out that the gluon-gluon-Z' anomaly automatically cancels, and the new states need not to be coloured, reducing their impact on LHC searches [108]. On the other hand, they will enter the calculation of loop induced processes such as two photons decays that are not calculable in an anomalous theory and are relevant for indirect searches [110, 113]. (Anomalous models can be studied within a specific EFT framework, in which the required additional heavy fermions are integrated out, resulting in a set of effective Chern-Simons terms that must be added to the theory [114])

4.2. The $\mathrm{U}(1)'$ *Model.* This model is one of the simplest possible extensions of the SM, in which the gauge group is enlarged by an additional $\mathrm{U}(1)'$, spontaneously broken by the vev of a scalar field s, singlet under the SM, that gives mass to the dark gauge boson Z'. As mentioned above, interesting features come from this construction. First, the invariance of the SM Yukawas force the Higgs to be charged under $\mathrm{U}(1)'$ whenever the charges of the left- and right-handed SM fermions differ from one another. Second, and consequently, the Higgs kinetic term includes interactions

with the Z' boson, that induce after EW symmetry breaking a $ZZ'h$ that may have an impact on indirect detection [110]. Moreover, the dark Higgs s enriches the phenomenology, both at the LHC and in the calculation of annihilation rates. Finally, in consistent models that implement gauge anomaly cancellation the SM leptons must typically be charged and couple to the Z', which is therefore constrained by resonant di-lepton searches. (The coupling to leptons can be avoided by adding new fermions with nontrivial transformations under the SM gauge group such that all anomalies cancel [115], or in models where the DM carries a non-zero baryon number [116–119].) This constraint may be evaded if the Z' is lighter than the SM Z, thus escaping resonant searches [120].

A number of studies have addressed DM Z' models with respect to LHC, direct and indirect searches, as well as its cosmological implications [53, 121–126]. If DM is a Dirac fermion, its nonrelativistic scattering off nuclei is spin-independent, and direct detection constrain the DM mass to be larger than $\sim$ 1 TeV [125]. Such a strong constraint is lifted if the DM is a Majorana fermion, since the vector bilinear $\overline{\chi}\gamma_\mu\chi$ vanishes exactly and only the axial-vector one is left. In models in which the mediator couples to leptons with a coupling similar in magnitude to the one to quarks (as required by anomaly cancellation) resonant di-lepton searches forces the Z' to be heavier than $\sim$ 3 − 4 TeV, depending on the couplings and on the structure of fermionic charges [127]. Di-jet searches can exclude $m_{Z'} \lesssim 2.5$ TeV for a coupling $g_q \approx 0.25$, see [128]. Mono-jet searches are typically weaker than the di-jet ones, reaching $m_{Z'} \lesssim 1.5$ TeV for $g_q = 0.25$, $g_\chi = 1$ and for $m_\chi < m_{Z'}/2$ [129].

The dark Higgs becomes relevant when the annihilation rate is concerned. Indeed, the sZ' annihilation channel proceeds in s-wave and, therefore, it dominates the cross section for indirect detection and for the relic abundance calculation [130], together with the ss, $Z'Z'$, and Zh channels [130, 131]. In particular, the additional channels and operators increase the DM annihilation rate, thus reducing the relic abundance and alleviating constraints from DM overproduction in the early universe. Moreover, mono-dark-Higgs signals can be looked for at the LHC, with the typical signature being DM produced in association with a scalar resonance s decaying to a highly boosted $b\bar{b}$ pair [131]. In this case, the expected LHC sensitivity extends up to $m_{Z'} \lesssim 3.5$ TeV, $m_\chi \lesssim 600$ GeV for $m_s = 50$ GeV, or higher for heavier s. In general, such a model can be viewed as a model with two mediators that in some limit may reduce to a spin-1 or to a spin-0 mediator [53].

4.3. Two Higgs Doublets (plus One Singlet) Models and DM. Models in which the (pseudo-)scalar mediator that couples to DM obtains its coupling to SM quarks from mixing with a second Higgs doublet have received a significant attention recently. With respect to the scenario in which the singlet mixes directly with the SM Higgs discussed in Section 4.1.1, in this model the Higgs branching ratios and signal strength are not modified. Moreover, both a scalar and a pseudo-scalar mediator can be accommodated without adding new sources of CP violation. Indeed, in the presence of a second doublet, there are 8 spin-0 fields, three of which get 'eaten' by the $Z, W^\pm$ after symmetry breaking, thus leaving one charged scalar field, two neutral ones and one neutral pseudo-scalar, which the dark mediator can mix with. The pseudo-scalar case is particularly interesting in view of the fact that its low energy effective vertex $\overline{q}i\gamma_5 q\overline{\chi}i\gamma_5\chi$ leads to the both spin- and momentum-suppressed non relativistic interaction $(\vec{s}_\chi \cdot \vec{q})(\vec{s}_N \cdot \vec{q})$ [132, 133], on which constrains from direct detection are poor.

A thorough discussion of 2HDM (not related to DM) is given in [134]. The model of interest here, where the 2HDM is complemented with an additional pseudo-scalar mediator and with a DM fermion, is described in detail in [135]. In general, the model counts many free parameters, many of which can be fixed by requiring that Higgs and precision EW tests are not spoiled, and by the requirement of the stability of the scalar potential. In particular, one of the two Higgs states is assumed to have SM-like couplings, while the second doublet couples to SM vectors only at loop level: this is the so-called *alignment/decoupling limit*. Moreover, the neutral scalar, pseudo-scalar, and the charged components of the second Higgs doublet are assumed to have the same mass. A typical choice is then to fix the DM Yukawa coupling to 1, and the DM mass to a benchmark value of 10 GeV. The model then consists of 4 free parameters, which are typically chosen to be the mass of the pseudo-scalars m_a, m_A, the ratio of the VEVs $\tan\beta = v_1/v_2$ and the $a - A$ mixing angle θ.

In the context of DM, many search channels have been used to constrain this class of models. In particular, searches for mono-jet/γ/Z/W/H, non-resonant dijets, single top as well as $t\bar{t}$, $b\bar{b}$, $b\bar{b}Z$, all in association with missing transverse energy, have been explored [62, 101, 104, 105, 135–142]. As usual, constraints come also from visible channels (i.e., where no invisible DM particle is produced), as well as indirect detection and cosmology. Finally, all the usual concerns about 2HDM coming from flavour physics, EW precision tests, invisible Higgs decays, vacuum stability and perturbative unitarity apply too.

The Higgs' width to invisibles constrains is $m_a \gtrsim 100$ GeV, while flavour constraints forces are $\tan\beta \gtrsim 1$. The most powerful searches are then the mono-Z and the mono-H ones that can exclude $\tan\beta$ up to 2 for values of m_a up to $200 - 350$ GeV, depending on the values of m_A and $\sin\theta$. For further details we refer the reader to [135].

Interestingly, since in such a model the coupling of DM to the heavy quarks is naturally enhanced, the Galactic Centre excess could be explained by a model which is testable at the LHC [139, 143].

Let us just mention another related possibility, which is the one of a second inert Higgs doublet, which does not couple to SM fermions except for its mixing with the Higgs. The lightest component of this doublet is a perfect candidate for scalar DM [144].

5. Conclusions

The question of which DM models should be adopted in defining new search strategies and in presenting experimental results is a pressing one, primarily for LHC searches. Simplified DM models are a possible answer to this question, living in between the effective operators approach (with a limited

applicability at the LHC) and the realm of well-motivated BSM theories.

From a bottom-up viewpoint, the idea of simplified models is to expand the effective operators including mediator particles in the description, thus avoiding the energy limitations of the EFT approach and adding a richer phenomenology, new search channels, etc. In a top-down framework, instead, simplified models can be seen as a way to simplify the phenomenology of complex new physics models in such a way to restrict to the phenomena related to DM.

In order not to deal with unphysical results, the vanilla simplified models have to be supplied with additional constraints, couplings, and states, in a kind of second-order improvement. The typical consequence is that the strongest LHC constraints on the dark sector come from many possible observables other than DM production processes (as the mono-X searches) and di-jet searches (e.g., di-lepton resonances, mixing with Z boson and electroweak precision tests, Higgs width to invisibles, perturbative unitarity, and so on). This comes with no surprise, since the high energy reach of the LHC consent to explore a large variety of phenomena above the weak scale, without restricting to the lightest stable state of this new physics sector. This is quite the opposite with respect to what happens with direct and indirect searches, which are intrinsically limited to constrain the properties of the DM particle.

Theoretically consistent simplified models tend to loose part of their generality and to mimic richer BSM theories. For example, models containing a vector mediator and a dark Higgs may descend from gauged $U(1)'$ constructions, while models featuring two Higgs doublets and a (pseudo-)scalar singlet resemble the Higgs sector of the NMSSM.

Simplified models cannot (or only partially) be viewed as an exhaustive toolbox to constrain all possible WIMP scenarios at once. For this reason, it is of extreme importance that the LHC collaborations publish their results on simple, search-specific, models in such a way that they are recastable for any other model (as it is for cut-and-count analyses). In turn, theoreticians should keep working in close contact with experimentalists in order to maximise the utility of the simplified models tool-kit. Finally, the use of (truncated) EFT should not be disregarded, since this is the most model-independent approach and it is economical from the point of view of the reduced dimensionality of its parameter space.

Conflicts of Interest

The author declares that there are no conflicts of interest regarding the publication of this paper.

Acknowledgments

The author is grateful to Michael Duerr and Davide Racco for the many useful comments on this manuscript.

References

[1] J. Goodman, M. Ibe, A. Rajaraman, W. Shepherd, T. M. Tait, and H. Yu, "Constraints on dark matter from colliders," *Physical Review D: Covering Particles, Fields, Gravitation, and Cosmology*, vol. 82, no. 11, 2010.

[2] M. Beltrán, D. Hooper, E. W. Kolb, Z. A. Krusberg, and T. M. Tait, "Maverick dark matter at colliders," *Physical Review D: Covering Particles, Fields, Gravitation, and Cosmology*, vol. 2010, no. 9, 2010.

[3] J. Goodman, M. Ibe, A. Rajaraman, W. Shepherd, T. M. Tait, and H. Yu, "Constraints on light Majorana dark matter from colliders," *High Energy Physics - Phenomenology*, vol. 695, no. 1-4, pp. 185–188, 2011.

[4] Y. Bai, P. J. Fox, and R. Harnik, "The Tevatron at the frontier of dark matter direct detection," *Physical Review D: Covering Particles, Fields, Gravitation, and Cosmology*, vol. 2010, no. 12, 2010.

[5] P. J. Fox, R. Harnik, J. Kopp, and Y. Tsai, "LEP shines light on dark matter," *Physical Review D: Covering Particles, Fields, Gravitation, and Cosmology*, vol. 84, 2011.

[6] A. Rajaraman, W. Shepherd, T. M. Tait, and A. M. Wijangco, "LHC bounds on interactions of dark matter," *Physical Review D: Covering Particles, Fields, Gravitation, and Cosmology*, vol. 84, no. 9, 2011.

[7] P. J. Fox, R. Harnik, J. Kopp, and Y. Tsai, "Missing energy signatures of dark matter at the LHC," *Physical Review D: Covering Particles, Fields, Gravitation, and Cosmology*, vol. 85, no. 5, 2012.

[8] I. M. Shoemaker and L. Vecchi, "Unitarity and monojet bounds on models for DAMA, CoGeNT, and CRESST-II," *Physical Review D: Covering Particles, Fields, Gravitation, and Cosmology*, vol. 86, no. 1, 2012.

[9] R. C. Cotta, J. L. Hewett, M. Le, and T. G. Rizzo, "Bounds on dark matter interactions with electroweak gauge bosons," *Physical Review D: Covering Particles, Fields, Gravitation, and Cosmology*, vol. 88, no. 11, 2013.

[10] H. K. Dreiner, M. Huck, M. Krämer, D. Schmeier, and J. Tattersall, "Illuminating dark matter at the ILC," *Physical Review D: Covering Particles, Fields, Gravitation, and Cosmology*, vol. 87, no. 7, 2013.

[11] Y. J. Chae and M. Perelstein, "Dark matter search at a linear collider: effective operator approach," *Journal of High Energy Physics*, vol. 5, no. 138, 2013.

[12] P. J. Fox and C. Williams, "Next-to-leading order predictions for dark matter production at hadron colliders," *Physical Review D: Particles, Fields, Gravitation and Cosmology*, vol. 87, no. 5, 2013.

[13] A. De Simone, A. Monin, A. Thamm, and A. Urbano, "On the effective operators for dark matter annihilations," *Journal of Cosmology and Astroparticle Physics*, no. 2, 2013.

[14] H. Dreiner, D. Schmeier, and J. Tattersall, "Contact interactions probe effective dark-matter models at the LHC," *EPL (Europhysics Letters)*, vol. 102, no. 5, 2013.

[15] J.-Y. Chen, E. W. Kolb, and L.-T. Wang, "Dark matter coupling to electroweak gauge and Higgs bosons: An effective field theory approach," *Physics of the Dark Universe*, vol. 2, no. 4, pp. 200–218, 2013.

[16] G. Busoni, A. De Simone, E. Morgante, and A. Riotto, "On the validity of the effective field theory for dark matter searches at the LHC," *Physics Letters B*, vol. 728, pp. 412–421, 2014.

[17] G. Busoni, A. De Simone, J. Gramling, E. Morgante, and A. Riotto, "On the validity of the effective field theory for dark matter searches at the LHC, part II: complete analysis for the s-channel," *Journal of Cosmology and Astroparticle Physics*, no. 6, 2014.

[18] G. Busoni, A. D. Simone, T. Jacques, E. Morgante, and A. Riotto, "On the Validity of the Effective Field Theory for Dark Matter Searches at the LHC, Part III: Analysis for the t-channel," *Journal of Cosmology and Astroparticle Physics*, vol. 2014, no. 1409, 2014.

[19] D. Racco, A. Wulzer, and F. Zwirner, "Robust collider limits on heavy-mediator Dark Matter," *Journal of High Energy Physics*, vol. 2015, no. 5, 2015.

[20] E. Dudas, Y. Mambrini, S. Pokorski, and A. Romagnoni, "(In)visible Z-prime and dark matter," *Journal of High Energy Physics*, vol. 2009, 2009.

[21] J. Goodman and W. Shepherd, "LHC Bounds on UV-Complete Models of Dark Matter," *High Energy Physics - Phenomenology*, 2011.

[22] H. An, X. Ji, and L. Wang, "Light dark matter and Z′ dark force at colliders," *Journal of High Energy Physics*, vol. 2012, no. 7, 2012.

[23] M. T. Frandsen, F. Kahlhoefer, A. Preston, S. Sarkar, and K. Schmidt-Hoberg, "LHC and Tevatron bounds on the dark matter direct detection cross-section for vector mediators," *Journal of High Energy Physics*, vol. 2012, no. 7, 2012.

[24] R. C. Cotta, A. Rajaraman, T. M. Tait, and A. M. Wijangco, "Particle physics implications and constraints on dark matter interpretations of the CDMS signal," *Physical Review D: Particles, Fields, Gravitation and Cosmology*, vol. 90, no. 1, 2014.

[25] J. Abdallah et al., "Simplified Models for Dark Matter and Missing Energy Searches at the LHC," *High Energy Physics - Phenomenology*, 2014.

[26] S. Malik, C. McCabe, H. Araujo, A. Belyaev, C. Boehm et al., "Interplay and Characterization of Dark Matter Searches at Colliders and in Direct Detection Experiments," *Physics of the Dark Universe*, vol. 9-10, pp. 51–58, 2015.

[27] J. Abdallah et al., "Simplified Models for Dark Matter Searches at the LHC," *Physics of the Dark Universe*, vol. 9-10, pp. 8–23, 2015.

[28] D. Abercrombie et al., "Dark Matter Benchmark Models for Early LHC Run-2 Searches: Report of the ATLAS/CMS Dark Matter Forum," 2015, https://arxiv.org/abs/1507.00966.

[29] A. De Simone and T. Jacques, "Simplified models vs. effective field theory approaches in dark matter searches," *The European Physical Journal C*, vol. 76, no. 7, 2016.

[30] G. Arcadi, M. Dutra, P. Ghosh et al., "The waning of the WIMP? A review of models, searches, and constraints," *The European Physical Journal C*, vol. 78, no. 3, 2018.

[31] A. Albert et al., "Towards the next generation of simplified Dark Matter models," *Physics of the Dark Universe*, vol. 16, pp. 49–70, 2017.

[32] F. Kahlhoefer, "Review of LHC dark matter searches," *International Journal of Modern Physics A*, vol. 32, 2017.

[33] E. Morgante, *Aspects of WIMP Dark Matter searches at colliders and other probes [Ph.D. thesis]*, Springer Theses, Geneva, Switzerland, 2017.

[34] G. D'Ambrosio, G. F. Giudice, G. Isidori, and A. Strumia, "Minimal flavor violation: An Effective field theory approach," *Nuclear Physics B*, vol. 645, pp. 155–187, 2002.

[35] M. J. Dolan, F. Kahlhoefer, C. McCabe, and K. Schmidt-Hoberg, "A taste of dark matter: flavour constraints on pseudoscalar mediators," *Journal of High Energy Physics*, vol. 2015, no. 3, 2015.

[36] P. Agrawal, M. Blanke, and K. Gemmler, "Flavored dark matter beyond Minimal Flavor Violation," *Journal of High Energy Physics*, vol. 2014, no. 10, 2014.

[37] O. Buchmueller, M. J. Dolan, and C. McCabe, "Beyond effective field theory for dark matter searches at the LHC," *Journal of High Energy Physics*, vol. 2014, no. 1, 2014.

[38] G. Busoni, A. D. Simone, T. Jacques, E. Morgante, and A. Riotto, "Making the most of the relic density for dark matter searches at the LHC 14 TeV Run," *Journal of Cosmology and Astroparticle Physics*, vol. 2015, 2015.

[39] S. Bruggisser, F. Riva, and A. Urbano, "Strongly Interacting Light Dark Matter," *SciPost Physics*, vol. 3, no. 3, 2017.

[40] S. Bruggisser, F. Riva, and A. Urbano, "The last gasp of dark matter effective theory," *Journal of High Energy Physics*, vol. 2016, no. 11, 2016.

[41] G. Busoni et al., "Recommendations on presenting LHC searches for missing transverse energy signals using simplified s-channel models of dark matter," 2016, https://arxiv.org/abs/1603.04156.

[42] A. Albert et al., "Recommendations of the LHC Dark Matter Working Group: Comparing LHC searches for heavy mediators of dark matter production in visible and invisible decay channels," 2017, https://arxiv.org/abs/1703.05703.

[43] A. Choudhury, K. Kowalska, L. Roszkowski, E. M. Sessolo, and A. J. Williams, "Less-simplified models of dark matter for direct detection and the LHC," *Journal of High Energy Physics*, vol. 2016, 2016.

[44] CMS collaboration, A. M. Sirunyan et al., "Search for new physics in final states with an energetic jet or a hadronically decaying W or Z boson and transverse momentum imbalance at $\sqrt{s} = 13$ TeV," *Physical Review D97*, vol. 092005, no. 9, 2018.

[45] O. Lebedev and Y. Mambrini, "Axial dark matter: The case for an invisible Z," *Physics Letters B*, vol. 734, pp. 350–353, 2014.

[46] O. Buchmueller, M. J. Dolan, S. A. Malik, and C. McCabe, "Characterising dark matter searches at colliders and direct detection experiments: vector mediators," *Journal of High Energy Physics*, vol. 2015, no. 1, 2015.

[47] P. Harris, V. V. Khoze, M. Spannowsky, and C. Williams, "Constraining dark sectors at colliders: Beyond the effective theory approach," *Physical Review D: Particles, Fields, Gravitation and Cosmology*, vol. 91, no. 5, 2015.

[48] M. R. Buckley, D. Feld, and D. Gonçalves, "Scalar simplified models for dark matter," *Physical Review D: Particles, Fields, Gravitation and Cosmology*, vol. 91, no. 1, 2015.

[49] Q. Xiang, X. Bi, P. Yin, and Z. Yu, "Searches for dark matter signals in simplified models at future hadron colliders," *Physical Review D: Particles, Fields, Gravitation and Cosmology*, vol. 91, no. 9, 2015.

[50] P. Harris, V. V. Khoze, M. Spannowsky, and C. Williams, "Closing up on dark sectors at colliders: From 14 to 100 TeV," *Physical Review D: Particles, Fields, Gravitation and Cosmology*, vol. 93, no. 5, 2016.

[51] M. Fairbairn and J. Heal, "Complementarity of dark matter searches at resonance," *Physical Review D: Particles, Fields, Gravitation and Cosmology*, vol. 90, no. 11, 2014.

[52] M. Chala, F. Kahlhoefer, M. McCullough, G. Nardini, and K. Schmidt-Hoberg, "Constraining dark sectors with monojets and dijets," *Journal of High Energy Physics*, vol. 2015, no. 7, 2015.

[53] M. Duerr, F. Kahlhoefer, K. Schmidt-Hoberg, T. Schwetz, and S. Vogl, "How to save the WIMP: global analysis of a dark matter model with two s-channel mediators," *Journal of High Energy Physics*, vol. 2016, no. 9, 2016.

[54] M. Fairbairn, J. Heal, F. Kahlhoefer, and P. Tunney, "Constraints on Z′ models from LHC dijet searches and implications for dark matter," *Journal of High Energy Physics*, vol. 2016, no. 9, 2016.

[55] T. Jacques and K. Nordström, "Mapping monojet constraints onto simplified dark matter models," *Journal of High Energy Physics*, vol. 2015, no. 6, 2015.

[56] A. J. Brennan, M. F. McDonald, J. Gramling, and T. D. Jacques, "Collide and conquer: constraints on simplified dark matter models using mono-X collider searches," *Journal of High Energy Physics*, vol. 2016, no. 5, 2016.

[57] P. Gondolo, P. Ko, and Y. Omura, " Light dark matter in leptophobic ," *Physical Review D: Particles, Fields, Gravitation and Cosmology*, vol. 85, no. 3, 2012.

[58] H. An, R. Huo, and L.-T. Wang, "Searching for low mass dark portal at the LHC," *Physics of the Dark Universe*, vol. 2, no. 1, pp. 50–57, 2013.

[59] T. Lin, E. W. Kolb, and L. Wang, "Probing dark matter couplings to top and bottom quarks at the LHC," *Physical Review D: Particles, Fields, Gravitation and Cosmology*, vol. 88, no. 6, 2013.

[60] U. Haisch and E. Re, "Simplified dark matter top-quark interactions at the LHC," *Journal of High Energy Physics*, vol. 2015, no. 6, 2015.

[61] C. Arina, M. Backović, E. Conte et al., "A comprehensive approach to dark matter studies: exploration of simplified top-philic models," *Journal of High Energy Physics*, vol. 2016, no. 11, 2016.

[62] U. Haisch, P. Pani, and G. Polesello, "Determining the CP nature of spin-0 mediators in associated production of dark matter and $t\bar{t}$ pairs," *Journal of High Energy Physics*, vol. 2017, no. 2, 2017.

[63] CMS. collaboration, "Search for dark matter in association with a top quark pair at sqrt(s)=13 TeV," CMS-PAS-EXO-16-005.

[64] CMS collaboration, "Search for dark matter in association with a top quark pair at $\sqrt{s} = 13TeV$ in the dilepton channel," CMS-PAS-EXO-16-028.

[65] N. F. Bell, A. J. Galea, J. B. Dent, T. D. Jacques, L. M. Krauss, and T. J. Weiler, "Searching for dark matter at the LHC with a mono-Z," *Physical Review D: Particles, Fields, Gravitation and Cosmology*, vol. 86, no. 9, 2012.

[66] S. Chang, R. Edezhath, J. Hutchinson, and M. Luty, "Effective WIMPs," *Physical Review D: Particles, Fields, Gravitation and Cosmology*, vol. 89, no. 1, 2014.

[67] H. An, L. Wang, and H. Zhang, "Dark matter with t-channel mediator: a simple step beyond contact interaction," *Physical Review D: Particles, Fields, Gravitation and Cosmology*, vol. 2014, 2014.

[68] Y. Bai and J. Berger, "Fermion portal dark matter," *Journal of High Energy Physics*, vol. 2013, no. 11, 2013.

[69] A. DiFranzo, K. I. Nagao, A. Rajaraman, and T. M. Tait, "Simplified models for dark matter interacting with quarks," *Journal of High Energy Physics*, vol. 2013, no. 11, 2013.

[70] M. Papucci, A. Vichi, and K. M. Zurek, "Monojet versus the rest of the world I: t-channel models," *Journal of High Energy Physics*, vol. 2014, no. 11, 2014.

[71] M. Garny, A. Ibarra, S. Rydbeck, and S. Vogl, "Majorana dark matter with a coloured mediator: collider vs direct and indirect searches," *Journal of High Energy Physics*, vol. 2014, no. 6, 2014.

[72] M. Garny, A. Ibarra, and S. Vogl, "Signatures of Majorana dark matter with t-channel mediators," *International Journal of Modern Physics D*, vol. 24, 2015.

[73] P. Agrawal, B. Batell, D. Hooper, and T. Lin, "Flavored dark matter and the Galactic Center gamma-ray excess," *Physical Review D: Particles, Fields, Gravitation and Cosmology*, vol. 90, no. 6, 2014.

[74] B. Batell, T. Lin, and L. Wang, "Flavored dark matter and R-parity violation," *Journal of High Energy Physics*, vol. 2014, no. 1, 2014.

[75] J. Andrea, B. Fuks, and F. Maltoni, "Monotops at the LHC," *Physical Review D: Particles, Fields, Gravitation and Cosmology*, vol. 84, no. 7, 2011.

[76] J. F. Kamenik and J. Zupan, "Discovering dark matter through flavor violation at the LHC," *Physical Review D: Particles, Fields, Gravitation and Cosmology*, vol. 84, no. 11, 2011.

[77] A. Kumar and S. Tulin, "Top-flavored dark matter and the forward-backward asymmetry," *Physical Review D: Particles, Fields, Gravitation and Cosmology*, vol. 87, no. 9, 2013.

[78] J. Agram, J. Andrea, M. Buttignol, E. Conte, and B. Fuks, "Monotop phenomenology at the Large Hadron Collider," *Physical Review D: Particles, Fields, Gravitation and Cosmology*, vol. 89, no. 1, 2014.

[79] C. Kilic, M. D. Klimek, and J. Yu, "Signatures of top flavored dark matter," *Physical Review D: Particles, Fields, Gravitation and Cosmology*, vol. 91, no. 5, 2015.

[80] M. Garny, J. Heisig, B. Lülf, and S. Vogl, "Coannihilation without chemical equilibrium," *Physical Review D: Particles, Fields, Gravitation and Cosmology*, vol. 96, no. 10, 2017.

[81] M. Garny, J. Heisig, M. Hufnagel, and B. Lülf, "Top-philic dark matter within and beyond the WIMP paradigm," *Physical Review D: Particles, Fields, Gravitation and Cosmology*, vol. 97, no. 7, 2018.

[82] W. Altmannshofer, P. J. Fox, R. Harnik, G. D. Kribs, and N. Raj, "Dark matter signals in dilepton production at hadron colliders," *Physical Review D: Particles, Fields, Gravitation and Cosmology*, vol. 91, no. 11, 2015.

[83] R. M. Capdevilla, A. Delgado, A. Martin, and N. Raj, "Characterizing dark matter at the LHC in Drell-Yan events," *Physical Review D: Particles, Fields, Gravitation and Cosmology*, vol. 97, no. 3, 2018.

[84] S. Kraml, U. Laa, K. Mawatari, and K. Yamashita, "Simplified dark matter models with a spin-2 mediator at the LHC," *The European Physical Journal C*, vol. 77, no. 5, 2017.

[85] C. Englert, M. McCullough, and M. Spannowsky, "S-channel dark matter simplified models and unitarity," *Physics of the Dark Universe*, vol. 14, pp. 48–56, 2016.

[86] R. M. Godbole, G. Mendiratta, and T. M. Tait, "A simplified model for dark matter interacting primarily with gluons," *Journal of High Energy Physics*, vol. 2015, no. 8, 2015.

[87] R. M. Godbole, G. Mendiratta, A. Shivaji, and T. M. Tait, "Mono-jet signatures of gluphilic scalar dark matter," *Physics Letters B*, vol. 772, pp. 93–99, 2017.

[88] O. Ducu, L. Heurtier, and J. Maurer, "LHC signatures of a Z ′ mediator between dark matter and the SU(3) sector," *Journal of High Energy Physics*, vol. 2016, no. 3, 2016.

[89] G. Arcadi, Y. Mambrini, and F. Richard, "Z-portal dark matter," *Journal of Cosmology and Astroparticle Physics*, vol. 2015, 2015.

[90] GAMBIT collaboration, P. Athron et al., "Status of the scalar singlet dark matter model," *The European Physical Journal C*, vol. 77, pp. 568–1705, 2017.

[91] G. Arcadi, C. Gross, O. Lebedev, S. Pokorski, and T. Toma, "Evading direct dark matter detection in Higgs portal models," *Physics Letters B*, vol. 769, pp. 129–133, 2017.

[92] G. Arcadi, P. Ghosh, Y. Mambrini, M. Pierre, and F. S. Queiroz, "$Z^{'}$ portal to Chern-Simons Dark Matter," *Journal of Cosmology and Astroparticle Physics*, vol. 2017, 2017.

[93] X. He and J. Tandean, "New LUX and PandaX-II results illuminating the simplest Higgs-portal dark matter models," *Journal of High Energy Physics*, vol. 2016, no. 12, 2016.

[94] C. Chang, X. He, and J. Tandean, "Two-Higgs-doublet-portal dark-matter models in light of direct search and LHC data," *Journal of High Energy Physics*, vol. 2017, no. 4, 2017.

[95] C. Chang, X. He, and J. Tandean, "Exploring Spin-3/2 Dark Matter with Effective Higgs Couplings," *Physical Review D: Particles, Fields, Gravitation and Cosmology*, vol. 96, no. 7, 2017.

[96] A. Delgado, A. Martin, and N. Raj, "Forbidden dark matter at the weak scale via the top portal," *Physical Review D: Particles, Fields, Gravitation and Cosmology*, vol. 95, no. 3, 2017.

[97] N. F. Bell, Y. Cai, J. B. Dent, R. K. Leane, and T. J. Weiler, "Dark matter at the LHC: Effective field theories and gauge invariance," *Physical Review D: Particles, Fields, Gravitation and Cosmology*, vol. 92, no. 5, 2015.

[98] S. Baek, P. Ko, M. Park, W. Park, and C. Yu, "Beyond the dark matter effective field theory and a simplified model approach at colliders," *Physics Letters B*, vol. 756, pp. 289–294, 2016.

[99] S. Baek, P. Ko, and W. Park, "Search for the Higgs portal to a singlet fermionic dark matter at the LHC," *Journal of High Energy Physics*, vol. 2012, no. 2, 2012.

[100] S. Baek, P. Ko, W.-I. Park, and E. Senaha, "Vacuum structure and stability of a singlet fermion dark matter model with a singlet scalar messenger," *Journal of High Energy Physics*, vol. 2012, no. 11, 2012.

[101] N. F. Bell, G. Busoni, and I. W. Sanderson, "Self-consistent Dark Matter simplified models with an s-channel scalar mediator," *Journal of Cosmology and Astroparticle Physics*, vol. 2017, 2017.

[102] K. Ghorbani, "Fermionic dark matter with pseudo-scalar Yukawa interaction," *Journal of Cosmology and Astroparticle Physics*, vol. 1501, 2015.

[103] K. Ghorbani and L. Khalkhali, "Mono-Higgs signature in a fermionic dark matter model," *Journal of Physics G: Nuclear and Particle Physics*, vol. 44, no. 10, 2017.

[104] S. Baek, P. Ko, and J. Li, "Minimal renormalizable simplified dark matter model with a pseudoscalar mediator," *Physical Review D: Particles, Fields, Gravitation and Cosmology*, vol. 95, no. 7, 2017.

[105] D. Goncalves, P. A. N. Machado, and J. M. No, "Simplified Models for Dark Matter Face their Consistent Completions," *Physical Review D: Covering Particles, Fields, Gravitation, and Cosmology*, vol. 95, 2017.

[106] N. F. Bell, Y. Cai, and R. K. Leane, "Mono-W Dark Matter Signals at the LHC: Simplified Model Analysis," *Journal of Cosmology and Astroparticle Physics*, vol. 1601, 2016.

[107] U. Haisch, F. Kahlhoefer, and T. M. Tait, "On mono- W signatures in spin-1 simplified models," *Physics Letters B*, vol. 760, pp. 207–213, 2016.

[108] F. Kahlhoefer, K. Schmidt-Hoberg, T. Schwetz, and S. Vogl, "Implications of unitarity and gauge invariance for simplified dark matter models," *Journal of High Energy Physics*, vol. 2016, no. 2, 2016.

[109] N. F. Bell, Y. Cai, and R. K. Leane, "Impact of mass generation for spin-1 mediator simplified models," *Journal of Cosmology and Astroparticle Physics*, vol. 2017, 2017.

[110] T. Jacques, A. Katz, E. Morgante, D. Racco, M. Rameez, and A. Riotto, "Complementarity of DM searches in a consistent simplified model: the case of $Z^{'}$," *Journal of High Energy Physics*, vol. 2016, no. 10, 2016.

[111] Y. Cui and F. D'Eramo, "Surprises from complete vector portal theories: New insights into the dark sector and its interplay with Higgs physics," *Physical Review D: Particles, Fields, Gravitation and Cosmology*, vol. 96, no. 9, 2017.

[112] S. Weinberg, *The quantum theory of fields*, vol. 2 of *Modern applications*, Cambridge University Press, 2013.

[113] M. Duerr, P. Fileviez Pérez, and J. Smirnov, "Gamma lines from Majorana dark matter," *Physical Review D: Particles, Fields, Gravitation and Cosmology*, vol. 93, no. 2, 2016.

[114] A. Ismail, A. Katz, and D. Racco, "On dark matter interactions with the Standard Model through an anomalous Z*I*," *Journal of High Energy Physics*, vol. 2017, no. 165, 2017.

[115] J. Ellis, M. Fairbairn, and P. Tunney, "Anomaly-free dark matter models are not so simple," *Journal of High Energy Physics*, no. 8, 2017.

[116] M. Duerr, P. Fileviez Perez, and M. B. Wise, "Gauge Theory for Baryon and Lepton Numbers with Leptoquarks," *Physical Review Letters*, vol. 11, 2013.

[117] M. Duerr and P. Fileviez Pérez, "Baryonic dark matter," *Physics Letters B*, vol. 732, pp. 101–104, 2014.

[118] P. Fileviez Pérez, S. Ohmer, and H. H. Patel, "Minimal theory for lepto-baryons," *Physics Letters B*, vol. 735, pp. 283–287, 2014.

[119] S. Ohmer and H. H. Patel, "Leptobaryons as Majorana dark matter," *Physical Review D: Particles, Fields, Gravitation and Cosmology*, vol. 92, no. 5, 2015.

[120] A. Alves, G. Arcadi, Y. Mambrini, S. Profumo, and F. S. Queiroz, "Augury of darkness: the low-mass dark $Z^{'}$ portal," *Journal of High Energy Physics*, vol. 2017, no. 4, 2017.

[121] A. Alves, S. Profumo, and F. S. Queiroz, "The dark Z' portal: direct, indirect and collider searches," *Journal of High Energy Physics*, vol. 2014, 2014.

[122] G. Arcadi, Y. Mambrini, M. H. Tytgat, and B. Zaldıvar, "Invisible $Z^{'}$ and dark matter: LHC vs LUX constraints," *Journal of High Energy Physics*, vol. 2014, no. 3, 2014.

[123] A. Alves, A. Berlin, S. Profumo, and F. S. Queiroz, "Dark Matter Complementarity and the $Z^{'}$ Portal," *Physical Review D*, vol. 92, 2015.

[124] K. Ghorbani and H. Ghorbani, "Two-portal dark matter," *Physical Review D: Particles, Fields, Gravitation and Cosmology*, vol. 91, no. 12, 2015.

[125] A. Alves, A. Berlin, S. Profumo, and F. S. Queiroz, "Dirac-fermionic dark matter in $U(1)_X$ models," *Journal of High Energy Physics*, vol. 76, pp. 1–33, 2015.

[126] G. Arcadi, M. D. Campos, M. Lindner, A. Masiero, and F. S. Queiroz, "Dark sequential Z' portal: Collider and direct detection experiments," *Physical Review D*, 2018.

[127] ATLAS collaboration, M. Aaboud et al., "Search for new high-mass phenomena in the dilepton final state using 36 fb^{-1} of proton-proton collision data at $\sqrt{s} = 13TeV$ with the ATLAS detector," *Journal of High Energy Physics*, vol. 10, 2017.

[128] ATLAS collaboration, M. Aaboud et al., "Search for new phenomena in dijet events using 37 fb^{-1} of pp collision data collected at $\sqrt{s} = 13TeV$ with the ATLAS detector," *Physical Review D*, vol. 96, 2017.

[129] ATLAS collaboration, "Search for dark matter and other new phenomena in events with an energetic jet and large missing transverse momentum using the ATLAS detector," ATLAS-CONF-2017-060.

[130] N. F. Bell, Y. Cai, and R. K. Leane, "Dark Forces in the Sky: Signals from Z' and the Dark Higgs," *Journal of Cosmology and Astroparticle Physics*, 2016.

[131] M. Duerr, A. Grohsjean, F. Kahlhoefer, B. Penning, K. Schmidt-Hoberg, and C. Schwanenberger, "Hunting the dark Higgs," *Journal of High Energy Physics*, vol. 2017, no. 4, 2017.

[132] J. Fan, M. Reece, and L. Wang, "Non-relativistic effective theory of dark matter direct detection," *Journal of Cosmology and Astroparticle Physics*, vol. 2010, no. 11, 2010.

[133] A. L. Fitzpatrick, W. Haxton, E. Katz, N. Lubbers, and Y. Xu, "The effective field theory of dark matter direct detection," *Journal of Cosmology and Astroparticle Physics*, vol. 2013, 2013.

[134] G. Branco, P. Ferreira, L. Lavoura, M. Rebelo, M. Sher, and J. P. Silva, "Theory and phenomenology of two-Higgs-doublet models," *Physics Reports*, vol. 516, no. 1-2, pp. 1–102, 2012.

[135] M. Bauer, U. Haisch, and F. Kahlhoefer, "Simplified dark matter models with two Higgs doublets: I. Pseudoscalar mediators," *Journal of High Energy Physics*, vol. 2017, no. 5, 2017.

[136] J. M. No, "Looking through the pseudoscalar portal into dark matter: Novel mono-Higgs and mono-Z signatures at the LHC," *Physical Review D*, vol. 93, no. 3, 2016.

[137] A. Angelescu and G. Arcadi, "Dark matter phenomenology of SM and enlarged Higgs sectors extended with vector-like leptons," *The European Physical Journal C*, 2017.

[138] S. Banerjee, D. Barducci, G. Bélanger, B. Fuks, A. Goudelis, and B. Zaldivar, "Cornering pseudoscalar-mediated dark matter with the LHC and cosmology," *Journal of High Energy Physics*, vol. 2017, no. 7, 2017.

[139] P. Tunney, J. M. No, and M. Fairbairn, "Probing the pseudoscalar portal to dark matter via $\overline{b}bZ(\longrightarrow \ell\ell) + \not{E}T$: From the LHC to the Galactic Center excess," *Physical Review D: Particles, Fields, Gravitation and Cosmology*, vol. 96, no. 9, 2017.

[140] N. F. Bell, G. Busoni, and I. W. Sanderson, "Two Higgs doublet dark matter portal," *Journal of Cosmology and Astroparticle Physics*, vol. 2018, no. 01, 2018.

[141] G. Arcadi, M. Lindner, F. S. Queiroz, W. Rodejohann, and S. Vogl, "Pseudoscalar mediators: a WIMP model at the neutrino floor," *Journal of Cosmology and Astroparticle Physics*, vol. 1803, no. 42, 2018.

[142] P. Pani and G. Polesello, "Dark matter production in association with a single top-quark at the LHC in a two-Higgs-doublet model with a pseudoscalar mediator," *High Energy Physics - Phenomenology*, vol. 21, pp. 8–15, 2018.

[143] S. Ipek, D. McKeen, and A. E. Nelson, "A Renormalizable Model for the Galactic Center Gamma Ray Excess from Dark Matter Annihilation," *Physical Review D: Particles, Fields, Gravitation and Cosmology*, vol. 90, 2014.

[144] L. L. Honorez, E. Nezri, J. F. Oliver, and M. H. G. Tytgat, "The inert doublet model: an archetype for dark matter," *Journal of Cosmology and Astroparticle Physics*, vol. 2007, 2007.

Hindawi
Advances in High Energy Physics
Volume 2018, Article ID 3010514, 23 pages
https://doi.org/10.1155/2018/3010514

Review Article

Impact of Cosmic-Ray Physics on Dark Matter Indirect Searches

Daniele Gaggero[1] **and Mauro Valli**[2]

[1]*GRAPPA Institute, Institute of Physics, University of Amsterdam, 1098 XH Amsterdam, Netherlands*
[2]*INFN, Sezione di Roma, P.le A. Moro 2, 00185 Roma, Italy*

Correspondence should be addressed to Mauro Valli; mauro.valli@roma1.infn.it

Received 2 February 2018; Accepted 30 April 2018; Published 17 December 2018

Academic Editor: Farinaldo Queiroz

The quest for the elusive dark matter (DM) that permeates the Universe (and in general the search for signatures of physics beyond the Standard Model at astronomical scales) provides a unique opportunity and a tough challenge to the high energy astrophysics community. In particular, the so-called DM *indirect searches*—mostly focused on a class of theoretically well-motivated DM candidates such as the weakly interacting massive particles—are affected by a complex astrophysical background of cosmic radiation. The understanding and modeling of such background require a deep comprehension of an intricate classical plasma physics problem, i.e., the interaction between high energy charged particles, accelerated in peculiar astrophysical environments, and magnetohydrodynamic turbulence in the interstellar medium of our galaxy. In this review we highlight several aspects of this exciting interplay between the most recent claims of DM annihilation/decay signatures from the sky and the galactic cosmic-ray research field. Our purpose is to further stimulate the debate about viable astrophysical explanations, discussing possible directions that would help breaking degeneracy patterns in the interpretation of current data. We eventually aim to emphasize how a deep knowledge on the physics of CR transport is therefore required to tackle the DM indirect search program at present and in the forthcoming years.

1. Exotica: Where to Find Them?

The particle dark matter (DM) [1] discovery may potentially undertake a different path than the beaten track of collider searches [2] and direct detection experiments [3]. Early Universe thermal relics, in particular, may be well-motivated DM candidates [4–6] expected to annihilate (or decay) even in today galactic halos, producing Standard Model (SM) particle yields. Therefore, the measurement of charged particle and gamma-ray fluxes of cosmic origin in a wide energy range—say from few MeV all the way up to the multi-TeV domain—may be a quite unique tool at our disposal in order to probe the putative particle nature of DM [7–9].

It is widely recognized that the indirect extraction of a DM signal in this context is an extremely challenging task. The DM problem in general and the indirect searches in particular have been already presented in comprehensive review papers (see, e.g., [10, 11]). Here, we wish to focus our attention on the important interplay between particle DM signatures and the background signals expected from astrophysics, discussing in particular the phenomenological relevance of cosmic-ray physics.

As far as charged particles are concerned, the first consideration in order is that high energy protons, nuclei, and electrons are injected in copious amounts as cosmic rays (CRs) by different classes of astrophysical sources (such as shocks associated with supernova explosions or superbubbles or possibly accretion-powered mildly relativistic jets), which provide a huge and irreducible background. On the other hand, the paucity of antiparticles, mostly produced by secondary interactions of CRs, could in principle drastically improve the signal-to-noise ratio in favor of a putative DM detection, within a rather low expected astrophysical background; this possibility of detecting Early Universe relics by studying galactic antiparticles was first outlined in the early 1980s in several pioneering papers (e.g., [12, 13]) and has been studied in much larger detail in particular during the last decade, mainly thanks to the dramatic improvement in the quality of the data provided by PAMELA [14] and

AMS-02 [15] experiments. For a recent discussion on cosmic antimatter opportunities, see, for example, [16, 17].

Despite the low background, even in the case of antimatter searches the large uncertainties involved in the modeling of both conventional astrophysical production and galactic transport play a major role and have hindered a firm DM detection so far, although some recent tentative claims (in particular, among others, [18–22]) have triggered an important debate in the community. In Sections 4, 5, and 6 we will describe in detail the current status for positron, antiproton and antinuclei indirect searches: our purpose is to provide a case-by-case discussion mostly focused on the relevance of CR transport physics in antimatter channels for DM indirect detection.

While charged antiparticles may be promising indirect messengers of the particle DM nature, they do not retain the directionality from their emission point and, hence, cannot provide the morphological characterization of a DM signal: this possibility is accomplished instead with the analysis of gamma-ray data (for early studies, see, e.g., [23–25]; more recently, [26, 27]). If DM particles eventually decay or annihilate into gamma radiation, it is crucial to identify the most promising regions of the sky where either the expected signal is large, or the astrophysical background is low: among the most important targets, we can certainly mention the inner galaxy (which satisfies the first criterion) and the DM-dominated satellite galaxies orbiting around our galaxy. The most tentative claims and interesting bounds from the study of the gamma-ray sky will be reviewed in detail in Section 7.

Before going through an extensive discussion of all these channels for DM indirect searches, in the next two sections we will set up the stages of this review by briefly presenting some relevant aspects of DM models connected with the scope of the present paper and then highlighting the several key aspects of the galactic CR transport problem. Those concepts will be recalled all across the paper when the most relevant interpretations of CR and gamma-ray anomalies are discussed.

2. Targeting DM Indirect Searches on High Energy Physics

The quest for the fundamental origin of DM may require considering a priori an impressive range of energy scales (see [28, 29] for interesting historical retrospectives). For instance, sitting on the extremes of the viable mass window for DM searches, today we may be looking for imprints on the cosmological matter power spectrum of super-light candidates such as axion-like particles [30–32] from the string landscape [33, 34], as well as aiming to detect the gravitational echoes of massive black hole merging [35, 36], possibly originated from primordial density fluctuations in the Early Universe [37, 38].

However, the phenomenology of DM candidates may be intriguingly correlated to the long-standing puzzles pertaining to the realm of the SM (see, e.g., [11, 39] for broad reviews on the topic). Of particular significance, one of the main driving forces of research on High Energy Physics has been the quadratic UV sensitivity of the Higgs boson mass to any new physics energy scale above the electroweak one [40]. On general grounds, the attention of this review is mostly paid to DM candidates motivated by New Physics at the electroweak scale. Many extensions of the SM theory addressing the electroweak hierarchy problem can indeed accommodate such DM candidate in their spectrum; see, e.g., [5] for a review on the widely mentioned case of supersymmetry; [41, 42] for higher dimensional theories aimed at stabilizing the electroweak scale; [43–46] for examples of strongly coupled UV completions. Moreover, DM candidates sitting around the electroweak scale may also be well-motivated in the context of nonnatural theories addressing other possible SM issues, such as proton stability and/or gauge coupling unification; see, e.g., [47–49] for the case of supersymmetry; [50–53] for interesting universal/warped extra-dimensional proposals.

In all these scenarios, the DM particle is usually stable due to its charge under a (discrete) symmetry of the new theory, while a benchmark range of masses and couplings can be eventually individuated on the basis of the UV guiding principles. Most importantly, the emerging DM phenomenology from these studies typically falls in the experimental window of sensitivities for antimatter and gamma-ray searches discussed in the next sections.

Marginalizing over the specific details of UV models, the DM reference framework we mainly refer to, in this review, corresponds to Early Universe cold thermal relics. Assumed to be in thermal equilibrium with the primordial plasma at the very early stages, DM decoupling as nonrelativistic species eventually leads to [54] (for more details, see also [55]):

$$\frac{\Omega}{0.25} \sim \frac{3 \times 10^{-26}\,\mathrm{cm^3\,s^{-1}}}{\langle \sigma v \rangle} \simeq \frac{10^{-8}\,\mathrm{GeV^{-2}}}{\sigma}. \tag{1}$$

Ω is the DM cosmological relative abundance observed today [56]; $\langle \sigma v \rangle$ is the DM thermally averaged particle annihilation cross section. In the last step we make use of the approximation $\langle \sigma v \rangle \simeq \sigma\, c/3$, expected to be valid for a WIMP at the time of chemical decoupling in the Early Universe. By means of dimensional analysis, we can naively estimate the DM annihilation cross section in terms of its mass m and dimensionless coupling constant g, obtaining

$$m \sim \left(\frac{g^2}{10^{-1}}\right)\left(\frac{10^{-4}\,\mathrm{GeV^{-1}}}{\sqrt{\sigma}}\right)\mathrm{TeV}; \tag{2}$$

(1) in conjunction with the estimate in (2) characterizes the so-called *Weakly Interacting Massive Particle (WIMP) miracle*: a cold thermal relic charged under weak interactions and with mass close by the electroweak scale naturally accounts for the present DM abundance.

The WIMP mass range may be bracketed from below according to the seminal works in [57, 58] as $m \gtrsim 10$ GeV, while it may be bracketed from the above unitarity arguments on the DM cross section pinpoint to $m \lesssim 10^2$ TeV [59] (but caveats exist [60]). Typical expectations from the WIMP paradigm may be notably disregarded by the presence

of resonant regimes, near mass thresholds, and coannihilation with other particles in the thermal bath [61]. Many other examples of variants to the standard WIMP freeze-out scenario have been investigated in literature [62–70]. Nonperturbative effects such as Sommerfeld enhancement [71–74] and bound-state formation [75–80] have also more recently acknowledged to be of possible dramatic impact in the broad context of WIMP phenomenology.

Importantly, (1) shows that the DM relic abundance is mostly sensitive to the annihilation cross section. It follows that a WIMP-less miracle is perfectly conceivable [81], opening on general grounds a broader range of viable mass scales (for a supersymmetric setup, down to the MeV scale within gauge-mediation breaking) and couplings for the phenomenology of DM thermal relics. Therefore, indirect signals from WIMP-like scenarios—whose signatures have been comprehensively inspected in [82, 83] and are of particular importance for this review—are after all **(1)** intimately connected to the possibility of being effectively visible today and **(2)** possibly connected to the tantalizing discovery of New Physics near the electroweak scale [84].

3. Miniguide to Galactic CR Physics

3.1. Origin of CRs. A clear identification of the classes of astrophysical sources able to accelerate particles from GeV all the way up to PeV energies (and, for extragalactic accelerators, up to $\sim 10^{20}$ eV) is crucial for DM indirect detection.

We will not digress here on the long debate about the origin of CRs and their acceleration mechanisms (see, e.g., [85] for an excellent review). For the purpose of this review, let us start by mentioning the *supernova paradigm* as the main guideline. Supernova remnants (SNRs) were proposed as potential sources out of energy budget arguments in [86, 87]; the picture was better defined later in terms of SNRs located in our own galaxy [88, 89]; however, a physical process capable of such a powerful CR acceleration had not been proposed yet at that time. Later, the theory of *diffusive shock acceleration* was presented in four famous seminal papers [90–93] and is currently considered the main reference framework in the field.

However, it is important to keep in mind that other classes of sources (e.g., pulsar wind nebulae for leptonic CRs [94], OB associations [95], and X-ray binaries [96]) and several other acceleration mechanisms have been proposed as well. As we will see below, many of these potential accelerators are expected to play a role in the explanation of some tentative claims of DM detection.

3.2. CR Transport: Preliminary Considerations. Let us now turn our attention to a crucial aspect of CR physics, which has an extremely relevant impact on DM indirect searches, i.e., CR propagation in our galaxy.

The usual starting point is a collection of several key observations that characterize the cosmic-ray flux.

(i) The isotropy of the arrival direction (at the level of $\sim 10^{-3}$ in the TeV-PeV range, recently measured with high precision by many experiments [97–102]).

(ii) The much larger abundance of Lithium, Beryllium, and Boron compared to the solar system abundances, which is naturally interpreted as the signature of the interaction of *primary* species such as protons and heavy nuclei with a column density of interstellar gas as large as few g/cm^2: such a *grammage* implies that the primary species have crossed the galactic disk many times.

(iii) The presence of a diffuse gamma-ray emission across the whole galactic disk, already predicted in the early 1960s [103] and first measured by pioneering satellite experiments such as OSO-3 (1967) and SAS-2 (1972); afterwards, COS-B and EGRET provided even more accurate results; nowadays, Fermi-LAT has provided a state-of-the art description of this emission in the 30 MeV-1000 GeV range, as detailed below.

These pieces of information, combined together, suggest a "conventional scenario" for CR transport that was shaped by the pioneering work of Ginzburg and colleagues (see [104] and references therein and [105]), based on a random walk through the galaxy governed by the quasilinear theory of pitch-angle scattering on Alfvénic turbulence (QLT), first presented in the 1960s [106, 107].

3.3. The CR Transport Equation. Magnetohydrodynamic turbulence—which is ubiquitous in the interstellar medium (ISM) and covers a very wide range of scales from astronomical units (AUs) to kpc [108]—is widely considered as the main responsible for this diffusive regime. In more detail, the relativistic motion of charged particles in our galactic environment is affected by the presence of a coherent large-scale magnetic field component, $\vec{B}$ [109, 110], on top of which magnetic inhomogeneities, $\delta\vec{B}$, are propagating. These fluctuations in the magnetized interstellar medium (ISM) are associated with a turbulent cascade that is believed to be either initiated at large scales $\sim 10^2$ pc (by supernova explosions, differential rotation of the galactic disk, or other mechanisms [111]) or (especially at small scales) triggered by CR themselves via *streaming instability* [112, 113]. This cascade has been usually considered, in the basic scenario of QLT, as isotropic and mainly composed of *Alfvén waves*, i.e., transverse magnetic perturbations moving at the Alfvén speed[1]:

$$v_A \simeq 2 \times 10^6 \frac{\left|\vec{B}\right|}{\mu\mathrm{G}} \sqrt{\frac{\mathrm{cm}^{-3}}{\rho_{\mathrm{ISM}}}}\ \mathrm{cm\,s}^{-1}. \tag{3}$$

Following in part the approach of [114], we recap here the main features of QLT (see also [104, 105]).

The rationale of QLT is to consider the interaction of a charged particle of momentum $\vec{p} = m\vec{v}$ with magnetic inhomogeneities $\delta\vec{B}$ that are sufficiently small (with respect to the regular field $\vec{B}$) at the scale of interest. The process is well described by a stochastic equation for the *pitch angle*, defined as $\mu = \cos(\hat{p} \wedge \vec{B})$. On average the variance of the pitch angle can be shown to feature a *resonance condition*

[105]. According to it, the particle only interacts with the inhomogeneities of wavelength $\sim 2\pi/k$ matching the particle Larmor gyroradius r_L [2]:

$$\left\langle \frac{\Delta\mu\Delta\mu}{\Delta t} \right\rangle = \frac{\pi\nu}{\mu r_L^2} \frac{\left|\overrightarrow{\delta B}\right|^2}{\left|\overrightarrow{B}\right|^2} \left(1-\mu^2\right) \delta\left(k - \frac{1}{\mu r_L}\right). \quad (4)$$

Let us now consider an ensemble of particles described by a phase-space distribution $f(\overrightarrow{x}, \overrightarrow{p}, t)$, with probability density $\Psi(\overrightarrow{p}, \Delta\overrightarrow{p})$ for transitions $\overrightarrow{p} \longrightarrow \overrightarrow{p} + \Delta\overrightarrow{p}$ in momentum space, due to interactions with stochastic fluctuations in the magnetized environment. We can state that, after a lapse Δt, *in the Alfvén wave rest frame* (primed), the evolved phase-space distribution must be equal to

$$f\left(\overrightarrow{x}' + \overrightarrow{v}' \cdot \Delta t, \overrightarrow{p}', t + \Delta t\right) = \int d\Delta\overrightarrow{p}' \Psi\left(\overrightarrow{p}' - \Delta\overrightarrow{p}', \Delta\overrightarrow{p}'\right) f\left(\overrightarrow{x}', \overrightarrow{p}' - \Delta\overrightarrow{p}', t\right) \quad (5)$$

with $\overrightarrow{v}'$ being the CR particle velocity in the wave frame.

We assume that detailed balance holds; i.e., a transition $\overrightarrow{p}' \longrightarrow \overrightarrow{p}' - \Delta\overrightarrow{p}'$ described by a probability $\Psi(\overrightarrow{p}', -\Delta\overrightarrow{p}')$ is equivalent to the one described by $\Psi(\overrightarrow{p}' - \Delta\overrightarrow{p}', \Delta\overrightarrow{p}')$. Applying this principle in the limit of $\Delta p'/p' \ll 1$ (originating from $|\delta\overrightarrow{B}|/|\overrightarrow{B}| \ll 1$) that characterizes QLT, we can write

$$\left\langle \Delta p_i' \right\rangle_{\Delta\overrightarrow{p}'} = \frac{1}{2} \sum_j \frac{\partial}{\partial p_j'} \left\langle \Delta p_i' \Delta p_j' \right\rangle_{\Delta\overrightarrow{p}'}, \quad (6)$$

where $\langle \ldots \rangle_{\Delta\overrightarrow{p}'} \equiv \int d\Delta\overrightarrow{p}' \Psi(\overrightarrow{p}', \Delta\overrightarrow{p}')$ and a Taylor expansion of $\Psi(\overrightarrow{p}', \Delta\overrightarrow{p}')$ has been performed.

Assuming the static limit, i.e., $\Delta t/t \ll 1$, starting from a Taylor expansion of (5), with the help of (6) we finally get, in the same wave frame,

$$\frac{\partial f}{\partial t} + \overrightarrow{v}' \frac{\partial f}{\partial \overrightarrow{x}'} = \frac{\partial}{\partial \overrightarrow{p}'} \left(D_{\overrightarrow{p}'\overrightarrow{p}'} \frac{\partial f}{\partial \overrightarrow{p}'} \right). \quad (7)$$

This is a Boltzmann equation where in the right-hand side the "collision operator" qualifies Brownian motion in momentum space with *diffusion coefficient*

$$D_{p_i' p_j'} \equiv \frac{1}{2} \left\langle \frac{\Delta p_i' \Delta p_j'}{\Delta t} \right\rangle_{\Delta\overrightarrow{p}'} \quad \text{for } i, j = 1, 2, 3, \quad (8)$$

describing indeed the momentum isotropization due to CR stochastic scattering with Alfvén waves.[3]

Let us now perform a transformation to the galactic rest frame. In this frame of reference, (7) features a spatial diffusion operator *along the direction of the regular field* as well. This is the most important term that governs CR transport in the galaxy. The spatial diffusion coefficient D_{zz} is related to D_{pp} by [115]

$$D_{zz} D_{pp} \propto v_A^2 p^2, \quad (9)$$

for $\overrightarrow{B} = B\hat{z}$. Inspired and guided by the results of QLT, a general transport equation is usually considered, mainly based on the aforementioned process of diffusion in both position and momentum space, but featuring a wider set of terms associated with other physical phenomena. The full equation reads

$$\frac{\partial N}{\partial t} + \overrightarrow{\nabla}\left(\overrightarrow{u} N\right) - \frac{1}{3}\frac{\partial}{\partial p}\left[p\left(\overrightarrow{\nabla}\cdot\overrightarrow{u}\right)N\right] - \overrightarrow{\nabla}\left(D_{\overrightarrow{x}\overrightarrow{x}}\overrightarrow{\nabla}N\right) - \frac{\partial}{\partial p}\left[p^2 D_{pp}\frac{\partial}{\partial p}\left(\frac{N}{p^2}\right)\right] + \frac{\partial}{\partial p}\left(\frac{dp}{dt}N\right) = Q_0 + Q_{\text{sec}} - \frac{N}{\tau_N}, \quad (10)$$

with $N(\overrightarrow{x}, p, t)$ and $Q(\overrightarrow{x}, p, t)$ being, respectively, the CR density species and CR injecting density source per unit of momentum. In the left-hand side, the diffusion term is usually *isotropic* and described by a scalar, position-independent coefficient, despite the fact that QLT predicts a highly anisotropic transport along the regular field direction (see, e.g., the discussion in [116]). The scalar spatial diffusion coefficient is generally taken as

$$D = \frac{c r_L}{\mathcal{F}(k)}, \quad (11)$$

where $\mathcal{F}(k)$ is defined as the (normalized) power associated with the turbulent modes with wave number $k \propto 1/p$ resonating with the particles carrying momentum p. Since the turbulent power scales as a power law, the rigidity dependence of the diffusion coefficient is usually parametrized as

$$D = D_0 \left(\frac{p}{p_0}\right)^{\delta}, \quad (12)$$

with D_0 and δ as free parameters to be fixed by comparison with CR data. The spatial dependence of such normalization that stems from the spatial variations of the turbulent power is usually neglected with some relevant exceptions [116–121].

The momentum diffusion is also called *stochastic reacceleration*, and the relation 10 is assumed to hold.

The left-hand side also involves an advection term originally present in (7) as well, now characterized by the bulk velocity of the plasma in the lab frame: galactic winds affecting CR motion may be described by such a term, together with adiabatic energy losses, involving velocity gradients even of $\mathcal{O}(10^2)$ km s^{-1} kpc^{-1} perpendicularly to the galactic disk.

The physics of advective-diffusive transport is enriched by two more relevant phenomena included in (10): net energy losses and spallation. In fact, we need to consider CR energy loss processes, characterized by the continuous loss rate dp/dt, particularly important, e.g., at high energies for light charged species such as leptons (see, e.g., [122, 123]).

Eventually, on the right-hand side of (10),

(i) the primary source term Q_0 captures the primary accelerators of CRs: as mentioned above, while the *supernova paradigm* is still the most accredited one, other classes of sources can certainly be at work;

(ii) the secondary source term $Q_{\rm sec}$ describes the production of a given species from spallation of the heavier ones onto interstellar gas;

(iii) a loss term due to inelastic collisions characterized by an interaction time τ_N is also introduced.

An important remark is needed at this point. Our picture of MHD turbulence has dramatically improved during the latest decades: according to the current scenarios [124, 125], MHD turbulence is composed of an *anisotropic* cascade of both Alfvén waves, and isotropic fast magnetosonic modes, as theoretically demonstrated and numerically confirmed by several simulations. As a consequence of the anisotropy of the Alfvénic cascade, the scattering efficiency on Alfvén waves turns out to be very low [126], posing a tough challenge to the whole scenario discussed above. Among others, a possible solution [127, 128] is that magnetosonic modes dominate gyroresonance interaction for most of the pitch-angle range.

However, although the actual microphysics underlying the CR random walk is still far from being exhaustively addressed, the QLT can still be considered a useful guideline to be taken as a reference, and (10) should be understood as a phenomenological tool to tame the complexity of the plasma physics problem, allowing us to make predictions against a plethora of data.

3.4. Modeling CR Transport: A Glimpse. In order to solve the complicated CR transport equation (for each CR species), today we have at our disposal several public numerical codes, equipped with different numerical and astrophysical ingredients, aimed at solving (10), most notably (in chronological order): `GALPROP`[129–132], `DRAGON` [123, 133–135], and `PICARD` [136, 137]. A semianalytical approach is instead followed by the `USINE` project [138].

While a detailed and realistic study of galactic CR propagation requires the extensive use of those numerical or complex semianalytical methods, we can extract some physical insight useful for the next sections looking at a simplified version of (10).

Indeed, at the basis of CR transport, an important hierarchic game of scales may be conceived: convective and reacceleration effects are typically related to low-energy regimes, while energy loss rates are negligible for high energy hadrons such as protons or heavier nuclei. So, for energies $E \gtrsim$ few GeV, the galactic motion of heavy species can be approximately described to be in a purely diffusive regime: then, we may trade the spatial diffusion operator for an effective time of confinement, τ_D, i.e.,

$$\vec{\nabla}\left(D_{\vec{x}\vec{x}}\vec{\nabla}N\right) \longrightarrow \frac{N}{\tau_D}, \tag{13}$$

and treat the galaxy as a box where CRs perform a random walk-up to the box boundaries, beyond which they leak out. In the steady-state limit of this simplified framework, CR secondary species, produced by the interaction of source-injected (namely, primary) CR particles, can be estimated as

$$N_s = Q_s\tau_D \propto N_p\tau_D. \tag{14}$$

Hence, the timescale for confinement of CRs in the galaxy is intimately linked to relative abundances of secondary and primary species. As anticipated in the above, antimatter species are typically produced as secondaries, and therefore (14) is of direct relevance for DM indirect searches in antimatter channels.

Note that, by dimensional analysis, $\tau_D \sim H^2/D$, where H captures the typical size of the box. Therefore, secondary fluxes are sensitive to both the spatial diffusion coefficient and the height of the CR propagation halo. As we will discuss below, our current poor knowledge of the value of H generally translates into an important source of uncertainty in DM indirect detection studies.

As stated above, the spatial diffusion coefficient scales as a power law with rigidity. Supplementing (14) with such expectation, we have a theoretical prediction that nicely fits the trend of available experimental data [140]: at energies above few GeV, the measurements of local CR secondary-over-primary observables like B/C are indeed compatible with a power-law behavior (with index δ) of the diffusion coefficient. Typical estimates of this parameter are in the range $0.3 < \delta < 0.6$ [141–145], with a normalization at GeV corresponding to $D_0 \simeq 10^{28}$ cm^2 s^{-1}, but pertain only to a local measurement (see [118] for a possible indirect inference of δ across the galaxy).

4. The Antiproton Channel

In the conventional scenario sketched above, antiprotons are produced in the galactic environment by *spallation* of heavy nuclei and protons onto interstellar gas.

The early measurements of the antiproton flux date back to the 1970s and early 1980s; a first tentative claim of anomaly with respect to the conventional expectations based on the picture of nuclear spallation goes back to [146]. However, DM connections were not outlined at that time: cosmic antiprotons were considered a promising channel for DM searches only some years later, in several seminal papers (see, for instance, [12, 147, 148] and, more recently, [149]).

A dramatic improvement in the accuracy of the data was provided by the PAMELA collaboration in 2009 [150] (with further refinement in [151]): the measurement showed a reasonably good agreement with conventional models based on purely secondary origin, as confirmed by [141, 152]. A note here is in order about the meaning of *conventional model*: in what follows, we will use this expression for a model based on the simplest version of (10), taking a single class of sources (SNRs) at work, with antiparticles produced only as secondary products from primary spallation, and featuring constant and homogeneous diffusion, tuned on local CR data.

Given the absence of significant unexpected spectral features (such as bumps), the potential constraining power of PAMELA dataset for DM searches was soon demonstrated in a series of papers (from the early ones as [153, 154] to the more recent [155]), which provided a comprehensive discussion on the upper bound on the WIMP annihilation cross section from the detection of cosmic antiprotons. The most relevant point made in those papers is the crucial role of CR transport.

A major source of uncertainty, in particular, is the size of the diffusive halo H introduced in the previous section, i.e., the volume, where galactic CRs are effectively confined by the presence of a turbulent magnetic field. Models of CR transport based on larger diffusion halos usually feature larger average values of the diffusion coefficient in order to correctly reproduce the secondary/primary ratio data: therefore, in these scenarios, the antiproton flux probes a larger region of the galaxy and exhibits a larger constraining power. On the other hand, cases where one assumes a very thin halo (smaller than $\simeq$ 2 kpc) turn out to be much less restricting on the particle DM properties indirectly probed.

Another source of uncertainty certainly lies on the properties of CR transport in a much smaller environment: the Heliosphere. We refer to [155] and references therein for a comprehensive discussion on this aspect.

As a consequence of this complicated puzzle, it was not possible to firmly exclude some relevant tentative DM claims made in other channels (see the gamma-ray section for more details), and the most severe limitation came from the poor constraints we actually have on the size of the galactic CR diffusion halo. A possible improvement in this direction may come from more accurate measurements of the Beryllium isotopes and from a careful analysis of the current and forthcoming data on the vertical profile (with respect to the galactic plane) of the synchrotron emission from the galaxy (following [156, 157], we point out that the current data seem to favor large values for the size of the diffusion halo).

In 2015 a much more accurate dataset was published by the AMS-02 collaboration [20]. The debate on the antiproton channel has then included tentative claims of anomalies with respect to the conventional scenario, possibly explained in terms of DM indirect detection.

First of all, the AMS-02 collaboration itself initially claimed the presence of an excess at high energies over 100 GeV. Right after, the significance of this anomaly was better characterized [139, 143, 158], pointing only to a mild overshooting of the expected background. The relevance of this putative discrepancy and the estimated impact of the different sources of uncertainty on the model predictions is well depicted in Figure 1 (taken from [139]).[4]

Taking at face-value the original tentative claim from AMS, the interpretation of the excess requires scenarios beyond the conventional on of CR transport pictured in the miniguide of Section 3. For instance, a mechanism that may be at work and explain the discrepancy is the *secondary production at the accelerator*: the idea, proposed before AMS data in [159] as a possible explanation to the positron ratio anomaly (see Section 6), is that secondary products of hadronic interactions inside the sources can participate in the acceleration process and subsequently escape into the interstellar medium as an extra component featuring a very flat spectrum. In [160] this scenario was applied to (pre-AMS) antiproton data as well, and the authors demonstrated that the boron-over-carbon ratio has much constraining power for this interpretation.

More recently, refined Bayesian analyses that include the official AMS data on this observable as well (see, e.g., [144]) confirm the presence of a mild discrepancy between the

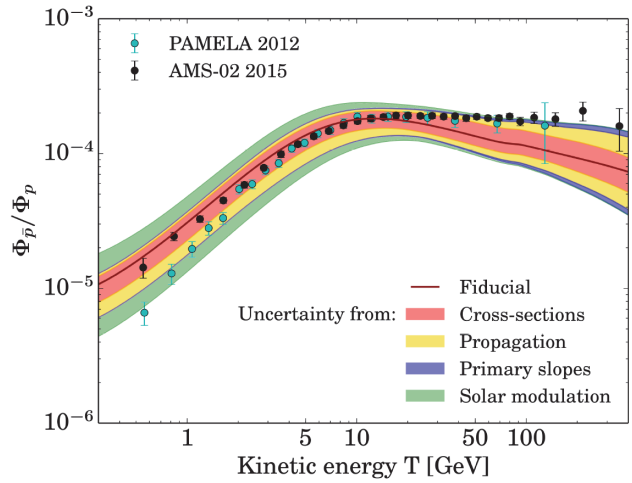

Figure 1: Impact of cross section, CR transport, and modulation uncertainties on the conventional predictions for the antiproton compared to the related dataset collected by the AMS-02 collaboration. Figure 1 is reproduced from Giesen et al. (2015) [139] (under the Creative Commons Attribution License/public domain).

regions of the parameter space pointed by AMS antiproton and B/C data.

However, spatial-dependent diffusion setups (e.g., the phenomenological two-zone models as those considered in [161, 162], designed to capture both CR transport in preexisting SNR-driven galactic turbulence, and confinement by CR-driven turbulence via streaming instability) seem to solve the discrepancy, as well as the latest scenarios that include secondary production at the accelerator [163].

DM interpretations for the high energy discrepancy are also still viable for quite large values of the DM particle mass (as shown, e.g., in [164–166]), in particular for light mediator scenarios. At the same time, the constraining power of AMS data in the energy range where no relevant feature or anomaly is present has been most recently explored in [167, 168].

On the other hand, on the low-energy side, a possible indication of a DM signal for DM masses near 80 GeV has been found [168–170], with a hadronic annihilation cross section close to the thermal value: interestingly, this tentative claim is compatible with the DM interpretation of the galactic center gamma-ray excess (see Section 7). Again, more investigation of the transport uncertainties (both in standard and beyond-standard scenarios) and more detailed combined studies of this signal together with constraints from other probes (e.g., the observation of dwarf spheroidals in the gamma-ray band) will be crucial in order to confirm the existence of this anomaly.

5. The Avenue for Antinuclei

A milestone campaign for imprints of particle DM on the observable CR radiation may correspond to the discovery of galactic light antinuclei such as antideuteron ($^2\overline{\mathrm{H}}$) [171–174] and antihelium-3 ($^3\overline{\mathrm{He}}$) [175, 176]. At present, no compelling evidence for a detection of antimatter with mass number

$A \geq 2$ has been experimentally corroborated in the measurement of galactic CR fluxes. A notable upper limit on the flux of cosmic antideuteron has been set by the BESS facility—reporting at the 95% of confidence level $\Phi_{^2\overline{\mathrm{H}}} \lesssim 2 \times 10^{-4}$ $(\mathrm{m}^2\ \mathrm{s\ sr\ GeV/n})^{-1}$ for kinetic energy per nucleon $0.17 \leq \mathrm{T} \leq 1.15$ GeV/n [177]—while the BESS-Polar collaboration currently constrains antihelium-to-helium flux to be smaller than 10^{-7} in the interval of probed rigidities, 1.6 – 14 GV [178].

Today, the AMS-02 mission is operating in the direction to perform the first historical observation of cosmic light antinuclei, with promising projected sensitivities [179]. A tentative claim of few antihelium events—possibly measured by the AMS-02 collaboration—might be already at hand, waiting for a firmer experimental response in the upcoming years; see, for instance, [180].

The phenomenological relevance of the avenue for antinuclei in relation to DM indirect searches stems from the kinematics of spallation processes producing CR secondaries: the energy threshold associated with the production of one antideuteron is roughly 2.5 greater than the one required to produce a secondary antiproton. Moreover, the same energy threshold is a monotonic increasing function of the mass number A. Therefore, the low-energy flux of cosmic antinuclei is expected to be small [181], opening a *low-energy window*—related to kinetic energies per nucleon between ~0.1 and few GeV/n—for large signal-to-background ratios from exotica.

The physics of CR accelerators and of propagation impacting the prediction for antinuclei fluxes at Earth sits on the very similar grounds of the one discussed for the antiproton channel. On the one hand, the unknowns stemming from galactic CR propagation affecting the predicted galactic fluxes for antideuteron and antihelium should be correlated to the galactic antiproton spectrum and boron-to-carbon ratio data. On the other one, the injection of antinuclei in the galactic interstellar medium is intimately connected to the antiproton production mechanism. As discussed in the previous section, the latter may be sourced from in situ acceleration in the downstream region of supernova remnant shockwaves. Such mechanism generally yields a source term distinguished into a A-component, referred to as CR secondaries accelerated by the shock, and a B-component, related to standard spallation processes sourced by CR primaries. Most recent analyses on the topic have included also these extra contributions in their predictions [182–184].

Figure 2, from [182], reports the maximum contribution to the antideuteron flux with respect to the typical unknowns from CR physics, properly calibrated on antiproton AMS-02 data. The components from production in supernovae (SNR-A and SNR-B bands) are found to be subdominant, giving (at most) a 10% effect with respect to the main standard component, obtained by considering the interactions of CR primaries with the interstellar medium (black line). Figure 2 also shows predictions for some benchmark exotica such as annihilating DM particles with masses of $\mathcal{O}(100)$ GeV and 100% branching ratios into $b\bar{b}$ or W^+W^- final states, together with the expectations from exotica that gained recent interest [35, 36] such as primordial black holes [185, 186]. The plot

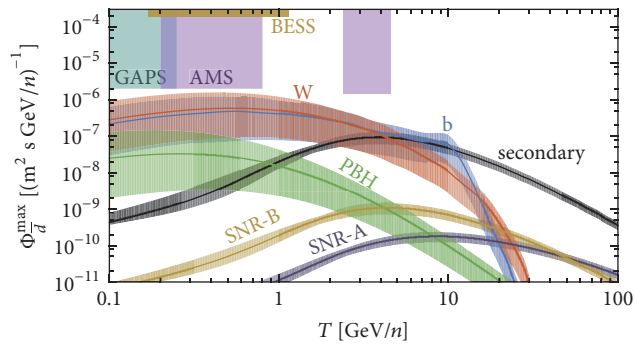

Figure 2: Maximum $^2\overline{\mathrm{H}}$ flux compatible with AMS-02 data from evaporation of primordial black holes (green) and DM particle annihilation (blue and brown), compared with current and projected sensitivities from BESS, AMS, and GAPS experiments. Maximum flux for the expected astrophysical background is also shown: in black color the contribution from CR spallation processes with the interstellar medium and the subleading SNR-A and SNR-B ones. Bands bracket uncertainties from force-field approximated solar modulation and an event-by-event coalescence model. Figure 2 is reproduced from Herms et al. (2016) [182] (under the Creative Commons Attribution License/public domain).

clearly highlights the importance in the aforementioned low-energy window. However, contrary to common wisdom [179], Figure 2 also underlines the unlucky possibility that within the forthcoming years current and future experimental facilities may not be sensitive to antideuteron yields from DM/exotica production.

At this point, it is important to stress that unknowns stemming from the physics of CR accelerators and galactic transport should not be retained to be the major source of uncertainty in the prediction of cosmic antinuclei fluxes. The bands reported in Figure 2, while including the effects of solar modulation—typically studied within the force-field approximation [188] and better investigated in [189] by means of numerical tools [190, 191]—are most importantly related to the coalescence model adopted to establish antideuteron formation. At present, the prediction of antinuclei fluxes seems to strongly depend on the assumptions made to describe antiproton-antineutron fusion [179]. Nowadays, state-of-the-art analyses can avoid to rely on simplistic analytical modeling [192], making instead use of Monte Carlo event generators and available data from colliders. Large systematics on the formation of antideuteron and antihelium can be understood on the basis of the sensitivity of these studies on the hadronization model implemented and the experimental dataset considered; see, e.g., [179, 193]. Interestingly, a recent work focused on the description of nuclear coalescence via a physical modeling for the fusion of nucleons into composite nuclei [194], and exploiting two-particle correlation measurements [195] has pointed out the possibility that the production cross section in pp collisions for antihelium-3 may have been underestimated by up to two orders of magnitude. Consequently, a putative detection of cosmic $^3\overline{\mathrm{He}}$ events related to kinetic energies greater than 1 GeV/n may actually be within the reach of AMS-02 in few years [17].

Therefore, we may conclude that searches for antinuclei, while being potentially exposed to CR propagation details, are mainly plagued by the assumptions and the systematics involved in the estimate of the poorly known production cross section. This can have a dramatic impact on our present ability to make projections for a concrete signal detection of antideuterons and antihelium-3. At the same time, these uncertainties leave us hope to foresee a spectacular discovery of exotica such as DM in the peculiar window of low-energy antinuclei events.

6. The Positron Channel

The positron channel has been under the spotlight for a long time in the DM indirect detection community. As mentioned in Section 1, the paucity of those particles makes them an ideal target for DM searches, and the presence of a significant anomaly (with respect to the conventional expectations) has further increased the interest around this observable during the latest decade.

Let us start by clarifying, also in this case, what we mean by "conventional" predictions. In the context of a simplified treatment of acceleration and transport—as described in the miniguide of CR physics—a slightly different discussion is actually required for leptons in general. In fact, high energy leptons feature relevant energy losses especially at high energies, which implies a new timescale competing with the diffusion one. The simplified transport equation governing $e^{\pm}$ propagation is therefore of this kind:

$$\frac{\partial N}{\partial t} - D\Delta N - \frac{\partial}{\partial p}\left(\frac{dp}{dt}N\right) = Q \tag{15}$$

where inverse Compton scattering on the photon background and synchrotron radiation define the typical timescale for energy losses, $\tau_{E_{loss}}(p) \sim p/|dp/dt| \propto p^{-1}$. The solution of (15) is given by a Green function that boils down to

$$N \simeq \frac{Q(p)\,\tau_{E_{loss}}}{\sqrt{D(p)\,\tau_{E_{loss}}}}. \tag{16}$$

For primary electrons this result implies a scaling $\propto p^{-\alpha_e-\delta/2-1/2}$, where $\alpha_{\rm CR}$ is the CR injected spectral index.

In the standard scenarios, positrons in the galaxy are believed to originate, like antiprotons, as an *entirely secondary* component arising from the collisions of relativistic protons with the ISM gas according to a chain like $p + H \longrightarrow \cdots \longrightarrow \pi^{\pm} \longrightarrow \mu^{\pm} + \cdots \longrightarrow e^{\pm} + \ldots$. The source function of positrons is then expected to scale as

$$q_{e^+} \propto N_p n_H \sigma_{p\longrightarrow e^+} \propto Q_p \tau_{diff} \propto p^{-\alpha_p-\delta}, \tag{17}$$

where we have implemented the rather simplistic approximation of an energy independent cross section $\sigma_{p\longrightarrow e^+}$, used the fact that the relevant timescale for propagation of high energy protons is the diffusion timescale, and defined α_p as the spectral index for the proton injection source function. Plugging this result in (17), we can predict the scaling of the propagated positron flux over the electron one:

$$\frac{N_{e^+}}{N_{e^-}} \propto p^{-\alpha_p+\alpha_e-\delta}, \tag{18}$$

with α_e being the spectral index at injection for the electron source distribution.

In the framework of diffusive shock acceleration, the injected spectral index should not differ much among different species. Consequently, the ratio of secondary positrons over primary electrons is predicted to *decrease* with increasing energy, unless a (very unlikely) large difference between the source spectral indexes for protons and electrons is assumed *ad hoc*.

The rise at high energy in the positron fraction originally discovered by PAMELA in 2009 [18] and subsequently confirmed by Fermi-LAT and AMS-02 [19] collaborations constitutes then a substantial deviation from the standard prediction of (18) and appears robust with respect to uncertainties in CR transport models, implemented in a more realistic way (see, however, [196]). The release of the data on the absolute positron spectrum [197] confirmed and strengthened this conclusion.

The detection immediately triggered a debate in the community (see, e.g., [198, 199] and references therein). A natural explanation in terms of nearby astrophysical accelerators of primary $e^+ + e^-$ pairs, e.g., pulsar wind nebulae (already invoked in [94] as potential contributors to the leptonic flux), was soon considered as a very promising one; see Figure 3 for a recent realization of this scenario, compared to up-to-date experimental data. Other astrophysical interpretations were proposed (see, e.g., [200]), including the already mentioned secondary production at accelerators [159].

On the other hand, many DM interpretations were invoked as well: the tough challenges for model building are in this case the large annihilation cross section required to sustain the measured positron flux at high energy and the strong constraints originating from other channels (including gamma rays, CMB, and antiprotons); we refer [201] for an early review on the topic. The Early Universe bounds [202, 203] are particularly difficult to evade, and one has to invoke, for instance, nonthermal mechanisms (see, e.g., [204] for a recent two-component scenario in which the heavier DM species is produced as a thermal relic in the Early Universe and decays to the lighter species over cosmological timescales) or Breit-Wigner enhancement of present-time annihilation (already proposed in 2009 to explain the boost factor required by PAMELA data [205, 206] and recently reconsidered, e.g., in [207, 208], as a way to evade the stringent CMB constraints).

More interestingly, nowadays it is possible to challenge the widely debated pulsar hypothesis in several ways, and the uncertainties in CR transport play a major role.

First of all, it is possible to look for an anisotropy in the arrival direction of high energy leptons. The Fermi-LAT collaboration has released two papers in 2010 and 2017 on this topic, with stringent upper limits [209, 210]. The compatibility between the pulsar models and those limits has

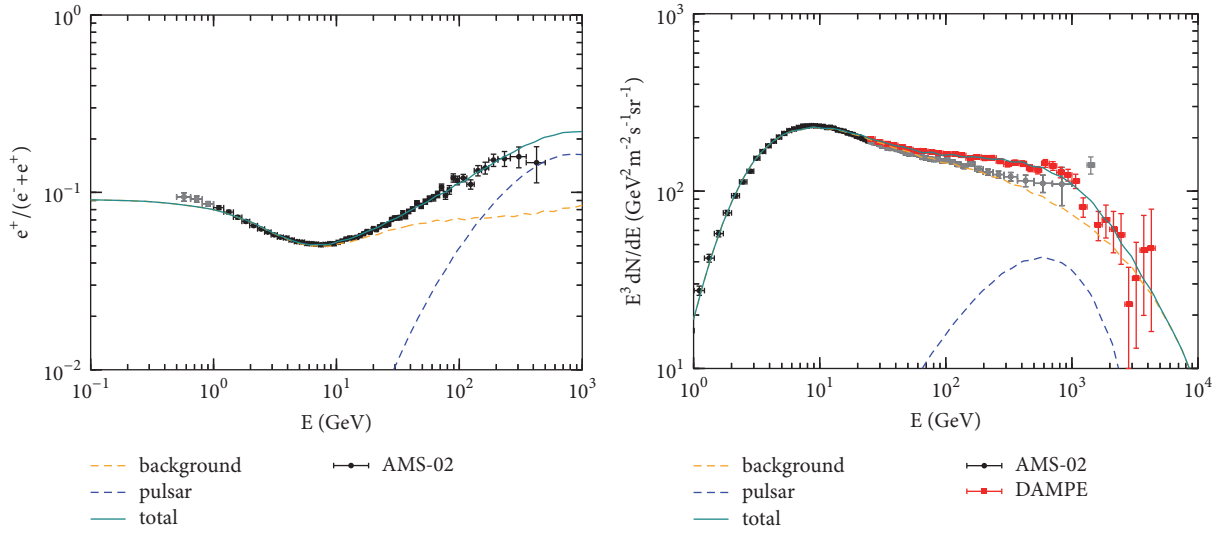

FIGURE 3: The most recent leptonic data from AMS and DAMPE, interpreted within a pulsar scenario. Figure 3 is reproduced from Yuan et al. (2017) [187] (under the Creative Commons Attribution License/public domain).

been studied several times in the literature (see, e.g., [211]) and is still matter of debate: as shown recently in [212], it is possible to build scenarios that are compatible with the most recent upper limits, where few nearby pulsars contribute at high energy and a collection of more distant ones dominates the low-energy positron flux; see also [213]. We also stress that it is problematic to rule out any pulsar scenario exploiting the anisotropy upper limits alone, due to the fact that we can only observe a subset of the nearby pulsar in radio and gamma rays, given the highly collimated emission (see [214]).

Moreover, the gamma-ray observatories may now allow to identify the emission from the leptons leaving nearby known pulsars. Along this track, a detection of a TeV halo around Geminga has recently been reported in [215]: in that paper a naive estimate of the diffusion coefficient in the vicinity of Geminga is presented, which turns out to be much smaller than the average galactic one inferred by secondary-to-primary ratios, posing a challenge both to CR transport models and to the pulsar interpretation of the positron anomaly as well; see also the follow-up detailed discussion in [216].

Very recently, the antiproton and positron channels were critically reexamined in [217]. In that paper it is noticed that the ratio between the positron (or antiproton) flux to the proton one is consistent with the secondary production rates in the conventional picture. Based on these considerations, the author suggests that galactic positrons and antiprotons may have a common origin as secondaries in hadronic interactions, probably produced in the local interstellar environment, so that diffusion and energy loss do not act for enough time to leave an observable imprint on the spectrum. If confirmed, this would imply a completely different propagation scenario characterized by a much lower residence time ($\sim$ 1 Myr) compared to current benchmark values: such scenario would also accommodate the spectral break in the electron spectrum reported by HESS [218], but not the electron slope, which is actually steeper than the antiproton and positron one: in such alternative framework, the e^-/p discrepancy could in principle be generated at source, by not-yet identified mechanisms. The take-home message of this discussion is that the positron channel is far from being understood, and the nature of the emission above $\simeq$ 30 GeV remains mysterious. However, DM interpretations of this anomaly seem disfavored with respect to several alternative astrophysical scenarios, in particular the pulsar hypothesis. Possible avenues towards a clearer understanding of these issues are **(1)** more detailed studies of the leptonic CR anisotropy (that can in principle provide a smoking gun of the pulsar scenario or in alternative strongly constrain the scenario itself); **(2)** more data beyond TeV energies: experiments such as DAMPE[5] and CALET[6] are already operating, and the first results from DAMPE [219] already showed some interesting features to be confirmed and further investigated [187] (as shown in Figure 3), while the measurement on $e^+ + e^-$ spectrum from 10 GeV to 3 TeV has been recently released by CALET collaboration [220]; **(3)** more investigations of the interplay with the high energy gamma-ray observations, such as the TeV halo around Geminga, aimed at characterizing the diffusion properties of leptons in the vicinity of the sources; **(4)** also in this case, a better characterization of the diffusion halo size, for instance, by means of analyses focused on the radio emission, following, e.g., the approach of [156, 157].

7. Gamma-Ray Opportunities

The ubiquitous flux of high energy CR nuclei and leptons may be able to transform the galaxy into a huge pion factory and an efficient machine to up-scatter diffuse photons emitted by stars and reprocessed by dust grains. These processes, namely, π^0 decay and inverse Compton scattering, with the addition of the (usually subdominant) bremsstrahlung emission, yield a diffuse flux of high energy photons from the MeV to the

multi-TeV energy domain, reaching the current sensitivity of space missions such as Fermi-LAT and AGILE, and ground-based facilities such as HESS, MAGIC, VERITAS, and HAWC.

Therefore, the observable gamma-ray sky can give us today a quite unique diagnostics of CR transport far from the solar system environment. The *galactic diffuse gamma-ray emission* stemming from CR interactions with the ambient gas and radiation field constitutes indeed the bulk of photons measured along the galactic plane region [221]. It depends on our observational knowledge of emitting targets [222], namely, the indirect tracing of gas column densities [223, 224] through, e.g., observed CO emissivities, or the characterization of the low-energy photon background, the so-called *interstellar radiation field* [225]. Moreover, it crucially relies on the details about CR propagation across the galaxy [226].

In the last few years important progress has been pursued in the development of phenomenological viable models for galactic CR propagation, able to match the observed GeV–TeV photon data from the galactic plane region, while reproducing local CR measurements [117, 118]. In the next future, a more systematic study of gamma-ray data in symbiosis with the analysis of local CR observables may offer us the most important chance to pin down the exact features underlying (10) (see, for example, [116, 227]) in a data-driven fashion [162, 228–230].

Looping over uncertainties both on the side of emitting targets and possibly also on the underlying CR transport properties is a challenging task [221, 231]. However, such an attempt is particularly welcome in order to constrain particle DM properties [226, 232, 233]. As previously mentioned, anomalies in the gamma-ray sky may be extremely compelling for indirect DM searches. State-of-the-art N-body simulations (see, e.g., [234, 235]) predict an extended DM halo embedding and surrounding the Milky Way, with a central density peaking in correspondence to the galactic center (GC). Then, within a scenario where DM particles pair-annihilate (or decay) eventually to gamma-ray photon yields, the GC region is likely the brightest possible target for DM indirect searches, being relatively close to us ($\sim$ 8 kpc).

The kinematics of DM thermal relics annihilating today in the halo may actually give rise to peculiar photon energy spectra. In particular, gamma-ray photon lines would not have any well-known astrophysical counterpart. Therefore, monochromatic lines in the GeV–TeV range produced by DM particle pairs annihilating into two-body final state channels with one or two photons give rise to a potential smoking-gun signature. However, in a standard scenario of electrically neutral particles [236], DM rate to monoenergetic photons will exhibit loop-suppression (see, e.g., [237, 238] for the benchmark of neutralino DM). Interestingly, a hint in favor of such a spectacular signature has been found in 2012 from dedicated analyses of Fermi-LAT data in an extended region of the galactic center [239, 240], showing a peak in the photon spectrum at an energy ~130 GeV with significance of the excess at $\sim 3\sigma$ level. After an optimal observational strategy has been carried out for the purpose [241, 242], the updated analysis from the Fermi-LAT collaboration does not support any longer the original evidence for such a spectral feature in the dataset [243], suggesting previous claims to be related only to a statistical fluke. While current lack of detection of gamma-ray lines place important upper limits on today's DM annihilation cross section/decay rate into monochromatic photons in the GeV–TeV energy window [243, 244], the search for pronounced spectral features in the gamma-ray sky remains one of the most tantalizing observational programs within the WIMP mass reach [27].

Interestingly enough, within almost an entire decade, an increasing number of studies focused on the GC region, repeatedly showing the existence of a statistically significant signal in Fermi-LAT data possibly correlated with spectral and morphological features of prompt gamma-ray emission from DM pair annihilation [245–263]. Originally, the analysis of Fermi-LAT data in 2009 concerning the innermost two degrees around the GC leads the authors of [247, 248] to discover the existence of a bump-like feature in the photon spectrum exceeding the estimated astrophysical background with high statistical significance. Peaking around $\sim$ 3 GeV and fitting an approximately spherical morphology, the signal found could be immediately associated with annihilating DM particles with mass range and cross section remarkably within the WIMP ballpark. Strengthening such compelling interpretation [252] and successively [254] focused on a region of interest (ROI) extended up to ten degrees in latitude, in correspondence to the low-latitude part of the Fermi bubbles [264], finding new evidence for the gamma-ray excess even at few kpc of distance from the GC. Eventually, in [257] an optimized analysis implementing specific cuts to Fermi-LAT events—improving the resolution of the gamma-ray maps—could reach a statistical preference at the $\sim 30\sigma$ level for the inclusion of a WIMP-like template in the fit to the dataset. These claims triggered several phenomenological studies on the New Physics direction to undertake in order to explain this anomaly (see, e.g., [265–272]).

It is important to note that a close investigation about the impact of the galactic diffuse emission—related to CR physics—on the robustness of the aforementioned evidence in favor of a DM indirect detection came only four years after [247], with the studies in [258, 259]. In particular, [259] analyzed the uncertainties related to the galactic diffuse modeling explicitly inspecting the systematics of 60 models with different characterization of CR transport physics and emitting target properties. Most importantly, the authors in [259] derived in a more data-driven way the overall systematics in the ROI of $20^\circ \times 20^\circ$ centered at the GC by looking at the residuals obtained from a large number of control ROI along the whole galactic plane, using their 60 galactic diffuse emission models for a principal component analysis. The systematics found in [259] associated with the GC excess signal enlarged the set of viable DM best-fit scenarios [269, 270] and opened a new window for the interpretation of the anomaly in terms of a population of point sources such as millisecond pulsars (MPs) [273], a scenario originally proposed in [274] and successively supported in [251, 253, 256, 275], while criticized in [276, 277].

Alternative astrophysical explanations in terms of outburst events of hadronic [278] or leptonic [279] origin turned out to be not favored by data [280]. On the other hand, a currently viable alternative scenario for the GeV gamma-ray spectral feature may be provided by the depletion of low-energy photons in molecular clouds as observed in the central molecular zone [263] (see also, for comparison, the sophisticated data-analysis and deconvolution technique presented in [281]).

Notably, the different CR injection terms (Q_0 appearing in (10)) adopted in all the aforementioned analyses correspond to radial distributions that in the GC proximity do not correlate well with the expected high-star formation rate present in the inmost few hundred parsecs around the GC [282], the so-called central molecular zone (CMZ). Multiwavelength observations of the CMZ [283] point indeed to an environment with large amount of molecular gas [284], hosting high-mass OB stars [285], and potential progenitors for standard CR acceleration sites such as supernova remnants [286]. These pieces of information motivated [245] to reanalyze the GC excess implementing a novel steady-state CR source term capturing the CMZ star-forming activity. The three panels in Figure 4 from [245] show the residual count maps of photons falling in the energy range of 1–10 GeV, within a ROI of $10^\circ \times 10^\circ$ centered at the GC. From left to right, the result within a benchmark scenario originally identified in [259] to optimize the study of the GC anomaly at the GeV and the remarkable improvement in the outcome of the fit to Fermi-LAT data when adding a DM component (central panel) or when revisiting the whole galactic diffuse emission background on the basis of the novel steady source term peaked at the GC (right panel).

This result has been successively corroborated and refined in [260, 287], with the implementation of the high-resolution galactic gas distribution obtained in [223], able to resolve spiral arms and the galactic bar, and most importantly providing kinematic resolution towards the GC, with the help of hydrodynamic simulations. These HII density maps have been consequently correlated to the CR source injection term by means of a simple model of star formation; see [288], in order to provide an improved modeling of CR physics at the GC.

The relevance of the galactic diffuse emission modeling when assessing the significance of the GeV excess at the GC has been further acknowledged by the Fermi-LAT collaboration [289]. In [289], injected CR electrons as in [260], together with the uncertainties on the interstellar radiation field, have been shown to play a major role in the characterization of the gamma-ray anomaly. As also marked by the right-bottom panel of Figure 4, noisy residual photon counts around the GC in the analyses of [245, 260, 289] still leave room for an extra component in the description of gamma-ray data. Notably, two independent studies implementing different statistical techniques for clustering patterns in the observed photon count maps have followed, showing very high evidence in favor of a hitherto undetected population of point sources, able to fully account for the GeV gamma-ray excess [290, 291]. The results of these two works reached remarkably similar conclusions, giving substantial credit to the MSP-like interpretation of the gamma-ray signal at the GC (see [292, 293] for discussions about the luminosity function of the putative MSPs at the GC) and triggering relevant dedicated searches [294]. Nonnegligible mismodeling of astrophysical backgrounds and foregrounds may affect the details on the prediction for such unresolved population of point sources within the galactic bulge; see, e.g., [261]. A recent novel tool, `SkyFACT`, developed in [295], based on image reconstruction and adaptive spatiospectral template regression, has allowed for dramatic improvements in the quality of the fits to gamma-ray data through fine-grained variations of galactic diffuse emission modeling. Exploiting this powerful package, a novel investigation on the morphology of the excess in connection with the stellar distribution of the bar/boxy bulge in the inner galaxy provides strong support to the MSP hypothesis [296].

In conclusion, the GC GeV excess remains a widely studied signal in the astro-particle community. The updated comprehensive analysis carried out by the Fermi-LAT collaboration [262] fairly summarizes the most relevant factors affecting the characterization of the signal: **(1)** the details on CR production and propagation, especially in the GC proximity; **(2)** the templates for the interstellar gas and radiation field in the inner galaxy; **(3)** the emissivity and morphology of the Fermi bubbles towards low latitudes; **(4)** the list of point sources near the GC identified within a given background model.

The take-home message of this long debate is likely twofold: the existence of an extended emission from the inner galaxy peaked at few GeV is well established; however, the characterization of this emission, i.e., the morphology and its intensity, strongly depends on the assumptions of the CR source distribution (and probably also on the details of the interactions with the molecular environments). Interestingly, the interpretation in terms of unresolved point sources, possibly associated with a population of millisecond pulsars—currently supported by wavelet and photon count statistics analyses—is testable in the future with more sensitive radio facilities [297]. As a final outlook, let us mention that a recent spatially extended gamma-ray signal from the center of M31 galaxy [298] has further renewed the interest on the GC anomaly and, for instance, may possibly shed new light on the existence of galactic bulge MSP populations [299].

Let us now move away from the GC region and consider another very relevant potential discovery window. Contrary to the complex astrophysical environment characterizing the CMZ and the GC, dwarf spheroidal galaxies of the Milky Way (dSphs) stand out as very promising targets in the gamma-ray band due to the corresponding low astrophysical background and foreground [300, 301]. Being relatively close to us and associated with fairly large DM densities, the gamma-ray campaign on dSphs has been soon realized to be one of the most potentially sensitive probes to particle DM properties [302–304]. At present, dSph gamma-ray upper-bounds are remarkably probing the benchmark thermal relic scenario within the WIMP mass window [305–308]. Such upper limits may be at odds with naive DM interpretations of the GC excess [309, 310], while depending crucially on the estimated

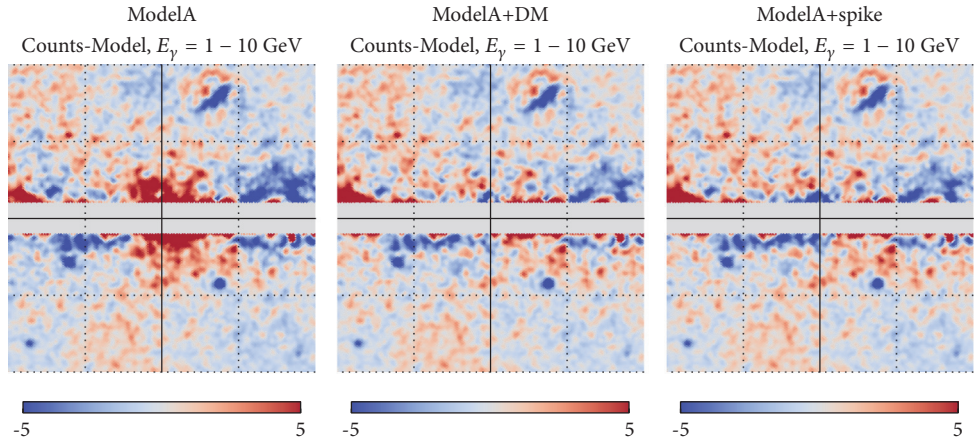

Figure 4: Importance of the cosmic-ray contribution to the galactic center excess at few GeV from the analysis of Fermi-LAT data. The three panels refer to the residual photon count maps discussed in [245]. Figure 4 is reproduced from Gaggero et al. (2015) [245] (under the Creative Commons Attribution License/public domain).

DM content in these galaxies, potentially affected by several systematics [311–314].

Interestingly, hints for a gamma-ray signal possibly compatible with the one observed at the GC have been found in the analysis of some of the most recently discovered Milky Way ultra-faint satellites; see, e.g., the case of Reticulum II [315–317]. According to the latest joint analysis of Fermi-LAT and Dark Energy Survey collaborations, the significance of these excesses remains at present well below the 3σ level [307]. Moreover, dedicated searches in the radio-band have not found any counterpart of the putative gamma-ray DM signal [318]. Note that—from the perspective of a signal detection—a broad multiwavelength program for indirect DM searches in dSphs would be indeed promising [319, 320]. However, in opposition to the case of gamma rays, constraints on DM annihilation/decay derived from the observation of dSphs in the radio and/or X band turn out to be subject to a larger set of astrophysical uncertainties, including CR transport physics [321].

8. Future Prospects: From MeV to Multi-TeV

The future of indirect searches is particularly bright.

In the gamma-ray band, two new regions of the spectrum will be explored. On the low-energy side, the MeV-GeV domain can be probed by planned experiments such as e-ASTROGAM [322][7] and AMEGO[8] (other previously proposed missions include, *e.g.*, COMPAIR [323] and ADEPT [324]), which could be realized in the mid- and long-term future in the late 2020s). All those experiments will feature a 2-3-order-of-magnitude increase in sensitivity [325, 326] with respect to previous instruments operating in this window like COMPTEL and EGRET [327, 328] and a remarkable energy resolution especially below $\simeq$ 10 GeV, where the detection principle is based on Compton scattering instead of pair production. This will guarantee a high constraining power as far as sharp spectral features (e.g., lines originating from DM annihilation) are concerned [329]. On theoretical grounds, vanilla WIMP scenario in this domain of energy scales may not be adequate due to the Lee-Weinberg bound [57, 58]. Interesting models designed to offer an explanation for a 511 keV emission line detected in the inner galaxy may be instead well probed [330, 331].

On the other end, in the TeV domain, while many Imaging Atmospheric Cherenkov Telescopes (MAGIC [332], HESS[9], and VERITAS[10]) and air-shower arrays (such as Milagro[11] and HAWC[12] [333]) have already been providing relevant results and have provided stringent constraints on DM annihilation [334], CTA will provide a further, unprecedented increase in sensitivity above the TeV. We want to emphasize that, as mentioned in Section 2, the most naive version of the *WIMP miracle* naturally yields a predicted mass for the DM candidate in that ballpark. CTA can probe the DM sector in different ways [335–338].

In connection with the main topic of this review, we stress once again that the GC region appears promising also in this context, which implies that a more careful modeling of the γ-ray diffuse emission from the inner galaxy will be required. The diffusion properties, again, play then a central role: in particular, the CR spectrum in the inner galaxy is currently a matter or debate, and Fermi-LAT data seem to hint towards a hardening in the inner galaxy [118, 229, 230]. `DRAGON`-based models [116, 118] featuring inhomogeneous or anisotropic diffusion, which are key features of this specific numerical package, allow reproducing Fermi-LAT data and providing TeV predictions [119, 228] which seem to be in accord with a collection of data from different experiments, including the bright and diffuse galactic Ridge emission measured by HESS over the latest decade [339–341]. These kind of studies will be even more important in the forthcoming years, due to the necessity, that we have stressed several times along this paper, of a good characterization of the astrophysical backgrounds. The study of dwarf spheroidal galaxies will also benefit from the expected increase in sensitivity in the TeV domain, and the expected performance of CTA in this channel is remarkable [342–344].

As far as charged particle channels are concerned, the antiparticle/antinuclear avenue is particularly promising

despite the relevant uncertainties. In fact, new high-quality data are expected by many experiments: besides AMS-02, the already operating DAMPE [345] space experiment, CALET [346], on board the International Space Station, and the next-generation balloon ISS-CREAM [347] have the opportunity to probe in particular the leptonic channel all the way up to the multi-TeV range with unprecedented energy resolution and sensitivity; planned experiments such as HERD[13] will provide a further very relevant extension in the covered energy range and sensitivity, and—on the antinuclei side—we are looking forward to experiments such as GAPS [348], a balloon experiment expected to operate in 2020 and optimized specifically for low-energy antinuclei signatures, thanks to a novel detection technique based on exotic atom capture and decay.

To conclude this *grand tour*, let us emphasize once again the opportunity offered by the tremendous increase in experimental accuracy we are already witnessing in these days, and we will be further exploiting with the upcoming years. In our opinion, in order to take full advantage of these developments, interdisciplinarity is the main avenue. The guaranteed outcome of the research program aimed at indirectly detecting particle dark matter by means of astronomical data certainly involves a more profound understanding of the CR physics outlined across this review. It is therefore crucial to deepen and broaden the connections between the research fields we have described above: both the high energy astrophysics and the particle physics community would unquestionably benefit from a cutting-edge increasing crossover.

Conflicts of Interest

The authors declare that there are no conflicts of interest regarding the publication of this article.

Acknowledgments

Thanks are due to Dario Grasso, Gianfranco Bertone, Piero Ullio, and Stefano Gabici for all their invaluable teachings about dark matter and cosmic-ray physics. The authors thank Alfredo Urbano and Carmelo Evoli for batting around a few interesting ideas on how to improve the manuscript.

Endnotes

1. The Alfvén speed is supersonic in most typical ISM environments: hot HII regions, warm intercloud gas, and molecular gas, with $\beta \equiv (v_s/v_A)^2 \simeq 0.1 \div 0.3$ everywhere [349].
2. As a reference, the reader can keep in mind that the energy scales from GeV to PeV, characteristic of galactic CRs, resonate with scales from $\mathcal{O}$(AU) to $\mathcal{O}$(pc).
3. Equivalently, in term of pitch angle, in the direction along the regular field we can write

$$\frac{\partial f}{\partial t} + v\mu\frac{\partial f}{\partial x} = \frac{\partial}{\partial \mu}\left(D_{\mu\mu}\frac{\partial f}{\partial \mu}\right). \quad (*)$$

4. We outline in particular the relevant role of the cross-section uncertainties (see also [135] and references therein). In this regard, there has been a remarkable activity in the latest years both concerning semiempirical parametrizations (tuned on experimental datasets) and Monte Carlo event generators: as far as the former category is concerned, new models have been proposed based on the data provided by the NA49 and BRAHMS collaborations [350–353]; concerning the latter, several codes (e.g., EPOS 1.99 [354], SIBYLL [355], and QGSJET-II-04 [356]) have been recently tuned to LHC data (see, e.g., [354, 356]).
5. http://dpnc.unige.ch/dampe/.
6. http://calet.phys.lsu.edu/.
7. e-ASTROGAM is proposed as ESA M5 mission.
8. See pcos.gsfc.nasa.gov/physpag/probe/AMEGO_probe.pdf
9. www.mpi-hd.mpg.de/hfm/HESS.
10. veritas.sao.arizona.edu/.
11. http://umdgrb.umd.edu/cosmic/milagro.html.
12. umdgrb.umd.edu/hawc/index.php.
13. http://herd.ihep.ac.cn/.

References

[1] J. Silk et al., *Particle Dark Matter: Observations, Models and Searches*, Cambridge University Press, 2010, http://www.cambridge.org/uk/catalogue/catalogue.asp?isbn=9780521763684.

[2] J. Abdallah et al., "Simplified Models for Dark Matter Searches at the LHC," *Physics of the Dark Universe*, vol. 9-10, pp. 8–23, 2015.

[3] T. Marrodan Undagoitia and L. Rauch, "Dark matter direct-detection experiments," *Journal of Physics G: Nuclear and Particle Physics*, vol. 43, 2016.

[4] J. Ellis, J. S. Hagelin, D. V. Nanopoulos, K. Olive, and M. Srednicki, "Supersymmetric relics from the big bang," *Nuclear Physics B*, vol. 238, no. 2, pp. 453–476, 1984.

[5] G. Jungman, M. Kamionkowski, and K. Griest, "Supersymmetric dark matter," *Physics Reports*, vol. 267, pp. 195–373, 1996.

[6] K. A. Olive, "Lectures on Dark Matter," in *Proceedings of Particle Physics and Cosmology: The Quest for Physics beyond the Standard Model(s), TASI 2002, June 3-28, 2002*, pp. 797–851, Theoretical Advanced Study Institute, Boulder, Colorado, USA, 2003.

[7] Y. B. Zeldovich, A. A. Klypin, M. Y. Khlopov, and V. M. Chechetkin, "Astrophysical constraints on the mass of heavy stable neutral leptons," *Soviet Journal of Nuclear Physics*, vol. 31, pp. 664–669, 1980, Yad.Fiz. 31 (1980) 1286-1294.

[8] D. Maurin, R. Taillet, F. Donato, P. Salati, A. Barrau, and G. Boudoul, "Galactic Cosmic Ray Nuclei as a Tool for Astroparticle Physics," *Recent Research Developments in Astrophysics*, 2002.

[9] L. E. Strigari, "Galactic Searches for Dark Matter," *Physics Reports*, vol. 531, no. 1, 2013.

[10] L. Bergstrom, "Non-baryonic dark matter - observational evidence and detection methods," *Reports on Progress in Physics*, vol. 63, p. 793, 2000.

[11] G. Bertone, D. Hooper, and J. Silk, "Particle dark matter: evidence, candidates and constraints," *Physics Reports*, vol. 405, pp. 279–390, 2005.

[12] J. Silk and M. Srednicki, "Cosmic-Ray Antiprotons as a Probe of a Photino-Dominated Universe," *Physical Review Letters*, vol. 53, p. 624, 1984.

[13] F. W. Stecker, S. Rudaz, and T. F. Walsh, "Galactic Antiprotons from Photinos," *Physical Review Letters*, vol. 55, p. 2622, 1985.

[14] P. Picozza et al., "PAMELA - a payload for antimatter matter exploration and light-nuclei astrophysics," *Astroparticle Physics*, vol. 27, pp. 296–315, 2007.

[15] A. Kounine, "The alpha magnetic spectrometer on the international space station," *International Journal of Modern Physics E*, vol. 21, 2012.

[16] A. Reinert and M. W. Winkler, "A precision search for WIMPs with charged cosmic rays," *Journal of Cosmology and Astroparticle Physics*, 2017.

[17] K. Blum, R. Sato, and E. Waxman, *Cosmic-ray Antimatter*, 2017, http://inspirehep.net/record/1624395.

[18] O. Adriani, G. C. Barbarino, and G. A. Bazilevskaya, "An anomalous positron abundance in cosmic rays with energies 1.5–100 GeV," *Nature*, vol. 458, pp. 607–609, 2009.

[19] M. Aguilar, G. Alberti, B. Alpat et al., "First Result from the Alpha Magnetic Spectrometer on the International Space Station: Precision Measurement of the Positron Fraction in Primary Cosmic Rays of 0.5–350 GeV," *Physical Review Letters*, vol. 110, 2013.

[20] M. Aguilar, L. Ali Cavasonza, B. Alpat et al., "Antiproton flux, antiproton-to-proton flux ratio, and properties of elementary particle fluxes in primary cosmic rays measured with the alpha magnetic spectrometer on the international space station," *Physical Review Letters*, vol. 117, 2016.

[21] A. Cuoco, M. Krämer, and M. Korsmeier, "Novel dark matter constraints from antiprotons in light of AMS-02," *Physical Review Letters*, vol. 118, 2017.

[22] A. Cuoco, J. Heisig, M. Korsmeier, and M. Kramer, "A combined dark matter study of AMS-02 antiprotons and Fermi-LAT gamma rays," in *Proceedings of the 2017 European Physical Society Conference on High Energy Physics (EPS-HEP 2017)*, Venice, Italy, July 5-12, 2017.

[23] L. Bergström and H. Snellman, "Observable monochromatic photons from cosmic photino annihilation," *Physical Review D*, vol. 37, 1988.

[24] S. Rudaz, "Annihilation of heavy-neutral-fermion pairs into monochromatic γ rays and its astrophysical implications," *Physical Review D*, vol. 39, 1989.

[25] G. F. Giudice and K. Griest, "Rate for annihilation of galactic dark matter into two photons," *Physical Review D*, vol. 2549, 1989.

[26] L. Bergström, P. Ullio, and J. H. Buckley, "Observability of gamma rays from dark matter neutralino annihilations in the milky way halo," *Astroparticle Physics*, vol. 9, pp. 137–162, 1998.

[27] T. Bringmann and C. Weniger, "Gamma ray signals from dark matter: Concepts, status and prospects," *Physics of the Dark Universe*, vol. 1, pp. 194–217, 2012.

[28] G. Bertone and D. Hooper, "A history of dark matter," *Reviews of Modern Physics*, 2016.

[29] J. de Swart, G. Bertone, and J. van Dongen, "How dark matter came to matter," *Nature Astronomy*, 2017.

[30] W. Hu, R. Barkana, and A. Gruzinov, "Fuzzy Cold Dark Matter: The Wave Properties of Ultralight Particles," *Physical Review Letters*, vol. 85, 2000.

[31] D. J. E. Marsh, "Axion cosmology," *Physics Reports*, vol. 643, pp. 1–79, 2016.

[32] L. Hui, J. P. Ostriker, S. Tremaine, and E. Witten, "Ultralight scalars as cosmological dark matter," *Physical Review D*, vol. 95, 2017.

[33] P. Svrvcek and E. Witten, "Axions in string theory," *Journal of High Energy Physics*, vol. 6, article no. 51, 2006.

[34] A. Arvanitaki, S. Dimopoulos, S. Dubovsky, N. Kaloper, and J. March-Russell, "String axiverse," *Physical Review D*, vol. 81, 2010.

[35] B. P. Abbott et al., "Observation of Gravitational Waves from a Binary Black Hole Merger," *Physical Review Letters*, vol. 116, 2016.

[36] S. Bird, I. Cholis, J. B. Muñoz et al., "Did LIGO detect dark matter?" *Physical Review Letters*, vol. 116, 2016.

[37] G. F. Chapline, "Cosmological effects of primordial black holes," *Nature (London)*, vol. 251, pp. 251-252, 1975.

[38] B. Carr, F. Kühnel, and M. Sandstad, "Primordial black holes as dark matter," *Physical Review D*, vol. 94, 2016.

[39] J. L. Feng, "Dark matter candidates from particle physics and methods of detection," *Annual Review of Astronomy and Astrophysics*, vol. 48, pp. 495–545, 2010.

[40] G. F. Giudice, "Naturally speaking: the naturalness criterion and physics at the LHC," in *Perspectives on LHC Physics*, 2008.

[41] M. Regis, M. Serone, and P. Ullio, "A dark matter candidate from an extra (Non-Universal) dimension," *Journal of High Energy Physics*, vol. 03, article no. 84, 2007.

[42] G. Panico, E. Pontón, J. Santiago, and M. Serone, "Dark matter and electroweak symmetry breaking in models with warped extra dimensions," *Physical Review D*, vol. 77, 2008.

[43] T. A. Ryttov and F. Sannino, "Ultraminimal technicolor and its dark matter technicolor interacting massive particles," *Physical Review D*, vol. 78, 2008.

[44] A. Belyaev, M. T. Frandsen, S. Sarkar, and F. Sannino, "Mixed dark matter from technicolor," *Physical Review D*, vol. 83, 2011.

[45] M. Frigerio, A. Pomarol, F. Riva, and A. Urbano, "Composite scalar dark matter," *Journal of High Energy Physics*, vol. 7, article no. 15, 2012.

[46] S. Bruggisser, F. Riva, and A. Urbano, "Strongly interacting light dark matter," *SciPost Physics*, vol. 3, no. 17, 2017.

[47] G. F. Giudice and A. Romanino, "Split Supersymmetry," *Nuclear Physics B*, vol. 699, pp. 65–89, 2004, Erratum to: "Split Supersymmetry," Nuclear Physics B, vol. 706, p. 487, 2005.

[48] N. Arkani-Hamed, S. Dimopoulos, G. F. Giudice, and A. Romanino, "Aspects of Split Supersymmetry," *Nuclear Physics B*, vol. 709, pp. 3–46, 2005.

[49] A. Masiero, S. Profumo, and P. Ullio, "Neutralino dark matter detection in split supersymmetry scenarios," *Nuclear Physics B*, vol. 712, pp. 86–114, 2005.

[50] G. Servant and T. M. P. Tait, "Is the lightest kaluza-klein particle a viable dark matter candidate?" *Nuclear Physics B*, vol. 650, pp. 391–419, 2003.

[51] K. Agashe and G. Servant, "Warped unification, proton stability and dark matter," *Physical Review Letters*, vol. 93, 2004.

[52] K. Agashe and G. Servant, "Baryon number in warped grand unified theories: model building and (dark matter related) phenomenology," *Journal of Cosmology and Astroparticle Physics*, vol. 2005, no. 02, 2005.

[53] D. Hooper and S. Profumo, "Dark matter and collider phenomenology of universal extra dimensions," *Physics Reports*, vol. 453, pp. 29–115, 2007.

[54] P. Gondolo and G. Gelmini, "Cosmic abundances of stable particles: Improved analysis," *Nuclear Physics B*, vol. 360, no. 1, pp. 145–179, 1991.

[55] S. Profumo, *An Introduction to Particle Dark Matter*, World Scientific, 2017.

[56] P. A. R. Ade et al., "Planck 2015 results. XIII. Cosmological parameters," *Astronomy and Astrophysics*, vol. 594, no. A13, 2016.

[57] M. I. Vysotsky, A. D. Dolgov, and Y. B. Zeldovich, "Cosmological limits on the masses of neutral leptons," *JETP Letters*, vol. 26, p. 188, 1977.

[58] B. W. Lee and S. Weinberg, "Cosmological lower bound on heavy-neutrino masses," *Physical Review Letters*, vol. 39, no. 4, 1977.

[59] K. Griest and M. Kamionkowski, "Unitarity limits on the mass and radius of dark-matter particles," *Physical Review Letters*, vol. 64, no. 6, 1990.

[60] K. Harigaya, M. Ibe, K. Kaneta, W. Nakano, and M. Suzuki, "Thermal relic dark matter beyond the unitarity limit," *Journal of High Energy Physics*, vol. 2016, no. 8, 2016.

[61] K. Griest and D. Seckel, "Three exceptions in the calculation of relic abundances," *Physical Review D: Particles, Fields, Gravitation and Cosmology*, vol. 43, no. 10, 1991.

[62] E. D. Carlson, M. E. Machacek, and L. J. Hall, "Self-interacting dark matter," *The Astrophysical Journal*, vol. 398, pp. 43–52, 1992.

[63] M. Pospelov, A. Ritz, and M. Voloshin, "Secluded WIMP dark matter," *Physics Letters B*, vol. 662, no. 1, pp. 53–61, 2008.

[64] Y. Hochberg, E. Kuflik, T. Volansky, and J. G. Wacker, "Mechanism for thermal relic dark matter of strongly interacting massive particles," *Physical Review Letters*, vol. 113, no. 17, 2014.

[65] F. D'Eramo and J. Thaler, "Semi-annihilation of dark matter," *Journal of High Energy Physics*, vol. 2010, no. 06, 2010.

[66] R. T. D'Agnolo and J. T. Ruderman, "Light dark matter from forbidden channels," *Physical Review Letters*, vol. 115, no. 6, 2015.

[67] D. Pappadopulo, J. T. Ruderman, and G. Trevisan, "Dark matter freeze-out in a nonrelativistic sector," *Physical Review D: Particles, Fields, Gravitation and Cosmology*, vol. 94, no. 3, 2016.

[68] J. A. Dror, E. Kuflik, and W. H. Ng, "Codecaying dark matter," *Physical Review Letters*, vol. 117, no. 21, 2016.

[69] R. T. D'Agnolo, D. Pappadopulo, and J. T. Ruderman, "Fourth exception in the calculation of relic abundances," *Physical Review Letters*, vol. 119, no. 6, 2017.

[70] F. D'Eramo, N. Fernandez, and S. Profumo, "When the universe expands too fast: relentless dark matter," *Journal of Cosmology and Astroparticle Physics*, vol. 2017, no. 5, 2017.

[71] N. Arkani-Hamed, D. P. Finkbeiner, T. R. Slatyer, and N. Weiner, "A theory of dark matter," *Physical Review D: Particles, Fields, Gravitation and Cosmology*, vol. 79, no. 1, 2009.

[72] J. L. Feng, M. Kaplinghat, and H.-B. Yu, "Halo-shape and relic-density exclusions of sommerfeld-enhanced dark matter explanations of cosmic ray excesses," *Physical Review Letters*, vol. 104, no. 15, 2010.

[73] J. L. Feng, M. Kaplinghat, and H.-B. Yu, "Sommerfeld enhancements for thermal relic dark matter," *Physical Review D: Particles, Fields, Gravitation and Cosmology*, vol. 82, no. 8, 2010.

[74] A. Hryczuk, R. Iengo, and P. Ullio, "Relic densities including Sommerfeld enhancements in the MSSM," *Journal of High Energy Physics*, vol. 2011, no. 3, 2011.

[75] W. Shepherd, T. M. Tait, and G. Zaharijas, "Bound states of weakly interacting dark matter," *Physical Review D: Particles, Fields, Gravitation and Cosmology*, vol. 79, no. 5, 2009.

[76] B. von Harling and K. Petraki, "Bound-state formation for thermal relic dark matter and unitarity," *Journal of Cosmology and Astroparticle Physics*, vol. 2014, no. 12, 2014.

[77] H. An, M. B. Wise, and Y. Zhang, "Effects of bound states on dark matter annihilation," *Physical Review D*, vol. 93, no. 11, 2016.

[78] M. Cirelli, P. Panci, K. Petraki, F. Sala, and M. Taoso, "Dark Matter's secret liaisons: phenomenology of a dark U(1) sector with bound states," *Journal of Cosmology and Astroparticle Physics*, vol. 2017, no. 05, 2017.

[79] A. Mitridate, M. Redi, J. Smirnov, and A. Strumia, "Cosmological implications of dark matter bound states," *Journal of Cosmology and Astroparticle Physics*, vol. 2017, no. 05, 2017.

[80] S. Biondini and M. Laine, "Thermal dark matter co-annihilating with a strongly interacting scalar," *Journal of High Energy Physics*, vol. 2018, no. 4, 2018.

[81] J. L. Feng and J. Kumar, "Dark-Matter particles without weak-scale masses or weak interactions," *Physical Review Letters*, vol. 101, no. 23, 2008.

[82] M. Cirelli, G. Corcella, A. Hektor et al., "PPPC 4 DM ID: a poor particle physicist cookbook for dark matter indirect detection," *Journal of Cosmology and Astroparticle Physics*, vol. 2011, no. 03, 2011, Erratum: "PPPC 4 DM ID: a poor particle physicist cookbook for dark matter indirect detection," Journal of Cosmology and Astroparticle Physics, vol. 2012, no. 10, 2012.

[83] J. Buch, M. Cirelli, G. Giesen, and M. Taoso, "PPPC 4 DM secondary: a Poor Particle Physicist Cookbook for secondary radiation from Dark Matter," *Journal of Cosmology and Astroparticle Physics*, vol. 2015, no. 09, 2015.

[84] G. Arcadi, M. Dutra, P. Ghosh et al., "The waning of the WIMP? A review of models, searches, and constraints," *The European Physical Journal C*, 2017.

[85] A. R. Bell, "Cosmic ray acceleration," *Astroparticle Physics*, vol. 43, pp. 56–70, 2013.

[86] W. Baade and F. Zwicky, *Contributions from the Mount Wilson Observatory*, vol. 3, 1934.

[87] W. Baade and F. Zwicky, "Remarks on super-novae and cosmic rays," *Physical Review*, vol. 46, no. 1, 1934.

[88] P. Morrison, "On the origins of cosmic rays," *Reviews of Modern Physics*, vol. 29, 1957.

[89] V. L. Ginzburg, "The nature of cosmic radio emission and the origin of cosmic rays," *Il Nuovo Cimento*, vol. 3, pp. 38–48, 1956.

[90] R. D. Blandford and J. P. Ostriker, "Particle acceleration by astrophysical shocks," *The Astrophysical Journal Letters*, vol. 221, pp. L29–L32, 1978.

[91] A. R. Bell, "The acceleration of cosmic rays in shock fronts. I," *Monthly Notices of the Royal Astronomical Society*, vol. 182, pp. 147–156, 1978.

[92] W. I. Axford, E. Leer, and G. Skadron, "The acceleration of cosmic rays by shock waves," in *Proceedings of the 15th International Cosmic Ray Conference*, vol. 11, pp. 132–137, 1977.

[93] G. F. Krymskii, "A regular mechanism for the acceleration of charged particles on the front of a shock wave," *Akademiia Nauk SSSR Doklady*, vol. 234, pp. 1306–1308, 1977.

[94] F. A. Aharonian, A. M. Atoyan, and H. J. Voelk, "High energy electrons and positrons in cosmic rays as an indicator of the existence of a nearby cosmic tevatron," *Astronomy and Astrophysics*, vol. 294, pp. L41–L44, 1995.

[95] R. P. Murphy, M. Sasaki, W. R. Binns et al., "Galactic cosmic ray origins and OB associations: evidence from SuperTIGER

observations of elements $_{26}$Fe through $_{40}$Zr," *The Astrophysical Journal*, vol. 831, 2016.

[96] S. Heinz and R. Sunyaev, "Cosmic rays from microquasars: A narrow component to the CR spectrum?" *Astronomy and Astrophysics*, vol. 390, no. 2, pp. 751–766, 2002.

[97] T. Antoni, W. D. Apel, A. F. Badea et al., "Large-Scale Cosmic-Ray Anisotropy with KASCADE," *The Astrophysical Journal*, vol. 604, no. 2, pp. 687–692, 2004.

[98] A. A. Abdo, B. T. Allen, T. Aune et al., "The large-scale cosmic-ray anisotropy as observed with milagro," *The Astrophysical Journal*, vol. 698, no. 2, pp. 2121–2130, 2009.

[99] M. Aglietta, V. V. Alekseenko, B. Alessandro et al., "Evolution of the cosmic-ray anisotropy above 10^{14}eV," *Astrophysical Journal Letters*, vol. 692, no. 2, pp. L130–L133, 2009.

[100] M. Amenomori, X. J. Bi, D. Chen et al., "Northern sky galactic cosmic ray anisotropy between 10 and 1000 TeV with the tibet air shower array," *The Astrophysical Journal*, vol. 836, no. 2, 2017.

[101] M. G. Aartsen, R. Abbasi, Y. Abdou et al., "Observation of cosmic-ray anisotropy with the icetop air shower array," *The Astrophysical Journal*, vol. 765, no. 1, 2013.

[102] R. Abbasi, Y. Abdou, T. Abu-Zayyad et al., "Observation of anisotropy in the galactic cosmic-ray arrival directions at 400 TeV with icecube," *The Astrophysical Journal*, vol. 746, no. 1, 2012.

[103] J. B. Pollack and G. G. Fazio, "Production of π mesons and gamma radiation in the galaxy by cosmic rays," *Physical Review*, vol. 131, no. 6, pp. 2684–2691, 1963.

[104] V. L. Ginzburg and S. I. Syrovatskii, *The Origin of Cosmic Rays*, Elsevier, 1964.

[105] V. S. Berezinskii, S. V. Bulanov, V. A. Dogiel, and V. S. Ptuskin, *Astrophysics of Cosmic Rays*, North-Holland, 1990.

[106] J. R. Jokipii, "Cosmic-ray propagation. I. Charged particles in a random magnetic field," *The Astrophysical Journal*, vol. 146, 1966.

[107] J. R. Jokipii and E. N. Parker, "Random walk of magnetic lines of force in astrophysics," *Physical Review Letters*, vol. 21, no. 1, pp. 44–47, 1968.

[108] J. W. Armstrong, B. J. Rickett, and S. R. Spangler, "Electron density power spectrum in the local interstellar medium," *The Astrophysical Journal*, vol. 443, no. 1, pp. 209–221, 1995.

[109] R. Jansson and G. R. Farrar, "The galactic magnetic field," *The Astrophysical Journal Letters*, vol. 761, no. 1, 2012.

[110] P. Terral and K. Ferrière, "Constraints from Faraday rotation on the magnetic field structure in the Galactic halo," *Astronomy & Astrophysics*, vol. 600, 2017.

[111] B. G. Elmegreen and J. Scalo, "Interstellar turbulence I: Observations and processes," *Annual Review of Astronomy and Astrophysics*, vol. 42, pp. 211–273, 2004.

[112] C. J. Cesarsky, "Cosmic-ray confinement in the galaxy," *Annual Review of Astronomy and Astrophysics*, vol. 18, pp. 289–319, 1980.

[113] P. Blasi, E. Amato, and P. D. Serpico, "Spectral breaks as a signature of cosmic ray induced turbulence in the galaxy," *Physical Review Letters*, vol. 109, no. 6, 2012.

[114] P. Blasi, "The origin of galactic cosmic rays," *Astronomy and Astrophysics Reviews*, vol. 21, no. 70, 2013.

[115] J. Skilling, "Cosmic ray streaming—I effect of Alfvén waves on particles," *Monthly Notices of the Royal Astronomical Society*, vol. 172, no. 3, pp. 557–566, 1975.

[116] S. S. Cerri, D. Gaggero, A. Vittino, C. Evoli, and D. Grasso, "A signature of anisotropic cosmic-ray transport in the gamma-ray sky," *Journal of Cosmology and Astroparticle Physics*, vol. 2017, no. 10, 2017.

[117] C. Evoli, D. Gaggero, D. Grasso, and L. Maccione, "Common solution to the cosmic ray anisotropy and gradient problems," *Physical Review Letters*, vol. 108, no. 21, 2012.

[118] D. Gaggero, M. Taoso, A. Urbano, M. Valli, and P. Ullio, "Gamma-ray sky points to radial gradients in cosmic-ray transport," *Physical Review D*, vol. 91, no. 8, 2015.

[119] D. Gaggero, D. Grasso, A. Marinelli, M. Taoso, and A. Urbano, "Diffuse cosmic rays shining in the Galactic center: A novel interpretation of H.E.S.S. and Fermi-LAT gamma-ray data," *Physical Review Letters*, vol. 119, 2017.

[120] N. Tomassetti, "Cosmic-ray protons, nuclei, electrons, and antiparticles under a two-halo scenario of diffusive propagation," *Physical Review D*, vol. 92, 2015.

[121] J. Feng, N. Tomassetti, and A. Oliva, "Bayesian analysis of spatial-dependent cosmic-ray propagation: astrophysical background of antiprotons and positrons," *Physical Review D*, vol. 94, no. 12, 2016.

[122] A. W. Strong, I. V. Moskalenko, and V. S. Ptuskin, "Cosmic-ray propagation and interactions in the galaxy," *Annual Review of Nuclear and Particle Science*, vol. 57, pp. 285–327, 2007.

[123] C. Evoli, D. Gaggero, A. Vittino et al., "Cosmic-ray propagation with DRAGON2: I. Numerical solver and astrophysical ingredients," *Journal of Cosmology and Astroparticle Physics*, vol. 2017, no. 2, article no. 015, 2017.

[124] S. Sridhar and P. Goldreich, "Toward a theory of interstellar turbulence. I. Weak Alfvénic turbulence," *The Astrophysical Journal*, vol. 432, no. 2, pp. 612–621, 1994.

[125] P. Goldreich and S. Sridhar, "Toward a theory of interstellar turbulence. II. Strong Alfvénic turbulence," *The Astrophysical Journal*, vol. 438, no. 2, pp. 763–775, 1995.

[126] B. D. G. Chandran, "Scattering of energetic particles by anisotropic magnetohydrodynamic turbulence with a goldreich-sridhar power spectrum," *Physical Review Letters*, vol. 85, no. 22, 2000.

[127] H. Yan and A. Lazarian, "Scattering of cosmic rays by magnetohydrodynamic interstellar turbulence," *Physical Review Letters*, vol. 89, no. 28, 2002.

[128] H. Yan and A. Lazarian, "Cosmic ray propagation: nonlinear diffusion parallel and perpendicular to mean magnetic field," *The Astrophysical Journal*, vol. 673, no. 2, 2008.

[129] A. W. Strong and G. Youssefi, "Propagation models for CR nucleons and electrons and predictions of the galactic gamma-ray spectrum," in *Proceedings of the 24th International Cosmic Ray Conference*, vol. 3, p. 48, 1995.

[130] A. W. Strong and I. V. Moskalenko, "Propagation of cosmic-ray nucleons in the galaxy," *The Astrophysical Journal*, vol. 509, no. 1, 1998.

[131] I. V. Moskalenko and A. W. Strong, "Production and propagation of cosmic-ray positrons and electrons," *The Astrophysical Journal*, vol. 493, no. 2, 1998.

[132] A. W. Strong and I. V. Moskalenko, "New developments in the GALPROP CR propagation model," in *Proceedings of the 27th International Cosmic Ray Conference*, vol. 5, pp. 1942–1945, 2001.

[133] C. Evoli, D. Gaggero, D. Grasso, and L. Maccione, "Cosmic-ray nuclei, antiprotons and gamma-rays in the galaxy: a new diffusion model," *Journal of Cosmology and Astroparticle Physics*, vol. 2008, no. 10, 2008.

[134] D. Gaggero, L. Maccione, G. Di Bernardo, C. Evoli, and D. Grasso, "Three-dimensional model of cosmic-ray lepton propagation reproduces data from the alpha magnetic spectrometer

on the international space station," *Physical Review Letters*, vol. 111, no. 2, 2013.

[135] C. Evoli, D. Gaggero, A. Vittino, M. Di Mauro, D. Grasso, and M. N. Mazziotta, "Cosmic-ray propagation with DRAGON2: II. Nuclear interactions with the interstellar gas," *Journal of Cosmology and Astroparticle Physics*, vol. 2018, 2018.

[136] R. Kissmann, "PICARD: A novel code for the Galactic Cosmic Ray propagation problem," *Astroparticle Physics*, vol. 55, pp. 37–50, 2014.

[137] M. Werner, R. Kissmann, A. W. Strong, and O. Reimer, "Spiral arms as cosmic ray source distributions," *Astroparticle Physics*, vol. 64, pp. 18–33, 2015.

[138] D. Maurin, F. Donato, R. Taillet, and P. Salati, "Cosmic rays below Z = 30 in a diffusion model: New constraints on propagation parameters," *The Astrophysical Journal*, vol. 555, no. 2, 2001.

[139] G. Giesen, M. Boudaud, Y. Génolini et al., "AMS-02 antiprotons, at last! Secondary astrophysical component and immediate implications for dark matter," *Journal of Cosmology and Astroparticle Physics*, vol. 2015, 2015.

[140] M. Aguilar, L. Ali Cavasonza, G. Ambrosi et al., "Precision measurement of the boron to carbon flux ratio in cosmic rays from 1.9 GV to 2.6 TV with the alpha magnetic spectrometer on the international space station," *Physical Review Letters*, vol. 117, no. 23, 2016.

[141] R. Trotta, G. Jóhannesson, I. V. Moskalenko, T. A. Porter, R. Ruiz De Austri, and A. W. Strong, "Constraints on cosmic-ray propagation models from a global bayesian analysis," *The Astrophysical Journal*, vol. 729, no. 2, 2011.

[142] G. Jóhannesson, R. R. de Austri, A. C. Vincent et al., "Bayesian analysis of cosmic ray propagation: evidence against homogeneous diffusion," *The Astrophysical Journal*, vol. 824, no. 1, 2016.

[143] C. Evoli, D. Gaggero, and D. Grasso, "Secondary antiprotons as a galactic dark matter probe," *Journal of Cosmology and Astroparticle Physics*, vol. 2015, no. 12, 2015.

[144] Q. Yuan, S.-J. Lin, K. Fang, and X.-J. Bi, "Propagation of cosmic rays in the AMS-02 era," *Physical Review D*, vol. 95, no. 8, 2017.

[145] J.-S. Niu and T. Li, "Galactic cosmic-ray model in the light of AMS-02 nuclei data," *Physical Review D*, vol. 97, no. 2, 2017.

[146] A. Buffington and S. M. Schindler, "Recent cosmic-ray antiproton measurements and astrophysical implications," *The Astrophysical Journal Letters*, vol. 247, pp. L105–L109, 1981.

[147] J. Ellis, R. A. Flores, K. Freese, S. Ritz, D. Seckel, and J. Silk, "Cosmic ray constraints on the annihilations of relic particles in the galactic halo," *Physics Letters B*, vol. 214, no. 3, pp. 403–412, 1988.

[148] S. Rudaz and F. W. Stecker, "Cosmic-ray antiprotons, positrons, and gamma rays from halo dark matter annihilation," *The Astrophysical Journal*, vol. 325, pp. 16–25, 1988.

[149] L. Bergström, J. Edsjö, and P. Ullio, "Cosmic antiprotons as a probe for supersymmetric dark matter?" *The Astrophysical Journal*, vol. 526, no. 1, 1999.

[150] O. Adriani, G. C. Barbarino, G. A. Bazilevskaya et al., "New measurement of the antiproton-to-proton flux ratio up to 100 GeV in the cosmic radiation," *Physical Review Letters*, vol. 102, no. 5, 2009.

[151] O. Adriani, G. C. Barbarino, G. A. Bazilevskaya et al., "PAMELA results on the cosmic-ray antiproton flux from 60 MeV to 180 GeV in kinetic energy," *Physical Review Letters*, vol. 105, no. 12, 2010.

[152] G. Di Bernardo, C. Evoli, D. Gaggero, D. Grasso, and L. Maccione, "Unified interpretation of cosmic ray nuclei and antiproton recent measurements," *Astroparticle Physics*, vol. 34, no. 5, pp. 274–283, 2010.

[153] T. Bringmann and P. Salati, "Galactic antiproton spectrum at high energies: Background expectation versus exotic contributions," *Physical Review D: Particles, Fields, Gravitation and Cosmology*, vol. 75, no. 8, 2007.

[154] F. Donato, D. Maurin, P. Brun, T. Delahaye, and P. Salati, "Constraints on WIMP dark matter from the high energy PAMELA $\overline{p}/p$ Data," *Physical Review Letters*, vol. 102, no. 7, 2009.

[155] M. Cirelli, D. Gaggero, G. Giesen, M. Taoso, and A. Urbano, "Antiproton constraints on the GeV gamma-ray excess: a comprehensive analysis," *Journal of Cosmology and Astroparticle Physics*, vol. 2014, no. 12, 2014.

[156] A. W. Strong, E. Orlando, and T. R. Jaffe, "The interstellar cosmic-ray electron spectrum from synchrotron radiation and direct measurements," *Astronomy and Astrophysics*, vol. 534, 2011.

[157] G. Di Bernardo, C. Evoli, D. Gaggero, D. Grasso, and L. Maccione, "Cosmic ray electrons, positrons and the synchrotron emission of the Galaxy: consistent analysis and implications," *Journal of Cosmology and Astroparticle Physics*, vol. 2013, no. 03, 2013.

[158] R. Kappl, A. Reinert, and M. W. Winkler, "AMS-02 antiprotons reloaded," *Journal of Cosmology and Astroparticle Physics*, vol. 2015, no. 10, 2015.

[159] P. Blasi, "Origin of the positron excess in cosmic rays," *Physical Review Letters*, vol. 103, no. 5, 2009.

[160] P. Mertsch and S. Sarkar, "AMS-02 data confront acceleration of cosmic ray secondaries in nearby sources," *Physical Review D: Particles, Fields, Gravitation and Cosmology*, vol. 90, no. 6, 2014.

[161] J. Feng, N. Tomassetti, and A. Oliva, "Bayesian analysis of spatial-dependent cosmic-ray propagation: Astrophysical background of antiprotons and positrons," *Physical Review D: Particles, Fields, Gravitation and Cosmology*, vol. 94, no. 12, 2016.

[162] Y.-Q. Guo and Q. Yuan, "Understanding the spectral hardenings and radial distribution of Galactic cosmic rays and Fermi diffuse gamma-rays with spatially-dependent propagation," *Physical Review D: Particles, Fields, Gravitation and Cosmology*, vol. 97, no. 6, 2018.

[163] I. Cholis, D. Hooper, and T. Linden, "Possible evidence for the stochastic acceleration of secondary antiprotons by supernova remnants," *Physical Review D*, vol. 95, no. 12, 2017.

[164] S.-J. Lin, X.-J. Bi, P.-F. Yin, and Z.-H. Yu, "Implications for dark matter annihilation from the AMS-02 $\overline{p}/p$ ratio," *Physical Review D*, vol. D95, no. 6, 2017.

[165] X.-J. Huang, C.-C. Wei, Y.-L. Wu, W.-H. Zhang, and Y.-F. Zhou, "Antiprotons from dark matter annihilation through light mediators and a possible excess in AMS-02 $\overline{p}/p$ data," *Physical Review D*, vol. 95, no. 6, 2017.

[166] J. Feng and H.-H. Zhang, "Dark matter search in space: combined analysis of cosmic ray antiproton-to-proton flux ratio and positron flux measured by AMS-02," *The Astrophysical Journal*, vol. 858, no. 2, 2018.

[167] S.-J. Lin, X.-J. Bi, J. Feng, P.-F. Yin, and Z.-H. Yu, "Systematic study on the cosmic ray antiproton flux," *Physical Review D: Particles, Fields, Gravitation and Cosmology*, vol. 96, no. 12, 2017.

[168] A. Cuoco, M. Krämer, and M. Korsmeier, "Novel dark matter constraints from antiprotons in light of AMS-02," *Physical Review Letters*, vol. 118, no. 19, 2017.

[169] A. Cuoco, J. Heisig, M. Korsmeier, and M. Krämer, "Probing dark matter annihilation in the Galaxy with antiprotons and gamma rays," *Journal of Cosmology and Astroparticle Physics*, vol. 2017, no. 10, 2017.

[170] M.-Y. Cui, Q. Yuan, Y.-L. S. Tsai, and Y.-Z. Fan, "Possible dark matter annihilation signal in the AMS-02 antiproton data," *Physical Review Letters*, vol. 118, no. 19, 2017.

[171] F. Donato, N. Fornengo, and P. Salati, "Antideuterons as a signature of supersymmetric dark matter," *Physical Review D: Particles, Fields, Gravitation and Cosmology*, vol. 62, no. 4, 2000.

[172] H. Baer and S. Profumo, "Low energy antideuterons: shedding light on dark matter," *Journal of Cosmology and Astroparticle Physics*, vol. 2005, no. 12, 2005.

[173] R. Duperray, B. Baret, D. Maurin et al., "Flux of light antimatter nuclei near Earth, induced by cosmic rays in the Galaxy and in the atmosphere," *Physical Review D: Particles, Fields, Gravitation and Cosmology*, vol. 71, no. 8, 2005.

[174] F. Donato, N. Fornengo, and D. Maurin, "Antideuteron fluxes from dark matter annihilation in diffusion models," *Physical Review D: Particles, Fields, Gravitation and Cosmology*, vol. 78, no. 4, 2008.

[175] E. Carlson, A. Coogan, T. Linden, S. Profumo, A. Ibarra, and S. Wild, "Antihelium from dark matter," *Physical Review D: Particles, Fields, Gravitation and Cosmology*, vol. 89, no. 7, 2014.

[176] M. Cirelli, N. Fornengo, M. Taoso, and A. Vittino, "Anti-helium from dark matter annihilations," *Journal of High Energy Physics*, vol. 2014, no. 8, 2014.

[177] H. Fuke et al., "Search for cosmic-ray antideuterons," *Physical Review Letters*, vol. 95, no. 8, 2005.

[178] K. Abe et al., "Search for antihelium with the BESS-polar spectrometer," *Physical Review Letters*, vol. 108, no. 13, 2012.

[179] T. Aramaki et al., "Review of the theoretical and experimental status of dark matter identification with cosmic-ray antideuterons," *Physics Reports*, vol. 618, pp. 1–37, 2016.

[180] A. Coogan and S. Profumo, "Origin of the tentative AMS antihelium events," *Physical Review D: Particles, Fields, Gravitation and Cosmology*, vol. 96, no. 8, 2017.

[181] P. Chardonnet, J. Orloff, and P. Salati, "The production of antimatter in our galaxy," *Physics Letters B*, vol. 409, no. 1-4, pp. 313–320, 1997.

[182] J. Herms, A. Ibarra, A. Vittino, and S. Wild, "Antideuterons in cosmic rays: sources and discovery potential," *Journal of Cosmology and Astroparticle Physics*, vol. 2017, no. 02, 2017.

[183] N. Tomassetti and A. Oliva, "Production and acceleration of antinuclei in supernova shockwaves," *The Astrophysical Journal Letters*, vol. 844, no. 2, 2017.

[184] M. Korsmeier, F. Donato, and N. Fornengo, "Prospects to verify a possible dark matter hint in cosmic antiprotons with antideuterons and antihelium," *Physical Review D*, vol. 7, no. 10, 2017.

[185] P. Kiraly, J. Szabelski, J. Wdowczyk, and A. W. Wolfendale, "Antiprotons in the cosmic radiation," *Nature*, vol. 293, pp. 120–122, 1981.

[186] M. S. Turner, "Could primordial black holes be the source of the cosmic ray antiprotons?" *Nature*, vol. 297, pp. 379–381, 1982.

[187] Q. Yuan, L. Feng, P.-F. Yin et al., *Interpretations of the DAMPE electron data*, 2017, https://inspirehep.net/record/1639414.

[188] L. J. Gleeson and W. I. Axford, "Solar modulation of galactic cosmic rays," *The Astrophysical Journal*, vol. 154, p. 1011, 1968.

[189] N. Fornengo, L. Maccione, and A. Vittino, "Dark matter searches with cosmic antideuterons: status and perspectives," *Journal of Cosmology and Astroparticle Physics*, vol. 2013, no. 09, 2013.

[190] L. Maccione, "Low energy cosmic ray positron fraction explained by charge-sign dependent solar modulation," *Physical Review Letters*, vol. 110, no. 8, 2013.

[191] A. Vittino, C. Evoli, and D. Gaggero, "Cosmic-ray transport in the heliosphere with HelioProp," in *Proceedings of the 35th International Cosmic Ray Conference (ICRC 2017)*, Bexco, Busan, Korea, 2017.

[192] A. Schwarzschild and C. Zupancic, "Production of tritons, deuterons, nucleons, and mesons by 30-GeV protons on A1, Be, and Fe targets," *Physical Review*, vol. 129, no. 2, 1963.

[193] S.-J. Lin, X.-J. Bi, and P.-F. Yin, *Expectations of the cosmic antideuteron flux*, 2018, https://inspirehep.net/record/1645899.

[194] K. Blum, K. C. Y. Ng, R. Sato, and M. Takimoto, "Cosmic rays, antihelium, and an old navy spotlight," *Physical Review D: Particles, Fields, Gravitation and Cosmology*, vol. 96, no. 10, 2017.

[195] M. A. Lisa, S. Pratt, R. Soltz, and U. Wiedemann, "Femtoscopy in relativistic heavy ion collisions: two decades of progress," *Annual Review of Nuclear and Particle Science*, vol. 55, pp. 357–402, 2005.

[196] N. J. Shaviv, E. Nakar, and T. Piran, "Inhomogeneity in cosmic ray sources as the origin of the electron spectrum and the PAMELA anomaly," *Physical Review Letters*, vol. 103, no. 11, 2009.

[197] M. Aguilar et al., "Electron and positron fluxes in primary cosmic rays measured with the alpha magnetic spectrometer on the international space station," *Physical Review Letters*, vol. 113, no. 12, 2014.

[198] P. D. Serpico, "Possible causes of a rise with energy of the cosmic ray positron fraction," *Physical Review D*, vol. 79, no. 2, 2009.

[199] D. Grasso, S. Profumo, A. W. Strong et al., "On possible interpretations of the high energy electron-positron spectrum measured by the fermi large area telescope," *Astroparticle Physics*, vol. 32, no. 2, pp. 140–151, 2009.

[200] P. D. Serpico, "Astrophysical models for the origin of the positron "excess"," *Astroparticle Physics*, vol. 39-40, pp. 2–11, 2012.

[201] X.-G. He, "Dark matter annihilation explanation for $e^{\pm}$ excesses in cosmic ray," *Modern Physics Letters A*, vol. 24, no. 27, pp. 2139–2160, 2009.

[202] T. R. Slatyer, N. Padmanabhan, and D. P. Finkbeiner, "CMB constraints on WIMP annihilation: Energy absorption during the recombination epoch," *Physical Review D: Particles, Fields, Gravitation and Cosmology*, vol. 80, no. 4, 2009.

[203] S. Galli, F. Iocco, G. Bertone, and A. Melchiorri, "CMB constraints on dark matter models with large annihilation cross section," *Physical Review D: Particles, Fields, Gravitation and Cosmology*, vol. 80, no. 2, 2009.

[204] J. Buch, P. Ralegankar, and V. Rentala, "Late decaying 2-component dark matter scenario as an explanation of the AMS-02 positron excess," *Journal of Cosmology and Astroparticle Physics*, vol. 2017, no. 10, 2017.

[205] M. Ibe, H. Murayama, and T. T. Yanagida, "Breit-Wigner enhancement of dark matter annihilation," *Physical Review D: Particles, Fields, Gravitation and Cosmology*, vol. 79, no. 9, 2009.

[206] W.-L. Guo and Y.-L. Wu, "Enhancement of dark matter annihilation via Breit-Wigner resonance," *Physical Review D: Particles, Fields, Gravitation and Cosmology*, vol. 79, no. 5, 2009.

[207] Y. Bai, J. Berger, and S. Lu, "Supersymmetric resonant dark matter: a thermal model for the AMS-02 positron excess," *Physical Review D: Particles, Fields, Gravitation and Cosmology*, vol. 97, no. 11, 2018.

[208] Q.-F. Xiang, X.-J. Bi, S.-J. Lin, and P.-F. Yin, "A dark matter model that reconciles tensions between the cosmic-ray $e^{\pm}$ excess and the gamma-ray and CMB constraints," *Physics Letters B*, vol. 773, pp. 448–454, 2017.

[209] M. Ackermann et al., "Searches for cosmic-ray electron anisotropies with the fermi large area telescope," *Physical Review D: Particles, Fields, Gravitation and Cosmology*, vol. 82, no. 9, 2010.

[210] S. Abdollahi et al., "Search for cosmic-ray electron and positron anisotropies with seven years of fermi large area telescope data," *Physical Review Letters*, vol. 118, no. 9, 2017.

[211] G. Di Bernardo, C. Evoli, D. Gaggero, D. Grasso, L. Maccione, and M. N. Mazziotta, "Implications of the cosmic ray electron spectrum and anisotropy measured with Fermi-LAT," *Astroparticle Physics*, vol. 34, no. 7, pp. 528–538, 2011.

[212] J. C. Joshi and S. Razzaque, "A self-consistent model of cosmic-ray fluxes and positron excess: Roles of nearby pulsars and a sub-dominant source population," *Journal of Cosmology and Astroparticle Physics*, vol. 2017, no. 9, 2017.

[213] S. Manconi, M. Di Mauro, and F. Donato, "Dipole anisotropy in cosmic electrons and positrons: inspection on local sources," *Journal of Cosmology and Astroparticle Physics*, vol. 2017, no. 01, 2017.

[214] P. Mertsch, "Cosmic ray electrons and positrons from discrete stochastic sources," *Journal of Cosmology and Astroparticle Physics*, vol. 2011, no. 02, 2011.

[215] A. U. Abeysekara et al., "Extended gamma-ray sources around pulsars constrain the origin of the positron flux at Earth," *Science*, vol. 358, pp. 911–914, 2017.

[216] R. López-Coto and G. Giacinti, "Constraining the properties of the magnetic turbulence in the Geminga region using HAWC γ-ray data," *Monthly Notices of the Royal Astronomical Society*, vol. 479, pp. 4526–4534, 2018.

[217] P. Lipari, "Interpretation of the cosmic ray positron and antiproton fluxes," *Physical Review D*, vol. 95, no. 6, 2017.

[218] F. Aharonian et al., "Energy spectrum of cosmic-ray electrons at TeV energies," *Physical Review Letters*, vol. 101, no. 26, 2008.

[219] DAMPE Collaboration, "Direct detection of a break in the teraelectronvolt cosmic-ray spectrum of electrons and positrons," *Nature*, vol. 552, pp. 63–66, 2017.

[220] O. Adriani et al., "Energy spectrum of cosmic-ray electron and positron from 10 GeV to 3 TeV observed with the calorimetric electron telescope on the international space station," *Physical Review Letters*, vol. 119, no. 18, 2017.

[221] M. Ackermann et al., "Fermi-LAT observations of the diffuse gamma-ray emission: implications for cosmic rays and the interstellar medium," *The Astrophysical Journal*, vol. 750, no. 1, 2012.

[222] I. Cholis, M. Tavakoli, C. Evoli, L. Maccione, and P. Ullio, "Diffuse galactic gamma rays at intermediate and high latitudes. I. Constraints on the ISM properties," *Journal of Cosmology and Astroparticle Physics*, vol. 2012, no. 05, 2012.

[223] M. Pohl, P. Englmaier, and N. Bissantz, "Three-dimensional distribution of molecular gas in the barred milky way," *The Astrophysical Journal*, vol. 677, no. 1, 2008.

[224] M. Tavakoli, *Three dimensional distribution of atomic hydrogen in the milky way*, 2012, https://arxiv.org/abs/1207.6150.

[225] T. A. Porter, I. V. Moskalenko, and A. W. Strong, "Inverse compton emission from galactic supernova remnants: effect of the interstellar radiation field," *The Astrophysical Journal Letters*, vol. 648, no. 1, 2006.

[226] M. Tavakoli, I. Cholis, C. Evoli, and P. Ullio, "Constraints on dark matter annihilations from diffuse gamma-ray emission in the Galaxy," *Journal of Cosmology and Astroparticle Physics*, vol. 2014, no. 01, 2014.

[227] A. D. Erlykin and A. W. Wolfendale, "Cosmic rays in the inner galaxy and the diffusion properties of the interstellar medium," *Astroparticle Physics*, vol. 42, pp. 70–75, 2013.

[228] D. Gaggero, D. Grasso, A. Marinelli, A. Urbano, and M. Valli, "The gamma-ray and neutrino sky: a consistent picture of fermi-lat, milagro, and icecube results," *The Astrophysical Journal Letters*, vol. 815, no. 2, 2015.

[229] F. Acero et al., "Development of the model of galactic interstellar emission for standard point-source analysis of fermi large area telescope data," *The Astrophysical Journal Supplement Series*, vol. 223, no. 2, 2016.

[230] R. Yang, F. Aharonian, and C. Evoli, "Radial distribution of the diffuse γ-ray emissivity in the Galactic disk," *Physical Review D: Particles, Fields, Gravitation and Cosmology*, vol. 93, no. 12, 2016.

[231] E. Nezri, J. Lavalle, and R. Teyssier, "Indirect dark matter searches: Towards a consistent top-bottom approach for studying the gamma-ray signals and associated backgrounds," *Physical Review D: Particles, Fields, Gravitation and Cosmology*, vol. 86, no. 6, 2012.

[232] E. Charles et al., "Sensitivity projections for dark matter searches with the fermi large area telescope," *Physics Reports*, vol. 636, pp. 1–46, 2016.

[233] J. Conrad and O. Reimer, "Indirect dark matter searches in gamma- and cosmic rays," *Nature Physics*, vol. 13, pp. 224–231, 2017.

[234] V. Springel, S. D. M. White, C. S. Frenk et al., "Prospects for detecting supersymmetric dark matter in the Galactic halo," *Nature*, vol. 456, no. 4, pp. 73–76, 2008.

[235] M. Schaller et al., "Dark matter annihilation radiation in hydrodynamic simulations of Milky Way haloes," *Monthly Notices of the Royal Astronomical Society*, vol. 455, no. 4, pp. 4442–4451, 2016.

[236] M. Taoso, G. Bertone, and A. Masiero, "Dark matter candidates: a ten-point test," *Journal of Cosmology and Astroparticle Physics*, vol. 2008, no. 03, 2008.

[237] L. Bergstrom and P. Ullio, "Full one-loop calculation of neutralino annihilation into two photons," *Nuclear Physics B*, vol. 504, no. 1-2, pp. 27–44, 1997.

[238] P. Ullio and L. Bergström, "Neutralino annihilation into a photon and a Z boson," *Physical Review D: Particles, Fields, Gravitation and Cosmology*, vol. 57, no. 3, 1998.

[239] T. Bringmann, X. Huang, A. Ibarra, S. Vogl, and C. Weniger, "Fermi LAT search for internal bremsstrahlung signatures from dark matter annihilation," *Journal of Cosmology and Astroparticle Physics*, vol. 2012, no. 07, 2012.

[240] C. Weniger, "A tentative gamma-ray line from dark matter annihilation at the fermi large area telescope," *Journal of Cosmology and Astroparticle Physics*, vol. 2012, no. 8, 2012.

[241] D. P. Finkbeiner, M. Su, and C. Weniger, "Is the 130 GeV line real? A search for systematics in the Fermi-LAT data," *Journal of Cosmology and Astroparticle Physics*, vol. 2013, no. 01, 2013.

[242] C. Weniger, M. Su, D. P. Finkbeiner, T. Bringmann, and N. Mirabal, *Closing in on the fermi line with a new observation strategy*, 2013, https://arxiv.org/abs/1305.4710.

[243] M. Ackermann et al., "Updated search for spectral lines from galactic dark matter interactions with pass 8 data from the fermi large area telescope," *Physical Review D*, vol. 91, no. 12, 2015.

[244] H. Abdalla et al., "H.E.S.S. limits on line-like dark matter signatures in the 100 GeV to 2 TeV energy range close to the Galactic Centre," *Physical Review Letters*, vol. 117, no. 15, 2016.

[245] D. Gaggero, M. Taoso, A. Urbano, M. Valli, and P. Ullio, "Towards a realistic astrophysical interpretation of the gamma-ray Galactic center excess," *Journal of Cosmology and Astroparticle Physics*, vol. 2015, no. 12, 2015.

[246] V. Vitale, A. Morselli, and for the Fermi/LAT Collaboration, *Indirect search for dark matter from the center of the milky way with the fermi-large area telescope*, 2009, https://arxiv.org/abs/0912.3828.

[247] L. Goodenough and D. Hooper, *Possible evidence for dark matter annihilation in the inner milky way from the fermi gamma ray space telescope*, 2009, https://arxiv.org/abs/0910.2998.

[248] D. Hooper and L. Goodenough, "Dark matter annihilation in the galactic center as seen by the fermi gamma ray space telescope," *Physics Letters B*, vol. 697, no. 5, pp. 412–428, 2011.

[249] A. Boyarsky, D. Malyshev, and O. Ruchayskiy, "A comment on the emission from the Galactic Center as seen by the Fermi telescope," *Physics Letters B*, vol. 705, no. 3, pp. 165–169, 2011.

[250] D. Hooper and T. Linden, "On the origin of the gamma rays from the galactic center," *Physical Review D*, vol. 84, no. 12, 2011.

[251] K. N. Abazajian and M. Kaplinghat, "Detection of a gamma-ray source in the galactic center consistent with extended emission from dark matter annihilation and concentrated astrophysical emission," *Physical Review D*, vol. 86, no. 8, 2012, Erratum: vol. 87, no. 12, 2013.

[252] D. Hooper and T. R. Slatyer, "Two emission mechanisms in the fermi bubbles: a possible signal of annihilating dark matter," *Physics of the Dark Universe*, vol. 2, no. 3, pp. 118–138, 2013.

[253] C. Gordon and O. Macías, "Dark matter and pulsar model constraints from Galactic Center Fermi-LAT gamma-ray observations," *Physical Review D: Particles, Fields, Gravitation and Cosmology*, vol. 88, no. 8, 2013, Erratum: vol. 89, no. 4, 2014.

[254] W.-C. Huang, A. Urbano, and W. Xue, *Fermi bubbles under dark matter scrutiny. Part I: astrophysical analysis*, 2013, https://arxiv.org/abs/1307.6862.

[255] O. Macias and C. Gordon, "Contribution of cosmic rays interacting with molecular clouds to the galactic center gamma-ray excess," *Physical Review D*, vol. 89, no. 6, 2014.

[256] K. N. Abazajian, N. Canac, S. Horiuchi, and M. Kaplinghat, "Astrophysical and dark matter interpretations of extended gamma-ray emission from the Galactic Center," *Physical Review D: Particles, Fields, Gravitation and Cosmology*, vol. 90, no. 2, 2014.

[257] T. Daylan, D. P. Finkbeiner, D. Hooper et al., "The characterization of the gamma-ray signal from the central Milky Way: A case for annihilating dark matter," *Physics of the Dark Universe*, vol. 12, pp. 1–23, 2016.

[258] B. Zhou, Y.-F. Liang, X. Huang et al., "GeV excess in the Milky Way: The role of diffuse galactic gamma-ray emission templates," *Physical Review D: Particles, Fields, Gravitation and Cosmology*, vol. 91, no. 12, 2015.

[259] F. Calore, I. Cholis, and C. Weniger, "Background model systematics for the Fermi GeV excess," *Journal of Cosmology and Astroparticle Physics*, vol. 2015, no. 03, 2015.

[260] E. Carlson, S. Profumo, and T. Linden, "Cosmic-ray injection from star-forming regions," *Physical Review Letters*, vol. 117, no. 11, 2016.

[261] S. Horiuchi, M. Kaplinghat, and A. Kwa, "Investigating the uniformity of the excess gamma rays towards the galactic center region," *Journal of Cosmology and Astroparticle Physics*, vol. 2016, no. 11, 2016.

[262] M. Ackermann et al., "The fermi galactic center gev excess and implications for dark matter," *The Astrophysical Journal*, vol. 840, no. 1, 2017.

[263] W. de Boer, L. Bosse, I. Gebauer, A. Neumann, and P. L. Biermann, "Molecular clouds as origin of the Fermi gamma-ray GeV excess," *Physical Review D: Particles, Fields, Gravitation and Cosmology*, vol. 96, no. 4, 2017.

[264] M. Su, T. R. Slatyer, and D. P. Finkbeiner, "Giant gamma-ray bubbles from fermi-LAT: Active galactic nucleus activity or bipolar galactic wind?" *The Astrophysical Journal*, vol. 724, no. 2, 2010.

[265] W.-C. Huang, A. Urbano, and W. Xue, "Fermi bubbles under dark matter scrutiny part II: Particle physics analysis," *Journal of Cosmology and Astroparticle Physics*, vol. 2014, no. 04, 2014.

[266] A. Alves, S. Profumo, F. S. Queiroz, and W. Shepherd, "Effective field theory approach to the Galactic Center gamma-ray excess," *Physical Review D: Particles, Fields, Gravitation and Cosmology*, vol. 90, no. 11, 2014.

[267] A. Berlin, D. Hooper, and S. D. McDermott, "Simplified dark matter models for the Galactic Center gamma-ray excess," *Physical Review D: Particles, Fields, Gravitation and Cosmology*, vol. 89, no. 11, 2014.

[268] M. Abdullah, A. DiFranzo, A. Rajaraman, T. M. Tait, P. Tanedo, and A. M. Wijangco, "Hidden on-shell mediators for the galactic center γ-ray excess," *Physical Review D: Particles, Fields, Gravitation and Cosmology*, vol. 90, no. 3, 2014.

[269] P. Agrawal, B. Batell, P. J. Fox, and R. Harnik, "WIMPs at the galactic center," *Journal of Cosmology and Astroparticle Physics*, vol. 2015, no. 05, 2015.

[270] F. Calore, I. Cholis, C. McCabe, and C. Weniger, "A tale of tails: Dark matter interpretations of the Fermi GeV excess in light of background model systematics," *Physical Review D: Particles, Fields, Gravitation and Cosmology*, vol. 91, no. 6, 2015.

[271] M. Kaplinghat, T. Linden, and H.-B. Yu, "Galactic center excess in gamma rays from annihilation of self-interacting dark matter," *Physical Review Letters*, vol. 114, no. 21, 2015.

[272] C. Karwin, S. Murgia, T. M. P. Tait, T. A. Porter, and P. Tanedo, "Dark matter interpretation of the Fermi-LAT observation toward the galactic center," *Physical Review D: Particles, Fields, Gravitation and Cosmology*, vol. 95, no. 10, 2017.

[273] J. Petrović, P. D. Serpico, and G. Zaharijas, "Millisecond pulsars and the Galactic Center gamma-ray excess: the importance of luminosity function and secondary emission," *Journal of Cosmology and Astroparticle Physics*, vol. 2015, no. 02, 2015.

[274] K. N. Abazajian, "The Consistency of Fermi-LAT observations of the galactic center with a millisecond pulsar population in the central stellar cluster," *Journal of Cosmology and Astroparticle Physics*, vol. 2011, no. 3, 2011.

[275] Q. Yuan and B. Zhang, "Millisecond pulsar interpretation of the Galactic center gamma-ray excess," *Journal of High Energy Astrophysics*, vol. 3-4, pp. 1–8, 2014.

[276] D. Hooper, I. Cholis, T. Linden, J. M. Siegal-Gaskins, and T. R. Slatyer, "Millisecond pulsars cannot account for the inner Galaxy's GeV excess," *Physical Review D: Particles, Fields, Gravitation and Cosmology*, vol. 88, no. 8, 2013.

[277] I. Cholis, D. Hooper, and T. Linden, "Challenges in explaining the Galactic Center gamma-ray excess with millisecond pulsars," *Journal of Cosmology and Astroparticle Physics*, vol. 2015, no. 06, 2015.

[278] E. Carlson and S. Profumo, "Cosmic ray protons in the inner galaxy and the galactic center gamma-ray excess," *Physical Review D*, vol. 90, no. 2, 2014.

[279] J. Petrovi, P. D. Serpico, and G. Zaharija, "Galactic Center gamma-ray "excess" from an active past of the galactic centre?" *Journal of Cosmology and Astroparticle Physics*, vol. 2014, no. 10, 2014.

[280] I. Cholis, C. Evoli, F. Calore, T. Linden, C. Weniger, and D. Hooper, "The galactic center GeV excess from a series of leptonic cosmic-ray outbursts," *Journal of Cosmology and Astroparticle Physics*, vol. 2015, no. 12, 2015.

[281] M. Selig, V. Vacca, N. Oppermann, and T. A. Enßlin, "The denoised, deconvolved, and decomposed fermi γ-ray sky - An application of the D^3PO algorithm," *Astronomy and Astrophysics*, vol. 581, 2015.

[282] D. F. Figer, R. M. Rich, S. S. Kim, M. Morris, and E. Serabyn, "An Extended Star Formation History for the Galactic Center from hubble space telescope NICMOS observations," *The Astrophysical Journal*, vol. 601, no. 1, 2004.

[283] R. M. Crocker, D. I. Jones, F. Aharonian et al., "Wild at heart: the particle astrophysics of the galactic centre," *Monthly Notices of the Royal Astronomical Society*, vol. 413, no. 2, pp. 763–788, 2011.

[284] K. Ferriere, W. Gillard, and P. Jean, "Spatial distribution of interstellar gas in the innermost 3 kpc of our galaxy," *Astronomy and Astrophysics*, vol. 467, pp. 611–627, 2007.

[285] D. F. Figer et al., "Massive stars in the arches cluster," *The Astrophysical Journal*, vol. 581, no. 1, 2002.

[286] T. Montmerle, "On gamma-ray sources, supernova remnants, OB associations, and the origin of cosmic rays," *Astrophysical Journal*, vol. 231, pp. 95–110, 1979.

[287] E. Carlson, T. Linden, and S. Profumo, "Improved cosmic-ray injection models and the Galactic Center gamma-ray excess," *Physical Review D: Particles, Fields, Gravitation and Cosmology*, vol. 94, no. 6, 2016.

[288] M. Schmidt, "The rate of star formation," *Astrophysical Journal*, vol. 129, p. 243, 1959.

[289] M. Ajello et al., "Fermi-LAT observations of high-energy γ-ray emission toward the galactic center," *The Astrophysical Journal*, vol. 819, no. 1, 2016.

[290] R. Bartels, S. Krishnamurthy, and C. Weniger, "Strong support for the millisecond pulsar origin of the galactic center GeV excess," *Physical Review Letters*, vol. 116, no. 5, 2016.

[291] S. K. Lee, M. Lisanti, B. R. Safdi, T. R. Slatyer, and W. Xue, "Evidence for unresolved γ-ray point sources in the inner galaxy," *Physical Review Letters*, vol. 116, no. 5, 2016.

[292] D. Hooper and G. Mohlabeng, "The gamma-ray luminosity function of millisecond pulsars and implications for the GeV excess," *Journal of Cosmology and Astroparticle Physics*, vol. 2016, no. 03, 2016.

[293] H. Ploeg, C. Gordon, R. Crocker, and O. Macias, "Consistency between the luminosity function of resolved millisecond pulsars and the galactic center excess," *Journal of Cosmology and Astroparticle Physics*, vol. 2017, no. 08, 2017.

[294] M. Ajello et al., *Characterizing the population of pulsars in the inner Galaxy with the Fermi Large Area Telescope*, 2017, https://arxiv.org/abs/1711.04778.

[295] E. Storm, C. Weniger, and F. Calore, "SkyFACT: high-dimensional modeling of gamma-ray emission with adaptive templates and penalized likelihoods," *Journal of Cosmology and Astroparticle Physics*, vol. 2017, no. 08, 2017.

[296] R. Bartels, E. Storm, C. Weniger, and F. Calore, *The Fermi-LAT GeV excess traces stellar mass in the galactic bulge*, 2017, https://arxiv.org/abs/1705.00009.

[297] F. Calore, M. Di Mauro, F. Donato, J. W. Hessels, and C. Weniger, "Radio detection prospects for a bulge population of millisecond pulsars as suggested by Fermi-LAT observations of the inner galaxy," *The Astrophysical Journal*, vol. 827, no. 2, 2016.

[298] M. Ackermann et al., "Observations of M31 and M33 with the fermi large area telescope: a galactic center excess in andromeda?" *The Astrophysical Journal*, vol. 836, no. 2, 2017.

[299] C. Eckner, X. Hou, P. D. Serpico et al., "Millisecond pulsar origin of the Galactic center excess and extended gamma-ray emission from Andromeda - a closer look," *The Astrophysical Journal*, vol. 862, no. 1, 79 pages, 2018.

[300] G. Lake, "Detectability of γ-rays from clumps of dark matter," *Nature*, vol. 346, pp. 39-40, 1990.

[301] N. W. Evans, F. Ferrer, and S. Sarkar, "A travel guide to the dark matter annihilation signal," *Physical Review D: Particles, Fields, Gravitation and Cosmology*, vol. 69, no. 12, 2004.

[302] L. E. Strigari, S. M. Koushiappas, J. S. Bullock, and M. Kaplinghat, "Precise constraints on the dark matter content of Milky Way dwarf galaxies for gamma-ray experiments," *Physical Review D: Particles, Fields, Gravitation and Cosmology*, vol. 75, no. 8, 2007.

[303] L. E Strigari, S. M. Koushiappas, J. S. Bullock et al., "The most dark-matter-dominated galaxies: predicted gamma-ray signals from the faintest milky way dwarfs," *The Astrophysical Journal*, vol. 678, no. 2, 2008.

[304] M. Ackermann et al., "Constraining dark matter models from a combined analysis of milky way satellites with the fermi large area telescope," *Physical Review Letters*, vol. 107, no. 24, 2011.

[305] M. Ackermann et al., "Searching for dark matter annihilation from milky way dwarf spheroidal galaxies with six years of fermi large area telescope data," *Physical Review Letters*, vol. 115, no. 23, 2015.

[306] M. L. Ahnen et al., "Limits to dark matter annihilation cross-section from a combined analysis of MAGIC and Fermi-LAT observations of dwarf satellite galaxies," *Journal of Cosmology and Astroparticle Physics*, vol. 2016, no. 02, 2016.

[307] A. Albert et al., "Searching for dark matter annihilation in recently discovered milky way satellites with Fermi-LAT," *The Astrophysical Journal*, vol. 834, no. 2, 2017.

[308] S. Archambault et al., "Dark matter constraints from a joint analysis of dwarf spheroidal galaxy observations with VERITAS," *Physical Review D: Particles, Fields, Gravitation and Cosmology*, vol. 95, no. 8, 2017.

[309] K. N. Abazajian and R. E. Keeley, "Bright gamma-ray Galactic Center excess and dark dwarfs: Strong tension for dark matter annihilation despite Milky Way halo profile and diffuse emission uncertainties," *Physical Review D*, vol. 93, no. 8, 2016.

[310] R. Keeley, K. Abazajian, A. Kwa, N. Rodd, and B. Safdi, "What the Milky Way's Dwarfs tell us about the Galactic Center extended gamma-ray excess," *Physical Review D*, vol. 97, no. 10, 2018.

[311] V. Bonnivard, C. Combet, D. Maurin, and M. G. Walker, "Spherical Jeans analysis for dark matter indirect detection in dwarf spheroidal galaxies - impact of physical parameters and

triaxiality," *Monthly Notices of the Royal Astronomical Society*, vol. 446, no. 3, pp. 3002–3021, 2015.

[312] P. Ullio and M. Valli, "A critical reassessment of particle Dark Matter limits from dwarf satellites," *Journal of Cosmology and Astroparticle Physics*, vol. 2016, no. 07, 2016.

[313] K. Hayashi, K. Ichikawa, S. Matsumoto, M. Ibe, M. N. Ishigaki, and H. Sugai, "Dark matter annihilation and decay from non-spherical dark halos in galactic dwarf satellites," *Monthly Notices of the Royal Astronomical Society*, vol. 461, no. 3, pp. 2914–2928, 2016.

[314] K. Ichikawa, M. N. Ishigaki, S. Matsumoto et al., "Foreground effect on the J-factor estimation of classical dwarf spheroidal galaxies," *Monthly Notices of the Royal Astronomical Society*, vol. 468, no. 3, pp. 2884–2896, 2017.

[315] A. Geringer-Sameth, M. G. Walker, S. M. Koushiappas et al., "Indication of gamma-ray emission from the newly discovered dwarf galaxy reticulum II," *Physical Review Letters*, vol. 115, no. 8, 2015.

[316] D. Hooper and T. Linden, "On the gamma-ray emission from reticulum II and other dwarf galaxies," *Journal of Cosmology and Astroparticle Physics*, vol. 2015, no. 09, 2015.

[317] V. Bonnivard, C. Combet, D. Maurin et al., "Dark matter annihilation and decay profiles for the reticulum ii dwarf spheroidal galaxy," *The Astrophysical Journal Letters*, vol. 808, no. 2, 2015.

[318] M. Regis, L. Richter, and S. Colafrancesco, "Dark matter in the Reticulum II dSph: a radio search," *Journal of Cosmology and Astroparticle Physics*, vol. 2017, no. 07, 2017.

[319] S. Colafrancesco, S. Profumo, and P. Ullio, "Detecting dark matter WIMPs in the Draco dwarf: A multiwavelength perspective," *Physical Review D: Particles, Fields, Gravitation and Cosmology*, vol. 75, no. 2, 2007.

[320] S. Profumo and P. Ullio, *Multi-wavelength searches for particle dark matter*, 2010, https://arxiv.org/abs/1001.4086.

[321] M. Regis, S. Colafrancesco, S. Profumo, W. J. G. de Blok, M. Massardi, and L. Richter, "Local Group dSph radio survey with ATCA (III): constraints on particle dark matter," *Journal of Cosmology and Astroparticle Physics*, vol. 2014, no. 10, 2014.

[322] A. De Angelis, V. Tatischeff, I. A. Grenier et al., *Science with e-ASTROGAM (A space mission for MeV-GeV gamma-ray astrophysics)*, 2017, https://arxiv.org/abs/1711.01265.

[323] A. A. Moiseev et al., *Compton-pair production space telescope (ComPair) for MeV gamma-ray astronomy*, 2015, https://arxiv.org/abs/1508.07349.

[324] S. D. Hunter et al., "A Pair Production Telescope for Medium-Energy Gamma-Ray Polarimetry," *Astroparticle Physics*, vol. 59, pp. 18–28, 2014.

[325] R. Essig, E. Kuflik, S. D. McDermott, T. Volansky, and K. M. Zurek, "Constraining light dark matter with diffuse X-ray and gamma-ray observations," *Journal of High Energy Physics*, vol. 2013, no. 11, 2013.

[326] K. K. Boddy and J. Kumar, "Indirect detection of dark matter using mev-range gamma-ray telescopes," *Physical Review D*, vol. 92, no. 2, 2015.

[327] A. W. Strong, H. Bloemen, R. Diehl, W. Hermsen, and V. Schoenfelder, "COMPTEL skymapping: a new approach using parallel computing," *Astrophysical Letters and Communications*, vol. 39, p. 209, 1999.

[328] S. D. Hunter et al., "EGRET observations of the diffuse gamma-ray emission from the galactic plane," *The Astrophysical Journal*, vol. 481, no. 1, 1997.

[329] R. Bartels, D. Gaggero, and C. Weniger, "Prospects for indirect dark matter searches with MeV photons," *Journal of Cosmology and Astroparticle Physics*, vol. 2017, no. 05, 2017.

[330] C. Bœhm and Y. Ascasibar, "More evidence in favor of light dark matter particles?" *Physical Review D: Particles, Fields, Gravitation and Cosmology*, vol. 70, no. 11, 2004.

[331] C. Boehm, D. Hooper, J. Silk, M. Casse, and J. Paul, "MeV Dark Matter: Has It Been Detected?" *Physical Review Letters*, vol. 92, no. 10, 2004.

[332] E. Lorenz and The MAGIC Collaboration, "Status of the 17 m ⌀ MAGIC telescope," *New Astronomy Reviews*, vol. 48, no. 5-6, pp. 339–344, 2004.

[333] A. U. Abeysekara, R. Alfaro, C. Alvarez et al., "The sensitivity of HAWC to high-mass dark matter annihilations," *Physical Review D*, vol. 90, no. 12, 2014.

[334] A. Abramowski, F. Acero, F. Aharonian et al., "Search for a dark matter annihilation signal from the galactic center halo with H.E.S.S," *Physical Review Letters*, vol. 106, no. 16, 2011.

[335] M. Doro, J. Conrad, D. Emmanoulopoulos et al., "Dark matter and fundamental physics with the cherenkov telescope array," *Astroparticle Physics*, vol. 43, pp. 189–214, 2013.

[336] H. Silverwood, C. Weniger, P. Scott, and G. Bertone, "A realistic assessment of the CTA sensitivity to dark matter annihilation," *Journal of Cosmology and Astroparticle Physics*, vol. 2015, no. 03, 2015.

[337] J. Conrad, "CTA in the Context of Searches for Particle Dark Matter - a glimpse," in *Proceedings of the 6th International Symposium on High Energy Gamma-Ray Astronomy*, vol. 1792 of *American Institute of Physics Conference Series*, 2017.

[338] A. Morselli, *The dark matter programme of the cherenkov telescope array*, 2017, https://arxiv.org/abs/1709.01483.

[339] F. Aharonian, A. G. Akhperjanian, A. R. Bazer-Bachi et al., "Discovery of very-high-energy gamma-rays from the galactic centre ridge," *Nature*, vol. 439, pp. 695–698, 2006.

[340] H.E.S.S. Collaboration, "Acceleration of petaelectronvolt protons in the galactic centre," *Nature*, vol. 531, pp. 476–479, 2016.

[341] H.E.S.S. Collaboration, "Characterising the VHE diffuse emission in the central 200 parsecs of our Galaxy with H.E.S.S," *Astronomy and Astrophysics*, vol. 612, 2018.

[342] M. Hatten, C. Combet, G. Maier, and D. Maurin, "Dark matter substructure modelling and sensitivity of the cherenkov telescope array to galactic dark halos," *Journal of Cosmology and Astroparticle Physics*, vol. 2016, no. 09, 2016.

[343] V. Lefranc, G. A. Mamon, and P. Panci, "Prospects for annihilating Dark Matter towards Milky Way's dwarf galaxies by the Cherenkov Telescope Array," *Journal of Cosmology and Astroparticle Physics*, vol. 2016, no. 09, 2016.

[344] V. Lefranc, E. Moulin, P. Panci, F. Sala, and J. Silk, "Dark Matter in γ lines: Galactic Center vs. dwarf galaxies," *Journal of Cosmology and Astroparticle Physics*, vol. 2016, no. 09, 2016.

[345] J. Chang, G. Ambrosi, Q. An et al., "The dark matter particle explorer mission," *Astroparticle Physics*, vol. 95, pp. 6–24, 2017.

[346] P. S. Marrocchesi, "CALET: a high energy astroparticle physics experiment on the ISS," in *Proceedings of the MG14 Meeting on General Relativity*, 2015.

[347] E. S. Seo, T. Anderson, D. Angelaszek et al., "Cosmic ray energetics and mass for the international space station (ISS-CREAM)," *Advances in Space Research*, vol. 53, no. 10, pp. 1451–1455, 2014.

[348] R. A. Ong, T. Aramaki, R. Bird et al., *The GAPS experiment to search for dark matter using low-energy antimatter*, 2017, https://arxiv.org/abs/1710.00452.

[349] V. S. Ptuskin, I. V. Moskalenko, F. C. Jones, A. W. Strong, and V. N. Zirakashvili, "Dissipation of magnetohydrodynamic waves on energetic particles: Impact on interstellar turbulence and cosmic-ray transport," *The Astrophysical Journal*, vol. 642, no. 2, pp. 902–916, 2006.

[350] R. P. Duperray, C.-Y. Huang, K. V. Protasov, and M. Buénerd, "Parameterization of the antiproton inclusive production cross section on nuclei," *Physical Review D*, vol. 68, no. 9, 2003.

[351] M. di Mauro, F. Donato, A. Goudelis, and P. D. Serpico, "New evaluation of the antiproton production cross section for cosmic ray studies," *Physical Review D: Particles, Fields, Gravitation and Cosmology*, vol. 90, no. 8, 2014.

[352] R. Kappl and M. W. Winkler, "The cosmic ray antiproton background for AMS-02," *Journal of Cosmology and Astroparticle Physics*, vol. 2014, no. 9, 2014.

[353] M. W. Winkler, "Cosmic ray antiprotons at high energies," *Journal of Cosmology and Astroparticle Physics*, vol. 2017, no. 2, 2017.

[354] T. Pierog, I. Karpenko, J. M. Katzy, E. Yatsenko, and K. Werner, "EPOS LHC: Test of collective hadronization with data measured at the CERN Large Hadron Collider," *Physical Review C: Nuclear Physics*, vol. 92, no. 3, 2015.

[355] R. Engel, T. K. Gaisser, T. Stanev, and P. Lipari, "Air shower calculations with the new version of SIBYLL," in *Proceedings of the 26th International Cosmic Ray Conference: Invited, Rapporteur, and Highlight Papers*, vol. 1, pp. 415–418, Salt Lake City, Utah, UT, USA, August 17-25, 1999.

[356] S. Ostapchenko, "Monte Carlo treatment of hadronic interactions in enhanced Pomeron scheme: QGSJET-II model," *Physical Review D: Particles, Fields, Gravitation, and Cosmology*, vol. 83, no. 1, 2011.

Hindawi
Advances in High Energy Physics
Volume 2018, Article ID 4078657, 21 pages
https://doi.org/10.1155/2018/4078657

Research Article

Neutrino Mass, Coupling Unification, Verifiable Proton Decay, Vacuum Stability, and WIMP Dark Matter in SU(5)

Biswonath Sahoo, Mainak Chakraborty, and M. K. Parida

Centre of Excellence in Theoretical and Mathematical Sciences, Siksha 'O'Anusandhan (Deemed to be University), Khandagiri Square, Bhubaneswar 751030, Odisha, India

Correspondence should be addressed to M. K. Parida; minaparida@soa.ac.in

Received 5 April 2018; Accepted 24 May 2018; Published 6 August 2018

Academic Editor: Farinaldo Queiroz

Nonsupersymmetric minimal SU(5) with Higgs representations 24_H and 5_H and standard fermions in $\bar{5}_F \oplus 10_F$ is well known for its failure in unification of gauge couplings and lack of predicting neutrino masses. Like standard model, it is also affected by the instability of the Higgs scalar potential. We note that extending the Higgs sector by 75_H and 15_H not only leads to the popular type-II seesaw ansatz for neutrino masses with a lower bound on the triplet mass $M_\Delta > 2\times10^9$ GeV, but also achieves precision unification of gauge couplings without proliferation of nonstandard light Higgs scalars or fermions near the TeV scale. Consistent with recent LUX-2016 lower bound, the model easily accommodates a singlet scalar WIMP dark matter near the TeV scale which resolves the vacuum stability issue even after inclusion of heavy triplet threshold effect. We estimate proton lifetime predictions for $p \longrightarrow e^+\pi^0$ including uncertainties due to input parameters and threshold effects due to superheavy Higgs scalars and superheavy $X^{\pm4/3}, Y^{\pm1/3}$ gauge bosons. The predicted lifetime is noted to be verifiable at Super Kamiokande and Hyper Kamiokande experiments.

1. Introduction

Standard model (SM) of strong and electroweak interactions has been established by numerous experimental tests, yet evidences on neutrino mass [1–5], the phenomena of dark matter [6–25] , and baryon asymmetry of the universe (BAU) [8, 26–29] call for beyond standard model (BSM) physics. It is well known that grand unified theories (GUTs) [30–37] are capable of addressing a number of limitations of the SM effectively. There are interesting theories on neutrino mass generation mechanisms [38–45] based upon various seesaw mechanisms such as type-I, type-II, type-III [46–62], linear [63, 64], and inverse [65–75]. Interesting models for Dirac neutrino mass origin of the neutrino oscillation data have been also proposed [76, 77]. In the absence of experimental evidence of supersymmetry so far, nonsupersymmetric (non-SUSY) GUTs are being extensively exploited by reconciling to the underlying gauge hierarchy problem through fine-tuning [78, 79]. Higher rank GUTs like SO(10) and E_6 can not define a unique symmetry breaking path to the SM gauge theory because of large number of possibilities with one and more intermediate symmetry breakings consistent with electroweak precision data on $\sin^2\theta_W(M_Z)$, $\alpha_S(M_Z)$, and $\alpha(M_Z)$ [80–82]. On the other hand, the rank-4 minimal SU(5) [32] with Higgs representations 5_H and 24_H defines only one unique symmetry breaking path to the standard model

$$SU(5) \longrightarrow SM. \tag{1}$$

Type-I seesaw [46–52] needs nonstandard heavy right-handed neutrino, linear and inverse seesaw both need non-standard fermions and scalars, and type-III seesaw [38–45, 58–62] needs only nonstandard fermionic extension for their implementation. Out of these popular seesaw mechanisms, type-II seesaw mechanism is the one which needs a heavy nonstandard triplet scalar [52–57, 59]. With a second triplet scalar, it is also capable of predicting baryon asymmetry of the universe [57] which is one of the main motivations behind this investigation. This neutrino mass generation mechanism, gauge coupling unification, dark matter, and vacuum stability are the focus of the present work.

Like the minimal SM, with its 15 fermions per generation and the standard Higgs doublet $\phi(2, 1/2, 1)$, the minimal SU(5) with Higgs representations 5_H and 24_H predicts neutrinos to be massless subject to a tiny $\mathcal{O}(10^{-5})$ eV contribution due to nonrenormalizable Planck scale effect which is nearly 4 orders smaller than the requirement of neutrino oscillation data. As the particle spectrum below the GUT symmetry breaking scale is identically equal to the SM spectrum, like SM, the minimal GUT fails to unify gauge couplings [83–87]. Also it predicts instability of the Higgs quartic coupling at mass scales $\mu \geq 5 \times 10^9$ GeV [88–90] after which the coupling continues to be increasingly negative at least up to the unification scale.

A number of interesting models have been suggested for coupling unification by populating the grand desert and for enhancing proton lifetime predictions [60–62, 91–98]. In these models a number of fermion or scalar masses below the GUT scale have been utilised to achieve unification. Interesting possibility of type-III seesaw [60–62] with experimentally verifiable dilepton production [99] at LHC has been also investigated.

The other shortcoming of minimal non-SUSY SU(5) is its inability to predict dark matter which appears to belong to two distinct categories: (i) the weakly interacting massive particle (WIMP) dark matter of bounded mass < 100 TeV and (ii) the decaying dark matter which has been suggested to be a possible source of PeV energy IceCube neutrinos.

In this work we implement a novel mechanism for coupling unification and neutrino masses together. When SU(5) is extended by the addition of its Higgs representations 75_H and 15_H, it achieves two objectives: (i) neutrino mass and mixing generation through type-II seesaw mechanism and (ii) precision gauge coupling unification with experimentally accessible proton lifetime.

But this does not cure the vacuum instability problem persisting in the model as well as the need for WIMP dark matter prediction. Out of these two, as we note in this work, when the dark matter prediction is successfully inducted into the model, the other problem on vacuum stability is automatically resolved.

In contrast to the popular belief on low proton lifetime prediction of the minimal SU(5) [35], we estimate new precise and enhanced predictions of this model including threshold effects [100–108] of heavy particles near the GUT scale. Predicted lifetimes are found to be within the accessible ranges of Superkamiokande and Hyperkamiokande experimental search programmes [109].

This paper is organised in the following manner. In Section 2 we discuss neutrino mass generation mechanism in extended SU(5). Section 3 deals with the problem of gauge coupling unification. In Section 4 we make proton lifetime prediction including possible uncertainties. Embedding WIMP scalar DM in SU(5) is discussed in Section 5 with a brief outline on the current experimental status. Resolution of vacuum stability issue is explained in Section 6. We summarise and conclude in Section 7. Renormalization group equations for gauge and Higgs quartic couplings are discussed in the Appendix.

2. Neutrino Mass Through Type-II Seesaw in SU(5)

As noted in Section 1, in contrast to many possible alternative symmetry breaking paths to SM from non-SUSY SO(10) and E_6 [80–82], SU(5) predicts only one symmetry breaking path which enhances its verifiable predictive capability. Fifteen SM fermions are placed in two different SU(5) representations:

$$\overline{5}_F = \begin{pmatrix} d_1^C \\ d_2^C \\ d_3^C \\ e^- \\ -\nu_e \end{pmatrix}_L, \qquad 10_F = \begin{pmatrix} 0 & u_2^C & -u_3^C & u_1 & d_1 \\ -u_2^C & 0 & u_1^C & u_2 & d_2 \\ u_3^C & -u_1^C & 0 & u_3 & d_3 \\ -u_1 & -u_2 & -u_3 & 0 & e^C \\ -d_1 & -d_2 & -d_3 & -e^C & 0 \end{pmatrix}_L. \tag{2}$$

Lack of RHν in these representations gives vanishing Dirac neutrino mass and vanishing Majorana neutrino mass at renormalizable level. Planck scale induced small Majorana masses can be generated through nonrenormalizable dim.5 interaction

$$-\mathscr{L}_{NR} = \frac{\kappa_{ij}}{M_{\text{Planck}}} \overline{5}_{F_i} \overline{5}_{F_j} 5_H 5_H + h.c, \tag{3}$$

leading to $m_\nu \sim 10^{-5}$ eV which is too low to explain neutrino oscillation data. Mechanism of Dirac neutrino mass generation has been discussed [76, 77] matching the neutrino oscillation data. Using extensions of the minimal GUT type-III seesaw origin of neutrino mass has been discussed where the nonstandard fermionic triplet $\Sigma_F(3, 0, 1)$ mediates the seesaw. This model can be experimentally tested by the production of like-sign dilepton signals at LHC.

Type-II seesaw mechanism for neutrino mass [53–57] does not need any nonstandard fermion but needs only the nonstandard left-handed Higgs scalar triplet $\Delta_L(3, -1, 1)$ with $Y = -2$ which directly couples with the a dilepton pair. It also directly couples to standard Higgs doublet ϕ. As such the standard Higgs VEV can be transmitted as a small induced VEV generating Majorana mass term for the light neutrinos. As this $\Delta_L(3, -1, 1)$ is contained in the symmetric SU(5) scalar representation 15_H, the scalar sector of the minimal GUT needs to include 15_H in addition to 5_H and 24_H.

The Yukawa Lagrangian

$$-\mathscr{L}^{(II)} = l_{L_i}^T C i\tau_2 Y_{ij} \left(\frac{\vec{\tau}.\vec{\Delta_L}}{\sqrt{2}} \right)^\dagger l_{L_j} + h.c, \tag{4}$$

combined with the relevant part of the Higgs potential

$$\mathscr{V}_{II} = M_\Delta^2 Tr\left[\Delta_L^\dagger \Delta_L\right] + \mu_\Delta \tilde{\phi}^\dagger \left(\frac{\vec{\tau}.\vec{\Delta_L}}{\sqrt{2}} \right) \phi + h.c. \tag{5}$$

gives rise to the type-II seesaw contribution. In our notation $l_{L_i}^T = (\nu_{L_i}, e_{L_i})$ (i = generation index) and $\phi^T = (\phi^+, \phi^0)$ which are the lepton and scalar doublet of $SU(2)_L$. Here $\widetilde{\phi} = i\tau_2\phi^*$, $\overrightarrow{\tau} = (\tau_1, \tau_2, \tau_3)$ (τ_i are the 2×2 Pauli spin matrices) and, similarly, the scalar triplet Δ_L in the adjoint representation of $SU(2)_L$ is expressed as $\overrightarrow{\Delta_L} = (\Delta_L^1, \Delta_L^2, \Delta_L^3)$. The Majorana type Yukawa coupling Y is a 3×3 matrix in flavor space and C is the charge conjugation matrix. Then

$$\left(\frac{\overrightarrow{\tau}.\overrightarrow{\Delta_L}}{\sqrt{2}}\right) = \frac{1}{\sqrt{2}}\left(\tau_1\Delta_L^1 + \tau_2\Delta_L^2 + \tau_3\Delta_L^3\right) = \begin{pmatrix} \frac{\Delta^+}{\sqrt{2}} & \Delta^{++} \\ \Delta^0 & -\frac{\Delta^+}{\sqrt{2}} \end{pmatrix}_L \tag{6}$$

where different components are given by

$$\Delta_L^0 = \frac{1}{\sqrt{2}}\left(\Delta_L^1 + i\Delta_L^2\right), \quad \Delta_L^+ = \Delta_L^3, \quad \Delta_L^{++} = \frac{1}{\sqrt{2}}\left(\Delta_L^1 - i\Delta_L^2\right) \tag{7}$$

A diagrammatic representation for type-II seesaw generation of neutrino mass is shown in Figure 1. From the Feynman diagram shown in Figure 1 the induced VEV of the scalar triplet is

$$v_L = \frac{\mu_\Delta v^2}{2M_\Delta^2}, \tag{8}$$

leading to the type-II seesaw formula

$$m_\nu = 2Yv_L. \tag{9}$$

It is necessary to explain the origin of the $B - L$ breaking scale μ_Δ that occurs in (4), (5), and (8) as well as the Feynman diagram of Figure 1. SU(5) invariance permits the triplet coupling $\mu_\Delta 15_H^\dagger 5_H 5_H$ leading to SM invariant coupling $\mu_\Delta \Delta_L \phi\phi$. Therefore, in one approach, μ_Δ may be treated as explicitly lepton number violating parameter. Alternatively, it is also possible to attribute a spontaneous lepton number violating origin to this parameter. Since the SM model gauge theory has to remain unbroken down to the electroweak scale, the lepton number violating scale can be generated by the VEV of a Higgs scalar that transforms as a singlet under SM. Such a singlet $S_{BL}(1, 0, 1)$ carrying $B - L = -2$ occurs in the Higgs representation 50_H [36, 110]. The part of the SU(5) invariant potential that generates this scale is

$$V_{BL} = \lambda_5 50_H 15_H 5_H 5_H + h.c, \tag{10}$$

leading to $\mu_\Delta = \lambda_5 < S_{BL} >$. The $U(1)_{B-L}$ symmetric origin of μ_{Δ_L} becomes more transparent if one treats SU(5) as the remnant of $SU(5) \times U(1)_{B-L}$ or higher rank GUTs like SO(10) and E_6. If unification constraint as discussed below is ignored, the order of magnitude of μ_Δ can be anywhere in the range $\mathcal{O}(\mathcal{M}_W) - \mathcal{O}(\mathcal{M}_{\text{Planck}})$. But as we will find in the subsequent sections, gauge coupling unification in the present SU(5) framework imposes the lower bound $\mu_\Delta \simeq M_\Delta \geq 10^{9.23}$ GeV.

2.1. Type-II Seesaw Fit to the Neutrino Oscillation Data

2.1.1. Neutrino Mass Matrix from Oscillation Data. The effective light neutrino mass matrix (m_ν) is diagonalised by a unitary matrix U (in PMNS parametrisation which is written as U_{PMNS}) and yields three mass eigenvalues (m_1, m_2, m_3). The light neutrino mass matrix (m_ν) can be reconstructed as

$$m_\nu = U_{PMNS}\text{diag}\left(m_1, m_2, m_3\right)U_{PMNS}^T, \tag{11}$$

where PMNS matrix is parameterised using the PDG convention [111] as

$$U_{\text{PMNS}} = \begin{pmatrix} c_{12}c_{13} & s_{12}c_{13} & s_{13}e^{-i\delta} \\ -s_{12}c_{23} - c_{12}s_{23}s_{13}e^{i\delta} & c_{12}c_{23} - s_{12}s_{23}s_{13}e^{i\delta} & s_{23}c_{13} \\ s_{12}s_{23} - c_{12}c_{23}s_{13}e^{i\delta} & -c_{12}s_{23} - s_{12}c_{23}s_{13}e^{i\delta} & c_{23}c_{13} \end{pmatrix} \text{diag}\left(e^{i\alpha_M/2}, e^{i\beta_M/2}, 1\right) \tag{12}$$

where $s_{ij} = \sin\theta_{ij}, c_{ij} = \cos\theta_{ij}$ with $(i, j = 1, 2, 3)$, δ is the Dirac CP phase, and (α_M, β_M) are Majorana phases.

Here we present our numerical analysis within 3σ and 1σ limits of experimental data. As we do not have any experimental information about Majorana phases, they are varied in the whole 2π interval randomly. From the set of randomly generated values we pick only one set of (α_M, β_M) and use them for our numerical estimations. The procedure adopted here can be repeated to derive corresponding solutions for the Majorana coupling matrix Y for other sets of randomly chosen Majorana phases. Although very recently 3σ and 1σ limits of Dirac CP phase have been announced [1], we prefer to use only their central value as an example. For our present analysis we choose a single set of (α_M, β_M) from a number of sets derived by random sampling and also a single value of δ close to the best fit value. For our analysis all possible

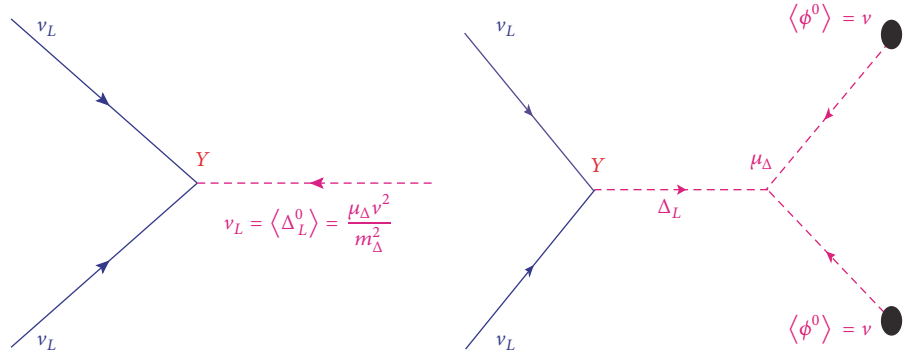

FIGURE 1: Schematic representation of generation of type-II term corresponding to (4) (a) and combination of (5)(b) where dashed line as triplet propagator supplies the damping factor M_Δ^{-2} to the induced vev v_L.

values of the solar and atmospheric mass squared differences and mixing angles have been taken which lie within the 3σ (or 1σ) limit of the oscillation data as determined by recent global analysis [1]. Summary of the global analysis is presented in Table 1. At first we analyze the limits imposed on the neutrino Yukawa couplings by 3σ oscillation constraints taking into account both the mass ordering of light neutrinos, normal ordering (NO), and inverted ordering (IO). In this case we use only one fixed value of the lightest neutrino mass eigenvalue and the other two mass eigenvalues are calculated using the experimental values of the mass squared differences. In this 3σ case we represent the bounds on the elements of Yukawa matrix in a tabular form. Later we proceed to estimate the bounds on the Y matrix elements imposed by 1σ experimental constraints of oscillation observables. In this analysis instead of fixed lightest neutrino mass eigenvalue, we vary it in the range (0–0.2) eV. The other two mass eigenvalues are calculated using 1σ ranges of solar and atmospheric mass squared differences. As already explained we use a single set of randomly chosen (α_M, β_M) and the central value of δ quoted in the Table 1. The variation of Y matrix elements is expressed in terms of their moduli ($|Y_{ij}|$) and the corresponding phases (ϕ_{ij})) with m_1 are shown graphically in Figures 2, 3, and 4 in the NO case. It is clear from the plots that for each single value of m_1 there is a band of allowed values of $|Y_{ij}|$ and ϕ_{ij}. This band signifies the 1σ allowed range of the corresponding matrix element for that single value of m_1. To represent the 1σ bounds in a more transparent manner we produce another set of plots as in Figures 5 and 6 where we show the allowed values of $|Y_{ij}|$ and ϕ_{ij} for a fixed value of m_1. It is to be noted that in this present work graphical representation is done for normally ordered light neutrinos only. Similar kind of exercise can be carried out for inverted mass ordering also.

2.1.2. Majorana Yukawa Coupling for 3σ Bounds of Neutrino Oscillation Data. We now estimate the m_ν matrix for the normally ordered (NO) case. For this purpose we take the mass of the lightest neutrino as $m_1 = 0.00127$ eV. Then using the 3σ ranges of solar and atmospheric mass squared differences for NO case, as mentioned in Table 1, the other two neutrino mass eigenvalues are calculated. Obviously we get a range of values of m_2 and m_3. Plugging in these mass eigenvalues along with all possible combinations and the mixing angles within the 3σ bound in (11) we obtain large number of sets of m_ν matrix. Thus we also get respective bounds on the elements of the m_ν matrix (or equivalently on the Yukawa coupling matrix Y) corresponding to the 3σ oscillation constraints. As mentioned earlier we use single set of randomly chosen Majorana phases while the Dirac CP phase is chosen close to its central value. The effective light neutrino mass matrix m_ν and the coupling matrix Y are connected through the induced VEV v_l which is obtained by assuming the dimensionful coupling $\mu_\Delta \sim M_\Delta$ where $M_\Delta = 10^{12}$ GeV and the electroweak VEV is 246 GeV. With these considerations we estimate the 3σ bound on the elements of Y matrix and present them in Table 2. In the inverted mass ordering the smallest mass eigenvalue is m_3 which is set to be equal to 0.00127 eV. The other two eigenvalues are calculated using the 3σ limit of the solar and atmospheric mass squared differences. In this case also we are able to put a bound on the modulus and phase of the Yukawa coupling matrix following the same procedure as done in the case of NO. The constrained parameters $(|Y_{ij}|, \phi_{ij})$ for inverted mass ordering are given in Table 3.

As we have taken a most general complex symmetric structure of the m_ν matrix (or in other words the Yukawa coupling matrix Y) without imposing any kinds specific flavor symmetry, it does not have any definite prediction of the Dirac CP violating phase δ. Any value of δ in the given 3σ range can be accommodated. In this regard few remarks about the present experimental status of the Dirac CP phase are in order. The recent global analysis of oscillation data done in [1] has made it clear that value of the Dirac CP phase $\delta = \pi/2$ is more or less ruled out. In normal mass ordering (NO) $\delta = \pi/2$ is disfavored at more than 4σ confidence level whereas for inverted mass ordering (IO) it is more stringent, where $\delta = \pi/2$ is ruled out at more than 6σ. The best fit value of δ in NO and IO is near 1.2π and 1.5π, respectively. For the sake of simplicity we work with only the best fit values. We have also estimated the highest and lowest values of the CP violating measure, the Jarlskog invariant (J_{CP} =

Table 1: Input data from neutrino oscillation experiments [1].

Quantity	best fit values	3σ ranges	2σ ranges	1σ ranges
$\Delta m^2_{21}\,[10^{-5}eV^2]$	7.55	7.05 – 8.14	7.20 – 7.94	7.39 – 7.55
$\lvert\Delta m^2_{31}\rvert\,[10^{-3}eV^2]\,(NO)$	2.50	2.41 – 2.60	2.44 – 2.57	2.47 – 2.53
$\lvert\Delta m^2_{31}\rvert\,[10^{-3}eV^2]\,(IO)$	2.42	2.31 – 2.51	2.34 – 2.47	2.38 – 2.46
$\theta_{12}/^\circ$	34.5	31.5 – 38.0	32.2 – 36.8	33.5 – 35.7
$\theta_{23}/^\circ(NO)$	47.7	41.8 – 50.7	43.1 – 49.8	46 – 48.9
$\theta_{23}/^\circ(IO)$	47.9	42.2 – 50.7	44.5 – 48.9	46.2 – 48.9
$\theta_{13}/^\circ(NO)$	8.45	8 – 8.9	8.2 – 8.8	8.31 – 8.61
$\theta_{13}/^\circ(IO)$	8.53	8.1 – 9	8.3 – 8.8	8.38 – 8.67
$\delta/^\circ(NO)$	218	157 – 349	182 – 315	191 – 256
$\delta/^\circ(IO)$	281	202 – 349	229 – 328	254 – 304

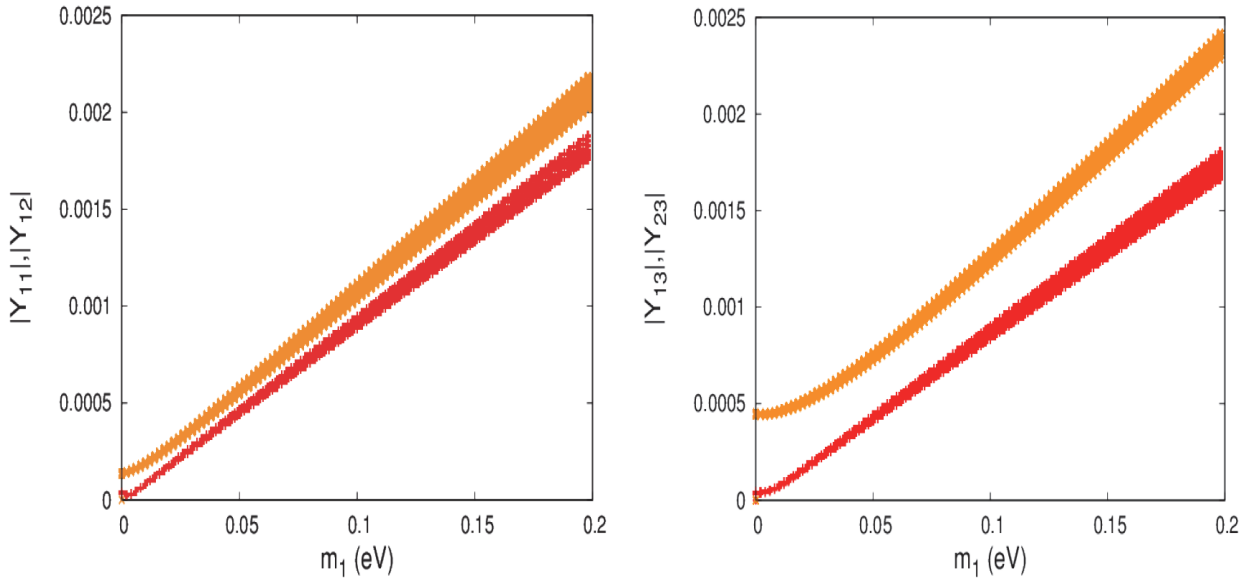

(a) (b)

Figure 2: Determination of moduli of Y matrix elements within 1σ uncertainty of oscillation data as a function of lightest neutrino mass eigenvalues m_1. Phase angles used are randomly chosen Majorana phases $\alpha_M = 37.91^\circ, \beta_M = 157.91^\circ$ and central value of the Dirac phase $\delta = 216^\circ$. In (a) red and yellow regions denote 1σ allowed values $|Y_{11}|$ and $|Y_{12}|$, respectively. In (b) red patch gives values of $|Y_{13}|$ whereas yellow region denotes the same for $|Y_{23}|$ within the same uncertainty of the oscillation data.

$-s_{12}c_{12}s_{13}c_{13}^2 s_{23}c_{23}\sin\delta$) for both the mass orderings. For NO: $J_{CP} = 0.0175 - 0.0212$, for IO: $J_{CP} = 0.0302 - 0.0365$ when δ is kept fixed at its best fit value whereas all other observables are varying in their respective 3σ ranges.

2.1.3. Majorana Yukawa Coupling for 1σ Bounds of Neutrino Oscillation Data. Here we follow exactly the same methodology as the previous case, however the numerical calculations are done with 1σ ranges of oscillation data instead of 3σ range. Here we are exploring the normally ordered case only. Unlike the previous case the lightest neutrino mass eigenvalue m_1 is not kept fixed; it is varied over a range of $(0 - 0.2)$ eV and the corresponding variations of the modulus and phase of Majorana Yukawa couplings are depicted in Figures 2, 3, and 4. The 1σ allowed ranges of those quantities for a fixed m_1 are also shown in Figures 5 and 6.

3. Gauge Coupling Unification in the Scalar Extended SU(5)

3.1. Lower Bound on the Scalar Triplet Mass. Exercising utmost economy in populating the grand desert, it was noted that the presence of the scalar component $\kappa(3,0,8) \subset 75_H$ at an intermediate mass $\simeq 10^{10}$ GeV could achieve gauge coupling unification at $M_{GUT} \simeq 10^{15}$ GeV [112] but no neutrino oscillation data was available at that time. Using the most recent electroweak precision data [111, 113, 114], in this work we find that this intermediate scalar mass is now reduced by one order, $M_\kappa = 10^{9.23}$ GeV. Similarly the GUT scale is now determined with high precision including all possible theoretical and experimental uncertainties. Noting the result of this work as discussed in Section 2 that type-II seesaw realisation of neutrino mass needs M_Δ

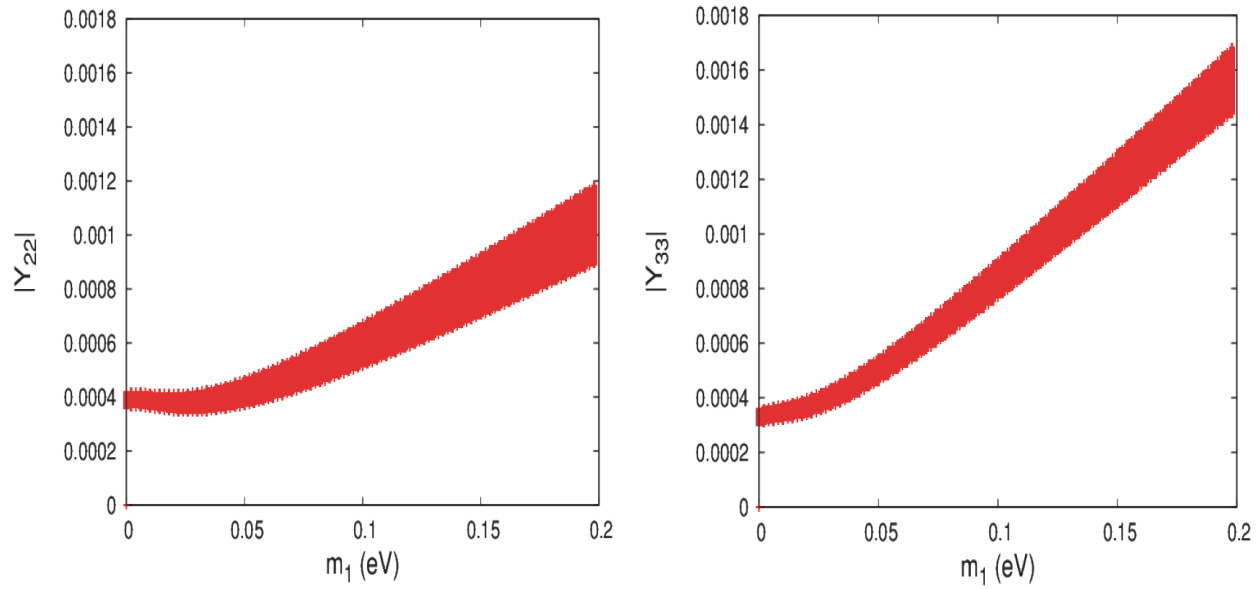

(a) (b)

FIGURE 3: Determination of moduli of Y matrix elements within 1σ uncertainty of oscillation data as a function of lightest neutrino mass eigenvalues m_1 as shown in (a) for $|Y_{22}|$, and in (b) for $|Y_{33}|$. Phase angles used are the same as in Figure 2.

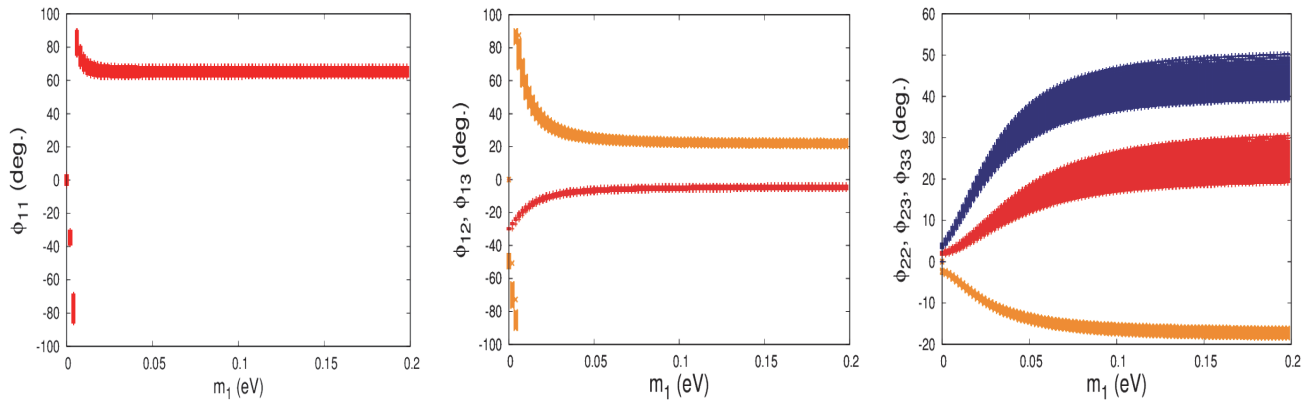

(a) (b) (c)

FIGURE 4: Determination of phases of Y matrix elements as a function of lightest neutrino mass eigenvalues m_1 within 1σ allowed uncertainty of oscillation data. Phase angles used are the same as in Figure 2. In (a) red region denotes values of ϕ_{11}. In (b) red and yellow regions denote allowed values ϕ_{12} and ϕ_{13}, respectively. In (c) red, yellow, and blue patches give allowed values of ϕ_{22}, ϕ_{23}, and ϕ_{33}, respectively.

substantially lower than the GUT scale leads to the natural apprehension that the presence $\Delta_L(3,-1,1)$ at intermediate mass scale would destroy precision unification achieved by $\kappa(3,0,8)$. This apprehension is logically founded on the basis that nonvanishing contributions to the $SU(2)_L$ and $U(1)_Y$ beta functions would misalign the fine structure constants $\alpha_{2L}(\mu)$ and $\alpha_Y(\mu)$ from the $\kappa(3,0,8)$ realised unification paths substantially for all mass scales $\mu > M_\Delta$.

We prevent any such deviation from the $\kappa(3,0,8)$-realisation of precision coupling unification by assuming all the components of $15_H \subset SU(5)$ to have the identical degenerate mass M_Δ which is bounded in the following manner:

$$M_\kappa \leq \left(M_\Delta = M_{15_H}\right) \leq M_{GUT}. \tag{13}$$

Thus, in order to safeguard precision unification, it is essential that $M_\Delta = M_{15_H} \geq M_\kappa$ in the present scalar extended SU(5) model (the upper limit is due to our observation that type-II seesaw scale is lower than the GUT scale although, strictly speaking, $M_\Delta = M_{15_H} > M_{GUT}$ is possible if type-II seesaw contribution to neutrino mass is ignored).

Thus type-II seesaw realisation of neutrino mass and precision unification in SU(5) needs the additional scalar representations 15_H and 75_H.

3.2. RG Solutions to Mass Scales. For realistic unification of gauge couplings we use one loop equations [115]

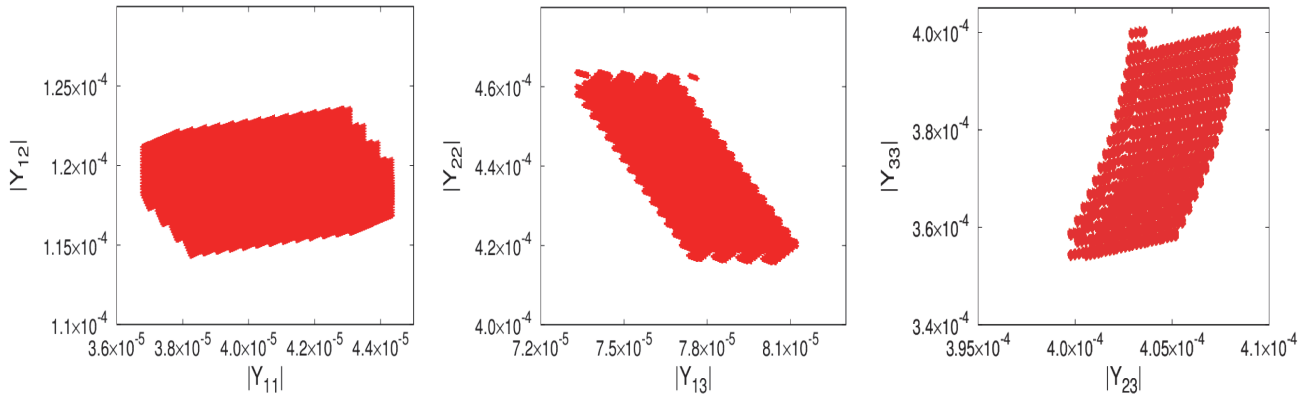

(a) (b) (c)

FIGURE 5: Determination of moduli of Y matrix elements for a fixed value of lightest mass eigenvalue $m_1 = 0.00127$ eV. Phase angles used for computation are $\alpha_M = 124.37^\circ, \beta_M = 86.27^\circ$ (randomly chosen), and $\delta = 216^\circ$. Neutrino oscillation observables are varied within 1σ range. (a) Variation of $|Y_{11}|$ with $|Y_{12}|$, (b) $|Y_{13}|$ versus $|Y_{22}|$, and (c) $|Y_{23}|$ versus $|Y_{33}|$.

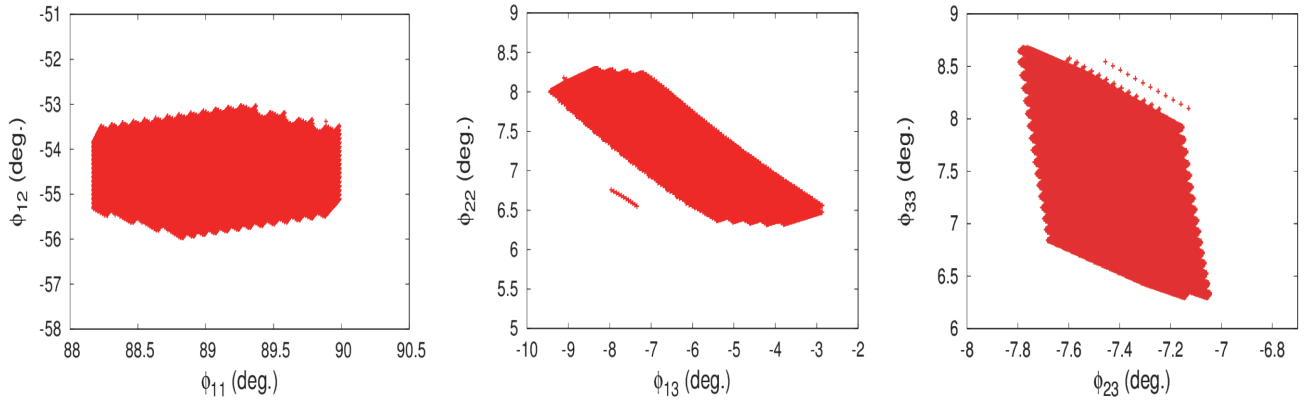

(a) (b) (c)

FIGURE 6: Determination of phases of Y matrix elements for fixed value of lightest mass eigenvalue $m_1 = 0.001$ eV. Phase angles used for computation are the same as in Figure 5. Neutrino oscillation observables are varied within 1σ range; (a) variation of ϕ_{11} with ϕ_{12}, (b) ϕ_{13} versus ϕ_{22}, and (c) ϕ_{23} versus ϕ_{33}.

supplemented by top-quark threshold effects [83] and two-loop corrections [116]

$$\mu\frac{\partial g_i(\mu)}{\partial\mu} = \frac{a_i}{16\pi^2}g_i^3 + \frac{1}{(16\pi^2)^2}\left[\Sigma_j b_{ij}g_i^3 g_j^2 - \kappa_i y_{\text{top}}^2\right] \quad (14)$$

In the range of mass scale $\mu = M_Z - M_U$ we include top-quark Yukawa coupling (y_{top}) contribution at the two-loop level with the coefficients in (14) $\kappa_{1Y} = 17/10, \kappa_{2L} = 3/2, \kappa_{3C} = 2$ and the RG evolution equation [83]

$$\mu\frac{\partial y_{top}}{\partial\mu} = \frac{y_{top}}{16\pi^2}\left(\frac{9}{2}y_{top}^2 - \frac{17}{20}g_{1Y}^2 - \frac{9}{4}g_{2L}^2 - 8g_{3C}^2\right) \quad (15)$$

The beta function coefficients in three different mass ranges $\mu = M_Z \longrightarrow M_\kappa$, $\mu = M_\sigma - M_\Delta$, and $\mu = M_\Delta - M_U$ are

$\underline{\mu = M_Z \longrightarrow M_\kappa :}$

$$a_Y = \frac{41}{10}, \quad a_{2L} = -\frac{19}{6}, \quad a_{3C} = -7, \quad (16)$$

$\underline{\mu = M_\kappa \longrightarrow M_\Delta :}$

$$a'_Y = \frac{41}{10}, \quad a'_{2L} = -\frac{1}{2}, \quad a'_{3C} = -\frac{11}{2}, \quad (17)$$

Table 2: Numerical values of the moduli ($|Y_{ij}|$) and phases (ϕ_{ij}) ($i, j = 1, 2, 3$) of Yukawa coupling matrix for normally ordered (NO) light neutrino masses corresponding to 3σ global fit of neutrino oscillation data. Lightest neutrino mass eigenvalue is kept fixed at $m_1 = 0.00127$ eV for the sake of simplicity. Randomly chosen Majorana phases $\alpha_M = 74.84^\circ$, $\beta_M = 112.85^\circ$ and the central value of the Dirac phase $\delta = 218^\circ$ have been used.

$\lvert Y_{11}\rvert$	$\lvert Y_{12}\rvert$	$\lvert Y_{13}\rvert$	$\lvert Y_{22}\rvert$	$\lvert Y_{23}\rvert$	$\lvert Y_{33}\rvert$
$(1.74 - 3.95) \times 10^{-5}$	$(1.13 - 1.44) \times 10^{-4}$	$(4.09 - 6.71) \times 10^{-5}$	$(3.20 - 4.67) \times 10^{-4}$	$(4.07 - 4.35) \times 10^{-4}$	$(3.05 - 4.5) \times 10^{-4}$
ϕ_{11} (deg.)	ϕ_{12} (deg.)	ϕ_{13} (deg.)	ϕ_{22} (deg.)	ϕ_{23} (deg.)	ϕ_{33} (deg.)
$(-65.24) - (-61.73)$	$(-48.50) - (-44.22)$	$(-17.48) - 8.27$	$4.67 - 10.6$	$(-6.81) - (-5.34)$	$3.77 - 10.0$

Table 3: Numerical values of the moduli ($|Y_{ij}|$) and phases (ϕ_{ij}) ($i, j = 1, 2, 3$) of Yukawa coupling matrix Y for invertedly ordered (IO) light neutrino masses corresponding to 3σ global fit of neutrino oscillation data. Lightest neutrino mass eigenvalue is kept fixed at $m_3 = 0.00127$ eV. Phase angles used are the same as in Table 2.

$\lvert Y_{11}\rvert$	$\lvert Y_{12}\rvert$	$\lvert Y_{13}\rvert$	$\lvert Y_{22}\rvert$	$\lvert Y_{23}\rvert$	$\lvert Y_{33}\rvert$
$(4.38 - 5.3) \times 10^{-4}$	$(4.29 - 5.5) \times 10^{-4}$	$(3.55 - 4.87) \times 10^{-4}$	$(8.83 - 23.5) \times 10^{-5}$	$(2.13 - 2.89) \times 10^{-4}$	$(2.84 - 4.0) \times 10^{-4}$
ϕ_{11} (deg.)	ϕ_{12} (deg.)	ϕ_{13} (deg.)	ϕ_{22} (deg.)	ϕ_{23} (deg.)	ϕ_{33} (deg.)
52.96	$(-6.51)-(-3.16)$	0.5	$(-60) - (-32.31)$	$(-69.16) - (-51.39)$	$(-78.89) - (-61.92)$
68.35		4.5			

$\mu = M_\Delta \longrightarrow M_U$:

$$a_Y'' = \frac{79}{15},$$
$$a_{2L}'' = \frac{2}{3}, \tag{18}$$
$$a_{3C}'' = -\frac{13}{3}.$$

We have used the most recent electroweak precision data [114]

$$\alpha_S(M_Z) = 0.1182 \pm 0.0005,$$
$$\sin^2\theta_W(M_Z) = 0.23129 \pm 0.00005, \tag{19}$$
$$\alpha^{-1}(M_Z) = 127.94 \pm 0.02.$$

Using RGEs and the combinations $1/\alpha(M_Z) - (8/3)1/\alpha_{2L}(M_Z)$ and $1/\alpha(M_Z) - (8/3)1/\alpha_{3C}(M_Z)$, we have derived analytic formulas for the unification scale and intermediate scale(M_κ) treating $SU(2)_L$ triplet scalar scale (M_Δ) constant as

$$\ln\frac{M_U^0}{M_Z} = \frac{2\pi}{187\alpha}\left(7 - \frac{80\alpha}{3\alpha_{3C}} + 8s_W^2\right) + \Delta_U$$
$$\ln\frac{M_\kappa^0}{M_Z} = \frac{12\pi}{187\alpha}\left(5 + \frac{23\alpha}{3\alpha_{3C}} - 21s_W^2\right) + \Delta_\kappa \tag{20}$$
$$\frac{1}{\alpha_{G^0}} = \frac{3}{8\alpha} + \frac{1}{187\alpha}\left(\frac{347}{8} + \frac{466\alpha}{3\alpha_{3C}} - 271s_W^2\right) + \Delta_{\alpha_G}$$

where $s_W^2 = \sin^2\theta_W(M_Z)$ and the first term in (20) represent one loop contributions. The terms Δ_I^i, $i = U, \kappa, \alpha_G$, denote the threshold corrections due to unification scale (M_U), intermediate scale (M_κ), and GUT fine structure constant ($1/\alpha_G$).

Excellent unification of gauge couplings is found for

$$M_U^0 = 10^{15.2+0.0312}\text{GeV},$$
$$M_\kappa^0 = 10^{9.23}\text{GeV}, \tag{21}$$
$$\alpha_{G_0}^{-1} = 41.79$$

where the number 0.0312 in the exponent is due to GUT scale matching of inverse fine structure constant that is present even if all superheavy masses are exactly at $\mu = M_U^0$ [101, 103–105].

3.3. Effects of 15_H on Unification. It is well known that when a complete GUT representation is superimposed on an already realised unification pattern in non-SUSY GUTs [117, 118], the GUT scale is unchanged but the inverse fine structure constants change their slopes and deviate from the original paths proportionately so as to increase the unification coupling. As an example in non-SUSY SO(10) [117, 118], at first a precision unification frame has been achieved with the modification of the TeV scale spectrum of the minimal SUSY GUT by taking out the full scalar super partner content of the spinorial super field representation $16 \subset SO(10)$. Then the resulting TeV scale spectrum is [117, 118]

$$\chi\left(2, -\frac{1}{2}, 1\right),$$
$$F_\phi\left(2, \frac{1}{2}, 1\right),$$

$$F_\chi\left(2,-\frac{1}{2},1\right),$$
$$F_\sigma\,(3,0,1)\,,$$
$$F_b\,(1,0,1)\,,$$
$$F_c\,(1,0,8) \tag{22}$$

which may be recognised to be the same as the corresponding spectrum in the split-SUSY case supplemented by the additional scalar doublet $\chi(2,-1/2,1)$. In 3.3 F_i's represent nonstandard fermions. Further adjustment of masses of these particles around TeV scale has been noted to achieve degree of precision coupling unification higher than MSSM [117]. After having thus achieved a precision unification, the full 15_H is superimposed at the type-II seesaw scale M_Δ of the nonsupersymmetrised unification framework. Analogous to MSSM, this model [118] predicts a number of fermions as in 3.3 at the TeV scale which must be verified experimentally at accelerator energies.

In contrast, the present model has only the standard Higgs doublet $\phi(2,1/2,1)$ and the WIMP DM scalar singlet $\xi(1,0,1)$ near TeV scale as discussed below. Although the TeV scale DM has not been confirmed yet by direct experiments, LUX-16 or Femi-LAT-like experiments may detect it. Moreover, as shown below, the present model ensures vacuum stability through this WIMP dark matter candidate whereas in [118] the vacuum stability and DM issues are yet to be answered. Further, the SM coupling unification scale in [118] being close to the SUSY GUT scale, $M_U \sim 10^{16}$ GeV, predicts proton lifetime nearly 60 times larger than the current experimental limit without threshold effect which is expected to introduce larger uncertainty compared to the present model. It may be more difficult to verify this model by ongoing proton decay experiments. But the present model including such uncertainties is within the experimentally accessible limits. The origin of invariant GUT scale in the presence of 15_H in the present model is due to the invariance of the beta function differences which is $-7/6$ in this model

$$\Delta a_i = \left(a_i' - a_i''\right) = -\left(\frac{7}{6}\right), \quad (i = 1,2,3)\,. \tag{23}$$

This results in a change in the inverse GUT coupling constant α_G^{-1} which occurs due to the RG predicted modification

$$\frac{1}{\alpha_G} = \frac{1}{\alpha_{G^0}} - \frac{1}{561\alpha}\left(\frac{229}{2} + \frac{134\alpha}{3\alpha_{3C}} - 350 s_W^2\right) + \frac{7}{12\pi}\ln\left(\frac{M_\Delta}{M_Z}\right). \tag{24}$$

Thus the result of type-II seesaw motivated insertion of 15_H into the $\kappa-$ realised unification framework is to decrease in the inverse GUT fine structure constant while keeping mass scales same as in (21)"

$$\alpha_G^{-1} = 37.765. \tag{25}$$

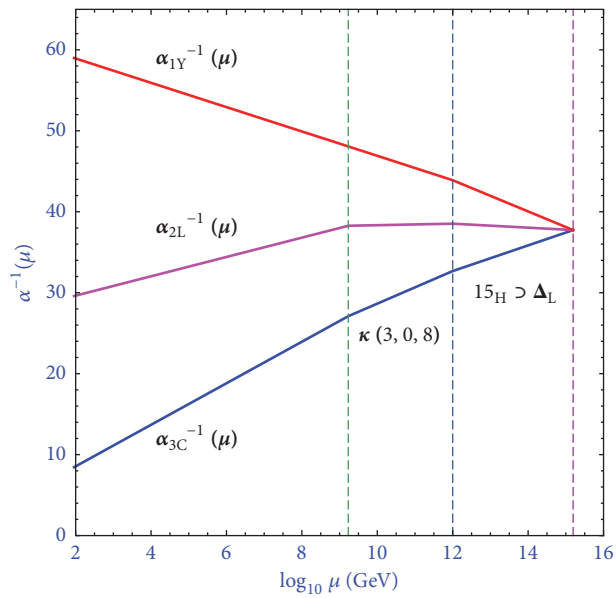

Figure 7: Unification of SM gauge couplings in the presence of $\kappa(3,0,8)$ at $M_\kappa = 10^{9.23}$ GeV and $15_H \subset SU(5)$ at $M_{15} = 10^{12}$ GeV as discussed in the text. The vertical dashed lines represent the intermediate scale masses and GUT scales.

which is a 9.6% effect. It is essential to take this effect into consideration in the top-down approach for consistency with the precision value of the electromagnetic fine structure constant $\alpha^{-1}(M_Z) = 127.9 \pm 0.01$ [114]. More important is its visible effect on proton lifetime prediction. It is clear from α_G^{-2} dependence in (36) of Section 4, (21), and (25) that the this intermediate type-II seesaw scale has a proton lifetime reduction by 19% that further reduces for lower seesaw scales, $M_\Delta < 10^{12}$ GeV. But the reduction effect decreases as M_Δ increases such that the proton lifetime remains unchanged for the limiting value $M_\Delta = M_{15_H} = M_U$.

In Figure 7 we have shown evolution of inverse fine structure constants of three gauge couplings of SM against mass scales depicting precision unification at $M_U^0 = 10^{15.2}$ GeV.

3.3.1. Implications for Lepton Number and Flavor Violations. It is evident from (13) and (21) that the numerical lower bound on the masses of three members of the triplet in $\Delta_L(3,-1,1)$ is

$$M_{\Delta^0} \simeq M_{\Delta^-} \simeq M_{\Delta^{--}} \geq 10^{9.23}\text{GeV}. \tag{26}$$

Out of these we have discussed in Section 2 how the mediation of M_{Δ^0} gives type-II seesaw contribution to neutrino masses matching with available neutrino oscillation data at 1σ-3σ levels for all types of hierarchies: NH, IH, and QD. As a result the Higgs-Yukwa interaction and induced VEV

of the neutral component of the triplet in the present SU(5) model give similar predictions as in the triplet extended SM based analyses [119] or in the left-right symmetric models and SO(10) with large W_R boson mass [45, 120]. Currently a number of experimental investigations are underway to detect the double beta decay process that would establish Majorana nature of neutrino. The most important difference from such SM based phenomenological analyses is that in the present SU(5) model with type-II seesaw all the parameters of the neutrino oscillation data are theoretically predicted by the seesaw mechanism. Even though $M_{\Delta^0} \geq 10^{9.23}$ GeV, it predicts the double beta decay lifetime close to the observable limit of $\tau_{\beta\beta} \sim 5 \times 10^{25}$ yrs for QD type light neutrino masses $\widehat{m}_i \sim 0.2$ eV. On the other hand for NH type of hierarchy the predicted decay rate is much lower with lifetime $\tau_{\beta\beta} \gg 10^{29}$ yrs. Another theoretical contribution to the double beta decay process is due to the mediation of the doubly charged component Δ^{--} through the physical process $W^-W^- \longrightarrow \Delta^{--} \longrightarrow e^-e^-$ which is negligible because of additional damping of the amplitude caused by the inverse square of its heavy mass $M_{\Delta^{--}} \geq 10^{9.23}$ GeV. The charged component Δ^- also mediates a new loop contributions to lepton flavor violating processes such as $l_\alpha \longrightarrow l_\beta + \gamma$. Again, because of heavy triplet mass the respective contribution to branching ratio turns out to be much smaller than the corresponding prediction with *SM* (supplemented by the oscillation data): $Br.(\mu \longrightarrow e\gamma) < 10^{-53}$ [45, 120]. Similarly the tree level mediation of the LFV process $\mu \longrightarrow ee\overline{e}$ by Δ^{--} is severely damped out compared to the loop mediated $W-$boson contribution.

3.4. Threshold Effects on the GUT Scale. In the single step breaking model discussed in this work, GUT threshold effects due to superheavy degrees of freedom in different SU(5) representations are expected as major sources of uncertainties on unification scale and proton lifetime prediction. We have estimated the threshold uncertainties following the partially degenerate assumption introduced in [121, 122] which states that the superheavy components belonging to the same GUT representation are degenerate with a single mass scale.

The analytic formulas for GUT threshold effects on the unification scale, intermediate scale, and GUT fine structure constant are

$$\begin{aligned}
\Delta_I^{\kappa} &= \Delta \ln \frac{M_\kappa}{M_Z} = \frac{1}{2244}\left(123\lambda_{2L} - 215\lambda_Y + 92\lambda_{3C}\right),\\
\Delta_I^{U} &= \Delta \ln \frac{M_U}{M_Z} = \frac{5}{3366}\left(3\lambda_{2L} + 13\lambda_Y - 16\lambda_{3C}\right),\\
\Delta_I^{\alpha_G} &= \Delta\left(\frac{1}{\alpha_G}\right)\\
&= \frac{1}{80784\pi}\left(-948\lambda_{2L} - 2425\lambda_Y + 5056\lambda_{3C}\right).
\end{aligned} \tag{27}$$

In (27) $\lambda_i, i = 2L, Y, 3C$ are matching functions due to superheavy scalars (S) and gauge bosons (V) to the three gauge couplings,

$$\alpha_i^{-1}\left(M_U\right) = \alpha_G^{-1} - \frac{\lambda_i\left(M_U\right)}{12\pi}, \tag{28}$$

$$\begin{aligned}
\lambda_i^S\left(M_U\right) &= \sum_j Tr\left(t_{iSj}^2 \widehat{p}_{Sj} \ln \frac{M_j^S}{M_U}\right),\\
\lambda_i^V\left(M_U\right) &= \sum_l Tr\left(t_{iVl}^2\right) - 21\sum_l Tr\left(t_{iVl}^2 \ln \frac{M_l^V}{M_U}\right),
\end{aligned} \tag{29}$$

where t_{iS} and t_{iV} represent the matrix representations due to broken generators of scalars and gauge bosons. The term $\widehat{p}_{Sj}$ denotes the projection operator that removes the Goldstone components from the scalars contributing to spontaneous symmetry breaking.

The decomposition of different SU(5) representations under G_{213} with respect to their superheavy components and values of corresponding matching functions is presented in Table 4.

Using the values of matching function $\lambda^i(M_U)$ from Table 4 in (27) we estimate corrections to different mass scales due to superheavy masses as

$$\begin{aligned}
\Delta \ln \frac{M_\kappa}{M_Z} &= 0.0026738\eta_5 + 0.23262\eta_{24} - 1.24599\eta_{75},\\
\Delta \ln \frac{M_U}{M_Z} &= -0.0160428\eta_5 - 0.0623886\eta_{24}\\
&\quad + 1.142602\eta_{75},\\
\Delta\left(\frac{1}{\alpha_G}\right) &= 0.0160999\eta_5 + 0.0522951\eta_{24}\\
&\quad + 0.0462547\eta_{75}.
\end{aligned} \tag{30}$$

Maximising the uncertainty in M_U leads to

$$\begin{aligned}
\Delta \ln\left(\frac{M_U}{M_Z}\right) &= \pm 0.22103\eta_{SH},\\
\Delta \ln\left(\frac{M_\kappa}{M_Z}\right) &= \pm 1.48128\eta_{SH},\\
\Delta\left(\frac{1}{\alpha_G}\right) &= \pm 0.02214\eta_{SH},
\end{aligned} \tag{31}$$

where $\eta_{SH} = \ln(M_{SH}/M_U)$ and $M_{SH}/M_U = n(1/n)$ with plausible allowed values of real number $n = 1 - 10$.

We also note that the degenerate superheavy gauge bosons contribute a significant correction to unification scale

$$\left(\frac{M_U}{M_U^0}\right)_V = 10^{\pm 0.65508}. \tag{32}$$

Adding all corrections together we obtain

$$M_U = 10^{15.2312 \pm 0.11 \pm 0.221\eta_S \pm 0.655\eta_V}\,\text{GeV}. \tag{33}$$

The first uncertainty (± 0.11) represents uncertainty in input parameters given in (19).

Table 4: Superheavy components of SU(5) representations under the SM gauge group G_{213} used to estimate GUT threshold effects.

$SU(5)$representations	G_{213} submultiplet	$(\lambda_{2L}, \lambda_{1Y}, \lambda_{3C})$
5_H	$C_1(1, -1/3, 3)$	$\left(0, \frac{2}{3}, 1\right)$
24_H	$D_1(3, 0, 1)$	$(2, 0, 0)$
	$D_2(1, 0, 8)$	$(0, 0, 3)$
75_H	$E_1(1, 10/3, 3)$	$\left(0, 5, \frac{1}{2}\right)$
	$E_2(2, 5/3, 3)$	$\left(\frac{3}{2}, \frac{5}{2}, 1\right)$
	$E_3(1, -10/3, \bar{3})$	$\left(0, 5, \frac{1}{2}\right)$
	$E_4(2, -5/3, \bar{3})$	$\left(\frac{3}{2}, \frac{5}{2}, 1\right)$
	$E_5(2, -5/3, \bar{6})$	$(3, 5, 5)$
	$E_6(2, 5/3, 6)$	$(3, 5, 5)$
	$E_7(1, 0, 8)$	$(0, 0, 3)$
15_H	$\Delta_L(3, -1, 1)$	$\left(4, \frac{18}{5}, 0\right)$
	$H_2(2, 1/6, 3)$	$\left(3, \frac{1}{5}, 2\right)$
	$H_3(1, 2/3, 6)$	$\left(0, \frac{16}{5}, 5\right)$
24_V	$V_1\left(2, -\frac{5}{6}, 3\right)$	$\left(\frac{3}{4}, \frac{5}{4}, \frac{1}{2}\right)$
	$V_2\left(2, \frac{5}{6}, \bar{3}\right)$	$\left(\frac{3}{4}, \frac{5}{4}, \frac{1}{2}\right)$

4. Proton Lifetime Prediction

Currently the measured value on the lower limit of the proton lifetime for the decay mode $p \longrightarrow e^+\pi^0$ is [109, 123–126]

$$\tau_p^{expt.} \geq 1.6 \times 10^{34} \text{ yrs.} \tag{34}$$

Including strong and electroweak renormalization effects on the d = 6 operator and taking into account quark mixing, chiral symmetry breaking effects, and lattice gauge theory estimations, the decay rates are [37, 127, 128]

$$\begin{aligned}\Gamma\left(p \longrightarrow e^+\pi^0\right) &= \left(\frac{m_p}{64\pi f_\pi^2}\frac{{\alpha_G}^4}{{M_U}^4}\right)\left|A_L\right|^2\left|\overline{\alpha_H}\right|^2\left(1 + D' + F\right)^2 \times R,\end{aligned} \tag{35}$$

where $R = [A_{SR}^2 + A_{SL}^2(1 + |V_{ud}|^2)^2]$ for $SU(5)$, $V_{ud} = 0.974$ = the $(1,1)$ element of V_{CKM} for quark mixings, and $A_{SL}(A_{SR})$ is the short-distance renormalization factor in the left (right) sectors. In (35) $A_L = 1.25$ = long distance renormalization factor but $A_{SL} \simeq A_{SR} = 2.542$. These are numerically estimated by evolving the dim.6 operator for proton decay by using the anomalous dimensions of [129] and the beta function coefficients for gauge couplings of this model. In (35) M_U = degenerate mass of superheavy gauge bosons, $\overline{\alpha}_H$ = hadronic matrix elements, m_p =proton mass = 938.3 MeV, f_π = pion decay constant = 139 MeV, and the chiral Lagrangian parameters are $D = 0.81$ and $F = 0.47$. With $\alpha_H = \overline{\alpha_H}(1 + D' + F) = 0.012\text{GeV}^3$ estimated from lattice gauge theory computations [130–132], we obtain $A_R \simeq A_L A_{SL} \simeq A_L A_{SR} \simeq 2.726$ and the expression for the inverse decay rate is

$$\Gamma^{-1}\left(p \longrightarrow e^+\pi^0\right) = \frac{4}{\pi}\frac{f_\pi^2}{m_p}\frac{M_U^4}{\alpha_G^2}\frac{1}{\alpha_H^2 A_R^2}\frac{1}{F_q}, \tag{36}$$

where the GUT fine structure constant $\alpha_G = 0.0263$ and the factor $F_q = (1 + (1 + |V_{ud}|^2)^2) \simeq 4.8$. This formula has the same form as given in [127] which has been modified here for the SU(5) case.

Using the estimated values of the model parameters, (36) gives

$$\tau_p^{SU(5)} \simeq 10^{33.110 \pm 0.440 \pm 0.884|\eta_S| \pm 2.62|\eta_V|} \text{ yrs.} \tag{37}$$

Numerical estimations on proton lifetime are shown in Table 5 for different splitting factors of superheavy masses.

It is interesting to note that despite three Higgs representations $5_H, 24_H, 75_H$, major contribution to threshold uncertainty in the model is only due to superheavy gauge bosons. When all superheavy gauge boson masses are identically equal to M_U, superheavy scalar mass splitting by a factor 20(1/20) from the GUT scale gives $\eta_S = 1.3(-1.3)$ leading to $[\tau_p]_{max} = 1.80 \times 10^{34}$ yrs. which is consistent with the current experimental bound.

5. Scalar Dark Matter in SU(5)

5.1. Phenomenological and Experimental Constraints. The existence of dark matter (DM) in our galaxy has been established beyond any doubt through its gravitational effects by numerous observations [133]. Hence the hunt for DM has

Table 5: Upper limits on predicted proton lifetime as a function of superheavy scalar (S) and gauge boson(V) mass splittings as defined in the text. The factor $10^{\pm 0.44}$ represents uncertainty due to input parameters.

$\frac{M_S}{M_U}$	$\frac{M_V}{M_U}$	$\tau_P(yrs)$	$\frac{M_S}{M_U}$	$\frac{M_V}{M_U}$	$\tau_P(yrs)$
10	1	$9.77 \times 10^{33\pm0.44}$	5	5	$3.59 \times 10^{35\pm0.44}$
10	2	$6.00 \times 10^{34\pm0.44}$	3	6	$3.68 \times 10^{35\pm0.44}$
8	3	$1.42 \times 10^{35\pm0.44}$	1	10	$5.32 \times 10^{35\pm0.44}$
6	4	$2.35 \times 10^{35\pm0.44}$	20	1	$1.80 \times 10^{34\pm0.44}$

been assumed to be of paramount importance for the particle physics community to understand its nature in particular and that of the universe in general. To this end, experiments using a wide range of approaches are being pursued worldwide and giving a large spectrum of interpretations of the DM candidates with masses ranging from a few eV to PeV or even beyond, from axions to wimpzillas and decaying dark matter.

Our motivation in this section is to explore whether SU(5) model can accommodate a scalar singlet (= ξ) as a candidate DM which might be instrumental in contributing to the observed relic density or may be detected through ongoing direct or indirect search experiments. The local DM density is observed with some uncertainty to be 0.4GeV/cm^3 [134]. Earlier measurements by WMAP [8] and more recent observation by PLANCK satellite [29] indicate 85% of matter content of the Universe to be DM with its relic density

$$\Omega_{\text{dm}} h^2_{\text{Hubble}} = 0.1198 \pm 0.0026 \tag{38}$$

where h_{Hubble} is the Hubble parameter. Various attractive models have been proposed to explain the observed relic density of dark matter and its stability with half-life greater than the age of the universe, $\tau_{DM} > 10^{17}$s. Attempts in this direction include addition of scalar or fermionic dark matter candidates to the RH neutrino (RHν) extended SM. Following the work of Lee-Weinberg [135] and in big-bang cosmology, a weakly interacting massive particle (WIMP) has enjoyed a special status as a DM candidate as it can naturally explain the observed relic density. Model independent upper bound on the WIMP DM mass has been also derived from perturbative unitarity [136] with $M_{\text{WIMP}} \leq 100$ TeV. Recently extensive investigations have been made to explore possible special symmetries underlying the dynamics of DM [137–139].

5.1.1. Direct Detection of Dark Matter. Since DM particles are electrically neutral and cosmologically stable, they are referred to as missing energy at colliders where searches for DM mainly focus on the detection of visible signals like jets and charged leptons. At colliders we can study DM either through investigating its direct detection signals or indirect detection signals. The scalar singlet DM in our model may be discovered through direct and indirect signals. In particular, XENON1T experiment may discover or rule out the scalar singlet DM for reasonable values of DM mass and Higgs portal coupling, rejecting its nonperturbative values higher than 1.5 TeV [140, 141] .

Several terrestrial experiments like CDMS [142, 143], DAMA/NAI [144, 145], XEXNON100 [16], and LUX [18] are still going on around the globe for direct detection of dark matter. These underground detectors are constructed using various targets made up of Xe, Ge, NaI, etc. in an attempt to explore either electronic or nuclear scatterings at low energies. In this case, the recoil energy is usually observed from the scattering between DM particles and nucleons [146] or from scattering between electrons and dark matter. The direct search experiments, XENON100 [16] and LUX, predict an upper bound in the $M_{DM} - \sigma_{DM}$ plane where σ_{DM} represents DM elastic scattering cross section and M_{DM} stands for DM mass. These experiments furnish very stringent bounds on dark matter-nucleon scattering cross section for different DM masses. For example, LUX and XENON100 experiments predict similar DM-nucleon cross section bound at around 10^{-44}cm^2 for a DM mass of 1000 GeV whereas XENON1T search predicts a smaller cross section bound $2 \times 10^{-46}\text{cm}^2$ for the same DM mass keeping the DM relic density in the right ballpark [147, 148]. A concise review of current status of scalar singlet dark matter is available in [149] where references to most of the recent experimental and phenomenological investigations are available. In general, for elastic scattering of a DM particle off nucleons, either a standard Higgs or a Z-boson exchange is needed in the t-channel of the dominant tree diagrams. Even though the singlet scalar DM $\xi(1, 0, 1)$ has no gauge interaction, still it can elastically scatter off nucleons in direct search experiments through Higgs exchange via quartic Higgs portal interaction

$$V_{\text{Port}} = \frac{\lambda_{\phi\xi}}{2} \phi^\dagger \phi \xi^2 + h.c, \tag{39}$$

where the standard Higgs VEV and the portal quartic coupling $\lambda_{\phi\xi}$ contribute directly to the cross section in the lowest order.

Although till today no signals in direct detection experiments have been observed except for the controversial DAMA modulation signal, direct detection searches still have the potential to unravel the mystery of DM because of the fact that if a signal is observed, we can correlate the scattering cross section and mass of the DM particle with its local density.

5.1.2. Indirect Detection of Dark Matter. In indirect dark matter detection (IDMD) experiments, the DM particles may annihilate or decay to standard model particles or other exotic final states in a region of high DM density and finally manifest as a visible signal in form of gamma rays, cosmic rays, neutrinos, and positrons or antiparticles. Such events

are expected to exhibit excesses over the desired abundance of the particles in the cosmos. The IDMD searches like Fermi-LAT [19], AMS [150], HESS [151], MAGIC [152], ATIC [153], DAMPE [154], PLANCK [29], ICECUBE [20, 21], etc. basically look for these excesses in the universe to confirm the detection of DM annihilation. For example, DM could be detected through the observation of neutrino fluxes by ICECUBE telescope arising from annihilation dark matter. The IceCube neutrino events have been recently interpreted to be consistent with decaying dark matter mass in the PeV range or larger.

Recently IDMD searches gave several hints for DM detection like lines at 3.5 KeV [155, 156], 130 GeV [157, 158], and the gamma ray excess from the galactic centre [159]. However, no conclusive and consistent information has emerged so far. These signals have been attributed to either astrophysical sources or instrumental effects [160, 161].

Recent data from LUX-2016 and Fermi-LAT [18, 19] have constrained the DM mass as well as its unknown Higgs portal coupling. It can be shown that $\lambda_{\phi\xi} \sim \mathcal{O}(0.01)$ can generate the right relic density with low mass ξ of order 50 GeV. On the other hand direct DM searches from the LUX-16 data have ruled out the existence of scalar DM ξ over a wider mass range $M_\xi \simeq 70 - 500$ GeV. In summary, the scalar dark matter mass can be on the lower side

$$M_\xi < 60\text{GeV}, \tag{40}$$

contributing prominently to relic density, or on the higher side

$$100\text{TeV} > M_\xi > 500\ \text{GeV}. \tag{41}$$

In (41) the LHS is due to the perturbative unitarity bound [135] and the RHS is due to [18].

5.2. Embedding in SU(5). Besides the SU(5) Higgs representations $5_H, 24_H, 15_H$, and 75_H, we further extend its scalar sector by the scalar singlet DM $\xi(1, 0, 1)$ which we assume to be also a SU(5) singlet. Obviously it has no direct gauge boson interaction of any kind. But it has interaction with SM Higgs through Higgs portal of the type shown in (39). Then it can have gauge interaction in higher orders. In any theoretical model, the stability of DM must be ensured such that its lifetime is longer than the lifetime of the universe. Usually a discrete symmetry Z_2 is imposed to safeguard the stability.

We assign all the fermions in $\bar{5}_F$, 10_F, and consequently the SM fermions, to possess $Z_2 = -1$. The Higgs representations $5_H, 24_H, 15_H$, and 75_H are assigned $Z_2 = +1$. Needless to mention that the SM Higgs doublet ϕ, $\kappa(3, 0, 8)$, and $\Delta_L(3, 0, 1)$ have the same value of $Z_2 = +1$. Out of all the scalars only the DM singlet scalar is assigned odd value of $Z_2 = -1$. This assignment prevents direct Yukawa interaction of ξ and ensures its desired stability.

6. Vacuum Stability in SU(5) through Scalar DM

Despite the above predictions on neutrino masses and mixings, coupling unification, and proton lifetime, the SU(5) model with Higgs representations still has the vacuum instability problem. This problem in the SM arises as the standard Higgs potential solely controlled by the standard Higgs field becomes unstable for large values of the field at scales $\mu \geq M_{\text{Inst.}} = 5 \times 10^9$ GeV. As there is no other field so far in the extended SU(5) model for $\mu < M_\Delta (= 10^{12} - 10^{15}\text{GeV})$ to couple through its Higgs portal, the instability problem turns out to be similar to SM. As we have embedded the scalar singlet DM candidate in SU(5) we now investigate the possibility of resolving the vacuum instability through Higgs partial interaction [88, 89, 149].

6.1. RG Equations and Parameters for Higgs Potential. As noted above the standard model Higgs potential

$$V_{SM} = -{\mu_\phi}^2 \phi^\dagger \phi + \lambda_\phi \left(\phi^\dagger \phi\right)^2 \tag{42}$$

develops instability as the Higgs quartic coupling λ_ϕ runs negative at an energy scale $10^9 - 10^{10}$GeV by the renormalization group running. Apart from other interesting suggestions [88, 89] an alternative popular solution to the vacuum instability problem is to extend the SM by a gauge singlet real scalar(ξ) which gives positive contribution to the Higgs quartic coupling and prevents it from becoming negative [88, 162–164]. It is worth mentioning that this scalar singlet can act as potential dark matter candidate termed as weakly interacting massive particle (WIMP) with an extra discrete symmetry $Z_2 : \xi \longrightarrow -\xi$ imposed on it. The scalar singlet is odd under Z_2 symmetry while all other scalars being even and SM fermions being odd under this symmetry. Hence it can not couple to SM particle and become stable. This also matches the discrete symmetry properties of SU(5) representations discussed above. Thus it can serve as a suitable WIMP dark matter particle which is also identified as the SU(5) singlet scalar. The unbroken discrete symmetry of the singlet scalar upto the Planck scale has two important consequences: (i) the ξ VEV is forbidden and (ii) the modified SM potential develops VEV and minima only due to the SM Higgs. The scalar $\kappa(3, 0, 8)$ has no coupling with ϕ. Even if Δ_L and some of its associates have coupling with ϕ, because of their heavy mass, $M_\Delta \gg M_W$, they are treated to have decoupled from the Lagrangian at energy scales below $\mu \sim M_\Delta$.

$\underline{\mu < M_\Delta}$

The potential of the model is modified in presence of the scalar singlet and a new term arises due to interaction of SM doublet (ϕ) with scalar singlet (ξ) and self-interaction of ξ

$$V(\xi, \phi) = V_{\text{SM}} + \frac{\lambda_{\phi\xi}}{2} \phi^\dagger \phi \xi^2 + \frac{\mu_\xi^2}{2} \xi^2 + \frac{\lambda_\xi}{24} \xi^4 \tag{43}$$

where λ_ξ is dark matter self-coupling, $\lambda_{\phi\xi}$ is standard Higgs and extra Higgs scalar interaction coupling or Higgs portal

coupling and μ_ξ is quadratic coupling of extra Higgs scalar. From electroweak scale, up to $\mu = 10^{12}$ GeV, the effective potential is $V'(\xi,\phi) = V_{SM} + V(\xi,\phi)$.

$\underline{\mu > M_\Delta}$

The introduction of the scalar triplet Δ_L of mass $M_\Delta \sim 10^{12}$ GeV changes the Higgs potential further by additional terms $V(\phi,\Delta_L)$ (arising out of interaction of SM doublet with scalar triplet and self-interaction of scalar triplet) and $V(\xi,\Delta_L)$ (arising out of interaction of scalar singlet DM and scalar triplet)

$$V(\xi,\phi,\Delta_L) = V(\xi,\phi) + V(\phi,\Delta_L) + V(\xi,\Delta_L) \tag{44}$$

where

$$\begin{aligned} V(\phi,\Delta_L) &= M_\Delta^2 \mathrm{Tr}\left(\Delta_L^\dagger \Delta_L\right) + \frac{\lambda_1}{2}\left[\mathrm{Tr}\left(\Delta_L^\dagger \Delta_L\right)\right]^2 \\ &+ \frac{\lambda_2}{2}\left(\left[\mathrm{Tr}\left(\Delta_L^\dagger \Delta_L\right)\right]^2 - \mathrm{Tr}\left[\left(\Delta_L^\dagger \Delta_L\right)^2\right]\right) \\ &+ \lambda_4\left(\phi^\dagger\phi\right)\mathrm{Tr}\left(\Delta_L^\dagger \Delta_L\right) \\ &+ \lambda_5 \phi^\dagger\left[\Delta_L^\dagger, \Delta_L\right]\phi \\ &+ \left(\mu_\Delta \widetilde{\phi}^\dagger\left(\frac{\overrightarrow{\tau}.\overrightarrow{\Delta_L}}{\sqrt{2}}\right)^\dagger \phi + \mathrm{h.c.}\right) \\ V(\xi,\Delta_L) &= \lambda_{\xi\Delta_L}\left(\xi^\dagger\xi\right)\left(\Delta_L^\dagger\Delta_L\right). \end{aligned} \tag{45}$$

Sufficiently below the mass scale $\mu = M_\Delta = 10^{12}$ GeV, our model has two scalars: the first one is the SM Higgs(ϕ) given by $\phi = (1/\sqrt{2})(\phi^+, v + h + i\phi^0)^T$ and the second one is extra scalar singlet(ξ) added to the SM. The mass of the extra singlet is given by

$$M_{DM}^2 = \mu_\xi^2 + \frac{\lambda_{\phi\xi}}{2}v^2. \tag{46}$$

We use the standard Higgs mass $m_h = 125$GeV.

Direct detection experiments [18, 19] impose constraints on the Higgs portal coupling ($\lambda_{\phi\xi}$) and dark matter mass [164, 165] derived from observed DM relic density

$$M_{DM} \sim 3300 \times \lambda_{\phi\xi} \tag{47}$$

or

$$\lambda_{\phi\xi} \sim 0.0003 \times M_{DM}, \tag{48}$$

for $M_{DM} \gg m_{\mathrm{top}}$. To be consistent with (41) we use $M_{DM} = m_\xi \sim 1$TeV throughout this work. Similar analysis can be carried out for all values of DM mass > 500 GeV.

These constraint on $\lambda_{\phi\xi}$ given in (48) can be also considerably relaxed if there is more than one WIMP DM candidate of the same or different species including fermions [110, 166].

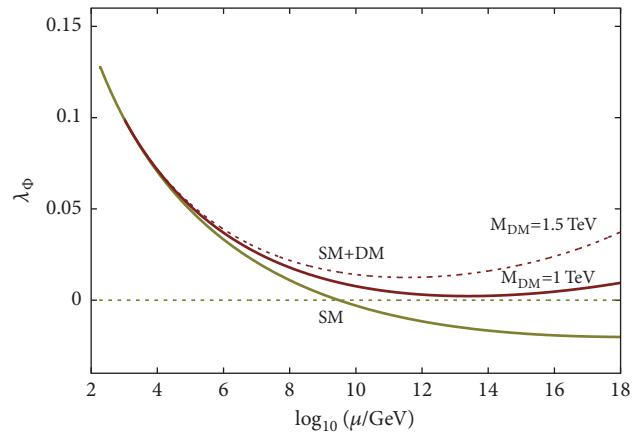

Figure 8: Running of Higgs quartic coupling.

6.2. RG Evolution of Quartic Coupling. Like other couplings of every non-Abelian gauge theory, it is well known that the SM Higgs potential is modified by quantum corrections determined by perturbative renormalization group equations (RGEs) for its running couplings $\eta(\mu)$

$$\frac{d\eta}{dt} = \sum_j \frac{\eta^{(j)}}{(16\pi^2)^j} \tag{49}$$

where $t = \log\mu$, μ is renormalization scale, $\eta(\mu)$ =different couplings (quartic or gauge, or others) at scale μ, and $j = j^{th}$ loop order. The one-loop RG-coefficients of different couplings are presented in the Appendix. For the stability of the Higgs potential (see (43)), the value of self-coupling including corrections must remain positive throughout the course of its evolution up to the Planck scale.

The running of Higgs quartic coupling $\lambda_\phi(\mu)$ with energy scale μ is shown in Figure 8.

In the figure, at first, we have neglected possible threshold effects due to Higgs triplet at $\mu = M_\Delta$ being determined as one of the solutions to neutrino oscillation data. Negligible Δ_L- threshold effect can also result for $\mu_\Delta \ll M_\Delta$. We have used the initial values of different coupling constants at top-quark mass scale ($\mu = m_{\mathrm{top}}$) as given in Table 6 and subsequently evolved them from m_t to Planck scale with the help of RGEs.

From Figure 8, it is clear that the desired quartic coupling remains stable up to the Planck scale for $\lambda_{\phi\xi} = 0.36$ and $M_{DM} = 1$ TeV.

6.3. Higgs Triplet Threshold Effect. Threshold effect due to heavier Higgs masses which couple to ϕ through their portals has been discussed in general [88, 89] and in specific cases [167, 168]. In our case the Higgs triplet mass used to fit the neutrino oscillation data is $M_\Delta \sim 10^{12}$ GeV and its induced VEV is $\mathcal{O}(1-10)$ eV. In such a case the threshold effect caused by the triplet VEV correction term is [88]

$$\Delta\lambda_\phi = \lambda_{\phi\Delta}\frac{v_L^2}{M_\Delta^2} \sim 10^{-36} \tag{50}$$

Table 6: Initial values of coupling constants at top quark mass.

Coupling constants	$\lambda_\phi(m_t)$	$\lambda_\xi(m_t)$	$\lambda_{\phi\xi}(m_t)$	$g_{1Y}(m_t)$	$g_{2L}(m_t)$	$g_{3C}(m_t)$	$y_t(m_t)$
Initial values	0.1296	0.1	0.36	0.35	0.64	1.16	0.94

The remaining threshold effect could be due the self-energy correction or the trilinear term $\mu_\Delta \Delta_L \phi\phi + h.c$ in the Higgs potential giving rise to threshold correction to quartic coupling

$$\Delta\lambda_\phi \equiv \lambda_{\mathrm{TH}} = \frac{\mu_\Delta^2}{M_\Delta^2} \tag{51}$$

Denoting the effective Higgs quartic coupling by $\lambda'(\mu)$ for $\mu \geq M_\Delta$ this is related to the quartic coupling $\lambda_\phi(\mu)$ at $\mu = M_\Delta$ [88]

$$\lambda_\phi(M_\Delta) = \lambda'(M_\Delta) - \lambda_{\mathrm{TH}}. \tag{52}$$

This correction comes into play when the running mass scale is $\mu \sim M_\Delta$ and larger.

We point out that the same values of Majorana Yukawa coupling elements of Y derived in Section 2 are valid up to a scale factor for a wide range of values of trilinear coupling mass parameter $\mu_\Delta < M_\Delta^0$ for which this threshold effect is well within the perturbative regime. We note from (8) that the mass formula gives the scaling relation

$$Y = Y^0 \frac{v_L^0}{v_L} = Y^0 \frac{\mu_\Delta^0}{\mu_\Delta}, \tag{53}$$

where we have used the zero superscript for values at $\mu_\Delta^0 = M_\Delta = 10^{12}$ GeV. Thus, for the values of neutrino mass and mixing given by the oscillation data, a new set of elements of Y are derived for any $\mu_\Delta < \mu_\Delta^0$ by multiplying all the vales given in Tables 2 and 3 by the same scale factor μ_Δ^0/μ_Δ.

In Figure 9 we have presented evolution of Higgs quartic couplings below and above $\mu = M_\Delta$ for $\lambda_{\mathrm{TH}} = 0.1$. Using the notations of the Appendix, we have used the initial values of different coupling constants at scalar triplet mass scale (M_Δ) as $\lambda_1 = \lambda_2 = \lambda_4 = 0.1$ and $\lambda_5 = 0.1$.

For all the three curves given in Figure 9 the scalar DM mass has been fixed at $M_{\mathrm{DM}} = 1$ TeV consistent with LUX:2016 data. The curve labeled as SM+DM+Δ includes threshold effect $\lambda_{\mathrm{TH}} = 0.1$ at $\mu = M_\Delta = 10^{12}$ GeV corresponding to $\mu_\Delta \sim (1/3)M_\Delta$. We have checked that even after including the heavy scalar threshold effect the quartic coupling remains perturbatively positive upto the Planck scale for $\mu_\Delta/M_\Delta \simeq 0.5$. (Denoting $\Phi_H = 24_H$, above the mass scale $\mu > M_{\mathrm{GUT}}$ we impose the well known discrete symmetry $\Phi_H \longrightarrow -\Phi_H$ which is usually assumed in the minimal SU(5) model. Without loss of generality we further assume the Higgs portal coupling $\lambda_{5_H,75_H}$ to be negligible.)

Thus, the issue of vacuum stability of SM Higgs potential is resolved through the embedding of ξ as a WIMP dark matter candidate in SU(5) even after including the heavy Higgs triplet threshold effect which could be verified by direct search experiments and LHC.

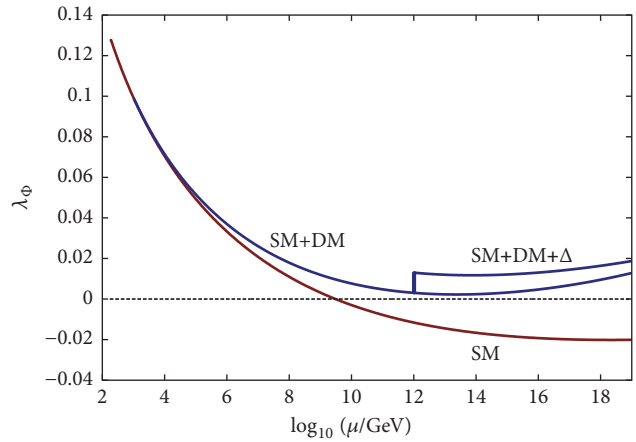

Figure 9: Running of standard Higgs quartic coupling including heavy triplet scalar threshold effect at $\mu = M_\Delta = 10^{12}$ GeV derived from fits to neutrino oscillation data. The curves labeled as SM, SM+DM, and SM+DM+Δ denote contributions due to SM alone, SM plus DM, and SM plus DM plus Higgs triplet threshold effect, respectively, as described in the text. The scalar DM mass has been fixed at $M_{\mathrm{DM}} = 1.0$ TeV consistent with LUX:2016 experimental data.

7. Summary and Conclusion

In this work we have attempted to resolve four limitations of the minimal SU(5) model by extending its scalar sector beyond 5_H and 24_H. Added presence of 15_H and 75_H is noted to account for precision coupling unification with experimentally verifiable proton lifetime for $p \longrightarrow e^+\pi^0$, and type-II seesaw ansatz for neutrino masses. The left-handed triplet Higgs mass in this model is bounded from below ($M_\Delta = M_{15_H}$) $\geq$ ($M_\kappa = 10^{9.23}$) GeV. Proton lifetime is predicted by taking into account sources of theoretical uncertainties due to GUT threshold effects and those due to electroweak precision parameters. Type-II seesaw scale effect on proton lifetime prediction is also discussed. The limitation due to vacuum stability of the Higgs potential in SU(5) is resolved by the inclusion of a scalar singlet near the TeV scale that acts as a WIMP dark matter candidate. All the fermions and this scalar are assigned to be odd under a dark matter stabilising Z_2 discrete symmetry whereas the SM Higgs is even. The scalar dark matter mass is consistent with current experimental LUX-2016 bound on direct search experiments. Renormalization group evolution of SM Higgs quartic coupling modified by Higgs portal coupling of this scalar DM completely alleviates the vacuum instability problem. We emphasize that no nonstandard Higgs field, except the scalar DM singlet, is present in this model below the κ mass $M_\kappa = 10^{9.23}$ GeV.

We thus conclude that such SM limitations as neutrino mass, coupling unification, proton lifetime, WIMP dark matter, and vacuum stability can be effectively resolved by extending the scalar sector of SU(5) to include $5_H, 24_H, 75_H, 15_H$, and 1_H. At present we need no extension on the established fermion structure of the SM and SU(5) or their minimal gauge structure. The remaining limitations on baryon asymmetry generation and/or the possibility of decaying dark matter projected to manifest as PeV energy IceCube neutrinos will be addressed elsewhere [169, 170].

Appendix

Renormalization Group Equations for Higgs Scalar Couplings

The RGEs for scalar quartic couplings [60–62, 168] in our model at one loop level are given by

$$16\pi^2 \frac{dC}{dt} = \beta_C \quad \left(C = \lambda_\phi, \lambda_{\phi\xi}, \lambda_\xi, \lambda_1, \lambda_2, \lambda_4, \lambda_5\right) \tag{A.1}$$

where

$$\begin{aligned}
&\beta_{\lambda_\phi} \\
&= 24\lambda_\phi^2 + 12\lambda_\phi y_t^2 - 6y_t^4 - 3\lambda_\phi\left(g_{1Y}^2 + 3g_{2L}^2\right) \\
&\quad + \frac{3}{8}\left[2g_{2L}^4 + \left(g_{1Y}^2 + g_{2L}^2\right)^2\right] + \frac{\lambda_{\phi\xi}^2}{2} \\
&\beta_{\lambda_{\phi\xi}} \\
&= \left\{4\lambda_{\phi\xi} + 12\lambda_\phi + 6y_t^2 - \frac{3}{2}\left(g_{1Y}^2 + 3g_{2L}^2\right) + \lambda_\xi\right\}\lambda_{\phi\xi} \\
&\beta_{\lambda_\xi} = 3\lambda_\xi^2 + 12\lambda_{\phi\xi}^2
\end{aligned} \tag{A.2}$$

For Standard model RG running in the energy scale $\mu < M_{DM}$, the term $\lambda_{\phi\xi}/2$ in β_{λ_ϕ} in (A.3) is to be ignored. The RGEs for SM gauge couplings and top-quark Yukawa coupling at two-loop level are given by

$$\begin{aligned}
\frac{dy_t}{dt} &= \frac{1}{16\pi^2}\left(\frac{9}{2}y_t^2 - \frac{17}{12}g_{1Y}^2 - \frac{9}{4}g_{2L}^2 - 8g_{3C}^2\right)y_t \\
&\quad + \frac{1}{\left(16\pi^2\right)^2}\left[-\frac{23}{4}g_{2L}^4 - \frac{3}{4}g_{2L}^2 g_{1Y}^2 + \frac{1187}{216}g_{1Y}^4\right. \\
&\quad + 9g_{2L}^2 g_{3C}^2 + \frac{19}{9}g_{3C}^2 g_{1Y}^2 - 108g_{3C}^4 \\
&\quad + \left(\frac{225}{16}g_{2L}^2 + \frac{131}{16}g_{1Y}^2 + 36g_{3C}^2\right)y_t^2 \\
&\quad \left. + 6\left(-2y_t^4 - 2y_t^2\lambda_\phi + \lambda_\phi^2\right)\right] \\
\frac{dg_{1Y}}{dt} &= \frac{1}{16\pi^2}\left(\frac{41}{6}g_{1Y}^3\right) + \frac{1}{\left(16\pi^2\right)^2}\left(\frac{199}{18}g_{1Y}^2\right. \\
&\quad \left. + \frac{9}{2}g_{2L}^2 + \frac{44}{3}g_{3C}^2 - \frac{17}{6}y_t^2\right)g_{1Y}^3 \\
\frac{dg_{2L}}{dt} &= \frac{1}{16\pi^2}\left(-\frac{19}{6}g_{2L}^3\right) + \frac{1}{\left(16\pi^2\right)^2}\left(\frac{3}{2}g_{1Y}^2\right. \\
&\quad \left. + \frac{35}{6}g_{2L}^2 + 12g_{3C}^2 - \frac{3}{2}y_t^2\right)g_{2L}^3 \\
\frac{dg_{3C}}{dt} &= \frac{1}{16\pi^2}\left(-7g_{3C}^3\right) + \frac{1}{\left(16\pi^2\right)^2}\left(\frac{11}{6}g_{1Y}^2 + \frac{9}{2}g_{2L}^2\right. \\
&\quad \left. - 26g_{3C}^2 - 2y_t^2\right)g_{3C}^3
\end{aligned} \tag{A.3}$$

After $\mu = 10^{12}$ GeV the scalar triplet Δ_L is introduced and we use the modified RG equations of λ_ϕ and other couplings relevant for this scalar triplet.

$$\begin{aligned}
\beta_{\lambda_\phi} &= \lambda_\phi\left[12\lambda_\phi - \left(\frac{9}{5}g_{1Y}^2 + 9g_{2L}^2\right) + 12y_t^2\right] \\
&\quad + \frac{9}{4}\left(\frac{3}{25}g_{1Y}^4 + \frac{2}{5}g_{1Y}^2 g_{2L}^2 + g_{2L}^4\right) + 6\lambda_4^2 + 4\lambda_5^2 \\
&\quad - 12y_t^4,
\end{aligned} \tag{A.4}$$

$$\begin{aligned}
\beta_{\lambda_1} &= \lambda_1\left[14\lambda_1 + 4\lambda_2 - \left(\frac{36}{5}g_{1Y}^2 + 24g_{2L}^2\right)\right. \\
&\quad \left. + 4\mathrm{tr}\,[T]\right] + \frac{108}{25}g_{1Y}^4 + \frac{72}{5}g_{1Y}^2 g_{2L}^2 + 18g_{2L}^4 + 2\lambda_2^2 \\
&\quad + 4\lambda_4^2 + 4\lambda_5^2 - 8\mathrm{tr}\left[T^2\right],
\end{aligned} \tag{A.5}$$

$$\begin{aligned}
\beta_{\lambda_2} &= \lambda_2\left[12\lambda_1 + 3\lambda_2 - \left(\frac{36}{5}g_{1Y}^2 + 24g_{2L}^2\right)\right. \\
&\quad \left. + 4\mathrm{tr}\,[T]\right] - \frac{144}{5}g_{1Y}^2 g_{2L}^2 + 12g_{2L}^4 - 8\lambda_5^2 \\
&\quad + 8\mathrm{tr}\left[T^2\right],
\end{aligned} \tag{A.6}$$

$$\begin{aligned}
\beta_{\lambda_4} &= \lambda_4\left[6\lambda_\phi + 8\lambda_1 + 2\lambda_2 + 4\lambda_4\right. \\
&\quad \left. - \left(\frac{9}{2}g_{1Y}^2 + \frac{33}{2}g_{2L}^2\right) + 6y_t^2 + 2\mathrm{tr}\,[T]\right] + \frac{27}{25}g_{1Y}^4 \\
&\quad + 6g_{2L}^4 + 8\lambda_5^2 - 4\mathrm{tr}\left[T^2\right],
\end{aligned} \tag{A.7}$$

$$\begin{aligned}
\beta_{\lambda_5} &= \lambda_5\left[2\lambda + 2\lambda_1 - 2\lambda_2 + 8\lambda_4 - \left(\frac{9}{2}g_{1Y}^2 + \frac{33}{2}g_{2L}^2\right)\right. \\
&\quad \left. + 6y_t^2 + 2\mathrm{tr}\,[T]\right] - \frac{18}{5}g_{1Y}^2 g_{2L}^2 + 4\mathrm{tr}\left[T^2\right],
\end{aligned} \tag{A.8}$$

where T is defined as $T = Y^{\dagger}Y$ and its beta function is expressed through the relation

$$\beta_T = T\left[6T - 3\left(\frac{3}{5}g_{1Y}^2 + 3g_{2L}^2\right) + 2tr\left[T\right]\right]. \quad (A.9)$$

Data Availability

The data used to support the findings of this study are available from the corresponding author upon request.

Conflicts of Interest

The authors declare that they have no conflicts of interest.

Acknowledgments

M. K. Parida acknowledges financial support under the Project ddd SB/S2/HEP-011/2013 from the Department of Science and Technology, Government of India. Financial support from Siksha 'O' Anusandhan (SOA), Deemed to be University, to Mainak Chakraborty for a Postdoctoral fellowship and to Biswonath Sahoo for a Ph. D. research fellowship is acknowledged.

References

[1] P. F. de Salas, D. V. Forero, C. A. Ternes, M. Tortola, and J. W. Valle, "Status of neutrino oscillations 2018: 3σ hint for normal mass ordering and improved CP sensitivity," *Physics Letters. B. Particle Physics, Nuclear Physics and Cosmology*, vol. 782, pp. 633–640, 2018.

[2] T. Schwetz, M. Tórtola, and J. W. Valle, "Global neutrino data and recent reactor fluxes: the status of three-flavour oscillation parameters," *New Journal of Physics* , vol. 13, no. 6, p. 063004, 2011.

[3] D. Forero, M. Tortola, and J. Valle, "Neutrino oscillations refitted," *Physical Review D: Particles, Fields, Gravitation and Cosmology*, vol. 90, no. 9, Article ID 093006, 10 pages, 2014.

[4] G. L. Fogli, E. Lisi, A. Marrone, D. Montanino, A. Palazzo, and A. M. Rotunno, "Global analysis of neutrino masses, mixings and phases: entering the era of leptonic CP violation searches," *Physical Review D: Particles, Fields, Gravitation and Cosmology*, vol. 86, Article ID 013012, 2012.

[5] J. Bergström, M. C. Gonzalez-Garcia, M. Maltoni, and T. Schwetz, "Bayesian global analysis of neutrino oscillation data," *Journal of High Energy Physics*, vol. 2015, no. 9, 2015.

[6] F. Zwicky, "Die rotverschiebung von extragalaktischen nebeln," *Helvetica Physica Acta*, vol. 6, pp. 110–127, 1933.

[7] F. Zwicky, "Republication of: The redshift of extragalactic nebulae," *General Relativity and Gravitation*, vol. 41, pp. 207–224, 2009.

[8] WMAP Collaboration, D. N. Spergel et al., "Wilkinson Microwave Anisotropy Probe(WMAP) three year results: implications for cosmology," *The Astrophysical Journal Supplement Series*, vol. 170, Article ID 0603449, p. 377, 2007.

[9] J. Einasto, ""Dark Matter", Astronomy and Astrophysics 2010," in *Encyclopedia of Life Support Systems (EOLSS)*, O. Engvold, R. Stabell, B. Czerny, and J. Lattanzio, Eds., Eolss Publishers, Oxford,UK, 2010, Developed under the Auspices of the UNESCO.

[10] G. R. Blumenthal, S. M. Faber, J. R. Primack, and M. J. Rees, "Formation of galaxies and large-scale structure with cold dark matter," *Nature*, vol. 311, no. 5986, pp. 517–525, 1984.

[11] J. Angle et al., "A search for light dark matter in XENON10 data," *Physical Review Letters*, vol. 107, Article ID 051301, 2011.

[12] J. Angle et al., "Erratum: Search for light dark matter in XENON10 data," *Physical Review Letters*, vol. 110, 2013.

[13] L. E. Strigari, "Galactic searches for dark matter," *Physics Reports*, vol. 531, no. 1, pp. 1–88, 2013.

[14] V. C. Rubin and W. K. Ford, "Rotation of the andromeda nebula from a spectroscopic survey of emission regions," *The Astrophysical Journal*, vol. 159, p. 379, 1970.

[15] D. Clowe, M. Bradač, A. H. Gonzalez et al., "A direct empirical proof of the existence of dark matter," *The Astrophysical Journal*, vol. 648, no. 2, pp. L109–L113, 2006.

[16] E. Aprile et al., "Dark Matter Results from 225 Live Days of XENON100 Data," *Physical Review Letters*, vol. 109, Article ID 181301, 2012.

[17] D. S. Akerib et al., "First results from the LUX dark matter experiment at the Sanford Underground Research Facility," *Physical Review Letters*, vol. 112, Article ID 091303, 2014.

[18] D. S. Akerib et al., "Results from a Search for Dark Matter in the Complete LUX Exposure," *Physical Review Letters B*, vol. 118, no. 2, Article ID 021303, 2017.

[19] M. Ajello et al., "Fermi-LAT Observations of High Energy γ-ray Emission Toward the Galactic Center," *The Astrophysical Journal*, vol. 819, no. 1, p. 44, 2016, arXiv:1511.02938.

[20] M. G. Aartsen, "Evidence for high-energy extraterrestrial neutrinos at the IceCube detector," *Science*, vol. 342, no. 6161, Article ID 1242856, 2013.

[21] M. G. Artsen et al., "Observation of High-Energy Astrophysical Neutrinos in Three Years of IceCube Data," *Physical Review Letters*, vol. 113, Article ID 101101, 2014.

[22] M. G. Artsen et al., "Lowering IceCube's Energy Threshold for Point Source Searches in the Southern Sky," *The Astrophysical Journal*, vol. 824, no. 2, 2016.

[23] IceCube, ANTARES Collaboration, S. Adrian-Martinez et al., "The First Combined Search for Neutrino-Point Sources in the Southern Hemisphere," *The Astrophysical Journal*, vol. 823, no. 1, p. 65, 2016.

[24] CMS Collaboration, A. M. Sirunyan et al., "Search for dark matter produced in association with heavy-flavor quarks in proton-proton collisions at sqrt(s)=13 TeV," High Energy Physics, 2017, CMS-EXO-16-005, CERN-EP-2017-087.

[25] A. M. Sirunyan et al., "Search for associated production of dark matter with a Higgs boson decaying to bb or $\gamma\gamma$ at s=13 TeV," in *JHEP*, vol. 1710, 180 edition, 2017, arXiv:1703.05236.

[26] D. N. Spergel et al., "First year Wilkinson Microwave Anisotropy Probe (WMAP) Observations: Determination of Cosmological Parameters," *The Astrophysical Journal Supplement Series*, vol. 148, p. 175, 2003.

[27] WMAP Collaboration, E. Komatsu et al., "Seven-Year Wilkinson Microwave Anisotropy Probe (WMAP) Observations: Cosmological Interpretation," *The Astrophysical Journal Supplement Series*, vol. 192, p. 18, 2011, arXiv:1001.4538.

[28] WMAP Collaboration, G. Hindshaw et al., "Five-Year Wilkinson Microwave Anisotropy Probe (WMAP) Observations: Data Processing, Sky Maps and Basic Results," *The Astrophysical Journal Supplement Series*, vol. 180, p. 225, 2009, arXiv:0803.0732.

[29] Planck Collaboration, P. A. Ade et al., "Planck 2015 results. XIII. Cosmological parameter," *Astron Astrophys*, vol. 59, p. pp, 2015, arXiv:1502.01589.

[30] J. C. Pati and A. Salam, "Lepton number as the fourth 'color'," *Physical Review D: Particles, Fields, Gravitation and Cosmology*, vol. 10, no. 1, pp. 275–289, 1974.

[31] J. C. Pati and A. Salam, "Erratum: Lepton number as the fourth 'color'," *Physical Review D: Particles, Fields, Gravitation and Cosmology*, vol. 11, pp. 275–289, 1975.

[32] H. Georgi and S. L. Glashow, "Unity of all elementary-particle forces," *Physical Review Letters*, vol. 32, no. 8, pp. 438–441, 1974.

[33] H. Georgi, "The State of the Art—Gauge Theories," in Particles and Fields, Williamsburg, Virginia (1974), AIP Conf. Proc. 23 (1975) 575.

[34] H. Fritzsch and P. Minkowski, "Unified interactions of leptons and hadrons," *Annals of Physics*, vol. 93, no. 1-2, pp. 193–266, 1975.

[35] P. Langacker, "Grand unified theories and proton decay," *Physics Reports*, vol. 72, no. 4, pp. 185–385, 1981.

[36] R. Slansky, "Group theory for unified model building," *Physics Reports*, vol. 79, no. 1, pp. 1–128, 1981.

[37] P. Nath and P. Fileviez Perez, "Proton stability in grand unified theories, in strings and in branes," *Physics Reports*, vol. 441, no. 5-6, pp. 191–317, 2007.

[38] G. Senjanovic, "Neutrino mass: from LHC to grand unification," *La Rivista del Nuovo Cimento*, vol. 34, pp. 1–68, 2011.

[39] G. Senjanovic and V. Tello, "Origin of Neutrino Mass," in *Proceedings of the 18th International Conference From the Planck Scale to the Electroweak Scale*, p. 141, Ioannina, Greece, May 2015.

[40] G. Altarelli, "Neutrinos Today: An Introduction," in *Proceedings of the in Proceedings: 49th Recontres de Moriond on Electroweak Interactons and Unified Theories*, Thuile, Italy, 2014.

[41] A. Y. Smirnov, "Theories of Neutrino Masses and Mixings," *Il Nuovo Cimento C*, vol. 37, no. 3, 2014.

[42] R. N. Mohapatra, "From old symmetries to new symmetries: Quarks, leptons and B - L," *50 Years of Quarks*, pp. 245–263, 2015.

[43] R. N. Mohapatra, "Neutrino mass as a signal of TeV scale physics," *Nuclear Physics B*, vol. 908, pp. 423–435, 2016.

[44] O. G. Miranda and J. W. Valle, "Neutrino oscillations and the seesaw origin of neutrino mass," *Nuclear Physics B*, vol. 908, pp. 436–455, 2016.

[45] M. K. Parida and B. P. Nayak, "Singlet Fermion Assisted Dominant Seesaw with Lepton Flavor and Number Violations and Leptogenesis," *Advances in High Energy Physics*, vol. 2017, Article ID 4023493, 24 pages, 2017.

[46] P. Minkowski, "$\mu \longrightarrow e\gamma$ at a rate of one out of 10^9 muon decays?" *Physics Letters B*, vol. 67, pp. 421–428, 1977.

[47] M. Gell-Mann, P. Ramond, and R. Slansky, *Supergravity*, P. van Nieuwenhuizen and D. Freedman, Eds., North-Holland, 1979.

[48] S.L. Glashow, in Quarks and Leptons, Cargèse, eds. M. Lévy et al., Plenum, 1980, New-York, p. 707.

[49] T. Yanagida, in *Proceedings of the Workshop on the Unified Theory and the Baryon Number in the Universe*, O. Sawada and A. Sugamoto, Eds., p. 95, Tsukuba, 1979, KEK Report No. 79-18.

[50] R. N. Mohapatra and G. Senjanovic, "Neutrino mass and spontaneous parity nonconservation," *Physical Review Letters*, vol. 44, p. 912, 1980.

[51] J. Schechter and J. W. F. Valle, "Neutrino masses in $SU(2) \otimes U(1)$ theories," *Physical Review D: Particles, Fields, Gravitation and Cosmology*, vol. 22, p. 2227, 1980.

[52] J. Schechter and J. W. F. Valle, "Neutrino decay and spontaneous violation of lepton number," *Physical Review D: Particles, Fields, Gravitation and Cosmology*, vol. 25, p. 774, 1982.

[53] T. Cheng and L.-F. Li, "Neutrino masses, mixings, and oscillations in $SU(2) \times U(1)$ models of electroweak interactions," *Physical Review D: Particles, Fields, Gravitation and Cosmology*, vol. 22, no. 11, pp. 2860–2868, 1980.

[54] M. Magg, C. Wetterich, and B. Phys. Lett, "Neutrino mass problem and gauge hierarchy," *Physics Letters B*, vol. 94, pp. 61–64, 1980.

[55] G. Lazarides, Q. Shafi, and C. Wetterich, "Proton lifetime and fermion masses in an SO(10) model," *Nuclear Physics Section B*, vol. 181, no. 2, pp. 287–300, 1981.

[56] R. N. Mohapatra and G. Senjanović, "Neutrino masses and mixings in gauge models with spontaneous parity violation," *Physical Review D: Particles, Fields, Gravitation and Cosmology*, vol. 23, article 165, 1981.

[57] E. Ma and U. Sarkar, "Neutrino masses and leptogenesis with heavy higgs triplets," *Physical Review Letters*, vol. 80, no. 26, article 5716, 1998.

[58] R. Foot, H. Lew, X. G. He, and G. C. Joshi, "See-saw neutrino masses induced by a triplet of leptons," *Zeitschrift für Physik C: Particles and Fields*, vol. 44, no. 3, pp. 441–444, 1989.

[59] E. Ma, "Pathways to naturally small neutrino masses," *Physical Review Letters*, vol. 81, p. 1171, 1998.

[60] B. Bajc and G. Senjanovic, "Seesaw at LHC," *Journal of High Energy Physics. A SISSA Journal*, vol. 0708, no. 014, 2007.

[61] A. Arhrib, B. Bajc, D. K. Ghosh et al., " Collider signatures for the heavy lepton triplet in the type ," *Physical Review D: Particles, Fields, Gravitation and Cosmology*, vol. 82, no. 5, 2010.

[62] B. Bajc, M. Nemevsek, and G. Senjanovic, "Probing seesaw at LHC," *Physical Review D*, vol. 76, Article ID 055011, 2007.

[63] E. Akhmedova, M. Lindnerb, E. Schnapkab, and J. Vallec, "Left-right symmetry breaking in NJL approach," *Physics Letters B*, vol. 368, no. 4, pp. 270–280, 1996.

[64] M. Malinsky, J. Romao, and J. Valle, "Supersymmetric SO(10) seesaw mechanism with low $B-L$ scale," *Physical Review Letters*, vol. 95, Article ID 161801, 2005.

[65] R. N. Mohapatra and J. W. F. Valle, "Neutrino mass and baryon-number nonconservation in superstring models," *Physical Review D: Particles, Fields, Gravitation and Cosmology*, vol. 34, no. 5, pp. 1642–1645, 1986.

[66] R. N. Mohapatra, "Mechanism for understanding small neutrino mass in superstring theories," *Physical Review Letters*, vol. 56, no. 6, pp. 561–563, 1986.

[67] C. H. Albright, "Search for a solution of the superstring neutrino mass problem without a high intermediate energy scale," *Physics Letters B*, vol. 178, no. 2-3, pp. 219–225, 1986.

[68] E. Witten, "New issues in manifolds of SU(3) holonomy," *Nuclear Physics B*, vol. 268, no. 1, pp. 79–112, 1986.

[69] S. Nandi and U. Sarkar, "Solution to the neutrino-mass problem in superstring E6 theory," *Physical Review Letters*, vol. 56, no. 6, pp. 564–567, 1986.

[70] E. Ma, "Lepton-number nonconservation in E6 superstring models," *Physics Letters B*, vol. 191, no. 3, pp. 287–289, 1987.

[71] D. Wyler and L. Wolfenstein, "Massless neutrinos in left-hand symmetric models," *Nuclear Physics B*, vol. 218, no. 1, pp. 205–214, 1983.

[72] J. Bernabeu, A. Santamaria, and J. Vidal, "Lepton flavour nonconservation at high energies in a superstring inspired standard model," *Physics Letters B*, vol. 187, pp. 303–308, 1987.

[73] J. W. F. Valle, "Gauge theories and physics of neutrino mass," *Progress in Particle and Nuclear Physics*, pp. 91–171, 1991.

[74] M. K. Parida, R. L. Awasthi, and P. K. Sahu, "Proton decay and new contributions to $0\nu2\beta$ decay in SO(10) with low-mass $Z^{'}$ boson, observable $n-\overline{n}$ oscillation, lepton flavor violation, and rare kaon decay," *Journal of High Energy Physics*, vol. 2015, article 45, 2015.

[75] R. L. Awasthi and M. K. Parida, "Inverse seesaw mechanism in nonsupersymmetric SO(10), proton lifetime, nonunitarity effects, and a low-mass $Z^{'}$ boson," *Physical Review D: Particles, Fields, Gravitation and Cosmology*, vol. 86, no. 9, Article ID 093004, 2012.

[76] M. Reig, D. Restrepo, J. W. F. Valle, and O. Zapata, *Bound-state dark matter and Dirac neutrino mass*, arXiv:1803.08528.

[77] S. Centelles Chuliá, R. Srivastava, and J. W. Valle, "Seesaw roadmap to neutrino mass and dark matter," *Physics Letters. B. Particle Physics, Nuclear Physics and Cosmology*, vol. 781, pp. 122–128, 2018.

[78] S. Weinberg, *Living in the Universe, or Multi Universe*, B. J. Carr, Ed., Cambridge University Press, 2007.

[79] S. M. Barr, "New approach to flavor symmetry and an extended naturalness principle," *Physical Review D: Particles, Fields, Gravitation and Cosmology*, vol. 82, no. 5, 2010.

[80] D. Chang, R. N. Mohapatra, and M. K. Parida, "Decoupling of parity- and SU(2)R-breaking scales: a new approach to left-right symmetric models," *Physical Review Letters*, vol. 52, no. 13, pp. 1072–1075, 1984.

[81] D. Chang, R. N. Mohapatra, and M. K. Parida, "New approach to left-right-symmetry breaking in unified gauge theories," *Physical Review D: Particles, Fields, Gravitation and Cosmology*, vol. 30, no. 5, article 1052, 1984.

[82] D. Chang, R. N. Mohapatra, J. M. Gipson, R. E. Marshak, and M. K. Parida, "Experimental tests of new SO(10) grand unification," *Physical Review D: Particles, Fields, Gravitation and Cosmology*, vol. 31, no. 7, pp. 1718–1732, 1985.

[83] P. Langacker and N. Polonsky, "Uncertainties in coupling constant unification," *Physical Review D: Particles, Fields, Gravitation and Cosmology*, vol. 47, no. 9, pp. 4028–4045, 1993.

[84] E. Ma and D. Suematsu, "Fermion triplet dark matter and radiative neutrino mass," *Modern Physics Letters A*, vol. 24, no. 8, pp. 583–589, 2009.

[85] D. Meloni, T. Ohlsson, and S. Riad, "Renormalization Group Running of Fermion Observables in an Extended Non-Supersymmetric SO(10) Model," in *JHEP*, vol. 3, p. 45, 2017, arXiv:1612.07973.

[86] C. Das and M. Parida, "New formulas and predictions for running fermion masses at higher scales in SM, 2HDM, and MSSM," *The European Physical Journal C*, vol. 20, no. 1, pp. 121–137, 2001.

[87] M. K. Parida, P. K. Patra, and A. K. Mohanty, "Gravity-induced large grand-unification mass in SU(5) with higher-dimensional operators," *Physical Review D: Particles, Fields, Gravitation and Cosmology*, vol. 39, no. 1, pp. 316–322, 1989.

[88] J. Elias-Miró, J. R. Espinosa, G. F. Giudice, H. M. Lee, and A. Strumia, "Stabilization of the electroweak vacuum by a scalar threshold effect," *Journal of High Energy Physics*, vol. 2012, article 31, 2012.

[89] O. Lebedev, "On stability of the electroweak vacuum and the Higgs portal," *The European Physical Journal C*, vol. 72, no. 7, 2012.

[90] S. Chigusa, T. Moroi, and Y. Shoji, "Decay rate of electroweak vacuum in the standard model and beyond," *Physical Review D: Particles, Fields, Gravitation and Cosmology*, vol. 97, no. 11, 2018.

[91] E. Ma, "Efficacious additions to the Standard Model," *Physics Letters B*, vol. 625, no. 1-2, pp. 76–78, 2005.

[92] I. Doršner, S. Fajfer, A. Greljo, J. Kamenik, and N. Košnik, "Physics of leptoquarks in precision experiments and at particle colliders," *Physics Reports*, vol. 641, pp. 1–68, 2016.

[93] I. Doršner, " Scalar leptoquark in ," *Physical Review D: Particles, Fields, Gravitation and Cosmology*, vol. 86, no. 5, 2012.

[94] I. Doršner, S. Fajfer, and I. Mustać, " Light vectorlike fermions in a minimal ," *Physical Review D: Particles, Fields, Gravitation and Cosmology*, vol. 89, no. 11, 2014.

[95] I. Doršner, S. Fajfer, and N. Košnik, "Leptoquark mechanism of neutrino masses within the grand unification framework," *The European Physical Journal C*, vol. 77, no. 6, 2017.

[96] I. Doršner, S. Fajfer, and N. Košnik, "Heavy and light scalar leptoquarks in proton decay," *Physical Review D: Particles, Fields, Gravitation and Cosmology*, vol. 86, Article ID 015013, 2012.

[97] I. Doršner and P. F. Pérez, "Upper bound on the mass of the type III seesaw triplet in an SU(5) model," *Journal of High Energy Physics*, vol. 2007, 2007.

[98] P. F. Pérez, "Supersymmetric adjoint SU(5)," *Physical Review D: Particles, Fields, Gravitation and Cosmology*, vol. 76, no. 7, 2007.

[99] W.-Y. Keung and G. Senjanović, "Majorana neutrinos and the production of the right-handed charged gauge boson," *Physical Review Letters*, vol. 50, no. 19, pp. 1427–1430, 1983.

[100] S. Weinberg, "Effective gauge theories," *Physics Letters B*, vol. 91, no. 1, pp. 51–55, 1980.

[101] L. J. Hall, "Grand unification of effective gauge theories," *Nuclear Physics B*, vol. 178, no. 1, pp. 75–124, 1981.

[102] B. A. Ovrut and H. J. Schnitzer, "Effective field theory in background field gauge," *Physics Letters B*, vol. 110, no. 2, pp. 139–142, 1982.

[103] M. K. Parida, "Heavy particle effects in grand unified theories with fine-structure constant matching," *Physics Letters B*, vol. 196, no. 2, pp. 163–169, 1987.

[104] M. K. Parida and P. K. Patra, " Useful theorem on vanishing threshold contribution to ," *Physical Review Letters*, vol. 66, no. 7, pp. 858–861, 1991.

[105] M. K. Parida and P. K. Patra, " Theorem on vanishing multiloop radiative corrections to ," *Physical Review Letters*, vol. 68, no. 6, pp. 754–756, 1992.

[106] M. K. Parida and C. C. Hazra, "Superheavy-Higgs-scalar effects in effective gauge theories from SO(10) grand unification with low-mass right-handed gauge bosons," *Physical Review D: Particles, Fields, Gravitation and Cosmology*, vol. 40, no. 9, pp. 3074–3085, 1989.

[107] M. K. Parida and B. Sahoo, "Planck-scale induced left–right gauge theory at LHC and experimental tests," *Nuclear Physics B*, vol. 906, pp. 77–104, 2016.

[108] B. Sahoo and M. K. Parida, "Low mass right-handed gauge bosons from minimal grand unified theories," *Nuclear and Particle Physics Proceedings*, vol. 273–275, pp. 2642–2644, 2016.

[109] Superkamiokande Collaboration, K. Abe, Y. Haga, Y. Hayato, M. Ikeda, K. Iyogi et al., "Search for Proton Decay via p⟶e+π0 and p⟶ μ+π0 in 0.31 Megaton Years Exposoure of Water Cherenkov Detector," *Physical Review D*, vol. 95, no. 1, Article ID 012004, 2017.

[110] M. K. Parida, B. P. Nayak, R. Satpathy, and R. L. Awasthi, "Standard Coupling Unification in SO(10), Hybrid Seesaw Neutrino Mass, Leptogenesis, Dark Matter, and Proton Lifetime

Predictions," *Journal of High Energy Physics*, vol. 1704, no. 75, 2017.

[111] Particle Data Group, J. Beringer et al., "Review of Particle Physics (RPP)," *Physical Review D*, vol. 86, Article ID 010001, 2012.

[112] M. L. Kynshi and M. K. Parida, "Higgs scalar in the grand desert with observable proton lifetime in SU(5) and small neutrino masses in SO(10)," *Physical Review D: Particles, Fields, Gravitation and Cosmology*, vol. 47, no. 11, pp. R4830–R4834, 1993.

[113] K. Olive, K. Agashe, and C. Amsler, "Review of particle physics," *Chinese Physics C*, vol. 38, no. 9, Article ID 090001, 2014.

[114] K. Olive, "Review of Particle Physics," *Chinese Physics C*, vol. 40, no. 10, Article ID 100001, 2016.

[115] H. Georgi, H. R. Quinn, and S. Weinberg, "Hierarchy of interactions in unified gauge theories," *Physical Review Letters*, vol. 33, no. 7, pp. 451–454, 1974.

[116] D. R. Jones, " Two-loop ," *Physical Review D: Particles, Fields, Gravitation and Cosmology*, vol. 25, no. 2, pp. 581-582, 1982.

[117] M. K. Parida, "Radiative Seesaw in SO(10) with Dark Matter," *Physics Letters B*, vol. 704, pp. 206–210, 2011.

[118] R. N. Mohapatra and M. K. Parida, "Type-II seesaw dominance in nonsupersymmetric and split-supersymmetry SO(10) models and proton lifetime," *Physical Review D: Particles, Fields, Gravitation and Cosmology*, vol. 84, no. 9, Article ID 095021, 2011.

[119] J. Schechter and J. W. F. Valle, "Neutrinoless double-β decay in su(2) x u(1) theories," *Physical Review D: Particles, Fields, Gravitation and Cosmology*, vol. 25, no. 11, article 2951, 1982.

[120] B. P. Nayak and M. K. Parida, "New mechanism for Type-II seesaw dominance in SO(10) with low-mass Z$\prime$,RH neutrinos, and verifiable LFV, LNV and proton decay," *The European Physical Journal C*, vol. 75, article no. 183, 2015.

[121] R. N. Mohapatra and M. K. Parida, "Threshold effects on the mass-scale predictions in SO(10) models and solar-neutrino puzzle," *Physical Review D: Particles, Fields, Gravitation and Cosmology*, vol. 47, no. 1, pp. 264–272, 1993.

[122] D.-G. Lee, R. N. Mohapatra, M. K. Parida, and M. Rani, "Predictions for the proton lifetime in minimal nonsupersymmetric SO(10) models: an update," *Physical Review D: Particles, Fields, Gravitation and Cosmology*, vol. 51, no. 1, pp. 229–235, 1995.

[123] M. Shiozawa, talk presented at TAUP, Asilomar, CA, U.S.A., 8-13 September, 2013.

[124] J. C. Pati, "Advantages of unity with SU(4)-color: Reflections through neutrino oscillations, baryogenesis and proton decay," *International Journal of Modern Physics A*, vol. 32, no. 09, p. 1741013, 2017.

[125] Superkamiokande Collaboration, H. Nishino et al., "Search for Nucleon Decay into Charged Anti-lepton plus Meson in Super-Kamiokande I and II," *Physical Review D*, vol. 85, Article ID 112001, 2012.

[126] J. L. Raaf, "Recent Nucleon Decay Results from Super-Kamiokande," *Nuclear Physics B—Proceedings Supplements*, vol. 229-232, p. 559, 2012.

[127] K. S. Babu, J. C. Pati, and Z. Tavartkiladze, "Constraining proton lifetime in SO(10) with stabilized doublet-triplet splitting," *Journal of High Energy Physics*, vol. 2010, article 84, 2010.

[128] B. Bajc, I. Dorsner, and M. Nemevsek, "Minimal SO(10) Splits Supersymmetry," *Journal of High Energy Physics*, vol. 811, 2008.

[129] A. Buras, J. Ellis, M. Gaillard, and D. Nanopoulos, "Aspects of the grand unification of strong, weak and electromagnetic interactions," *Nuclear Physics B*, vol. 135, no. 1, pp. 66–92, 1978.

[130] Y. Aoki, C. Dawson, J. Noaki, and A. Soni, "Proton decay matrix elements with domain-wall fermions," *Physical Review D: Particles, Fields, Gravitation and Cosmology*, vol. 75, no. 1, 2007.

[131] Y. Aoki, E. Shintani, and A. Soni, "Proton Decay Matrix Elements on the Lattice," *Physical Review D*, vol. 89, no. 1, Article ID 014505, 2014.

[132] C. Muñoz, "Enhancement factors for supersymmetric proton decay in SU(5) and SO(10) with superfield techniques," *Physics Letters B*, vol. 177, no. 1, pp. 55–59, 1986.

[133] G. Bertone and D. Hooper, "A History of Dark Matter," *Reviews of Modern Physics*, 2016.

[134] R. Catena and P. Ullio, "A novel determination of the local dark matter density," *Journal of Cosmology and Astroparticle Physics*, vol. 1008, no. 004, 2010.

[135] B. W. Lee and S. Weinberg, "Cosmological lower bound on heavy-neutrino masses," *Physical Review Letters*, vol. 39, no. 4, pp. 165–168, 1977.

[136] K. Griest and M. Kamionkowski, "Unitarity limits on the mass and radius of dark-matter particles," *Physical Review Letters*, vol. 64, no. 6, pp. 615–618, 1990.

[137] G. Arcadi, M. Lindner, Y. Mambrini, M. Pierre, and F. S. Queiroz, "GUT models at current and future hadron colliders and implications to dark matter searches," *Physics Letters B*, vol. 771, pp. 508–514, 2017.

[138] Y. Mambrini, S. Profumo, and F. S. Queiroz, "Dark matter and global symmetries," *Physics Letters. B. Particle Physics, Nuclear Physics and Cosmology*, vol. 760, pp. 807–815, 2016.

[139] P. V. Dong, D. T. Huong, F. S. Queiroz, J. W. Valle, and C. A. Vaquera-Araujo, "The dark side of flipped trinification," *Journal of High Energy Physics*, vol. 4, p. 143, 2018.

[140] J. M. Cline, K. Kainulainen, P. Scott, and C. Weniger, "Update on scalar singlet dark matter," *Physical Review D*, vol. 88, Article ID 055025, 2013.

[141] J. M. Cline, K. Kainulainen, P. Scott, and C. Weniger, "Erratum: Update on scalar singlet dark matter," *Physical Review D: Particles, Fields, Gravitation and Cosmology*, vol. 92, no. 3, 2015.

[142] Z. Ahmed et al., "Results from a Low-Energy Analysis of the CDMS II Germanium Data," *Physical Review Letters*, vol. 106, Article ID 131302, 2011.

[143] R. Agnese et al., "Improved WIMP-search reach of the CDMS II germanium data," *Physical Review D*, vol. 92, no. 7, Article ID 072003, 2015.

[144] R. Bernabei, P. Belli, F. Cappella et al., "First results from DAMA/LIBRA and the combined results with DAMA/NaI," *The European Physical Journal C*, vol. 56, no. 3, pp. 333–355, 2008.

[145] R. Bernabei et al., "New results from DAMA/LIBRA," *European Physical Journal C*, vol. 67, p. 39, 2010.

[146] M. W. Goodman and E. Witten, "Detectability of certain dark-matter candidates," *Physical Review D: Particles, Fields, Gravitation and Cosmology*, vol. 31, no. 12, pp. 3059–3063, 1985.

[147] L. Baudis, "Dark matter detection," *Journal of Physics G: Nuclear and Particle Physics*, vol. 43, no. 4, p. 044001, 2016.

[148] M. Schumann, L. Baudis, L. Bütikofer, A. Kish, and M. Selvi, "Dark matter sensitivity of multi-ton liquid xenon detectors," *Journal of Cosmology and Astroparticle Physics*, vol. 1510, no. 10, 2015.

[149] I. Garg, S. Goswami, K. Vishnudath, and N. Khan, "Electroweak vacuum stability in presence of singlet scalar dark matter in

TeV scale seesaw models," *Physical Review D: Particles, Fields, Gravitation and Cosmology*, vol. 96, no. 5, 2017.

[150] M. Aguilar et al., "First Result from the Alpha Magnetic Spectrometer on the International Space Station: Precision Measurement of the Positron Fraction in Primary Cosmic Rays of 0.5350 GeV," *Physical Review Letters*, vol. 110, Article ID 141102, 2013.

[151] A. Abramowski et al., "Search for Photon-Linelike Signatures from Dark Matter Annihilations with H.E.S.S," *Physical Review Letters*, vol. 110, Article ID 041301, 2013.

[152] J. Albert et al., "VHE Gamma-Ray Observation of the Crab Nebula and its Pulsar with the MAGIC telescope," *The Astrophysical Journal*, vol. 674, p. 1037, 2008.

[153] J. Chang et al., "An excess of cosmic ray electrons at energies of 300-800 GeV," *Nature*, vol. 456, p. 362, 2008.

[154] P. Athron, C. Balazs, A. Fowlie, and Y. Zhang, "Model-independent analysis of the DAMPE excess," *Journal of High Energy Physics*, vol. 1802, no. 121, 2018.

[155] E. Bulbul, M. Markevitch, A. Foster, R. K. Smith, M. Loewenstein, and S. W. Randall, "Detection of an unidentified emission line in the stacked X-ray spectrum of galaxy clusters," *The Astrophysical Journal* , vol. 789, article 13, 2014.

[156] A. Boyarsky, O. Ruchayskiy, D. Iakubovskyi, and J. Franse, "Unidentified line in X-ray spectra of the andromeda galaxy and perseus galaxy cluster," *Physical Review Letters*, vol. 113, no. 25, Article ID 251301, 2014.

[157] T. Bringmann, X. Huang, A. Ibarra, S. Vogl, and C. Weniger, "Fermi LAT search for internal bremsstrahlung signatures from dark matter annihilation," *Journal of Cosmology and Astroparticle Physics*, vol. 1207, p. 054, 2012.

[158] C. Weniger, "A tentative gamma-ray line from Dark Matter annihilation at the Fermi Large Area Telescope," *Journal of Cosmology and Astroparticle Physics*, vol. 1208, no. 007, 2012.

[159] T. Daylan, D. P. Finkbeiner, D. Hooper et al., "The characterization of the gamma-ray signal from the central Milky Way: A case for annihilating dark matter," *Physics of the Dark Universe*, vol. 12, pp. 1–23, 2016.

[160] T. Jeltema and S. Profumo, "Discovery of a 3.5 keV line in the Galactic Centre and a critical look at the origin of the line across astronomical targets," *Monthly Notices of the Royal Astronomical Society*, vol. 450, no. 2, pp. 2143–2152, 2015.

[161] J. Petrović, P. D. Serpico, and G. Zaharijaš, "Galactic Center gamma-ray "excess" from an active past of the Galactic Centre?" *Journal of Cosmology and Astroparticle Physics*, vol. 1410, no. 10, p. 052, 2014.

[162] M. Gonderinger, Y. Li, H. Patel, and M. J. Ramsey-Musolf, "Vacuum stability, perturbativity, and scalar singlet dark matter," *Journal of High Energy Physics*, vol. 1001, no. 53, 2010.

[163] C. Chen and Y. Tang, "Vacuum stability, neutrinos, and dark matter," *Journal of High Energy Physics*, vol. 1204, no. 19, 2012.

[164] N. Khan and S. Rakshit, "Study of electroweak vacuum metastability with a singlet scalar dark matter," *Physical Review D: Particles, Fields, Gravitation and Cosmology*, vol. 90, no. 11, 2014.

[165] P. Athron et al., "Status of the scalar singlet dark matter model," *The European Physical Journal C*, vol. 77, no. 8, p. 568, 2017.

[166] M. Cirelli, A. Strumia, and M. Tamburini, "Cosmology and astrophysics of minimal dark matter," *Nuclear Physics B*, vol. 787, no. 1-2, pp. 152–175, 2007.

[167] A. Arhrib, R. Benbrik, M. Chabab et al., "Higgs potential in the type II seesaw model," *Physical Review D: Particles, Fields, Gravitation and Cosmology*, vol. 84, no. 9, 2011.

[168] N. Haba, H. Ishida, N. Okada, and Y. Yamaguchi, "Vacuum stability and naturalness in type-II seesaw," *The European Physical Journal C*, vol. 76, no. 6, 2016.

[169] D. Chang, R. N. Mohapatra, and M. K. Parida, "New mechanism for baryon generation in SO(10) models with low mass WR-boson," *Physics Letters B*, vol. 142, no. 1-2, pp. 55–58, 1984.

[170] R. Satpathy, M. Chakraborty, B. Sahoo, M. K. Parida, Work in progress.

Hindawi
Advances in High Energy Physics
Volume 2018, Article ID 5340935, 12 pages
https://doi.org/10.1155/2018/5340935

Review Article

Z' Portal Dark Matter in the Minimal $B - L$ Model

Satomi Okada

Graduate School of Science and Engineering, Yamagata University, Yamagata 990-8560, Japan

Correspondence should be addressed to Satomi Okada; satomi.the.great@gmail.com

Received 5 March 2018; Accepted 2 May 2018; Published 15 July 2018

Academic Editor: Farinaldo Queiroz

We consider a dark matter scenario in the context of the minimal extension of the Standard Model (SM) with a $B - L$ (baryon number minus lepton number) gauge symmetry, where three right-handed neutrinos with a $B - L$ charge -1 and a $B - L$ Higgs field with a $B - L$ charge $+2$ are introduced to make the model anomaly-free and to break the $B - L$ gauge symmetry, respectively. The $B - L$ gauge symmetry breaking generates Majorana masses for the right-handed neutrinos. We introduce a Z_2 symmetry to the model and assign an odd parity only for one right-handed neutrino, and hence the Z_2-odd right-handed neutrino is stable and the unique dark matter candidate in the model. The so-called minimal seesaw works with the other two right-handed neutrinos and reproduces the current neutrino oscillation data. We consider the case that the dark matter particle communicates with the SM particles through the $B - L$ gauge boson (Z'_{B-L} boson) and obtain a lower bound on the $B - L$ gauge coupling (α_{B-L}) as a function of the Z'_{B-L} boson mass ($m_{Z'}$) from the observed dark matter relic density. On the other hand, we interpret the recent LHC Run-2 results on the search for a Z' boson resonance to an upper bound on α_{B-L} as a function of $m_{Z'}$. These two constraints are complementary for narrowing down an allowed parameter region for this "Z' portal" dark matter scenario, leading to a lower mass bound of $m_{Z'} \geq 3.9$ TeV.

1. Introduction

In 2012, the Higgs boson, which is the last piece of the Standard Model (SM), was finally discovered by the A Toroidal LHC ApparatuS (ATLAS) and Compact Muon Solenoid (CMS) experiments at the Cern Large Hadron Collider (LHC) [1, 2]. The SM is the best theory to describe elementary particles and fundamental interactions among them (strong, weak, and electromagnetic interactions) and agrees with a number of experimental results in a high accuracy. For example, properties of the weak gauge bosons (W and Z) in the SM, such as their masses and couplings with the quarks and leptons, were measured at the Large Electron-Positron (LEP) collider with a very high degree of precision [3, 4]. Properties of the Higgs boson have also been measured to be consistent with the SM predictions at the LHC [5].

Despite its great success, there are some observational problems that the SM cannot account for. One of the major missing pieces of the SM is the neutrino mass matrix. Since, in contrast to the other fermions, right-handed partners of the SM left-handed neutrinos are missing in the SM particle content, the SM neutrinos cannot acquire their masses at the renormalizable level, even after the electroweak symmetry is broken. However, neutrino oscillation phenomena among three neutrino flavors have been confirmed by the Super-Kamiokande experiments in 1998 [6] and the Sudbury Neutrino Observatory (SNO) in 2001 [7]. Neutrino oscillation phenomena require neutrino masses and flavor mixings, and therefore we need a framework beyond the SM to incorporate them. The so-called type I seesaw mechanism [8–12] is a natural way for this purpose, where heavy Majorana right-handed neutrinos are introduced.

Another major missing piece of the SM is a candidate for the dark matter particle in the present universe. Based on the recent results of the precision measurements of the cosmic microwave background (CMB) anisotropy by the Wilkinson Microwave Anisotropy Probe (WMAP) [13] and the Planck satellite [14, 15], the energy budget of the present universe is determined to be composed of 73% dark energy, 23% cold dark matter, and only 4% from baryonic matter. Since the SM has no suitable candidate for the (cold) dark matter particle, we need to extend the SM to incorporate it. The

weakly interacting massive particle (WIMP) [16] has long been studied as one of the most promising candidates for the dark matter. Through its interaction with the SM particles, the WIMP was in thermal equilibrium in the early universe and the WIMP dark matter is a thermal relic from the early universe. Note that the relic density of the WIMP dark matter is independent of the history of the universe before it has been gotten in thermal equilibrium.

Among many possibilities, the minimal gauged $B - L$ extension of the SM [17–21] is a very simple way to incorporate neutrino masses and flavor mixings via the seesaw mechanism. In this extension, the accidental global $B - L$ (baryon number minus lepton number) symmetry in the SM is gauged. Associated with this gauging, three right-handed neutrinos with a $B - L$ charge -1 are introduced to cancel all the gauge and mixed-gravitational anomalies of the model. In other words, the right-handed neutrinos which play the essential role in the type I seesaw mechanism must be present for the theoretical consistency. SM gauge singlet Higgs boson with a $B - L$ charge -2 is also contained in the model and its vacuum expectation value (VEV) breaks the $B - L$ gauge symmetry. The Higgs VEV generates the $B - L$ gauge boson mass as well as Majorana masses of the right-handed neutrinos. After the electroweak symmetry breaking, the SM neutrino Majorana masses are generated through the seesaw mechanism. The mass spectrum of new particles introduced in the minimal $B - L$ model, the $B - L$ gauge boson (Z'_{B-L} boson), the right-handed Majorana neutrinos, and the $B - L$ Higgs boson, is controlled by the $B - L$ symmetry breaking scale. If the breaking scale lies around the TeV scale the minimal $B - L$ model can be tested at the LHC in the future.

Although the minimal $B - L$ model supplements the SM with the neutrino masses and mixings, a cold dark matter candidate is still missing. Towards a more complete scenario, we need to consider a further extension of the model. Ref. [22] has proposed a concise way to introduce a dark matter candidate to the minimal $B - L$ model, where instead of introducing a new particle as a dark matter candidate, a Z_2 symmetry is introduced and an odd parity is assigned only for one right-handed neutrino. Thanks to the Z_2 symmetry, the Z_2-odd right-handed neutrino becomes stable and hence plays the role of dark matter. On the other hand, the other two right-handed neutrinos are involved in the seesaw mechanism. It is known that the type I seesaw with two right-handed neutrinos is a minimal system to reproduce the observed neutrino oscillation data. This so-called minimal seesaw [23, 24] predicts one massless neutrino. Dark matter phenomenology in this model context has been investigated in [22, 25, 26]. The right-handed neutrino dark matter can communicate with the SM particles through (i) the Z'_{B-L} boson and (ii) two Higgs bosons which are realized as linear combinations of the SM Higgs and the $B - L$ Higgs bosons. The cases (i) and (ii) are, respectively, called "Z' portal" and "Higgs portal" dark matter scenarios. In the following, we focus on the "Z' portal" dark matter scenario. See [22, 25, 26] for extensive studies on the Higgs portal dark matter scenario.

In recent years, the Z' portal dark matter has attracted a lot of attention [27–64], where a dark matter candidate along with a new $U(1)$ gauge symmetry is introduced and the dark matter particle communicates with the SM particles through the $U(1)$ gauge boson (Z' boson). Through this Z' boson interaction, we can investigate a variety of dark matter physics, such as the dark matter relic density and the direct/indirect dark matter search. Very interestingly, the search for a Z' boson production by the LHC experiments can provide the information which is complementary to the information obtained by dark matter physics.

Note that the minimal $B-L$ model with the right-handed neutrino dark matter introduced above is a simple example of the Z' portal dark matter scenario. In this article, we consider this Z' portal dark matter scenario. Since the model is very simple, dark matter physics is controlled by only three free parameters, namely, the $B - L$ gauge coupling (α_{B-L}), the Z'_{B-L} boson mass ($m_{Z'}$), and the dark matter mass (m_{DM}). We first identify allowed parameter regions of the model by considering the cosmological bound on the dark matter relic density. We then consider the results from the search for a Z' boson resonance with dilepton final states to identify allowed parameter regions. Combining the cosmological and the LHC constraints, we find a narrow allowed region. This complementarity between the cosmological and the LHC constraints has been investigated in [46, 54]. The purpose of this article is to update the results in the references by employing the latest LHC results, along with a review of the minimal $B - L$ model with the right-handed neutrino dark matter.

The plan of this article is as follows: In the next section, we give a review of the minimal $B-L$ model. In Section 3, we introduce the minimal $B-L$ model with Z_2 symmetry, where one right-handed neutrino, which is a unique Z_2-odd particle in the model, is identified with the dark matter particle. In Section 4, the cosmological constraints on the right-handed neutrino dark matter are considered and an allowed parameter region is identified. In Section 5, we consider the LHC Run-2 constraints from the search for a narrow resonance with dilepton final states and find the constraints on our model parameters. Combining the results obtained in Section 3, we find an allowed region. The cosmological constraint and the LHC constraints are complementary for narrowing down the allowed parameter regions. Section 6 is devoted to conclusions.

2. The Minimal B–L Model

The SM Lagrangian at the tree-level is invariant under the global $U(1)_B$ and $U(1)_L$ transformations:

$$\begin{aligned} \psi &\longrightarrow \psi' = e^{iQ_B\theta_B}\psi, \\ \psi &\longrightarrow \psi' = e^{iQ_L\theta_L}\psi, \end{aligned} \tag{1}$$

where θ_B and θ_L are constant phases associated with the $U(1)_B$ and $U(1)_L$ transformations, and Q_B and Q_L are charges identified as a baryon number (B) and a lepton number (L) of the fermion ψ, respectively. The baryon number is a quantum number to characterize fermions. A quark (antiquark) has a baryon number 1/3 ($-1/3$), while SM lepton has 0. The lepton number is a quantum number similar to baryon

Table 1: Particle content of the minimal $B-L$ model.

	$SU(3)_C$	$SU(2)_L$	$U(1)_Y$	$U(1)_{B-L}$
q_L^i	**3**	**2**	1/6	1/3
u_R^i	**3**	**1**	2/3	1/3
d_R^i	**3**	**1**	−1/3	1/3
l_L^i	**1**	**2**	−1/2	−1
N_R^i	**1**	**1**	0	−1
e_R^i	**1**	**1**	−1	−1
H	**1**	**2**	−1/2	0
Φ	**1**	**1**	0	2

number. A lepton (antilepton) has a lepton number 1 (−1), while a quark has 0. Although these $U(1)$ symmetries are anomalous under the SM gauge group, the combination of $B-L$ is anomaly-free. The $B-L$ symmetry means that the SM Lagrangian is invariant under the global $U(1)_{B-L}$ transformation:

$$\psi \longrightarrow \psi' = e^{i(Q_B - Q_L)\theta_{B-L}}\psi, \tag{2}$$

where θ_{B-L} is a constant phase associated with the $U(1)_{B-L}$ transformation.

In the minimal $B-L$ model [17–21], this global $B-L$ symmetry in the SM is gauged, and hence this model is based on the gauge group $SU(3)_C \times SU(2)_L \times U(1)_Y \times U(1)_{B-L}$. Three right-handed neutrinos (N_R^i, $i = 1, 2, 3$, is a generation index) and an SM singlet scalar field (Φ) are introduced to make the theory anomaly-free and to break the $U(1)_{B-L}$ gauge symmetry, respectively. The particle content of the minimal $B-L$ model is listed in Table 1.

2.1. Gauge Sector. Lagrangian of the gauge bosons in the $B-L$ model is generally given by

$$\begin{aligned}\mathscr{L}^{B-L}_{\text{gauge}} = &-\frac{1}{2}\text{tr}\left[G_{\mu\nu}G^{\mu\nu}\right] - \frac{1}{2}\text{tr}\left[F_{\mu\nu}F^{\mu\nu}\right] - \frac{1}{4}B_{\mu\nu}B^{\mu\nu} \\ &- \frac{1}{4}B'_{\mu\nu}B'^{\mu\nu} - c_{\text{mix}}B_{\mu\nu}B'^{\mu\nu},\end{aligned} \tag{3}$$

where $G_{\mu\nu}$, $F_{\mu\nu}$, and $B_{\mu\nu}$ are the field strengths of the SM gauge fields of $SU(3)_C \times SU(2)_L \times U(1)_Y$, and

$$B'_{\mu\nu} = \partial_\mu\left(Z'_{B-L}\right)_\nu - \partial_\nu\left(Z'_{B-L}\right)_\mu \tag{4}$$

is the field strength for the new electrically neutral gauge boson (Z'_{B-L}) of $U(1)_{B-L}$. Note that we can generally introduce the last term for a kinetic mixing between the $U(1)_Y$ and the $U(1)_{B-L}$ gauge bosons. In fact, such a mixing term is generated through quantum corrections. Since we can always set $c_{\text{mix}} = 0$ at a fixed energy, we define the minimal $B-L$ model with $c_{\text{mix}} = 0$ at the scale of the $B-L$ symmetry breaking, for simplicity.

2.2. Scalar Sector. Lagrangian of the scalar sector in the minimal $B-L$ model is given by

$$\begin{aligned}\mathscr{L}^{B-L}_{\text{scalar}} = &\left(\mathscr{D}^\mu H\right)^\dagger\left(\mathscr{D}_\mu H\right) + \left(\mathscr{D}^\mu\Phi\right)^\dagger\left(\mathscr{D}_\mu\Phi\right) \\ &- V(H,\Phi),\end{aligned} \tag{5}$$

where H and Φ are the SM Higgs field and the SM singlet scalar field ($B-L$ Higgs), respectively, and the scalar potential is given by

$$\begin{aligned}V(H,\Phi) = &\lambda_H\left(H^\dagger H - \frac{v^2}{2}\right)^2 + \lambda_\Phi\left(\Phi^\dagger\Phi - \frac{v_{B-L}^2}{2}\right)^2 \\ &+ \lambda_{\text{mix}}\left(H^\dagger H - \frac{v^2}{2}\right)\left(\Phi^\dagger\Phi - \frac{v_{B-L}^2}{2}\right).\end{aligned} \tag{6}$$

Here, λ_H (> 0), λ_Φ (> 0) and λ_{mix} are real coupling constants, $v = 246$ GeV [65], and v_{B-L} is a real and positive constant. We will derive a condition for λ_{mix} to make the potential bounded from below. In this scalar potential, the SM Higgs doublet and $U(1)_{B-L}$ Higgs field develop the VEVs:

$$\begin{aligned}\langle H\rangle &= \frac{1}{\sqrt{2}}\begin{pmatrix}v\\0\end{pmatrix}, \\ \langle\Phi\rangle &= \frac{v_{B-L}}{\sqrt{2}}.\end{aligned} \tag{7}$$

We expand the Higgs fields around the VEVs such that

$$\begin{aligned}H &= \frac{1}{\sqrt{2}}\begin{pmatrix}v+h\\0\end{pmatrix}, \\ \Phi &= \frac{v_{B-L}+h'}{\sqrt{2}},\end{aligned} \tag{8}$$

where h, h' are physical Higgs bosons. Substituting this expansion into scalar potential (6), we read out the mass terms of the Higgs bosons as

$$\begin{aligned}V(H,\Phi) &\supset \lambda_H v^2 h^2 + \lambda_\Phi v_{B-L}^2 h'^2 + \lambda_{\text{mix}} v v_{B-L} h h' \\ &= \frac{1}{2}\begin{pmatrix}h & h'\end{pmatrix}\begin{pmatrix}2\lambda_H v^2 & \lambda_{\text{mix}} v v_{B-L}\\ \lambda_{\text{mix}} v v_{B-L} & 2\lambda_\Phi v_{B-L}^2\end{pmatrix}\begin{pmatrix}h\\h'\end{pmatrix} \\ &= \frac{1}{2}\begin{pmatrix}h & h'\end{pmatrix} M_{\text{scalar}}\begin{pmatrix}h\\h'\end{pmatrix}.\end{aligned} \tag{9}$$

In order for the scalar potential to be bounded from below, the mass matrix M_{scalar} must be positive definite; namely,

$$\det\left[M_{\text{scalar}}\right] = \left(4\lambda_H\lambda_\Phi - \lambda_{\text{mix}}^2\right)v^2 v_{B-L}^2 > 0, \tag{10}$$

and hence $|\lambda_{mix}| < 2\sqrt{\lambda_H \lambda_\Phi}$. Now we diagonalize the mass matrix by

$$\begin{pmatrix} h \\ h' \end{pmatrix} = \begin{pmatrix} \cos\alpha & \sin\alpha \\ -\sin\alpha & \cos\alpha \end{pmatrix} \begin{pmatrix} h_1 \\ h_2 \end{pmatrix}, \tag{11}$$

where h_1, h_2 are mass eigenstates, and the mixing angle is given by

$$\tan 2\alpha = -\frac{\lambda_{\text{mix}} v v_{B-L}}{\lambda_H v^2 - \lambda_\Phi v_{B-L}^2}. \tag{12}$$

The mass eigenstates are given by

$$\begin{aligned} m_{h_1}^2 &= \lambda_H v^2 + \lambda_\Phi v_{B-L}^2 \\ &\quad + \sqrt{\left(\lambda_H v^2 - \lambda_\Phi v_{B-L}^2\right)^2 + \left(\lambda_{\text{mix}} v v_{B-L}\right)^2}, \\ m_{h_2}^2 &= \lambda_H v^2 + \lambda_\Phi v_{B-L}^2 \\ &\quad - \sqrt{\left(\lambda_H v^2 - \lambda_\Phi v_{B-L}^2\right)^2 + \left(\lambda_{\text{mix}} v v_{B-L}\right)^2}. \end{aligned} \tag{13}$$

For simplicity, we assume a very small λ_{mix}, so that one mass eigenstate is an SM-like Higgs boson, and the other is almost a $B-L$ Higgs boson. Since the Higgs boson properties measured by the LHC experiments are consistent with the SM predictions [5], $|\lambda_{\text{mix}}| \ll 1$ is justified.

Let us now calculate the mass of the $B-L$ gauge boson Z'_{B-L}. The kinetic term of the $B-L$ Higgs field is given by

$$\mathscr{L}_{\text{scalar}}^{B-L\ \text{kin}} = \left(\mathscr{D}_\mu \Phi\right)^\dagger \left(\mathscr{D}^\mu \Phi\right), \tag{14}$$

where the covariant derivative is

$$\mathscr{D}_\mu = \partial_\mu - 2ig_{B-L}\left(Z'_{B-L}\right)_\mu, \tag{15}$$

and g_{B-L} is the coupling constant of $U(1)_{B-L}$ gauge interaction. Substituting $\Phi \longrightarrow \langle\Phi\rangle$, the Z'_{B-L} gauge boson mass is found to be

$$m_{Z'} = 2g_{B-L} v_{B-L}. \tag{16}$$

2.3. Yukawa Sector. Lagrangian of the Yukawa sector in the $B-L$ model is given by

$$\begin{aligned} \mathscr{L}_{\text{Yukawa}}^{B-L} \supset & -\sum_{i=1}^{3}\sum_{j=1}^{3} Y_D^{ij} \overline{l_L^i} H N_R^j - \frac{1}{2}\sum_{k=1}^{3} Y_N^k \Phi \overline{N_R^{kC}} N_R^k \\ & + H.c., \end{aligned} \tag{17}$$

where Y_D^{ij} and Y_N^k are Dirac Yukawa coupling constant and Majorana Yukawa coupling constant. Once the $B-L$ Higgs field Φ develops its VEV, the $B-L$ gauge symmetry is broken and the Majorana mass terms for the right-handed neutrinos are generated from the second term in the right-hand side. The seesaw mechanism is automatically implemented in the model after the electroweak symmetry breaking. Neutrino mass matrix is given by

$$M_{\text{neutrino}} = \begin{pmatrix} 0 & m_D \\ m_D^T & M \end{pmatrix}. \tag{18}$$

Here, m_D and M are Dirac and Majorana mass matrices, respectively, which are given by

$$\begin{aligned} m_D &= \frac{Y_D}{\sqrt{2}} v, \\ M &= \frac{Y_N}{\sqrt{2}} v_{B-L}. \end{aligned} \tag{19}$$

Assuming $|m_D^{ij}| \ll M^k$, we can block-diagonalize the mass matrix M_{neutrino} to be

$$\begin{pmatrix} 0 & m_D \\ m_D^T & M \end{pmatrix} \longrightarrow \begin{pmatrix} -m_D^T M^{-1} m_D & 0 \\ 0 & M \end{pmatrix}. \tag{20}$$

When we consider only one generation, the mass eigenvalues are simply

$$\begin{aligned} m_{\nu_l} &\simeq -\frac{m_D^2}{M}, \\ m_{\nu_h} &\simeq M. \end{aligned} \tag{21}$$

Because of the seesaw mechanism, a huge mass hierarchy between the light eigenstate (ν_l) and the heavy eigenstate (ν_h) is generated.

3. The Minimal $B-L$ Model with Z_2 Parity

In the previous section, we have discussed that the minimal $B-L$ extended SM incorporates the neutrino masses and mixings through the seesaw mechanism. In this section, we extend the model further to introduce a cold dark matter candidate in the model. Among many possibilities, we follow a very concise way proposed in [22] and introduce a Z_2 symmetry without extending the model particle content. We then assign an odd parity only for one right-handed neutrino N_R. The particle content is listed in Table 2. Except for the introduction of the Z_2 symmetry and the parity assignments, the particle content is identical to that of the minimal $B-L$ model in Table 1. The conservation of the Z_2 parity ensures the stability of the Z_2-odd N_R, and, therefore, this right-handed neutrino is a unique dark matter candidate in the model [22].

With the Z_2 symmetry, the Yukawa sector of the minimal $B-L$ model in (17) is modified to be

$$\begin{aligned} \mathscr{L}_{\text{Yukawa}}^{B-L} \supset & -\sum_{i=1}^{3}\sum_{j=1}^{2} Y_D^{ij} \overline{l_L^i} H N_R^j - \frac{1}{2}\sum_{k=1}^{2} Y_N^k \Phi \overline{N_R^{kC}} N_R^k \\ & - \frac{1}{2} Y_N \Phi \overline{N_R^C} N_R + H.c. \end{aligned} \tag{22}$$

Note that due to the Z_2 parity assignment only the two generation right-handed neutrinos are involved in the neutrino

Table 2: The particle content of the minimal $B-L$ extended SM with Z_2 symmetry. In addition to the SM particle content ($i = 1, 2, 3$), the three right-handed neutrinos [N_R^j ($j = 1, 2$) and N_R] and the $B-L$ Higgs field (Φ) are introduced. Because of the Z_2 parity assignment shown here, N_R is a unique (cold) dark matter candidate.

	$SU(3)_C$	$SU(2)_L$	$U(1)_Y$	$U(1)_{B-L}$	Z_2
q_L^i	**3**	**2**	1/6	1/3	+
u_R^i	**3**	**1**	2/3	1/3	+
d_R^i	**3**	**1**	-1/3	1/3	+
l_L^i	**1**	**2**	-1/2	-1	+
N_R^j	**1**	**1**	0	-1	+
N_R	**1**	**1**	0	-1	-
e_R^i	**1**	**1**	-1	-1	+
H	**1**	**2**	-1/2	0	+
Φ	**1**	**1**	0	2	+

Dirac Yukawa coupling. The renormalizable scalar potentials for the SM Higgs and the $B-L$ Higgs fields are the same as the minimal $B-L$ model, and the Higgs fields develop their VEVs. This $B-L$ symmetry breaking generates masses for the Majorana neutrinos N_R^j ($j = 1, 2$), the dark matter particle N_R, and the $B-L$ gauge boson (Z'_{B-L} boson):

$$m_N^j = \frac{Y_N^j}{\sqrt{2}} v_{B-L},$$
$$m_{\mathrm{DM}} = \frac{Y_N}{\sqrt{2}} v_{B-L}, \tag{23}$$
$$m_{Z'} = 2 g_{B-L} v_{B-L}.$$

The seesaw mechanism [8–12] is automatically implemented in the model after the electroweak symmetry breaking. Due to the Z_2 symmetry, only two right-handed neutrinos $N_R^{1,2}$ are relevant to the seesaw mechanism. This system is the so-called minimal seesaw [23, 24] which possesses a number of free parameters Y_D^{ij} and Y_N^k enough to reproduce the neutrino oscillation data with predicting one massless eigenstate. Since the lightest neutrino is massless in our model, the pattern of the light neutrino mass spectrum is either the normal hierarchy or the inverted hierarchy. The quasi-degenerate mass spectrum cannot be realized.

The dark matter particle can communicate with the SM particles in two ways: One is through the Higgs bosons. In the Higgs potential of (6), the SM Higgs boson and the $B-L$ Higgs boson mix with each other in the mass eigenstates (see (11) and (12)), and these Higgs boson mass eigenstates mediate the interactions between the dark matter particle and the SM particles. Dark matter physics with the Higgs interactions have been investigated in [22, 25, 26]. In this analysis, four free parameters are involved, namely, the dark matter mass, Yukawa coupling Y_N, the $B-L$ Higgs boson mass, and a mixing parameter between the SM Higgs and $B-L$ Higgs bosons. The other way for the dark matter particle to communicate with the SM particles is through the $B-L$ gauge interaction with the Z'_{B-L} gauge boson. In this case, only three free parameters (g_{B-L}, $m_{Z'}$, and m_{DM}) are involved in dark matter physics analysis. In this article, we concentrate on dark matter physics mediated by the Z'_{B-L} boson, namely, "Z' portal dark matter." Assuming $|\lambda_{\mathrm{mix}}| \ll 1$ in Higgs potential (6), the Higgs bosons mediated interactions are negligibly small, and the dark matter particle communicates with the SM particles only through the Z'_{B-L} boson. We may consider a supersymmetric extension of our model [30] to naturally realize this situation, where λ_{mix} is forbidden by supersymmetry. Although we do not consider the supersymmetric case, dark matter phenomenology in our model is essentially the same as the supersymmetric case (see [30]), when all the superpartners of the SM particles are heavier than the dark matter particle. See [25, 26, 30, 66] for studies on the Z'_{B-L} portal dark matter scenario with a limited parameter choice.

4. Cosmological Constraints on Z'_{B-L} Portal Dark Matter

The dark matter relic density is measured at the 68% limit as [67]

$$\Omega_{\mathrm{DM}} h^2 = 0.1198 \pm 0.0015. \tag{24}$$

We now evaluate the relic density of the dark matter N_R and identify an allowed parameter region that satisfies the upper bound on the dark matter relic density of $\Omega_{\mathrm{DM}} h^2 \leq 0.1213$. The relic density of dark matter N_R is evaluated by solving the Boltzmann equation:

$$\frac{dY_{\mathrm{DM}}}{dx} = -\frac{s \langle \sigma v_{\mathrm{rel}} \rangle}{xH(m_{\mathrm{DM}})} \left(Y_{\mathrm{DM}}^2 - \left(Y_{\mathrm{DM}}^{\mathrm{eq}} \right)^2 \right) \tag{25}$$

where $Y_{\mathrm{DM}} = n_{DM}/s$ is the yield of the dark matter particle with the dark matter number density (n_{DM}) and the entropy density (s), Y_{DM} in thermal equilibrium is denoted as $Y_{\mathrm{DM}}^{\mathrm{eq}}$, $x \equiv m_{\mathrm{DM}}/T$ (T is temperature of the universe) is time normalized by the dark matter mass, $H(m_{\mathrm{DM}})$ is the Hubble parameter at $T = m_{\mathrm{DM}}$, and $\langle \sigma v_{\mathrm{rel}} \rangle$ is the thermal average of the cross section for dark matter annihilation process times

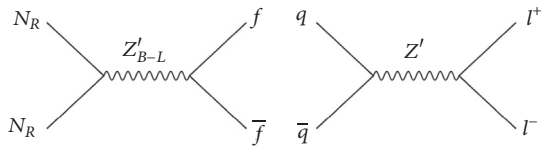

FIGURE 1: Left: Majorana neutrino dark matter (N_R) pair annihilation process into the SM fermions (f) through the Z'_{B-L} exchange in the s-channel, $N_R N_R \longrightarrow Z'_{B-L} \longrightarrow f\overline{f}$. Right: parton level process (quark (q) and antiquark ($\overline{q}$) annihilation process) to produce a dilepton final state (l^+l^-) through a Z' exchange in the s-channel at the LHC.

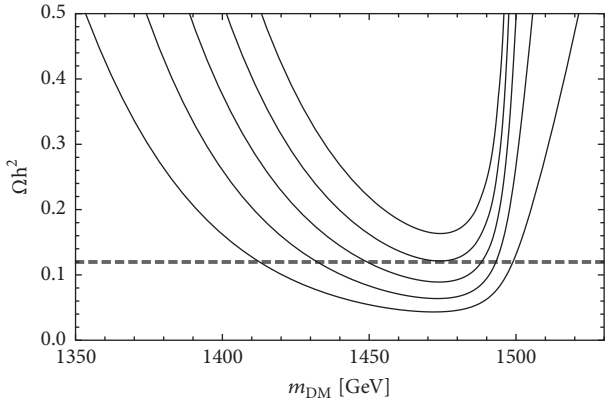

FIGURE 2: The relic abundance of the Z'_{B-L} portal right-hard neutrino dark matter as a function of the dark matter mass (m_{DM}) for $m_{Z'} = 3$ TeV and various values of the gauge coupling $\alpha_{B-L} = 0.001, 0.0014, 0.002, 0.003$, and 0.005 (solid lines from top to bottom). The two horizontal lines denote the range of the observed dark matter relic density, $0.1183 \leq \Omega_{\mathrm{DM}}h^2 \leq 0.1213$.

relative velocity. We give explicit formulas of the quantities in the Boltzmann equation:

$$s = \frac{2\pi^2}{45} g_* \frac{m_{\mathrm{DM}}^3}{x^3},$$

$$H\left(m_{\mathrm{DM}}\right) = \sqrt{\frac{4\pi^3}{45} g_*} \frac{m_{\mathrm{DM}}^2}{M_{pl}}, \tag{26}$$

$$sY_{\mathrm{DM}}^{\mathrm{eq}} = \frac{g_{\mathrm{DM}}}{2\pi^2} \frac{m_{\mathrm{DM}}^3}{x} K_2\left(x\right),$$

where $M_{pl} = 1.22 \times 10^{19}$ GeV is the Planck mass, g_* is the effective total degree of freedom for SM particles in thermal equilibrium ($g_* = 106.75$ is employed in the following analysis), $g_{\mathrm{DM}} = 2$ is the degree of freedom for the right-handed neutrino dark matter, and K_2 is the modified Bessel function of the second kind. In our Z'_{B-L} portal dark matter scenario, the dark matter particles pair-annihilate into the SM particles mainly through the s-channel Z'_{B-L} boson exchange (see the left panel of Figure 1). The thermal average of the annihilation cross section is calculated as

$$\left\langle \sigma v_{\mathrm{rel}} \right\rangle = \left(sY_{\mathrm{DM}}^{\mathrm{eq}}\right)^{-2} g_{\mathrm{DM}}^2 \frac{m_{\mathrm{DM}}}{64\pi^4 x} \times \int_{4m_{\mathrm{DM}}^2}^{\infty} ds\widehat{\sigma}\left(s\right) \sqrt{s} K_1\left(\frac{x\sqrt{s}}{m_{\mathrm{DM}}}\right), \tag{27}$$

where $\widehat{\sigma}(s) = 2(s - 4m_{\mathrm{DM}}^2)\sigma(s)$ is the reduced cross section with $\sigma(s)$ being the total annihilation cross section. The total cross section of the annihilation process $N_R N_R \longrightarrow Z'_{B-L} \longrightarrow f\overline{f}$ (f denotes an SM fermion) is calculated as

$$\sigma\left(s\right) = \pi\alpha_{B-L}^2 \frac{\sqrt{s\left(s - 4m_{\mathrm{DM}}^2\right)}}{\left(s - m_{Z'}^2\right)^2 + m_{Z'}^2\Gamma_{Z'}^2} \times \left[\frac{37}{9} + \frac{1}{3}\beta_t\left(1 - \frac{1}{3}\beta_t^2\right)\right] \tag{28}$$

with $\beta_t(s) = \sqrt{1 - 4m_t^2/s}$, top quark mass of $m_t = 173.34$ GeV [65], and the total decay width of Z'_{B-L} boson given by

$$\Gamma_{Z'} = \frac{\alpha_{B-L}}{6} m_{Z'} \left[\frac{37}{3} + \frac{1}{3}\beta_t\left(m_{Z'}^2\right)\left(3 - \beta_t\left(m_{Z'}^2\right)^2\right) + \left(1 - \frac{4m_{\mathrm{DM}}^2}{m_{Z'}^2}\right)^{2/3} \theta\left(\frac{m_{Z'}^2}{m_{\mathrm{DM}}^2} - 4\right)\right] \tag{29}$$

Here, we have taken $m_N^j > m_{Z'}/2$, for simplicity.

Solving the Boltzmann equation numerically, we evaluate the dark matter relic density by

$$\Omega_{\mathrm{DM}}h^2 = \frac{m_{\mathrm{DM}} s_0 Y\left(\infty\right)}{\rho_{crit}/h^2}, \tag{30}$$

where $Y(\infty)$ is the yield in the limit of $x \longrightarrow \infty$, $s_0 = 2890$ cm^{-3} is the entropy density of the present universe, and $\rho_{\mathrm{crit}}/h^2 = 1.05 \times 10^{-5}$ GeV/ cm^3 is the critical density. Note that we have only three parameters, $\alpha_{B-L} = g_{B-L}^2/(4\pi)$, $m_{Z'}$, and m_{DM}, in our analysis. For $m_{Z'} = 3$ TeV and various values of the gauge coupling α_{B-L}, Figure 2 depicts the resultant dark matter relic density as a function of its mass m_{DM}, along with the observed bounds $0.1183 \leq \Omega_{\mathrm{DM}}h^2 \leq 0.1213$ [67] (two horizontal dashed lines). The solid curves from top to bottom correspond to the results for $\alpha_{B-L} = 0.001, 0.0014, 0.002, 0.003$, and 0.005, respectively. We find that, in order to reproduce the observed relic density, the dark matter mass must be close to half of the Z'_{B-L} boson mass. In other words, normal values of the dark matter annihilation cross section lead to overabundance, and an enhancement of the cross section through the Z'_{B-L} boson resonance in the s-channel annihilation process is necessary. In Figure 2, we can see the maximum annihilation cross section occurs for

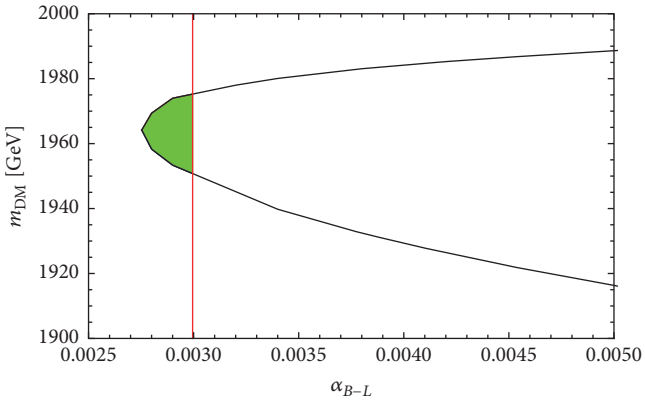

FIGURE 3: The dark matter mass as a function of α_{B-L} for $m_{Z'} = 4$ TeV. Along the solid (black) curve in each panel, $\Omega_{\rm DM}h^2 = 0.1198$ is satisfied. The vertical solid line (in red) represents the upper bound on α_{B-L} obtained from the ATLAS results [68] (see Figure 4). The (green) shaded region satisfies $\Omega_{\rm DM}h^2 \leq 0.1198$ and the ATLAS bound on $\alpha_{B-L} \leq 0.003$.

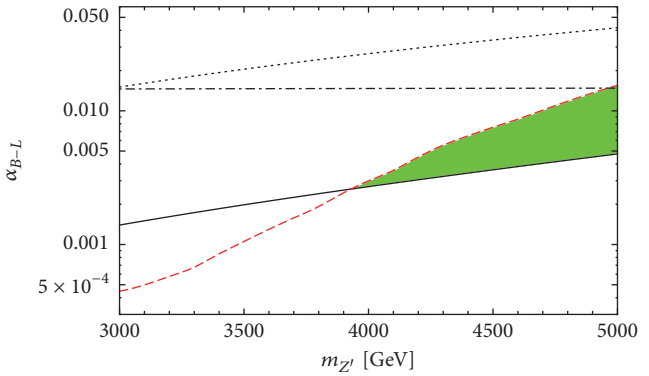

FIGURE 4: Allowed parameter region for the Z'_{B-L} portal dark matter scenario. The solid (black) line shows the lower bound on α_{B-L} as a function of $m_{Z'}$ to satisfy the cosmological upper bound on the dark matter relic abundance. The dashed line (in red) shows the upper bound on α_{B-L} as a function of $m_{Z'}$ from the search results for Z' boson resonance by the ATLAS collaboration [68]. The LEP bound is depicted as the dotted line. Combining these bounds, the allowed parameter region is depicted as the (green) shaded region. We also show a theoretical upper bound on α_{B-L} (dashed-dotted) to avoid the Landau pole of the running $B - L$ gauge coupling below the Planck mass M_{pl}.

$m_{\rm DM}$ slightly smaller than $m_{Z'}/2$ because of the effect from thermally averaging the cross section.

As can be seen (28), the dark matter annihilation cross section becomes smaller as the gauge coupling α_{B-L} is lowered, for a fixed $m_{\rm DM}$. This can be seen in Figure 2, where, for a fixed $m_{\rm DM}$, the resultant relic abundance becomes larger as α_{B-L} is lowered. As a result, there is a lower bound on α_{B-L} in order to satisfy the cosmological upper bound on the dark matter relic abundance $\Omega_{\rm DM}h^2 \leq 0.1213$. For a α_{B-L} value larger than the lower bound ($\alpha_{B-L} = 0.0014$ in Figure 2), we can find two values of m_{DM} which result in the center value of the observed relic abundance $\Omega_{\rm DM}h^2 = 0.1198$. In Figure 3, we show the dark matter mass yielding $\Omega_{\rm DM}h^2 = 0.1198$ as a function of α_{B-L}, for $m_{Z'} = 4$ TeV. As a reference, we also show the dotted lines corresponding to $m_{\rm DM} = m_{Z'}/2$. In Figure 2, we see that the minimum relic abundance is achieved by a dark matter mass which is very close to but smaller than $m_{Z'}/2$. Although the annihilation cross section of (28) has a peak at $\sqrt{s} = m_{Z'}$, the thermal averaged cross section given in (27) includes the integral of the product of the reduced cross section and the modified Bessel function K_1. Our results indicate that for $m_{\rm DM}$ taken to be slightly smaller than $m_{Z'}/2$, the thermal averaged cross section is larger than the one for $m_{\rm DM} = m_{Z'}/2$.

As mentioned above, for a fixed Z'_{B-L} boson mass, we can find a corresponding lower bound on the gauge coupling α_{B-L} in order for the resultant relic abundance not to exceed the cosmological upper bound $\Omega_{\rm DM}h^2 = 0.1213$. Figure 4 depicts the lower bound of α_{B-L} as a function of $m_{Z'}$ [solid (black) line]. Along this solid (black) line, we find that the dark matter mass is approximately given by $m_{\rm DM} \simeq 0.49 m_{Z'}$. The dark matter relic abundance exceeds the cosmological upper bound in the region below the solid (black) line. Along with the other constraints that will be obtained in the next section, Figure 4 is our main result in this section.

5. LHC Run-2 Constraints

The ATLAS and the CMS collaborations have been searching for a Z' boson resonance with dilepton final states (although the Z' boson resonance has been searched also with dijet final states [69], we can see that the constraints from this search are weaker than the one with dilepton final states) at the LHC Run-2 [70, 71] (for the process, see the right diagram in Figure 1) and have improved the upper limits of the Z' boson production cross section from those in the LHC Run-1 [72, 73]. Employing the LHC Run-2 results, in particular, the most recent ATLAS result with a 36/fb luminosity [68], we will derive an upper bound on α_{B-L} as a function of $m_{Z'}$. (The results in this article are the update of the results in [46, 54].) Since we have obtained in the previous section the lower bound on α_{B-L} as a function of $m_{Z'}$ from the constraint on the dark matter relic abundance, the LHC Run-2 results are complementary to the cosmological constraint. As a result, the parameter space of the Z'_{B-L} portal dark matter scenario is severally constrained once the two constraints are combined.

Let us consider the Z'_{B-L} boson production process, $pp \longrightarrow Z'_{B-L} + X \longrightarrow l^+l^- + X$, where X denotes hadron jets. The differential cross section is given by

$$\frac{d\sigma}{dM_{ll}} = \sum_{a,b} \int_{M_{ll}^2/E_{\rm CM}^2}^1 dx \frac{2M_{ll}}{xE_{\rm CM}^2} f_a\left(x, Q^2\right) f_b\left(\frac{M_{ll}^2}{E_{\rm CM}^2}, Q^2\right) \times \hat{\sigma}\left(q\bar{q} \longrightarrow Z'_{B-L} \longrightarrow l^+l^-\right), \quad (31)$$

where $E_{\rm CM} = 13$ TeV is the LHC Run-2 energy in the center-of-mass frame, M_{ll} is the invariant mass of the dilepton final

state, and f_a is the parton distribution function (PDF) for a parton "a." For the PDFs we utilize CTEQ6L [74] with $Q = m_{Z'}$ as the factorization scale. Here, the cross section for the colliding partons is given by

$$\widehat{\sigma} = \frac{4\pi\alpha_{B-L}^2}{81} \frac{M_{ll}^2}{\left(M_{ll}^2 - m_{Z'}^2\right)^2 + m_{Z'}^2\Gamma_{Z'}^2}. \tag{32}$$

In calculating the total cross section, we set a range of M_{ll} that is used in the analysis by the ATLAS and the CMS collaborations, respectively. We compare our results of the total cross section with the upper limits of the ATLAS and CMS results.

In the analysis by the ATLAS and the CMS collaborations, the so-called sequential SM Z' (Z'_{SSM}) model [75] has been considered as a reference model. We first analyze the sequential Z' model to check a consistency of our analysis with the one by the ATLAS collaboration [68]. In the sequential Z' model, the Z'_{SSM} boson has exactly the same couplings with quarks and leptons as the SM Z boson. With the couplings, we calculate the cross section of the process $pp \longrightarrow Z'_{SSM} + X \longrightarrow l^+l^- + X$ like (31). By integrating the differential cross section in the region of 128 GeV $\leq M_{ll} \leq$ 6000 GeV [72], we obtain the cross section of the dilepton production process as a function of Z'_{SSM} boson mass. Our result is shown as a solid line in the top panel in Figure 5, along with the plot presented by the ATLAS collaboration [68]. In the analysis in the ATLAS paper, the lower limit of the Z'_{SSM} boson mass is found to be 4.5 TeV, which is read from the intersection point of the theory prediction (diagonal dashed line) and the experimental cross section bound [horizontal solid curve (in red)]. In order to take into account the difference of the PDFs used in the ATLAS and our analysis and QCD corrections of the process, we have scaled our resultant cross section by a factor $k = 1.31$, with which we can obtain the same lower limit of the Z'_{SSM} boson mass as 4.5 TeV. We can see that our result with the factor of $k = 1.31$ is very consistent with the theoretical prediction (diagonal dashed line) presented in [68]. This factor is used in our analysis of the Z'_{B-L} production process. Now we calculate the cross section of the process $pp \longrightarrow Z'_{B-L} + X \longrightarrow l^+l^- + X$ for various values of α_{B-L}, and our results are shown in the bottom panel of Figure 5, along with the plot in [68]. The diagonal solid lines from left to right correspond to $\alpha_{B-L} = 10^{-5}, 10^{-4.5}, 10^{-4}, 10^{-3.5}, 10^{-3}, 10^{-2.5}, 10^{-2}$, and $10^{-1.8}$, respectively. From the intersections of the horizontal curve and diagonal solid lines, we can read off a lower bound on the Z'_{B-L} boson mass for a fixed α_{B-L} value. In this way, we have obtained the upper bound on α_{B-L} as a function the Z'_{B-L} boson mass, which is depicted in Figure 4 [dashed (red) line].

In Figure 4, we also show the LEP bound as the dotted line which is obtained from the search for effective 4 Fermi interactions mediated by the Z'_{B-L} boson [76]. An updated limit with the final LEP 2 data [4] is found to be [77]

$$\frac{m_{Z'}}{g_{B-L}} \geq 6.9 \text{ TeV} \tag{33}$$

at 95% confidence level. We find that the ATLAS bound at the LHC Run-2 is more severe than the LEP bound for the

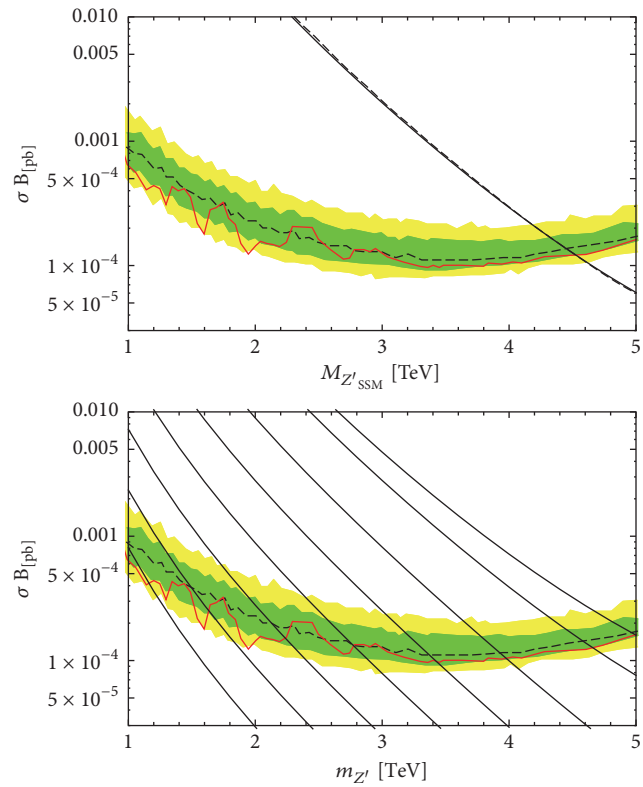

FIGURE 5: Top panel: the cross section as a function of the Z'_{SSM} mass (solid line) with $k = 1.31$, along with the ATLAS result in [68] from the combined dielectron and dimuon channels. Bottom panel: the cross sections calculated for various values of α_{B-L} with $k = 1.31$. The solid lines from left to right correspond to $\alpha_{B-L} = 10^{-5}, 10^{-4.5}, 10^{-4}, 10^{-3.5}, 10^{-3}, 10^{-2.5}, 10^{-2}$, and $10^{-1.8}$, respectively.

Z' boson mass range presented here. In order to avoid the Landau pole of the running $B - L$ coupling $\alpha_{B-L}(\mu)$, below the Plank mass ($1/\alpha_{B-L}(M_{pl}) > 0$), we find

$$\alpha_{B-L} < \frac{\pi}{6 \ln\left[M_{pl}/m_{Z'}\right]}, \tag{34}$$

which is shown as the dashed-dotted line in Figure 4. Here, the gauge coupling α_{B-L} used in our analysis for dark matter physics and LHC physics is defined as the running gauge coupling $\alpha_{B-L}(\mu)$ at $\mu = m_{Z'}$, and we have employed the renormalization group equation at the one-loop level with $m_N^1 = m_N^2 = m_\Phi = m_{Z'}$, for simplicity.

6. Conclusions

We have discussed a simple extension of the SM where the global $B - L$ symmetry in the SM is promoted to the $B - L$ gauge symmetry. In the minimal version of this extension, which is the so-called minimal $B - L$ model, we introduce three right-handed neutrinos with a $B - L$ charge -1 and the $B-L$ (SM singlet) Higgs field with a $B-L$ charge $+2$. The three right-handed neutrinos cancel all the gauge and gravitational anomalies caused by gauging the $B - L$ symmetry. The VEV of the $B - L$ Higgs field breaks the $B - L$ gauge symmetry

and generates the $B-L$ gauge boson (Z'_{B-L}) mass but also the Majorana masses for the right-handed neutrinos. The SM neutrino mass matrix is then generated after the electroweak symmetry breaking. In order to supplement the minimal $B-L$ model with a dark matter candidate, we have introduced a Z_2 symmetry and one right-handed neutrino of a unique Z_2-odd particle in the model plays the role of the dark matter. In this way, the minimal $B-L$ model with Z_2 symmetry supplements the major missing pieces of the SM, the neutrino mass matrix, and a dark matter candidate, while the original particle content of the minimal $B-L$ model is kept intact.

In this model context, we have investigated the "Z'_{B-L} portal" dark matter scenario, where the dark matter particle (Z_2-odd right-handed neutrino) mainly communicates with the SM particles through the Z'_{B-L} boson. We have only three free parameters in our analysis, namely, the gauge coupling (α_{B-L}), the dark matter mass (m_{DM}), and the Z'_{B-L} boson mass ($m_{Z'}$). We have derived the lower bound on α_{B-L} as a function of $m_{Z'}$ by using the cosmological bound on the dark matter relic abundance. On the other hand, the LHC Run-2 results on the search for a narrow resonance constrain the Z'_{B-L} production cross section at the LHC. We have interpreted the latest results by the ATLAS collaboration [68] and derived the upper bound on α_{B-L} as a function of $m_{Z'}$. Similar (but weaker) upper bounds on α_{B-L} have been obtained from the results by the LEP experiment and the perturbativity condition of the running $B-L$ gauge coupling below the Planck mass. After combining all constraints, we have obtained the allowed parameter space shown in Figure 4. We can see that the cosmological and the collider constraints are complementary for narrowing down the arrowed parameter space: $m_{Z'} \geq 3.9$ TeV. Since the SM background events for $m_{Z'} \gtrsim 3$ TeV are negligibly small (see [68]), we expect that the future search reaches for the Z' boson production scales as the luminosity of the LHC experiments. In the narrow decay width approximation (which is justified in our analysis), the Z'_{B-L} boson production cross section is proportional to α_{B-L}. Therefore, from Figure 4, we expect that the (green) shaded region will be covered in the future with a LHC luminosity about 120/fb.

Towards direct and indirect detection of dark matter particles, many experiments are in operation and also planned. Because of its Majorana nature, the right-handed neutrino dark matter has the axial vector coupling with the Z'_{B-L} boson, while the SM fermions have the vector couplings due to their $B-L$ charges. Hence, the elastic scattering amplitude between the dark matter particles and quarks through the Z'_{B-L} boson exchange is vanishing in the nonrelativistic limit, and our dark matter particle evades its direct detection. We can consider an indirect detection of the right-handed neutrino dark matter through cosmic rays from their pair annihilations in the galactic halo. However, because of the Majorana nature, the pair annihilation cross section is highly suppressed by a dark matter velocity at the present universe, and we find that the cosmic ray flux from the dark matter pair annihilations is far below the observable level for the parameter region shown in Figure 4.

If kinematically allowed, a pair of right-handed neutrinos involved in the seesaw mechanism can be produced from a Z'_{B-L} boson decay. Collider signatures of the right-handed neutrinos produced in this way have been studied (see, for example, [78–82] for recent studies). The right-handed neutrinos, once observed at the LHC, are clue to understand the mass generation mechanism of light neutrinos. In addition to the study of Z' boson production at the LHC, the search for right-handed neutrinos at the future LHC is worth investigating.

It is interesting to extend the minimal $B-L$ model to the so-called nonexotic $U(1)_X$ model [83]. In this model, the particle content remains the same, while the $U(1)_X$ charge of a particle is generalized as $Q_X = Yx_H + Q_{B-L}$, where Y and Q_{B-L} are $U(1)_Y$ and $U(1)_{B-L}$ charges of the particle, respectively, and x_H is a real parameter. In this $U(1)_X$ generalization, the minimal $B-L$ model is realized as a limit $x_H = 0$. For studies on the Z' portal dark matter scenario in the minimal $U(1)_X$ model, see [54]. With a special value of $x_H = -4/5$, we can consider the unification of the model into the gauge group $SU(5) \times U(1)_X$ [84].

Finally, our minimal $B-L$ model with the right-handed neutrino dark matter can also account for the origin of the baryon asymmetry in the universe through leptogenesis [85] with two Z_2-even right-handed neutrinos if they are almost degenerate (so-called resonant leptogenesis [86, 87]). See [88] for detailed analysis. Furthermore, if we introduce nonminimal gravitational coupling, the $B-L$ Higgs field plays the role of inflaton which causes cosmological inflation in the early universe. We can achieve the successful cosmological inflation scenario with a suitable choice of the nonminimal gravitational coupling constant. See, for example, [89–91].

Conflicts of Interest

The author declares that she has no conflicts of interest.

Acknowledgments

The author would like to thank Nobuchika Okada for collaborations.

References

[1] ATLAS Collaboration, G. Aad, T. Abajyan et al., "Observation of a new particle in the search for the Standard Model Higgs boson with the ATLAS detector at the LHC," *Physics Letters B*, vol. 716, pp. 1–29, 2012.

[2] CMS Collaboration, S. Chatrchyan, V. Khachatryan et al., "Observation of a new boson at a mass of 125 GeV with the CMS experiment at the LHC," *Physics Letters B*, vol. 716, pp. 30–61, 2012.

[3] LEP Collaborations, ALEPH Collaboration, DELPHI Collaboration et al., "A combination of preliminary electroweak measurements and constraints on the standard model," *High Energy Physics - Experiment*, vol. 2, p. 173, 2006.

[4] DELPHI, OPAL, LEP Electroweak, ALEPH, L3 Collaboration, and S. Schael, "Electroweak measurements in electron–positron collisions at W-boson-pair energies at LEP," *Physics Reports*, vol. 532, no. 4, pp. 119–244, 2013.

[5] CMS ATLAS Collaboration, G. Aad, B. Abbott et al., "Measurements of the Higgs boson production and decay rates and

constraints on its couplings from a combined ATLAS and CMS analysis of the LHC pp collision data at $\sqrt{s} = 7$ and 8 TeV," *Journal of High Energy Physics*, vol. 2016, no. 8, p. 45, 2016.

[6] Y. Fukuda and Super-Kamiokande Collaboration, "Evidence for oscillation of atmospheric neutrinos," *Physical Review Letters*, vol. 81, pp. 1562–1567, 1998.

[7] Q. R. Ahmad and SNO Collaboration, "Measurement of the rate of $\nu_e + d \longrightarrow p + p + e^-$ interactions produced by 8B solar neutrinos at the Sudbury Neutrino Observatory," *Physical Review Letters*, vol. 87, Article ID 071301, 2001.

[8] P. Minkowski, "$\mu \longrightarrow e\gamma$ at a rate of one out of 10^9 muon decays?" *Physics Letters B*, vol. 67, pp. 421–428, 1977.

[9] T. Yanagida, "Horizontal gauge symmetry and masses of neutrinos," in *Proceedings of the International Conference on the Seesaw Mechanism*, pp. 261–264, Institut Henri Poincaré, Paris, France, 1979.

[10] R. N. Mohapatra and G. Senjanovic, "Neutrino mass and spontaneous parity nonconservation," *Physical Review Letters*, vol. 44, p. 912, 1980.

[11] S. L. Glashow, "The future of elementary particle physics," *Nato Science Series B*, vol. 61, p. 687, 1980.

[12] M. Gell-Mann, P. Ramond, and R. Slansky, "Complex Spinors and Unified Theories," in *Conf. Proc. C790927*, pp. 315–321, 1979.

[13] G. Hinshaw, D. Larson, and WMAP Collaboration, "Nine-Year wilkinson microwave anisotropy probe (wmap) observations: cosmological parameter results," *The Astrophysical Journal Supplement Series*, vol. 208, p. 19, 2013.

[14] Planck Collaboration, P. A. R. Ade, N. Aghanim et al., "Planck 2013 results. XV. CMB power spectra and likelihood," *Astronomy & Astrophysics*, vol. 571, p. A15, 2013.

[15] Planck Collaboration and P. A. R. Ade, "Planck 2015 results. XIII. Cosmological parameters," *Astronomy & Astrophysics*, vol. 594, article A13, 63 pages, 2016.

[16] B. W. Lee and S. Weinberg, "Cosmological lower bound on heavy-neutrino masses," *Physical Review Letters*, vol. 39, no. 4, pp. 165–168, 1977.

[17] R. N. Mohapatra and R. E. Marshak, "Local B–L symmetry of electroweak interactions, majorana neutrinos, and neutron oscillations," *Physical Review Letters*, vol. 44, no. 20, pp. 1316–1319, 1980.

[18] R. E. Marshak and R. N. Mohapatra, "Quark-lepton symmetry and $B - L$ as the U(1) generator of the electroweak symmetry group," *Physics Letters B*, vol. 91, no. 2, pp. 222–224, 1980.

[19] C. Wetterich, "Neutrino masses and the scale of $B-L$ violation," *Nuclear Physics B*, vol. 187, no. 2, pp. 343–375, 1981.

[20] A. Masiero, J. F. Nieves, and T. Yanagida, "$B-L$ violating proton decay and late cosmological baryon production," *Physics Letters B*, vol. 116, no. 1, pp. 11–15, 1982.

[21] W. Buchmuller, C. Greub, and P. Minkowski, "Neutrino masses, neutral vector bosons and the scale of B–L breaking," *Physics Letters B*, vol. 267, no. 3, pp. 395–399, 1991.

[22] N. Okada and O. Seto, "Higgs portal dark matter in the minimal gauged," *Physical Review D: Particles, Fields, Gravitation and Cosmology*, vol. 82, no. 2, Article ID 023507, 2010.

[23] S. F. King, "Large mixing angle MSW and atmospheric neutrinos from single right-handed neutrino dominance and U(1) family symmetry," *Nuclear Physics B*, vol. 576, no. 1-3, pp. 85–105, 2000.

[24] P. Frampton, S. Glashow, and T. Yanagida, "Cosmological sign of neutrino CP violation," *Physics Letters B*, vol. 548, no. 3-4, pp. 119–121, 2002.

[25] N. Okada and Y. Orikasa, "Dark matter in the classically conformal $B - L$ model," *Physical Review D: Particles, Fields, Gravitation and Cosmology*, vol. 85, no. 11, Article ID 115006, 2012.

[26] T. Basak and T. Mondal, "Constraining minimal $U(1)_{B-L}$ model from dark matter observations," *Physical Review D: Particles, Fields, Gravitation and Cosmology*, vol. 89, no. 6, Article ID 063527, 2014.

[27] H. An, X. Ji, and L. Wang, "Light dark matter and $Z^{'}$ dark force at colliders," *Journal of High Energy Physics*, vol. 2012, no. 7, 2012.

[28] H. An, R. Huo, and L.-T. Wang, "Searching for low mass dark portal at the LHC," *Physics of the Dark Universe*, vol. 2, no. 1, pp. 50–57, 2013.

[29] D. E. Soper, M. Spannowsky, C. J. Wallace, and T. M. Tait, "Scattering of dark particles with light mediators," *Physical Review D: Particles, Fields, Gravitation and Cosmology*, vol. 90, no. 11, Article ID 115005, 2014.

[30] Z. M. Burell and N. Okada, "Supersymmetric minimal $B - L$ model at the TeV scale with right-handed Majorana neutrino dark matter," *Physical Review D: Particles, Fields, Gravitation and Cosmology*, vol. 85, no. 5, Article ID 055011, 2012.

[31] L. Basso, O. Fischer, and J. J. van der Bij, "Natural model with an inverse seesaw mechanism and leptonic dark matter," *Physical Review D: Particles, Fields, Gravitation and Cosmology*, vol. 87, no. 3, Article ID 035015, 2013.

[32] M. Das and S. Mohanty, "Leptophilic dark matter in gauged $L_\mu - L_\tau$ extension of MSSM," *Physical Review D: Particles, Fields, Gravitation and Cosmology*, vol. 89, no. 2, Article ID 025004, 2014.

[33] X. Chu, Y. Mambrini, J. Quevillon, and B. Zaldívar, "Thermal and non-thermal production of dark matter via $Z^{'}$-portal(s)," *Journal of Cosmology and Astroparticle Physics*, vol. 2014, no. 01, pp. 034-034, 2014.

[34] E. Dudas, L. Heurtier, Y. Mambrini, and B. Zaldivar, "Extra U(1), effective operators, anomalies and dark matter," *Journal of High Energy Physics*, vol. 2013, no. 11, p. 083, 2013.

[35] M. Lindner, D. Schmidt, and A. Watanabe, "Dark matter and $U(1)^{'}$ symmetry for the right-handed neutrinos," *Physical Review D: Particles, Fields, Gravitation and Cosmology*, vol. 89, no. 1, Article ID 013007, 2014.

[36] A. Alves, S. Profumo, and F. S. Queiroz, "The dark $Z^{'}$ portal: direct, indirect and collider searches," *Journal of High Energy Physics*, vol. 2014, article 63, 2014.

[37] J. Kopp, L. Michaels, and J. Smirnov, "Loopy constraints on leptophilic dark matter and internal bremsstrahlung," *Journal of Cosmology and Astroparticle Physics*, vol. 2014, no. 04, pp. 022-022, 2014.

[38] P. Agrawal, Z. Chacko, and C. B. Verhaaren, "Leptophilic Dark Matter and the Anomalous Magnetic Moment of the Muon," *Journal of High Energy Physics*, vol. 2014, no. 08, p. 147, 2014.

[39] D. Hooper, "$Z^{'}$ mediated dark matter models for the Galactic Center gamma-ray excess," *Physical Review D: Particles, Fields, Gravitation and Cosmology*, vol. 91, no. 3, Article ID 035025, 2015.

[40] E. Ma and R. Srivastava, "Dirac or inverse seesaw neutrino masses with $B - L$ gauge symmetry and S_3 flavor symmetry," *Modern Physics Letters A*, vol. 30, no. 26, Article ID 1530020, 9 pages, 2015.

[41] A. Alves, A. Berlin, S. Profumo, and F. S. Queiroz, "Dark Matter Complementarity and the $Z^{'}$ Portal," *Physical Review D*, vol. 92, no. 8, Article ID 083004, 2015.

[42] K. Ghorbani and H. Ghorbani, "Two-portal dark matter," *Physical Review D: Particles, Fields, Gravitation and Cosmology*, vol. 91, no. 12, 2015.

[43] B. Sánchez-Vega and E. Schmitz, "Fermionic dark matter and neutrino masses in a $B - L$ model," *Physical Review D: Particles, Fields, Gravitation and Cosmology*, vol. 92, no. 5, 2015.

[44] M. Duerr, P. Fileviez Pérez, and J. Smirnov, "Simplified Dirac dark matter models and gamma-ray lines," *Physical Review D: Particles, Fields, Gravitation and Cosmology*, vol. 92, no. 8, 2015.

[45] E. Ma, N. Pollard, R. Srivastava, and M. Zakeri, "Gauge B-L Model with Residual Z_3 Symmetry," *Physics Letters B*, vol. 750, pp. 135–138, 2015.

[46] N. Okada and S. Okada, "Z'_{BL} portal dark matter and LHC Run-2 results," *Physical Review D: Particles, Fields, Gravitation and Cosmology*, vol. 93, no. 7, 2016.

[47] N. Okada and N. Papapietro, "R-parity conserving minimal SUSY $B - L$ model," *High Energy Physics - Phenomenology*, vol. 1, p. 17, 2016.

[48] W. Chao, H. Guo, and Y. Zhang, "Majorana dark matter with B+L gauge symmetry," *Journal of High Energy Physics*, vol. 2017, no. 4, 2017.

[49] A. Biswas, S. Choubey, and S. Khan, "Galactic gamma ray excess and dark matter phenomenology in a $U(1)_{B-L}$ model," *Journal of High Energy Physics*, vol. 2016, no. 8, 2016.

[50] M. Fairbairn, J. Heal, F. Kahlhoefer, and P. Tunney, "Constraints on Z' models from LHC dijet searches and implications for dark matter," *Journal of High Energy Physics*, vol. 2016, no. 9, 2016.

[51] M. Klasen, F. Lyonnet, and F. S. Queiroz, "NLO+NLL collider bounds, Dirac fermion and scalar dark matter in the B–L model," *The European Physical Journal C*, vol. 77, no. 5, 2017.

[52] P. S. Bhupal Dev, R. N. Mohapatra, and Y. Zhang, "Naturally stable right-handed neutrino dark matter," *Journal of High Energy Physics*, vol. 2016, no. 11, 2016.

[53] W. Altmannshofer, S. Gori, S. Profumo, and F. S. Queiroz, "Explaining dark matter and B decay anomalies with an $L_\mu - L_\tau$ model," *Journal of High Energy Physics*, vol. 12, no. 106, 2016.

[54] N. Okada and S. Okada, "Z'-portal right-handed neutrino dark matter in the minimal $U(1)_X$ extended Standard Model," *Physical Review D: Particles, Fields, Gravitation and Cosmology*, vol. 95, no. 3, Article ID 035025, 2017.

[55] K. Kaneta, Z. Kang, and H.-S. Lee, "Right-handed neutrino dark matter under the B-L gauge interaction," *Journal of High Energy Physics*, vol. 2017, p. 31, 2017.

[56] A. Alves, G. Arcadi, Y. Mambrini, S. Profumo, and F. S. Queiroz, "Augury of darkness: the low-mass dark Z' portal," *Journal of High Energy Physics*, vol. 2017, no. 4, p. 164, 2017.

[57] S. Singirala, R. Mohanta, S. Patra, and S. Rao, "Majorana Dark Matter in a new $B - L$ model," *High Energy Physics - Phenomenology*, vol. 1, p. 21, 2017.

[58] G. Arcadi, M. Dutra, P. Ghosh et al., "The waning of the WIMP? A review of models, searches, and constraints," *The European Physical Journal C*, vol. 78, no. 3, 2018.

[59] Y. Cui and F. D'Eramo, "Surprises from complete vector portal theories: new insights into the dark sector and its interplay with Higgs physics," *Physical Review D: Particles, Fields, Gravitation and Cosmology*, vol. 96, no. 9, Article ID 095006, 2017.

[60] G. Arcadi, P. Ghosh, Y. Mambrini, M. Pierre, and F. S. Queiroz, "Z' portal to Chern-Simons dark matter," *Journal of Cosmology and Astroparticle Physics*, vol. 2017, no. 11, pp. 020-020, 2017.

[61] P. Bandyopadhyay, E. J. Chun, and R. Mandal, "Implications of right-handed neutrinos in B-L extended standard model with scalar dark matter," *Physical Review D*, vol. 97, no. 1, Article ID 015001, 2018.

[62] V. De Romeri, E. Fernandez-Martinez, J. Gehrlein, P. A. Machado, and V. Niro, "Dark Matter and the elusive Z' in a dynamical Inverse Seesaw scenario," *Journal of High Energy Physics*, vol. 2017, no. 10, 2017.

[63] D. Nanda and D. Borah, "Common origin of neutrino mass and dark matter from anomaly cancellation requirements of a $U(1)_{B-L}$ model," *Physical Review D: Particles, Fields, Gravitation and Cosmology*, vol. 96, no. 11, Article ID 115014, 2017.

[64] S. Profumo, F. S. Queiroz, J. Silk, and C. Siqueira, "Searching for secluded dark matter with H.E.S.S., Fermi-LAT, and Planck," *Journal of Cosmology and Astroparticle Physics*, vol. 2018, no. 03, pp. 010-010, 2018.

[65] Particle Data Group Collaboration and C. Patrignani, "Review of particle physics," *Chinese Physics C*, vol. 40, no. 10, Article ID 100001, 2016.

[66] S. Oda, N. Okada, and D. Takahashi, "Right-handed neutrino dark matter in the classically conformal $U(1)'$ extended standard model," *Physical Review D: Particles, Fields, Gravitation and Cosmology*, vol. 96, no. 9, Article ID 095032, 2017.

[67] Planck Collaboration, N. Aghanim, M. Arnaud et al., "Planck 2015 results. XI. CMB power spectra, likelihoods, and robustness of parameters," *Astronomy & Astrophysics*, vol. 594, p. A11, 2016.

[68] ATLAS Collaboration, M. Aaboud, G. Aad et al., "Search for new high-mass phenomena in the dilepton final state using 36 fb^{-1} of proton-proton collision data at $\sqrt{s} = 13$ TeV with the ATLAS detector," *Journal of High Energy Physics*, vol. 2017, no. 10, p. 182, 2017.

[69] M. Aaboud and ATLAS Collaboration, "Search for new phenomena in dijet events using 37 fb^{-1} of pp collision data collected at $\sqrt{s} = 13$ TeV with the ATLAS detector," *Physical Review D*, vol. 96, no. 5, Article ID 052004, 2017.

[70] ATLAS Collaboration, "Search for new high-mass resonances in the dilepton final state using proton-proton collisions at $\sqrt{s} = 13$ TeV with the ATLAS detector," in *Proceedings of the ATLAS-CONF-2016-045*, 2016.

[71] CMS Collaboration, "Search for a high-mass resonance decaying into a dilepton final state in 13 fb^{-1} of pp collisions at $\sqrt{s} = 13$ TeV," CMS-PAS-EXO-16-031.

[72] G. Aad and ATLAS Collaboration, "Search for high-mass dilepton resonances in pp collisions at $\sqrt{s} = 8$ TeV with the ATLAS detector," *Physical Review D*, vol. 5, Article ID 052005, 2014.

[73] CMS Collaboration, "Search for Resonances in the Dilepton Mass Distribution in pp Collisions at $\sqrt{s} = 8$ TeV," in *Proceedings of the CMS-PAS-EXO-12-061*, 2013.

[74] J. Pumplin, D. Robert Stump, J. Huston, H.-L. Lai, P. Nadolsky, and W.-K. Tung, "New generation of Parton distributions with uncertainties from global QCD analysis," *Journal of High Energy Physics*, vol. 2002, article 012, 2002.

[75] V. Barger, W. Y. Keung, and E. Ma, "Doubling of weak gauge bosons in an extension of the standard model," *Physical Review Letters*, vol. 44, no. 18, pp. 1169–1172, 1980.

[76] M. Carena, A. Daleo, B. A. Dobrescu, and T. M. Tait, "Z' gauge bosons at the Tevatron," *Physical Review D: Particles, Fields, Gravitation and Cosmology*, vol. 70, no. 9, Article ID 093009, 2004.

[77] J. Heeck, "Unbroken $B-L$ symmetry," *Physics Letters. B. Particle Physics, Nuclear Physics and Cosmology*, vol. 739, pp. 256–262, 2014.

[78] Z. Kang, P. Ko, and J. Li, "New avenues to heavy right-handed neutrinos with pair production at hadronic colliders," *Physical Review D: Particles, Fields, Gravitation and Cosmology*, vol. 93, no. 7, Article ID 075037, 2016.

[79] P. Cox, C. Han, and T. T. Yanagida, "LHC search for right-handed neutrinos in $Z^{'}$ models," *Journal of High Energy Physics*, vol. 2018, no. 1, p. 37, 2018.

[80] E. Accomando, L. D. Rose, S. Moretti, E. Olaiya, and C. H. Shepherd-Themistocleous, "Extra Higgs boson and $Z^{'}$ as portals to signatures of heavy neutrinos at the LHC," *Journal of High Energy Physics*, vol. 2018, no. 2, p. 109, 2018.

[81] A. Das, N. Okada, and D. Raut, "Enhanced pair production of heavy Majorana neutrinos at LHC," *Physical Review D*, vol. 97, Article ID 115023, 2018.

[82] A. Das, N. Okada, and D. Raut, "Heavy Majorana neutrino pair productions at the LHC in minimal U(1) extended Standard Model," *High Energy Physics - Phenomenology*, vol. 1, p. 21, 2017.

[83] T. Appelquist, B. A. Dobrescu, and A. R. Hopper, "Nonexotic neutral gauge bosons," *Physical Review D: Particles, Fields, Gravitation and Cosmology*, vol. 68, no. 3, Article ID 035012, 2003.

[84] N. Okada, S. Okada, and D. Raut, "$SU(5)\times U(1)_X$ grand unification with minimal seesaw and $Z^{'}$-portal dark matter," *Physics Letters B*, vol. 780, pp. 422–426, 2018.

[85] M. Fukugita and T. Yanagida, "Barygenesis without grand unification," *Physics Letters B*, vol. 174, no. 1, pp. 45–47, 1986.

[86] A. Pilaftsis, "CP violation and baryogenesis due to heavy Majorana neutrinos," *Physical Review D: Particles, Fields, Gravitation and Cosmology*, vol. 56, no. 9, pp. 5431–5451, 1997.

[87] A. Pilaftsis and T. E. J. Underwood, "Resonant leptogenesis," *Nuclear Physics B*, vol. 692, no. 3, pp. 303–345, 2004.

[88] S. Iso, N. Okada, and Y. Orikasa, "Resonant leptogenesis in the minimal," *Physical Review D: Particles, Fields, Gravitation and Cosmology*, vol. 83, no. 9, Article ID 093011, 2011.

[89] N. Okada, M. U. Rehman, and Q. Shafi, "Non-minimal B-L inflation with observable gravity waves," *Physics Letters B*, vol. 701, pp. 520–525, 2011.

[90] N. Okada and D. Raut, "Running non-minimal inflation with stabilized inflaton potential," *The European Physical Journal C*, vol. 77, no. 4, 2017.

[91] S. Oda, N. Okada, D. Raut, and D. Takahashi, "Nonminimal quartic inflation in classically conformal," *Physical Review D: Particles, Fields, Gravitation and Cosmology*, vol. 97, no. 5, Article ID 055001, 2018.

Hindawi
Advances in High Energy Physics
Volume 2018, Article ID 6828560, 15 pages
https://doi.org/10.1155/2018/6828560

Review Article

The Discreet Charm of Higgsino Dark Matter: A Pocket Review

Kamila Kowalska and Enrico Maria Sessolo

National Centre for Nuclear Research, Hoża 69, 00-681 Warsaw, Poland

Correspondence should be addressed to Enrico Maria Sessolo; enrico.sessolo@gmail.com

Received 9 February 2018; Accepted 12 June 2018; Published 11 July 2018

Academic Editor: Yann Mambrini

We give a brief review of the current constraints and prospects for detection of higgsino dark matter in low-scale supersymmetry. In the first part we argue, after performing a survey of all potential dark matter particles in the MSSM, that the (nearly) pure higgsino is the only candidate emerging virtually unscathed from the wealth of observational data of recent years. In doing so by virtue of its gauge quantum numbers and electroweak symmetry breaking only, it maintains at the same time a relatively high degree of model-independence. In the second part we properly review the prospects for detection of a higgsino-like neutralino in direct underground dark matter searches, collider searches, and indirect astrophysical signals. We provide estimates for the typical scale of the superpartners and fine tuning in the context of traditional scenarios where the breaking of supersymmetry is mediated at about the scale of Grand Unification and where strong expectations for a timely detection of higgsinos in underground detectors are closely related to the measured 125 GeV mass of the Higgs boson at the LHC.

1. Introduction

From the particle physics point of view, the simplest, most popular, and arguably most robust mechanism leading to the correct amount of cold dark matter (DM) in the early Universe is thermal freeze-out (see, e.g., [1–4]). Briefly stated, one assumes that the DM consists of one or more matter species that were originally in thermal equilibrium with the Standard Model (SM) after the Big Bang and that, as the Universe expanded and cooled down, "froze" out of equilibrium when their number density became too low for annihilation and creation processes to take place.

As is well known, in the context of the freeze-out mechanism the measurement of the relic abundance provided by WMAP and Planck, $\Omega_{\rm PL}h^2 = 0.1188 \pm 0.0010$ [5, 6], implies a rather specific value for the thermally averaged annihilation cross section of the DM into SM particles: $\langle\sigma v\rangle \approx 3\times10^{-26}\,\mathrm{cm}^3/\mathrm{s} \approx 1\,\mathrm{pb}$. Nevertheless, the thermal mechanism fails to provide any additional information on the nature of the DM itself since a cross section of that size can result from a discouraging wide range of DM mass values, spin quantum numbers, and DM-SM coupling strengths. Thus, in lack of more information, one has almost always to resort to some theoretical assumptions in order to narrow the search for DM down.

Since the 1990s, expectations about the scale of the new physics beyond the SM (BSM) have been driven by the theorists' discomfort with the hierarchy problem. This is the well-known fact that, in a low-energy effective theory that includes one or more light fundamental scalars (as likely is the SM with a Higgs boson), one expects enormous quantum corrections to the scalar's mass from the physics in the UV (the Planck scale, in the absence of anything else). Given the broad separation between the characteristic energies in play, this means that in order to get electroweak symmetry breaking (EWSB) one should fine tune the fundamental (unknown) Lagrangian parameters at the level, again in the absence of anything lighter than the Planck scale, of one part in $\sim 10^{28}$, unless, of course, additional degrees of freedom were present, preferably close to the Higgs mass itself (say $\sim 100 - 1000\,\mathrm{GeV}$).

Remarkably, simply on dimensional grounds, if one of these expected TeV-scale BSM particles were to be the DM, its coupling to the SM extracted from the freeze-out mechanism

would be of the size of the electroweak coupling constant, $g \approx (16\pi m_{\rm DM}^2 \cdot 1\,{\rm pb})^{1/4} \approx 0.1 - 1$. This fascinating coincidence, which, in light of its singling out specifically weakly interacting massive particles, or WIMPs, is known as the "WIMP miracle," maintains its attractiveness to these days, even if the LHC has failed to discover new particles below the scale of approximately 2 TeV [7, 8].

Arguably the most complete and well motivated of the known BSM theories still remains low-scale supersymmetry (SUSY) (see, e.g., [9], for a popular review). From the theoretical point of view, not only does SUSY provide possibly the most elegant solution to the hierarchy problem (if one allows for the possibility that, given the current LHC bounds, the theory might have to be amended to regain full naturalness), but it also leads to a more precise UV unification of the gauge couplings than in the SM alone; it provides a solid rationale for the measured value of the Higgs boson and top quark masses and, by extension, for radiative EWSB. From the phenomenological point of view, the Minimal Supersymmetric Standard Model (MSSM) contains all the necessary ingredients for successful baryogenesis and provides a framework for cosmic inflation. It thus makes sense that, of all possible candidates for WIMPs, through the years a lot of attention was dedicated to the particles of the MSSM.

In this review we give a compact summary of the subject of DM in the traditional MSSM. After briefly surveying the particles with the potential of providing a good DM candidate, we argue that the nearly pure higgsino neutralino survives to these days as perhaps the only one that is not in substantial tension with any phenomenological constraint. Interestingly, it does so in a relatively model-independent way, without the need of resorting to narrow or secluded regions of the parameter space. We will thus review the higgsino's prospects for detection in direct underground DM searches, indirect searches for DM in gamma-ray, and neutrino telescopes and at the LHC. Incidentally we will show that, in those models where SUSY breaking is transmitted to the visible sector at the scale of Grand Unification (GUT), the detection prospects of higgsino DM become tightly bound to the typical mass of the sfermions in the spectrum and, as a direct consequence, to the size of the Higgs boson mass.

In recent months several comprehensive reviews on the status of WIMP dark matter have appeared in the literature [10–13], one of which, coauthored by one of us, dedicated a full chapter to the MSSM neutralino with particular attention to the detection prospects of a $\sim$ 1 TeV higgsino. While that work is broader in scope, casting light on the experimental opportunities provided by neutralinos in the context of the wider picture of thermal DM models, DM constraints, and existing experimental anomalies, we concentrate here instead on the specific physical characteristics of higgsinos, underlining what we believe makes them currently stand out as the most interesting elements in the DM panorama of the MSSM. In this we are not dissimilar, perhaps, to recently appearing studies in the same tone [14, 15].

The structure of the review is as follows. In Section 2 we recall the particles of the MSSM that can provide a good DM candidate, classifying them according to their transformation properties under the SM gauge symmetry group. In Section 3 we single out the higgsino as the most promising candidate of the list and review its detection prospects in different and complementary experimental venues. We dedicate an additional subsection to the calculation of typical fine tuning and expectations for the scale of the superpartners in models constrained at the GUT scale. We summarize the main treated points and conclude in Section 4.

2. Dark Matter in the MSSM

One of the features making the MSSM very attractive from a phenomenological point of view is that its gauge symmetry structure originates directly from the supersymmetrization of the SM itself. As such, the fundamental gauge symmetry is $\mathrm{SU}(3) \times \mathrm{SU}(2) \times \mathrm{U}(1)$, and the dimensionless couplings are of the strong, electroweak, or SM Yukawa type.

One of the consequences is that a potentially viable DM particle is also expected to interact with SM-like strength. Since cosmological observations have long excluded the possibility of DM particles being charged under color [16] and, on the other hand, the DM is by definition "dark," or practically electrically neutral [3, 17], one is led to conclude that all viable DM candidates in the MSSM must be classifiable on the basis only of the SU(2) representation they belong to. Moreover, the available representations are limited to those that can be found in the SM: SU(2) singlets, doublets, and the adjoint.

Before we proceed to briefly review these three groups individually, we remind the reader that in order to make the lightest SUSY particle (LSP) stable on cosmological time scales, one introduces in the MSSM an additional discrete symmetry, R-parity [18–22], under which only the superpartners of the SM fermions, gauge bosons, and any Higgs scalar field are odd. The origin of R-parity is still an active subject of research, and addressing the issue goes beyond the scope of the present review. We just point out that R-parity violation is strongly constrained phenomenologically, by the proton decay rate and electroweak precision measurements [23].

The only particles of the MSSM that are electrically and color-neutral are the neutrinos, their scalar superpartners, called *sneutrinos*, and, finally, the *neutralinos*. Neutralinos, $\chi_{i=1,..,4}$, are Majorana fermion mass eigenstates emerging, after EWSB, from the diagonalization of the mass matrix of four electrically and color-neutral SUSY states (see [24–27] for early studies and [3] for a comprehensive, classic review). Two of these particles are *gauginos*, fermionic superpartners of the SM gauge bosons. The *bino*, $\widetilde{B}$, in particular, is the partner of the U(1) gauge boson, while the neutral *wino*, $\widetilde{W}$, is the partner of the SU(2) gauge boson W_3. The other two states are neutral *higgsinos*, $\widetilde{H}_u$ and $\widetilde{H}_d$, which belong to a vector-like pair of Higgs doublet superfields. If the lightest neutralino, hereafter, indicated simply with χ, is the LSP it can be the DM particle.

At the tree level, the neutralino mass matrix takes the following well-known form:

$$\mathbf{M}_{\chi} = \begin{bmatrix} M_1 & 0 & -\frac{g' v_d}{\sqrt{2}} & \frac{g' v_u}{\sqrt{2}} \\ 0 & M_2 & \frac{g v_d}{\sqrt{2}} & -\frac{g v_u}{\sqrt{2}} \\ -\frac{g' v_d}{\sqrt{2}} & \frac{g v_d}{\sqrt{2}} & 0 & -\mu \\ \frac{g' v_u}{\sqrt{2}} & -\frac{g v_u}{\sqrt{2}} & -\mu & 0 \end{bmatrix}, \quad (1)$$

where g and g' are SU(2) and U(1) gauge couplings, respectively, v_u and v_d are the vacuum expectation values (vev) of the neutral components of the scalar Higgs doublets, M_1 and M_2 are the soft SUSY-breaking bare masses of the bino and wino, respectively, and μ is the vector-like mass parameter of the Higgs doublet superfields.

In the remainder of this section we give an overview of the mentioned DM candidates of the MSSM, highlighting the strongest phenomenological constraints that can be applied in each case. We will not, however, discuss the neutrinos. It has been long known [28, 29] that the SM neutrinos do not provide, on their own, a viable candidate for cold DM. Their mass is $\mathcal{O}(<\text{eV})$, so that they are relativistic at the time of decoupling and therefore incur strong constraints from structure formation [30–32]. On the other hand, heavy right-handed neutrinos, whose existence might be postulated on the ground of the observed neutrino masses and could provide a naturally expected extension of the traditional MSSM, also do not provide a good candidate for DM because they are not protected by R-parity and therefore not stable over cosmological scales in most scenarios.

2.1. SU(2) Singlets

(Nearly) Pure Bino. The first SU(2) singlet DM candidate we present is the bino. Because of EWSB, a pure bino state does not exist in the MSSM, but the lightest neutralino behaves like a pure bino to a very good approximation, after the diagonalization of $\mathbf{M}_{\chi}$, if $|M_1| \ll M_2, \mu$.

The interactions of the bino-like neutralino with the SM fields are easily found by directly supersymmetrizing the SM gauge-fermion-fermion interaction and applying the R-parity conservation constraint. The resulting vertex takes the form bino-sfermion-fermion, $\mathscr{L} \supset -X_L \tilde{f}_L \overline{\chi} P_L f - X_R \tilde{f}_R \overline{\chi} P_R f$, where tree-level couplings, $X_{L,R} = \sqrt{2}\, g' Y_{L,R}$, are expressed in terms of the hypercharge assignment $Y_{L,R}$ of the fermion Weyl spinors.

The pair-annihilation of bino-like neutralinos in the early Universe proceeds at the leading order through the t-channel diagram shown in Figure 1(a). The region of the MSSM parameter space where $\Omega h^2 \approx 0.12$ is obtained in this way is historically known as the *bulk* [33, 34]. One can calculate the thermal cross section for binos, given approximately by the following [35]:

$$\langle \sigma v \rangle_{\tilde{B}} \approx \sum_{\tilde{f}} \frac{g'^4 Y_{\tilde{f}}^4}{2\pi} \frac{m_\chi^2 \left(m_{\tilde{f}}^4 + m_\chi^4 \right)}{\left(m_{\tilde{f}}^2 + m_\chi^2 \right)^4} \left(\frac{T_F}{m_\chi} \right), \quad (2)$$

in terms of the neutralino (bino) mass, m_χ, sfermions' mass $m_{\tilde{f}}$, hypercharge $Y_{\tilde{f}}$, and freeze-out temperature T_F, which parameterizes the dependence on velocity of the p-wave cross section, and is set here approximately at $T_F \approx (0.04-0.05) m_\chi$.

The bulk has been long known to be strongly constrained by direct SUSY searches at colliders. To give a semiquantitative estimate of these constraints, let us assume that only selectrons and smuons belong to the light SUSY spectrum, a reasonable ansatz in light of the strong LHC bounds on particles with color [36–38]. Assuming all four left- and right-handed slepton states have the same mass, and inserting $Y_{\tilde{f}_L} = -1/2$, $Y_{\tilde{f}_R} = -1$ in (2) one finds that the cross section is typically much smaller than ~ 1 pb, except in the range $m_\chi < m_{\tilde{f}} \lesssim 100$ GeV. A charged slepton mass of this size has been long excluded by direct searches at LEP [39].

If, instead of selectrons and smuons, the light sfermions happen to be status, the parameter space opens up a little, $m_{\tilde{\tau}_1} \lesssim 150$ GeV for $m_\chi \approx 50$ GeV, due to the nonnegligible mixing between left and right chiral slepton states, which introduces an s-wave component to the annihilation cross section (see, e.g., [40]). Nevertheless, LHC bounds on electroweak production [41], implying $m_{\tilde{\tau}_1} \gtrsim 109$ GeV, are by now becoming strongly constraining for these scenarios too, which will be probed even more deeply soon [42]. Finally, as we have mentioned, SUSY parameter space where bulk sfermions are charged under color is strongly excluded by LHC direct searches.

A way to evade the strong collider bounds is provided, if the bino-like neutralino and some other sparticles (sfermions $\tilde{f}$ or other gauginos) are nearly degenerate in mass, by the mechanism of coannihilation [43–45]. In this case the cross section of (2) should be replaced with an effective quantity that takes into account the thermal average of all annihilations and coannihilations of the kind $\chi\chi, \chi\tilde{f}, \tilde{f}\tilde{f} \longrightarrow$ SM SM, some of which are likely to be much more efficient than $\chi\chi \longrightarrow$ SM SM alone.

However, without any guidance from the theory in the UV, coannihilation of the bino with other sparticles can only be achieved in narrow slices of the parameter space, which require some tuning of the initial parameters to engineer the desired coincidence of neutralino and sfermion mass. And in models that are instead defined in terms of a limited number of free parameters in the UV, like the CMSSM [46], in which slepton or stop coannihilation with the bino can occur naturally for particular choices of the initial conditions, the preferred regions of the parameter space are incurring increasingly strong limits from direct LHC searches [13, 47–50]. Besides, with gaugino universality at the GUT scale, it is a struggle to fully accommodate the measured value of the Higgs mass at the LHC [47, 51] (this problem is resolved if the gluino mass is a free parameter, e.g., [52]). Thus, even if

coannihilation of the bino with other sparticles can still lead to viable regions of the parameter space in the most generic parametrizations of the MSSM [53], it is also perhaps not exceedingly attractive from a natural point of view.

R Sneutrino. The second SU(2) singlet DM candidate of the MSSM is the scalar "right-handed" sneutrino. The right-handed sneutrino does not properly belong to the MSSM, which in its original formulation features massless neutrinos, but naturally emerges in SM extensions with right-handed neutrinos, which can give rise to the neutrino mass via small Yukawa couplings (if the right-handed neutrino is Dirac), or through the see-saw mechanism (if the right-handed neutrino is Majorana, see, e.g., [54] and references therein).

The phenomenology of right-handed sneutrinos as DM, however interesting, is very model-dependent. In traditional see-saw models with large-scale Majorana mass the right-handed sneutrino is too heavy to be the DM. On the other hand, for a sneutrino of the "Dirac" type, or, in alternative, Majorana but such that the bare mass is of the order of the superpartners' mass [55, 56], the only really model-independent vertex with the SM involves a very small Yukawa coupling $\mathscr{L} \supset -y_{\nu_R} \bar{e}_L \widetilde{H}_u^{\pm}\, \widetilde{\nu}_R - y_{\nu_R} \bar{\nu}_L \widetilde{H}_u^{0}\, \widetilde{\nu}_R$. Thus, the induced t-channel processes similar to Figure 1(a), with sneutrinos (charginos) in place of neutralinos (sfermions), and a tiny coupling constant are not strong enough to get the correct Ωh^2.

On the other hand, the correct relic density can certainly be obtained thanks to the mixing with the left-handed sneutrino, and SUSY breaking can generate A-terms of the order of the SUSY scale, which provide large couplings to the SM Higgs boson. The phenomenology of these cases can be very rich and exceeds the scope of this review. We direct the reader to the vast literature on sneutrino DM for further details (see, e.g., [57–60], for early studies and bounds, and [61] for a recent LHC analysis).

2.2. SU(2) Doublets. We have seen that singlet DM candidates in the MSSM are accompanied by some uncomfortable features: they are either strongly constrained by collider bounds, are only viable in fine-tuned regions of the parameter space, or present a phenomenology that is highly model-dependent. We therefore move on to reviewing the next set of candidates, the SU(2) doublets.

(Nearly) Pure Higgsino. The most popular SU(2) doublet DM candidate, and the one that appears to us most attractive from a phenomenological point of view, is the higgsino, which is the main subject of this review. As was the case for the bino, there is no pure higgsino state after EWSB, but one obtains an almost pure higgsino-like neutralino by diagonalizing $\mathbf{M}_{\boldsymbol{\chi}}$ in (1) in the limit $|\mu| \ll M_1, M_2$.

As supersymmetry assigns a Weyl spinor to each complex state in the scalar Higgs doublets one counts four physical higgsino states, which, after EWSB, give rise to two Majorana neutralinos, χ_1 (or χ) and χ_2, and a Dirac chargino, $\chi^{\pm}$. When $|\mu| \ll M_1 \approx M_2$, the tree-level mass splitting between the two higgsino-like neutralinos is of approximately the size of $m_Z^2/M_{1,2}$ [9], and the splitting between the higgsino-like chargino and the lightest neutralino is approximately half of that. Moreover, radiative corrections also induce a nonnegligible and irreducible mass splitting (~100s MeV) between the charged and neutral states (see, e.g., [62, 63]).

To correctly compute the thermally averaged effective cross section that yields the DM relic abundance, one must take into account all possible annihilations and coannihilations of higgsino states. For m_χ above the W threshold the dominant final state is into W and Z bosons (Figures 1(b) and 1(c) give examples of possible diagrams for this processes), to which higgsino-like neutralinos and charginos couple through the electroweak charged and neutral currents [3]:

$$\begin{aligned}\mathscr{L} \supset & \left(-\frac{g}{2} W_\mu^+ \overline{\chi} \gamma^\mu \chi^- - \frac{g}{4\cos\theta_W} Z_\mu \overline{\chi}_1 \gamma^\mu \chi_2 + \text{h.c.}\right) \\ & - \frac{g}{2\cos\theta_W} Z_\mu \overline{\chi}^+ \gamma^\mu \left(1 - 2\sin^2\theta_W\right) \chi^-.\end{aligned} \tag{3}$$

The effective cross section can be obtained at the leading order in the limit of all four states being degenerate (see, e.g., [35]):

$$\langle \sigma v \rangle_{\widetilde{H}}^{(\text{eff})} \approx \frac{21 g^4 + 3 g^2 g'^2 + 11 g'^2}{512 \pi m_\chi^2}. \tag{4}$$

For heavy, very pure higgsinos, one should include in the calculation of $\langle \sigma v \rangle_{\widetilde{H}}^{(\text{eff})}$ corrections due to the Sommerfeld enhancement, a well-known nonperturbative effect originating from the fact that if a DM particle is much heavier than the electroweak gauge bosons and relatively slow, the weak force becomes effectively long-range and the impact of the nonrelativistic potential on the interaction cross section becomes significant [64, 65]. However, in the case of the higgsino the splitting between its charged and neutral components is almost always large enough to effectively wash out substantial nonperturbative effects originating from the resummation of ladder diagrams [66–68], so that in a first approximation (4) provides a fairly accurate estimate of $\langle \sigma v \rangle_{\widetilde{H}}^{(\text{eff})}$.

One can see that the cross section is typically much larger than ~ 1 pb, unless $m_\chi \approx 1$ TeV (the precise numerical value is more about 1.1 TeV, as we shall see). Thus, ~ 1 TeV higgsino is on its own a good candidate for the DM in the Universe [69], while a higgsino much lighter than 1 TeV requires one to assume the existence of an additional DM component (e.g., axion [70, 71]), needed to get $\Omega h^2 \approx 0.12$.

As we shall see in the next sections, ~ 1 TeV higgsino is generally associated with a large SUSY-breaking scale and for this reason it is not currently very constrained from a phenomenological point of view. However, its characteristic properties can give us hope for a timely detection in direct and indirect DM searches and even, if $m_\chi \ll 1$ TeV, in collider searches.

L Sneutrino. We conclude this subsection by reviewing the properties of the only other SU(2) doublet DM candidate in

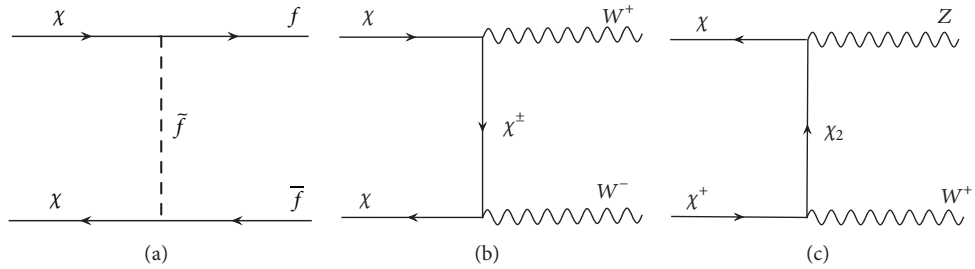

Figure 1: (a) The dominant early-Universe annihilation channel for a nearly pure bino-like neutralino. (b), (c) Examples of annihilation and coannihilation tree-level channels into gauge bosons for a predominantly higgsino-like neutralino.

the MSSM: the "left-handed" sneutrino, scalar superpartner of the SM left-handed neutrino.

The left-handed sneutrino is a complex scalar field with SU(2) × U(1) quantum numbers equal to the higgsino's. Like the higgsino, it has charged and neutral current couplings to the W and Z bosons, $\mathscr{L} \sim -ig/\sqrt{2}(W^+_\mu \tilde{\nu}^*_L \partial^\mu \tilde{e}^-_L + W^-_\mu \tilde{e}^+_L \partial^\mu \tilde{\nu}_L) - ig/(2\cos\theta_W) Z_\mu \tilde{\nu}^*_L \partial^\mu \tilde{\nu}_L$. The mass splitting of the charged and neutral components of the SU(2) doublet is, however, much larger for sneutrinos/sleptons than for higgsinos, being generated through hypercharge D-term contributions [9]: $m^2_{\tilde{e}_L} - m^2_{\tilde{\nu}_L} \approx -m^2_W \cos 2\beta$, where $\tan\beta \equiv v_u/v_d$. Thus, one should resist the temptation of interpreting (4) as an accurate estimate of the effective cross section for sneutrinos too, since the coannihilation of charged and neutral states becomes somewhat less efficient. It turns out [60] that the mass required to produce $\langle\sigma v\rangle^{(\mathrm{eff})}_{\tilde{\nu}_L} \approx 1$ pb is about $m_{\tilde{\nu}_L} \approx 600$–700 GeV. Sneutrinos lighter than that imply the existence of an additional component of DM.

A very important constraint on left-handed sneutrinos as DM arises because they, unlike the Majorana higgsino-like neutralinos, are not their own antiparticle, so that their elastic scattering with nuclei in direct detection experiments proceeds also through t-channel exchange of a Z boson. By virtue of the sneutrino's neutral current coupling, the spin-independent cross section is approximately given by a Fermi-like contact interaction, $\sigma^{\mathrm{SI}}_p \approx \mu^2_{\mathrm{red}} G^2_F/8\pi \approx 10^{-3}$ pb $= 10^{-39}\,\mathrm{cm}^2$, where reduced mass $\mu_{\mathrm{red}} \approx m_p$ for $m_{\tilde{\nu}_L} \gg m_p$. Cross sections of this size have been long excluded in underground detector searches [72, 73].

2.3. SU(2) Adjoint Triplet

(Nearly) Pure Wino. The only SU(2) triplet DM candidate in the MSSM is the wino-like neutralino, dominated by the fermionic superpartner of the W_3 weak gauge boson. The wino belongs to the adjoint representation of the gauge group (hypercharge $Y = 0$) and the wino-like neutralino emerges, after EWSB, from the diagonalization of (1) in the limit $|M_2| \ll M_1, \mu$. One finds a Majorana neutralino, χ, and a Dirac chargino, $\chi^\pm$, mass-degenerate at the tree level. In the context of UV complete models of SUSY-breaking, spectra with a light wino can arise, for example, in scenarios where SUSY breaking is transmitted via anomaly mediation [93, 94].

If the wino LSP is heavier than the electroweak gauge bosons, its dominant final state channel for annihilation (and coannihilation with charginos) in the early Universe is into W (but not Z) boson final states, to which it couples as $\mathscr{L} \sim -g\, W^\pm_\mu \overline{\chi} \gamma^\mu \chi^\mp$. The thermal annihilation cross section is dominated by coannihilations of the three wino states, similarly to what happens for the doublet higgsinos. Annihilation into fermion–antifermion final states through a t-channel sfermion exchange, reminiscent of the bino bulk mechanism, has been instead long excluded by LEP limits on the charged slepton masses.

Unlike higgsinos, in the wino case mass splitting between the charged and neutral fermion component of the SU(2) multiplet is generated exclusively by radiative corrections, $\Delta M_{\widetilde{W}} = (g^2/4\pi) m_W \sin^2(\theta_W/2) \approx 166$ MeV [95]. Note that the mass splitting is typically much smaller than for higgsinos, so that one cannot neglect the effects of the Sommerfeld resummation on the calculation of the thermal cross section. When one includes the Sommerfeld enhancement numerically, the correct relic density is obtained for $m_\chi \approx 2.7$–2.8 TeV [66–68]. For a lighter mass, winos do not saturate the relic abundance.

The Sommerfeld enhancement induces more dramatic modifications of the effective DM annihilation cross section when the average kinetic energy of the WIMP corresponds to speeds of the order of $10^{-3}c$, as in the present-day Universe. This fact has led to the derivation of powerful indirect astrophysical constraints on the annihilation cross section of wino-like neutralinos [91, 96–99]. By taking into account the effects of Sommerfeld-enhanced contributions to the annihilation of winos into monochromatic gamma rays, as well as bounds on the present-day cross section to W^+W^- from diffuse gamma radiation from the Galactic Center and Dwarf Spheroidal satellite galaxies (dSphs), measured in terrestrial and space telescopes HESS [89, 100] and Fermi-LAT/MAGIC [88], and from cosmic-ray (CR) antiproton data at AMS-02 [90, 91], one can derive strong independent constraints (albeit affected by significant systematic uncertainties) which steeply raise the stakes on the wino as a viable DM particle, especially in scenarios where it saturates the relic abundance.

2.4. Mixed Cases. The four neutralinos of the MSSM are all Majorana fermions that, after EWSB, remain neutral under $U(1)_{\mathrm{em}}$ and color. In the absence of a well-separated hierarchy

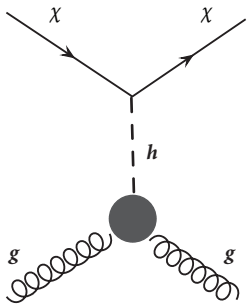

Figure 2: The main interaction between the neutralino and heavy nuclei in underground detectors in the limit of squarks and heavy Higgs bosons being much heavier than $m_h = 125$ GeV and in general outside of LHC reach.

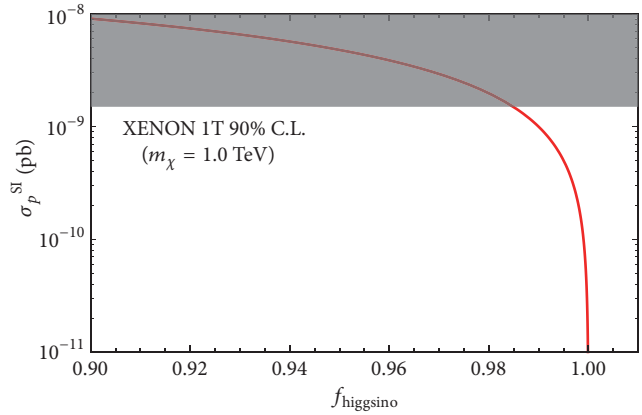

Figure 3: The neutralino-proton spin-independent cross section, σ_p^{SI}, for a typical case of predominantly higgsino-like neutralino DM with $m_\chi = 1.0$ TeV as a function of higgsino purity $f_{higgsino}$ ($\equiv f_h$).

among M_1, M_2, and μ, the lightest mass eigenstate will be an admixture of the SU(2) gauge multiplets discussed in Sections 2.1–2.3 but, unlike those cases, it will present properties that differ significantly from a pure gauge eigenstate.

When $|M_1| \approx |\mu|$ the neutralino is in a highly mixed bino/higgsino state. Mixed neutralinos of this kind (sometimes also called "well-tempered" [35]), originally observed in mSUGRA parameter space [101–103] but that can arise under different boundary conditions (e.g., [104, 105]), enjoyed some popularity, especially before the advent of the LHC, because they can easily lead to $\Omega h^2 \approx 0.12$ for values of the μ parameter as low as few hundreds GeV, which are favored to solve the hierarchy problem. However, the rapid progress made in the bounds on the spin-independent cross section of the neutralino scattering off nuclei in direct WIMP detection searches, combined with a failure to directly observe scalar fermions and heavy Higgs bosons at the LHC, have rendered scenarios where the lightest neutralino is a rich admixture of gaugino and higgsino much less appealing if not excluded altogether (see, e.g. [106], for a very recent update of the constraints on bino-higgsino, and [99] for wino-higgsino scenarios).

To briefly set the issue on quantitative grounds, let us estimate the strength of the coupling with which neutralino admixtures of higgsino and gaugino contribute to the spin-independent cross section. We recall that, in the limit of the squarks and heavy Higgs bosons being much heavier than $m_h = 125$ GeV, which has become a reasonable assumption after the first two runs of the LHC, the main interaction between the neutralino and heavy nuclei in underground detectors proceeds as in Figure 2, via t-channel exchange of the 125 GeV Higgs boson and an effective coupling to gluons through the heavy quark loops.

As the neutralino LSP-Higgs-neutralino LSP tree-level vertex directly stems from applying the gauge covariant derivative on the Higgs doublets, it is nonzero only for a gaugino/higgsino admixture. For $\tan\beta$ sufficiently large to ensure a predominantly SM-like Higgs boson ($\tan\beta > 3-4$ is a condition often fulfilled, for instance, in scenarios where EWSB is obtained radiatively via the renormalization group evolution of soft SUSY-breaking parameters constrained at some high scale, as it prevents certain soft masses from running tachyonic at the low scale.), the coupling to the nucleon can thus be expressed entirely in terms of the higgsino fraction (or *purity*), f_h, which depends on the elements of the unitary matrix, N, diagonalizing (1).

If $\mathrm{diag}[m_{\chi_1}, m_{\chi_2}, m_{\chi_3}, m_{\chi_4}] = N\mathbf{M}_{\boldsymbol{\chi}}N^\dagger$, one can define $f_h \equiv |N_{13}|^2 + |N_{14}|^2$ and express the coupling of interest as $\mathscr{L} \sim (g\sqrt{f_h(1-f_h)}/4)\overline{\chi}\chi h$. Note, incidentally, that deriving an explicit form for the elements of matrix N in terms of bare masses M_1, M_2, and μ is not a trivial task even at the tree level, and useful formulas in this regard can be found in several papers, for example, [107–110]. By simple inspection of (1), however, one can infer a rough approximation for the higgsino fraction in the limit of nearly pure higgsinos, $|\mu| \ll M_2 \approx M_1$:

$$1 - f_h \approx \frac{m_W^2}{\left(M_{1,2} - |\mu|\right)^2}. \tag{5}$$

Equation (5) becomes quite accurate for $f_h \gtrsim 0.999$.

The spin-independent cross section of the neutralino with protons (nucleons), $\sigma_p^{SI} = (4\mu_{red}^2/\pi)|\mathscr{A}_p|^2$, can be parameterized for moderate-to-large $\tan\beta$ simply as follows [3]:

$$\mathscr{A}_p(f_h) \approx a_{\mathrm{eff}}\frac{f_{TG}}{9}\frac{m_p}{v}\frac{g\sqrt{f_h(1-f_h)}}{m_h^2}, \tag{6}$$

in terms of the gluon fractional content of the proton, f_{TG} (we use the default value for `micrOMEGAs v4.3.1` [111], $f_{TG} = 0.92$), and a phenomenological fudge factor, $a_{\mathrm{eff}} \approx 0.9-1$, which takes into account the dependence of $\mathscr{A}_p$ on twist-two operators [112] and higher-order loop corrections [113].

We show in Figure 3 a plot of σ_p^{SI} as a function of purity f_h for a $m_\chi = 1$ TeV neutralino (to a first approximation the DM mass affects the cross section only through the reduced mass leading to $\mu_{red} \approx m_p$). One can see that, for admixtures dominated by the higgsino fraction, the most recent XENON-1T 90% CL upper bound [75] on σ_p^{SI} enforces

$f_h > 98\%$, so that viable DM candidates ought to be very close to a pure higgsino state.

Since the purity of well-tempered higgsino-dominated neutralinos stays well below 90% in those models attempting to provide a satisfactory solution to the hierarchy problem while saturating the relic abundance [35], we conclude that, barring increasingly narrow corners of the parameter space [106], these scenarios have become very hard to rescue or justify in light of the most recent direct detection bounds.

To conclude this subsection, we finally recall that, in cases where $|M_1| < |\mu| \lesssim 1 - 2$ TeV, one obtains scenarios where the mixed neutralino is predominantly bino-like, but also acquires couplings that originate from its admixture with higgsino states, so that additional mechanisms for obtaining $\langle \sigma v \rangle \approx 1$ pb with respect to Section 2.1 are possible.

These mechanisms, often called *funnels*, involve resonant or close-to-resonant s-channel annihilation of two neutralino LSPs via a nearly on-shell mediator which could be the Z boson (if $m_\chi \approx m_Z/2$) [25], the SM Higgs boson (if $m_\chi = 60 - 65$ GeV) [114], or one of the heavy Higgs bosons of the MSSM [33].

Note that the Z-funnel parameter space is strongly constrained by the LHC. The coupling of the lightest neutralino to the Z boson is due exclusively to the isospin neutral current, cf. Section 2.2, which means that in mixed bino-higgsino scenarios it is directly proportional to the higgsino fraction. As a consequence, f_h cannot take excessively small values or, in other words, μ cannot be much larger than $M_1 \approx m_Z/2$. The relative proximity of a mostly higgsino-like chargino and a mostly bino-like neutralino subjects this region of the parameter space to strong bounds from direct LHC multilepton searches [115].

Light and heavy Higgs boson funnels are less constrained from direct LHC SUSY searches than the Z funnel, since the direct coupling to the lightest neutralino is dependent on $\sqrt{f_h}$ and the mediator can be quite heavy. However, there exist complementary observables which can constrain these regions, like the branching ratio BR ($B_s \longrightarrow \mu^+\mu^-$) [116] and direct searches for heavy Higgs bosons in the $\tau\tau$ channel [117]. Moreover, as was the case for the coannihilations of the bino, most phenomenological scenarios require *ad hoc* arrangement of the parameters to obtain the right ratio of neutralino to scalar mass, although this is not necessarily the case for some parameter-space regions of GUT-constrained scenarios like the CMSSM, in which the renormalization group evolution (RGE) of soft masses from a handful of free parameters can lead more naturally to the right mass coincidence (see, e.g., [118, 119] for early studies).

3. Phenomenology of Higgsino Dark Matter

The discussion of Section 2 has led us to conclude that the sole DM candidate of the MSSM emerging almost unscathed from the wealth of observational data of recent years is the nearly pure higgsino. We therefore dedicate this section to the analysis of the prospects for detection of a higgsino-like neutralino in direct DM detection searches, collider searches, and indirect astrophysical signals, and spend a few words on alternative strategies in other experimental venues. We will also give some predictions for the scale of the superpartner particles in traditional models and briefly discuss the issue of fine tuning.

3.1. Prospects for Detection in Direct and Indirect Searches. We begin in Figure 4(a), where we plot the rescaled spin-independent neutralino-nucleon cross section versus neutralino mass for a nearly pure higgsino under CMSSM/mSUGRA boundary conditions [46] (We remind the reader that this means scanning simultaneously over 4 free parameters: m_0, the universal soft SUSY-breaking scalar mass at the GUT scale; $m_{1/2}$, the universal GUT-scale gaugino mass; A_0, the universal GUT-scale soft trilinear coupling; and $\tan\beta$, the ratio of the Higgs doublets' vevs. We scan them in this study over broad ranges: $m_0, m_{1/2} \in [0.1\,\text{TeV}, 30\,\text{TeV}]$, $A_0 \in [-30\,\text{TeV}, 30\,\text{TeV}]$, $\tan\beta \in [1, 62]$. Additionally, one chooses the sign of μ, which we set here to positive, as its sign does not much affect the region of parameter space with nearly pure higgsino DM (see, e.g., [47, 116]). Note that the chosen input mass ranges encompass the parameter space region shown in Figure 4 in its entirety. In it one finds $m_{1/2} \lesssim 0.6 m_0$, with 5 TeV $\lesssim m_0 \lesssim$ 25 TeV, 2.5 TeV $\lesssim m_{1/2} \lesssim$ 15 TeV due to the Higgs mass measurement, see discussion below.). The color code depicts the higgsino DM relic abundance. For the points of the parameter space corresponding to Ωh^2 below the Planck measurement [6], $\Omega_{\text{PL}} h^2 \approx 0.12$, we directly rescale σ_p^{SI} by $\xi = \Omega h^2/\Omega_{\text{PL}} h^2$, assuming implicitly that the fraction of higgsino DM we measure locally today traces closely its early time large-scale freeze-out value. Solid tilted lines show recent direct upper bounds from the PandaX-II [74] (maroon) and XENON1T [75] (blue) underground experiments. The latter is not much more constraining than an earlier bound from the now decommissioned LUX [76]. Dot-dashed lines show the projected reach of several upcoming and planned experiments.

We also show in Figure 4(a) as a thin black line the current lower bound on mass from direct searches for compressed electroweakinos in final states with two low-momentum leptons at the LHC ([82, 83], following a proposal and case studies by [120, 121]), which is sensitive to higgsino DM for mass splitting $m_{\chi_2} - m_{\chi_1} = 3 - 30$ GeV. One should also be aware of the estimated putative reach of the ILC in testing higgsinos [122], which we do not show in the plot for lack of space. It extends to approximately 240 GeV (480 GeV), independently of mass splitting, if the beam energy is set to $s = (500\,\text{GeV})^2$ ($s = 1000^2\,\text{GeV}^2$).

In Figure 4(b) we show the rescaled spin-dependent neutralino-proton elastic scattering cross section, $\xi\sigma_p^{\text{SD}}$, versus neutralino mass. We show with solid lines existing indirect upper bounds from observations of neutrinos from the Sun in the neutrino telescopes IceCube [84] (green) and Antares [85] (red), interpreted for a predominantly W^+W^- annihilation final state, which give a good approximation for the nearly pure higgsino case [53, 123]. Dashed lines of different colors give various projections for the future direct reach in σ_p^{SD} of underground detectors.

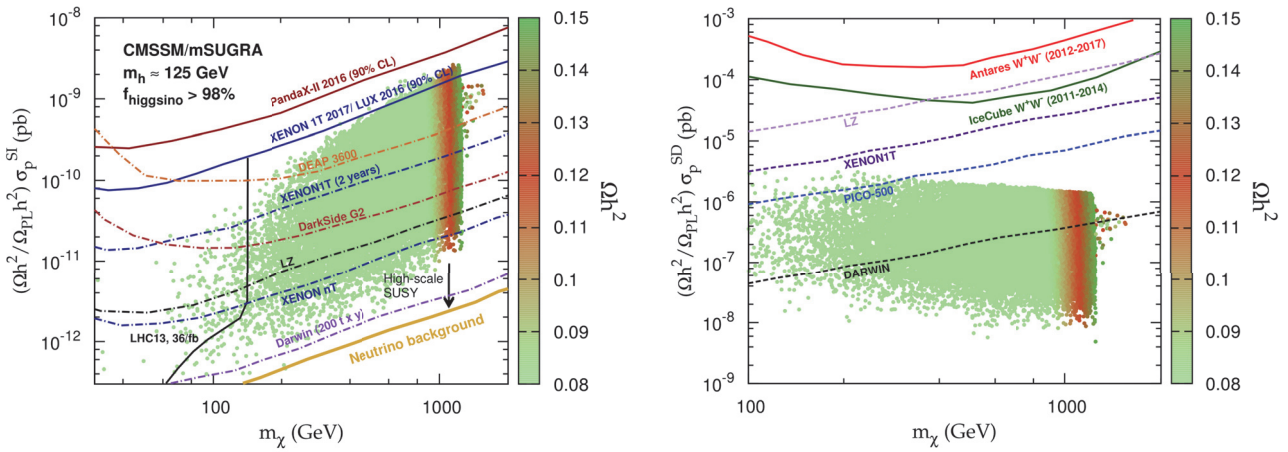

(a) (b)

FIGURE 4: (a) Spin-independent neutralino-nucleon cross section σ_p^{SI} rescaled by the relic abundance, as a function of neutralino mass m_χ, for a nearly pure higgsino with CMSSM/mSUGRA boundary conditions subject to $m_h \approx 125$ GeV and LHC Higgs bounds. Solid lines show the 90% CL upper bounds from PandaX-II [74] (maroon) and XENON1T [75] (LUX [76]) (blue). Dot-dashed lines show the projected reach for DEAP-3600 [77] (orange), XENON1T/nT [78] (blue), DarkSide G2 [79] (maroon), LZ [80] (black), DARWIN (purple) [81]. Thin solid black line shows the current lower bound on mass from direct searches at the LHC [82, 83]. (b) Rescaled spin-dependent neutralino nucleon cross section σ_p^{SD} as a function of neutralino mass m_χ, for the a nearly pure higgsino in the CMSSM/mSUGRA. Solid lines show the 90% CL indirect upper bounds from IceCube [84] (green) and Antares [85] (red). Dashed lines show projections for LZ [86] (violet), XENON1T [78] (purple), Pico-500 [87] (blue), and DARWIN [81] (black).

The relic density and DM observables are here calculated with `micrOMEGAs v4.3.1` [111]. The supersymmetric spectrum is calculated with `SPheno v4.0.3` [124, 125], and all model points are subject to LHC Higgs constraints from `HiggsSignals/HiggsBounds` [126–129] and to the Higgs mass measurement [130]. The Higgs mass is calculated, like the SUSY spectrum, with the latest version of `SPheno`, which yields, in the regime where soft SUSY-breaking masses are well above ~ 1 TeV, a value in excellent agreement with other numerical packages, `SusyHD` [131] and `FlexibleSUSY` [132]. The calculated value is subject to an overall estimated theory uncertainty of approximately 2 GeV [133], which we take into account in Figure 4. Note that when the SUSY spectrum lies in the several TeV regime or above, all electroweak precision and flavor observables, including the anomalous magnetic moment of the muon, are expected to roughly maintain their SM value.

We have chosen to show in Figure 4 the higgsino parameter space under CMSSM boundary conditions, which provide a reasonable ansatz for models with scalar universality inspired by supergravity, and more generally cast in a lean framework scenarios in which supersymmetry breaking is transmitted to the visible sector at some high scale (the GUT scale) and EWSB is obtained radiatively around the minima of the MSSM scalar potential. In models defined in this way one observes, for a higgsino-like neutralino, strong correlation between the Higgs boson mass and the allowed minimum value of σ_p^{SI}. We show this in Figure 5, where we plot the lower bound on σ_p^{SI} as a function of Higgs mass for a higgsino LSP of arbitrary mass. The correlation

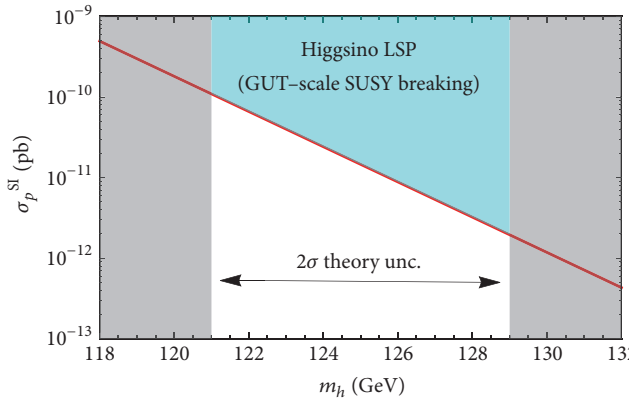

FIGURE 5: Lower bound on σ_p^{SI} as a function of Higgs mass for a higgsino LSP of arbitrary mass in generic models where the breaking of supersymmetry is transmitted at the GUT scale and the physical spectrum and EWSB are obtained after RGE to the low scale.

between minimum cross section and Higgs mass translates in Figure 4(a) into a lower bound on σ_p^{SI} when $m_\chi \approx 1$ TeV.

To qualitatively understand what is happening, let us recall from Section 2.4 that in order to push down σ_p^{SI} for a predominantly higgsino-like neutralino one must increase purity f_h or, in other words, raise the wino and bino masses, cf. (5). Very heavy winos/binos at the GUT scale feed through the RGE on the low-scale value of the soft SUSY-breaking up-type Higgs doublet mass, which carry SU(2) isospin and hypercharge and also tend to push down the right-handed

stop mass. This happens even in scenarios where the gluino mass is not universal and can be found relatively close to the higgsino, like those analyzed in [134].

In order to keep the Higgs doublet soft mass under control, so as to obtain a higgsino-like LSP after EWSB, and avoid tachyonic physical states, numerical scans are in this situation driven to large negative A_0 and/or larger soft scalar mass. Both solutions have the net effect of pushing up the Higgs boson mass and give rise to the behavior we observe in Figure 5 (The attractiveness, from the phenomenological point of view, of a lower bound on the neutralino scattering cross section determined by the Higgs mass measurement was pointed out early on in Bayesian analyses of the CMSSM/NUHM [13, 47, 116]. The exact minimal cross section depends strongly on the calculation of the Higgs mass itself, and on how it translates into mass predictions for the sparticles. In `SPheno v4.0.3`, $m_h \approx 125$ GeV leads to less optimistic expectations for the mean SUSY scale than in the versions of `SOFTSUSY` [135] or `FeynHiggs` [136] used in [47, 116]. Hence the parameter space in Figure 4(a) extends to lower σ_p^{SI} values than in those studies.).

There is no apparent lower bound on the scattering cross section if we relax the requirement of radiative EWSB from boundary conditions generated at the GUT scale. This is the case, for example, in models where the typical mass of scalar particles is by several orders of magnitude decoupled from the electroweak vev (see, e.g., [137–139]), and one does not expect to infer strict relations between the mechanism of SUSY-breaking and EWSB. The relic density alone determines then the mass of the higgsino-like DM, and purity f_h can be extremely close to 1. We generically indicate with a black arrow in Figure 4(a) the parameter space for higgsino DM in those models, which can extend well below the neutrino background floor [63, 140].

This highly inaccessible part of the higgsino parameter space proves particularly tricky to probe. For underabundant higgsinos, $\mu \ll 1$ TeV, interesting venues for detections can be provided, for very small mass splitting, $m_{\chi^\pm} - m_\chi \approx 150$ MeV, by future collider searches for disappearing tracks [141, 142]. If there is a sizable CP violating phase, future electron dipole moment experiments might be sensitive to parameter space with purity in excess of 99.99% [63]. And possibly new venues for detection are given by the cooling curve of white dwarfs [15]. Additional opportunities for the future detection of higgsino-like compressed spectra, in particular for long-lived particles with a relatively short lifetime, can arise then in electron-proton colliders [143].

We finally show in Figure 6 the status of indirect detection bounds and projections in gamma-ray searches in space and terrestrial telescopes for $\sim$ 1 TeV higgsino DM under CMSSM/mSUGRA boundary conditions (we implicitly assume that the chances for detection maximize if higgsinos saturate the relic abundance). In Figure 6(a), solid black line shows the most recent 90% CL upper bound on the present-day σv from the statistical combination of Fermi-LAT and MAGIC observations of dSphs [88], and the magenta line draws the recent bound from 10-year observation of the Galactic Center at HESS [89] under the Einasto profile assumption. We adopt the bounds in the W^+W^- final state interpretation, which give a good approximation for the $\sim$ 1 TeV higgsino.

For the W^+W^- final state we show in solid green the determination by [91] of the 95% CL upper bound on σv from antiproton CR data at AMS-02 [90], under the NFW profile assumption. Note that the bound is subject to uncertainties related to the choice of diffusion model for CR propagation in the Galaxy. Some of these choices can in fact weaken it [91], and push it up to approximately the level of the HESS limit. Finally, dashed blue line shows the projected statistical reach of CTA 500h, under the Einasto profile assumption [53, 144]. Note that including the systematic uncertainty from diffuse astrophysical radiation will most likely weaken the extent of the projected reach [123, 145]. Also note in Figure 6(a) that some model points are characterized by σv significantly above the thermal relic expectation, due to the presence of the heavy pseudoscalar Higgs mass at $m_A \approx 2m_\chi$ [47, 53]. Regions of the parameter space that allow for this serendipitous coincidence thus see their indirect detection prospects improve significantly.

We show in Figure 6(b), as a magenta solid line, the current 95% CL upper bound on the annihilation cross section (times velocity) to gamma-ray lines from the final 254h data at HESS [92] under the Einasto profile assumption. The line is compared to the cross section of our $\sim$ 1 TeV higgsino points, which lie well below the limit.

3.2. The Soft SUSY Scale and Fine Tuning. We conclude with a few words about the expected scale of the supersymmetric particles associated with higgsino DM. In truth, little is known in this regard, as the issue is highly model-dependent and there is not one only way of inferring the scale of SUSY breaking.

Of course, expressions similar to (5)-(6) can give us a lower bound on the scale of the electroweak gauginos for every given upcoming new constraint on σ_p^{SI}, but to be precise one should then take into account the rich parametric dependence of the full formulas. Equivalently, the Higgs mass measurement tells us that in all likelihood stops and gluinos sit well above the LHC reach, but little more than that is known, as expectations depend strongly on parameters like $\tan\beta$ and the trilinear coupling A_t.

Thus, without pretence of presenting any universally valid result, but to just show an example of a model where the measurement of the Higgs mass actually does provide predictions for the maximally allowed typical scale of the superpartners, we present in Figure 7(a) the distribution of the mean stop mass, $M_{\mathrm{SUSY}} = (m_{\tilde{t}_1}\, m_{\tilde{t}_2})^{1/2}$, under CMSSM/mSUGRA boundary conditions in the $(m_\chi, \xi\sigma_p^{\mathrm{SI}})$ plane with higgsino DM. One can see that by approximately the next round of XENON-1T data we will be starting to probe the 10 TeV range of the superpartners if the DM is entirely composed of higgsinos. Note also that, for higgsino mass $m_\chi \lesssim 140$ GeV, the LHC is already excluding, with direct soft-lepton bounds on electroweakinos, the parameter space corresponding to $M_{\mathrm{SUSY}} \lesssim 8 - 10$ TeV.

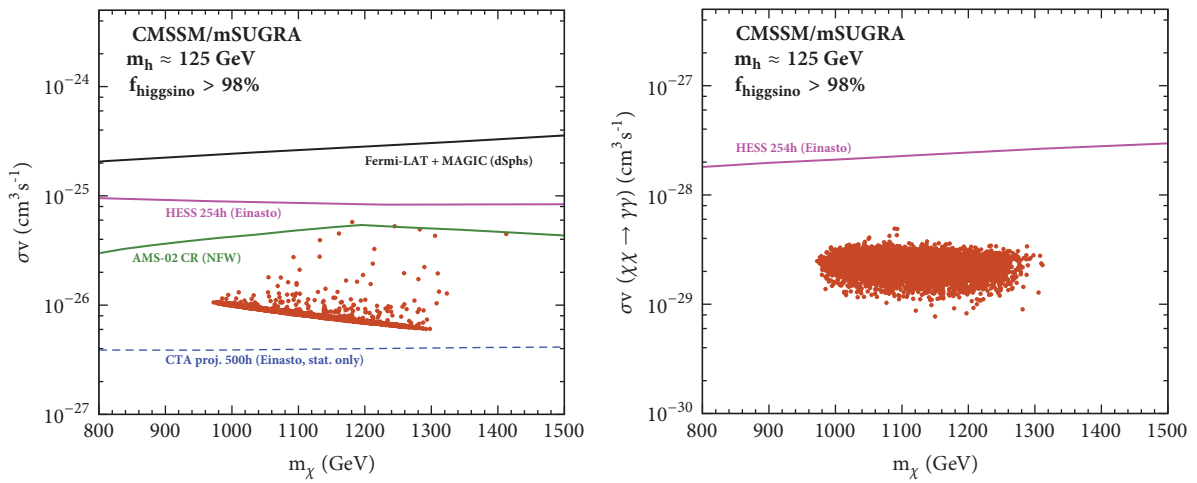

FIGURE 6: (a) Indirect detection bounds and projections in gamma-ray searches in space and terrestrial telescopes for ~ 1 TeV higgsino DM under CMSSM/mSUGRA boundary conditions. Solid black line shows 90% CL upper bounds on the present-day annihilation cross section to W^+W^- from the statistical combination of Fermi-LAT and MAGIC observations of dSphs [88]; solid magenta line shows the recent bound from 10-year observation of the Galactic Center at HESS [89] under the Einasto profile assumption; solid green line shows the upper bound from antiproton cosmic-ray (CR) data at AMS-02 [90] according to [91] for the NFW profile; and dashed blue line shows the projected reach of CTA 500h under the Einasto profile assumption [53]. (b) In magenta, the current 95% CL upper bound on the annihilation cross section (times velocity) to gamma-ray lines, $\sigma_{\gamma\gamma}v$, from HESS [92] under the Einasto profile assumption, compared to the cross section of our ~ 1 TeV higgsino points.

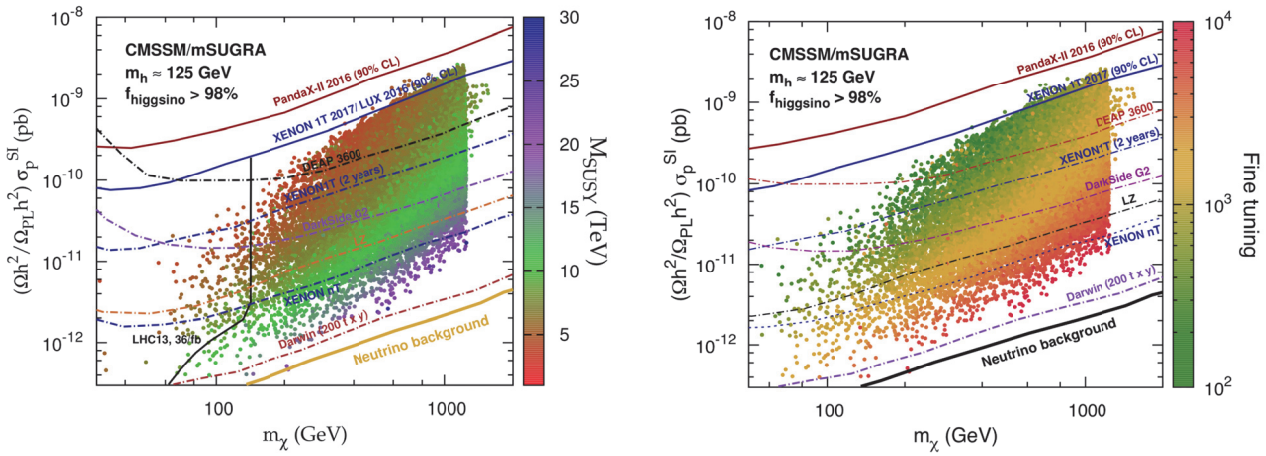

FIGURE 7: (a) A plot of $M_{\text{SUSY}} = (m_{\tilde{t}_1}\ m_{\tilde{t}_2})^{1/2}$ in the $(m_\chi, \xi\sigma_p^{\text{SI}})$ plane with higgsino DM under CMSSM/mSUGRA boundary conditions. (b) EWSB fine tuning for points with higgsino DM in the $(m_\chi, \xi\sigma_p^{\text{SI}})$ plane.

Finally, like all BSM models developed at least in part to deal with the hierarchy problem, after the first two runs of the LHC models with higgsino DM have become marred by a certain amount of EWSB fine tuning. The severity of this issue depends, of course, on the specific features of each model: how EWSB is obtained and the relation to the mass of the Higgs boson. In the context of the CMSSM, the fine tuning associated with higgsino DM is shown in Figure 7(b), where we plot in the $(m_\chi, \xi\sigma_p^{\text{SI}})$ plane the size of the usual Barbieri-Giudice measure [146, 147] (following the prescription of [148]) (We remind the reader that the Barbieri-Giudice measure is generally defined as $\max_{p_i}|\partial \log M_Z^2/\partial \log p_i|$, where p_i are the model's input parameters at the typical scale of the messengers for SUSY breaking. In the CMSSM these are the GUT-defined parameters $m_0, m_{1/2}, A_0, B_0, \mu_0$.). No point shows EWSB fine tuning of less than a part in 100, as direct

consequence of the Higgs mass measurement, and one can observe the well-known fact that higgsino points favored by expectations of naturalness correspond to $m_\chi < 1\,\text{TeV}$ and lead to $\Omega h^2 \ll 0.12$. For the specific case of the $\sim 1\,\text{TeV}$ higgsino, a failure to observe a signal in, say, the next round of XENON-1T data will imply a fine tuning greater than one part in 10^3, with rapid increase with each successive milestone exclusion (There exist ways of embedding the MSSM in UV completions that can lead to lower fine tuning for higgsino DM, see, e.g., [134, 149].).

However, we emphasize that a large fine tuning is by no means exclusive to the CMSSM, to higgsino DM, or even to SUSY in general (see, e.g., [150] for fine tuning in a non-SUSY scenario). As a matter of fact, the majority of phenomenological DM models found in the literature do not even attempt to construct a UV completion that could directly relate their free parameters to the physics of the high scale. It is very possible that once a discovery is finally made many of the suspended questions will start to find their answers. Higgsinos appear to be just in the perfect position to usher, in case of their eventual discovery, a new era of understanding.

4. Summary and Conclusions

The appealing theoretical features of the MSSM have made it, through the years, a natural favorite among the theoretical frameworks incorporating a possible DM particle. In this review, we have given a summary of the current status of phenomenological constraints on the DM candidates of the MSSM and have highlighted the growing consensus that, although available parameter space remains open for most DM aspirant particles, only one of them, the higgsino-like neutralino, is almost entirely free of tension from the increasing amount of observational data.

Much of what makes higgsinos very attractive is the fact that the current constraints are not evaded with specific arrangements of some model parameters, but rather as a consequence only of the higgsino isospin quantum numbers, which lead to a fairly large mass to produce Ωh^2 in agreement with observations, and of the mass splittings among its neutral and charged components, which stem directly from EWSB. As these are not exotic features, one reasonably expects that the higgsino parameter space will not remain unexplored indefinitely.

We have thus reviewed the excellent prospects for detection of higgsinos in the traditional experimental venues of direct DM detection in underground searches, indirect detection from astrophysical observations, and collider accelerators, all of which show reasons for optimism. The prospects are particularly enticing in supergravity-inspired scenarios with radiative EWSB, where the overall consistency of the theoretical picture requires a lower bound on the spin-independent cross section for higgsinos, determined indirectly but convincingly by the measured value of the Higgs boson mass.

For those models that might instead be characterized by very large scales for the superpartners (in agreement with the 125 GeV Higgs mass when $\tan\beta$ is close to 1), the prospects for detection are more tricky to assess, but not without hope. We have drawn the reader's attention to a few references that promoted alternative venues for the explorations of this more fleeting scenarios. Promising venues are given by the experimental determination of dipole moments, disappearing track signatures in colliders, and the measurement of cooling curves in white dwarfs and neutron stars.

Overall, we hope this might serve as an agile but comprehensive report on the consistency of the higgsino DM picture, and on the multiple opportunities that arise for its observation in the not so distant future.

Conflicts of Interest

The authors declare that there are no conflicts of interest regarding the publication of this article.

Acknowledgments

The authors would like to thank Luc Darmé for his comments on the manuscript and discussions. The use of the CIS computer cluster at the National Centre for Nuclear Research in Warsaw is gratefully acknowledged.

References

[1] E. W. Kolb and M. S. Turner, "The early universe," *Frontiers of Physics*, vol. 69, pp. 1–547, 1990.

[2] P. Gondolo and G. Gelmini, "Cosmic abundances of stable particles: improved analysis," *Nuclear Physics B*, vol. 360, no. 1, pp. 145–179, 1991.

[3] G. Jungman, M. Kamionkowski, and K. Griest, "Supersymmetric dark matter," *Physics Reports*, vol. 267, no. 5-6, pp. 195–373, 1996.

[4] S. Dodelson, *Modern Cosmology*, Academic Press, Amsterdam, the Netherlands, 2003, http://www.slac.stanford.edu/spires/find/books/www?cl=QB981:D62:2003.

[5] WMAP Collaboration, E. Komatsu et al., "Seven-year wilkinson microwave anisotropy probe (WMAP) observations: cosmological interpretation," *The Astrophysical Journal Supplement Series*, vol. 192, no. 18, 2011.

[6] Planck Collaboration, P. A. R. Ade et al., "Planck 2015 results. XIII. Cosmological parameters," *Astronomy & Astrophysic*, vol. 549, no. A13, 2016.

[7] https://indico.cern.ch/event/653848/contributions/2719894/attachments/1576222/2489420/CouncilTalk.pdf.

[8] https://indico.cern.ch/event/653848/contributions/2719895/attachments/1576169/2489824/CMSCERN-LHC25.pdf.

[9] S. P. Martin, "A Supersymmetry primer," *Advanced Series on Directions in High Energy Physics*, vol. 18, pp. 1–98, 1998.

[10] G. B. Gelmini, "Light weakly interacting massive particles," *Reports on Progress in Physics*, vol. 80, no. 8, p. 082201, 2017.

[11] G. Arcadi, M. Dutra, P. Ghosh et al., "The waning of the WIMP? A review of models, searches, and constraints," *The European Physical Journal C*, vol. 78, no. 3, p. 203, 2018.

[12] T. Plehn, "Yet another introduction to dark matter," *High Energy Physics—Phenomenology*, 2017.

[13] L. Roszkowski, E. M. Sessolo, and S. Trojanowski, "WIMP dark matter candidates and searches—current status and future prospects," *Reports on Progress in Physics*, vol. 81, no. 6, p. 066201, 2018.

[14] H. Baer, V. Barger, and H. Serce, "SUSY under siege from direct and indirect WIMP detection experiments," *Physical Review D: Particles, Fields, Gravitation and Cosmology*, vol. 94, no. 11, 2016.

[15] R. Krall and M. Reece, "Last electroweak WIMP standing: pseudo-dirac higgsino status and compact stars as future probes," *Chinese Physics C*, vol. 42, no. 4, 2018.

[16] G. D. Starkman, A. Gould, R. Esmailzadeh, and S. Dimopoulos, "Opening the window on strongly interacting dark matter," *Physical Review D: Particles, Fields, Gravitation and Cosmology*, vol. 41, no. 12, pp. 3594–3603, 1990.

[17] P. Smith and J. Bennett, "A search for heavy stable particles," *Nuclear Physics B*, vol. 149, no. 3, pp. 525–533, 1979.

[18] G. R. Farrar and P. Fayet, "Phenomenology of the production, decay, and detection of new hadronic states associated with supersymmetry," *Physics Letters B*, vol. 76, no. 5, pp. 575–579, 1978.

[19] S. Dimopoulos and H. Georgi, "Softly broken supersymmetry and SU(5)," *Nuclear Physics B*, vol. 193, no. 1, pp. 150–162, 1981.

[20] S. Weinberg, "Supersymmetry at ordinary energies. 1. Masses and conservation laws," *Physical Review D: Particles, Fields, Gravitation and Cosmology*, vol. 26, p. 287, 1982.

[21] N. Sakai and T. Yanagida, "Proton decay in a class of supersymmetric grand unified models," *Nuclear Physics B*, vol. 197, no. 3, pp. 533–542, 1982.

[22] S. Dimopoulos, S. Raby, and F. Wilzeck, "Proton decay in supersymmetric models," *Physics Letters B*, vol. 112, no. 2, pp. 133–136, 1982.

[23] R. Barbier et al., "R-parity violating supersymmetry," *Physics Reports*, vol. 420, pp. 1–202, 2005.

[24] J. R. Ellis, J. S. Hagelin, D. V. Nanopoulos, K. A. Olive, and M. Srednicki, "Supersymmetric relics from the big bang," *Nuclear Physics B*, vol. 238, no. 2, pp. 453–476, 1984.

[25] K. Griest, "Cross sections, relic abundance, and detection rates for neutralino dark matter," *Physical Review D: Particles, Fields, Gravitation and Cosmology*, vol. 38, p. 2357, 1988, Erratum: Physical Review D, vol. 39, pp. 3802, 1989.

[26] K. Griest, "Calculations of rates for direct detection of neutralino dark matter," *Physical Review Letters*, vol. 61, no. 6, pp. 666–669, 1988.

[27] K. Griest, M. Kamionkowski, and M. S. Turner, "Supersymmetric dark matter above the w mass," *Physical Review D: Particles, Fields, Gravitation and Cosmology*, vol. 41, no. 12, pp. 3565–3582, 1990.

[28] S. Tremaine and J. E. Gunn, "Dynamical role of light neutral leptons in cosmology," *Physical Review Letters*, vol. 42, no. 6, pp. 407–410, 1979.

[29] S. D. White, C. S. Frenk, and M. Davis, "Clustering in a neutrino-dominated universe," *The Astrophysical Journal*, vol. 274, pp. L1–L5, 1983.

[30] K. Abazajian, "Linear cosmological structure limits on warm dark matter," *Physical Review D: Particles, Fields, Gravitation and Cosmology*, vol. 73, no. 6, 2006.

[31] R. De Putter, O. Mena, E. Giusarma et al., "New neutrino mass bounds from sloan digital sky survey III data release 8 photometric luminous galaxies," *The Astrophysical Journal*, vol. 761, no. 12, 2012.

[32] V. N. Lukash, E. V. Mikheeva, and A. M. Malinovsky, "Formation of the large-scale structure of the Universe," *Physics-Uspekhi*, vol. 54, no. 10, pp. 983–1005, 2011.

[33] M. Drees and M. M. Nojiri, "The Neutralino relic density in minimal $N = 1$ supergravity," *Physical Review D: Particles, Fields, Gravitation and Cosmology*, vol. 47, pp. 376–408, 1993.

[34] H. Baer and M. Brhlik, "Cosmological relic density from minimal supergravity with implications for collider physics," *Physical Review D: Particles, Fields, Gravitation and Cosmology*, vol. 53, no. 2, pp. 597–605, 1996.

[35] N. Arkani-Hamed, A. Delgado, and G. F. Giudice, "The well-tempered neutralino," *Nuclear Physics B*, vol. 741, no. 1-2, pp. 108–130, 2006.

[36] CMS Collaboration, A. M. Sirunyan et al., "Search for new phenomena with the MT2 variable in the all-hadronic final state produced in proton-proton collisions at $\sqrt{s} = 13$ TeV," *The European Physical Journal C*, vol. 77, no. 10, p. 710, 2017.

[37] ATLAS Collaboration, M. Aaboud et al., "Search for top-squark pair production in final states with one lepton, jets, and missing transverse momentum using 36 fb^{-1} of $\sqrt{s} = 13$ TeV pp collision data with the ATLAS detector," *High Energy Physics—Experiment*, 2017.

[38] ATLAS Collaboration, M. Aaboud et al., "Search for squarks and gluinos in final states with jets and missing transverse momentum using 36 fb^{-1} of $\sqrt{s} = 13$ TeV pp collision data with the ATLAS detector," *Physical Review D*, vol. 97, 2018.

[39] Particle Data Group Collaboration, C. Patrignani et al., "Review of particle physics," *Chinese Physics C*, vol. 40, no. 10, 2016.

[40] K. Fukushima, C. Kelso, J. Kumar, P. Sandick, and T. Yamamoto, "MSSM dark matter and a light slepton sector: the incredible bulk," *Physical Review D: Particles, Fields, Gravitation and Cosmology*, vol. 90, no. 9, 2014.

[41] ATLAS Collaboration, G. Aad et al., "Search for the electroweak production of supersymmetric particles in $\sqrt{s} = 8$ TeV pp collisions with the ATLAS detector," *Physical Review D*, vol. 93, no. 5, 2016.

[42] ATLAS Collaboration, "Prospect for a search for direct stau production in events with at least two hadronic taus and missing transverse momentum at theHigh Luminosity LHC with the ATLAS Detector," ATL-PHYS-PUB-2016-021, CERN, Geneva, Switzerland, 2016, http://cds.cern.ch/record/2220805.

[43] K. Griest and D. Seckel, "Three exceptions in the calculation of relic abundances," *Physical Review D: Particles, Fields, Gravitation and Cosmology*, vol. 43, no. 10, pp. 3191–3203, 1991.

[44] J. Ellis, T. Falk, and K. A. Olive, "Neutralino-stau coannihilation and the cosmological upper limit on the mass of the lightest supersymmetric particle," *Physics Letters B*, vol. 444, no. 3-4, pp. 367–372, 1998.

[45] J. Ellis, T. Falk, K. A. Olive, and M. Srednicki, "Calculations of neutralino–stau coannihilation channels and the cosmologically relevant region of MSSM parameter space," *Astroparticle Physics*, vol. 13, no. 2-3, pp. 181–213, 2000, Erratum: Astroparticle Physics, vol. 15, article 413, 2001.

[46] G. L. Kane, C. F. Kolda, L. G. Roszkowski, and J. D. Wells, "Study of constrained minimal supersymmetry," *Physical Review D: Particles, Fields, Gravitation and Cosmology*, vol. 49, no. 11, pp. 6173–6210, 1994.

[47] L. Roszkowski, E. M. Sessolo, and A. J. Williams, "What next for the CMSSM and the NUHM: improved prospects for superpartner and dark matter detection," *Journal of High Energy Physics*, vol. 2014, no. 08, p. 067, 2014.

[48] P. Bechtle et al., "Killing the cMSSM softly," *The European Physical Journal C*, vol. 76, no. 2, p. 96, 2016.

[49] C. Han, K. Hikasa, L. Wu, J. M. Yang, and Y. Zhang, "Status of CMSSM in light of current LHC Run-2 and LUX data," *Physics Letters B*, vol. 769, pp. 470–476, 2017.

[50] GAMBIT Collaboration, P. Athron et al., "Global fits of GUT-scale SUSY models with GAMBIT," *The European Physical Journal C*, vol. 77, no. 12, p. 824, 2017.

[51] J. Ellis, J. L. Evans, F. Luo, K. A. Olive, and J. Zheng, "Stop coannihilation in the CMSSM and SubGUT models," *The European Physical Journal C*, vol. 78, no. 5, 2018.

[52] S. Akula and P. Nath, "Gluino-driven radiative breaking, Higgs boson mass, muon g-2, and the Higgs diphoton decay in supergravity unification," *Physical Review D: Particles, Fields, Gravitation and Cosmology*, vol. 87, no. 11, 2013.

[53] L. Roszkowski, E. M. Sessolo, and A. J. Williams, "Prospects for dark matter searches in the pMSSM," *Journal of High Energy Physics*, vol. 2015, no. 2, p. 014, 2015.

[54] R. N. Mohapatra, "Theories of neutrino masses and mixings," *High Energy Physics—Phenomenology*, 1999.

[55] N. Arkani-Hamed, L. Hall, H. Murayama, D. Smith, and N. Weiner, "Small neutrino masses from supersymmetry breaking," *Physical Review D: Particles, Fields, Gravitation and Cosmology*, vol. 64, no. 11, 2001.

[56] F. Borzumati and Y. Nomura, "Low-scale seesaw mechanisms for light neutrinos," *Physical Review D: Particles, Fields, Gravitation and Cosmology*, vol. 64, no. 5, 2001.

[57] D. Tucker-Smith and N. Weiner, "Inelastic dark matter," *Physical Review D*, vol. 64, 2001.

[58] D. Tucker-Smith and N. Weiner, "The Status of inelastic dark matter," *Physical Review D*, vol. 72, 2005.

[59] T. Asaka, K. Ishiwata, and T. Moroi, "Right-handed sneutrino as cold dark matter," *Physical Review D: Particles, Fields, Gravitation and Cosmology*, vol. 73, no. 5, 2006.

[60] C. Arina and N. Fornengo, "Sneutrino cold dark matter, a new analysis: relic abundance and detection rates," *Journal of High Energy Physics*, vol. 2007, no. 11, p. 029, 2007.

[61] C. Arina, M. E. Catalan, S. Kraml, S. Kulkarni, and U. Laa, "Constraints on sneutrino dark matter from LHC Run 1," *Journal of High Energy Physics*, vol. 2015, no. 5, p. 142, 2015.

[62] M. Drees, M. M. Nojiri, D. P. Roy, and Y. Yamada, "Light Higgsino dark matter," *Physical Review D: Particles, Fields, Gravitation and Cosmology*, vol. 56, pp. 276–290, 1997, Erratum: Physical Review D, vol. 64, article 039901, 2001.

[63] N. Nagata and S. Shirai, "Higgsino dark matter in high-scale supersymmetry," *Journal of High Energy Physics*, vol. 2015, no. 1, p. 029, 2015.

[64] J. Hisano, S. Matsumoto, and M. M. Nojiri, "Unitarity and higher-order corrections in neutralino dark matter annihilation into two photons," *Physical Review D: Particles, Fields, Gravitation and Cosmology*, vol. 67, no. 7, 2003.

[65] J. Hisano, S. Matsumoto, M. M. Nojiri, and O. Saito, "Non-perturbative effect on dark matter annihilation and gamma ray signature from the galactic center," *Physical Review D: Particles, Fields, Gravitation and Cosmology*, vol. 71, no. 6, 2005.

[66] J. Hisano, S. Matsumot, M. Nagai, O. Saito, and M. Senami, "Non-perturbative effect on thermal relic abundance of dark matter," *Physics Letters B*, vol. 646, no. 1, pp. 34–38, 2007.

[67] M. Cirelli, A. Strumia, and M. Tamburini, "Cosmology and astrophysics of minimal dark matter," *Nuclear Physics B*, vol. 787, no. 1-2, pp. 152–175, 2007.

[68] A. Hryczuk, R. Iengo, and P. Ullio, "Relic densities including Sommerfeld enhancements in the MSSM," *Journal of High Energy Physics*, vol. 2011, no. 3, p. 069, 2011.

[69] S. Profumo and C. E. Yaguna, "Statistical analysis of supersymmetric dark matter in the minimal supersymmetric standard model after WMAP," *Physical Review D: Particles, Fields, Gravitation and Cosmology*, vol. 70, no. 9, 2004.

[70] H. Baer, A. Lessa, S. Rajagopalan, and W. Sreethawong, "Mixed axion/neutralino cold dark matter in supersymmetric models," *Journal of Cosmology and Astroparticle Physics*, vol. 1106, no. 06, p. 031, 2011.

[71] H. Baer, A. Lessa, and W. Sreethawong, "Coupled Boltzmann calculation of mixed axion/neutralino cold dark matter production in the early universe," *Journal of Cosmology and Astroparticle Physics*, vol. 1201, no. 01, p. 036, 2012.

[72] T. Falk, K. A. Olive, and M. Srednicki, "Heavy sneutrinos as dark matter," *Physics Letters B*, vol. 339, no. 3, pp. 248–251, 1994.

[73] L. J. Hall, T. Moroi, and H. Murayama, "Sneutrino cold dark matter with lepton-number violation," *Physics Letters B*, vol. 424, no. 3-4, pp. 305–312, 1998.

[74] PandaX-II Collaboration, A. Tan et al., "Dark matter results from first 98.7 days of data from the PandaX-II experiment," *Physical Review Letters*, vol. 117, no. 12, 2016.

[75] XENON Collaboration, E. Aprile et al., "First dark matter search results from the XENON1T experiment," *Physical Review Letters*, vol. 119, no. 18, 2017.

[76] LUX Collaboration, D. S. Akerib et al., "Results from a search for dark matter in the complete LUX exposure," *Physical Review Letters*, vol. 118, no. 2, 2017.

[77] DEAP Collaboration, P. A. Amaudruz et al., "DEAP-3600 dark matter search," *Nuclear and Particle Physics Proceedings*, no. 273–275, pp. 340–346, 2016.

[78] XENON Collaboration, E. Aprile et al., "Physics reach of the XENON1T dark matter experiment," *Journal of Cosmology and Astroparticle Physics*, vol. 1604, no. 04, p. 027, 2016.

[79] C. E. Aalseth et al., "The darkside multiton detector for the direct dark matter search," *Advances in High Energy Physics*, vol. 2015, Article ID 541362, 8 pages, 2015.

[80] LUX Collaboration, LZ Collaboration, and M. Szydagis, "The present and future of searching for dark matter with LUX and LZ," in *Proceedings of the 38th International Conference on High Energy Physics*, vol. 220, Chicago, IL, USA, August 2016.

[81] DARWIN Collaboration, J. Aalbers et al., "DARWIN: towards the ultimate dark matter detector," *Journal of Cosmology and Astroparticle Physics*, vol. 1611, no. 017, 2016.

[82] ATLAS Collaboration, M. Aaboud et al., "Search for electroweak production of supersymmetric states in scenarios with compressed mass spectra at $\sqrt{s} = 13$ TeV with the ATLAS detector," *Physical Review D*, vol. 97, no. 5, 2018.

[83] CMS Collaboration, "Search for new physics in events with two low momentum opposite-sign leptons and missing transverse energy at $\sqrt{s} = 13$TeV," CMS-PAS-SUS 16-048, CERN, Geneva, Switzerland, 2017.

[84] IceCube Collaboration, M. G. Aartsen et al., "Search for annihilating dark matter in the Sun with 3 years of IceCube data," *The European Physical Journal C*, vol. 77, no. 3, p. 146, 2017.

[85] ANTARES Collaboration, S. Adrian-Martinez et al., "Limits on dark matter annihilation in the sun using the ANTARES neutrino telescope," *Physics Letters B*, vol. 759, pp. 69–74, 2016.

[86] LZ Collaboration, D. S. Akerib et al., "LUX-ZEPLIN (LZ) conceptual design report," *Physics—Instrumentation and Detectors*, 2015.

[87] https://indico.cern.ch/event/432527/contributions/1071434/attachments/1320962/1980949/PICO_Dark_Matter_Searches_ICHEP_2016.pdf.

[88] Fermi-LAT Collaboration, MAGIC Collaboration, M. L. Ahnen et al., "Limits to dark matter annihilation cross-section from a combined analysis of MAGIC and Fermi-LAT observations of dwarf satellite galaxies," *Journal of Cosmology and Astroparticle Physics*, vol. 2016, no. 02, p. 039, 2016.

[89] H.E.S.S. Collaboration, H. Abdallah et al., "Search for dark matter annihilations towards the inner Galactic halo from 10 years of observations with H.E.S.S," *Physical Review Letters*, vol. 117, no. 11, 2016.

[90] AMS Collaboration, M. Aguilar et al., "Antiproton flux, antiproton-to-proton flux ratio, and properties of elementary particle fluxes in primary cosmic rays measured with the alpha magnetic spectrometer on the international space station," *Physical Review Letters*, vol. 117, no. 9, 2016.

[91] A. Cuoco, J. Heisig, M. Korsmeier, and M. Krämer, "Constraining heavy dark matter with cosmic-ray antiprotons," *Journal of Cosmology and Astroparticle Physics*, vol. 1804, no. 04, p. 004, 2018.

[92] H.E.S.S. Collaboration, L. Rinchiuso, E. Moulin, A. Viana, C. Van Eldik, and J. Veh, "Dark matter gamma-ray line searches toward the Galactic Center halo with H.E.S.S I," in *Proceedings of the 35th International Cosmic Ray Conference (ICRC '17)*, vol. 893, 2017.

[93] L. Randall and R. Sundrum, "Out of this world supersymmetry breaking," *Nuclear Physics B*, vol. 557, pp. 79–118, 1999.

[94] G. F. Giudice, R. Rattazzi, M. A. Luty, and H. Murayama, "Gaugino mass without singlets," *Journal of High Energy Physics*, vol. 1998, no. 12, p. 027, 1998.

[95] M. Cirelli, N. Fornengo, and A. Strumia, "Minimal dark matter," *Nuclear Physics B*, vol. 753, no. 1-2, pp. 178–194, 2006.

[96] T. Cohen, M. Lisanti, A. Pierce, and T. R. Slatyer, "Wino dark matter under siege," *Journal of Cosmology and Astroparticle Physics*, vol. 1310, no. 10, p. 061, 2013.

[97] J. Fan and M. Reece, "In wino veritas? Indirect searches shed light on neutralino dark matter," *Journal of High Energy Physics*, vol. 2013, no. 10, p. 124, 2013.

[98] A. Hryczuk, I. Cholis, R. Iengo, M. Tavakoli, and P. Ullio, "Indirect detection analysis: wino dark matter case study," *Journal of Cosmology and Astroparticle Physics*, vol. 1407, no. 07, p. 031, 2014.

[99] M. Beneke, A. Bharucha, A. Hryczuk, S. Recksiegel, and P. Ruiz-Femenía, "The last refuge of mixed wino-Higgsino dark matter," *Journal of High Energy Physics*, vol. 2017, no. 1, 2017.

[100] H.E.S.S. Collaboration, A. Abramowski et al., "Search for photon-linelike signatures from dark matter annihilations with H.E.S.S," *Physical Review Letters*, vol. 110, 2013.

[101] K. L. Chan, U. Chattopadhyay, and P. Nath, ""Naturalness, weak scale supersymmetry and the prospect for the observation of supersymmetry at the Tevatron and at the CERN LHC," *Physical Review D: Particles, Fields, Gravitation and Cosmology*, vol. 58, no. 9, 1998.

[102] J. L. Feng, K. T. Matchev, and T. Moroi, "Focus points and naturalness in supersymmetry," *Physical Review D: Particles, Fields, Gravitation and Cosmology*, vol. 61, no. 7, 2000.

[103] J. L. Feng, K. T. Matchev, and F. Wilczek, "Neutralino dark matter in focus point supersymmetry," *Physics Letters B*, vol. 482, no. 4, pp. 388–399, 2000.

[104] H. Baer, A. Mustafayev, E. Park, and X. Tata, "Target dark matter detection rates in models with a well-tempered neutralino," *Journal of Cosmology and Astroparticle Physics*, vol. 2007, no. 0701, p. 017, 2007.

[105] H. Baer, A. Mustafayev, E. Park, and X. Tata, "Collider signals and neutralino dark matter detection in relic-density-consistent models without universality," *Journal of High Energy Physics*, vol. 2008, no. 05, p. 058, 2008.

[106] M. Badziak, M. Olechowski, and P. Szczerbiak, "Is well-tempered neutralino in MSSM still alive after 2016 LUX results?" *Physics Letters B*, vol. 770, pp. 226–235, 2017.

[107] M. M. El Kheishen, A. A. Shafik, and A. A. Aboshousha, "Analytic formulas for the neutralino masses and the neutralino mixing matrix," *Physical Review D: Particles, Fields, Gravitation and Cosmology*, vol. 45, pp. 4345–4348, 1992.

[108] S. Choi, J. Kalinowski, G. Moortgat–Pick, and P. Zerwas, "Analysis of the neutralino system in supersymmetric theories," *The European Physical Journal C*, vol. 22, no. 3, pp. 563–579, 2001.

[109] S. Y. Choi, M. Drees, and B. Gaissmaier, "Systematic study of the impact of CP violating phases of the MSSM on leptonic high-energy observables," *Physical Review D: Particles, Fields, Gravitation and Cosmology*, vol. 70, no. 1, 2004.

[110] V. Beylin, V. Kuksa, R. Pasechnik, and G. Vereshkov, "Diagonalization of the neutralino mass matrix and boson–neutralino interaction," *The European Physical Journal C*, vol. 56, no. 3, pp. 395–405, 2008.

[111] G. Belanger, F. Boudjema, A. Pukhov, and A. Semenov, "micrOMEGAs_3: a program for calculating dark matter observables," *Computer Physics Communications*, vol. 185, no. 3, pp. 960–985, 2014.

[112] M. Drees and M. M. Nojiri, "Neutralino-nucleon scattering reexamined," *Physical Review D: Particles, Fields, Gravitation and Cosmology*, vol. 48, no. 8, pp. 3483–3501, 1993.

[113] J. Hisano, S. Matsumoto, M. M. Nojiri, and O. Saito, "Direct detection of the Wino and Higgsino-like neutralino dark matter at one-loop level," *Physical Review D: Particles, Fields, Gravitation and Cosmology*, vol. 71, no. 1, 2005.

[114] J. Ellis, L. Roszkowski, and Z. Lalak, "Higgs effects on the relic supersymmetric particle density," *Physics Letters B*, vol. 245, no. 3-4, pp. 545–555, 1990.

[115] L. Calibbi, J. M. Lindert, T. Ota, and Y. Takanishi, "LHC tests of light neutralino dark matter without light sfermions," *Journal of High Energy Physics*, vol. 2014, no. 11, p. 106, 2014.

[116] K. Kowalska, L. Roszkowski, and E. M. Sessolo, "Two ultimate tests of constrained supersymmetry," *Journal of High Energy Physics*, vol. 2013, no. 6, p. 78, 2013.

[117] A. Arbey, M. Battaglia, and F. Mahmoudi, "Supersymmetric heavy Higgs bosons at the LHC," *Physical Review D: Particles, Fields, Gravitation and Cosmology*, vol. 88, no. 1, 2013.

[118] A. B. Lahanas, D. V. Nanopoulos, and V. C. Spanos, "Neutralino relic density in a universe with a nonvanishing cosmological constant," *Physical Review D: Particles, Fields, Gravitation and Cosmology*, vol. 62, no. 2, 2000.

[119] J. Ellis, T. Falk, G. Ganis, K. A. Olive, and M. Srednicki, "The CMSSM parameter space at large tanβ," *Physics Letters B*, vol. 510, no. 1–4, pp. 236–246, 2001.

[120] G. F. Giudice, T. Han, K. Wang, and L.-T. Wang, "Nearly degenerate gauginos and dark matter at the LHC," *Physical Review D: Particles, Fields, Gravitation and Cosmology*, vol. 81, Article ID 115011, 2010.

[121] P. Schwaller and J. Zurita, "Compressed electroweakino spectra at the LHC," *Journal of High Energy Physics*, vol. 2014, no. 3, article 060, 2014.

[122] K. Fujii et al., "The potential of the ILC for discovering new particles," *High Energy Physics—Phenomenology*, 2017.

[123] M. E. Cabrera-Catalan, S. Ando, C. Weniger, and F. Zandanel, "Indirect and direct detection prospect for TeV dark matter in the nine parameter MSSM," *Physical Review D: Particles, Fields, Gravitation and Cosmology*, vol. 92, no. 3, 2015.

[124] W. Porod, "SPheno, a program for calculating supersymmetric spectra, SUSY particle decays and SUSY particle production at e^+e^- colliders," *Computer Physics Communications*, vol. 153, no. 2, pp. 275–315, 2003.

[125] W. Porod and F. Staub, "SPheno 3.1: extensions including flavour, CP-phases and models beyond the MSSM," *Computer Physics Communications*, vol. 183, no. 11, pp. 2458–2469, 2012.

[126] P. Bechtle, S. Heinemeyer, O. Stål, T. Stefaniak, and G. Weiglein, "HiggsSignals: confronting arbitrary higgs sectors with measurements at the tevatron and the LHC," *The European Physical Journal C*, vol. 74, no. 2, article 2711, 2014.

[127] P. Bechtle, O. Brein, S. Heinemeyer, G. Weiglein, and K. E. Williams, "HiggsBounds: confronting arbitrary higgs sectors with exclusion bounds from LEP and the tevatron," *Computer Physics Communications*, vol. 181, no. 1, pp. 138–167, 2010.

[128] P. Bechtle, O. Brein, S. Heinemeyer, G. Weiglein, and K. E. Williams, "HiggsBounds 2.0.0: confronting neutral and charged Higgs sector predictions with exclusion bounds from LEP and the Tevatron," *Computer Physics Communications*, vol. 182, no. 12, pp. 2605–2631, 2011.

[129] P. Bechtle, O. Brein, S. Heinemeyer et al., "HiggsBounds-4: improved tests of extended Higgs sectors against exclusion bounds from LEP, the Tevatron and the LHC," *The European Physical Journal C*, vol. 74, no. 3, pp. 1–32, 2014.

[130] ATLAS, CMS Collaboration, G. Aad et al., "Combined measurement of the higgs boson mass in pp collisions at $\sqrt{s} = 7$ and 8 TeV with the ATLAS and CMS experiments," *Physical Review Letters*, vol. 114, 2015.

[131] J. P. Vega and G. Villadoro, "SusyHD: higgs mass determination in supersymmetry," *Journal of High Energy Physics*, vol. 2015, no. 7, p. 159, 2015.

[132] P. Athron, J. Park, T. Steudtner, D. Stöckinger, and A. Voigt, "Precise higgs mass calculations in (non-)minimal supersymmetry at both high and low scales," *Journal of High Energy Physics*, vol. 2017, no. 1, p. 079, 2017.

[133] F. Staub and W. Porod, "Improved predictions for intermediate and heavy supersymmetry in the MSSM and beyond," *The European Physical Journal C*, vol. 77, no. 5, 2017.

[134] K. Kowalska, L. Roszkowski, E. M. Sessolo, and S. Trojanowski, "Low fine tuning in the MSSM with higgsino dark matter and unification constraints," *Journal of High Energy Physics*, vol. 2014, no. 4, p. 166, 2014.

[135] B. C. Allanach, "SOFTSUSY: a program for calculating supersymmetric spectra," *Computer Physics Communications*, vol. 143, no. 3, pp. 305–331, 2002.

[136] T. Hahn, S. Heinemeyer, W. Hollik, H. Rzehak, and G. Weiglein, "High-precision predictions for the light CP-even higgs boson mass of the minimal supersymmetric standard model," *Physical Review Letters*, vol. 112, no. 14, 2014.

[137] L. J. Hall and Y. Nomura, "Spread supersymmetry," *Journal of High Energy Physics*, vol. 01, no. 082, 2012.

[138] P. J. Fox, G. D. Kribs, and A. Martin, "Split dirac supersymmetry: an ultraviolet completion of higgsino dark matter," *Physical Review D: Particles, Fields, Gravitation and Cosmology*, vol. 90, no. 7, 2014.

[139] K. Benakli, L. Darmé, and M. D. Goodsell, "(O)Mega split," *Journal of High Energy Physics*, vol. 2015, no. 11, 2015.

[140] R. J. Hill and M. P. Solon, "WIMP-nucleon scattering with heavy WIMP effective theory," *Physical Review Letters*, vol. 112, 2014.

[141] R. Mahbubani, P. Schwaller, and J. Zurita, "Closing the window for compressed dark sectors with disappearing charged tracks," *Journal of High Energy Physics*, vol. 2017, no. 6, p. 119, 2017.

[142] H. Fukuda, N. Nagata, H. Otono, and S. Shirai, "Higgsino dark matter or not: role of disappearing track searches at the LHC and future colliders," *Physics Letters B: Particle Physics, Nuclear Physics and Cosmology*, vol. 781, pp. 306–311, 2018.

[143] D. Curtin, K. Deshpande, O. Fischer, and J. Zurita, "Physics opportunities for long-lived particles at electron-proton colliders," *High Energy Physics—Phenomenology*, 2017.

[144] CTA Collaboration, J. Carr et al., "Prospects for indirect dark matter searches with the cherenkov telescope array (CTA)," in *Proceedings of the 34th International Cosmic Ray Conference (ICRC '15)*, vol. 1203, The Hague, The Netherlands, 2016.

[145] H. Silverwood, C. Weniger, P. Scott, and G. Bertone, "A realistic assessment of the CTA sensitivity to dark matter annihilation," *Journal of Cosmology and Astroparticle Physics*, vol. 2015, no. 03, p. 055, 2015.

[146] J. Ellis, K. Enqvist, D. Nanopoulos, and F. Zwirner, "Observables in low-energy superstring models," *Modern Physics Letters A*, vol. 1, no. 1, pp. 57–69, 1986.

[147] R. Barbieri and G. F. Giudice, "Upper bounds on supersymmetric particle masses," *Nuclear Physics B*, vol. 306, no. 1, pp. 63–76, 1988.

[148] G. G. Ross, K. Schmidt-Hoberg, and F. Staub, "Revisiting fine-tuning in the MSSM," *Journal of High Energy Physics*, vol. 2017, 21, no. 3, 2017.

[149] G. G. Ross, K. Schmidt-Hoberg, and F. Staub, "On the MSSM Higgsino mass and fine tuning," *Physics Letters B*, vol. 759, pp. 110–114, 2016.

[150] J. Barnard, D. Murnane, M. White, and A. G. Williams, "Constraining fine tuning in composite higgs models with partially composite leptons," *Journal of High Energy Physics*, vol. 2017, no. 49, 2017.

Hindawi
Advances in High Energy Physics
Volume 2018, Article ID 1825874, 13 pages
https://doi.org/10.1155/2018/1825874

Review Article

Long-Baseline Oscillation Experiments as a Tool to Probe High Energy Flavor Symmetry Models

Pedro Pasquini [1,2]

[1] *Instituto de Física Gleb Wataghin-UNICAMP, 13083-859 Campinas, SP, Brazil*
[2] *Northwestern University, Department of Physics & Astronomy, 2145 Sheridan Road, Evanston, IL 60208, USA*

Correspondence should be addressed to Pedro Pasquini; pedrosimpas@gmail.com

Received 2 February 2018; Revised 19 March 2018; Accepted 22 March 2018; Published 4 July 2018

Academic Editor: Giorgio Arcadi

We review the current status of neutrino oscillation experiments, mainly focusing on T2(H)K, NOνA, and DUNE. Their capability to probe high energy physics is found in the precision measurement of the CP phase and θ_{23}. In general, neutrino mass models predict correlations among the mixing angles that can be used to scan and shrink their parameter space. We updated previous analysis and presented a list of models that contain such structure.

1. Introduction

The upcoming sets of long-baseline neutrino experiments will establish a new standard in the search for new physics. Two distinct directions arise; the phenomenological approach consists of seeking new unobserved phenomena that are present in a large class of models. They were extensively studied in the literature and are subdivided into 3 main groups: Nonstandard Interactions (NSI) searches [1–14], Light Sterile Neutrinos [15–19], and Nonunitarity [20–28]. The second approach is more theory based and was less explored. It focuses on correlations among neutrino mixing angles predicted by high energy models. This opens the possibility of testing models that contain almost no low-energy phenomenological effects different from the Standard Model.

Since the discovery of neutrino oscillations, a plethora of models was realized to try to explain the origin of the neutrino masses. The first proposal was the see-saw mechanism [29–34] which tried to explain the smallness of neutrino masses (m_ν) through a heavy mass scale (M) $m_\nu \propto M^{-1}$. Another possible path uses loop mechanisms, in which neutrino masses can be suppressed at zeroth [35] or even first order [36]. Nevertheless, such theories usually do not explain the structure of the oscillation parameters, as they are merely free parameters.

This changes by the addition of discrete symmetry that controls the pattern of the leptonic mass matrix [37–39]; for a review on the subject see, e.g., [40, 41]. They can predict relations among the neutrino mixing angles [42–53] which can be used to constrain the parameter space of such theories [54].

This manuscript is divided into seven sections: In Section 2 we describe current and future neutrino oscillation experiments: T2K, NOνA, and DUNE and their simulation. In Section 3 we briefly discuss the statistical analysis and methods used to scan the parameter space. In Section 4 we present the sensitivity to neutrino mixing parameters expected in each experiment. In Section 5 we review the possibilities of using the θ_{23}-δ_{CP} correlation in long-baseline experiments by updating previous analysis of two models [55, 56]. In Section 6 we review the possibility of using the θ_{13}-θ_{23} correlation by combining long-baseline experiments with reaction measurements of θ_{13}. In Section 8 we present a summary of the results.

2. Long-Baseline Experiments and Their Simulation

Here we choose focusing on four experimental setups; two of them are already running: T2K [57] and NOνA [58]; and two

Table 1: Summary of neutrino experiments.

Experiment	Baseline	Size	Target	Expected POT	Peak Energy (GeV)	Status
T2K [57]	295 km	22.5 kt	Water	7.8×10^{21} (20×10^{21})	0.6	Running (10% total POT)
NOνA [58]	810 km	14 kt	Liq. Scintillator	3.6×10^{21}	2.0	Running (17% total POT)
DUNE [59]	1300 km	40 kt	Liq. Argon	1.47×10^{21}	2.5	Start data taking: 2026
T2HK [60]	295 km	2×190 kt	Water	1.56×10^{22}	0.6	Start data taking: 2026 (2032)

had their construction approved: DUNE [59] and T2HK [60]. Their sensitivity to the two most unknown parameters of the leptonic sector, the CP violation phase and the atmospheric mixing angle, makes them ideal to probe correlations among the mixing angles. As shown in [54], they can be used to shrink the parameter space of predictive models. A short description of each experiment can be found below and in Table 1.

(1) T2K. The Tokai to Kamiokande (T2K) experiment [57, 61] uses the Super-Kamiokande [62] as a far detector for the J-Park neutrino beam, which consists of an off-axis (by a 2.5° angle) predominantly muon neutrino flux with energy around 0.6 GeV. The Super-Kamiokande detector is a 22.5 kt water tank located at 295 from the J-Park facility. It detects neutrino through the Cherenkov radiation emitted by a charged particle created via neutrino interaction. There is also a near detector (ND280); thus the shape of the neutrino flux is well known, and the total normalization error reaches 5% for the signal and 10% for the background. T2K is already running and its current results can be found in [63] and reach 7×10^{20} POT of flux for each neutrino/antineutrino mode, which corresponds to 10% of the 7.8×10^{21} expected approved exposure. There are also plans for extending the exposure to 20×10^{21} POT.

(2) NOνA. The NuMI off-axis ν_e appearance (NOνA) [58, 64, 65] is an off-axis (by a 0.8° angle) that uses a neutrino beam from the Main Injector of Fermilab's beamline (NuMI). This beam consists of mostly muon neutrinos with energy around 2 GeV traveling through 810 km until arriving at the 14 kt Liquid Scintillator far detector placed at Ash River, Minnesota. The far and near detectors are highly active tracking calorimeters segmented by hundreds of PVP cells and can give a good estimate of the total signal and background within an error of 5% and 10% of total normalization error, respectively. The planned exposure consists of a 3.6×10^{21} POT that can be achieved in 6 years of running time, working in 50% in the neutrino mode and 50% in the antineutrino mode. NOνA is already running; current results can be found in [66, 67].

(3) DUNE. The Deep Underground Neutrino Experiment (DUNE) [59, 68–71] is a long-baseline next generation on-axis experiment also situated in Fermilab. It flux will be generated at the LBNF neutrino beam to target a 40 kt Liquid Argon time chamber projection (LarTPC) located 1300 km away from the neutrino source at Sanford Underground Research Facility (SURF). The beam consists of mostly muon neutrinos of energy around 2.5 GeV and expects a total exposure of 1.47×10^{21} POT running 3.5 years in neutrino mode and 3.5 years in antineutrino mode. The near and far detectors are projected to obtain a total signal (background) normalization uncertainty of 4% (10%). The experiment is expected to start taking data around 2026.

(4) T2HK. The Tokai to Hyper-Kamiokande (T2HK) [60, 72–75] is an upgrade of the successful T2K experiment at J-Park. It uses the same beam as its predecessor T2K, an off-axis beam from the J-Park facility 295 km away from its new far detector: two water Cherenkov tanks with 190 kt of fiducial mass each. The expected total power is 1.56×10^{22} POT to be delivered within 2.5 yrs of neutrino mode and 7.5 yrs of antineutrino mode in order to obtain a similar number of both neutrino types. The new design includes improvements in the detector systems and particle identification that are still in development. For simplicity, we take similar capability as the T2K experiment and will assume a 5% (10%) of signal (background) normalization error. The first data taking is expected to start with one tank in 2026 and the second tank in 2032.

In order to perform simulation of any neutrino experiment, the experimental collaboration uses Monte Carlo Methods, which can be performed through several event generators like GENIE [76], FLUKA [77], and many others. See PDG [78] for a review. Such technique requires an enormous computational power and detector knowledge, as it relies on the simulation of each individual neutrino interaction and how its products evolve inside of the detector. A simpler, but faster, simulation can be accomplished by using a semianalytic calculation of the event rate integral [79]:

$$N_i\left(\nu_\beta \longrightarrow \nu_\alpha\right) = \int_{E_i-\Delta E_i/2}^{E_i+\Delta E_i/2} K_{\nu_\alpha}\left(E, E'\right) \phi_{\nu_\beta}(E)\, P_{\beta\alpha}(E)\, \sigma(E)\, dE\, dE'. \quad (1)$$

N_i is the number of detected neutrinos with energy between $E_i - \Delta E_i/2$ and $E_i + \Delta E_i/2$. $\phi_{\nu_\beta}(E)$ describes the flux of neutrino ν_β arriving at the detector. $P_{\beta\alpha}$ is the oscillation probability and $\sigma(E)$ the detection cross section of the detection reaction.

$K_{\nu_\alpha}(E, E')$, also known as migration matrix, describes how the detector interprets α neutrino with energy E being detected at energy E' and summarizes the effect of the Monte Carlo simulation of the detector into a single function. A perfect neutrino detector is described by a delta function,

Table 2: Description of the possible hypothesis taken to generate the numerical analysis. Here, Standard-3ν means standard 3 neutrino oscillation.

Cases	pseudo-data	Null Hypothesis	Test Hypothesis
General	M_i	M_1	M_2
I	Standard-3ν	Standard-3ν	New Model
II	New Model	Standard-3ν	New Model
III	Standard-3ν	New Model	Standard-3ν
IV	New Model	New Model	Standard-3ν

$K_{\nu_\alpha}(E, E') = \delta(E - E')$, while a more realistic simulation can use a Gaussian function:

$$K_{\nu_\alpha}\left(E, E'\right) = \frac{e^{-(E-E')^2/2\delta E^2}}{\sqrt{2\pi}\delta E}, \tag{2}$$

where δE parametrizes the error in the neutrino energy detection or a migration matrix provided by the experimental collaboration.

The public available software GLoBES [79, 80] follows this approach and is commonly used to perform numerical simulation of neutrino experiments. There is also another tool, the NuPro package [81] that will be publicly released soon. All the simulations in this manuscript are performed using GLoBES.

3. Statistical Analysis and Probing Models: A Brief Discussion

We are interested in a rule to distinguish between two neutrino oscillation models that can modify the spectrum of detected neutrinos in a long-baseline neutrino experiment. From the experimental point of view, one may apply a statistical analysis to quantitatively decide between two (or more) distinct hypotheses given a set of data points H_{real}.

Each model (M_i) will define a probability distribution function (p.d.f.), $f(t \mid M_i)$, where the statistic test function t depends on the real data points and the model parameters θ_i, $i = 1, 2, \ldots$. The best fit of a model is defined as the values of the model parameters that maximize the p.d.f. function: $f_0(M_i) = \max[f(H_{\text{real}}, \theta_i^1 \mid M_i)]$. Thus, one can reject model M_2, over model M_1 by some certain confidence level n if

$$\frac{f_0\left(M_2\right)}{f_0\left(M_1\right)} \leq C_n. \tag{3}$$

C_n is a constant that depends on the probability test, the number of parameters, and the confidence level n.

From the theoretical point of view, the real data points were not yet measured; this means that in order to find the expected experimental sensitivity we need to produce pseudo-data points H_{real} by adding an extra assumption on which model is generating the yet-to-be-measured data points. That means there are various ways of obtaining sensitivity curves; each of them is described in Table 2.

Although one can always generate the pseudo-data points using any desired model at any point in its parameter space, the usual approach is to assume that the data points are generated by the standard 3 neutrino oscillation (Standard-3ν) model with parameters given by current best fit values. We will use this approach in the work. Current best fit values are described in Table 3 and were taken from [82].

Table 3: Current best fit values of Standard-3ν as given by [82]. Notice that Normal Hierarchy is assumed.

parameter	value	error
$\Delta m^2_{21}/10^{-5}$	7.56 eV^2	(19)
$\Delta m^2_{31}/10^{-3}$	2.55 eV^2	(4)
$\sin^2\theta_{12}$	0.321	(18)
$\sin^2\theta_{13}$	0.02155	(90)
$\sin^2\theta_{23}$	0.430	(20)
δ_{CP}/π	1.40	(31)

3.1. Frequentist Analysis. The chi-square test [78, 83, 84] is the most common statistical analysis chosen to test the compatibility between the experimental data and the expected outcome of a given neutrino experiment. It is based on the construction of a Gaussian chi-squared estimator (χ^2) so that $f(t \mid \text{Model}) = \text{N}e^{-\chi^2/2}$. This means that the best fit values are obtained by the set of values that globally minimizes the function χ^2. For long-baseline neutrino oscillation experiments the chi-square function can be divided into three factors:

$$\chi^2 = \chi^2_{\text{data}} + \chi^2_{\text{sys}} + \chi^2_{\text{prior}}, \tag{4}$$

where χ^2_{data} in the simplest case reduces to Poissonian Pearson's statistic

$$\chi^2_{\text{data}} = \sum_i^N \left[\frac{N_i^{\text{obs}} - (1-a)\,N_i^s - (1-b)\,N_i^b}{\sqrt{N_i^{\text{obs}}}}\right]^2. \tag{5}$$

N_i^{obs} is the number of observed neutrinos in the bin $i = 1, 2, 3 \cdots N$. It represents the pseudo-data points generated by a given model. N_i^s (N_i^b) is the signal (background) observed neutrino as expected by a given model and depends on the model parameters. χ^2_{sys} comprises the experimental uncertainties and systematics. For χ^2 in (5), it is given by

$$\chi^2_{\text{sys}} = \left(\frac{a}{\sigma_a}\right)^2 + \left(\frac{b}{\sigma_b}\right)^2. \tag{6}$$

Here, σ_a (σ_b) is the total normalization error in the signal (background) flux. Finally, χ^2_{prior} contains all the prior information one wishes to include in the model parameters. In this work we will assume $\chi^2_{\text{prior}} = 0$ unless stated otherwise.

The exponential nature of the chi-squared estimator makes it straightforward to find the confidence levels for the model parameters. It suffices to define the function

$$\Delta\chi^2 = \chi^2_{\text{min}}\left(\theta_i \mid M_2\right) - \chi^2_{\text{min}}\left(M_1\right), \tag{7}$$

where $\chi^2_{\text{min}}(M_1)$ is the chi-squared function assuming model M_1 calculated in its best fit and $\chi^2_{\text{min}}(\theta_i \mid M_2)$ is the chi-squared function assuming model M_2 minimized over all

the desired free parameters. Thus, the confidence levels are obtained by finding the solutions of

$$\Delta\chi^2 \leq A_n. \tag{8}$$

θ_i are all the fixed parameters of model M_2 and A_n are the constants that define the probability cuts and depend on the number of parameters in $\chi^2(\theta_i \mid M_2)$ and the confidence probability. For $n\sigma$ intervals and one parameter, $A_n = n^2$.

Notice that $\Delta\chi^2$ is in fact a function of the parameters one assumes to generate the pseudo-data points, which we call *True Values* and denote as θ_i(True), and the parameters of the model we wish to test, which we call *Test Values* and denote as θ_i(Test).

4. Measurement of Oscillation Parameters in Long-Baseline Experiments

The main goal of long-baseline experiments is to measure with high precision the two most unknown oscillation parameters: the CP phase and the atmospheric mixing angle θ_{23} through the measurement of the neutrino/antineutrino $\nu_\mu \to \nu_\mu$ survival and $\nu_\mu \to \nu_e$ transition of neutrinos from the beamline. Many authors studied the power of long-baseline experiments to obtain the neutrino mixing parameters [85–93]. Particularly, only the transition is sensitive to δ_{CP} and described, to first order in matter effects, by the probability function below.

$$\begin{aligned} P\left(\nu_\mu \longrightarrow \nu_e\right) &= 4c_{13}^2 s_{13}^2 s_{23}^2 \sin^2\Delta_{31} \\ &+ 8c_{13}^2 s_{12}s_{13}s_{23}\left(c_{12}c_{23}\cos\delta_{\mathrm{CP}} - s_{12}s_{13}s_{23}\right)\cos\Delta_{32} \\ &\cdot \cos\Delta_{31}\cos\Delta_{21} - 8c_{13}^2 c_{12}c_{23}s_{12}s_{13}s_{23}\sin\delta_{\mathrm{CP}}\sin\Delta_{32} \\ &\cdot \sin\Delta_{31}\sin\Delta_{21} + 4s_{12}^2 c_{13}^2\left(c_{12}^2 c_{23}^2 + s_{12}^2 s_{23}^2 s_{13}^2\right. \\ &\left. - 2c_{12}c_{23}s_{12}s_{23}s_{13}\cos\delta_{\mathrm{CP}}\right)\sin^2\Delta_{21} - 8c_{13}^2 s_{13}^2 s_{23}^2 \\ &\cdot \frac{aL}{4E}\left(1 - 2\sin_{13}^2\right)\cos\Delta_{32}\sin\Delta_{31} + 8c_{13}^2 s_{13}^2 s_{23}^2 \\ &\cdot \frac{a}{\Delta m_{31}^2}\left(1 - 2\sin_{13}^2\right)\sin^2\Delta_{31}, \end{aligned} \tag{9}$$

where $c_{ij} = \cos\theta_{ij}$, $s_{ij} = \sin\theta_{ij}$, $\Delta_{ij} = \Delta m_{ij}^2 L/4E$, and $a = 2\sqrt{2}G_{\mathrm{F}}n_e E$. G_{F} is the Fermi constant and n_e is the electron density in the medium. E is the neutrino energy and L is the baseline of the experiment and they are chosen to obey $L/E \sim 500$ in order to enhance the effect of the CP phase. The antineutrino probability is obtained by changing $a \to -a$ and $\delta_{\mathrm{CP}} \to -\delta_{\mathrm{CP}}$. Thus, the difference between neutrino and antineutrino comes from matter effects and the CP phase. It turns out that the T2HK is the most sensitivity to δ_{CP} as it has a bigger statistic and lower matter effect and can reach 8σ difference between CP conservation and maximal CP-nonconservation [73], in contrast with DUNE's 5.5σ [68]. In Figure 1 we plotted the expected allowed regions of θ_{23}(test) versus δ_{CP}(test) at 3σ for each experiment. We assumed the true value of the parameters as those given in Table 3. The

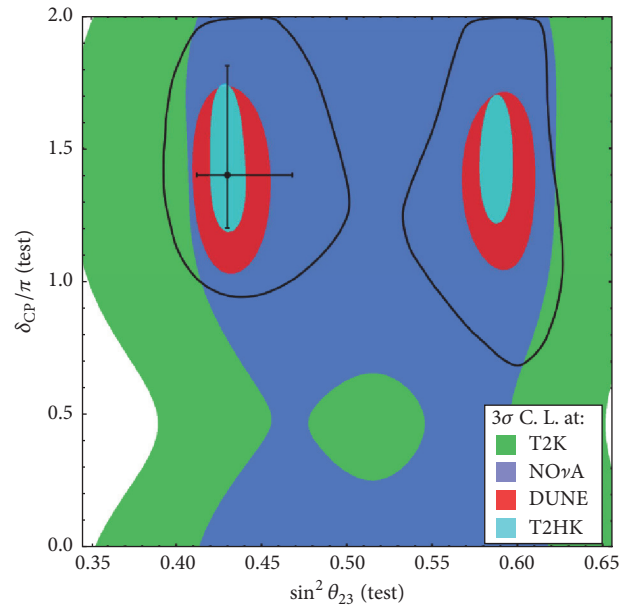

Figure 1: Expected sensitivity regions of $\sin^2\theta_{23}$(test) versus δ_{CP}(test) assuming as the true and test model the Standard-3ν paradigm for the three long-baseline detectors discussed: (1) T2K (green), (2) NOνA (blue), (3) DUNE (red), and (4) T2HK (cyan). The black curve is current 90% CL and the black point is the current best fit given in Table 3. Notice that within this assumptions the octant would remain unresolved even at 3σ CL.

black region is the current 90% CL region and the black points are the best fit points. T2HK is the most sensitive experiment in reconstructing both parameters, followed by DUNE. NOνA and T2K are the first experiments to measure a difference between matter and antimatter in the leptonic sector but cannot measure the CP phase with more than 3σ. Notice that the experiments cannot discover the correct octant of θ_{23} at 3σ; that is, they cannot tell if $\theta_{23} > \pi/4$ (High Octant) or $\theta_{23} < \pi/4$ (Lower Octant) unless they are supplemented by an external prior. This effect is independent of the value of θ_{23} as can be observed in Figure 2(a) where we plotted the reconstruction of θ_{23}(test) given a fixed true value of θ_{23}(true) of each experiment. The black line corresponds to current best fit and the gray area is the 1σ region. The x-like pattern of the region shows that given any true value of θ_{23} there is 3σ region in the correct octant and in the wrong octant. Nevertheless, the octant can be obtained if one incorporates a prior to the θ_{13} angle [94–98] and future prospects on the measurement of θ_{13} by reactor experiments will allow both DUNE and T2HK to measure the octant if the atmospheric angle is not all inside the region $0.47 < \sin^2\theta_{23} < 0.53$ [99].

For completeness, we show in Figure 2(a) the reconstruction of the δ_{CP}(test) given a fixed true value of δ_{CP}(true). The black line represents current best fit and the gray area shows the 1σ region. We do not show the plots for NOνA or T2K as they cannot reconstruct the CP phase at 3σ. The sensitivity is a little bit worse around maximum CP violation $\delta_{\mathrm{CP}} = \pi/2$ or

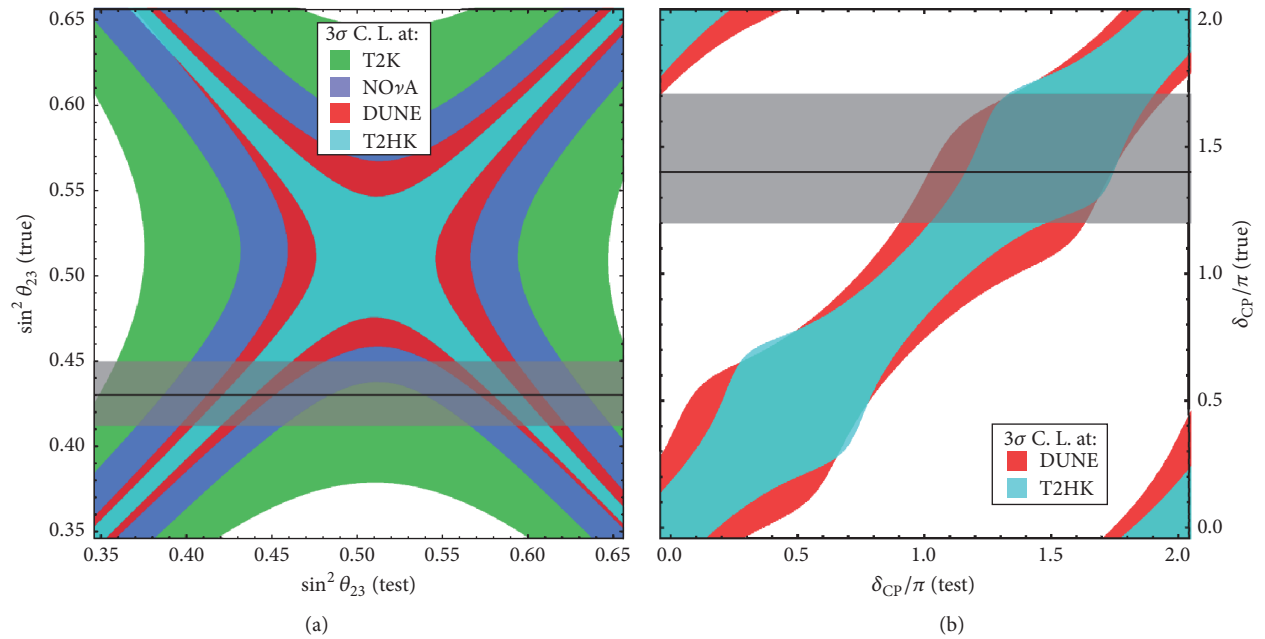

FIGURE 2: (a) and (b) correspond to the expected reconstruction of the oscillation parameter $\theta_{23}(\delta_{CP})$. The black line indicates the best fit value given in Table 3 and the gray area corresponds to its 1σ region. The colored areas represent the regions that the experiments cannot distinguish within more than 3σ for (1) T2K (green), (2) NOνA (blue), (3) DUNE (red), and (4) T2HK (cyan). In (b) we did not include T2K or NOνA as they cannot reconstruct the CP phase with more than 3σ.

$3\pi/2$ but in general it does not change much when one varies δ_{CP}(true).

5. θ_{23} and δ_{CP} Correlation and Probing Models

In spite of being with relatively low energy (<few GeV), neutrino experiments can be a tool to probe high energy physics. Many neutrino mass models predict relations such as neutrino mass sum rules [41, 100–106] that can be probed in neutrinoless double beta decay [107] and relations among the neutrino mixing parameters. To name but a few examples we cite [42–44, 108]. They can be put to test by a scan of the parameter space much like what was done by the LHC in search for new physics. Thus, inspired by the precision power of future long-baseline neutrino experiments, it was shown in [54] that models that predict a sharp correlation between the atmospheric angle and the CP phase can be used to put stringent bounds on parameters of such models.

In general, a predictive neutrino mass model $\mathcal{M}$ is constructed by imposing a symmetry on the Lagrangian and can be parametrized by a set of free parameters ϕ_i, $i = 1, 2, \ldots, N$, which can be translated into the usual neutrino mixing parameters from the neutrino mass matrix; that is,

$$\theta_{jk} \equiv \theta_{jk}(\phi_i), \qquad \delta_{CP} \equiv \delta_{CP}(\phi_i). \tag{10}$$

Because of the symmetry on the Lagrangian, not all possible mass matrices are allowed to be generated and the free parameters ϕ_i may not span the entire space of the mixing parameters θ_{ij} and δ_{CP}. Thus, in principle, it is possible to probe or even exclude a model if the real best fit falls into a region that the model $\mathcal{M}$ cannot predict. As an example, in Figure 3 we plot the allowed parameter space of two discrete symmetry based models, the Warped Flavor Symmetry (WFS) model [45] (a) and the Revamped A_4 Babu-Ma-Valle (BMV) model [109] (b). The black curves represent currently unconstrained (Standard-3ν) 90% CL regions for the neutrino parameters and the black point shows the best fit value, while the blue region represents the 3σ allowed parameter space of the two models. Notice that even for the 3σ range the model can only accommodate a much smaller region than the unconstrained one. This is a reflex of the symmetries forced upon those models by construction; in WFS a maximal CP phase implies $\theta_{23} = \pi/4$, and the smaller the CP violation is, the farther away from $\pi/4$ the atmospheric angle is, while in BMV a maximal CP phase implies a Lower Octant atmospheric mixing and it cannot fit a $|\theta_{23} - \pi/4| > 0.02\pi$.

By using this approach, a full scan of the parameter space was performed for those two models, in [55] for the WFS model and in [56] for the Revamped A_4 model.

We show in Figure 4 an updated version of their results. The colored regions represent regions of the parameter space in which the model *cannot* be excluded with more than 3σ for DUNE (red) and T2HK (cyan) experiment; both T2K and NOνA cannot probe the CP phase with more than 3σ; thus, they cannot exclude the model alone.

This means that if future long-baseline experiments measure a specific combination of δ_{CP} and θ_{23} as its best fit that does not fall into the colored regions, they may be able

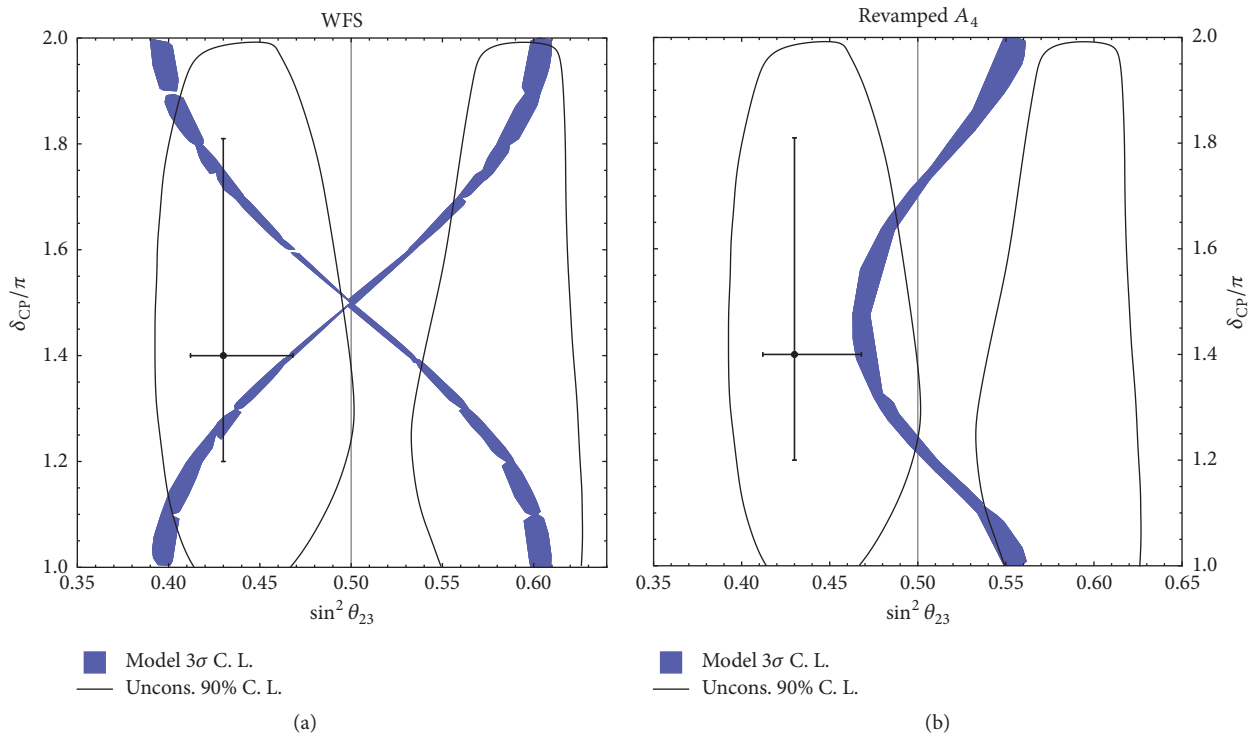

FIGURE 3: In blue are possible parameter values allowed by the two benchmark models: Warped Flavor Symmetry (a) and Revamped A_4-BMV (b). The regions are constructed by varying all the free parameters of the model and selecting those that are allowed at 3σ in current global fit analysis [82]. The black line corresponds to current 90% CL region and the black-dot is the best fit of Table 3. Normal Hierarchy is assumed.

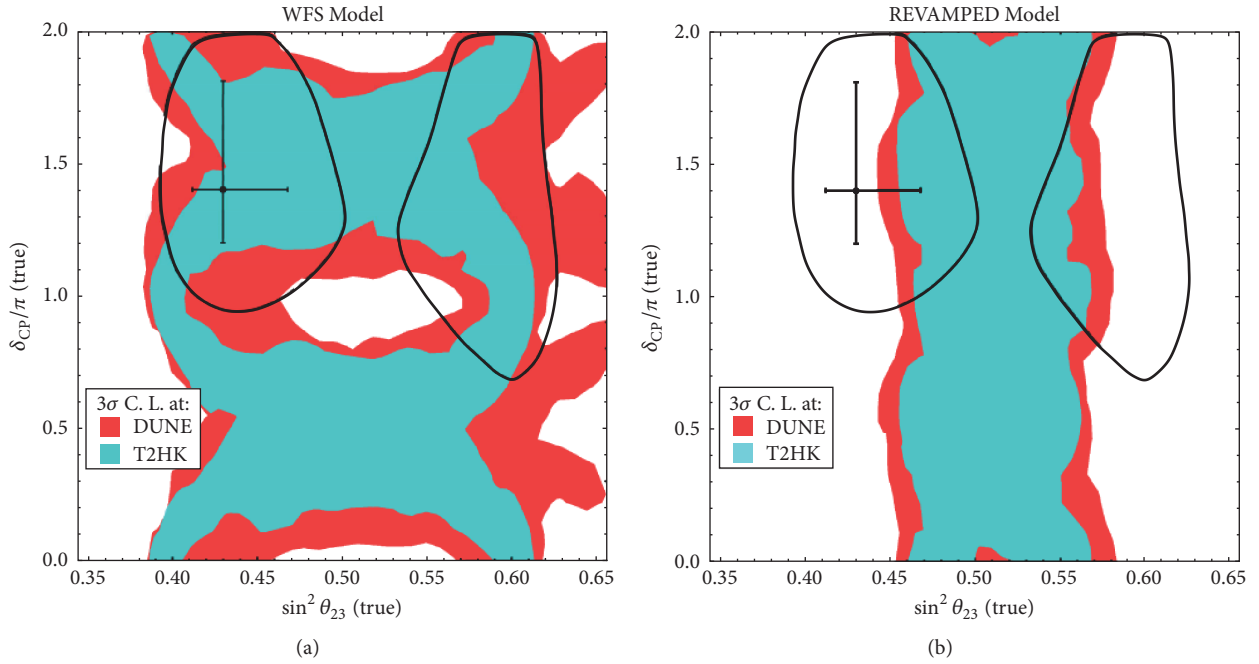

FIGURE 4: Expected sensitivity regions at which DUNE (Red) or T2HK (Cyan) would not exclude the WFS model (a) and the Revamped BMV model (b) at 3σ confidence level. The black contours correspond to 90% CL of current global fit [82].

to exclude the model. Therefore, those kinds of analysis are guidelines to decide which model can or cannot be tested given the future results of DUNE and T2HK and are worth performing in any model that contains predictive correlations among the CP phase and the atmospheric mixing, like [42–44, 110] and many others. It is also worth mentioning that combination of long-baseline measurements and reactors can greatly improve the sensitivity of the analysis.

6. θ_{13} and the Atmospheric Octant

The analysis in the last section can be extended to include another type of correlation that tries to explain the smallness of the reactor angle $\theta_{13} \sim O(10^\circ)$. A general approach common in many models [46–53] imposes a given symmetry on the mass matrix that predicts $\theta_{13} = 0$, which is later spontaneously broken to give a small correction $\delta\theta_{13} \sim O(10^\circ)$ to the reactor angle. It turns out that in order to generate nonzero θ_{13} one automatically generates corrections to other mixing angles $\delta\theta_{ij} \neq 0$.

This can be easily observed by considering a toy model that predicts the tri-bimaximal mixing matrix:

$$U_{\text{PMNS}} = U_{\text{TBM}} = \begin{pmatrix} \sqrt{\frac{2}{3}} & \sqrt{\frac{1}{3}} & 0 \\ \sqrt{\frac{1}{3}} & -\sqrt{\frac{1}{3}} & \sqrt{\frac{1}{2}} \\ -\sqrt{\frac{1}{3}} & \sqrt{\frac{1}{3}} & \sqrt{\frac{1}{2}} \end{pmatrix}. \quad (11)$$

Any consistent small correction to the mixing matrix should maintain its unitary character. Particularly, we can set a correction in the 2-3 planes via the matrix

$$\delta U_{23} = \begin{pmatrix} 1 & 0 & 0 \\ 0 & 1 & \delta\theta \\ 0 & -\delta\theta & 1 \end{pmatrix}. \quad (12)$$

Notice that $\delta U_{23} \cdot \delta U_{23}^{\dagger} = 1 + O(\delta\theta^2)$. If we change the mixing matrix (notice that the correction $\delta U_{23} \cdot U_{\text{TBM}}$ cannot produce a nonzero θ_{13}) by $U_{\text{PMNS}} = U_{\text{TBM}} \to U_{\text{TBM}} \cdot \delta U_{23}$ then $\theta_{13} = (1/\sqrt{3})|\pi/4 - \theta_{23}|$. The general case can be described by an initial mixing matrix $U_{\text{PMNS}} = U_0$ that is later corrected by a rotation matrix U_{ij}:

$$\begin{aligned} &U_{\text{PMNS}} = U_0 \longrightarrow \\ &U_{\text{PMNS}} = U_{ij} \cdot U_0 \text{ or } U_0 \cdot U_{ij} \end{aligned} \quad (13)$$

All the possible combinations of corrections from tri-bimaximal, bimaximal, and democratic mixing were considered in [111]. Particularly, one can investigate a general correlation of θ_{13} to the nonmaximality of the atmospheric angle:

$$\theta_{13} = F\left(\delta\theta_{23}\right), \quad (14)$$

Table 4: Summary of models containing reactor and atmospheric angle correlation. All the possible combinations of corrections from tri-bimaximal, bimaximal, and democratic mixing were considered in [111].

Model	f	θ_{13}^0 [rad]
[53]	$\sqrt{2}$	0
[50, 51]	0.35	[0, 0.35]
[49]	0.1 or 10	0.62
[52]	$1/\theta_0$	$[-1, 1]$
$U_{13} \cdot U_{\text{TBM}}$	6.3	0
$U_{12} \cdot U_{\text{TBM}}$	6.3	0
$U_{\text{TBM}} \cdot U_{23}$	$1/\sqrt{3}$	0
$U_{\text{BM}} \cdot U_{23}U_{13}$	1/2	0
$U_{\text{TBM}} \cdot U_{23}U_{12}$	2	0.157
$U_{\text{TBM}} \cdot U_{23}U_{13}$	$1/\sqrt{2}$	0
$U_{\text{TBM}} \cdot U_{13}U_{12}$	$2/\sqrt{2}$	0
$U_{\text{BM}} \cdot U_{13}U_{12}$	$\sqrt{3/2}$	0
$U_{\text{BM}} \cdot U_{23}U_{12}$	$\sqrt{3/2}$	0
$U_{\text{BM}} \cdot U_{23}U_{13}$	1/2	0

where F is a function of the correction $\delta\theta_{23} = |\pi/4 - \theta_{23}|$. Long-baseline experiments alone are not too sensitive to changes in the reactor angle; nevertheless, it was shown in [112] that it is possible to use such correlation to probe the parameter space of such models by combining long-baseline and reactor experiments.

This can be accomplished in a model-independent approach by series expanding (14):

$$\theta_{13} = f(0) + f'(0)\left|\frac{\pi}{4} - \theta_{23}\right| \equiv \theta_{13}^0 + f\left|\frac{\pi}{4} - \theta_{23}\right|. \quad (15)$$

This encompasses both the uncorrelated (Standard-3ν) case if one sets $f = 0$ and assumes θ_{13}^0 as a free parameter and the small correction case by setting $\theta_{13}^0 = 0$ and $f \neq 0$. In Table 4 we present many models that contain this kind of correlation and their possible parameters values for f and θ_{13}^0.

In Figure 6 we update the potential exclusion regions where models of the form $\theta_{13}^0 = 0$ can be excluded for each value of $\sin^2\theta_{23}$(true) at 3σ by DUNE + reactors and T2HK + reactors. The true value of θ_{13} is set to the central value of Table 3 and its error is assumed to be 3%. The colored regions represent the regions that *cannot* be excluded with more than 3σ. There we can see that models that contain strong correlations ($f > 1.9$) or weak correlations ($f < 0.8$) can be excluded from any set of atmospheric angles.

The general case for any θ_{13}^0 is presented in Figure 6(a) for DUNE and for T2HK in Figure 6(b) for three values of $\sin^2\theta_{23}$: 0.43 (green), 0.5 (cyan), and 0.6 (red). The region shrinks greatly as the true value of the atmospheric angle goes away from the maximal mixing θ_{23}(true) $= \pi/4$.

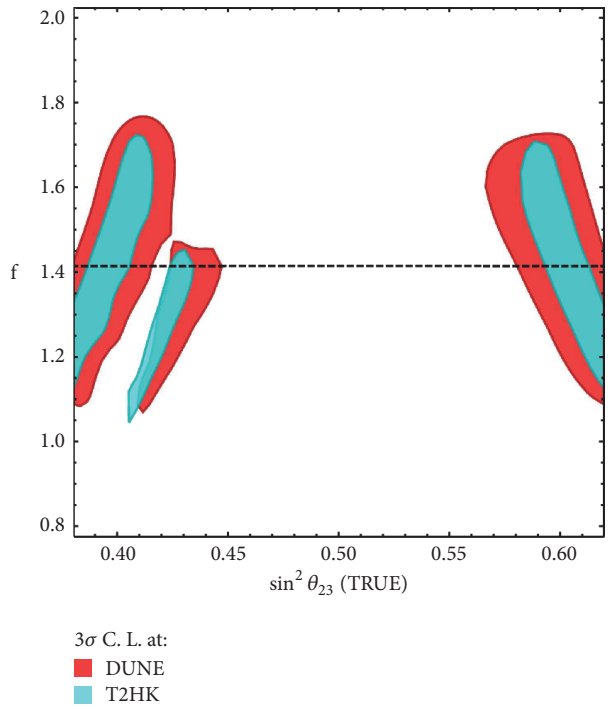

FIGURE 5: Regions that future neutrino long-baseline oscillation experiments cannot exclude the models that follow (15) at more than 3σ CL as a function of the true value of the atmospheric mixing angle for DUNE (red) and T2HK (cyan).

7. Going Beyond Flavor Models

Albeit flavor symmetry models are very common in the literature, mixing angles correlations are by no means exclusive to this class. Since long-baseline experiments are sensitive to the most unknown leptonic parameters, the possibility of using such correlations was studied not only in long-baseline but also in any neutrino experiment. The most common class is high energy model containing Nonstandard Interactions [1–14]; in particular, any model that produces nonstandard 4-point Fermi interaction between electron and the neutrinos can, in principle, be probed by experiments that contain matter interactions, as well as studies in special mixing matrix ansatz such as Golden Ratio and other symmetries [41, 47, 91, 111, 113–118]. Moreover, one can find assumptions on neutrino mass sum rules that can be tested [104–106, 119] and generalized CP symmetry schemes [120–125]. General class of models such as grand unifying theories (GUT) and large extra dimensions (LED) was studied in [126–128]. Cosmology can also present ways of testing predictive neutrino mass models in leptogenesis [129] and even baryogenesis [130].

8. Summary

The state of the art of long-baseline neutrino oscillation experiments is T2(H)K, NOν, and DUNE. They will be capable of reaching very good precision in the reactor and atmospheric mixing angle and will measure for the first time the CP violation phase. This will create an opportunity to put at test a plethora of neutrino mass models that predict values and correlations among the parameters of the PMNS matrix [54–56, 110, 131, 132].

Here we briefly discuss the fitting approach that quantifies the ability of long-baseline experiments to exclude predictive high energy models. Two types of correlations can be used: The θ_{23}-δ_{CP} correlation is found in many models containing a variety of symmetries [42–45]. Nevertheless, each model in the market may contain a different correlation, and most models are still in need to be analyzed. On the other hand, the θ_{13}-θ_{23} correlation can only be probed by combining long-baseline with reactor experiments, as the former are not sensible enough to θ_{13} variations. However, we can take a model-independent approach [112] that covers most models that try to explain the smallness of the θ_{13} angle trough an spontaneous symmetry breaking [46–53]. We present a set of Figures 4, 5, and 6 containing the potential exclusion regions of each model here analyzed that can be used as a benchmark when the future experiments start to run.

Conflicts of Interest

The author declares that there are no conflicts of interest regarding the publication of this article.

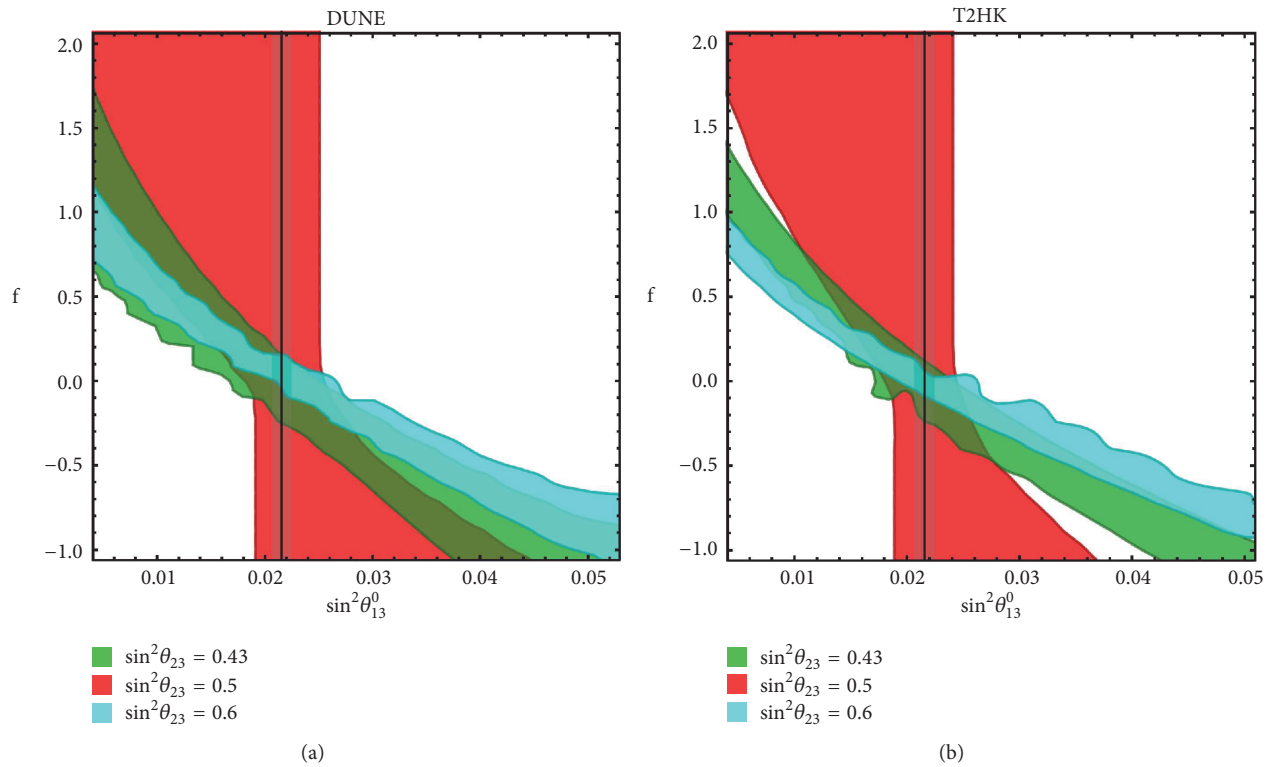

Figure 6: General parameter space regions that cannot be distinguished from the unconstrained relation hypothesis at more than 3σ by future long-baseline neutrino oscillation experiments in combination with reactor measurements as a function of the two parameters of (15): θ^0_{13} and f. The analysis assumed the central value of the reactor angle as the best fit given in Table 3 and three values for the atmospheric angle: (1) $\sin^2\theta_{23}$(true) = 0.43 (green), (2) $\sin^2\theta_{23}$(true) = 0.5 (red), and (3) $\sin^2\theta_{23}$(true) = 0.6 (cyan) for DUNE (a) and T2HK (b).

Acknowledgments

Pedro Pasquini was supported by FAPESP Grants 2014/05133-1, 2015/16809-9, and 2014/19164-6 and FAEPEX Grant no. 2391/17 and, also, by the APS-SBF collaboration scholarship.

References

[1] M. M. Guzzo, A. Masiero, and S. T. Petcov, "On the MSW effect with massless neutrinos and no mixing in the vacuum," *Physics Letters B*, vol. 260, no. 1-2, pp. 154–160, 1991.

[2] A. Bolanos, O. G. Miranda, A. Palazzo, M. A. Tortola, and J. W. F. Valle, "Probing nonstandard neutrino-electron interactions with solar and reactor neutrinos," *Physical Review D: Particles, Fields, Gravitation and Cosmology*, vol. 79, no. 11, Article ID 113012, 2009.

[3] Y. Farzan and M. Tortola, "Neutrino oscillations and Non-Standard Interactions," 2017, https://arxiv.org/abs/1710.09360.

[4] M. Ghosh and O. Yasuda, "Testing NSI suggested by the solar neutrino tension in T2HKK and DUNE," 2017, https://arxiv.org/abs/1709.08264.

[5] J. Tang and Y. Zhang, "Study of non-standard charged-current interactions at the MOMENT experiment," 2017, https://arxiv.org/abs/1705.09500.

[6] J. Liao, D. Marfatia, and K. Whisnant, "Nonstandard neutrino interactions at DUNE, T2HK and T2HKK," *Journal of High Energy Physics*, vol. 71, 2017.

[7] Y. Farzan, "Viable models for large non-standard neutrino interactions," in *Proceedings of the 18th International Workshop on Neutrino Factories, Superbeams, Beta beams (NuFact 2016)*, 7 pages, Quy Nhon, Vietnam, 2016, https://arxiv.org/abs/1612.04971.

[8] M. Blennow, P. Coloma, E. Fernandez-Martinez, J. Hernandez-Garcia, and J. Lopez-Pavon, "Non-unitarity, sterile neutrinos, and non-standard neutrino interactions," *Journal of High Energy Physics*, vol. 2017, no. 4, 2017.

[9] D. V. Forero and W. C. Huang, "Sizable NSI from the $SU(2)_L$ scalar doublet-singlet mixing and the implications in DUNE," *Journal of High Energy Physics*, vol. 2017, article 018, no. 3, 2017.

[10] S. F. Ge and A. Y. Smirnov, "Non-standard interactions and the CP phase measurements in neutrino oscillations at low energies," *Journal of High Energy Physics*, vol. 2016, no. 10, 2016.

[11] M. Masud and P. Mehta, "Nonstandard interactions and resolving the ordering of neutrino masses at DUNE and other long baseline experiments," *Physical Review D: Particles, Fields, Gravitation, and Cosmology*, vol. 94, no. 5, Article ID 053007, 2016.

[12] P. Coloma and T. Schwetz, "Erratum: Generalized mass ordering degeneracy in neutrino oscillation experiments [Phys. Rev. D 94, 055005 (2016)]," *Physical Review D: Particles, Fields, Gravitation, and Cosmology*, vol. 95, no. 7, Article ID 079903, 2017.

[13] K. Huitu, T. J. Kärkkäinen, J. Maalampi, and S. Vihonen, "Constraining the nonstandard interaction parameters in long baseline neutrino experiments," *Physical Review D: Particles,*

Fields, Gravitation, and Cosmology, vol. 93, no. 5, Article ID 053016, 2016.

[14] M. Blennow, S. Choubey, T. Ohlsson, D. Pramanik, and S. K. Raut, "A combined study of source, detector and matter non-standard neutrino interactions at DUNE," *Journal of High Energy Physics*, vol. 2016, no. 08, article no. 90, 2016.

[15] A. Boyarsky, D. Iakubovskyi, and O. Ruchayskiy, "Next decade of sterile neutrino studies," *Physics of the Dark Universe*, vol. 1, no. 1-2, pp. 136–154, 2012.

[16] K. M. Heeger, M. N. Tobin, B. R. Littlejohn, and H. P. Mumm, "Experimental parameters for a reactor antineutrino experiment at very short baselines," *Physical Review D: Covering Particles, Fields, Gravitation, and Cosmology*, vol. 87, no. 7, Article ID 073008, 2013.

[17] L. Gastaldo, C. Giunti, and E. Zavanin, "Light sterile neutrino sensitivity of 163Ho experiments," *Journal of High Energy Physics*, vol. 2016, no. 6, 2016.

[18] C. Giunti and E. M. Zavanin, "Appearance–disappearance relation in 3 + Ns short-baseline neutrino oscillations," *Modern Physics Letters A*, vol. 31, no. 01, p. 1650003, 2016.

[19] S. Gariazzo, C. Giunti, M. Laveder, Y. F. Li, and E. M. Zavanin, "Light sterile neutrinos," *Journal of Physics G: Nuclear and Particle Physics*, vol. 43, no. 3, Article ID 033001, 2016.

[20] O. Miranda, M. Tórtola, and J. Valle, "New Ambiguity in Probing," Physical Review Letters 6, 2016.

[21] D. Dutta and P. Ghoshal, "Probing CP violation with T2K, NOνA and DUNE in the presence of non-unitarity," *Journal of High Energy Physics*, vol. 2016, article 110, no. 9, 2016.

[22] D. Dutta, P. Ghoshal, and S. Roy, "Effect of non-unitarity on neutrino mass hierarchy determination at DUNE, NOνA and T2K," *Nuclear Physics B*, vol. 920, pp. 385–401, 2017.

[23] F. J. Escrihuela, D. V. Forero, O. G. Miranda, M. Tórtola, and J. W. F. Valle, "Probing CP violation with non-unitary mixing in long-baseline neutrino oscillation experiments: DUNE as a case study," *New Journal of Physics*, vol. 19, no. 9, Article ID 093005, 2017.

[24] S.-F. Ge, P. Pasquini, M. Tórtola, and J. W. F. Valle, "Measuring the leptonic *CP* phase in neutrino oscillations with nonunitary mixing," *Physical Review D: Particles, Fields, Gravitation, and Cosmology*, vol. 95, no. 3, Article ID 033005, 2017.

[25] J. Hernandez-Garcia and J. Lopez-Pavon, "Non-Unitarity vs sterile neutrinos at DUNE," https://arxiv.org/abs/1705.01840.

[26] C. R. Das, J. Maalampi, J. Pulido, and S. Vihonen, "Determination of the θ_{23} octant in long baseline neutrino experiments within and beyond the standard model," 2017, https://arxiv.org/abs/1708.05182.

[27] C. Soumya and R. Mohanta, "Non-unitarity lepton mixing in an inverse seesaw and its impact on the physics potential of long-baseline experiments," *High Energy Physics - Phenomenology*, 24 pages, 2017.

[28] S. Choubey and D. Pramanik, "Constraints on sterile neutrino oscillations using DUNE near detector," *Physics Letters B*, vol. 764, pp. 135–141, 2017.

[29] M. Magg and C. Wetterich, "Neutrino mass problem and gauge hierarchy," *Physics Letters B*, vol. 94, no. 1, pp. 61–64, 1980.

[30] R. N. Mohapatra and G. Senjanovic, "Neutrino mass and spontaneous parity nonconservation," *Physical Review Letters*, vol. 44, p. 912, 1980.

[31] J. Schechter and J. W. Valle, "Neutrino-oscillation thought experiment," *Physical Review D: Particles, Fields, Gravitation and Cosmology*, vol. 23, no. 7, pp. 1666–1668, 1981.

[32] C. Wetterich, "Neutrino masses and the scale of *B-L* violation," *Nuclear Physics B*, vol. 187, no. 2, pp. 343–375, 1981.

[33] R. Foot, H. Lew, X. G. He, and G. C. Joshi, "See-saw neutrino masses induced by a triplet of leptons," *Zeitschrift für Physik C: Particles and Fields*, vol. 44, no. 3, pp. 441–444, 1989.

[34] A. Abada, C. Biggio, F. Bonnet, M. B. Gavela, and T. Hambye, "Low energy effects of neutrino masses," *Journal of High Energy Physics*, vol. 2007, no. 12, article 061, 2007.

[35] F. Bonnet, M. Hirsch, T. Ota, and W. Winter, "Systematic study of the $d = 5$ Weinberg operator at one-loop order," *Journal of High Energy Physics*, vol. 2012, no. 153, 2012.

[36] D. Aristizabal Sierra, A. Degee, L. Dorame, and M. Hirsch, "Systematic classification of two-loop realizations of the Weinberg operator," *Journal of High Energy Physics*, vol. 2015, no. 3, 2015.

[37] S. F. King, A. Merle, S. Morisi, Y. Shimizu, and M. Tanimoto, "Neutrino mass and mixing: from theory to experiment," *New Journal of Physics* , vol. 16, Article ID 045018, 2014.

[38] N. Haba, J. Sato, M. Tanimoto, and K. Yoshioka, "Possible flavor mixing structures of lepton mass matrices," *Physical Review D: Particles, Fields, Gravitation and Cosmology*, vol. 64, no. 11, 2001.

[39] P. Chen, G.-J. Ding, F. Gonzalez-Canales, and J. W. F. Valle, "Classifying CP transformations according to their texture zeros: Theory and implications," *Physical Review D: Covering Particles, Fields, Gravitation, And Cosmology*, vol. 94, no. 3, Article ID 033002, 2016, http://dx.doi.org/10.1103/PhysRevD.94.033002.

[40] G. Altarelli and F. Feruglio, "Discrete flavor symmetries and models of neutrino mixing," *Reviews of Modern Physics*, vol. 82, no. 3, pp. 2701–2729, 2010.

[41] S. F. King and C. Luhn, "Neutrino mass and mixing with discrete symmetry," *Reports on Progress in Physics*, vol. 76, no. 5, Article ID 056201, 2013.

[42] A. E. Cárcamo Hernández and H. N. Long, "A highly predictive A_4 flavour 3-3-1 model with radiative inverse seesaw mechanism," 2017, https://arxiv.org/abs/1705.05246.

[43] A. Dev, "Gauged L_μ-L_τ Model with an Inverse Seesaw Mechanism for Neutrino Masses," 2017, https://arxiv.org/abs/1710.02878.

[44] S. Centelles Chuliá, R. Srivastava, and J. W. Valle, "Generalized bottom-tau unification, neutrino oscillations and dark matter: Predictions from a lepton quarticity flavor approach," *Physics Letters B*, vol. 773, pp. 26–33, 2017.

[45] P. Chen, G. Ding, A. D. Rojas, C. A. Vaquera-Araujo, and J. W. Valle, "Warped flavor symmetry predictions for neutrino physics," *Journal of High Energy Physics*, vol. 2016, no. 1, 2016.

[46] D. A. Dicus, S. F. Ge, and W. W. Repko, "Generalized hidden Z_2 symmetry of neutrino mixing," *Physical Review D: Particles, Fields, Gravitation and Cosmology*, vol. 83, no. 9, Article ID 093007, 2011.

[47] M. Sruthilaya, C. Soumya, K. N. Deepthi, and R. Mohanta, "Predicting leptonic CP phase by considering deviations in charged lepton and neutrino sectors," *New Journal of Physics*, vol. 17, no. 8, Article ID 083028, 2015.

[48] A. Dev, P. Ramadevi, and S. U. Sankar, "Non-zero θ_{13} and δ_{CP} in a neutrino mass model with A_4 symmetry," *Journal of High Energy Physics*, vol. 2015, article 034, no. 11, pp. 1–15, 2015.

[49] G. N. Li and X. G. He, "CP violation in neutrino mixing with $\delta = -\pi/2$ in A_4 Type-II seesaw model," *Physics Letters B*, vol. 750, pp. 620–626, 2015.

[50] D. N. Dinh, N. A. Ky, P. Q. Văn, and N. T. H. Vân, "A see-saw scenario of an A_4 flavour symmetric standard model," 2016, https://arxiv.org/abs/1602.07437.

[51] N. A. Ky, P. Q. Văn, and N. T. H. Vân, "Neutrino mixing model based on an $A_4 \times Z_3 \times Z_4$ flavor symmetry," *Physical Review D*, vol. 94, no. 9, Article ID 095009, 2016.

[52] A. E. Cárcamo Hernández, S. Kovalenko, J. W. F. Valle, and C. A. Vaquera-Araujo, "Predictive Pati-Salam theory of fermion masses and mixing," *Journal of High Energy Physics*, vol. 2017, article 118, no. 7, 2017.

[53] P. H. Frampton, T. W. Kephart, and S. Matsuzaki, "Simplified renormalizable T' model for tribimaximal mixing and Cabibbo angle," *Physical Review D: Particles, Fields, Gravitation and Cosmology*, vol. 78, no. 7, Article ID 073004, 2008.

[54] P. Pasquini, S. C. Chuliá, and J. W. F. Valle, "Neutrino oscillations from warped flavor symmetry: Predictions for long baseline experiments T2K, NOvA, and DUNE," *Physical Review D*, vol. 95, no. 9, Article ID 095030, 2017.

[55] S. S. Chatterjee, P. Pasquini, and J. Valle, "Probing atmospheric mixing and leptonic CP violation in current and future long baseline oscillation experiments," *Physics Letters B*, vol. 771, pp. 524–531, 2017.

[56] S. S. Chatterjee, M. Masud, P. Pasquini, and J. Valle, "Cornering the revamped BMV model with neutrino oscillation data," *Physics Letters B*, vol. 774, pp. 179–182, 2017.

[57] K. Duffy et al., "Current Status and Future Plans of T2K," *High Energy Physics - Experiment*, 2017, https://arxiv.org/abs/1705.01764.

[58] S. Childress and J. Strait, "Long baseline neutrino beams at Fermilab," *Journal of Physics: Conference Series*, vol. 408, Article ID 012007, 2013.

[59] R. Acciarri, M. A. Acero, M. Adamowski et al., "Long-Baseline Neutrino Facility (LBNF) and Deep Underground Neutrino Experiment (DUNE) Conceptual Design Report Volume 2: The Physics Program for DUNE at LBNF," *Instrumentation and Detectors*, 2016, https://arxiv.org/abs/1512.06148.

[60] K. Abe, H. Aihara, C. Andreopoulos et al., "Physics potential of a long-baseline neutrino oscillation experiment using a J-PARC neutrino beam and Hyper-Kamiokande," *Progress of Theoretical and Experimental Physics*, vol. 2015, no. 5, Article ID 053C02, 2015.

[61] K. Abe, J. Adam, H. Aihara et al., "Neutrino oscillation physics potential of the T2K experiment," *Progress of Theoretical and Experimental Physics*, vol. 2015, no. 4, Article ID 043C01, 2015.

[62] K. Abe et al., "Solar neutrino measurements in Super-Kamiokande-IV," *Physical Review D: Particles, Fields, Gravitation, and Cosmology*, vol. 94, no. 5, Article ID 052010, 2016.

[63] L. Haegel et al., "The latest T2K neutrino oscillation results," in *Proceedings of the The European Physical Society Conference on High Energy Physics (EPS-HEP 2017)*, 6 pages, Venice, Italy, July 2017.

[64] R. B. Patterson, "The NOvA experiment: status and outlook," *Nuclear Physics B - Proceedings Supplements*, vol. 235-236, pp. 151–157, 2013.

[65] S. K. Agarwalla, S. Prakash, S. K. Raut, and S. U. Sankar, "Potential of optimized NOνA for large θ_{13} & combined performance with a LArTPC & T2K," *Journal of High Energy Physics*, vol. 2012, Article ID 75, 2012.

[66] P. Adamson et al., "Constraints on Oscillation Parameters from ν_e Appearance and ν_μ Disappearance in NOvA," *Physical Review Letters*, vol. 118, no. 23, Article ID 231801, 2017.

[67] P. Adamson et al., "Measurement of the Neutrino Mixing Angle θ_{23} in NOvA," *Physical Review Letters*, vol. 118, no. 15, Article ID 151802, 2017.

[68] R. Acciarri et al., "Long-Baseline Neutrino Facility (LBNF) and Deep Underground Neutrino Experiment (DUNE) Conceptual Design Report Volume 1: The LBNF and DUNE Projects," 2016, https://arxiv.org/abs/1601.05471.

[69] J. Strait et al., "Long-Baseline Neutrino Facility (LBNF) and Deep Underground Neutrino Experiment (DUNE) Conceptual Design Report Volume 3: Long-Baseline Neutrino Facility for DUNE June 24, 2015," https://arxiv.org/abs/1601.05823.

[70] R. Acciarri et al., "Long-Baseline Neutrino Facility (LBNF) and Deep Underground Neutrino Experiment (DUNE) Conceptual Design Report, Volume 4 The DUNE Detectors at LBNF," 2016, https://arxiv.org/abs/1601.02984.

[71] E. Kemp, "The Deep Underground Neutrino Experiment: The precision era of neutrino physics," *Astronomische Nachrichten*, vol. 338, no. 9-10, p. 993, 2017.

[72] K. Abe et al., "Letter of Intent: The Hyper-Kamiokande Experiment — Detector Design and Physics Potential —," 2011, https://arxiv.org/abs/1109.3262.

[73] Hyper-Kamiokande Collaboration, "Hyper-Kamiokande Design Report," KEK-PREPRINT-2016-21, ICRR-REPORT-701-2016-1, 2016.

[74] K. Abe, Ke. Abe, H. Aihara et al., "The Hyper-Kamiokande Experiment," Tech. Rep., 2017, https://arxiv.org/abs/1705.00306.

[75] K. Abe, Ke. Abe, H. Aihara et al., "The Hyper-Kamiokande Experiment: Overview & Status," Tech. Rep., 2017, https://arxiv.org/abs/1704.05933.

[76] C. Andreopoulos, A. Bell, D. Bhattacharya et al., "The GENIE neutrino Monte Carlo generator," *Nuclear Instruments and Methods in Physics Research Section A: Accelerators, Spectrometers, Detectors and Associated Equipment*, vol. 614, no. 1, pp. 87–104, 2010.

[77] G. Battistoni, P. R. Sala, M. Lantz, A. Ferrari, and G. Smirnov, "Neutrino interactions: From theory to Monte Carlo simulations," in *Proceedings of the 45th Karpacz Winter School in Theoretical Physics*, vol. 40, p. 2491, Ladek-Zdroj, Poland, 2009.

[78] C. Patrignani, K. Agashe, G. Aielli et al., "Review of Particle Physics," *Chinese Physics C*, vol. 40, no. 10, Article ID 100001, 2016.

[79] P. Huber, M. Lindner, and W. Winter, "Simulation of long-baseline neutrino oscillation experiments with GLoBES: (General Long Baseline Experiment Simulator)," *Computer Physics Communications*, vol. 167, no. 3, pp. 195–202, 2005.

[80] P. Huber, J. Kopp, M. Lindner, M. Rolinec, and W. Winter, "New features in the simulation of neutrino oscillation experiments with GLoBES 3.0: (General Long Baseline Experiment Simulator)," *Computer Physics Communications*, vol. 177, no. 5, pp. 432–438, 2007.

[81] S.-F. Ge, "NuPro: a simulation package for neutrino properties," http://nupro.hepforge.org.

[82] P. F. de Salas, D. V. Forero, C. A. Ternes, M. Tortola, and J. W. F. Valle, "Status of neutrino oscillations 2017," 2017, https://arxiv.org/abs/1708.01186.

[83] F. James, *Statistical Methods in Experimental Physics*, 345 p, World Scientific, Hackensack, USA, 2006.

[84] W. G. Cochran, *The Annals of Mathematical Statistics 23- No3*, vol. 315, 1942.

[85] S. Prakash, S. K. Raut, and S. U. Sankar, "Getting the best out of T2K and NOνA," *Physical Review D: Covering Particles, Fields, Gravitation, and Cosmology*, vol. 86, no. 3, Article ID 033012, 2012.

[86] M. Ghosh, P. Ghoshal, S. Goswami, and S. K. Raut, "Evidence for leptonic CP phase from NOνA, T2K and ICAL: A chronological progression," *Nuclear Physics B*, vol. 884, pp. 274–304, 2014.

[87] M. Ghosh, S. Goswami, and S. K. Raut, "Maximizing the DUNE early physics output with current experiments," *The European Physical Journal C*, vol. 76, 114, 2016.

[88] M. Ghosh, P. Ghoshal, S. Goswami, N. Nath, and S. K. Raut, "New look at the degeneracies in the neutrino oscillation parameters, and their resolution by T2K, NOνA and ICAL," *Physical Review D: Covering Particles, Fields, Gravitation, and Cosmology*, vol. 93, no. 1, Article ID 013013, 2016.

[89] K. Chakraborty, K. N. Deepthi, and S. Goswami, "Spotlighting the sensitivities of T2HK,T2HKK and DUNE," 2017, https://arxiv.org/abs/1711.11107.

[90] S. Choubey, D. Dutta, and D. Pramanik, "Measuring the Sterile Neutrino CP Phase at DUNE and T2HK," 2017, https://arxiv.org/abs/1711.07464.

[91] S. K. Agarwalla, S. S. Chatterjee, S. T. Petcov, and A. V. Titov, "Addressing Neutrino Mixing Models with DUNE and T2HK," 2017, https://arxiv.org/abs/1711.02107.

[92] J. Evslin, S.-F. Ge, and K. Hagiwara, "The leptonic CP phase from T2(H)K and μ^+ decay at rest," *Journal of High Energy Physics*, vol. 02, no. 137, 2016.

[93] P. Ballett, S. F. King, S. Pascoli, N. W. Prouse, and T. Wang, "Sensitivities and synergies of DUNE and T2HK," *Physical Review D: Covering Particles, Fields, Gravitation, and Cosmology*, vol. 96, no. 3, Article ID 033003, 2017.

[94] N. Nath, M. Ghosh, and S. Goswami, "The physics of antineutrinos in DUNE and determination of octant and δ_{CP}," *Nuclear Physics B*, vol. 913, pp. 381–404, 2016.

[95] K. Bora, D. Dutta, and P. Ghoshal, "Determining the octant of θ_{23} at LBNE in conjunction with reactor experiments," *Modern Physics Letters A*, vol. 30, no. 14, Article ID 1550066, 22 pages, 2015.

[96] H. Minakata, H. Sugiyama, O. Yasuda, K. Inoue, and F. Suekane, "Erratum: Reactor measurement of θ_{13} and its complementarity to long-baseline experiments [Phys. Rev. D 68, 033017 (2003)]," *Physical Review D: Particles, Fields, Gravitation and Cosmology*, vol. 70, no. 5, Article ID 059901, 2004.

[97] S. K. Agarwalla, S. Prakash, and S. U. Sankar, "Resolving the octant of θ_{23} with T2K and NOνA," *Journal of High Energy Physics*, vol. 07, 131, 2013.

[98] A. Chatterjee, P. Ghoshal, S. Goswami, and S. K. Raut, "Octant sensitivity for large θ_{13} in atmospheric and long-baseline neutrino experiments," *Journal of High Energy Physics*, vol. 06, 010, 2013.

[99] S. Sachi Chatterjee, P. Pasquini, and J. W. F. Valle, "Resolving the atmospheric octant by an improved measurement of the reactor angle," *Physical Review D: Particles, Fields, Gravitation, and Cosmology*, vol. 96, no. 1, Article ID 011303, 2017.

[100] S. F. King, "Parameterizing the lepton mixing matrix in terms of deviations from tri-bimaximal mixing," *Physics Letters B*, vol. 659, no. 1-2, pp. 244–251, 2008.

[101] D. Hernandez and A. Yu. Smirnov, "Lepton mixing and discrete symmetries," *Physical Review D: Covering Particles, Fields, Gravitation, and Cosmology*, vol. 86, no. 5, Article ID 053014, 2012.

[102] D. Hernandez and A. Yu. Smirnov, "Discrete symmetries and model-independent patterns of lepton mixing," *Physical Review D: Covering Particles, Fields, Gravitation, and Cosmology*, vol. 87, no. 5, Article ID 053005, 2013.

[103] P. Ballett, S. F. King, C. Luhn, S. Pascoli, and M. A. Schmidt, "Testing atmospheric mixing sum rules at precision neutrino facilities," *Physical Review D: Particles, Fields, Gravitation and Cosmology*, vol. 89, no. 1, Article ID 016016, 2014.

[104] M. Spinrath, "Neutrino Mass Sum Rules," *Journal of Physics: Conference Series*, vol. 888, no. 1, Article ID 012176, 2017.

[105] F. Buccella, M. Chianese, G. Mangano, G. Miele, S. Morisi, and P. Santorelli, "A neutrino mass-mixing sum rule from SO(10) and neutrinoless double beta decay," *Journal of High Energy Physics*, vol. 2017, no. 4, 2017.

[106] J. Gehrlein, A. Merle, and M. Spinrath, "Predictivity of neutrino mass sum rules," *Physical Review D: Particles, Fields, Gravitation and Cosmology*, vol. 94, no. 9, 2016.

[107] S. F. King, A. Merle, and A. J. Stuart, "The power of neutrino mass sum rules for neutrinoless double beta decay experiments," *Journal of High Energy Physics*, vol. 2013, no. 12, article no. 5, 2013.

[108] T. Wang and Y.-L. Zhou, "Neutrino non-standard interactions as a portal to test flavour symmetries," 2018, https://arxiv.org/pdf/1801.05656.pdf.

[109] D. V. Forero, S. Morisi, J. C. Romão, and J. W. F. Valle, "Neutrino mixing with revamped A_4 flavor symmetry," *Physical Review D: Particles, Fields, Gravitation, and Cosmology*, vol. 88, no. 1, Article ID 016003, 2013.

[110] R. Srivastava, C. A. Ternes, M. Tórtola, and J. W. F. Valle, "Testing a lepton quarticity flavor theory of neutrino oscillations with the DUNE experiment," 2017, https://arxiv.org/abs/1711.10318.

[111] W. Chao and Y. j. Zheng, "Relatively large Theta13 from modification to the tri-bimaximal, bimaximal and democratic neutrino mixing matrices," *Journal of High Energy Physics*, vol. 2013, article 44, 2013.

[112] P. Pasquini, "Reactor and atmospheric neutrino mixing angles' correlation as a probe for new physics," *Physical Review D: Particles, Fields, Gravitation, and Cosmology*, vol. 96, no. 9, Article ID 095021, 2017.

[113] S. Pramanick, "Ameliorating the popular lepton mixings with A4 symmetry: A see-saw model for realistic neutrino masses and mixing," 2017, https://arxiv.org/abs/1711.03510.

[114] G.-J. Ding, S. F. King, and C.-C. Li, "Golden littlest seesaw," *Nuclear Physics B*, vol. 925, pp. 470–499, 2017.

[115] J. Zhang and S. Zhou, "Viability of exact tri-bimaximal, golden-ratio and bimaximal mixing patterns and renormalization-group running effects," *Journal of High Energy Physics*, vol. 09, 167, 2016.

[116] L. A. Delgadillo, L. L. Everett, R. Ramos, and A. J. Stuart, "Predictions for the Dirac CP-Violating Phase from Sum Rules," 2018, https://arxiv.org/abs/1801.06377.

[117] C. H. Albright, A. Dueck, and W. Rodejohann, "Possible alternatives to tri-bimaximal mixing," *The European Physical Journal C*, vol. 70, no. 4, pp. 1099–1110, 2010.

[118] A. D. Hanlon, S.-F. Ge, and W. W. Repko, "Phenomenological consequences of residual Z_2^s and Z symmetries," *Physics Letters B*, vol. 729, pp. 185–191, 2014.

[119] J. Barry and W. Rodejohann, "Neutrino mass sum-rules in flavor symmetry models," *Nuclear Physics B*, vol. 842, no. 1, pp. 33–50, 2011.

[120] J. Turner, "Predictions for leptonic mixing angle correlations and nontrivial Dirac *CP* violation from A_5 with generalized *CP* symmetry," *Physical Review D: Particles, Fields, Gravitation, and Cosmology*, vol. 92, no. 11, Article ID 116007, 2015.

[121] J. Turner, "Mixing angle and phase predictions from A5 with generalised CP," in *Proceedings of the Topical Research Meeting on Prospects in Neutrino Physics (NuPhys'14)*, London, UK, 2015, https://arxiv.org/abs/1506.06898.

[122] P. Ballett, S. Pascoli, and J. Turner, "Mixing angle and phase correlations from A_5 with generalized *CP* and their prospects for discovery," *Physical Review D: Particles, Fields, Gravitation, and Cosmology*, vol. 92, no. 9, Article ID 093008, 2015.

[123] L. L. Everett and A. J. Stuart, "Lepton sector phases and their roles in flavor and generalized *CP*symmetries," *Physical Review D: Particles, Fields, Gravitation, and Cosmology*, vol. 96, no. 3, Article ID 035030, 2017.

[124] J.-N. Lu and G.-J. Ding, "Alternative schemes of predicting lepton mixing parameters from discrete flavor and *CP* symmetry," *Physical Review D: Particles, Fields, Gravitation, and Cosmology*, vol. 95, no. 1, Article ID 015012, 2017.

[125] P. Chen, S. Centelles Chuliá, G.-J. Ding, R. Srivastava, and J. W. F. Valle, "Neutrino Predictions from Generalized CP Symmetries of Charged Leptons," 2018, https://arxiv.org/abs/1802.04275.

[126] S. F. King, "Unified models of neutrinos, flavour and *CP* Violation," *Progress in Particle and Nuclear Physics*, vol. 94, pp. 217–256, 2017.

[127] J. M. Berryman, A. de Gouvêa, K. J. Kelly, O. L. G. Peres, and Z. Tabrizi, "Large extra dimensions at the deep underground neutrino experiment," *Physical Review D: Particles, Fields, Gravitation, and Cosmology*, vol. 94, no. 3, Article ID 033006, 2016.

[128] M. Carena, Y.-Y. Li, C. S. Machado, P. A. N. Machado, and C. E. M. Wagner, "Neutrinos in large extra dimensions and short-baseline ν_e appearance," *Physical Review D: Particles, Fields, Gravitation, and Cosmology*, vol. 96, no. 9, Article ID 095014, 2017.

[129] C.-C. Li and G.-J. Ding, "Implications of residual *CP* symmetry for leptogenesis in a model with two right-handed neutrinos," *Physical Review D: Particles, Fields, Gravitation, and Cosmology*, vol. 96, no. 7, Article ID 075005, 2017.

[130] H. Borgohain and M. K. Das, "Perturbations to $\mu - \tau$ symmetry, lepton Number Violation and baryogenesis in left-right symmetric Model," 2018, https://arxiv.org/abs/1803.05710.

[131] S. F. Ge, D. A. Dicus, and W. W. Repko, "Z_2 symmetry prediction for the leptonic Dirac CP phase," *Physics Letters B*, vol. 702, no. 4, pp. 220–223, 2011.

[132] S.-F. Ge, D. A. Dicus, and W. W. Repko, "Residual Symmetries for Neutrino Mixing with a Large theta_13 and Nearly Maximal delta_D," *Physical Review Letters*, vol. 108, Article ID 041801, 2012.

Hindawi
Advances in High Energy Physics
Volume 2018, Article ID 3905848, 11 pages
https://doi.org/10.1155/2018/3905848

Review Article

Anomalies in $b \to s$ Transitions and Dark Matter

Avelino Vicente

Instituto de Física Corpuscular (CSIC-Universitat de València), Apdo. 22085, E-46071 Valencia, Spain

Correspondence should be addressed to Avelino Vicente; avelino.vicente@ific.uv.es

Received 20 March 2018; Accepted 28 May 2018; Published 24 June 2018

Academic Editor: Farinaldo Queiroz

Since 2013, the LHCb collaboration has reported on the measurement of several observables associated with $b \to s$ transitions, finding various deviations from their predicted values in the Standard Model. These include a set of deviations in branching ratios and angular observables, as well as in the observables R_K and R_{K^*}, specially built to test the possible violation of Lepton Flavor Universality. Even though these tantalizing hints are not conclusive yet, the $b \to s$ anomalies have gained considerable attention in the flavor community. Here we review new physics models that address these anomalies and explore their possible connection to the dark matter of the Universe. After discussing some of the ideas introduced in these works and classifying the proposed models, two selected examples are presented in detail in order to illustrate the potential interplay between these two areas of current particle physics.

1. Introduction

The Standard Model (SM) of particle physics provides an excellent description for a vast amount of phenomena and can be regarded as one of the most successful scientific theories ever built. In fact, with the recent discovery of the last missing piece, the Higgs boson, the particle spectrum is finally complete and the SM looks stronger than ever. However, and despite its enormous success, there are several indications that clearly point towards the existence of a more complete theory, with neutrino masses and the baryon asymmetry of the Universe as the most prominent examples.

Another open question is the nature of the dark matter (DM) that accounts for 27% of the energy density of the Universe [1]. Several ideas have been proposed to address this fundamental problem in current physics. Under the hypothesis that the DM is composed of particles, these cannot be identified with any of the states in the SM, hence demanding an extension of the model with new states and, possibly, new dynamics. Again, many directions exist. Interestingly, in scenarios involving New Physics (NP) at the TeV scale, the first signals from the new DM sector might be found in experiments not specially designed to look for them.

Rare decays stand among the most powerful tests of the SM. Since 2013, results obtained by the LHCb collaboration have led to an increasing interest in B physics, particularly in processes involving $b \to s$ transitions. Deviations from the SM expectations have been reported in several observables, some of them hinting at the violation of Lepton Flavor Universality (LFU), a central feature in the SM. Even though these anomalies could be caused by a combination of unfortunate fluctuations and, perhaps, a poor theoretical understanding of some processes, it is tempting to speculate about their possible origin in terms of NP models, in particular models linking them to other open problems.

This *minireview* will pursue this goal, focusing on NP scenarios that relate the $b \to s$ anomalies to DM. Several works [2–20] have already explored this connection, mostly by means of specific models that accommodate the observations in $b \to s$ transitions with a new dark sector. We will review some of the ideas introduced in these works and highlight those that deserve further exploration. We will also classify the proposed models into two general categories: (i) models in which the NP contributions to $b \to s$ transitions and DM production in the early Universe share a common mediator, and (ii) models with the DM particle running in loop diagrams that contribute to the solution of the $b \to s$ anomalies. After a general discussion, a selected example of each class will be presented in detail.

The rest of the manuscript is organized as follows. First, we review the anomalies in $b \to s$ transitions in Section 2 and interpret the experimental results in a model independent way in Section 3. In Section 4 we discuss and classify the proposed New Physics explanations to these anomalies that involve a link to the dark matter problem. Sections 5 and 6 present two simple example models that illustrate this connection. Finally, we summarize and draw our conclusions in Section 7.

2. Experimental Situation

We begin by discussing the present experimental situation. The observed anomalies in $b \to s$ transitions can be classified into two classes: (1) branching ratios and angular observables and (2) lepton flavor universality violating (LFUV) anomalies. Although they might be related (and caused by the same NP), they are conceptually different.

Branching Ratios and Angular Observables. using state-of-the-art computations of the hadronic form factors involved, one can compute branching ratios and angular observables for $b \to s$ processes such as $B \to K^* \ell^+ \ell^-$ and look for deviations from the SM predictions. For the comparison to be meaningful, one must have a good knowledge of all possible Quantum ChromoDynamics (QCD) effects that might pollute the theoretical calculation and we currently have at our disposal several methods to minimize or at least estimate the uncertainties. (The size of the hadronic uncertainties in different calculations is a matter of hot debate nowadays. We will not discuss this issue here but just refer to the recent studies regarding form factors [21, 22] and nonlocal contributions [23–28] for extended discussions.) In particular, a basis of optimized observables for the decay $B \to K^* \mu^+ \mu^-$, specially designed to reduce the hadronic uncertainties, was introduced in [29]. In 2013, the LHCb collaboration published results on these observables using their 1 fb^{-1} dataset, finding a 3.7σ deviation between the measurement and the SM prediction for the P_5' angular observable in one dimuon invariant mass bin [30]. A systematic deficit with respect to the SM predictions in the branching ratios of several processes, mainly $B_s \to \phi \mu^+ \mu^-$, was also reported by LHCb [31]. These discrepancies have been found later in other datasets. In 2015, LHCb confirmed these anomalies using their full Run 1 dataset with 3 fb^{-1} [32, 33], whereas in 2016 the Belle collaboration presented an independent measurement of P_5', compatible with the LHCb result [34, 35]. More recently, both ATLAS [36] and CMS [37] have also presented preliminary results on the $B \to K^* \mu^+ \mu^-$ angular observables, with relatively good agreement with LHCb.

LFUV Anomalies. One of the central features of the SM is that gauge bosons coupled with the same strength to all three families of leptons. This prediction can be tested by measuring observables such as the $R_{K^{(*)}}$ ratios, defined as [38]

$$R_{K^{(*)}} = \frac{\Gamma\left(B \longrightarrow K^{(*)} \mu^+ \mu^-\right)}{\Gamma\left(B \longrightarrow K^{(*)} e^+ e^-\right)}, \tag{1}$$

measured in specific dilepton invariant mass squared ranges $q^2 \in [q^2_{\min}, q^2_{\max}]$. In the SM, these ratios should be very approximately equal to one. Furthermore, hadronic uncertainties are expected to cancel very good approximation in these ratios, which implies that, in contrast to the previous class of anomalies, deviations in these observables cannot be explained by uncontrolled QCD effects and would be a clear indication of NP at work. For this reason, they are sometimes referred to as *clean observables*. Interestingly, in 2014, the LHCb collaboration measured R_K in the region $[1, 6]$ GeV^2 [39], finding a value significantly lower than one, while in 2017 similar measurements of the R_{K^*} ratio in two q^2 bins [40] were also found to depart from their SM expected values:

$$\begin{aligned} R_K &= 0.745^{+0.090}_{-0.074} \pm 0.036, \quad q^2 \in [1, 6] \text{ GeV}^2, \\ R_{K^*} &= 0.660^{+0.110}_{-0.070} \pm 0.024, \quad q^2 \in [0.045, 1.1] \text{ GeV}^2, \\ R_{K^*} &= 0.685^{+0.113}_{-0.069} \pm 0.047, \quad q^2 \in [1.1, 6.0] \text{ GeV}^2. \end{aligned} \tag{2}$$

The comparison between these experimental results and the SM predictions [41, 42],

$$\begin{aligned} R_K^{\text{SM}} &= 1.00 \pm 0.01, \quad q^2 \in [1, 6] \text{ GeV}^2, \\ R_{K^*}^{\text{SM}} &= 0.92 \pm 0.02, \quad q^2 \in [0.045, 1.1] \text{ GeV}^2, \\ R_{K^*}^{\text{SM}} &= 1.00 \pm 0.01, \quad q^2 \in [1.1, 6.0] \text{ GeV}^2, \end{aligned} \tag{3}$$

shows deviations from the SM at the 2.6σ level in the case of R_K, 2.2σ for R_{K^*} in the low-q^2 region, and 2.4σ for R_{K^*} in the central-q^2 region. Finally, Belle has recently measured the LFUV observable $Q_5 = P_5^{\mu\prime} - P_5^{e\prime}$, with the observable $P_5^{e\prime}$ defined for $B \to K^* e^+ e^-$ analogously to $P_5^{\mu\prime} \equiv P_5'$ for $B \to K^* \mu^+ \mu^-$ [43]. The result, although statistically not very significant, also points towards the violation of LFU [35].

Summarizing, there are at present two sets of experimental anomalies in processes involving $b \to s$ transitions at the quark level. While the relevance of the first set is currently a matter of discussion due to the possibility of unknown QCD effects faking the deviations from the SM, the second can only be explained by NP violating LFU. In principle, these two classes of anomalies can be completely unrelated but, as we will see in the next section, global analyses of all experimental data in $b \to s$ transitions indicate that a common explanation (in terms of a single effective operator) can address both sets in a satisfactory and economical way. This intriguing result has made the $b \to s$ anomalies a topic of great interest currently.

Finally, it is very interesting to note the existence of an independent set of anomalies in $b \to c$ transitions. Several experimental measurements of the ratios $R(D)$ and $R(D^*)$ have been found to depart from their SM predictions, with a global discrepancy at the $\sim 4\sigma$ level [44]. Recently, the $R(J/\psi)$ ratio has also been measured by the LHCb collaboration, finding again a deviation from the SM expected value [45]. Compared to the $b \to s$ anomalies, the $b \to c$ anomalies are of a different nature and, if real, they could have a completely different origin. For instance, they would involve a new

charged current, instead of a neutral one, hence requiring the new mediators to be much lighter to be able to compete with the SM W boson tree-level exchange. However, many authors have proposed models that can simultaneously address both sets of anomalies. We refer to [46] for a general discussion on combined explanations and ignore the $b \to c$ anomalies for the rest of this paper.

3. Model Independent Interpretation

The experimental tensions discussed in the previous section must be properly quantified and interpreted. **Quantification** is crucial to determine whether the anomalies can be explained by fluctuations in the data or they truly indicate a statistically significant deviation from the SM. Assuming that these tensions are caused by genuine NP, the ultimate goal is to construct a specific model in which they are solved. However, the first step in this direction must be a **model independent interpretation** of the experimental data in order to identify the ingredients that this new scenario must include. This is achieved by adopting an approach based on effective operators, valid under the assumption that all NP degrees of freedom lie at energies well above the relevant energy scales for the observables of interest.

The effective Hamiltonian for $b \to s$ transitions is usually written as

$$\mathscr{H}_{\text{eff}} = -\frac{4G_F}{\sqrt{2}} V_{tb} V_{ts}^* \frac{e^2}{16\pi^2} \sum_i \left(C_i \mathcal{O}_i + C_i' \mathcal{O}_i' \right) + \text{h.c.}. \quad (4)$$

Here G_F is the Fermi constant, e the electric charge, and V the Cabibbo-Kobayashi-Maskawa (CKM) matrix. $\mathcal{O}_i$ and $\mathcal{O}_i'$ are the effective operators that contribute to $b \to s$ transitions, and C_i and C_i' their Wilson coefficients. The most relevant operators for the interpretation of the $b \to s$ anomalies are

$$\begin{aligned} \mathcal{O}_9 &= \left(\bar{s}\gamma_\mu P_L b\right)\left(\bar{\ell}\gamma^\mu \ell\right), \\ \mathcal{O}_9' &= \left(\bar{s}\gamma_\mu P_R b\right)\left(\bar{\ell}\gamma^\mu \ell\right), \end{aligned} \quad (5)$$

$$\begin{aligned} \mathcal{O}_{10} &= \left(\bar{s}\gamma_\mu P_L b\right)\left(\bar{\ell}\gamma^\mu \gamma_5 \ell\right), \\ \mathcal{O}_{10}' &= \left(\bar{s}\gamma_\mu P_R b\right)\left(\bar{\ell}\gamma^\mu \gamma_5 \ell\right). \end{aligned} \quad (6)$$

Here $\ell = e, \mu, \tau$. In fact, the operators and Wilson coefficients carry flavor indices and we are omitting them to simplify the notation. When necessary, we will denote a particular lepton flavor with a superscript, e.g., C_9^μ and $\mathcal{O}_9^\mu$, for muons. It is also convenient to split the Wilson coefficients in two pieces: the SM contributions and the NP contributions, defining the following (similar splittings could be defined for the Wilson coefficients of the primed operators, C_9' and C_{10}', but in this case the SM contributions are suppressed and one has $C_9' \simeq C_9'^{\text{NP}}$ and $C_{10}' \simeq C_{10}'^{\text{NP}}$):

$$C_9 = C_9^{\text{SM}} + C_9^{\text{NP}}, \quad (7)$$

$$C_{10} = C_{10}^{\text{SM}} + C_{10}^{\text{NP}}. \quad (8)$$

The SM contributions have been computed at NNLO at $\mu_b = 4.8$ GeV, obtaining $C_9^{\text{SM}}(\mu_b) = 4.07$ and $C_{10}^{\text{SM}}(\mu_b) = -4.31$ (see [29] and references therein), leaving the NP contributions as parameters to be determined (or at least constrained) by using experimental data.

It is in principle possible to derive limits for the NP contributions considering each observable independently, but this approach would completely miss the global picture. The effective operators in (4) contribute to several observables and one expects the presence of NP to be revealed by a pattern of deviations from the SM expectations, rather than by a single anomaly. For this reason, global fits constitute the best approach to analyze the available experimental data. Interestingly, several independent fits [47–54] have found a remarkable tension between the SM and experimental data on $b \to s$ transitions which is clearly reduced with the addition of NP contributions. Although the numerical details (such as statistical significance) differ among different analyses, there is a general consensus on the following qualitative results:

(i) Global fits improve substantially with a negative contribution in $C_9^{\mu,\text{NP}}$, with $C_9^{\mu,\text{NP}} \sim -25\% \times C_9^{\mu,\text{SM}}$, leading to a total Wilson coefficient C_9^μ significantly smaller than the one in the SM.

(ii) NP contributions in other Wilson coefficients can also improve the fit, but only in a subdominant way. For instance, the anomalies can also be accommodated in scenarios with $C_9^{\mu,\text{NP}} = -C_{10}^{\mu,\text{NP}}$ or $C_9^{\mu,\text{NP}} = -C_9^{\prime\mu,\text{NP}}$, without a clear statistical preference with respect to the scenario with NP only in C_9^μ. (Such patterns for the Wilson coefficients are automatically obtained if the NP states coupled to SM fermions with specific chiralities. For instance, the relation $C_9^{\mu,\text{NP}} = -C_{10}^{\mu,\text{NP}}$ is obtained in models where the NP states only couple to the *left-handed* muons. Two examples of this class of models are shown in Sections 5 and 6.)

(iii) Other operators involving muons are perfectly compatible with their SM values. Similarly, no NP is required for operators involving electrons or tau leptons.

Armed with these results, model builders can construct specific models where all requirements are met and the anomalies explained. Similarly, one can extract interesting implications for model building by explaining the anomalies in terms of gauge invariant effective operators; see [55] for a recent analysis. Either way, the resulting profile of NP contributions reveals a pattern that was not predicted by any theoretical framework, such as supersymmetry, and many new models have been put forward. In the next Section we will discuss some of these models, in particular those linking the $b \to s$ anomalies to dark matter.

4. Linking the $b \to s$ Anomalies to Dark Matter

After discussing the current experimental situation in $b \to s$ transitions, let us focus on possible connections to the

dark matter problem. These have been explored in [2–20]. In general, the proposed models that solve the $b \to s$ anomalies and explain the origin of the dark matter of the Universe can be classified into two principal categories:

(i) **Portal models:** models in which the mediator responsible for the NP contributions to $b \to s$ transitions also mediates the DM production in the early Universe.

(ii) **Loop models:** models that induce the required NP contributions to $b \to s$ transitions with loops containing the DM particle.

In the case of **portal models**, the usual scenario considers a $U(1)$ gauge extension of the SM that leads to the existence of a new massive gauge boson after spontaneous symmetry breaking. The resulting Z' boson induces a new neutral current contribution in $b \to s$ transitions and mediates the production of DM particles in the early Universe via a Z' portal interaction. This setup was first considered in [2]. In this particular realization of the general idea, the SM fermions were assumed to be neutral under the new $U(1)_X$ gauge symmetry and the Z' couplings to quarks ($\bar{b}s$) and leptons ($\mu^+\mu^-$), necessary to explain the $b \to s$ anomalies, are generated at tree-level via mixing with new vector-like (VL) fermions. Additionally, the Z' boson also couples to the scalar field χ, the DM candidate in this model, automatically stabilized by an remnant $\mathbb{Z}_2$ symmetry after $U(1)_X$ breaking. This model will be reviewed in more detail in Section 5. Variants of this setup with fermionic DM also exist. In [6], a horizontal $U(1)_{B_1+B_2-2B_3}$ gauge symmetry is introduced, with B_i being the baryon number of the ith fermion family. The resulting Z' boson couples directly to the SM quarks, while the coupling to muons is obtained by introducing a VL lepton. This allows accommodating the anomalies in $b \to s$ transitions. Furthermore, the model also contains a Dirac fermion that is stable due to a remnant $\mathbb{Z}_2$ symmetry, in a similar fashion as in [2], which becomes the DM candidate. Similarly, [7] builds on the well-known $U(1)_{L_\mu - L_\tau}$ model of [56] and extends it to include a stable Dirac fermion with a relic density also determined by Z' portal interactions, while [20] considers a similar model but makes use of kinetic mixing between the Z' and the SM neutral gauge bosons. Reference [19] considers vector-like neutrino DM in a setup analogous to [2] extended with additional VL fermions. Reference [10] explored a pair of scenarios based on a $U(1)$ gauge symmetry supplemented with VL fermions and a fermionic DM candidate, of Dirac or Majorana nature. This paper focuses on effects in indirect detection experiments, aiming at an explanation of the excess of events in antiproton spectra reported by the AMS-02 experiment in 2016 [57]. Other works that adopt the standard Z' portal setup are [4, 12]. Finally, [11] considers a light mediator (not the usual heavy Z') that contributes to $b \to s$ transitions and decays predominantly into invisible final states, possibly made of light DM particles.

It is important to note that the phenomenology of these Z' portal models differs substantially from the standard Z' portal phenomenology. This is due to the fact that the Z' bosons in these models couple with different strengths to different fermion families, as required to accommodate the LFUV hints observed by the LHCb collaboration (R_K and R_{K^*}). For instance, DM annihilation typically yields muon and tau lepton pairs, but not electrons and positrons. Direct detection experiments are also more challenging in the standard Z' portal scenario, since the DM candidate typically does not couple to first generation quarks, more abundant in the nucleons.

In what concerns **loop models**, many variations are possible. To the best of our knowledge, the first model of this type that appeared in the literature is [13], based on previous work on loop models for the $b \to s$ anomalies, without connecting to the DM problem, in [58, 59]. In this model the SM particle content is extended with two VL pairs of $SU(2)_L$ doublets, with the same quantum numbers as the SM quark and lepton doublets, but charged under a global $U(1)_X$ symmetry. The model also contains the complex scalar X, singlet under the SM gauge symmetry and also charged under $U(1)_X$. With these states, one can draw a 1-loop diagram contributing to the $b \to s$ observables relevant to explaining the anomalies. Furthermore, if the global $U(1)_X$ is conserved, the lightest $U(1)_X$-charged state becomes stable. In this work, this state is assumed to be X, hence the DM candidate in the model. A more detailed discussion about this model can be found in Section 6. Two similar setups can be found in [18], where a different set of global symmetries are considered ($U(1) \times \mathbb{Z}_2$ and $U(1) \times \mathbb{Z}_3$) in order to stabilize a scalar DM candidate. This paper also includes right-handed neutrinos in order to accommodate nonzero neutrino masses with the type-I seesaw mechanism and explores the lepton flavor violating phenomenology of the model in detail. A Majorana fermionic DM candidate was considered in [16]. Similarly to the previously mentioned models, this scenario also addresses the $b \to s$ anomalies at 1-loop level introducing a minimal number of fields: just a VL quark (Ψ) and an inert scalar doublet (Φ), in addition to the fermion singlet that constitutes the DM candidate. The model is supplemented with a discrete $\mathbb{Z}_2$ symmetry to ensure the stability of the DM particle. Interestingly, the model can be tested in direct DM detection experiments as well as at the Large Hadron Collider (LHC), where the states Ψ and Φ can be pair-produced and lead to final states with hard leptons and missing energy. Finally, an extended loop model for the $b \to s$ anomalies, which also has an additional $U(1)$ gauge symmetry, contains a scalar DM candidate and explains neutrino masses that can be found in [17].

Finally, let us comment on other models and works that do not easily fit within any of the two categories mentioned above. The model in [3] is very similar to the model in [2]. It also extends the SM with a complex scalar, VL quarks, and leptons and a new $U(1)_X$ gauge symmetry that breaks down to a $\mathbb{Z}_2$ parity. However, the VL leptons carry different $U(1)_X$ charges, leading to a loop-induced $Z'\mu^+\mu^-$ coupling. This changes the DM phenomenology dramatically. The dominant mechanism for the DM production in the early Universe is not a Z' portal interaction, but t-channel exchange of VL leptons. The model in [9] can be regarded as a *hybrid* model, with features from both portal and loop models. The SM

symmetry group is extended with a new $U(1)_{\mu-\tau} \times \mathbb{Z}_2$ piece. The first factor leads to the existence of a massive Z' boson while the second one stabilizes a scalar DM candidate. The $Z'\bar{b}s$ coupling is generated with a loop containing the $\mathbb{Z}_2$-odd fields and the dominant DM production mechanism is a Z' portal interaction, mainly with leptons. The $Z'\bar{b}s$ coupling is also loop-generated in [14], but in this case production of DM particles takes place via a Higgs portal. Reference [8] proposes an extended Scotogenic model for neutrino masses [60] supplemented with a nonuniversal $U(1)$ gauge group. The DM candidate in this case is the lightest fermion singlet and is produced by Yukawa interactions. Finally, two models that address the $b \to s$ anomalies with leptoquarks and include DM candidates were introduced in [5, 15]. In the former the DM candidate is a component of an $SU(2)_L$ multiplet introduced to enhance the diphoton rate of a scalar in the model, whereas in the latter the DM candidate is a baryon-like composite state in a model with strong dynamics at the TeV scale.

Having reviewed and classified the proposed models, we now proceed to discuss in some detail two specific examples. These illustrate the main features of portal and loop models.

5. An Example Portal Model

We will now review the model introduced in [2], arguably one of the simplest scenarios to account for the $b \to s$ anomalies with a dark sector. Some of the ingredients of this model were already present in the model of [56], which is extended in the quark sector (following the same lines as in the lepton sector). It also includes a dark matter candidate that couples to the SM fields via the same mediator that leads to an explanation of the $b \to s$ anomalies, a heavy Z' boson. A variation of this scenario with a loop-induced coupling to muons appeared afterwards in [3], whereas the phenomenology of an extension to account for neutrino masses will be discussed in [61].

The model extends the SM gauge group with a new dark $U(1)_X$ factor, under which all the SM particles are assumed to be singlets. The *dark sector* contains two pairs of vector-like fermions, Q and L, as well as the complex scalar fields, ϕ and χ. Tables 1 and 2 show all the details about the gauge sector and the new scalars and fermions in the model. Q and L have the same representation under the SM gauge group as the SM doublets q and ℓ, and they can be decomposed under $SU(2)_L$ as

$$Q_{L,R} = \begin{pmatrix} U \\ D \end{pmatrix}_{L,R}, \qquad L_{L,R} = \begin{pmatrix} N \\ E \end{pmatrix}_{L,R}, \tag{9}$$

With the electric charges of U, D, N, and E being $+2/3$, $-1/3$, 0, and -1, respectively. In contrast to their SM counterparts, Q and L are vector-like fermions charged under the dark $U(1)_X$. In addition to the usual canonical kinetic terms, the new vector-like fermions Q and L have Dirac mass terms,

$$\mathscr{L}_m = m_Q \overline{Q} Q + m_L \overline{L} L, \tag{10}$$

as well as Yukawa couplings with the SM doublets q and ℓ and the scalar ϕ,

$$\mathscr{L}_Y = \lambda_Q \overline{Q_R} \phi q_L + \lambda_L \overline{L_R} \phi \ell_L + \text{h.c.}, \tag{11}$$

where λ_Q and λ_L are 3 component vectors. The scalar potential of the model can be split into different pieces,

$$\mathscr{V} = \mathscr{V}_{\text{SM}} + \mathscr{V}(H, \phi, \chi) + \mathscr{V}(\phi, \chi). \tag{12}$$

$\mathscr{V}_{\text{SM}}$ is the usual SM scalar potential containing quadratic and quartic terms for the Higgs doublet H. The new terms involving the scalars ϕ and χ are

$$\mathscr{V}(H, \phi, \chi) = \lambda_{H\phi} |H|^2 |\phi|^2 + \lambda_{H\chi} |H|^2 |\chi|^2 \tag{13}$$

and

$$\begin{aligned} \mathscr{V}(\phi, \chi) = {} & m_\phi^2 |\phi|^2 + m_\chi^2 |\chi|^2 + \frac{\lambda_\phi}{2} |\phi|^4 + \frac{\lambda_\chi}{2} |\chi|^4 \\ & + \lambda_{\phi\chi} |\phi|^2 |\chi|^2 + \left(\mu \phi \chi^2 + \text{h.c.}\right). \end{aligned} \tag{14}$$

All λ_i couplings are dimensionless, whereas μ has dimensions of mass and m_ϕ^2 and m_χ^2 have dimensions of mass^2. We will assume that the scalar potential parameters allow for the vacuum configuration

$$\left\langle H^0 \right\rangle = \frac{v}{\sqrt{2}}, \qquad \langle \phi \rangle = \frac{v_\phi}{\sqrt{2}}, \tag{15}$$

where H^0 is the neutral component of the Higgs doublet H. The scalar χ does not get a vacuum expectation value (VEV). Therefore, the scalar ϕ will be responsible for the spontaneous

Table 1: Gauge sector of the model of [2].

Field	Group	Coupling
B	$U(1)_Y$	g_1
W	$SU(2)_L$	g_2
g	$SU(3)_c$	g_3
B_X	$U(1)_X$	g_X

Table 2: New scalars and fermions in the model of [2].

Field	Spin	$SU(3)_c \times SU(2)_L \times U(1)_Y \times U(1)_X$
ϕ	0	$(\mathbf{1}, \mathbf{1}, 0, 2)$
χ	0	$(\mathbf{1}, \mathbf{1}, 0, -1)$
$Q_{L,R}$	$\frac{1}{2}$	$(\mathbf{3}, \mathbf{2}, \frac{1}{6}, 2)$
$L_{L,R}$	$\frac{1}{2}$	$(\mathbf{1}, \mathbf{2}, -\frac{1}{2}, 2)$

breaking of $U(1)_X$. This automatically leads to the existence of a new massive gauge boson, the Z' boson, with mass $m_{Z'} = 2g_X v_\phi$. In the absence of mixing between the $U(1)$ gauge bosons, the Z' boson can be identified with the original B_X boson in Table 1. We note that a Lagrangian term of the form $\mathscr{L} \supset \varepsilon F^Y_{\mu\nu} F_X^{\mu\nu}$, where $F^{X,Y}_{\mu\nu}$ are the usual field strength tensors for the $U(1)_{X,Y}$ groups, would induce this mixing. In order to avoid phenomenological difficulties associated with this mixing we will assume that $\varepsilon \ll 1$. Moreover, it can be shown that loop contributions to this mixing are kept under control if $m_Q \simeq m_L$ [2].

Let us now discuss how this model solves the $\boldsymbol{b \to s}$ **anomalies**. After the spontaneous breaking of $U(1)_X$, the Yukawa interactions in (11) lead to mixings between the vector-like fermions and their SM counterparts. This mixing results in Z' effective couplings to the SM fermions. If these are parametrized as [62, 63]

$$\mathscr{L} \supset \overline{f}_i \gamma^\mu \left(\Delta_L^{f_i f_j} P_L + \Delta_R^{f_i f_j} P_R \right) f_j Z'_\mu, \tag{16}$$

and one assumes $\lambda_Q^d = \lambda_L^e = \lambda_L^\tau = 0$ for the sake of simplicity, the Z' couplings to $\overline{b}s$ and $\mu^+\mu^-$, necessary to solve the $b \to s$ anomalies, are found to be

$$\begin{aligned} \Delta_L^{bs} &= \frac{2 g_X \lambda_Q^b \lambda_Q^{s*} v_\phi^2}{2m_Q^2 + \left(\left|\lambda_Q^s\right|^2 + \left|\lambda_Q^b\right|^2 \right) v_\phi^2}, \\ \Delta_L^{\mu\mu} &= \frac{2 g_X \left|\lambda_L^\mu\right|^2 v_\phi^2}{2m_L^2 + \left|\lambda_L^\mu\right|^2 v_\phi^2}. \end{aligned} \tag{17}$$

These couplings induce a tree-level contribution to the semileptonic four-fermion operators in (5) and (6), as shown schematically in Figure 1. More specifically, given that the SM fermions participating in the effective vertices are left-handed, see (11), the operators $\mathcal{O}_9$ and $\mathcal{O}_{10}$ are generated simultaneously, with [63]

$$C_9^{\mu,\mathrm{NP}} = -C_{10}^{\mu,\mathrm{NP}} = -\frac{\Delta_L^{bs} \Delta_L^{\mu\mu}}{V_{tb} V_{ts}^*} \left(\frac{\Lambda_v}{m_{Z'}} \right)^2, \tag{18}$$

where we have introduced

$$\Lambda_v = \left(\frac{\pi}{\sqrt{2} G_F \alpha} \right)^{1/2} \simeq 4.94\,\mathrm{TeV}, \tag{19}$$

with $\alpha = e^2/4\pi$ being the electromagnetic fine structure constant. Λ_v and the CKM elements appear in (18) in order to normalize the Wilson coefficients as defined in (5) and (6). By taking proper ranges for the model parameters, the required values for these Wilson coefficients, previously identified by the global fits to flavor data, can be easily obtained.

Finally, we move to the discussion on the **Dark Matter** phenomenology of the model. We note that the model does not include any *ad hoc* stabilizing symmetry for the DM candidate χ. However, this state is perfectly stable. This is due to the fact that the continuous $U(1)_X$ symmetry leaves

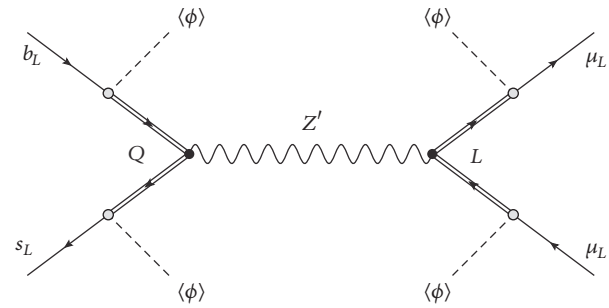

FIGURE 1: Generation of $\mathcal{O}_9$ and $\mathcal{O}_{10}$ in the model of [2]. The mixing between the SM fermions and the vector-like ones induces semi-Leptonic four-fermion interactions.

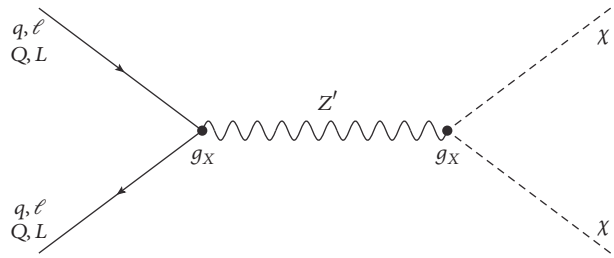

FIGURE 2: DM production via the Z' portal in the model of [2]. We notice that the vertex on the left of the diagram also participates in the explanation of the $b \to s$ anomalies (see Figure 1).

a remnant $\mathbb{Z}_2$ parity, under which χ is odd, after spontaneous symmetry breaking [64–66]. Therefore, the same symmetry that leads to the dynamics behind the $b \to s$ anomalies is also at the origin of the DM stabilization mechanism. Furthermore, the DM production in the early Universe can take place via $2 \leftrightarrow 2$ processes mediated by the Z' boson, thus establishing another link with the $b \to s$ anomalies. Indeed, purely gauge interactions open a Z' *portal* that induces $\overline{F}F \leftrightarrow \chi\chi^*$ annihilation processes, with $F = q, \ell, Q, L$, as shown in Figure 2. (Another possibility is the so-called *Higgs portal*, activated in this model with the scalar potential term $\lambda_{H\chi}|H|^2|\chi|^2$, which induces $HH^\dagger \leftrightarrow \chi\chi^*$ processes. This DM production mechanism will be subdominant for sufficiently small $\lambda_{H\chi}$). We notice that these processes match those in Figure 1 if one trades one of the fermion pairs for $\chi\chi^*$. Therefore, one can establish an interplay between flavor and DM physics in this scenario. Figure 3 illustrates this connection displaying contours for constant $\log(\Omega_{\mathrm{DM}} h^2)$ (the DM relic density) and the ratio $C_9^{\mu,\mathrm{NP}}/C_9^{\mu,\mathrm{SM}}$ in the $(g_X, m_{Z'})$ plane. This figure has been obtained with fixed $\lambda_Q^b = \lambda_Q^s = 0.025$, $\lambda_L^\mu = 0.5$, $m_Q = m_L = 1\,\mathrm{TeV}$, and $m_\chi^2 = 1\,\mathrm{TeV}^2$. The calculation of the flavor observables has been performed with `FlavorKit` [67], whereas the DM relic density has been evaluated with `MicrOmegas` [68]. We see that there is a region in parameter space, with moderately large $g_X \simeq 0.3$, where the observed DM relic density can be reproduced and a ratio $C_9^{\mu,\mathrm{NP}}/C_9^{\mu,\mathrm{SM}}$ in agreement with the global fits is obtained.

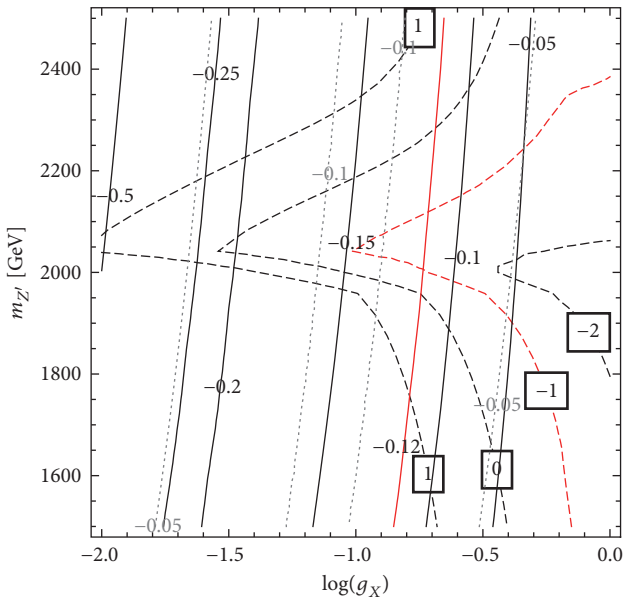

FIGURE 3: Contours for constant $C_9^{\mu,\mathrm{NP}}/C_9^{\mu,\mathrm{SM}}$ and $\log(\Omega_{\mathrm{DM}}h^2)$ (dashed black) in the $(g_X, m_{Z'})$ plane. For the ratio $C_9^{\mu,\mathrm{NP}}/C_9^{\mu,\mathrm{SM}}$ the full 1-loop results are shown via the black lines, while the dotted grey lines give the values using the tree-level approximation. Red lines indicate the preferred values for $C_9^{\mu,\mathrm{NP}}/C_9^{\mu,\mathrm{SM}}$ and $\log(\Omega_{\mathrm{DM}}h^2)$ from global fits and cosmological observations, respectively. Figure taken from [2].

We also note that the DM relic density tends to be large. In fact, in order to obtain a numerical value in the ballpark of $\Omega_{\mathrm{DM}}h^2 \simeq 0.1$ one has to be rather close to the resonant region with $m_{Z'} \simeq 2m_\chi$, which in this plot is located around $m_{Z'} = 2$ TeV.

Besides flavor and DM physics, the model has rich phenomenological prospects in other fronts. The new states can be discovered at the LHC in large portions of the parameter space. Although one typically assumes that the Z' boson couples predominantly to the second- and third-generation quarks ($|\lambda_Q^d| \ll 1$), the resulting suppressed production cross-sections at the LHC can still be sufficient for a discovery; see, for instance, [69]. Furthermore, the new VL fermions can also be produced and detected. In particular, the heavy VL quarks masses are already pushed beyond the TeV scale due to their efficient production in pp collisions. In what concerns direct and indirect DM detection, scenarios with a *dark* Z' portal have been discussed in [70, 71]. For more details about this model, its predictions, and the most relevant experimental constraints we refer to [2].

6. An Example Loop Model

We now turn our attention to the second class of models, those that explain the $b \to s$ anomalies via loop diagrams including DM particles. A simple but illustrative example of this category is that presented in [13]. Previous work on loop models for the b $\to$ s anomalies, without connecting to the DM problem, can be found in [58, 59].

The model introduces two VL fermions, Q and L, with the same gauge quantum numbers as the SM quark and lepton doublets, respectively. It also adds the complex scalar X, a complete singlet under the SM gauge symmetry. The new fields are charged under a global Abelian symmetry, $U(1)_X$, under which all SM fields are assumed to be singlets. As we will see below, this particle content is sufficient to address the $b \to s$ anomalies. Table 3 details the new fields and their charges under the gauge and global symmetries of the model.

The VL fermions Q and L can be decomposed as in (9), with their $SU(2)_L$ components having exactly the same electric charges as in that case. Therefore, the same Dirac mass terms as in (10) can be written. In addition, the symmetries of the model allow for the Yukawa couplings with the SM doublets q and ℓ and the scalar X

$$\mathscr{L}_Y = \lambda_Q \overline{Q_R} X q_L + \lambda_L \overline{L_R} X \ell_L + \text{h.c.}, \tag{20}$$

where λ_Q and λ_L are 3 component vectors. The scalar potential of the model contains the following terms:

$$\mathscr{V} = \mathscr{V}_{\mathrm{SM}} + m_X^2 |X|^2 + \lambda_X |X|^4 + \lambda_H |H|^2 |X|^2 . \tag{21}$$

All λ_i couplings are dimensionless, whereas m_X^2 has dimensions of mass^2. In the following, possible effects due to the λ_H coupling will be ignored, assuming $\lambda_H \ll 1$. We will also assume that the scalar potential parameters allow for a vacuum configuration with $\langle X \rangle = 0$. In this case, the global $U(1)_X$ symmetry is conserved and the lightest state with a nonvanishing charge under this symmetry is completely stable. Moreover, we note that the conservation of $U(1)_X$ prevents the VL fermions from mixing with the SM ones.

We move now to the solution of the ***b*** $\to$ ***s* anomalies** in the context of this model. It is straightforward to check that no NP contributions to $b \to s$ transitions are generated at tree-level in this model. (For instance, in contrast to the model discussed in Section 5, there is no SM-VL mixing, nor a Z' boson that can mediate these transitions at tree-level.) However, the semileptonic operators $\mathcal{O}_9$ and $\mathcal{O}_{10}$ are generated at the 1-loop level as shown in Figure 4. This diagram leads to

$$\begin{aligned} C_9^{\mu,\mathrm{NP}} &= -C_{10}^{\mu,\mathrm{NP}} \\ &= \frac{\lambda_Q^b \lambda_Q^{s*} |\lambda_L^\mu|^2}{64\pi^2 V_{tb} V_{ts}^*} \frac{\Lambda_v^2}{m_Q^2 - m_L^2} \left[f\left(\frac{m_X^2}{m_Q^2}\right) - f\left(\frac{m_X^2}{m_L^2}\right) \right], \end{aligned} \tag{22}$$

where Λ_v was introduced in (19) and $f(x)$ is the loop function

$$f(x) = \frac{1}{x-1} - \frac{\ln x}{(x-1)^2}. \tag{23}$$

This loop-level solution to the $b \to s$ anomalies corresponds to scenario A-I, model class b), in [59]. Figure 5 shows that the model can accommodate the R_K and R_{K^*} measurements by the LHCb collaboration. This figure has been obtained with fixed $|\lambda_Q^b \lambda_Q^s| = 0.15$, $m_L = 1$ TeV, and $m_Q = 1.1$ TeV. One finds that the 1 and 2σ regions for R_K and R_{K^*} almost overlap, and thus they can be accommodated in

Table 3: New scalars and fermions in the model of [13]. The $U(1)_X$ symmetry is global.

Field	Spin	$SU(3)_c \times SU(2)_L \times U(1)_Y$	$U(1)_X$
X	0	$(\mathbf{1},\mathbf{1},0)$	-1
$Q_{L,R}$	$\frac{1}{2}$	$(\mathbf{3},\mathbf{2},\frac{1}{6})$	1
$L_{L,R}$	$\frac{1}{2}$	$(\mathbf{1},\mathbf{2},-\frac{1}{2})$	1

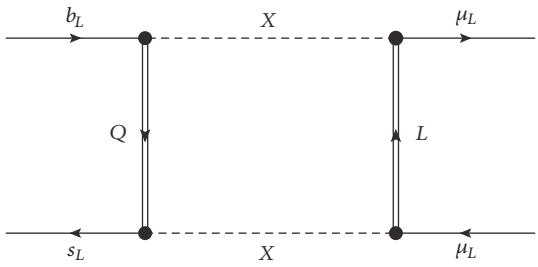

Figure 4: Generation of $\mathcal{O}_9$ and $\mathcal{O}_{10}$ in the model of [13]. Semi-Leptonic four-fermion operators are generated at the 1-loop level.

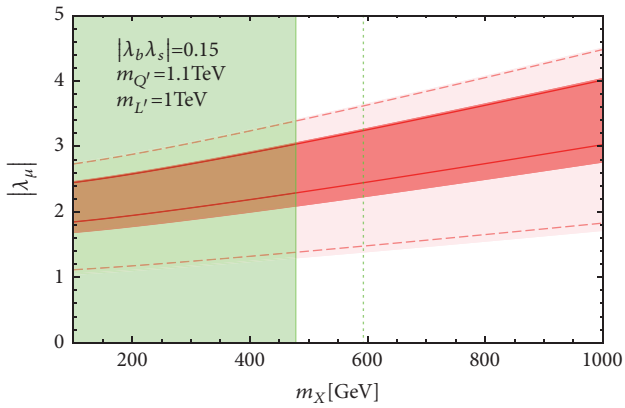

Figure 5: Required values for λ_L^μ (denoted as λ_μ in this figure) and m_X to explain the observed values of R_K and R_{K^*} in the model of [13]. This figure has been obtained with fixed $|\lambda_Q^b\lambda_Q^s| = 0.15$, $m_L = 1$ TeV, and $m_Q = 1.1$ TeV. The light (dark) red region corresponds to the R_K measurement at 1σ (2σ), whereas the red lines indicate the same regions for R_{K^*}. The green region is excluded due to $B_s - \overline{B_s}$ mixing for $m_Q = 1.1$ TeV. The excluded region would extend up to the dashed green line for $m_Q = 1$ TeV. Figure taken from [13].

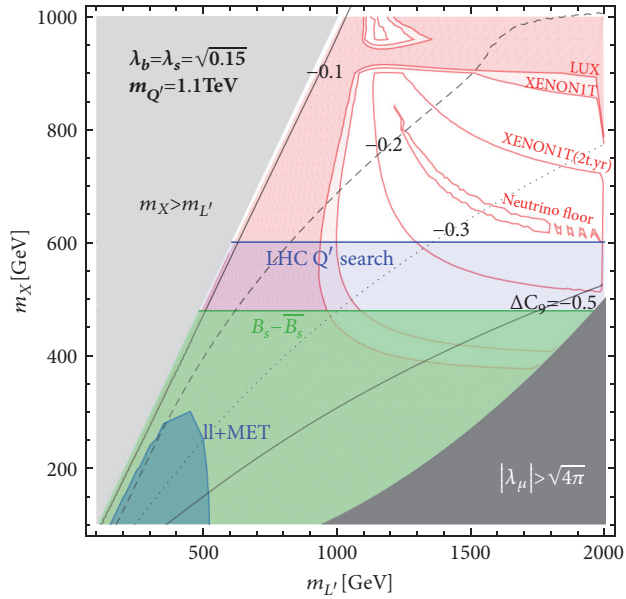

Figure 6: Contours of constant $C_9^{\mu,\mathrm{NP}}$ in the $m_L - m_X$ plane for the model of [13]. This figure has been obtained with fixed $\lambda_Q^b = \lambda_Q^s = \sqrt{0.15}$ and $m_Q = 1.1$ TeV, choosing λ_L^μ in order to reproduce the observed DM relic density. The colored regions are excluded by various constraints: heavy quark and lepton searches at the LHC (blue), $B_s - \overline{B_s}$ mixing (green), and direct DM detection experiments (red). The grey regions are excluded due to perturbativity constraints (dark grey region) or by demanding that X is the lightest $U(1)_X$-charged state (light grey region). Future direct DM detection prospects are also shown in this plot. Figure taken from [13].

the same region of parameter space. Furthermore, in order to be compatible with the bounds coming from $B_s - \overline{B_s}$ mixing one needs $|\lambda_Q^b\lambda_Q^s| \ll 1$, which implies a relatively large value of $|\lambda_L^\mu|$, $|\lambda_L^\mu| \gtrsim 2$. This feature, a hierarchy between the NP couplings to quarks and leptons, is shared by most models addressing the $b \to s$ anomalies. For a general discussion about the $B_s - \overline{B_s}$ mixing constraint in the context of the $b \to s$ anomalies we refer to [72].

Finally, let us discuss the **Dark Matter** phenomenology of the model. As explained above, the global $U(1)_X$ symmetry is assumed to be conserved, and this implies that a stable state must exist. Assuming that the lightest state charged under $U(1)_X$ is the neutral scalar X, it constitutes the DM candidate in the model. One then needs to determine whether the observed DM relic density can be achieved in the region of parameter space where the $b \to s$ anomalies are solved, without conflict with other experimental constraints. This is shown in Figure 6, where contours of $C_9^{\mu,\mathrm{NP}}$ are shown in the $m_L - m_X$ plane. This figure has been obtained with fixed $\lambda_Q^b = \lambda_Q^s = \sqrt{0.15}$ and $m_Q = 1.1$ TeV. For each parameter point, the value of λ_L^μ is chosen to reproduce the observed DM relic density, which is calculated using `MicrOmegas` [68]. Large values of $|\lambda_L^\mu|$ are obtained in this way. For this reason, the most relevant DM annihilation channels for the determination of the relic density with these parameter values are $XX^* \leftrightarrow \mu^+\mu^-, \nu\nu$. Even though the experimental constraints, in particular those from direct LHC searches for extra quarks, reduce the allowed parameter space substantially, one finds valid regions with $C_9^{\mu,\mathrm{NP}} \sim -0.3$. This value would explain the $b \to s$ anomalies at 2σ; see, for

instance, [48]. Interestingly, the model is testable in future direct DM detection experiments, such as XENON1T, as shown in Figure 6. In the region of parameter space selected for this figure, the dominant process leading to DM-nucleon scattering is 1-loop photon exchange, with leptons running in the loop. The loop suppression is compensated by the large λ_L^μ coupling.

The new states in this model can be discovered at the LHC. For instance, the heavy VL charged lepton can be produced in Drell-Yan processes. Due to the required large values for the λ_L^μ coupling, this exotic state is expected to decay mainly to a DM particle X (invisible at the LHC) and a muon. Since $U(1)_X$ conservation requires the X particles to be produced in pairs, the expected signature is the observation of two energetic muons and large missing energy. Similar events replacing the muons by jets (mainly b jets) are expected for the VL quarks. We conclude the discussion of this model by referring for more details to the original work in [13].

7. Summary and Discussion

In this minireview we have discussed New Physics models that address the $b \to s$ anomalies and link them to the dark matter of the Universe. The interplay between these two areas of particle physics may offer novel model building directions as well as additional phenomenological tests for the proposed scenarios. We have shown that most of the proposed models can be classified into two categories: (i) models in which the $b \to s$ anomalies and the DM production mechanism share a common mediator (such as a heavy Z' boson), and (ii) models that induce the NP contributions to explain the $b \to s$ anomalies via loops including the DM particle. These generic ideas have been illustrated with two particular realizations (the models introduced in [2, 13]), which clearly show that the combination of flavor physics and dark matter leads to new scenarios with a rich phenomenology.

The introduction of a dark sector in a model for the $b \to s$ anomalies can also have phenomenological consequences besides the existence of a DM candidate. For instance, both problems, the dark matter of the Universe and the $b \to s$ anomalies, might be connected to another long-standing question in particle physics: the muon anomalous magnetic moment [4, 73–75]. Furthermore, it is interesting to note that the introduction of dark matter in some models can help alleviate some of the most stringent constraints. Indeed, the LHC bounds on some mediators become weaker if they have invisible decay channels [76]. We believe that this is a promising line of research to be pursued in order to fully assess the validity of some scenarios that are currently under experimental tension.

We are living an exciting moment in flavor physics, with several interesting anomalies in B-meson decays. Whether real or not, only time can tell. New LHCb analyses based on larger datasets are expected to appear in the near future, possibly shedding new light on these anomalies. In the longer term, fundamental contributions from the Belle II experiment will also be crucial to settle the issue [77]. In the meantime, an intense model building effort is opening new avenues with rich phenomenological scenarios. The possible connection to one of the central problems in current physics, the nature of the dark matter of the Universe, would definitely be a fascinating outcome of this endeavour.

Conflicts of Interest

The author declares that there are no conflicts of interest regarding the publication of this paper.

Acknowledgments

The author is grateful to Junichiro Kawamura, Shohei Okawa, and Yuji Omura for clarifications regarding [13] and to Javier Virto for comments about the manuscript. They are also very grateful to their collaborators in the subjects discussed in this review and acknowledge financial support from the Grants FPA2017-85216-P and SEV-2014-0398 (MINECO) and PROMETEOII/2014/084 (Generalitat Valenciana).

References

[1] Planck Collaboration, P. A. R. Ade et al., "Planck 2015 results. XIII. Cosmological parameters," *Astronomy & Astrophysics*, vol. 594, 2016.

[2] D. A. Sierra, F. Staub, and A. Vicente, "Shedding light on the b→s anomalies with a dark sector," *Physical Review D: Particles, Fields, Gravitation and Cosmology*, vol. 92, no. 1, Article ID 015001, 2015.

[3] G. Bélanger, C. Delaunay, and S. Westhoff, "A Dark matter relic from muon anomalies," *Physical Review D: Particles, Fields, Gravitation and Cosmology*, vol. 92, no. 5, Article ID 055021, 2015.

[4] B. Allanach, F. S. Queiroz, A. Strumia, and S. Sun, "Z' models for the LHCb and g-2 muon anomalies," *Physical Review D: Particles, Fields, Gravitation and Cosmology*, vol. 93, no. 5, Article ID 055045, 2016, Erratum: Phys. Rev.D95,no.11,119902(2017).

[5] M. Bauer and M. Neubert, "Flavor anomalies, the 750 GeV diphoton excess, and a dark matter candidate," *Physical Review D: Particles, Fields, Gravitation and Cosmology*, vol. 93, no. 11, 2016.

[6] A. Celis, W. Feng, and M. Vollmann, "Dirac dark matter and b→sl+l- with U(1) gauge symmetry," *Physical Review D: Particles, Fields, Gravitation and Cosmology*, vol. 95, no. 3, Article ID 035018, 2017.

[7] W. Altmannshofer, S. Gori, S. Profumo, and F. S. Queiroz, "Explaining dark matter and B decay anomalies with an Lμ-Lτ model," *Journal of High Energy Physics*, vol. 12, no. 106, 2016.

[8] P. Ko, T. Nomura, and H. Okada, "A flavor dependent gauge symmetry, predictive radiative seesaw and LHCb anomalies," *Physics Letters. B. Particle Physics, Nuclear Physics and Cosmology*, vol. 772, pp. 547–552, 2017.

[9] P. Ko, T. Nomura, and H. Okada, "Explaining B→K(*)l+l- anomaly by radiatively induced coupling in U(1)μ-τ gauge symmetry," *Physical Review D: Particles, Fields, Gravitation and Cosmology*, vol. 95, no. 11, Article ID 111701, 2017.

[10] J. M. Cline, J. M. Cornell, D. London, and R. Watanabe, "Hidden sector explanation of," *Physical Review D: Particles, Fields, Gravitation and Cosmology*, vol. 95, no. 9, Article ID 095015, 2017.

[11] F. Sala and D. M. Straub, "A new light particle in B decays?" *Physics Letters B*, vol. 774, pp. 205–209, 2017.

[12] J. Ellis, M. Fairbairn, and P. Tunney, "Anomaly-free models for flavour anomalies," *The European Physical Journal C*, vol. 78, no. 3, 2018.

[13] J. Kawamura, S. Okawa, and Y. Omura, "Interplay between the b→sll anomalies and dark matter physics," *Physical Review D: Particles, Fields, Gravitation and Cosmology*, vol. 96, no. 7, Article ID 075041, 2017.

[14] S. Baek, "Dark matter contribution to b→sμ+μ- anomaly in local U(1)Lμ-Lτ model," *Physics Letters B*, vol. 781, pp. 376–382, 2018.

[15] J. M. Cline, "B decay anomalies and dark matter from vectorlike confinement," *Physical Review D: Particles, Fields, Gravitation and Cosmology*, vol. 97, no. 1, Article ID 015013, 2018.

[16] J. M. Cline and J. M. Cornell, "R(K(∗)) from dark matter exchange," *Physics Letters B*, vol. 782, pp. 232–237, 2018.

[17] L. Dhargyal, "A simple model to explain the observed muon sector anomalies, small neutrino masses, baryon-genesis and dark-matter," https://arxiv.org/abs/1711.09772.

[18] C.-W. Chiang and H. Okada, "A simple model for explaining muon-related anomalies and dark matter," https://arxiv.org/abs/1711.07365.

[19] A. Falkowski, S. F. King, E. Perdomo, and M. Pierre, "Flavourful Z$\prime$ portal for vector-like neutrino Dark Matter and RK(∗)," https://arxiv.org/abs/1803.04430.

[20] G. Arcadi, T. Hugle, and F. S. Queiroz, "The Dark Lμ–Lτ Rises via Kinetic Mixing," https://arxiv.org/abs/1803.05723.

[21] S. Jäger and J. M. Camalich, "On B → V$\ell\ell$ at small dilepton invariant mass, power corrections, and new physics," *Journal of High Energy Physics*, vol. 2013, no. 5, 2013.

[22] S. Descotes-Genon, L. Hofer, J. Matias, and J. Virto, "On the impact of power corrections in the prediction of B → K *μ+μ– observables," *Journal of High Energy Physics*, vol. 2014, no. 12, 2014.

[23] A. Khodjamirian, T. Mannel, A. Pivovarov, and Y. Wang, "Charm-loop effect in B → K (*) ℓ + ℓ– and B → K *γ," *Journal of High Energy Physics*, vol. 2010, no. 9, 2010.

[24] M. Ciuchini, M. Fedele, E. Franco et al., "B → K∗ℓ + ℓ– decays at large recoil in the Standard Model: a theoretical reappraisal," *Journal of High Energy Physics*, vol. 2016, no. 6, 2016.

[25] B. Capdevila, S. Descotes-Genon, L. Hofer, and J. Matias, "Hadronic uncertainties in B→K*μ+μ-: a state-of-the-art analysis," *Journal of High Energy Physics*, vol. 2017, no. 4, 2017.

[26] V. G. Chobanova, T. Hurth, F. Mahmoudi, D. M. Santos, and S. Neshatpour, "Large hadronic power corrections or new physics in the rare decay B → K ∗μ + μ–?" *Journal of High Energy Physics*, vol. 2017, no. 7, 2017.

[27] C. Bobeth, M. Chrzaszcz, D. van Dyk, and J. Virto, "Long-distance effects in B→K∗$\ell\ell$ from Analyticity," https://arxiv.org/abs/1707.07305.

[28] T. Blake, U. Egede, P. Owen, G. Pomery, and K. A. Petridis, "An empirical model of the long-distance contributions to B0→K*0μ+μ- transitions," *The European Physical Journal C*, vol. 78, no. 453, 2018.

[29] S. Descotes-Genon, T. Hurth, J. Matias, and J. Virto, "Optimizing the basis of B → K *ℓ + ℓ– observables in the full kinematic range," *Journal of High Energy Physics*, vol. 2013, no. 5, 2013.

[30] LHCb Collaboration, R. Aaij et al., "Measurement of Form-Factor-Independent Observables in the Decay B0→K*0μ+μ-," *Physical Review Letters*, vol. 118, no. 12, 2017.

[31] LHCb Collaboration, R. Aaij et al., "Differential branching fraction and angular analysis of the decay Bs0→ $\phi\mu$+μ-," *JHEP*, vol. 7, no. 84, 2013.

[32] LHCb Collaboration, R. Aaij et al., "Angular analysis of the B0→K*0μ+μ- decay using 3 fb -1 of integrated luminosity," *JHEP*, vol. 2, no. 104, 2016.

[33] LHCb Collaboration, R. Aaij et al., "Angular analysis and differential branching fraction of the decay Bs0→ $\phi\mu$+μ-," *JHEP*, vol. 09, no. 179, 2015.

[34] Belle Collaboration, A. Abdesselam et al., "Angular analysis of B0→K*(892)0l+l-," in *in Proceedings, LHCSki - A First Discussion of 13 TeV Results: Obergurgl*, Austria, 2016, arXiv:1604.04042.

[35] Belle Collaboration, S. Wehle et al., "Lepton-Flavor-Dependent Angular Analysis of B→K*l+l-," *Phys. Rev. Lett*, vol. 118, no. 11, Article ID 111801, 2017.

[36] ATLAS Collaboration, "Angular analysis of Bd0→K*μ+μ- decays in pp collisions at s=8 TeV with the ATLAS detector," in *Proceedings of the collision8 TeV with the ATLAS detector*, pp. 2017-023, 2017.

[37] CMS Collaboration, "Measurement of the P1 and P5' angular parameters of the decay B0?K*0μ+μ- in proton-proton collisions at s=8TeV," *CMS-PAS-BPH-15-008*, 2017.

[38] G. Hiller and F. Krüger, "More model-independent analysis of b→s processes," *Physical Review D: Particles, Fields, Gravitation and Cosmology*, vol. 69, no. 7, 2004.

[39] LHCb Collaboration, R. Aaij et al., "Test of lepton universality using B+→K+l+l- decays," *Physical Review Letters*, vol. 113, Article ID 151601, 2014.

[40] LHCb Collaboration, R. Aaij et al., "Test of lepton universality with B 0 → K *0 ℓ + ℓ– decays," *Journal of High Energy Physics*, vol. 2017, no. 55, 2017.

[41] S. Descotes-Genon, L. Hofer, J. Matias, and J. Virto, "Global analysis of b→sll anomalies," *Journal of High Energy Physics*, vol. 1606, article 092, no. 6, 2016.

[42] M. Bordone, G. Isidori, and A. Pattori, "On the Standard Model predictions for RK and RK*," *The European Physical Journal C*, vol. 76, no. 8, 2016.

[43] B. Capdevila, S. Descotes-Genon, J. Matias, and J. Virto, "Assessing lepton-flavour non-universality from B →K ∗$\ell\ell$ angular analyses," *Journal of High Energy Physics*, vol. 2016, no. 10, 2016.

[44] Heavy flavor averaging group, http://www.slac.stanford.edu/xorg/hfag/semi/fpcp17/RDRDs.html.

[45] LHCb Collaboration, R. Aaij et al., "Measurement of the Ratio of Branching Fractions B(B+c→J/$\psi\tau$+$\nu\tau$)/B(B+c→J/$\psi\mu$+$\nu\mu$)," *Physical Review Letters*, vol. 120, Article ID 121801, 2018.

[46] D. Buttazzo, A. Greljo, G. Isidori, and D. Marzocca, "B-physics anomalies: a guide to combined explanations," *Journal of High Energy Physics*, vol. 2017, no. 11, 2017.

[47] B. Capdevila, A. Crivellin, S. Descotes-Genon, J. Matias, and J. Virto, "Patterns of New Physics in b → sℓ+ℓ– transitions in the light of recent data," *Journal of High Energy Physics*, vol. 2018, no. 1, 2018.

[48] W. Altmannshofer, P. Stangl, and D. M. Straub, "Interpreting hints for lepton flavor universality violation," *Physical Review D: Particles, Fields, Gravitation and Cosmology*, vol. 96, no. 5, 2017.

[49] G. D'Amico, M. Nardecchia, P. Panci et al., "Flavour anomalies after the RK* measurement," *Journal of High Energy Physics*, vol. 2017, no. 9, 2017.

[50] G. Hiller and I. Nišandžić, "RK and RK* beyond the standard model," *Physical Review D: Particles, Fields, Gravitation and Cosmology*, vol. 96, no. 3, Article ID 035003, 2017.

[51] L. Geng, B. Grinstein, S. Jäger, J. Martin Camalich, X. Ren, and R. Shi, "Towards the discovery of new physics with lepton-universality ratios of b→sll decays," *Physical Review D: Particles, Fields, Gravitation and Cosmology*, vol. 96, no. 9, 2017.

[52] M. Ciuchini, A. M. Coutinho, M. Fedele et al., "On flavourful Easter eggs for New Physics hunger and lepton flavour universality violation," *The European Physical Journal C*, vol. 77, no. 10, 2017.

[53] A. K. Alok, B. Bhattacharya, A. Datta, D. Kumar, J. Kumar, and D. London, "New Physics in b→sμ+μ- after the Measurement of RK*," *Physical Review D: Particles, Fields, Gravitation and Cosmology*, vol. 96, no. 9, 2017.

[54] T. Hurth, F. Mahmoudi, D. Martínez Santos, and S. Neshatpour, "Lepton nonuniversality in exclusive b→sll decays," *Physical Review D: Particles, Fields, Gravitation and Cosmology*, vol. 96, no. 9, 2017.

[55] A. Celis, J. Fuentes-Martín, A. Vicente, and J. Virto, "Gauge-invariant implications of the LHCb measurements on lepton-flavor nonuniversality," *Physical Review D: Particles, Fields, Gravitation and Cosmology*, vol. 96, no. 3, 2017.

[56] W. Altmannshofer, S. Gori, M. Pospelov, and I. Yavin, "Quark flavor transitions in Lμ-Lτ models," *Physical Review D: Particles, Fields, Gravitation and Cosmology*, vol. 89, no. 9, 2014.

[57] AMS Collaboration, M. Aguilar et al., "Antiproton Flux, Antiproton-to-Proton Flux Ratio, and Properties of Elementary Particle Fluxes in Primary Cosmic Rays Measured with the Alpha Magnetic Spectrometer on the International Space Station," *Physical Review Letters*, vol. 117, no. 9, Article ID 091103, 2016.

[58] B. Gripaios, M. Nardecchia, and S. Renner, "Linear flavour violation and anomalies in B physics," *Journal of High Energy Physics*, vol. 2016, no. 6, 2016.

[59] P. Arnan, L. Hofer, F. Mescia, and A. Crivellin, "Loop effects of heavy new scalars and fermions in b→sμ+μ-," *Journal of High Energy Physics*, vol. 2017, no. 4, 2017.

[60] E. Ma, "Verifiable radiative seesaw mechanism of neutrino mass and dark matter," *Physical Review D: Particles, Fields, Gravitation and Cosmology*, vol. 73, Article ID 077301, 2006.

[61] P. Rocha-Moran and A. Vicente, "Lepton flavor violation in a Z' model for the $b \to s$ anomalies," In press.

[62] A. J. Buras, F. De Fazio, and J. Girrbach, "The anatomy of Z′ and Z with flavour changing neutral currents in the flavour precision era," *Journal of High Energy Physics*, vol. 2013, no. 2, 2013.

[63] W. Altmannshofer and D. M. Straub, "New physics in b→s transitions after LHC run 1," *The European Physical Journal C*, vol. 75, no. 8, 2015.

[64] L. M. Krauss and F. Wilczek, "Discrete gauge symmetry in continuum theories," *Physical Review Letters*, vol. 62, no. 11, pp. 1221–1223, 1989.

[65] B. Petersen, M. Ratz, and R. Schieren, "Patterns of remnant discrete symmetries," *Journal of High Energy Physics*, vol. 2009, no. 08, article 111, 2009.

[66] D. A. Sierra, M. Dhen, C. S. Fong, and A. Vicente, "Dynamical flavor origin of ZN symmetries," *Physical Review D: Particles, Fields, Gravitation and Cosmology*, vol. 91, no. 9, 2015.

[67] W. Porod, F. Staub, and A. Vicente, "A flavor kit for BSM models," *The European Physical Journal C*, vol. 74, no. 8, article 2992, 2014.

[68] G. Belanger, F. Boudjema, A. Pukhov, and A. Semenov, "micrOMEGAs_3: a program for calculating dark matter observables," *Computer Physics Communications*, vol. 185, no. 3, pp. 960–985, 2014.

[69] A. Greljo, G. Isidori, and D. Marzocca, "On the breaking of lepton flavor universality in B decays," *Journal of High Energy Physics*, vol. 2015, no. 7, 2015.

[70] A. Alves, S. Profumo, and F. S. Queiroz, "The dark Z' portal: direct, indirect and collider searches," *Journal of High Energy Physics*, vol. 2014, article 63, 2014.

[71] A. Alves, A. Berlin, S. Profumo, and F. S. Queiroz, "Dark Matter Complementarity and the Z' Portal," *Physical Review D*, vol. 92, no. 8, Article ID 083004, 2015.

[72] L. Di Luzio, M. Kirk, and A. Lenz, "Updated Bs-mixing constraints on new physics models for b→sℓ+ℓ− anomalies," *Physical Review D*, vol. 97, Article ID 095035, 2018.

[73] G. Bélanger and C. Delaunay, "A Dark Sector for gμ-2, RK and a Diphoton Resonance," *Physical Review D: Particles, Fields, Gravitation and Cosmology*, vol. 94, no. 7, Article ID 075019, 2016.

[74] S. Di Chiara, A. Fowlie, S. Fraser et al., "Minimal flavor-changing Z′ models and muon g-2 after the RK* measurement," *Nuclear Physics B*, vol. 923, pp. 245–257, 2017.

[75] K. Kowalska and E. M. Sessolo, "Expectations for the muon g-2 in simplified models with dark matter," *Journal of High Energy Physics*, vol. 2017, no. 9, article 112, 2017.

[76] D. A. Faroughy, A. Greljo, and J. F. Kamenik, "Confronting lepton flavor universality violation in B decays with high- pT tau lepton searches at LHC," *Physics Letters B*, vol. 764, pp. 126–134, 2017.

[77] J. Albrecht, F. Bernlochner, M. Kenzie, S. Reichert, D. Straub, and A. Tully, "Future prospects for exploring present day anomalies in flavour physics measurements with Belle II and LHCb," https://arxiv.org/abs/1709.10308.

Hindawi
Advances in High Energy Physics
Volume 2018, Article ID 9132381, 7 pages
https://doi.org/10.1155/2018/9132381

Research Article

Lower Mass Bound on the W' Mass via Neutrinoless Double Beta Decay in a 3-3-1 Model

A. C. O. Santos [1,2] **and P. Vasconcelos** [1]

[1] *Departamento de Física, Universidade Federal da Paraíba, Caixa Postal 5008, 58051-970 João Pessoa, PB, Brazil*
[2] *Centre for Cosmology, Particle Physics and Phenomenology (CP3), Université Catholique de Louvain, 1348 Louvain-la-Neuve, Belgium*

Correspondence should be addressed to A. C. O. Santos; antonio_santos@fisica.ufpb.br

Received 10 November 2017; Revised 19 February 2018; Accepted 3 April 2018; Published 23 May 2018

Academic Editor: Jose W. F. Valle

The discovery of neutrino masses has raised the importance of studies in the context of neutrinoless double beta decay ($0\nu\beta\beta$), which constitutes a landmark for lepton number violation (LNV). The standard interpretation is that the light massive neutrinos that we observed oscillating in terrestrial experiments mediate double beta decay. In the minimal 3-3-1 model (3-3-1M), object of our study, there is an additional contribution that stems from the mixing between a new charged vector boson, W', and the Standard Model W boson. Even after setting this mixing to be very small, we show that tight constraints arise from the nonobservation of $0\nu\beta\beta$. Indeed, we derive bounds on the mass of the W' gauge boson that might exceed those from collider probes and most importantly push the scale of symmetry breaking beyond its validity, leading to an exclusion bound for the minimal 3-3-1 model.

1. Introduction

The Standard Model (SM) has thrived after a multitude of precision tests at low and high energy scales [1]. However, the existence of neutrino masses is one of the main motivations for physics beyond the SM [2]. If neutrinos are majorana particles, neutrinoless double beta decay ($0\nu\beta\beta$) should occur. Double beta decay is the transition of a nucleus with mass and atomic number A and Z to a nucleus with A and $Z+2$, accompanied by the emission of two electrons only. Its possible discovery will represent an irrefutable proof of lepton number violation, LNV. The standard diagram that leads to such lepton number violation process is exhibited in Figure 1.

At present, a lot of experiments using different isotopes and techniques are operating or under development in the search for neutrinoless double beta decay (see [3]). In this work we investigate the implications of the nonobservation of neutrinoless double beta decay in the context of 3-3-1 models [4–9]. 3-3-1 models are plausible extensions of the SM where fermions are placed in the fundamental or adjoint representation of $SU(3)$. Generally these models while being consistent with colliders data [10, 11] nicely explain why we have three fermion generations [5, 12, 13], accommodate neutrino masses [14–16], and may feature several dark matter candidates [17, 18] to the dark matter problem. Moreover, they could also address low energy anomalies [19, 20] and might feature interesting astrophysical [21, 22] and collider phenomenology via the presence of exotic gauge bosons which are popularly used in many different contexts [23, 24]. See [25–31] for many other exciting phenomenological studies.

In this work, we focus our attention on the minimal 3-3-1 model (3-3-1M), one of the possible versions of 3-3-1 models, in which the electric operator takes the form $Q = T_3 + \beta T_8 + X$ considering T_i as $\lambda^a/2$ (Gell-Mann matrices with $a = 1, \ldots, 8$), $\beta = -\sqrt{3}$ for $SU(3)_L$ (see explanation below), and X as $U(1)_X$ charge, where no new leptons are evoked (right-handed neutrinos as well), thus featuring a minimal fermion content. Since we are dealing with an extended gauge group, there will be additional gauge bosons, one of them being singly charged, W', due to the chosen charge operator parameter. This new gauge boson might induce the

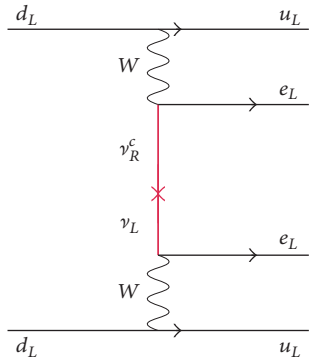

FIGURE 1: Canonical $0\nu\beta\beta$ due to light massive neutrinos.

neutrinoless double beta decay if it mixes with the W boson. In order to successfully explain neutrino masses in this model without the use of nonrenormalizable operators [14], a scalar sextet should be introduced [32, 33]. This scalar sextet embeds the scalar triplet model, often used in the context of neutrino masses [34–37]. The first component of the scalar sextet is a neutral field which is often assumed to yield a null vacuum expectation value (vev). In this work we make assumption otherwise. If such scalar acquires a nonvanishing vev then W' mixes with the SM W boson, giving rise to new contributions to the neutrinoless double beta decay. This scenario has been investigated before in the context of majoron in [38–41]. Here we revisit the implications in a more general setting in perspective with other existing colliders constraints. We will ignore contributions arising from the scalar fields because they yield less restrictive bounds [39] and because a bound on the W' mass is already implied into a lower mass bound on the entire particle spectrum of model, since the W' mass is directly connected to the scale of symmetry breaking of the model. It is worth mentioning that in this work our parameter space provides a very small $Z - Z'$ mixing and does not bring relevant constraints coming from STU parameters [41, 42].

We will show that if W' does feature a mixing with the SM W boson then limits stemming from neutrinoless double beta decay supersede LHC probes, highlighting the importance of multiple new physics searches probes.

The paper is organized as follows: In Section 2 we describe the model and explain how the $W' - W$ mass mixing can be generated. In Section 3 we derive the contributions to neutrinoless double beta decay. In Section 4 we draw our conclusions.

2. The Model

In the minimal 3-3-1 model leptons are arranged as

$$L^{\ell} = \begin{pmatrix} \nu_{\ell} \\ \ell \\ \ell^c \end{pmatrix}_L \sim (3, 0), \tag{1}$$

where $\sim$ represents the way the triplet transforms under $SU(3)_L \otimes U(1)_N$, with $\ell = e, \mu, \tau$, representing the three known generations. Notice that the third component of the lepton triplet is the right-handed lepton. The quarks are placed as follows:

$$Q_{1L} = \begin{pmatrix} u_1 \\ d_1 \\ J_1 \end{pmatrix}_L \sim \left(3, \frac{2}{3}\right),$$
$$Q_{iL} = \begin{pmatrix} d_i \\ -u_i \\ J_i \end{pmatrix}_L \sim \left(\overline{3}, -\frac{1}{3}\right), \quad i = 2, 3. \tag{2}$$

Here u_{aL} and d_{aL} ($a = 1, 2, 3$) correspond, respectively, to flavors u, c, t and d, s, b of the Standard Model (SM) quarks. The first generation transforms as a triplet, while the second and third generations transform as antitriplets under $SU(3)_L$. In addition to the left-handed field we have right-handed quarks as singlets under $SU(3)_L$: $u_{aR} \sim (1, 2/3)$, $d_{aR} \sim (1, -1/3)$, $J_{1R} \sim (1, 5/3)$, $J_{iR} \sim (1, -4/3)$, with $a = 1, 2, 3$ and $i = 2, 3$. J_1 and J_i are exotic quarks predicted by the model with electric charges of 5/3 and $-4/3$, respectively. These exotic quarks are also known as leptoquarks in the literature [43, 44].

The mass generation mechanism relies firstly on the presence of three scalar triplets; namely,

$$\eta = \begin{pmatrix} \eta^0 \\ \eta_1^- \\ \eta_2^+ \end{pmatrix},$$
$$\rho = \begin{pmatrix} \rho^+ \\ \rho^0 \\ \rho^{++} \end{pmatrix}, \tag{3}$$
$$\chi = \begin{pmatrix} \chi^- \\ \chi^{--} \\ \chi^0 \end{pmatrix},$$

with them transforming as $(3, 0)$, $(3, 1)$, and $(3, -1)$ under $SU(3)_L \otimes U(1)_N$, respectively. These scalar triplets couple with the fermions fields through the following Yukawa Lagrangian:

$$\begin{aligned} -\mathscr{L}_Y = {} & \frac{1}{2}\sum_{\ell\ell'} G^{\ell\ell'} \epsilon^{lmn} \left[\overline{(L_l^{\ell})^c} L_m^{\ell'} \eta_n\right] + G_{1a}^u \overline{Q}_{1L} \eta u_{aR} \\ & + G_{1a}^d \overline{Q}_{1L} \rho d_{aR} + G_{11}^{J1} \overline{Q}_{1L} \chi J_{1R} + G_{2a}^s \overline{Q}_{2L} \eta^* d_{aR} \\ & + G_{2a}^c \overline{Q}_{2L} \rho^* u_{aR} + G_{2i}^{J2} \overline{Q}_{2L} \chi^* J_{iR} \\ & + G_{3a}^b \overline{Q}_{3L} \eta^* d_{aR} + G_{3a}^t \overline{Q}_{3L} \rho^* u_{aR} \\ & + G_{3i}^{J3} \overline{Q}_{3L} \chi^* J_{iR} + \text{h.c.}, \end{aligned} \tag{4}$$

with $\ell, \ell' = e, \mu, \tau$. Equation (4) is sufficient to generate masses to charged leptons and quarks but neutrinos remain

massless. In order to obtain nonzero neutrino masses, a scalar sextet should be introduced:

$$S = \begin{pmatrix} \sigma_1^0 & \frac{h_2^-}{\sqrt{2}} & \frac{h_1^+}{\sqrt{2}} \\ \frac{h_2^-}{\sqrt{2}} & H_1^{--} & \frac{\sigma_2^0}{\sqrt{2}} \\ \frac{h_1^+}{\sqrt{2}} & \frac{\sigma_2^0}{\sqrt{2}} & H_2^{++} \end{pmatrix} \sim (\mathbf{6}, \mathbf{0}). \tag{5}$$

The presence of such scalar sextet gives rise to the Yukawa term,

$$\mathscr{L}_Y^S = -\frac{1}{2}\sum_{\ell\ell'} G\overline{(L^\ell)^c} S^* L^{\ell'}, \tag{6}$$

with $L^c = C\overline{L}^T$, C being the charge conjugate matrix.

Expanding (6) we have explicitly

$$\begin{aligned} \mathscr{L}_Y^S \supset -\frac{1}{2}\sum_{\ell\ell'} G_{\ell\ell'} \Bigg[& \overline{(\nu_{\ell L})^c}\nu_{\ell' L}\sigma_1^0 + \overline{(\ell_L)^c}\ell'_L H_1^{++} \\ & + \overline{\ell_R}\left(\ell'^c\right)_L H_2^{--} + \left(\overline{(\ell_L)^c}\nu_{\ell' L} + \overline{(\nu_{\ell L})^c}\ell'_L\right)\frac{h_2^+}{\sqrt{2}} \\ & + \left(\overline{\ell_R}\nu_{\ell' L} + \overline{(\nu_{\ell L})^c}\left(\ell'^c\right)_L\right)\frac{h_1^-}{\sqrt{2}} \\ & + \left(\overline{\ell_R}\ell'_L + \overline{(\ell_L)^c}\left(\ell'_R\right)^c\right)\frac{\sigma_2^0}{\sqrt{2}}\Bigg] + \text{h.c.} \end{aligned} \tag{7}$$

Notice that a new contribution to the charged lepton masses arises if $v_{\sigma_2} \neq 0$. Moreover, neutrinos remain massless unless $\langle\sigma_1^0\rangle \neq 0$. Typically, this scalar sextet is absent in 3-3-1 studies, and consequently neutrino masses are not addressed. In this work, we discuss a more general setting, where the scalar sextet is present and $v_{\sigma_{1,2}} \neq 0$. In this setup, the spontaneous symmetry breaking occurs as follows: firstly, χ^0 develops vev (v_χ), breaking $SU(3)_L \otimes U(1)_N$ into $SU(2)_L \otimes U(1)_Y$. Later ρ^0 and η^0 acquire a nonzero vev with $v_\rho \sim v_\eta$, breaking $SU(2) \otimes U(1)_Y$ into $U(1)_{QED}$, that is, the electromagnetism gauge group.

This symmetry breaking pattern generates mass to all SM fermions and gauge bosons. We highlight that, due to the enlarged gauge group, 3-3-1 models feature five new gauge bosons. In the minimal 3-3-1 model they are identified as $W'^{\pm}$, $U^{\pm\pm}$, and Z'. An important result of the spontaneous symmetry breaking is the rising of a mass mixing between the W and W' bosons that yields the mass mixing matrix:

$$\begin{pmatrix} W_\mu^+ & W_\mu'^+ \end{pmatrix}\begin{pmatrix} M_W^2 & M_{WW'}^2 \\ M_{WW'}^2 & M_{W'}^2 \end{pmatrix}\begin{pmatrix} W^{\mu-} \\ W'^{\mu-} \end{pmatrix}, \tag{8}$$

where

$$M_{WW'}^2 = \frac{g^2}{2}\left(2v_{\sigma_1}v_{\sigma_2}\right), \tag{9}$$

$g = e/s_W$, and

$$\begin{aligned} M_W^2 &= \frac{g^2}{2}\left(v_\eta^2 + v_\rho^2 + v_{\sigma_2}^2 + v_{\sigma_1}^2\right), \\ M_{W'}^2 &= \frac{g^2}{2}\left(v_\eta^2 + v_\chi^2 + v_{\sigma_2}^2 + v_{\sigma_1}^2\right). \end{aligned} \tag{10}$$

If we take $v_{\sigma_{1,2}} = 0$, then $M_{WW'}^2 = 0$, and consequently $v_\eta^2 + v_\rho^2 = v^2$, where $v = 175\,\text{GeV}$. In this way, the W mass is correctly obtained. After diagonalization we find two mass eigenstates W_1^+ and W_2^+ with

$$\begin{aligned} M_{W_{1,2}} = \frac{1}{2}\Bigg[& \left(M_W^2 + M_{W'}^2\right) \\ & \pm \left(\left(M_W^2 - M_{W'}^2\right)^2 + 4M_{WW'}^4\right)^{1/2}\Bigg], \end{aligned} \tag{11}$$

which are related to the mass eigenvectors via

$$\begin{pmatrix} W^+ \\ W'^+ \end{pmatrix} = \begin{pmatrix} c_\theta & -s_\theta \\ s_\theta & c_\theta \end{pmatrix}\begin{pmatrix} W_1^+ \\ W_2^+ \end{pmatrix}, \tag{12}$$

with

$$\tan 2\theta = \frac{-2M_{WW'}^2}{\left(M_W^2 - M_{W'}^2\right)}. \tag{13}$$

Considering the limit $M_{WW'}^2 \to 0$, we get $M_{W_1} = M_W$ and $M_{W_2} = M_{W'}$. The charged currents associated with these gauge bosons are

$$\begin{aligned} \mathscr{L}_{cc} \supset & \frac{g}{\sqrt{2}}\left[\overline{u}_L\gamma^\mu V_{CKM} d_L - \overline{\nu}_L\gamma^\mu\left(U_\nu V_\ell\right) l_L\right] W_\mu^+ \\ & + \frac{g}{\sqrt{2}}\left[\overline{l^c}_L\gamma^\mu\left(V_l U_\nu^\dagger\right)\nu_L\right] W_\mu'^+ + \text{h.c.}, \end{aligned} \tag{14}$$

where V_l and U_ν are the mixing matrices for the charged leptons and neutrinos, with $\nu_L = (\nu_{eL}, \nu_{\mu L}, \nu_{\tau L})$ and $l_L = (e_L, \mu_L, \tau_L)$. There is also a term involving the doubly charged gauge boson, but it is not relevant for our reasoning [40].

We have gathered all ingredients to now discuss the neutrinoless double beta decay in the minimal 3-3-1 model.

3. The Neutrinoless Double Beta Decay

Neutrinoless double beta decay is a landmark process in particle physics. It is defined as the transition of a nucleus into another nucleus with an atomic number larger by two units and the emission of two electrons only:

$$(A, Z) \longrightarrow (A, Z+2) + 2e^-. \tag{15}$$

Since there are no leptons in the initial state, but two in the final state, the observation of neutrinoless double beta decay constitutes an irrefutable proof that lepton number is violated by nature. In the past decades, there has been a substantial improvement on the bound over the half-life of

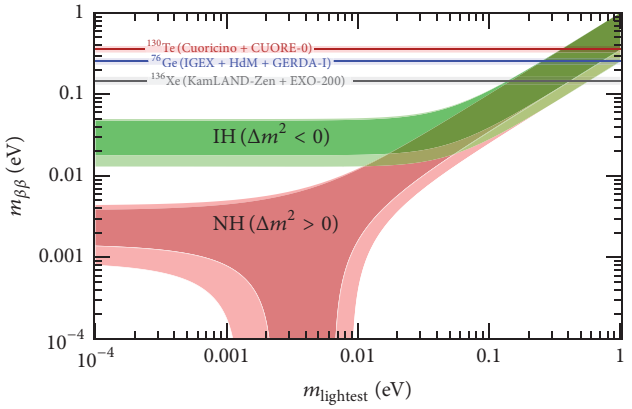

FIGURE 2: Updated prediction on $m_{\beta\beta}$ from neutrino oscillations as a function of the lightest neutrino mass according to the current neutrino data. In the figure, both normal and inverted hierarchy schemes for neutrino masses are displayed. Figure taken from [45]. In the figure is also visible the current limit from KamLAND-Zen.

the neutrinoless double beta decay [45]. These bounds can be later translated into upper limits on the effective majorana mass defined as

$$m_{\beta\beta} = \left| \sum_{i=e,\mu,\tau} U_{ei}^2 m_{\nu_i} \right|. \tag{16}$$

The effective majorana mass term grows inversely with the half-life. A stronger lower bound on the half-life of the neutrinoless double beta decay implies a stronger bound on the effective majorana mass term (see Figure 2). The strongest bound today comes from KamLAND-Zen [46], $t_{1/2} > 2.6 \times 10^{25}$ yrs, implying that

$$m_{\beta\beta}^{\text{current}} < 0.15\,\text{eV}. \tag{17}$$

In the foreseeable future, CUORE is expected to achieve $^{130}\text{Te} > 9.5 \times 10^{25}$ yrs [45] which translates into

$$m_{\beta\beta}^{\text{CUORE}} < 0.073\,\text{eV}. \tag{18}$$

A projected limit further into the future with nEXO of $t_{1/2} > 10^{27}$ yrs for ^{136}Xe is expected, which then would yield

$$m_{\beta\beta}^{\text{nEXO}} < 0.01\,\text{eV}. \tag{19}$$

Now from the current and projected experimental sensitivity we will approach the theoretical aspects of this observable. That said, the amplitude in Figure 1 is proportional to

$$A_1 \propto \frac{g^4 m_{\beta\beta}}{M_W^4 \langle p^2 \rangle} c_\theta^4 = \frac{32 G_F^2 m_{\beta\beta}}{\langle p^2 \rangle} c_\theta^4, \tag{20}$$

where $\langle p^2 \rangle$ is the average of the four-momentum transfer squared, which is approximately $(100\,\text{MeV})^2$.

Moreover, one should observe that the amplitude for the diagram in Figure 3 is proportional to

$$A_2 \propto 32 G_F^2 \left(\frac{M_W}{M_{W'}} \right)^2 \frac{c_\theta^3 s_\theta}{\sqrt{\langle p^2 \rangle}}. \tag{21}$$

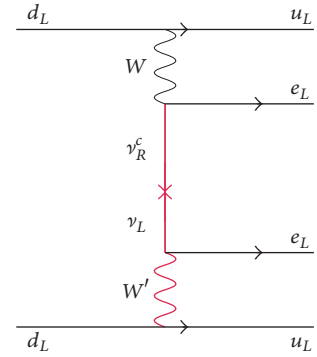

FIGURE 3: Novel 331 contribution for double beta decay due to light massive neutrinos.

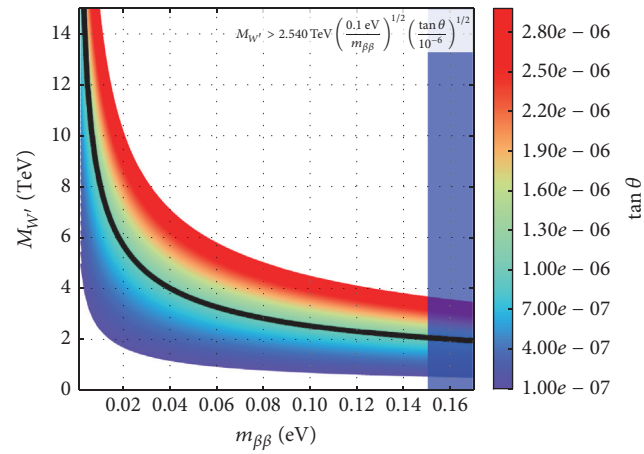

FIGURE 4: Temperature plot of the lower mass bound on the W' mass as function of $m_{\beta\beta}$ and $\tan\theta$. The black curve is drawn simply to guide the eye and check that, indeed for $\tan\theta \sim 10^{-6}$ and $m_{\beta\beta} \sim 0.1$ eV, we find the lower mass bound $M_{W'} \gtrsim 2.5$ TeV.

Bearing in mind that θ should be small in order not to alter the SM W properties, then $A_2/A_1 < 1$. This results in

$$\frac{A_2}{A_1} = \left(\frac{M_W}{M_{W'}} \right)^2 \frac{\sqrt{\langle p^2 \rangle}}{m_{\beta\beta}} \tan\theta < 1. \tag{22}$$

Therefore we get the lower mass bound:

$$M_{W'} > 2.540\,\text{TeV} \left(\frac{0.1\,\text{eV}}{m_{\beta\beta}} \right)^{1/2} \times \left(\frac{\tan\theta}{10^{-6}} \right)^{1/2}. \tag{23}$$

In Figure 4 we exhibited this lower mass bound on the W' mass. It is quite visible that even for small $\tan\theta$ the bound on W' is rather strong. It is important to make it clear that the 3-3-1M models give us other contributions beyond the one depicted in Figure 3, as pointed out by [47], but they are of much smaller intensity and therefore do not give new better results.

However, equation (23) is not very useful to us because the W' mass also appears in $\tan\theta$. Therefore, these quantities are not independent; they are strongly correlated. Bearing in

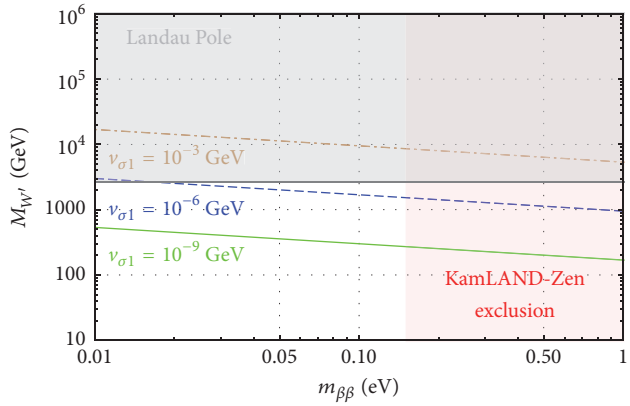

FIGURE 5: Lower mass bound on the W' mass from the nonobservation of the neutrinoless double beta decay with different choices for the vev of scalar field σ_1 which controls the parameter $M^2_{WW'}$ in (24). The gray solid area denotes Landau pole upper limit [12, 50] and light red denotes the KamLAND-Zen exclusion [46].

mind that we are working in the regimen where $\theta \ll 1$, then $\tan\theta \sim \theta$ and we can solve for $M_{W'}$ to find

$$M_{W'} > 50.4\,\text{TeV}\left(\frac{0.1\,\text{eV}}{m_{\beta\beta}}\right)^{1/4}\left(M^2_{WW'}\right)^{1/4}. \quad (24)$$

This equation can give rise to more robust bounds on the W' mass since the parameters that go into it are the majorana effective mass $m_{\beta\beta}$ and $M^2_{WW'}$ term, which depends on vevs of the scalar fields σ_1 and σ_2. Since the Standard Model W mass does not come mostly from vevs of these scalar fields as long as they are much smaller than v_{SM}, then our choices for v_{σ_1} and v_{σ_2} are in principle completely arbitrary.

To have a clear vision of what (24) represents, we show the lower mass bounds on the W' mass in Figure 5. There we select $v_{\sigma 2} = 3\,\text{GeV}$; larger values are ruled out by the ρ-parameter [39, 48] and vary $v_{\sigma 1}$. Notice that, depending on the value adopted for $v_{\sigma 1}$, neutrinoless double beta decay might yield very strong constraints on the W' mass. In particular for $m_{\beta\beta} \sim 0.1\,\text{eV}$ we get a lower mass bound on the W' mass that varies from 300 GeV to about 9.5 TeV. The latter is achieved if $v_{\sigma 1} = 10^{-3}$ GeV.

One shortcoming of our lower mass bound on the W' mass is its dependence on the choice for vevs. Anyways, these constitute an independent bound on the W' mass which can be much stronger than the limit on the W' arising from colliders searches. Notice that our W' does not couple only to ordinary quarks; therefore it cannot be produced resonantly at the LHC via s-channel processes. Nevertheless, one can use LHC limits on the Z' mass to convert into a lower mass limit on the W' mass, since both masses are dictated by the same quantity, v_χ, the scale of symmetry breaking of the 3-3-1 symmetry. Indeed one can find that $M_{W'} \sim 0.32 v_\chi$ and $M_{Z'} \sim 0.4 v_\chi$. Limits from dilepton searches at the LHC at 14 TeV with $\sim 23\,\text{fb}^{-1}$ exclude $M_{Z'} < 4\,\text{TeV}$ (see Figure 9 inside [49]). With a projection with $100\,\text{fb}^{-1}$ of data, extrapolating the luminosity effect, one would exclude $M_{Z'} < 4.7\,\text{TeV}$. These two limits translate into $M_{W'} > 3.2\,\text{TeV}$ and $M_{W'} > 3.7\,\text{TeV}$, respectively.

Therefore, we can conclude that the neutrinoless double beta decay offers a complementary probe to collider physics and, depending on choices for $v_{\sigma 1}$, it can offer the most restrictive bound on this gauge boson mass. We emphasize that the mixing angle θ is quite small since it is dictated by $M^2_{WW'}/M^2_{W'}$, rendering our conclusions robust.

4. Validity of the Minimal 3-3-1 Model

It has been shown that the 3-3-1M is valid up to energies of 5.7 TeV or so due the presence of a Landau pole [12, 50]. The collider bounds on the Z' and W' mentioned above already pose a strong tension on the model since these mass limits translate into $v_\chi \approx 10\,\text{TeV}$ and $v_\chi \approx 12\,\text{TeV}$. With the addition of new exotic fermions that can contribute to the renormalization group equations, this tension can be alleviated. As can be seen in Figure 5, for $m_{\beta\beta} \sim 0.1$ eV and $v_{\sigma 1} \sim 10^{-6}$ GeV, the lower mass bound on W' lies around 1.6 TeV, which implies that $v_\chi > 3.6$ TeV.

This would constitute a strong but valid claim, under the assumptions made. Neutrinoless double beta decay under certain assumptions already excludes the minimal 3-3-1 model, imposing that the scale of symmetry breaking of the model should lie beyond its validity (for previous bounds on this model see [51–59]).

These findings are valid for $m_{\beta\beta} \sim 0.1\,\text{eV}$, but if we consider the nEXO sensitivity which is expected to reach $m_{\beta\beta} \sim 0.01$ eV, the impact that our study brings to the minimal 3-3-1 model is even more profound. Even for $v_{\sigma 1} \sim 10^{-6}$ GeV, we would already impose $v_\chi \geq 6$ TeV.

In summary, neutrinoless double beta decay offers an orthogonal probe to the minimal 3-3-1 model. If the vevs of the fields in the scalar sextet are sufficiently small, neutrinoless double beta decay does not favor the original version of the minimal 3-3-1 model.

5. Conclusions

We discussed neutrinoless double beta decay in the context of the minimal 3-3-1 model. It features a minimal fermion content, arguably rendering it more predictive in comparison to other models based on this 3-3-1 gauge group. In the past decades, we have observed a significant improvement in the bound of the neutrinoless double beta decay. We exploit this fact to obtain a lower mass bound on the W' boson that arises due to the enlarged gauge group. Our limits are based mostly on the charged current and the vev of a scalar field that generates neutrino masses and induces the $W - W'$ mixing. This mixing leads to a sizable contribution to neutrinoless double beta decay.

We obtained a fully analytic expression that represents a lower mass bound on the W' mass. Depending on the vev adopted for this scalar field (σ_1), neutrinoless double beta decay might offer the most restrictive limit on the W' surpassing those of collider probes. Moreover, since the W' mass is directly connected to the scale of symmetry breaking

of the model, a lower mass bound on the gauge boson represents also a lower bound on the scale of symmetry breaking. In particular, if $v_{\sigma 1} > 0.1$ GeV, current limits on the half-life of the neutrinoless double beta decay strongly disfavored out the minimal 3-3-1 model.

Conflicts of Interest

The authors declare that there are no conflicts of interest regarding the publication of this paper.

Acknowledgments

This work was supported by Coordenação de Aperfeiçoamento de Pessoal de Nível Superior (Capes-PDSE-88881.135139/2016-01). The authors are also grateful to Farinaldo Queiroz and Diego Cogollo for discussions and suggestions.

References

[1] C. Patrignani et al., "Review of Particle Physics," *Chinese Physics C*, vol. 40, no. 10, Article ID 100001, 2016.

[2] W. Rodejohann, "Neutrino-less double beta decay and particle physics," *International Journal of Modern Physics E*, vol. 20, no. 9, pp. 1833–1930, 2011.

[3] H. Päs and W. Rodejohann, "Neutrinoless double beta decay," *New Journal of Physics* , vol. 17, no. 11, Article ID 115010, 2015.

[4] M. Singer, J. W. F. Valle, and J. Schechter, "Canonical neutral-current predictions from the weak-electromagnetic gauge group SU(3) × U(1)," *Physical Review D: Particles, Fields, Gravitation and Cosmology*, vol. 22, no. 3, pp. 738–743, 1980.

[5] F. Pisano and V. Pleitez, "SU(3) ⊗ U(1) model for electroweak interactions," *Physical Review D: Particles, Fields, Gravitation and Cosmology*, vol. 46, no. 1, pp. 410–417, 1992.

[6] R. Foot, O. F. Hernández, F. Pisano, and V. Pleitez, "Lepton masses in an $SU(3)_L$ x $U(1)_N$ gauge model," *Physical Review D: Particles, Fields, Gravitation and Cosmology*, vol. 47, no. 9, pp. 4158–4161, 1993.

[7] P. Frampton, "Chiral dilepton model and the flavor question," *Physical Review Letters*, vol. 69, no. 20, pp. 2889–2891, 1992.

[8] R. Foot, H. N. Long, and T. A. Tran, "*SU(3)L⊗U(1)N* and *SU(4)L⊗U(1)N* gauge models with right-handed neutrinos," *Physical Review D: Particles, Fields, Gravitation and Cosmology*, vol. 50, no. 1, pp. R34–R38, 1994.

[9] H. N. Long, "The 331 model with right handed neutrinos," *Physical Review D: Particles, Fields, Gravitation and Cosmology*, vol. 53, pp. 437–445, 1996, https://arxiv.org/abs/hep-ph/9504274.

[10] A. Alves, E. Ramirez Barreto, A. G. Dias, C. A. de S. Pires, F. S. Queiroz, and P. S. Rodrigues da Silva, "Explaining the Higgs decays at the LHC with an extended electroweak model," *The European Physical Journal C*, vol. 73, no. 2, article no. 2288, pp. 1–9, 2013.

[11] W. Caetano, C. A. de S. Pires, P. S. Rodrigues da Silva, D. Cogollo, and F. S. Queiroz, "Explaining ATLAS and CMS results within the reduced minimal 3-3-1 model," *The European Physical Journal C*, vol. 73, no. 10, article no. 2607, pp. 1–10, 2013.

[12] A. G. Dias, R. Martinez, and V. Pleitez, "Concerning the Landau pole in 3-3-1 models," *The European Physical Journal C*, vol. 39, no. 1, pp. 101–107, 2005.

[13] A. G. Dias, "Evading the few TeV perturbative limit in 3-3-1 models," *Physical Review D: Particles, Fields, Gravitation and Cosmology*, vol. 71, no. 1, Article ID 015009, 2005.

[14] C. A. de S. Pires, F. Queiroz, and P. S. Rodrigues da Silva, "A minimal 3-3-1 model with naturally sub-eV neutrinos," *Physical Review D: Particles, Fields, Gravitation and Cosmology*, vol. 82, no. 6, Article ID 065018, 2010, https://arxiv.org/abs/1003.1270v2.

[15] W. Caetano, D. Cogollo, C. A. D. S. Pires, and P. S. R. Da Silva, "Combining type I and type II seesaw mechanisms in the minimal 3-3-1 model," *Physical Review D: Particles, Fields, Gravitation and Cosmology*, vol. 86, no. 5, Article ID 055021, 2012.

[16] D. Cogollo, H. Diniz, and C. A. de S. Pires, "keV right-handed neutrinos from type II seesaw mechanism in a 3-3-1 model," *Physics Letters B*, vol. 677, no. 5, pp. 338–342, 2009.

[17] S. Profumo and F. S. Queiroz, "Constraining the Z' mass in 331 models using direct dark matter detection," *The European Physical Journal C*, vol. 74, no. 7, article no. 2960, pp. 1–12, 2014.

[18] A. Alves, G. Arcadi, P. V. Dong, L. Duarte, F. S. Queiroz, and J. W. F. Valle, "R-parity as a residual gauge symmetry: probing a theory of cosmological dark matter," *Physics Letters B*, vol. 772, pp. 825–831, 2017.

[19] D. Cogollo, F. S. Queiroz, and P. Vasconcelos, "Flavor changing neutral current processes in a reduced minimal scalar sector," *Modern Physics Letters A*, vol. 29, no. 32, Article ID 1450173, 2014.

[20] F. S. Queiroz, C. Siqueira, and J. W. F. Valle, "Constraining flavor changing interactions from LHC Run-2 dilepton bounds with vector mediators," *Physics Letters B*, vol. 763, pp. 269–274, 2016.

[21] A. Alves, S. Profumo, F. S. Queiroz, and W. Shepherd, "Effective field theory approach to the Galactic Center gamma-ray excess," *Physical Review D: Particles, Fields, Gravitation and Cosmology*, vol. 90, no. 11, Article ID 115003, 2014.

[22] M. D. Campos, F. S. Queiroz, C. E. Yaguna, and C. Weniger, "Search for right-handed neutrinos from dark matter annihilation with gamma-rays," *Journal of Cosmology and Astroparticle Physics*, vol. 2017, no. 7, article no. 016, 2017.

[23] A. Alves, A. Berlin, S. Profumo, and F. S. Queiroz, "Dirac-fermionic dark matter in $U(1)_X$ models," *Journal of High Energy Physics*, vol. 2015, article 76, pp. 1–33, 2015.

[24] A. Alves, A. Berlin, S. Profumo, and F. S. Queiroz, "Dark Matter Complementarity and the Z' Portal," *Physical Review D*, vol. 92, no. 8, Article ID 083004, 2015.

[25] A. Doff and C. Siqueira, "Composite Higgs models, Technicolor and the muon anomalous magnetic moment," *Physics Letters B*, vol. 754, pp. 294–301, 2016.

[26] J. G. Ferreira, C. A. de S. Pires, J. G. Rodrigues, and P. S. Rodrigues da Silva, "Embedding cosmological inflation, axion dark matter and seesaw mechanism in a 3-3-1 gauge model," *Physics Letters B*, vol. 771, pp. 199–205, 2017.

[27] O. Rodríguez, R. H. Benavides, W. A. Ponce, and E. Rojas, "Flipped versions of the universal 3-3-1 and the left-right symmetric models in [SU (3)] 3: A comprehensive approach," *Physical Review D: Particles, Fields, Gravitation and Cosmology*, vol. 95, no. 1, Article ID 014009, 2017.

[28] C. A. de S. Pires, P. S. R. Da Silva, A. C. O. Santos, and C. Siqueira, "Higgs mass and right-handed sneutrino WIMP in a supersymmetric 3-3-1 model," *Physical Review D: Particles, Fields, Gravitation and Cosmology*, vol. 94, no. 5, Article ID 055014, 2016.

[29] J. S. Borges and R. O. Ramos, "Symmetry breaking patterns of the 3-3-1 model at finite temperature," *The European Physical Journal C*, vol. 76, no. 6, 2016.

[30] P. V. Dong, D. Q. Phong, D. V. Soa, and N. C. Thao, The economical 3-3-1 model revisited,.

[31] J. G. Ferreira, C. A. de S. Pires, P. S. Rodrigues da Silva, and C. Siqueira, "On the Higgs-like boson in the minimal supersymmetric 3-3-1 model," *The European Physical Journal C*, vol. 78, no. 225, 2018.

[32] J. C. Montero, C. A. de S. Pires, and V. Pleitez, "Neutrino masses through the seesaw mechanism in 3-3-1 models," *Physical Review D: Particles, Fields, Gravitation and Cosmology*, vol. 65, no. 9, Article ID 095001, 2002.

[33] J. C. Montero, C. A. de S. Pires, and V. Pleitez, "Lepton masses from a TeV scale in a 3-3-1 model," *Physical Review D: Particles, Fields, Gravitation and Cosmology*, vol. 66, no. 11, Article ID 113003, 2002.

[34] R. N. Mohapatra, A. Pérez-Lorenzana, and C. A. de Sousa Pires, "Type II seesaw and a gauge model for the bimaximal mixing explanation of neutrino puzzles," *Physics Letters B*, vol. 474, no. 3-4, pp. 355–360, 2000.

[35] P. Gu, H. Zhang, and S. Zhou, "Minimal type II seesaw model," *Physical Review D: Particles, Fields, Gravitation and Cosmology*, vol. 74, no. 7, Article ID 076002, 2006.

[36] E. K. Akhmedov and M. Frigerio, "Interplay of type I and type II seesaw contributions to neutrino mass," *Journal of High Energy Physics*, vol. 2007, no. 01, 2007.

[37] M. Reig, J. W. F. Valle, and C. A. Vaquera-Araujo, "Realistic $SU(3)_c \otimes SU(3)_L \otimes U(1)_X$ model with a type II Dirac neutrino seesaw mechanism," *Physical Review D: Particles, Fields, Gravitation and Cosmology*, vol. 94, no. 3, Article ID 033012, 2016.

[38] J. C. Montero, C. A. de S. Pires, and V. Pleitez, "Spontaneous breaking of a global symmetry in a 3-3-1 model," *Physical Review D: Particles, Fields, Gravitation and Cosmology*, vol. 60, Article ID 115003, 1999.

[39] J. C. Montero, C. A. de Sousa Pires, and V. Pleitez, "Comment on 'Majoron emitting neutrinoless double beta decay in the electroweak chiral gauge extensions'," *Physical Review D: Particles, Fields, Gravitation and Cosmology*, vol. 60, no. 9, Article ID 098701, 1999.

[40] J. C. Montero, C. A. de Sousa Pires, and V. Pleitez, "Neutrinoless double beta decay with and without Majoron-like boson emission in a 3-3-1 model," *Physical Review D: Particles, Fields, Gravitation and Cosmology*, vol. 64, no. 9, Article ID 096001, 2001.

[41] J. C. Montero, C. A. de S. Pires, and V. Pleitez, "Seesaw tau lepton mass and calculable neutrino masses in a 3-3-1 model," *Physical Review D: Particles, Fields, Gravitation and Cosmology*, vol. 65, no. 9, Article ID 093017, 2002.

[42] P. V. Dong and D. T. Si, "Discriminating the minimal 3-3-1 models," *Physical Review D: Particles, Fields, Gravitation and Cosmology*, vol. 90, no. 11, Article ID 117703, 2014.

[43] F. S. Queiroz, K. Sinha, and A. Strumia, "Leptoquarks, dark matter, and anomalous LHC events," *Physical Review D: Particles, Fields, Gravitation and Cosmology*, vol. 91, no. 3, Article ID 035006, 2015.

[44] B. Allanach, A. Alves, F. S. Queiroz, K. Sinha, and A. Strumia, "Interpreting the CMS $\ell^+\ell^- jj$+ missing transverse energy excess with a leptoquark model," *Physical Review D: Particles, Fields, Gravitation and Cosmology*, vol. 92, no. 5, Article ID 055023, 2015.

[45] S. Dell'Oro, S. Marcocci, M. Viel, and F. Vissani, "Neutrinoless double beta decay: 2015 review," *Advances in High Energy Physics*, vol. 2016, Article ID 2162659, 37 pages, 2016.

[46] K. Asakura et al., "Results from KamLAND-Zen," Article ID 170003, 1666, 2015, AIP Conf. Proc.

[47] D. V. Soa, P. V. Dong, T. T. Huong, and H. N. Long, "Bilepton contributions to the neutrinoless double beta decay in the economical 3-3-1 model," *Journal of Experimental and Theoretical Physics*, vol. 108, no. 5, pp. 757–763, 2009.

[48] S. Shelly Sharma, "Reply to "Comment on 'Majoron emitting neutrinoless double beta decay in the electroweak chiral gauge extensions' "," *Physical Review D: Particles, Fields, Gravitation and Cosmology*, vol. 60, no. 9, Article ID 098702, 1999.

[49] Y. A. Coutinho, V. S. Guimarães, and A. A. Nepomuceno, "Bounds on Z′ from 3-3-1 model at the LHC energies," *Physical Review D: Particles, Fields, Gravitation and Cosmology*, vol. 87, no. 11, Article ID 115014, 2013.

[50] R. Martínez and F. Ochoa, "The Landau pole and Ź decays in the 331 dilepton model," *The European Physical Journal C*, vol. 51, no. 3, pp. 701–711, 2007.

[51] R. A. Diaz, R. Martínez, and F. Ochoa, "Scalar sector of the $SU(3)_c \otimes SU(3)_L \otimes U(1)_X$ model," *Physical Review D: Particles, Fields, Gravitation and Cosmology*, vol. 69, no. 9, Article ID 095009, 2004.

[52] R. A. Diaz, R. Martinez, and F. Ochoa, "$SU(3)_c \otimes SU(3)_L \otimes U(1)_X$ models for β arbitrary and families with mirror fermions," *Physical Review D: Particles, Fields, Gravitation and Cosmology*, vol. 72, no. 3, Article ID 035018, 2005.

[53] G. A. Gonzalez-Sprinberg, R. Martinez, and O. Sampayo, "Bilepton and exotic quark mass limits in 331 models from Z > b anti-b decay," *Physical Review D: Particles, Fields, Gravitation and Cosmology*, vol. 71, Article ID 115003, 2005.

[54] F. Ochoa and R. Martínez, "Family dependence in $SU(3)_c \otimes SU(3)_L \otimes U(1)_X$ models," *Physical Review D: Particles, Fields, Gravitation and Cosmology*, vol. 72, no. 3, Article ID 035010, 2005.

[55] A. E. Carcamo Hernandez, R. Martínez, and F. Ochoa, "Z and Z' decays with and without FCNC in 331 models," *Physical Review D: Particles, Fields, Gravitation and Cosmology*, vol. 73, no. 3, Article ID 035007, 2006.

[56] A. G. Dias, A. Doff, C. A. De S. Pires, and P. S. Rodrigues Da Silva, "Neutrino decay and neutrinoless double beta decay in a 3-3-1 model," *Physical Review D: Particles, Fields, Gravitation and Cosmology*, vol. 72, no. 3, Article ID 035006, pp. 1–8, 2005.

[57] J. M. Cabarcas, D. Gómez Dumm, and R. Martinez, "Phenomenological aspects of the exotic T quark in 331 models," *The European Physical Journal C*, vol. 58, no. 4, pp. 569–578, 2008.

[58] R. Martinez and F. Ochoa, "Heavy quark signals from radiative corrections to the Z-prime boson decay in 3-3-1 models," *Physical Review D: Particles, Fields, Gravitation and Cosmology*, vol. 80, Article ID 075020, 2009.

[59] J. M. Cabarcas, D. G. Dumm, and R. Martinez, "Flavor-changing neutral currents in 331 models," *Journal of Physics G: Nuclear and Particle Physics*, vol. 37, no. 4, Article ID 045001, 2010.

Hindawi
Advances in High Energy Physics
Volume 2018, Article ID 5806743, 16 pages
https://doi.org/10.1155/2018/5806743

Research Article

Investigating the Hybrid Textures of Neutrino Mass Matrix for Near Maximal Atmospheric Neutrino Mixing

Madan Singh

Department of Physics, National Institute of Technology, Kurukshetra, Haryana 136119, India

Correspondence should be addressed to Madan Singh; singhmadan179@gmail.com

Received 22 December 2017; Accepted 5 April 2018; Published 14 May 2018

Academic Editor: Jose W. F. Valle

We have studied that the implication of a large value of the effective Majorana neutrino mass in case of neutrino mass matrices has either two equal elements and one zero element (popularly known as hybrid texture) or two equal cofactors and one zero minor (popularly known as inverse hybrid texture) in the flavor basis. In each of these cases, four out of sixty phenomenologically possible patterns predict near maximal atmospheric neutrino mixing angle in the limit of large effective Majorana neutrino mass. This feature remains irrespective of the experimental data on solar and reactor mixing angles. In addition, we have also performed the comparative study of all the viable cases of hybrid and inverse hybrid textures at 3σ CL.

1. Introduction

In leptonic sector, the reactor mixing angle (θ_{13}) has been established to a reasonably good degree of precision [1–6], and its nonzero and relatively large value has not only provided an opportunity in exploring CP violation and the neutrino mass ordering in the future experiments but has also highlighted the puzzle of neutrino mass and mixing pattern. In spite of the significant developments made over the years, there are still several intriguing questions in the neutrino sector which remain unsettled. For instance, the present available data is unable to throw any light on the neutrino mass spectrum, which may be normal/inverted and may even be degenerate. Another important issue is the determination of octant of atmospheric mixing angle θ_{23}, which may be greater than or less than or equal to 45^0. The determination of the nature of neutrinos whether Dirac or Majorana also remains an open question. The observation of neutrinoless double beta ($0\nu\beta\beta$) decay would eventually establish the Majorana nature of neutrinos.

The effective Majorana mass term related to $0\nu\beta\beta$ decay can be expressed as

$$|M|_{ee} = \left|m_1 c_{12}^2 c_{13}^2 e^{2i\rho} + m_2 s_{12}^2 c_{13}^2 e^{2i\sigma} + m_3 s_{13}^2\right|. \quad (1)$$

Data from KamLAND-Zen experiment has presented an improved search for neutrinoless double-beta ($0\nu\beta\beta$) decay [7] and it is found that $|M|_{ee} < (0.061–0.165)$ eV at 90% (or $<2\sigma$) CL. For recent reviews on $0\nu\beta\beta$ decay see [8–13].

In the lack of any convincing theory, several phenomenological ideas have been proposed in the literature so as to restrict the form of neutrino mass matrix, such as some elements of neutrino mass matrix that are considered to be zero or equal [14–21] or some cofactors of neutrino mass matrix to be either zero or equal [19, 22–27]. Specifically, mass matrices with zero textures (or cofactors) have been extensively studied [14–18, 22–24] due to their connections to flavor symmetries. In addition, texture structures with one zero element (or minor) and an equality between two independent elements (or cofactors) in neutrino mass matrix have also been studied in the literature [20, 21, 26, 27]. Such form of texture structures sets to one constraint equation and thus reduces the number of real free parameters of neutrino mass matrix to seven. Hence they are considered as predictive as the well-known two-zero textures and can also be realised within the framework of seesaw mechanism. Out of sixty possibilities, only fifty-four are found to be compatible with the neutrino oscillation data [21] for texture structures having one zero element and equal matrix elements in the

neutrino mass matrix (1TEE), while for texture with one vanishing minor and equal cofactors in the neutrino mass matrix (1TEC) only fifty-two cases are able to survive the data [26, 27].

The purpose of present paper is to investigate the implication of large effective neutrino mass $|M|_{ee}$ on 1TEE and 1TEC structures of neutrino mass matrix, while taking into account the assumptions of [28, 29]. The consideration of large $|M|_{ee}$ is motivated by the extensive search for this parameter in the ongoing $0\nu\beta\beta$ experiments. The implication of large $|M|_{ee}$ has earlier been studied for the viable cases of texture two-zero and two-vanishing minor, respectively [28, 29]. Grimus et al. [30] also predicted the near maximal atmospheric mixing for two-zero textures when supplemented with the assumption of quasi-degenerate mass spectrum. However, the observation made in all these analyses is independent of solar and reactor mixing angles. Motivated by these works, we find that only four out of sixty cases are able to predict near maximal θ_{23} for 1TEE and 1TEC, respectively. In addition, the analysis also hints towards the indistinguishable feature of 1TEE and 1TEC. To present the indistinguishable nature of the 1TEE and 1TEC texture structures, we have then carried out a comparative study of all the viable cases of 1TEE and 1TEC at 3σ CL. The similarity between texture zero structures with one mass ordering and corresponding cofactor zero structures with the opposite mass ordering has earlier been noted in [31–33]. In [19], the strong similarities have also been noted between the texture structures with two equalities of elements and structures with two equalities of cofactors in neutrino mass matrix, with opposite mass ordering.

The rest of the paper is planned in the following manner. In Section 2, we shall discuss the methodology to obtain the constraint equations. Section 3 is devoted to numerical analysis. In the end we will summarize our result.

2. Methodology

The effective Majorana neutrino mass matrix (M_ν) contains nine parameters which include three neutrino masses (m_1, m_2, m_3), three mixing angles (θ_{12}, θ_{23}, θ_{13}), and three CP violating phases (δ, ρ, σ). In the flavor basis, the Majorana neutrino mass matrix can be expressed as follows:

$$M_\nu = P_l U P_\nu M^{\mathrm{diag}} P_\nu^T U^T P_l^T, \tag{2}$$

where $M^{\mathrm{diag}} = \mathrm{diag}(m_1, m_2, m_3)$ is the diagonal matrix of neutrino masses and U is the flavor mixing matrix, and

$$P_\nu = \begin{pmatrix} e^{i\rho} & 0 & 0 \\ 0 & e^{i\sigma} & 0 \\ 0 & 0 & 1 \end{pmatrix}, \qquad P_l = \begin{pmatrix} e^{i\phi_e} & 0 & 0 \\ 0 & e^{i\phi_\mu} & 0 \\ 0 & 0 & e^{i\phi_\tau} \end{pmatrix}, \tag{3}$$

where P_ν is diagonal phase matrix containing Majorana neutrinos ρ, σ. P_l is unobservable phase matrix and depends on phase convention. Equation (2) can be rewritten as

$$M_\nu = P_l U \begin{pmatrix} \lambda_1 & 0 & 0 \\ 0 & \lambda_2 & 0 \\ 0 & 0 & \lambda_3 \end{pmatrix} U^T P_l^T, \tag{4}$$

where $\lambda_1 = m_1 e^{2i\rho}$, $\lambda_2 = m_2 e^{2i\sigma}$, $\lambda_3 = m_3$. For the present analysis, we consider the following parameterization of U [20]:

$$U = \begin{pmatrix} c_{12}c_{13} & s_{12}c_{13} & s_{13} \\ -c_{12}s_{23}s_{13} - s_{12}c_{23}e^{-i\delta} & -s_{12}s_{23}s_{13} + c_{12}c_{23}e^{-i\delta} & s_{23}c_{13} \\ -c_{12}c_{23}s_{13} + s_{12}s_{23}e^{-i\delta} & -s_{12}c_{23}s_{13} - c_{12}s_{23}e^{-i\delta} & c_{23}c_{13} \end{pmatrix}, \tag{5}$$

where $c_{ij} = \cos\theta_{ij}$, $s_{ij} = \sin\theta_{ij}$. Here, U is a 3×3 unitary matrix consisting of three flavor mixing angles ($\theta_{12}, \theta_{23}, \theta_{13}$) and one Dirac CP-violating phase δ.

For hybrid texture structure (1TEE) of M_ν, we can express the ratios of neutrino mass eigenvalues in terms of the mixing matrix elements as [21]

$$\frac{\lambda_1}{\lambda_3} = \frac{P\left(U_{a3}U_{b3}U_{\alpha2}U_{\beta2} - U_{a2}U_{b2}U_{\alpha3}U_{\beta3}\right) + \left(U_{a2}U_{b2}U_{c3}U_{d3} - U_{a3}U_{b3}U_{c2}U_{d2}\right)}{P\left(U_{a2}U_{b2}U_{\alpha1}U_{\beta1} - U_{a1}U_{b1}U_{\alpha2}U_{\beta2}\right) + \left(U_{a1}U_{b1}U_{c2}U_{d2} - U_{a2}U_{b2}U_{c1}U_{d1}\right)},$$
$$\frac{\lambda_2}{\lambda_3} = \frac{P\left(U_{a1}U_{b1}U_{\alpha3}U_{\beta3} - U_{a3}U_{b3}U_{\alpha1}U_{\beta1}\right) + \left(U_{a3}U_{b3}U_{c1}U_{d1} - U_{a1}U_{b1}U_{c3}U_{d3}\right)}{P\left(U_{a2}U_{b2}U_{\alpha1}U_{\beta1} - U_{a1}U_{b1}U_{\alpha2}U_{\beta2}\right) + \left(U_{a1}U_{b1}U_{c2}U_{d2} - U_{a2}U_{b2}U_{c1}U_{d1}\right)}, \tag{6}$$

where $P = e^{i(\phi_\alpha + \phi_\beta - \phi_c - \phi_d)}$ is a phase factor. Similarly, in case of inverse hybrid texture structure (1TEC) of M_ν, we can express the ratios of mass eigenvalues as [26, 27] follows:

$$\frac{\lambda_1}{\lambda_3} = \frac{A_1B_2 - A_2B_1}{A_2B_3 - A_3B_2},$$
$$\frac{\lambda_2}{\lambda_3} = \frac{A_1B_2 - A_2B_1}{A_3B_1 - A_1B_3}, \tag{7}$$

where

$$A_i = \left(U_{pj}U_{qj}U_{rk}U_{sk} - U_{tj}U_{uj}U_{vk}U_{wk}\right) + \left(j \longleftrightarrow k\right),$$

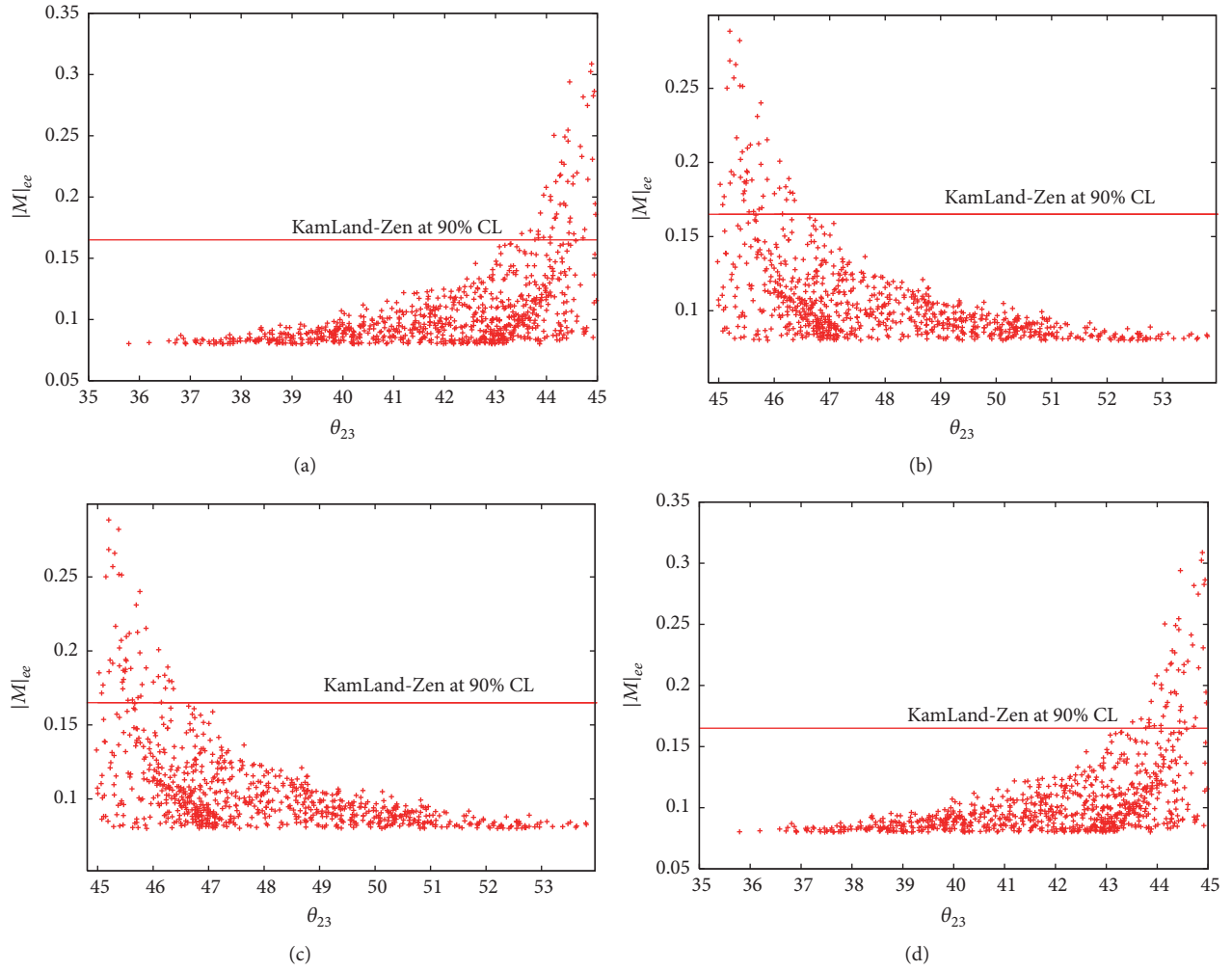

FIGURE 1: Correlation plots for textures B_2 ((a) NO and (b) IO) and C_7 for ((c) NO and (d) IO) at 3σ CL for 1TEE. The symbols have their usual meaning. The horizontal line indicates the upper limit on effective neutrino mass term $|M|_{ee}$ (i.e., $|M|_{ee} < 0.165$ eV) at 90% CL, given in KamLAND-Zen experiment [7].

$$\begin{aligned} B_i = {} & (-1)^{m+n} Q \left(U_{aj}U_{bj}U_{ck}U_{dk} - U_{ej}U_{fj}U_{gk}U_{hk}\right) \\ & - (-1)^{m'+n'} \left(U_{a'j}U_{b'j}U_{c'k}U_{d'k} - U_{e'j}U_{f'j}U_{g'k}U_{h'k}\right) \\ & + \left(j \longleftrightarrow k\right), \end{aligned} \tag{8}$$

with (i, j, k) a cyclic permutation of (1, 2, 3) and $Q = e^{i(\phi_a+\phi_b+\phi_c+\phi_d-\phi_{a'}-\phi_{b'}-\phi_{c'}-\phi_{d'})}$ is phase factor.

Using the above expressions, we can obtain the magnitude of neutrino mass ratios, $\alpha \equiv |\lambda_1|/|\lambda_3|$ and $\beta \equiv |\lambda_2|/|\lambda_3|$ in each texture structure, and the Majorana phases (ρ, σ) can be given as $\rho = (1/2)\arg(\lambda_1/\lambda_3)$ and $\sigma = (1/2)\arg(\lambda_2/\lambda_3)$.

The solar and atmospheric mass squared differences $(\delta m^2, \Delta m^2)$, where δm^2 corresponds to solar mass-squared difference and Δm^2 corresponds to atmospheric mass-squared difference, can be defined as [20]

$$\delta m^2 = \left(m_2^2 - m_1^2\right),$$

$$\Delta m^2 = m_3^2 - \frac{1}{2}\left(m_1^2 + m_2^2\right). \tag{9}$$

The experimentally determined solar and atmospheric neutrino mass-squared differences can be related to neutrino mass ratios (α, β) as

$$R_\nu \equiv \frac{\delta m^2}{|\Delta m^2|} = \frac{2\left(\beta^2 - \alpha^2\right)}{|2 - (\beta^2 + \alpha^2)|}, \tag{10}$$

and the three neutrino masses can be determined in terms of α, β as

$$\begin{aligned} m_3 &= \sqrt{\frac{\delta m^2}{\beta^2 - \alpha^2}}, \\ m_2 &= m_3\beta, \\ m_1 &= m_3\alpha. \end{aligned} \tag{11}$$

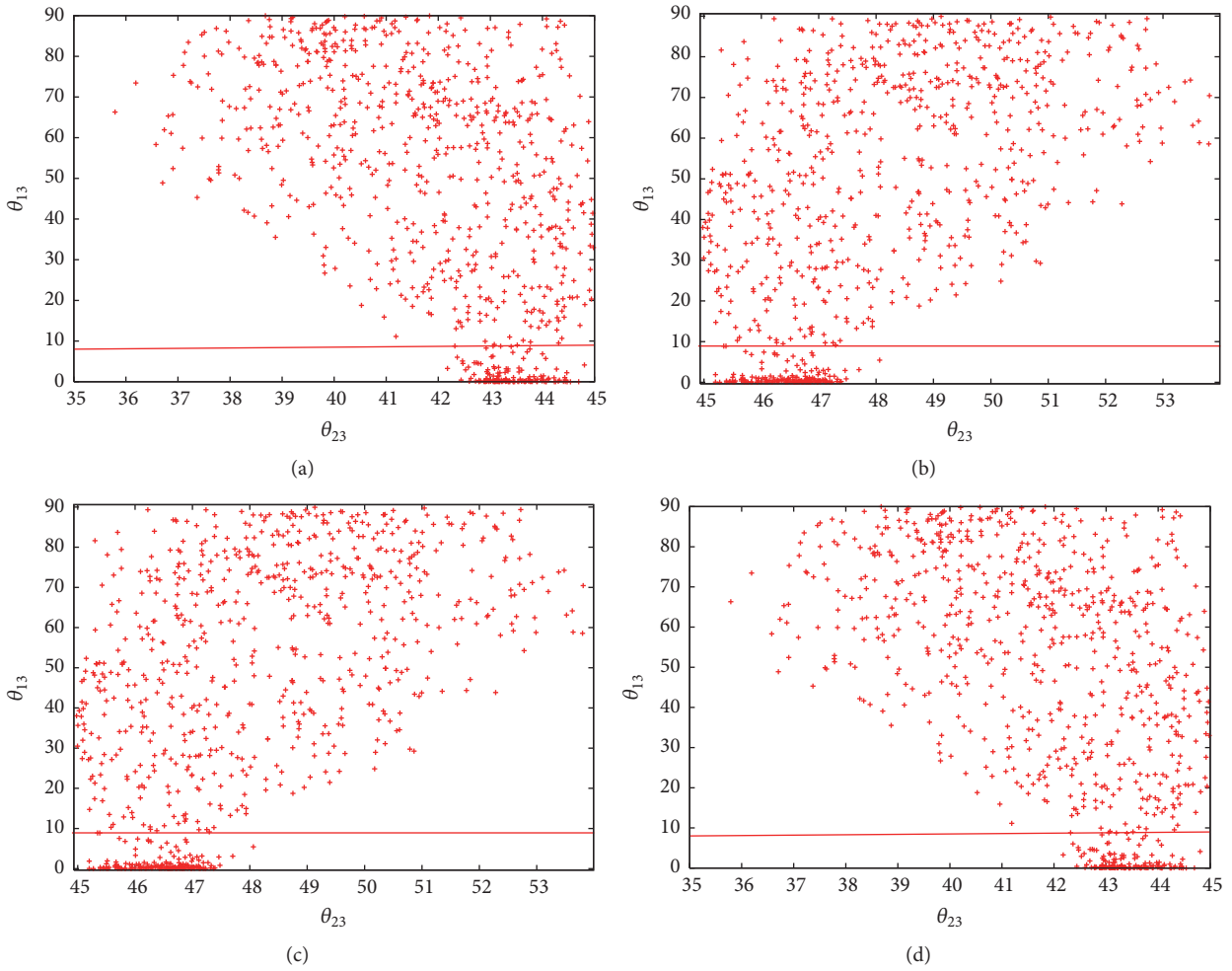

FIGURE 2: Correlation plots for textures B_2 ((a) NO and (b) IO) and C_7 for ((c) NO and (d) IO) at 3σ CL for 1TEE. The symbols have their usual meaning. The horizontal line indicates the upper limit on reactor mixing angle $\theta_{13} < 8.9^0$, as given in Table 1.

Among the sixty logically possible cases of 1TEE or 1TEC texture structures, there are certain pair, which exhibit similar phenomenological implications and are related via permutation symmetry [21, 26, 27]. This corresponds to permutation of the 2-3 rows and 2-3 columns of M_ν. The corresponding permutation matrix can be given by

$$P_{23} = \begin{pmatrix} 1 & 0 & 0 \\ 0 & 0 & 1 \\ 0 & 1 & 0 \end{pmatrix}. \tag{12}$$

With the help of permutation symmetry, one obtains the following relations among the neutrino oscillation parameters:

$$\begin{aligned} \theta_{12}^X &= \theta_{12}^Y, \\ \theta_{23}^X &= 90^\circ - \theta_{23}^Y, \\ \theta_{13}^X &= \theta_{13}^Y, \\ \delta^X &= \delta^Y - 180^\circ, \end{aligned} \tag{13}$$

where X and Y denote the cases related to 2-3 permutation. The following pair among sixty cases are related via permutation symmetry:

(A_1, A_1); (A_2, A_8); (A_3, A_7); (A_4, A_6); (A_5, A_5); (A_9, A_{10}); (B_1, C_1)

(B_2, C_7); (B_3, C_6); (B_4, C_5); (B_5, C_4); (B_6, C_3) (B_7, C_2); (B_8, C_{10})

(B_9, C_9); (B_{10}, C_8); (D_1, F_2); (D_2, F_1); (D_3, F_4); (D_4, F_3)

(D_5, F_5); (D_6, F_9); (D_7, F_8); (D_8, F_7); (D_9, F_6); (D_{10}, F_{10})

(E_1, E_2); (E_3, E_4); (E_5, E_5); (E_6, E_9); (E_7, E_8); (E_{10}, E_{10}).

Clearly we are left with only thirty-two independent cases. It is worthwhile to mention that cases A_1, A_5, E_5, and E_{10} are invariant under the permutations of 2 and 3 rows and columns.

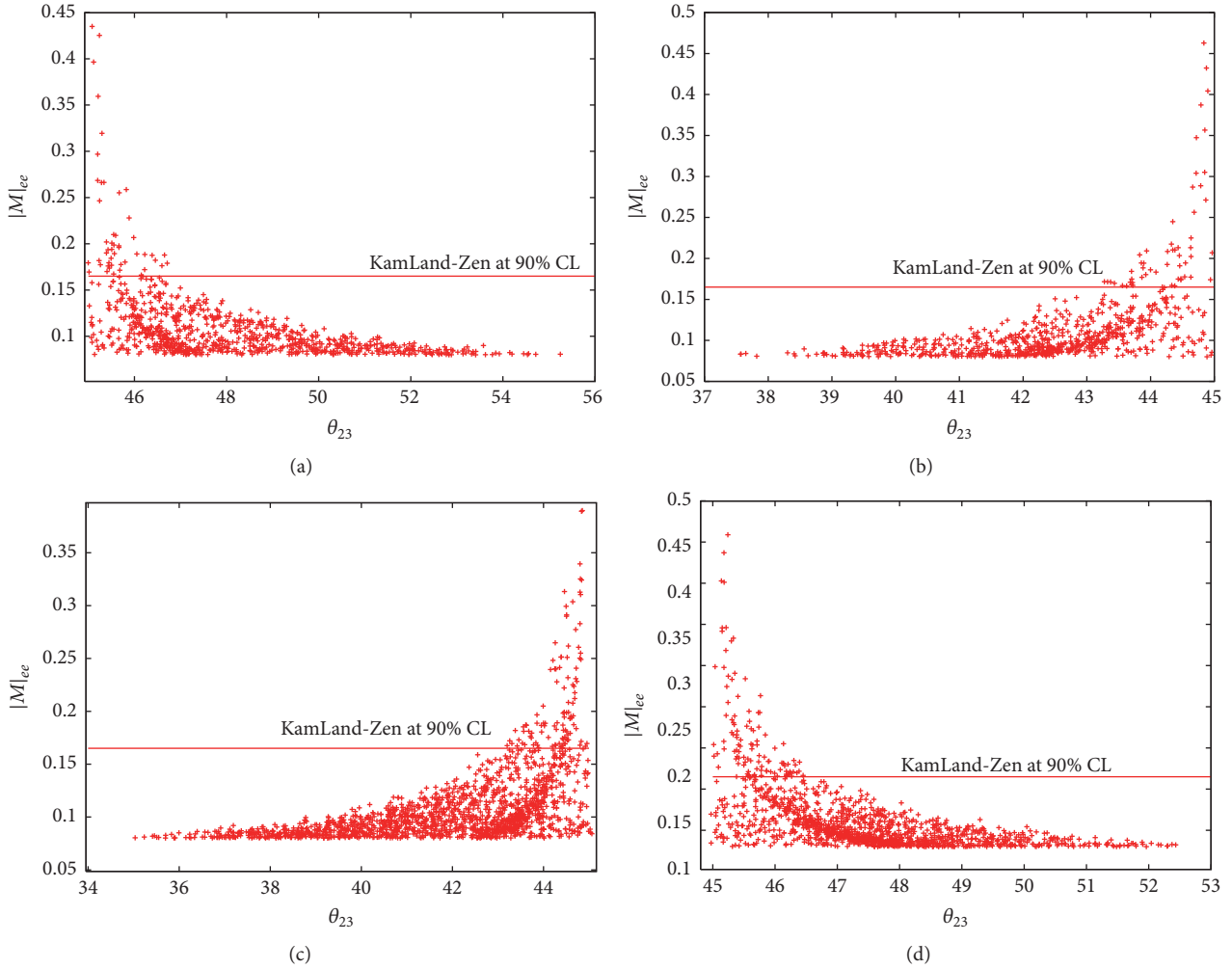

FIGURE 3: Correlation plots for textures B_2 ((a) NO and (b) IO) and C_7 for ((c) NO and (d) IO) at 3σ CL for 1TEC. The symbols have their usual meaning. The horizontal line indicates the upper limit on effective neutrino mass term $|M|_{ee}$ (i.e., $|M|_{ee} < 0.165$ eV) at 90% ($<2\sigma$)CL, given in KamLAND-Zen experiment [7].

3. Numerical Analysis

The experimental constraints on neutrino parameters at 3σ confidence levels (CL) are given in Table 1. The classification of sixty phenomenologically possible cases of 1TEE and 1TEC is done in the nomenclature, given by Wang et al. in [26, 27]. All the sixty cases are divided into six categories A, B, C, D, and E (Table 2). In [26, 27], it is found that the phenomenological results of cases belonging to 1TEC (or 1TEE) are almost similar to each other due to permutation symmetry. For the purpose of calculation, we have used the latest experimental data on neutrino mixing angles $(\theta_{12}, \theta_{23}, \theta_{13}, \delta m^2)$ and mass squared differences $(\Delta m^2, \delta)$ at 3σ CL [5, 6].

3.1. Near Maximal Atmospheric Mixing for 1TEE and 1TEC Texture Structures. As a first step of the analysis, all the sixty cases of 1TEE and 1TEC have been investigated in the limit of large $|M|_{ee}$. For the analysis, we have incorporated the assumptions of [28, 29], wherein authors have considered the lower bound on $|M|_{ee}$ to be large (i.e., $|M|_{ee} > 0.08$ eV). The upper bound on $|M|_{ee}$ is chosen to be more conservative; that is, $|M|_{ee} < 0.5$ eV at 3σ CL [10]. The input parameters $(\theta_{12}, \theta_{23}, \theta_{13}, \delta m^2, \Delta m^2, \delta)$ are generated by the method of random number generation. The three neutrino mixing angles and Dirac-type CP-violating phase δ are varied between 0^0 to 90^0 and 0^0 to 360^0, respectively. However, the mass-squared differences $(\delta m^2, \Delta m^2)$ are varied randomly within their 3σ experimental range [5, 6]. For the numerical analysis, we follow the same procedure as discussed in [20]. The main results and discussion are summarized as follows.

In Figures 1, 2, 3, 4, 5, and 6, it is explicitly shown that the octant of θ_{23} is well restricted for B_2, C_7, D_3, F_4 of 1TEE and 1TEC texture structures, respectively. However, for the remaining cases, the value of θ_{23} is unconstrained like other oscillation parameters. Apart from restricting the octant of θ_{23}, the analysis also ensures the quasi-degenerate mass ordering for these cases similar to the observation of [28–30]. From Figures 1(a), 1(b), 3(a), and 3(b), it is clear that,

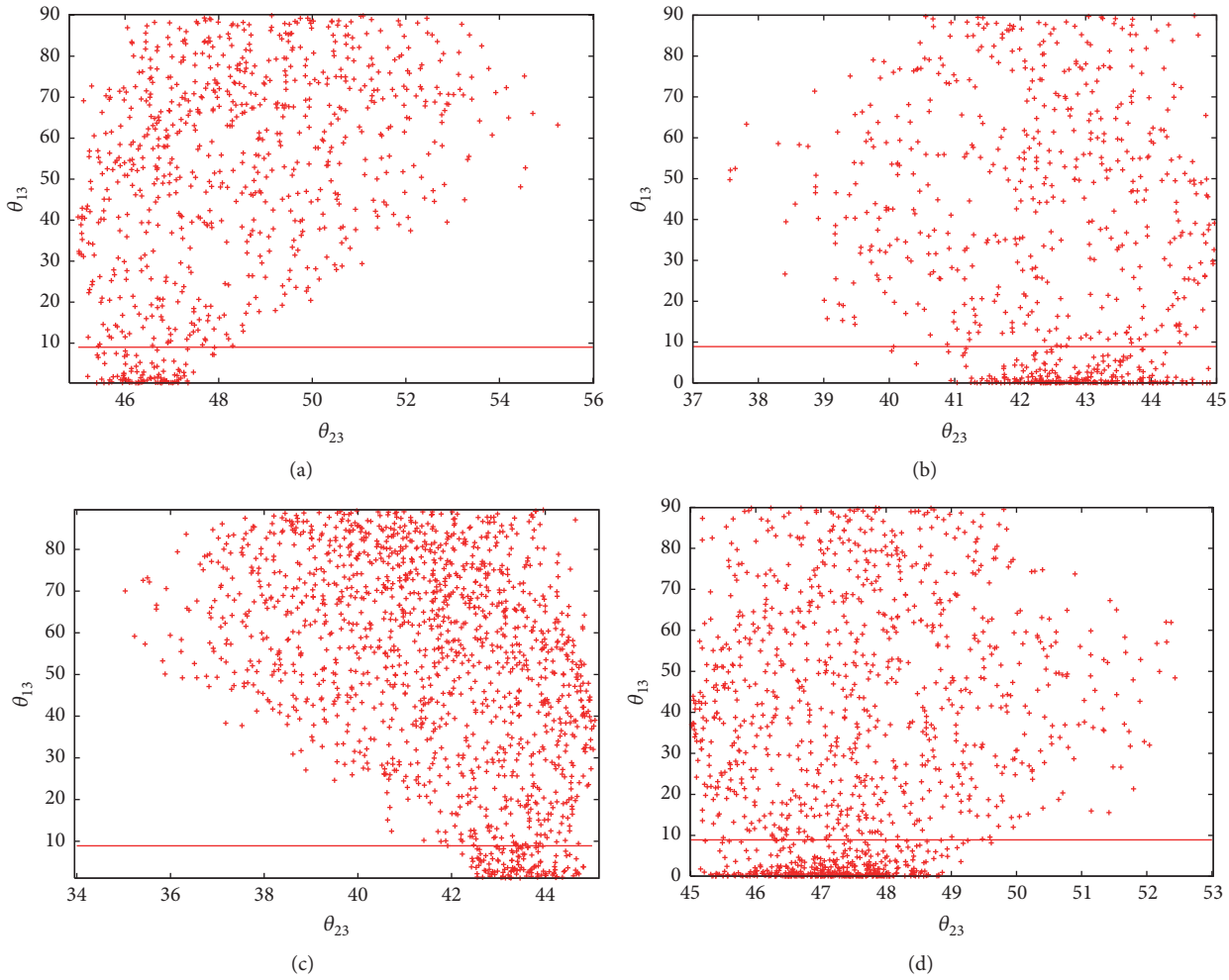

FIGURE 4: Correlation plots for textures B_2 ((a) NO and (b) IO) and C_7 for ((c) NO and (d) IO) at 3σ CL for 1TEC. The symbols have their usual meaning. The horizontal line indicates the upper limit on reactor mixing angle $\theta_{13} < 8.9^0$, as given in Table 1.

TABLE 1: Current neutrino oscillation parameters from global fits at 3σ confidence level [5, 6]. NO (IO) refers to normal (inverted) neutrino mass ordering.

Parameter	Best fit	3σ
δm^2 $[10^{-5}\,\text{eV}^2]$	7.50	7.03–8.09
$\lvert\Delta m^2_{31}\rvert$ $[10^{-3}\,\text{eV}^2]$ (NO)	2.52	2.407–2.643
$\lvert\Delta m^2_{31}\rvert$ $[10^{-3}\,\text{eV}^2]$ (IO)	2.52	2.39–2.63
θ_{12}	33.56°	31.3°–35.99°
θ_{23} (NO)	41.6°	38.4°–52.8°
θ_{23} (IO)	50.0°	38.8°–53.1°
θ_{13} (NO)	8.46°	7.99°–8.90°
θ_{13} (IO)	8.49°	8.03°–8.93°
δ (NO)	261°	0°–360°
δ (IO)	277°	145°–391°

for increasing value of $|M|_{ee}$, atmospheric mixing angle θ_{23} approaches to maximal value for the structure B_2 of 1TEE and 1TEC for both normal ordering (NO) and inverted ordering (IO). In Figures 2 and 4, it is explicitly shown that for cases B_2 and C_7 the quadrant of θ_{23} is already decided without the experimental input of the mixing angles. For 1TEE, we have $\theta_{23} < 45^0$ for NO and $\theta_{23} > 45^0$ for IO, whereas for 1TEC, $\theta_{23} > 45^0$ for NO, while $\theta_{23} < 45^0$ for IO (Figures 2(a), 2(b), 4(a), and 4(b)). Clearly the correlation plots of case B_2 are indistinguishable for 1TEE and 1TEC, if neutrino mass

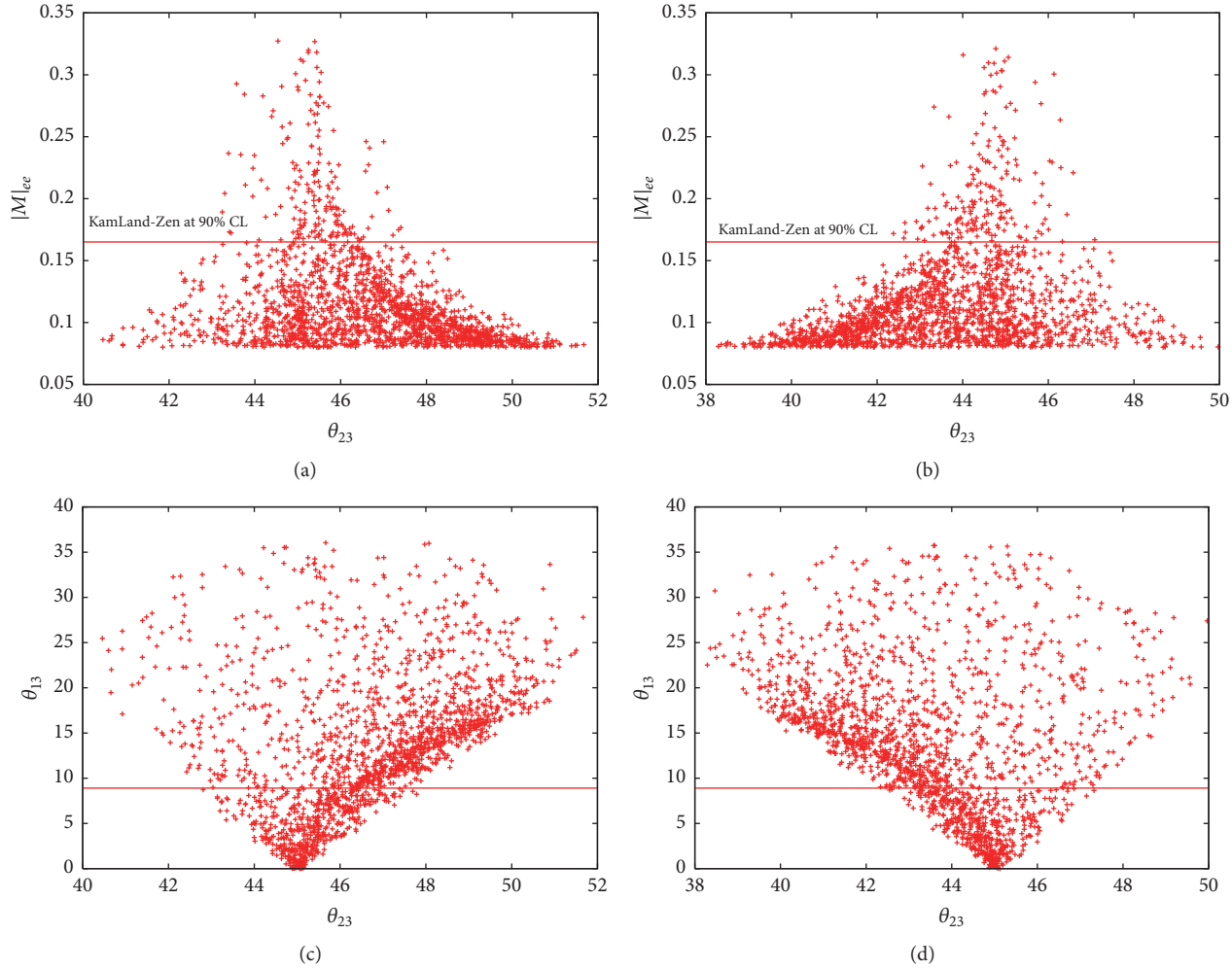

FIGURE 5: Correlation plots for textures D_3 ((a), (c)) and F_4 ((b), (d)) with IO for 1TEE at 3σ CL. The symbols have their usual meaning. In (a) and (b), colored horizontal line indicates the upper limit on effective neutrino mass term $|M|_{ee}$ (i.e., $|M|_{ee} < 0.165$ eV) at 90 ($<2\sigma$)% CL, given in KamLAND-Zen experiment [7]. In (c) and (d), we have shown the upper limit on reactor mixing angle θ_{13}.

ordering is not considered as also pointed out earlier. Similar conclusion can be drawn for structure C_7 since both are related through 2-3 exchange symmetry (Figures 2(c), 2(d), 4(c), and 4(d)). Apart from the prediction of near maximality of θ_{23}, cases B_2 and C_7 also predict $\delta \simeq 90^0, 270^0$ for 1TEE and 1TEC, respectively, if experimental range of mixing angles is considered as in Table 2. Figures 2(a) and 2(c) for NO and Figures 2(b) and 2(d) for IO depict the 2-3 interchange symmetry between cases B_2 and C_7 for 1TEE. Similar phenomenological observation is shown for 1TEC in Figures 4(a), 4(c), 4(b), and 4(d), respectively.

Similarly, cases D_3 and F_4 of 1TEE also predict near maximal atmospheric mixing angle (θ_{23}) for IO (Figures 5(a) and 5(b)). Interestingly the parameter space of reactor mixing angle θ_{13} is found to be constrained between 0^0 and 35^0 (Figures 5(c) and 5(d)). In Figures 5(c) and 5(d), it is clear that, for the allowed experimental range of θ_{13} (8.5^0–9.8^0), θ_{23} inches closer to 45^0. Similar predictions have been noted for cases D_3 and F_4 of 1TEC, however, for normal mass ordering (NO) (Figures 6(a), 6(b), 6(c), and 6(d)).

3.2. Comparing the Results for 1TEE and 1TEC Texture Structures. In this subsection, we compare the results of all the viable structures of 1TEE and 1TEC in neutrino mass matrix. It is worthwhile to mention that the present refinements of the experimental data do not limit the number of viable cases in 1TEE and 1TEC textures respectively. The number of viable cases obtained is the same as predicted in [21, 26, 27] for 1TEE and 1TEC, respectively. For executing the analysis, we vary the allowed ranges of three neutrino mixing angles ($\theta_{12}, \theta_{23}, \theta_{13}$) and mass squared differences ($\delta m^2, \Delta m^2$) within their 3σ confidence level. To facilitate the comparison, we have encapsulated the the predictions regarding three CP violating phases (ρ, σ, δ) and neutrino masses $m_{1,2,3}$ for all the allowed texture structures of 1TEE and 1TEC, respectively (Tables 3, 4, 5, and 6).

Category A. In Category A, there are 10 possible cases out of which only four ($A_{1,4,5,6}$) are allowed for 1TEE at 3σ CL, and in addition inverted mass ordering (IO) is ruled out for all these cases. On the other hand, only three ($A_{1,4,6}$) are allowed

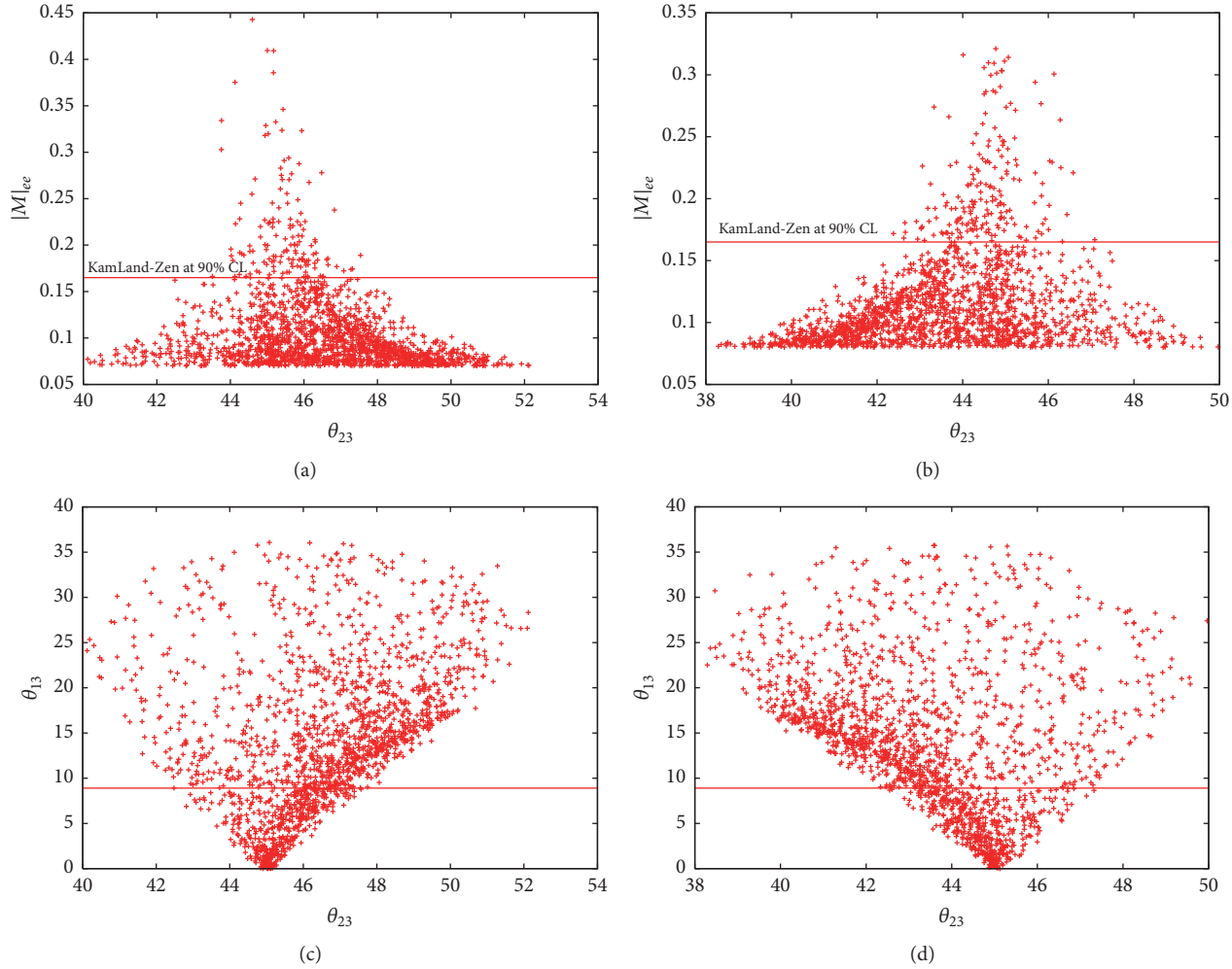

FIGURE 6: Correlation plots for textures D_3 ((a), (c)) and F_4 ((b), (d)) with NO for 1TEC at 3σ CL. The symbols have their usual meaning. In (a) and (b), colored horizontal line indicates the upper limit on effective neutrino mass term $|M|_{ee}$ (i.e., $|M|_{ee} < 0.165$ eV) at 90 ($<2\sigma$)% CL, given in KamLAND experiment [7]. In (c) and (d), we have shown the upper limit on reactor mixing angle θ_{13}.

for 1TEC with current oscillation data, while normal mass ordering (NO) is ruled out for these cases. For 1TEE, ρ, σ, δ remain unconstrained; however, for 1TEC, only δ remains unconstrained, while Majorana phases (ρ, σ) are restricted near 0^0 pertaining to viable cases. From Table 3, it is clear that lower bound on lowest neutrino mass (m_1 (NO) or m_3 (IO)) is nearly equal or less than 1 meV for 1TEE and 1TEC.

Category B (C). In Category B, all the ten possible cases are allowed for both 1TEE and 1TEC, respectively, at 3σ CL; however, cases $B_{1,6,7}$ allow only NO for 1TEE, while the same allow only IO for 1TEC (Table 4). Cases $B_{2,3,4,5,8,9,10}$ allow both NO and IO for 1TEE and 1TEC, respectively. As mentioned in [26, 27], cases of Category B are related to the cases belonging to Category C through permutation symmetry; therefore, we can obtain the results for Category C from B. We find that cases $C_{1,2,3}$ allow only NO for 1TEE, while the same allow IO for 1TEC.

Textures B_1 (NO), B_3 (NO, IO), B_5 (NO, IO), B_6 (NO), B_7 (NO), B_8 (NO), B_{10} (NO), C_1 (NO), C_2 (NO), C_3 (NO), C_4 (NO, IO), C_6 (NO, IO), C_8 (NO), and C_{10} (NO) held nearly no constraint on Dirac CP violating phase (δ) for 1TEE and 1TEC, respectively, but with opposite neutrino mass ordering (Table 4). Only cases B_2 (NO), B_4 (IO), C_7 (NO), and C_5 (IO) for 1TEE and B_2 (IO), B_4 (NO), C_7 (IO), and C_5 (NO) for 1TEC show significant reduction in the parameter space of δ. It is found that δ is restricted near 90^0 and 270^0 for 1TEE and 1TEC, respectively (Table 4). These predictions are significant considering the latest hint on δ near 270^0 [5, 6]. Therefore all the above cases discussed are almost indistinguishable for 1TEE and 1TEC, if neutrino mass ordering is not considered.

Category D(F). All the ten possible cases belonging to Category D are acceptable with neutrino oscillation data at 3σ CL for 1TEE and 1TEC, respectively (Table 5). However cases $D_{1,2,4,5,6,7,9}$ favor both NO and IO for 1TEE and 1TEC, while D_3, D_8, and D_{10} are acceptable only for IO in case of 1TEE; however, the same cases allowed NO in case of 1TEC. Similarly, the results for cases belonging to Category F can be derived from Category D.

Table 2: Sixty phenomenologically possible hybrid texture structures of M_ν at 3σ C.L where the triangles "$\triangle$" denote equal and nonzero elements (or cofactors) and "0" denotes the vanishing element (or minor). "$\times$" denotes the nonzero elements or cofactor.

	A	B	C	D	E	F
1	$\begin{pmatrix} 0 & \triangle & \triangle \\ \triangle & \times & \times \\ \triangle & \times & \times \end{pmatrix}$	$\begin{pmatrix} \triangle & 0 & \triangle \\ 0 & \times & \times \\ \triangle & \times & \times \end{pmatrix}$	$\begin{pmatrix} \triangle & \triangle & 0 \\ \triangle & \times & \times \\ 0 & \times & \times \end{pmatrix}$	$\begin{pmatrix} \triangle & \triangle & \times \\ \triangle & 0 & \times \\ \times & \times & \times \end{pmatrix}$	$\begin{pmatrix} \triangle & \triangle & \times \\ \triangle & \times & 0 \\ \times & 0 & \times \end{pmatrix}$	$\begin{pmatrix} \triangle & \triangle & \times \\ \triangle & \times & \times \\ \times & \times & 0 \end{pmatrix}$
2	$\begin{pmatrix} 0 & \triangle & \times \\ \triangle & \triangle & \times \\ \times & \times & \times \end{pmatrix}$	$\begin{pmatrix} \times & 0 & \triangle \\ 0 & \triangle & \times \\ \triangle & \times & \times \end{pmatrix}$	$\begin{pmatrix} \triangle & \times & 0 \\ \times & \triangle & \times \\ 0 & \times & \times \end{pmatrix}$	$\begin{pmatrix} \triangle & \times & \triangle \\ \times & 0 & \times \\ \triangle & \times & \times \end{pmatrix}$	$\begin{pmatrix} \triangle & \times & \triangle \\ \times & \times & 0 \\ \triangle & 0 & \times \end{pmatrix}$	$\begin{pmatrix} \triangle & \times & \triangle \\ \times & \times & \times \\ \triangle & \times & 0 \end{pmatrix}$
3	$\begin{pmatrix} 0 & \times & \triangle \\ \times & \times & \triangle \\ \triangle & \triangle & \times \end{pmatrix}$	$\begin{pmatrix} \times & 0 & \triangle \\ 0 & \times & \triangle \\ \triangle & \triangle & \times \end{pmatrix}$	$\begin{pmatrix} \triangle & \times & 0 \\ \times & \times & \triangle \\ 0 & \triangle & \times \end{pmatrix}$	$\begin{pmatrix} \triangle & \times & 0 \\ \times & 0 & \triangle \\ 0 & \triangle & \times \end{pmatrix}$	$\begin{pmatrix} \triangle & \times & \times \\ \times & \triangle & 0 \\ \times & 0 & \times \end{pmatrix}$	$\begin{pmatrix} \triangle & \times & \times \\ \times & \triangle & \times \\ \times & \times & 0 \end{pmatrix}$
4	$\begin{pmatrix} 0 & \times & \times \\ \times & \triangle & \triangle \\ \times & \triangle & \times \end{pmatrix}$	$\begin{pmatrix} \times & 0 & \triangle \\ 0 & \times & \times \\ \triangle & \times & \triangle \end{pmatrix}$	$\begin{pmatrix} \triangle & \times & 0 \\ \times & \times & \times \\ 0 & \times & \triangle \end{pmatrix}$	$\begin{pmatrix} \triangle & \times & \times \\ \times & 0 & \times \\ \times & \times & \triangle \end{pmatrix}$	$\begin{pmatrix} \triangle & \times & \times \\ \times & \times & 0 \\ \times & 0 & \triangle \end{pmatrix}$	$\begin{pmatrix} \triangle & \times & \times \\ \times & \times & \triangle \\ \times & \triangle & 0 \end{pmatrix}$
5	$\begin{pmatrix} 0 & \times & \times \\ \times & \triangle & \times \\ \times & \times & \triangle \end{pmatrix}$	$\begin{pmatrix} \triangle & 0 & \times \\ 0 & \triangle & \times \\ \times & \times & \times \end{pmatrix}$	$\begin{pmatrix} \times & \triangle & 0 \\ \triangle & \triangle & \times \\ 0 & \times & \times \end{pmatrix}$	$\begin{pmatrix} \times & \triangle & \triangle \\ \triangle & 0 & \times \\ \triangle & \times & \times \end{pmatrix}$	$\begin{pmatrix} \times & \triangle & \triangle \\ \triangle & \times & 0 \\ \triangle & 0 & \times \end{pmatrix}$	$\begin{pmatrix} \times & \triangle & \triangle \\ \triangle & \times & \times \\ \triangle & \times & 0 \end{pmatrix}$
6	$\begin{pmatrix} 0 & \times & \times \\ \times & \times & \triangle \\ \times & \triangle & \triangle \end{pmatrix}$	$\begin{pmatrix} \triangle & 0 & \times \\ 0 & \times & \triangle \\ \times & \triangle & \times \end{pmatrix}$	$\begin{pmatrix} \times & \triangle & 0 \\ \triangle & \times & \triangle \\ 0 & \triangle & \times \end{pmatrix}$	$\begin{pmatrix} \times & \triangle & \times \\ \triangle & 0 & \triangle \\ \times & \triangle & \times \end{pmatrix}$	$\begin{pmatrix} \times & \triangle & \times \\ \triangle & \triangle & 0 \\ \times & 0 & \times \end{pmatrix}$	$\begin{pmatrix} \times & \triangle & \times \\ \triangle & \triangle & \times \\ \times & \times & 0 \end{pmatrix}$
7	$\begin{pmatrix} 0 & \triangle & \times \\ \triangle & \times & \triangle \\ \times & \triangle & \times \end{pmatrix}$	$\begin{pmatrix} \triangle & 0 & \times \\ 0 & \times & \times \\ \times & \times & \triangle \end{pmatrix}$	$\begin{pmatrix} \times & \triangle & 0 \\ \triangle & \times & \times \\ 0 & \times & \triangle \end{pmatrix}$	$\begin{pmatrix} \times & \triangle & \times \\ \triangle & 0 & \times \\ \times & \times & \triangle \end{pmatrix}$	$\begin{pmatrix} \times & \triangle & \times \\ \triangle & \times & 0 \\ \times & 0 & \triangle \end{pmatrix}$	$\begin{pmatrix} \times & \triangle & \times \\ \triangle & \times & \triangle \\ \times & \triangle & 0 \end{pmatrix}$
8	$\begin{pmatrix} 0 & \times & \triangle \\ \times & \times & \times \\ \triangle & \times & \triangle \end{pmatrix}$	$\begin{pmatrix} \times & 0 & \times \\ 0 & \triangle & \triangle \\ \times & \triangle & \times \end{pmatrix}$	$\begin{pmatrix} \times & \times & 0 \\ \times & \triangle & \triangle \\ 0 & \triangle & \times \end{pmatrix}$	$\begin{pmatrix} \times & \times & \triangle \\ \times & 0 & \triangle \\ \triangle & \triangle & \times \end{pmatrix}$	$\begin{pmatrix} \times & \times & \triangle \\ \times & \triangle & 0 \\ \triangle & 0 & \times \end{pmatrix}$	$\begin{pmatrix} \times & \times & \triangle \\ \times & \triangle & \times \\ \triangle & \times & 0 \end{pmatrix}$
9	$\begin{pmatrix} 0 & \times & \triangle \\ \times & \triangle & \times \\ \triangle & \times & \times \end{pmatrix}$	$\begin{pmatrix} \times & 0 & \times \\ 0 & \triangle & \times \\ \times & \times & \triangle \end{pmatrix}$	$\begin{pmatrix} \times & \times & 0 \\ \times & \triangle & \times \\ 0 & \times & \triangle \end{pmatrix}$	$\begin{pmatrix} \times & \times & \triangle \\ \times & 0 & \times \\ \triangle & \times & \triangle \end{pmatrix}$	$\begin{pmatrix} \times & \times & \triangle \\ \times & \times & 0 \\ \triangle & 0 & \triangle \end{pmatrix}$	$\begin{pmatrix} \times & \times & \triangle \\ \times & \times & \triangle \\ \triangle & \triangle & 0 \end{pmatrix}$
10	$\begin{pmatrix} 0 & \triangle & \times \\ \triangle & \times & \times \\ \times & \times & \triangle \end{pmatrix}$	$\begin{pmatrix} \times & 0 & \times \\ 0 & \times & \triangle \\ \times & \triangle & \triangle \end{pmatrix}$	$\begin{pmatrix} \times & \times & 0 \\ \times & \times & \triangle \\ 0 & \triangle & \triangle \end{pmatrix}$	$\begin{pmatrix} \times & \times & \times \\ \times & 0 & \triangle \\ \times & \triangle & \triangle \end{pmatrix}$	$\begin{pmatrix} \times & \times & \times \\ \times & \triangle & 0 \\ \times & 0 & \triangle \end{pmatrix}$	$\begin{pmatrix} \times & \times & \times \\ \times & \triangle & \triangle \\ \times & \triangle & 0 \end{pmatrix}$

Cases D_1 (IO), D_2 (IO), D_3 (IO), D_4 (IO), D_5 (NO, IO), D_6 (IO), D_7 (NO, IO), D_8 (IO), D_9 (NO, IO), D_{10} (IO), F_1 (IO), F_2 (IO), F_3 (IO), F_4 (IO), F_5 (NO, IO), F_6 (IO), F_7 (NO, IO), F_8 (IO), F_9 (NO, IO), and F_{10} (IO) predict literally no constraints on δ for 1TEE. These cases give identical predictions for 1TEC, but for opposite mass ordering. For cases D_1 (NO), D_2 (NO), D_4 (NO), D_6 (NO), F_1 (NO), F_2 (NO), F_4 (NO), and F_6 (NO), the parameter space of δ is found to be well constrained for 1TEE. These cases give similar predictions regarding the parameter space of δ for 1TEC, but for IO.

Category E. In Category E, all the ten possible cases are allowed for 1TEE at 3σ CL, while only nine other than E_5 are

Table 3: The allowed ranges of Dirac CP-violating phase δ, the Majorana phases ρ, σ, and three neutrino masses m_1, m_2, m_3 for the experimentally allowed cases of Category A. Masses are in eV. "×" denotes the nonviability of case for a particular mass ordering.

Cases	1TEE		1TEC	
	NO	IO	NO	IO
A_1	$\rho = -90^0$–90^0	×	×	$\rho = -0.0277^0 - -0.0220^0 \oplus 0.0214^0$–$0.0274^0$
	$\sigma = -90^0$–90^0	×	×	$\sigma = -0.0273^0$–0.0271^0
	$\delta = 0^0$–360^0	×	×	$\delta = 0^0$–360^0
	$m_1 = 0.00147$–0.0106	×	×	$m_1 = 0.0430$–0.0534
	$m_2 = 0.00849$–0.0139	×	×	$m_2 = 0.0439$–0.0541
	$m_3 = 0.0437$–0.0551	×	×	$m_3 = 0.000904$–0.00504
A_2 (A_8)	×	×	×	×
A_3 (A_7)	×	×	×	×
A_4 (A_6)	$\rho = -90^0$–90^0	×	×	$\rho = -0.0275^0 - -0.0222^0 \oplus 0.0215^0$–$0.0269^0$
	$\sigma = -90^0$–90^0	×	×	$\sigma = -0.0250^0$–0.0268^0
	$\delta = 0^0$–360^0	×	×	$\delta = 0^0$–360^0
	$m_1 = 0.00148$–0.0106	×	×	$m_1 = 0.0431$–0.0534
	$m_2 = 0.00850$–0.0139	×	×	$m_2 = 0.0439$–0.0540
	$m_3 = 0.0437$–0.0551	×	×	$m_3 = 0.000950$–0.00504
A_5 (A_5)	$\rho = -90^0$–90^0	×	×	×
	$\sigma = -90^0$–90^0	×	×	×
	$\delta = 0^0$–360^0	×	×	×
	$m_1 = 0.00163$–0.0105	×	×	×
	$m_2 = 0.00854$–0.0137	×	×	×
	$m_3 = 0.0438$–0.0545	×	×	×
A_9 (A_{10})	×	×	×	×

acceptable in case of 1TEC (Table 6). Cases $E_{1,2,3,4,6,7,8,9}$ allow only inverted mass ordering (IO) for 1TEE, while the same textures allow only normal mass ordering (NO) for 1TEC. Cases E_5 and E_{10} allow both NO and IO for 1TEE; however E_5 is ruled out for both NO and IO for 1TEC at 3σ CL. Similar to cases belonging to Category D, $E_{1,2,3,4,5,6,7,8,9}$ (IO) cover full range of ρ, σ, δ for 1TEE, whereas the same cases (except E_5) give identical predictions for 1TEC, but for NO. For E_5 (NO) and E_{10} (NO), phases ρ, σ, δ are somewhat restricted at 3σ CL for 1TEE, while only for E_{10} (IO), the parameter space of ρ, σ, δ seems to be restricted for 1TEC (Table 6).

To summarize our discussion, we have investigated all the viable cases of 1TEE and 1TEC texture structures in the limit of large effective neutrino mass $|M|_{ee}$. It is found that only four cases are able to produce near maximal atmospheric mixing for 1TEE and 1TEC, respectively. However, the predictions remain true irrespective of the experimental data on solar and reactor mixing angle. The observation also hints towards the indistinguishable feature of 1TEE and 1TEC texture structures, but for opposite mass ordering. In order to depict the indistinguishability, we have carried out a comparative study of 1TEE and 1TEC texture structures using the current experimental data at 3σ CL. From our discussion we find that most of the cases belonging to 1TEE and 1TEC are almost indistinguishable as far as the neutrino oscillation parameters are concerned, but with opposite neutrino mass ordering. The indistinguishable nature of 1TEE and 1TEC is more prominent for quasi-degenerate mass ordering. For the cases where lower bound on lowest neutrino mass is very small (<1 meV), there is noticeable deviation in the predictions for 1TEE and 1TEC (Tables 3, 4, 5, and 6). This point is also discussed by Liao et. al. in [31]. In addition, the parameter space of δ for most of the cases belonging to 1TEE and 1TEC remains unrestricted, while only eight cases show maximal restriction for δ. Since no presently feasible experiment has been able to determine the neutrino mass ordering, therefore, we cannot distinguish 1TEE and 1TEC structures using the present oscillation data. However, the currently running and forthcoming neutrino experiments aimed at distinguishing the mass ordering of neutrinos will test our phenomenological results. Also the ongoing and future neutrinoless double beta decay experiments are capable of measuring $|M|_{ee}$ term, which would, in turn, either confirm or rule out our assumption of large $|M|_{ee}$.

Conflicts of Interest

The author declares that there are no conflicts of interest regarding the publication of this paper.

Table 4: The allowed ranges of Dirac CP-violating phase δ, the Majorana phases ρ, σ, and three neutrino masses m_1, m_2, m_3 for the experimentally allowed cases of Category B (C). Masses are in eV. "×" denotes the nonviability of case for a particular mass ordering.

Cases	1TEE		1TEC	
	NO	IO	NO	IO
B_1 (C_1)	$\rho = -90^0$–90^0	×	×	$\rho = -0.0277^0$–0.0279^0
	$\sigma = -90^0$–90^0	×	×	$\sigma = -0.0284^0$–0.0284^0
	$\delta = 0^0$–360^0	×	×	$\delta = 0^0$–360^0
	$m_1 = 0.00550$–0.0298	×	×	$m_1 = 0.0439$–0.0597
	$m_2 = 0.0101$–0.0310	×	×	$m_2 = 0.0447$–0.0604
	$m_3 = 0.0443$–0.0605	×	×	$m_3 = 0.000754$–0.0297
B_2 (C_7)	$\rho = -2.76^0$–2.81^0	$\rho = -7.74^0$–7.75^0	$\rho = -90^0$–90^0	$\rho = -4.46^0$–4.40^0
	$\sigma = -10.48^0$–10.22^0	$\sigma = -8.84^0$–9.22^0	$\sigma = -90^0$–90^0	$\sigma = -5.41^0$–5.39^0
	$\delta = 77.3^0$–$94.27^0 \oplus 266.3^0$–284^0	$\delta = 84.01^0$–$98.7^0 \oplus 262.19^0$–276.6^0	$\delta = 86.22^0$–273.3^0	$\delta = 81.56^0$–$96.48^0 \oplus 263.7^0$–278.4^0
	$m_1 = 0.0235$–0.314	$m_1 = 0.0453$–0.277	$m_1 = 0.00548$–0.267	$m_1 = 0.0507$–0.419
	$m_2 = 0.0242$–0.0310	$m_2 = 0.0465$–0.274	$m_2 = 0.00806$–0.316	$m_2 = 0.0508$–0.419
	$m_3 = 0.0485$–0.0315	$m_3 = 0.0117$–0.271	$m_3 = 0.0428$–0.320	$m_3 = 0.0249$–0.414
B_3 (C_6)	$\rho = -90^0$– – $5.9^0 \oplus 5.9^0$–90^0	$\rho = -90^0$–90^0	$\rho = -90^0$–90^0	$\rho = -90^0$–90^0
	$\sigma = -90^0$– – $5.9^0 \oplus 5.9^0$–90^0	$\sigma = -90^0$–90^0	$\sigma = -90^0$–90^0	$\sigma = -90^0$–90^0
	$\delta = 7.47^0$–356^0	$\delta = 8.3^0$–$173^0 \oplus 187^0$–351^0	$\delta = 5.16^0$–$178^0 \oplus 183.7^0$–353.6^0	$\delta = 0^0$–360^0
	$m_1 = 0.0153$–0.331	$m_1 = 0.0459$–0.335	$m_1 = 0.00504$–0.485	$m_1 = 0.0427$–0.505
	$m_2 = 0.0161$–0.331	$m_2 = 0.0461$–0.334	$m_2 = 0.00920$–0.483	$m_2 = 0.0445$–0.503
	$m_3 = 0.0445$–0.0335	$m_3 = 0.0136$–0.330	$m_3 = 0.0416$–0.480	$m_3 = 0.00884$–0.500
B_4 (C_5)	$\rho = -19.07^0$–19.75^0	$\rho = -4.80^0$–4.66^0	$\rho = -43.13^0$–40.12^0	$\rho = -16.38^0$–18.8^0
	$\sigma = -90^0$–90^0	$\sigma = -2.83^0$–3.12^0	$\sigma = -43^0$–40.1^0	$\sigma = -41.43^0$–40.59^0
	$\delta = 0^0$–$100^0 \oplus 260.2^0$–360^0	$\delta = 84.68^0$–$94.7^0 \oplus 265.08^0$–275.5^0	$\delta = 88.04^0$–$124.4^0 \oplus 230.09^0$–272^0	$\delta = 5.56^0$–$13.82^0 \oplus 255.7^0$–307.3^0
	$m_1 = 0.00681$–0.318	$m_1 = 0.0488$–0.314	$m_1 = 0.0105$–0.373	$m_1 = 0.0444$–0.420
	$m_2 = 0.00969$–0.0317	$m_2 = 0.0486$–0.312	$m_2 = 0.0129$–0.369	$m_2 = 0.0447$–0.416
	$m_3 = 0.0421$–0.0321	$m_3 = 0.0202$–0.310	$m_3 = 0.0435$–0.374	$m_3 = 0.0103$–0.418
B_5 (C_4)	$\rho = -20.83^0$–20.79^0	$\rho = -90^0$– – $11.3^0 \oplus 11.3^0$–90^0	$\rho = -90^0$–90^0	$\rho = -24.19^0$–24.45^0
	$\sigma = -36.3^0$–36^0	$\$\sigma = -90^0$– – $14.3^0 \oplus 14.8^0$–90^0	$\sigma = -90^0$–90^0	$\sigma = -27.7^0$–27.4^0
	$\delta = 0^0$–$177.5^0 \oplus 182^0$–360^0	$\delta = 0^0$–$168^0 \oplus 192.5^0$–360^0	$\delta = 9.33^0$–$172.4^0 \oplus 187.20$–350.4^0	$\delta = 0^0$–$179.3^0 \oplus 180.6^0$–360^0
	$m_1 = 0.00965$–0.330	$m_1 = 0.0761$–0.330	$m_1 = 0.0603$–0.498	$m_1 = 0.0440$–0.498
	$m_2 = 0.0113$–0.0330	$m_2 = 0.0762$–0.330	$m_2 = 0.0608$–0.496	$m_2 = 0.0447$–0.499
	$m_3 = 0.0421$–0.0332	$m_3 = 0.0603$–0.328	$m_3 = 0.0629$–0.500	$m_3 = 0.0103$–0.499
B_6 (C_3)	$\rho = -90^0$–90^0	×	×	$\rho = -90^0$–90^0
	$\sigma = -90^0$–90^0	×	×	$\sigma = -90^0$–90^0
	$\delta = 0^0$–360^0	×	×	$\delta = 0^0$–360^0
	$m_1 = 0.0147$–0.324	×	×	$m_1 = 0.0452$–0.454
	$m_2 = 0.00161$–0.324	×	×	$m_2 = 0.0451$–0.451
	$m_3 = 0.0445$–0.324	×	×	$m_3 = 0.00161$–0.450

Table 4: Continued.

Cases	1TEE		1TEC	
	NO	IO	NO	IO
B_7 (C_2)	$\rho = -26.25^0 - 26.43^0$	×	×	$\rho = -30.92^0 - 30.42^0$
	$\sigma = -50.28^0 - 50.2^0$	×	×	$\sigma = -41.9^0 - 43.8^0$
	$\delta = 0^0 - 177.5^0 \oplus 182^0 - 360^0$	×	×	$\delta = 0^0 - 360^0$
	$m_1 = 0.00883 - 0.331$	×	×	$m_1 = 0.0447 - 0.498$
	$m_2 = 0.00121 - 0.329$	×	×	$m_2 = 0.0451 - 0.498$
	$m_3 = 0.0421 - 0.334$	×	×	$m_3 = 0.00804 - 0.498$
B_8 (C_{10})	$\rho = -90^0 - 90^0$	$\rho = -90^0 - 90^0$	$\rho = -90^0 - 90^0$	$\rho = -90^0 - 90^0$
	$\sigma = -90^0 - 90^0$	$\sigma = -90^0 - 90^0$	$\sigma = -90^0 - 90^0$	$\sigma = -90^0 - 90^0$
	$\delta = 0^0 - 166.5^0 \oplus 196.5^0 - 360^0$	$\delta = 45.05^0 - 135^0 \oplus 224.5^0 - 314.6^0$	$\delta = 45.86^0 - 315.05^0$	$\delta = 0^0 - 360^0$
	$m_1 = 0.00127 - 0.279$	$m_1 = 0.0418 - 0.279$	$m_1 = 0.00498 - 0.381$	$m_1 = 0.0427 - 0.303$
	$m_2 = 0.00691 - 0.277$	$m_2 = 0.0429 - 0.307$	$m_2 = 0.00736 - 0.382$	$m_2 = 0.0428 - 0.302$
	$m_3 = 0.0409 - 0.280$	$m_3 = 0.00398 - 0.305$	$m_3 = 0.0407 - 0.384$	$m_3 = 0.00342 - 0.298$
B_9 (C_9)	$\rho = -90^0 - 90^0$	$\rho = -90^0 - 90^0$	$\rho = -90^0 - 90^0$	$\rho = -90^0 - 90^0$
	$\sigma = -90^0 - 90^0$	$\sigma = -90^0 - 90^0$	$\sigma = -90^0 - 90^0$	$\sigma = -90^0 - 90^0$
	$\delta = 5.55^0 - 354^0$	$\delta = 12^0 - 171.7^0 \oplus 189.7^0 - 352.7^0$	$\delta = 8.32^0 - 175.9^0 \oplus 186^0 - 350.47^0$	$\delta = 0^0 - 360^0$
	$m_1 = 0.00338 - 0.279$	$m_1 = 0.0435 - 0.319$	$m_1 = 0.00622 - 0.487$	$m_1 = 0.0447 - 0.486$
	$m_2 = 0.00831 - 0.277$	$m_2 = 0.0445 - 0.319$	$m_2 = 0.00681 - 0.486$	$m_2 = 0.0451 - 0.487$
	$m_3 = 0.0423 - 0.282$	$m_3 = 0.00398 - 0.317$	$m_3 = 0.00914 - 0.486$	$m_3 = 0.00458 - 0.480$
B_{10} (C_8)	$\rho = -90^0 - 90^0$	$\rho = -90^0 - 90^0$	$\rho = -90^0 - 90^0$	$\rho = -90^0 - 90^0$
	$\sigma = -90^0 - 90^0$	$\sigma = -90^0 - 90^0$	$\sigma = -90^0 - 90^0$	$\sigma = -90^0 - 90^0$
	$\delta = 0^0 - 360^0$	$\delta = 44.64^0 - 136.5^0 \oplus 224.6^0 - 314.2^0$	$\delta = 1.92^0 - 313.04^0$	$\delta = 0^0 - 360^0$
	$m_1 = 0.00163 - 0.294$	$m_1 = 0.0425 - 0.277$	$m_1 = 0.00516 - 0.348$	$m_1 = 0.0427 - 0.365$
	$m_2 = 0.00691 - 0.293$	$m_2 = 0.0423 - 0.275$	$m_2 = 0.00806 - 0.346$	$m_2 = 0.0453 - 0.365$
	$m_3 = 0.0409 - 0.299$	$m_3 = 0.00380 - 0.272$	$m_3 = 0.0416 - 0.348$	$m_3 = 0.00879 - 0.391$

Table 5: The allowed ranges of Dirac CP-violating phase δ, the Majorana phases ρ, σ, and three neutrino masses m_1, m_2, m_3 for the experimentally allowed cases of Category D (F). Masses are in eV. "×" denotes the nonviability of case for a particular mass ordering.

Cases	1TEE		1TEC	
	NO	IO	NO	IO
D_1 (F_2)	$\rho = -90^0$–90^0	$\rho = -90^0$–90^0	$\rho = -90^0$–90^0	$\rho = -90^0$–90^0
	$\sigma = -90^0$–90^0	$\sigma = -90^0$–90^0	$\sigma = -90^0$–90^0	$\sigma = -90^0$–90^0
	$\delta = 30.185^0$–322.6^0	$\delta = 0^0$–360^0	$\delta = 0^0$–360^0	$\delta = 31.79^0$–318.66^0
	$m_1 = 0.0541$–0.224	$m_1 = 0.00432$–0.252	$m_1 = 0.00331$–0.603	$m_1 = 0.0731$–0.501
	$m_2 = 0.0538$–0.224	$m_2 = 0.00437$–0.251	$m_2 = 0.00800$–0.606	$m_2 = 0.0719$–0.500
	$m_3 = 0.0679$–0.230	$m_3 = 0.00343$–0.248	$m_3 = 0.0371$–0.604	$m_3 = 0.0593$–0.496
D_2 (F_1)	$\rho = -50.28^0$–60.48^0	$\rho = -90^0$–90^0	$\rho = -90^0$–90^0	$\rho = -63.3^0$–64^0
	$\sigma = -90^0$–90^0	$\sigma = -90^0$–90^0	$\sigma = -90^0$–90^0	$\sigma = -89.37^0$–86.25^0
	$\delta = 87.19^0$–297.4^0	$\delta = 0^0$–360^0	$\delta = 0^0$–$64.34^0 \oplus 295.7^0$–360^0	$\delta = 70.50^0$–295.77^0
	$m_1 = 0.124$–0.293	$m_1 = 0.0422$–0.263	$m_1 = 0.00542$–0.0277	$m_1 = 0.128$–0.581
	$m_2 = 0.125$–0.294	$m_2 = 0.0430$–0.262	$m_2 = 0.00993$–0.0291	$m_2 = 0.130$–0.582
	$m_3 = 0.132$–0.295	$m_3 = 0.00552$–0.257	$m_3 = 0.0440$–0.0600	$m_3 = 0.120$–0.579
D_3 (F_4)	×	$\rho = -90^0$–90^0	$\rho = -90^0$–90^0	×
	×	$\sigma = -90^0$–90^0	$\sigma = -90^0$–90^0	×
	×	$\delta = 0^0$–360^0	$\delta = 0^0$–$64.34^0 \oplus 295.7^0$–360^0	×
	×	$m_1 = 0.0439$–0.308	$m_1 = 0.0161$–0.474	×
	×	$m_2 = 0.0445$–0.308	$m_2 = 0.0164$–0.471	×
	×	$m_3 = 0.00888$–0.304	$m_3 = 0.0416$–0.469	×
D_4 (F_3)	$\rho = -58.71^0$–59.35^0	$\rho = -90^0$–90^0	$\rho = -90^0$–90^0	$\rho = -61.4^0$–61.5^0
	$\sigma = -88.90^0$–87.18^0	$\sigma = -90^0$–90^0	$\sigma = -90^0$–90^0	$\sigma = -90^0$–90^0
	$\delta = 75.87^0$–285.58^0	$\delta = 0^0$–360^0	$\delta = 18.12^0$–318.75^0	$\delta = 77.86^0$–286.15^0
	$m_1 = 0.0574$–0.287	$m_1 = 0.00429$–0.254	$m_1 = 0.0102$–0.795	$m_1 = 0.0711$–0.424
	$m_2 = 0.0575$–0.286	$m_2 = 0.00430$–0.254	$m_2 = 0.0147$–0.796	$m_2 = 0.0740$–0.424
	$m_3 = 0.0679$–0.291	$m_3 = 0.00969$–0.202	$m_3 = 0.0369$–0.790	$m_3 = 0.0564$–0.418
D_5 (F_5)	$\rho = -90^0$–90^0	$\rho = -90^0$–90^0	$\rho = -90^0$–90^0	$\rho = -90^0$–90^0
	$\sigma = -90^0$–90^0	$\sigma = -90^0$–90^0	$\sigma = -90^0$–90^0	$\sigma = -90^0$–90^0
	$\delta = 0^0$–360^0	$\delta = 0^0$–360^0	$\delta = 0^0$–360^0	$\delta = 0^0$–360^0
	$m_1 = 0.0337$–0.334	$m_1 = 0.0431$–0.335	$m_1 = 0.00255$–0.509	$m_1 = 0.0538$–0.505
	$m_2 = 0.0338$–0.334	$m_2 = 0.0434$–0.334	$m_2 = 0.00370$–0.505	$m_2 = 0.0539$–0.506
	$m_3 = 0.0541$–0.334	$m_3 = 0.00940$–0.330	$m_3 = 0.0351$–0.510	$m_3 = 0.0305$–0.500
D_6 (F_9)	$\rho = -65.09^0$–58.48^0	$\rho = -90^0$–90^0	$\rho = -23.03^0$– − $7.74^0 \oplus 7.66^0$–22.14^0	$\rho = -18.42^0$– − $6.56^0 \oplus 6.77^0$–18.27^0
	$\sigma = -90^0$–90^0	$\sigma = -90^0$–90^0	$\sigma = -68.53^0$– − $38.75^0 \oplus 37.86^0$–69.0^0	$\sigma = -71.1^0$– − $46.2^0 \oplus 46.2^0$–70.48^0
	$\delta = 64.2^0$–288.1^0	$\delta = 0^0$–360^0	$\delta = 109.68^0$–$150.05^0 \oplus 210.4^0$–250.2^0	$\delta = 118.19^0$–$154.2^0 \oplus 206.7^0$–242.3^0
	$m_1 = 0.0974$–0.323	$m_1 = 0.0446$–0.277	$m_1 = 0.0202$–0.456	$m_1 = 0.108$–0.398
	$m_2 = 0.0965$–0.0321	$m_2 = 0.0448$–0.277	$m_2 = 0.0204$–0.456	$m_2 = 0.109$–0.396
	$m_3 = 0.107$–0.0326	$m_3 = 0.00888$–0.324	$m_3 = 0.0451$–0.456	$m_3 = 0.0962$–0.396

Table 5: Continued.

Cases	1TEE		1TEC	
	NO	IO	NO	IO
D_7 (F_8)	$\rho = -90^0$–90^0	$\rho = -90^0$–90^0	$\rho = -90^0$–90^0	$\rho = -90^0$–90^0
	$\sigma = -90^0$–90^0	$\sigma = -90^0$–90^0	$\sigma = -90^0$–90^0	$\sigma = -90^0$–90^0
	$\delta = 0^0$–360^0	$\delta = 0^0$–360^0	$\delta = 0^0$–360^0	$\delta = 0^0$–360^0
	$m_1 = 0.0478$–0.273	$m_1 = 0.0439$–0.333	$m_1 = 0.00663$–0.436	$m_1 = 0.0647$–0.437
	$m_2 = 0.0479$–0.273	$m_2 = 0.0454$–0.333	$m_2 = 0.0103$–0.434	$m_2 = 0.0649$–0.438
	$m_3 = 0.0644$–0.300	$m_3 = 0.00806$–0.330	$m_3 = 0.0416$–0.438	$m_3 = 0.0439$–0.491
D_8 (F_7)	×	$\rho = -90^0$–90^0	$\rho = -90^0$–90^0	×
	×	$\sigma = -90^0$–90^0	$\sigma = -90^0$–90^0	×
	×	$\delta = 0^0$–360^0	$\delta = 0^0$–$64.34^0 \oplus 295.7^0$–360^0	×
	×	$m_1 = 0.0451$–0.0938	$m_1 = 0.00941$–0.0803	×
	×	$m_2 = 0.0459$–0.0941	$m_2 = 0.0125$–0.0804	×
	×	$m_3 = 0.00121$–0.0790	$m_3 = 0.0445$–0.0953	×
D_9 (F_6)	$\rho = -90^0$–90^0	$\rho = -90^0$–90^0	$\rho = -90^0$–90^0	$\rho = -90^0$–90^0
	$\sigma = -90^0$–90^0	$\sigma = -90^0$–90^0	$\sigma = -90^0$–90^0	$\sigma = -90^0$–90^0
	$\delta = 0^0$–360^0	$\delta = 0^0$–360^0	$\delta = 0^0$–360^0	$\delta = 0^0$–360^0
	$m_1 = 0.0492$–0.300	$m_1 = 0.0455$–0.310	$m_1 = 0.00769$–0.436	$m_1 = 0.0647$–0.411
	$m_2 = 0.0496$–0.300	$m_2 = 0.0456$–0.310	$m_2 = 0.00932$–0.434	$m_2 = 0.0638$–0.412
	$m_3 = 0.0638$–0.303	$m_3 = 0.00969$–0.306	$m_3 = 0.0426$–0.438	$m_3 = 0.0458$–0.407
D_{10} (F_{10})	×	$\rho = -90^0$–90^0	$\rho = -90^0$–90^0	×
	×	$\sigma = -90^0$–90^0	$\sigma = -90^0$–90^0	×
	×	$\delta = 0^0$–360^0	$\delta = 0^0$–$64.34^0 \oplus 295.7^0$–360^0	×
	×	$m_1 = 0.0432$–0.102	$m_1 = 0.00201$–0.0793	×
	×	$m_2 = 0.0442$–0.102	$m_2 = 0.00870$–0.0795	×
	×	$m_3 = 0.00301$–0.0901	$m_3 = 0.0435$–0.0932	×

Table 6: The allowed ranges of Dirac CP-violating phase δ, the Majorana phases ρ, σ, and three neutrino masses m_1, m_2, m_3 for the experimentally allowed cases of Category E. Masses are in eV. "×" denotes the nonviability of case for a particular mass ordering.

Cases	1TEE		1TEC	
	NO	IO	NO	IO
E_1 (E_2)	×	$\rho = -90^0 - 90^0$	$\rho = -90^0 - 90^0$	×
	×	$\sigma = -90^0 - 90^0$	$\sigma = -90^0 - 90^0$	×
	×	$\delta = 0^0 - 360^0$	$\delta = 0^0 - 64.34^0 \oplus 295.7^0 - 360^0$	×
	×	$m_1 = 0.0511 - 0.0804$	$m_1 = 0.00283 - 0.0629$	×
	×	$m_2 = 0.0516 - 0.0805$	$m_2 = 0.00878 - 0.0634$	×
	×	$m_3 = 0.0264 - 0.0678$	$m_3 = 0.0440 - 0.0809$	×
E_3 (E_4)	×	$\rho = -90^0 - 90^0$	$\rho = -90^0 - 90^0$	×
	×	$\sigma = -90^0 - 90^0$	$\sigma = -90^0 - 90^0$	×
	×	$\delta = 0^0 - 360^0$	$\delta = 0^0 - 64.34^0 \oplus 295.7^0 - 360^0$	×
	×	$m_1 = 0.0439 - 0.333$	$m_1 = 0.00914 - 0.499$	×
	×	$m_2 = 0.0457 - 0.333$	$m_2 = 0.00115 - 0.504$	×
	×	$m_3 = 0.00888 - 0.333$	$m_3 = 0.0432 - 0.500$	×
E_5	$\rho = -90^0 - - 156 \oplus 29.3 - 90^0$	$\rho = -90^0 - 90^0$	×	×
	$\rho = -90^0 - - 156 \oplus 29.3 - 90^0$	$\sigma = -90^0 - 90^0$	×	×
	$\delta = 29.3^0 - 153.5^0 \oplus 206.5^0 - 334^0$	$\delta = 0^0 - 360^0$	×	×
	$m_1 = 0.130 - 0.332$	$m_1 = 0.0439 - 0.269$	×	×
	$m_2 = 0.132 - 0.330$	$m_2 = 0.0451 - 0.270$	×	×
	$m_3 = 0.137 - 0.334$	$m_3 = 0.0103 - 0.262$	×	×
E_6 (E_9)	×	$\rho = -90^0 - 90^0$	$\rho = -90^0 - 90^0$	×
	×	$\sigma = -90^0 - 90^0$	$\sigma = -90^0 - 90^0$	×
	×	$\delta = 0^0 - 360^0$	$\delta = 0^0 - 360^0$	×
	×	$m_1 = 0.0511 - 0.333$	$m_1 = 0.00914 - 0.499$	×
	×	$m_2 = 0.0517 - 0.333$	$m_2 = 0.00115 - 0.504$	×
	×	$m_3 = 0.0273 - 0.333$	$m_3 = 0.0432 - 0.500$	×
E_7 (E_8)	×	$\rho = -90^0 - 90^0$	$\rho = -90^0 - 90^0$	×
	×	$\sigma = -90^0 - 90^0$	$\sigma = -90^0 - 90^0$	×
	×	$\delta = 0^0 - 360^0$	$\delta = 0^0 - 360^0$	×
	×	$m_1 = 0.0511 - 0.0908$	$m_1 = 0.0225 - 0.0469$	×
	×	$m_2 = 0.0517 - 0.0911$	$m_2 = 0.0238 - 0.0480$	×
	×	$m_3 = 0.0273 - 0.0746$	$m_3 = 0.0494 - 0.0708$	×
E_{10}	$\rho = -90^0 - - 28.6^0 \oplus 26.01^0 - 90^0$	$\rho = -18.15^0 - 18.08^0$	$\rho = -90^0 - 90^0$	$\rho = -90^0 - - 19^0 \oplus 19.5^0 - 90^0$
	$\sigma = -90^0 - - 28.6^0 \oplus 26.01^0 - 90^0$	$\sigma = -90^0 - - 6.41^0 \oplus 6.09^0 - 90^0$	$\sigma = -90^0 - 90^0$	$\sigma = -90^0 - - 19^0 \oplus 19.5^0 - 90^0$
	$\delta = 25.35^0 - 151.92^0 \oplus 206.97^0 - 332.3^0$	$\delta = 0^0 - 177^0 \oplus 184.3^0 - 357.5^0$	$\delta = 0^0 - 360^0$	$\delta = 23.75^0 - 161.97^0 \oplus 198.9^0 - 339^0$
	$m_1 = 0.136 - 0.331$	$m_1 = 0.0431 - 0.334$	$m_1 = 0.00156 - 0.481$	$m_1 = 0.141 - 0.481$
	$m_2 = 0.137 - 0.331$	$m_2 = 0.0445 - 0.334$	$m_2 = 0.00571 - 0.480$	$m_2 = 0.142 - 0.492$
	$m_3 = 0.143 - 0.334$	$m_3 = 0.00969 - 0.330$	$m_3 = 0.0404 - 0.484$	$m_3 = 0.133 - 0.491$

Acknowledgments

The author would like to thank the Director, National Institute of Technology Kurukshetra, for providing necessary facilities to work.

References

[1] Y. Abe, C. Aberle, T. Akiri et al., "Indication of Reactor $\overline{\nu}_e$ Disappearance in the Double Chooz Experiment," *Physical Review Letters*, vol. 108, no. 13, Article ID 131801, 2012.

[2] F. P. An, J. Z. Bai, A. B. Balantekin et al., "Observation of Electron-Antineutrino Disappearance at Daya Bay," *Physical Review Letters*, vol. 108, no. 17, Article ID 171803, 2012.

[3] J. K. Ahn, S. Chebotaryov, J. H. Choi et al., "Observation of reactor electron antineutrinos disappearance in the RENO experiment," *Physical Review Letters*, vol. 108, no. 19, Article ID 191802, 2012.

[4] K. Abe, J. Adam, H. Aihara et al., "Observation of Electron Neutrino Appearance in a Muon Neutrino Beam," *Physical Review Letters*, vol. 112, no. 6, Article ID 061802, 8 pages, 2014.

[5] I. Esteban, M. C. Gonzalez-Garcia, and M. Maltoni, "Updated fit to three neutrino mixing: exploring the accelerator-reactor complementarity," *Journal of High Energy Physics*, vol. 87, 2017.

[6] P. F. de Salas, D. V. Forero, C. A. Ternes, M. Tortola, and J. W. F. Valle, "Status of neutrino oscillations 2017," https://arxiv.org/abs/1708.01186.

[7] A. Gando, Y. Gando, T. Hachiya et al., "Search for Majorana Neutrinos Near the Inverted Mass Hierarchy Region with KamLAND-Zen," *Physical Review Letters*, vol. 117, no. 8, Article ID 082503, 2016.

[8] J. B. Albert, D. J. Auty, and P. S. Barbeau, "Search for Majorana neutrinos with the first two years of EXO-200 data," *Nature*, vol. 510, pp. 229–234, 2014.

[9] S. Dell'Oro, S. Marcocci, M. Viel, and F. Vissani, "Neutrinoless Double Beta Decay: 2015 Review," *Advances in High Energy Physics*, vol. 2016, Article ID 2162659, 37 pages, 2016.

[10] W. Rodejohann, "Neutrino-less double beta decay and particlE," *International Journal of Modern Physics E*, vol. 20, article 1833, 2011.

[11] F. T. Avignone III, S. R. Elliott, and J. Engel, "Double beta decay, Majorana neutrinos, and neutrino mass," *Reviews of Modern Physics*, vol. 80, article 481, 2008.

[12] J. J. Gómez-Cadenas, J. Martin-Albo, M. Mezzetto, F. Monrabal, and M. Sorel, "The search for neutrinoless double beta decay," *La Rivista del Nuovo Cimento*, vol. 29, no. 2, 2012.

[13] S. M. Bilenky and C. Giunti, "Neutrinoless double-beta decay: a brief review," *Modern Physics Letters A*, vol. 27, no. 13, Article ID 1230015, 22 pages, 2012.

[14] P. H. Frampton, S. L. Glashow, and D. Marfatia, "Zeroes of the neutrino mass matrix," *Physics Letters B*, vol. 536, no. 1-2, pp. 79–82, 2002.

[15] Z.-Z. Xing, "Texture zeros and majorana phases of the neutrino mass matrix," *Physics Letters B*, vol. 530, no. 1-4, pp. 159–166, 2002.

[16] J. Liao, D. Marfatia, and K. Whisnant, "Texture and cofactor zeros of the neutrino mass matrix," *Journal of High Energy Physics*, vol. 13, 2014.

[17] D. Meloni, A. Meroni, and E. Peinado, "Two-zero Majorana textures in the light of the Planck results," *Physical Review D*, vol. 89, no. 5, Article ID 053009, 2014.

[18] P. O. Ludl and W. Grimus, "A complete survey of texture zeros in the lepton mass matrices," *Journal of High Energy Physics*, vol. 9, 2014.

[19] S. Dev, R. R. Gautam, and L. Singh, "Neutrino mass matrices with two equalities between the elements or cofactors," *Physical Review D: Particles, Fields, Gravitation and Cosmology*, vol. 87, Article ID 073011, 2013.

[20] J.-Y. Liu and S. Zhou, "Hybrid textures of Majorana neutrino mass matrix and current experimental tests," *Physical Review D: Particles, Fields, Gravitation and Cosmology*, vol. 87, no. 9-1, Article ID 093010, 2013.

[21] S. Kaneko, H. Sawanaka, and M. Tanimoto, *Journal of High Energy Physics*, vol. 73, Article ID 0508, 2005.

[22] L. Lavoura, "Zeros of the inverted neutrino mass matrix," *Physics Letters B*, vol. 609, no. 3-4, pp. 317–322, 2005.

[23] E. I. Lashin and N. Chamoun, "Zero minors of the neutrino mass matrix," *Physical Review D: Particles, Fields, Gravitation and Cosmology*, vol. 78, no. 7, Article ID 073002, 2008.

[24] E. I. Lashin and N. Chamoun, "One vanishing minor in the neutrino mass matrix," *Physical Review D: Particles, Fields, Gravitation and Cosmology*, vol. 80, no. 9, Article ID 093004, 2009.

[25] J. Liao, D. Marfatia, and K. Whisnant, "Texture and cofactor zeros of the neutrino mass matrix," *Journal of High Energy Physics*, vol. 13, Article ID 1409, 2014.

[26] W. Wang, "Neutrino mass textures with one vanishing minor and two equal cofactors," *The European Physical Journal C*, vol. 73, article 2551, 2013.

[27] S. Dev, R. R. Gautam, and L. Singh, "Hybrid textures of the right-handed Majorana neutrino mass matrix," *Physical Review D: Particles, Fields, Gravitation and Cosmology*, vol. 88, Article ID 033008, 2013.

[28] S. Dev, R. R. Gautam, L. Singh, and M. Gupta, "Hybrid textures of the right-handed Majorana neutrino mass matrix," *Physical Review D: Particles, Fields, Gravitation and Cosmology*, vol. 90, Article ID 013021, 2014.

[29] S. Dev, S. Gupta, R. R. Gautam, and L. Singh, "Near maximal atmospheric mixing in neutrino mass matrices with two vanishing minors," *Physics Letters B*, vol. 706, no. 2-3, pp. 168–176, 2011.

[30] W. Grimus and P. O. Ludl, "Maximal atmospheric neutrino mixing from texture zeros and quasi-degenerate neutrino masses," *Physics Letters B*, vol. 700, no. 5, pp. 356–361, 2011.

[31] J. Liao, D. Marfatia, and K. Whisnant, "Dual models of the neutrino mass spectrum," *Physical Review D: Particles, Fields, Gravitation and Cosmology*, vol. 89, no. 1, Article ID 013009, 2014.

[32] J. Liao, D. Marfatia, and K. Whisnant, "Seesaw mechanism with four texture zeros in the neutrino Yukawa matrix," *Physical Review D: Particles, Fields, Gravitation and Cosmology*, vol. 87, no. 7, Article ID 073013, 2013.

[33] J. Liao, D. Marfatia, and K. Whisnant, "One diagonal texture or cofactor zero of the neutrino mass matrix," *Physical Review D: covering particles, fields, gravitation, and cosmology*, vol. 88, no. 3, Article ID 033011, 2013.

Hindawi
Advances in High Energy Physics
Volume 2018, Article ID 4809682, 11 pages
https://doi.org/10.1155/2018/4809682

Research Article

Neutrino Mass and the Higgs Portal Dark Matter in the ESSFSM

Najimuddin Khan [1,2]

[1] *Theoretical Physics Division, Physical Research Laboratory, Ahmedabad 380009, India*
[2] *Centre for High Energy Physics, Indian Institute of Science, Bangalore 560012, India*

Correspondence should be addressed to Najimuddin Khan; khanphysics.123@gmail.com

Received 20 November 2017; Accepted 8 February 2018; Published 13 March 2018

Academic Editor: Farinaldo Queiroz

We extend the standard model with three right-handed singlet neutrinos and a real singlet scalar. We impose two Z_2 and Z_2' symmetries. We explain the tiny neutrino mass-squared differences with two Z_2- and Z_2'-even right-handed neutrinos using type I seesaw mechanism. The Z_2-odd fermion and the Z_2'-odd scalar can both serve as viable dark matter candidates. We identify new regions in the parameter space which are consistent with relic density of the dark matter from recent direct search experiments LUX-2016 and XENON1T-2017 and LHC data.

1. Introduction

The found Higgs boson at the Large Hadron Collider (LHC) [1–3] completes the search for the particle content of the standard model (SM). The hierarchy problem related to the Higgs boson mass has motivated a plethora of models such as supersymmetry, and extra dimensions in which the fine-tuning is reconsidered. However, an inevitable consequence of these models is that the new physics should lie close to the TeV scale. Nonobservations [4] of any new physics from the collider experiments imply that the Higgs hierarchy issue is reverting back to being an unsolved open problem.

In addition, the SM is unable to explain some physical phenomena in nature such as the existence of massive neutrinos, the presence of dark matter (DM), the observed matter-antimatter asymmetry, and so forth. In the SM, by construction, the neutrinos are massless as it does not include right-handed neutrinos. However, from the neutrino oscillation experiments, we got convinced that at least two neutrinos have nonzero mass. The neutrino oscillation experiments have given information about the mass-squared differences between neutrino mass eigenstates. However the individual value of the masses is not yet known. It has been seen that the sum of the three neutrino masses is less than ~0.1 eV [5–7] which is consistent with the cosmological measurements. Individual masses and the basic nature of neutrinos, that is, whether they are Dirac or Majorana particles, are still an open question.

As neutrino masses are very tiny compared to the other fermion masses, it is believed that the mechanism behind neutrino mass generation is different from the other fermions. The other fermions are obtained mass through the Higgs mechanism. The most popular natural explanation of small neutrino masses is the seesaw mechanism. There are broadly three classes of such models, namely, type I, type II, and type III seesaw models requiring involvement of right-handed neutrinos, a $SU(2)_L$ triplet scalar with hypercharge $Y = 2$ and $SU(2)_L$ hyperchargeless triplet fermions, respectively. The minimal scenario in this respect is the canonical type I seesaw mechanism, in which the SM is extended by a right-handed Majorana neutrinos [8–14]. The TeV-scale seesaw mechanism has been discussed in [15–17]. Including extra scalar fields, it has been studied in [18–21].

Various kinds of astrophysical observations, such as anomalies in the galactic rotation curves, gravitational lensing effects in the Bullet cluster, and excess gamma rays (The excess gamma rays from the galactic centers may come from other sources like pulsars.) from the galactic centers, have indicated the existence of DM in the Universe. The cosmological measurements of tiny anisotropies in Cosmic Microwave Background Radiation (CMBR) by the WMAP and Planck Collaboration [5] suggest that the Universe is

made of 69% dark energy, 27% dark matter, and 4% ordinary matter.

Astrophysical and cosmological data can tell us about the total amount/density of the DM of the Universe. There is still no consensus on what it is composed of and the properties are still unknown. The possibilities of different kinds of baryonic or nonbaryonic DM candidates have been discussed in [22]. The weakly interacting massive particles (WIMPs) are the best viable DM candidates. No evidence of the WIMP has been found from the direct detection experiments such as XENON100 [23], LUX [24, 25], and XENON1T [26]. As these DM-nucleon scattering experiments still have not found any signature in the detector, these experiments have ruled out low mass (10–50 GeV) regions in the parameter space of a Z- and Higgs h-portal DM. Recent LUX-2016 [25] data has also excluded the mass range 65–550 GeV of a h-portal fermionic (it depends on the mixing angle between Higgs and singlet scalar) DM model [27] and scalar DM models [27–29]. It indicates that we may need the multicomponent DM particles to explain the experimental data. We may detect these DMs in the more efficient detector in the future experiments. Multicomponent DM model is needed [30] to explain the Galactic Center gamma ray excess [31] and the colliding galaxy cluster [32–34] simultaneously. Multicomponent DM models have been considered in [35, 36] in various models which also include neutrino, Axion, and supersymmetric particles. Various models with two WIMP candidates could lead to typical signatures at different mass scale and have been studied in [37–58].

We add three right-handed $SU(2)$ singlet fermions and a singlet scalar to the SM. We also impose two Z_2 and Z_2' symmetries. All SM and the first two fermion fields are even under these Z_2 and Z_2' transformations. The Dirac mass terms can be formed using these fermions and the SM neutrinos. We use type I seesaw mechanism to explain the tiny neutrino mass-squared differences and the mixing angles which are observed by the neutrino oscillation experiments. The third Z_2-odd fermion and Z_2'-odd scalar both can serve as viable DM particles in this work. Moreover, the requisite rate of annihilation is ensured by postulating some Z_2 and Z_2' preserving dimension-four and dimension-five operators for the scalar and fermion particles, respectively. The four-point interaction term of the extra fermions and scalar can be obtained from other five-dimensional operators [59]. The interaction term of the third fermion and the scalar allows a larger region of the parameter space than what we would have had with a single DM particle (either fermion or scalar) alone. This interplay brings an enriched DM phenomenology compared to the other models having fermion or scalar DM particle. The region of DM masses 65–550 GeV of a fermionic or scalar Higgs portal DM model is excluded from the present LUX experimental data. In this model, we show that the region with masses 50–550 GeV up to 300 TeV is still allowed by the direct search experiments. Hence, we feel a desirable feature of our model for future study.

The plan of the paper is as follows. In Section 2, we present the theoretical framework of our extended singlet scalar fermionic standard model (ESSFSM). We also discuss the diagonalization procedure to get the neutrino mass matrix and the relic density calculation of two dark matter particles. We show the detailed constraints on this model in Section 3. We present our numerical results and show the allowed region in the parameter spaces from the neutrino mass and mixing angle, relic density, and direct detection in Section 4. Finally, we conclude in Section 5.

Table 1: The $Z_2 \times Z_2'$ quantum numbers. u represents the *up-type* quarks of the three generations u, c, t and d stand for the *down-type* quarks d, s, b. The charged leptons are denoted by $l = e, \mu, \tau$ with the corresponding left-handed neutrinos ν_l. Φ is the SM Higgs doublet. G^+ (G^0) stand for the charged (neutral) Goldstone boson. L, R stand for left- and right-handed chirality of fermions.

Fields	Charged under $SU(2) \times Z_2 \times Z_2'$ transformation		
	$SU(2)$	Z_2	Z_2'
$Q_L = \begin{pmatrix} u_L \\ d_L \end{pmatrix}$	2	1	1
u_R, d_R	1	1	1
$L = \begin{pmatrix} \nu_l \\ l^- \end{pmatrix}$	2	1	1
l_R	1	1	1
$\Phi = \begin{pmatrix} G^+ \\ \frac{h + v + iG^0}{\sqrt{2}} \end{pmatrix}$	2	1	1
$\nu_{s,1}, \nu_{s,2}$	1	1	1
$\nu_{s,3}$	1	−1	1
S	1	1	−1

2. Theoretical Framework of the Model

In this section, we give a description of our model. We add three right-handed neutrinos and a scalar to the SM Lagrangian. These extra particles are singlet under $SU(2)$ transformation. We impose two Z_2 and Z_2' symmetries such that the SM fields and first two right-handed neutrinos are even under these Z_2 and Z_2' transformations. The third right-handed neutrino is odd (even) under Z_2 (Z_2') transformation whereas the scalar field is even (odd) under Z_2 (Z_2') transformation. The $Z_2 \times Z_2'$ quantum numbers of the SM fields and extra right-handed neutrinos and scalar fields are summarized in Table 1. The $Z_2 \times Z_2'$-even neutrinos are free to mix with the usual SM neutrinos and therefore generate the neutrino masses through type I seesaw mechanism. These symmetries prohibited the coupling of an odd number of the third fermion and/or the scalar particle to the SM particles. The part of Lagrangian that is invariant under $SU(2) \times U(1) \times Z_2 \times Z_2'$ transformation is given by

$$\mathscr{L} = \frac{i}{2}\overline{\nu}_{s,a}\not{\partial}\nu_{s,a} - \frac{1}{2}\overline{M}_{\nu_{s,a}}\overline{\nu}_{s,a}\nu^c_{s,a} + \frac{1}{2}\partial_\mu S \partial^\mu S - \frac{\mu_S}{2}S^2 - \frac{\lambda_S}{4!}S^4, \tag{1}$$

where summation over a is implied, with $a = 1, 2, 3$ denoting generation indices for the right-handed fermions. c stands for the charge conjugation. The mutual interaction terms of the SM Higgs, left-handed leptons, the extra scalar, and fermions are given by

$$\begin{aligned}\mathscr{L}_{\text{mix}} = &-Y_{\nu,ab}\overline{L}_a\Phi^c\nu_{s,b} - \overline{M}_{\nu_s,mn}\overline{\nu}_{s,m}\nu^c_{s,n} - \frac{\kappa}{2}|\Phi|^2 S^2 \\ &+ \frac{C_{h,mn}}{\Lambda_{h,mn}}|\Phi|^2\,\overline{\nu}_{s,m}\nu^c_{s,n} + \frac{C_{h,a}}{\Lambda_{h,a}}|\Phi|^2\,\overline{\nu}_{s,a}\nu^c_{s,a} \\ &+ \frac{C_{S,mn}}{\Lambda_{S,mn}}S^2\overline{\nu}_{s,m}\nu^c_{s,n} + \frac{C_{S,a}}{\Lambda_{S,a}}S^2\overline{\nu}_{s,a}\nu^c_{s,a} + \text{h.c.}\end{aligned} \tag{2}$$

Φ is the SM Higgs doublet, $\Phi \equiv (G^+, (v + h + iG^0)/\sqrt{2})^T$, where $G^\pm$ and G^0 are the Goldstone bosons, and h is the SM Higgs. Φ^c stands for charge conjugate of Φ. $L \equiv (\nu_l, l)^T$ with $l = e, \mu$ and τ being the left-handed lepton doublet. $b = 1, 2$ does not assume the third index as the third fermion is odd under Z_2-symmetry. The indices $m \neq n = 1, 2$; hence the second term in (2) generates the mixing mass term between two Z_2- and Z_2' -even neutrinos. After electroweak (EW) symmetry breaking, the fourth term, that is, the dimension-five operator also gives an additional mixing mass term. The Higgs to extra neutrinos couplings are also generated from the dimension-five operators (fourth and fifth term in (2)). This will lead to the Higgs boson decay into these extra neutrons. As the Z_2- and Z_2'-even neutrinos are considered to be very heavy, the partial decay width of the Higgs to these neutrinos is zero. As we are allowing these dimension-five operators in the Lagrangian, for completeness, we also add the other dimension-five operators $(C_{S,mn}/\Lambda_{S,mn})S^2\overline{\nu}_{s,m}\nu^c_{s,n}$ and $(C_{S,a}/\Lambda_{S,a})S^2\overline{\nu}_{s,a}\nu^c_{s,a}$, which in turn give more room in the parameter space to maneuver. In this work, we focus on the dominant dimension-five operators related to the neutrino and Higgs portal dark matter physics, that is, those involving at least one Higgs and neglecting other possible operators which are allowed by the SM gauge and $Z_2 \times Z_2'$ symmetries. Λ's are the cut-off scales for the new physics. In our calculation, we assume $\Lambda_{h,a} = \Lambda_{S,a} = \Lambda_{h,mn} = \Lambda_{S,mn} \equiv \Lambda$. $C_{h,a}$, $C_{S,a}$, $C_{h,mn}$, and $C_{S,mn}$ are dimensionless coupling parameters. The cut-off scale Λ and $C_{h,12}$ and the Yukawa couplings $Y_{\nu,ab}$ are important to explain the neutrino oscillation observables, whereas Λ, $C_{h,3}$, $C_{S,3}$, and κ could change the masses and coupling strength of DM particles to the Higgs. In addition, these could alter the self-annihilation interaction probability of the heavier DM particles into the lighter DM particles. Hence, these parameters play a crucial role to calculate the relic density of the DM particles $\nu_{s,3}$ and S. The masses of the DM particles are given by

$$\begin{aligned}M_{\nu_{s,3}} &= \overline{M}_{\nu_{s,3}} - \frac{C_{h,3}}{\Lambda}v^2, \\ M_S^2 &= \mu_S^2 + \frac{1}{2}\kappa v^2,\end{aligned} \tag{3}$$

and the coupling strength of the DM candidates with the Higgs can be written as

$$\begin{aligned}h\overline{\nu}_{s,3}\nu_{s,3} &: \frac{C_{h,3}}{\Lambda}, \\ hSS &: \frac{\kappa}{2}v.\end{aligned} \tag{4}$$

The parameter $C_{S,3}$ is responsible for the annihilation of $SS \leftrightarrow \overline{\nu}_{s,3}\nu_{s,3}$. This process reduces the number density of the heavier DM till the freeze-out.

It is also important to note that the gauge boson B_μ and/or W^i_μ interactions terms are not present in the kinetic part of the Lagrangian (see (1)). Therefore, this model does not have any extra gauge-boson contribution to the DM-nucleus scattering cross section which is allowing larger region in the parameter space from the direct detection experiments. This is the specialty of the presence of real singlet scalar and fermion in the ESSFSM.

2.1. Diagonalization Procedure of Type I Seesaw Matrix and Nonunitarity of PMNS Matrix. Here, we show the diagonalization procedure [60, 61] of type I seesaw mechanism to generate tiny neutrino mass-squared difference [62, 63]. In this model, 5×5 neutrino mass matrix in the basis (ν_l, ν_s) can be written as

$$M_\nu = \begin{pmatrix} 0 & M_D \\ M_D^T & M_{\nu_s}\end{pmatrix}, \tag{5}$$

where the Dirac mass M_D and Majorana mass M_{ν_s} terms can be written as

$$\begin{aligned}M_D &= \begin{pmatrix} Y_{\nu,11}v & Y_{\nu,12}v \\ Y_{\nu,21}v & Y_{\nu,22}v \\ Y_{\nu,31}v & Y_{\nu,32}v\end{pmatrix}, \\ M_{\nu_s} &= \begin{pmatrix} M_{11} & M_{12} \\ M_{12} & M_{22}\end{pmatrix}.\end{aligned} \tag{6}$$

Here, $M_{11} = \overline{M}_{\nu_s,1} - (C_{h,1}/\Lambda)v^2$, $M_{22} = \overline{M}_{\nu_s,2} - (C_{h,2}/\Lambda)v^2$, and $M_{12} = \overline{M}_{\nu_s,12} - (C_{h,12}/\Lambda)v^2$

Using 5×5 unitary matrices [64, 65], one can diagonalize the neutrino mass matrix M_ν in (5). It is given by

$$U^T M_\nu U = M_\nu^{\text{diag}}, \tag{7}$$

where $M_\nu^{\text{diag}} = \text{diag}(m_i, M_j)$ with mass eigenvalues m_i $(i = 1, 2, 3)$ for three light neutrinos and M_j $(j = 1, 2)$ for two heavy neutrinos, respectively. In this calculation, we have two nonzero mass eigenstates of light neutrinos. We consider m_1 to be zero. In the limit $M_D^2 \ll M_{\nu_s}^2$, the matrix U can be expressed as follows [61]:

$$\begin{aligned}U = WT &= \begin{pmatrix} U_L & V \\ S & U_H\end{pmatrix} \\ &= \begin{pmatrix} \left(1 - \frac{1}{2}\epsilon\right)U_\nu & M_D^*\left(M_{\nu_s}^{-1}\right)^* U_R \\ -M_{\nu_s}^{-1}M_D^T U_\nu & \left(1 - \frac{1}{2}\epsilon'\right)U_R\end{pmatrix},\end{aligned} \tag{8}$$

where U_L, V, S and U_H are $3\times3, 2\times3, 3\times2$ and 2×2 matrices, respectively, which are not unitary. The unitary W matrix which brings the full 5×5 neutrino matrix in the block diagonal forms as

$$W^T\begin{pmatrix}0 & \widehat{M}_D\\ M_D^T & M_{\nu_s}\end{pmatrix}W=\begin{pmatrix}m_{\text{light}} & 0\\ 0 & M_{\text{heavy}}\end{pmatrix}. \tag{9}$$

Another unitary matrix $T=\text{diag}(U_\nu, U_R)$ matrix again diagonalizes the mass matrices in the light and heavy sectors are appearing in the upper and lower block of the block diagonal matrix, respectively. In the above-stated limit, one can then write the light neutrino mass matrix to the leading order as

$$m_{\text{light}}=M_D M_{\nu_s}^{-1}M_D^T. \tag{10}$$

In (8), U_L corresponds to the PMNS matrix which acquires a nonunitary correction $(1-\epsilon/2)$ due to the presence of heavy neutrinos. The characterizations of nonunitarity are denoted by the notations ϵ and ϵ'. These are given by the following [60]:

$$\begin{aligned}\epsilon&=M_D^* M_{\nu_s}^{-1*}M_{\nu_s}^{-1}M_D^T,\\ \epsilon'&=M_{\nu_s}^{-1}M_D^T M_D^* M_{\nu_s}^{-1*}.\end{aligned} \tag{11}$$

2.2. Relic Density Calculation of the Two-Component Dark Matter. In order to calculate the relic abundance of two-component DM in the present formalism, we need to solve the relevant coupled Boltzmann equations [66]:

$$\begin{aligned}&\frac{dn_{\nu_{s,3}}}{dt}+3Hn_{\nu_{s,3}}\\ &\quad=-\langle\sigma v\rangle_{\nu_{s,3}\nu_{s,3}\to XX}\left(n_{\nu_{s,3}}^2-n_{\nu_{s,3}\text{eq}}^2\right)\\ &\qquad-\langle\sigma v\rangle_{\nu_{s,3}\nu_{s,3}\to SS}\left(n_{\nu_{s,3}}^2-\frac{n_{\nu_{s,3}\text{eq}}^2}{n_{S_{\text{eq}}}^2}n_S^2\right),\\ &\frac{dn_S}{dt}+3Hn_S\\ &\quad=-\langle\sigma v\rangle_{SS\to XX}\left(n_S^2-n_{S_{\text{eq}}}^2\right)\\ &\qquad-\langle\sigma v\rangle_{SS\to\nu_{s,3}\nu_{s,3}}\left(n_S^2-\frac{n_{S_{\text{eq}}}^2}{n_{\nu_{s,3}\text{eq}}^2}n_{\nu_{s,3}}^2\right),\end{aligned} \tag{12}$$

where Z_2-even (SM, $\nu_{s,2}$ and $\nu_{s,2}$) particles are denoted by X. In addition, the heavier X can decay into lighter particles. $\langle\sigma v\rangle$ is the average effective annihilation cross sections of the DM candidates which include all $n\geq2$-body final state particles. The first term on the right-hand side of (12) indicates the contribution of annihilation to SM particles whereas the second term in both equations takes care of the contribution of the self-scattering of DM particles. The contributions from the processes $\nu_{s,3}S\to\nu_{s,3}S$ are zero as it does not alter the number density. In the very early Universe, both of the DM candidates are in thermal and chemical equilibrium. In the nonrelativistic case, if the temperature T of the Universe is less than the DM masses, then the equilibrium number density takes the form $n_{\text{DM eq}}=(M_{\text{DM}}T/2\pi)^{3/2}\exp(-M_{\text{DM}}/T)$. As the temperature was falling down, some species are decoupled and contributing to the relic density. The heavier DM candidate particle decouples earlier than the lighter one. In the present Universe, they both were frozen out and giving a partial contribution in the total relic abundance Ω_{tot}. If the individual contributions of the fermion and scalar are $\Omega_{\nu_{s,3}}$ and Ω_S, then the total relic abundance Ω_{tot} can be written as

$$\Omega_{\text{DM}}=\Omega_{\nu_{s,3}}+\Omega_S, \tag{13}$$

where $\Omega_{\nu_{s,3}}=(M_{\nu_{s,3}}/\rho_c)n_{\nu_{s,3}}(T_0)$ and $\Omega_{\nu_{s,3}}=(M_S/\rho_c)n_S(T_0)$. $\rho_c\sim1.05\times10^{-5}h^2\,\text{GeVcm}^{-3}$ stands for the critical density of the present Universe; $h=0.72$ is the Hubble parameter. $n(T_0)$ is the number density of the DM at temperature T_0 today.

One can note that if the masses of the DM particles are degenerate, then the Boltzmann equations (12) become decoupled; that is, self-scattering cross sections of the process $\nu_{s,3}\nu_{s,3}\leftrightarrow SS$ are very small compared to the self-annihilation cross section of the DM. These equations describe the evolution of each DM independently. In our calculation, we use the `micrOMEGAs` [66] and solve the above coupled Boltzmann equations to calculate the individual number density of the DM particles in the present Universe.

3. Constraints on the Model

The parameter spaces of this model are constrained from various theoretical considerations like absolute vacuum stability, perturbation, and unitarity of the scattering matrix. The absolute stability of the Higgs potential demands that the scalar potential should not approach to negative infinity along any direction of the field space at large field values. The required conditions are $\lambda>0$, $\lambda_S>0$, and $\kappa>-\sqrt{2\lambda\lambda_s}/\sqrt{2}$, where λ is the Higgs quartic coupling [29]. Lagrangian of our model remains perturbative [67, 68] for $|\lambda|\lesssim4\pi/3$, $|\kappa|\lesssim8\pi$, $|\lambda_S(\Lambda)|\lesssim8\pi, C_{h,a}\lesssim8\pi$, and $C_{S,a}\lesssim8\pi$. The parameters of the scalar part of Lagrangian (see (1) and (2)) of this model are constrained by the unitarity of the scattering matrix (S-matrix). One can obtain the S-matrix by using various scalar-scalar, gauge boson-gauge boson, and scalar-gauge boson scattering amplitudes. We use the equivalence theorem [69–71] to reproduce the S-matrix for this model [68]. The unitary bounds demand that the eigenvalues of this matrix should be less than 8π which imply $\lambda\leq8\pi$ and $|12\lambda+\lambda_S\pm\sqrt{16\kappa^2+(-12\lambda+\lambda_S)^2}|\leq32\pi$.

The observed neutrino mass-squared differences and mixing angles by the neutrino oscillation experiments put stringent constraints on the parameter space of this model. The Higgs signal strength and the decay width measured by the LHC, the relic density, and direct-indirect searches of DM all alone restrict the allowed parameter space considerably. We discuss these in the following.

3.1. Bounds from the Neutral Fermion Mass and Mixing Angles. The global analysis of neutrino oscillation measurements

provides the neutrino oscillation parameters for both normal and inverted hierarchies scenario. These can be found in [62, 63]. The measurements of the electroweak precision observables along with other experimental data put severe constraints on the light neutrino mixing matrix U_L. The detailed analysis has been given in Refs [72, 73].

The L3 collaboration at the LEP had analyzed the decay channels $N \to e^{\pm}W^{\mp}$ to find the evidence of the heavy neutrino. No signature had been found for the mass range in between 80 GeV (with $|V_{\alpha i}|^2 \leq 2 \times 10^{-5}$) and 205 GeV (with $|V_{\alpha i}|^2 \leq 1$) [74]. V is the light-heavy mixing matrix, given in (8). This puts a lower bound on the mass of the heavy neutrino and the mixing matrix elements $V_{\alpha i}$. $|V_{\alpha i}|^2 \gtrsim 10^{-5}$ and $3 < M_{1,2} < M_Z$ regions have also been ruled out from the invisible decay width of the Z-boson [75–77].

The experimental data [78] $\mathrm{Br}(\mu \to e\gamma) < 4.2 \times 10^{-13}$ of the flavor changing decay processes has restricted the arbitrary Yukawa coupling Y_ν. In this model, the branching ratio can be written as follows [79]:

$$\mathrm{Br}\left(\mu \longrightarrow e\gamma\right) = \frac{3\alpha}{8\pi}\left|V_{ei}V_{i\mu}^{\dagger} f\left(x\right)\right|^2, \tag{14}$$

where $x = (M_i^2/M_W^2)$, $i = 1, 2$, stands for the mass of heavy neutrinos and $f(x)$ is the slowly varying function can be found in [79].

3.2. Bounds from the Higgs Signal Strength at the LHC. The dominant contribution of the Higgs h-production cross section is coming through the gluon fusion. In this work, the Higgs to diphoton signal strength $\mu_{\gamma\gamma}$ can be written as

$$\begin{aligned}\mu_{\gamma\gamma} &\simeq \frac{\sigma\left(gg \to h \to \gamma\gamma\right)_{\mathrm{ESSFSM}}}{\sigma\left(gg \to h \to \gamma\gamma\right)_{\mathrm{SM}}} \\ &= \frac{\sigma\left(gg \to h\right)_{\mathrm{ESSFSM}}}{\sigma\left(gg \to h\right)_{\mathrm{SM}}} \frac{\mathrm{Br}\left(h \to \gamma\gamma\right)_{\mathrm{ESSFSM}}}{\mathrm{Br}\left(h \to \gamma\gamma\right)_{\mathrm{SM}}}.\end{aligned} \tag{15}$$

The production cross section of h is the same as in the SM. Then $\mu_{\gamma\gamma}$ can be written as

$$\mu_{\gamma\gamma} = \frac{\Gamma_{h,\mathrm{SM}}^{\mathrm{total}}}{\Gamma_{h,\mathrm{ESSFM}}^{\mathrm{total}}}, \quad \text{as } \frac{\Gamma_h^{\mathrm{total}}}{M_h} \longrightarrow 0. \tag{16}$$

As we do not have any extra charged particle, the decay width $\Gamma(h \to \gamma\gamma)$ is the same as in the SM. If the extra particles (scalar and fermions) have the mass less than half of the Higgs mass $M_h/2$, then the diphoton signal strength could be changed due to the invisible decay of the Higgs boson. Using the global fit analysis [80] that such an invisible branching ratio is less than ~20%, so the decay width in (16) provides a suppression of about ~80–100 percent. The present combined value of $\mu_{\gamma\gamma}$ by the ATLAS and CMS collaborations is $1.14^{+0.19}_{-0.18}$ [81]. As the partial decay width of the Higgs to the heavy Z_2- and Z_2'-even neutrinos is zero, it cannot alter $\mu_{\gamma\gamma}$. We also check that the mass region $M_{\mathrm{DM}} < 55\,\mathrm{GeV}$ of the Z_2'-odd scalar and Z_2-odd neutrino DM along with $|\kappa| \gtrsim 0.004$ and/or $|C_{h,3}| \gtrsim 0.2$ is excluded at 2σ.

3.3. Relic Density and Direct Search Limits. The relic density of DM all alone restricts the allowed parameter space. The parameter space of this model should also satisfy the combined WMAP and Planck [82] imposed dark matter relic density constraint $\Omega_{\mathrm{tot}}h^2 = 0.1198 \pm 0.0026$. In our calculation, we use the `micrOMEGAs` [66] to calculate the total relic density of the two DM particles. In this model, we find the correct relic density for the dark matter particles mass $M_{\mathrm{DM}} < 55\,\mathrm{GeV}$. However, these regions in the parameter spaces are ruled out from the invisible Higgs decay width and direct search data. In the following, we discuss the detailed constraints from direct detection of two-component dark matter particles.

The WIMPs, in particular, those that have nonvanishing weak interactions with the SM and therefore can be tested. They are actively being searched for in the direct detection experiments which look for their nuclear scatterings in the deep underground detectors. If the DM scatters from atomic nucleus, then it leaves their signature in form of a recoiled nucleus. However, no confirmed detection of the DM in the experimental laboratory has been made so far. If a discovery is within the reach of a near-future direct detection experiment, then these experiments will be able to constrain the WIMP properties such as its mass, DM-nucleus scattering cross section, and possibly spin.

As we have two-component DM, it is very difficult to distinguish these DM particles in the direct detection experiment. The local number density of the DM particles in the solar neighborhood is important in determining the total number of event rate in the experiment. It is not entirely straightforward to determine which component dominates the event rate. There have been only a few works regarding the direct detection of multicomponent DM [83–85]. The signal rate generated from two-component DM in the detector is different compared to a single-component DM and it completely depends on the DM masses and local densities in the solar neighborhood. The particle masses will determine their individual rates (see section 3.2 of [85]) that can distinguish one- or two-component DM if the DM particles have different masses.

Presently, nonobservation of DM in the direct detection experiments such as XENON100 [23], LUX [24, 25], and XENON1T [26] sets a limit on WIMP-nucleon scattering cross section for given DM masses. The most stringent bound is set by the XENON1T [26] and LUX 2016 [25] exclusion data. The region above the green line in Figure 2 is excluded. We translate the LUX exclusion data into some allowed or excluded zones in the parameter spaces of our model comprising $C_{h,3}$, $M_{\nu_{s,3}}$, κ, M_S and $C_{S,3}$. In this model, the Feynman diagrams for the scattering of DM particles $\nu_{s,3}, S$ with the nuclei are shown in Figure 1. In the limit $M_{\mathrm{DM}}(M_{\nu_{s,3}}, M_S) \gg M_N$, the fermion-nucleon and scalar-nucleon scattering cross sections are roughly given by

$$\begin{aligned}\sigma_{\nu_{s,3},N} &= X_N\left(\frac{C_{h,3}}{\Lambda M_{\nu_{s,3}}}\right)^2, \\ \sigma_{S,N} &= \frac{X_N}{2}\left(\frac{\kappa}{M_S}\right)^2,\end{aligned} \tag{17}$$

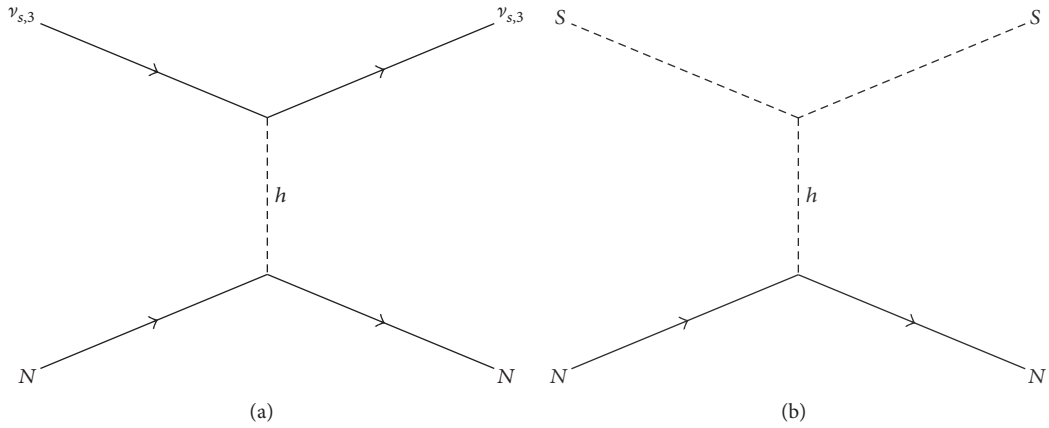

Figure 1: (a) Lowest order Feynman diagram for singlet neutrino-nucleus elastic scattering via the Higgs mediation. (b) A similar diagram for the singlet scalar-nucleus elastic scattering.

where $X_N = (m_r m_N f/\sqrt{\pi} M_h^2)^2$ and $f \approx 0.3$ is the form factor of the nucleus. m_r represents the reduced mass of the nucleus and the scattered DM particle.

Using (17), we calculate the DM-nucleon cross sections for the two dark matter components of different mass. The region in the parameter space for which DM-nucleon cross section falls above the green line in Figure 2 is ruled out by the recent LUX-2016 [25] exclusion data. The region above the purple line is ruled out by the recent XENON-2017 [26] data.

4. Numerical Results

We explain the neutrino mass using type I seesaw mechanism. We show that our results are compatible with the various constraints such as the charged lepton flavor violating decay $\mu \to e\gamma$. In addition, the extra Z_2-odd fermion and the Z_2'-odd scalar both can serve as viable DM particles producing the relic density in the right ballpark. We show that the regions in the parameter space are consistent with the Planck/WMAP as well as LUX-2016 and XENON-2017 data. In this study, we use `FeynRules` [86] along with `micrOMEGAs` [66] to compute the relic density of the DM candidates $\nu_{s,3}$ and S. We will discuss these in the following.

4.1. Neutrino Oscillation Parameters. We obtain tiny neutrino mass through type I seesaw mechanism. We use the input parameters such as the new Yukawa couplings $Y_{\nu,ij}$ ($i = 1, 2, 3$ and $j = 1, 2$), dimensionless couplings $C_{h,1}$, $C_{h,2}$, $C_{h,12}$, and the mass terms $\overline{M}_{\nu_s,1}$, $\overline{M}_{\nu_s,2}$, and $\overline{M}_{\nu_s,12}$. In our calculation, we assume cut-off scale for the new physics is $\Lambda = 10$ TeV. In order to explain successful leptogenesis [87, 88], we need complex Yukawa coupling to have nonzero CP-violation. The detailed discussion can be found in [61]. The presence of the extra Majorana neutrinos will allow for neutrinoless double β-decay [12]. In this work, we use the nonzero and real Yukawa couplings $Y_{\nu,12} = Y_{\nu,23}$ ($\equiv y_\nu$). Other Yukawa couplings are taken to zero. We chose the values of parameters $\overline{M}_{\nu_s,12}$ and $C_{h,12}$ such that the off-diagonal components of the heavy mass matrix M_{ν_s} become zero (see (6)). We consider three heavy neutrino masses $\mathcal{O}(10^{11})$ GeV, $\mathcal{O}(10^5)$ GeV, and $\mathcal{O}(10^3)$ GeV and the corresponding three different Yukawa couplings y_ν to obtain tiny the neutrino masses. We present these benchmark points and the corresponding low-energy variables in Table 2. These variables are consistent with the experimental data. As the cut-off scale for the new physics Λ is very large, the dimensionless couplings C_h (within perturbative limit) could not alter the neutrino mass considerably.

4.2. New Regions in the DM Parameter Space. We have seen that the region in the parameter space $M_{\rm DM} < \mathcal{O}(500)$ GeV of a single Higgs portal WIMP DM particle is ruled out by the recent LUX experiment. Hence, it becomes important to show that these regions in the parameter space are still alive in the ESSFSM. In Table 3, we present five benchmark points for this model which are producing right relic density and allowed by the recent nonobservation of DM-nucleon scattering in the LUX experiment. The DM mass regions below the half of the Higgs mass are also consistent with the Higgs invisible decay width [80]. If the mass difference between the fermionic and scalar DM particles is very large, then it is expected that lighter one will dominate over the heavier one in contributing to the relic density. For $M_{\nu_{s,3}} \simeq M_S$ and tiny interaction coupling $C_{S,3}$, the contribution of these DM particles is nearly equal to the total relic density, whereas the interaction coupling $C_{S,3} \sim \mathbf{O}(1)$ and a huge mass difference in the DM particles with particular Higgs portal couplings κ and $C_{h,3}$ can produce equal relic density in the Universe. For example, see benchmark points I–IV. The lighter DM mass near 60 GeV will always dominate over the heavier one because the contribution of self-annihilation processes DM, DM $\to b\bar{b}$ into the relic density is larger than the other processes. The other processes can dominate over the DM, DM $\to b\bar{b}$ process for the choice of the large Higgs portal coupling κ. In this case, the relic density and the direct detection data restrict such a choice of κ.

Table 2: Three lists of benchmark points used in our analysis. Using these BPs, we have obtained the outputs for our model which are satisfying all the low energy constraints.

Parameters	Benchmark points for Z_2- and Z_2'-even fermions		
	BM-I	BM-II	BM-III
M_{11} GeV	1.2×10^{11}	7.1×10^{5}	6.9×10^{3}
$C_{h,1}$	0.1	0.01	0
M_{22} GeV	1.4×10^{12}	2.36×10^{5}	2.41×10^{3}
$C_{h,2}$	0.1	0.01	0
M_{12} GeV	0	0	0
y_ν	0.01	10^{-5}	10^{-6}
Outputs	Corresponding low-energy variables		
$\Delta m^2_{21}/10^{-5}$ eV^2	7.5001	7.2909	7.7197
$\Delta m^2_{31}/10^{-3}$ eV^2	2.55234	2.63959	2.5312
θ_{12}	0.5883	0.5774	0.5720
θ_{23}	0.7953	0.7854	0.7803
θ_{13}	0.1476	0.1473	0.1469
δ_{PMNS} rad	10^{-5}	10^{-4}	10^{-3}
α rad	1.7	1.8	1.9
m_i eV	0, 0.0087, 0.0505	0, 0.0085, 0.0514	0, 0.0088, 0.0505
Br($\mu \to e\gamma$)	3.0×10^{-48}	1.9×10^{-37}	1.69×10^{-33}

Table 3: Lists of benchmark points used in our analysis. Using these BPs we obtain the relic density in the right ballpark allowed by LUX-2016 direct detection data.

Benchmark points	Parameters					Relic density Ωh^2	Percentage of DM		DM-N cross section in [zb]	
	$M_{\nu_{s,3}}$ GeV	$C_{h,3}$	M_S GeV	κ	$C_{S,3}$		Fermion	Scalar	Fermion	Scalar
BP-I	260	0.05	59	0.0015	0.1	0.1271	39.12	61.88	0.33	0.0054
BP-II	130	0.01	60	0.001	0.1	0.1263	40.68	59.32	0.013	0.0023
BP-III	86	−0.01	59.8	0.0012	0.1	0.1129	53.10	46.90	0.013	0.0033
BP-IV	62	−0.01	60.9	0.0016	0.1	0.1156	69.76	30.24	0.013	0.0058
BP-V	59	0.02	250	0.0025	0.1	0.1201	99.6	0.4	0.053	0.0008

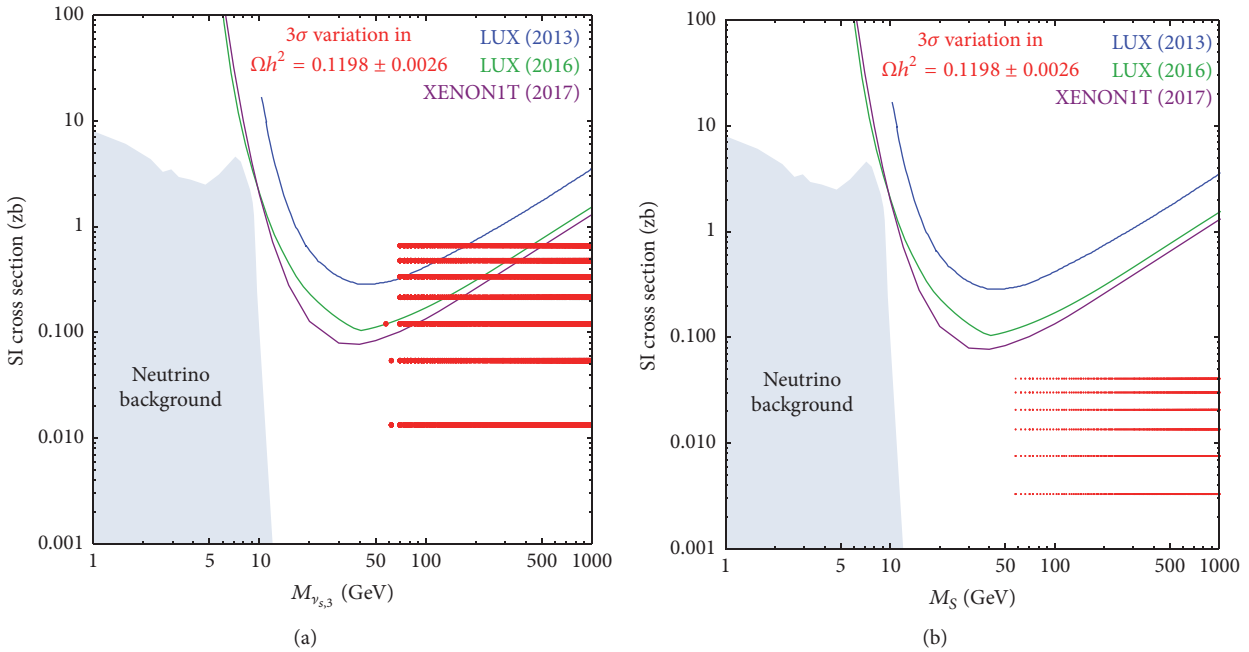

Figure 2: WIMP-nucleon cross section versus DM mass keeping $C_{S,3} = 0.1$. The gray region indicates the neutrino background. Note that each plot contains only 10^7 data (red) points. Larger data points can fill the gap between the red bands.

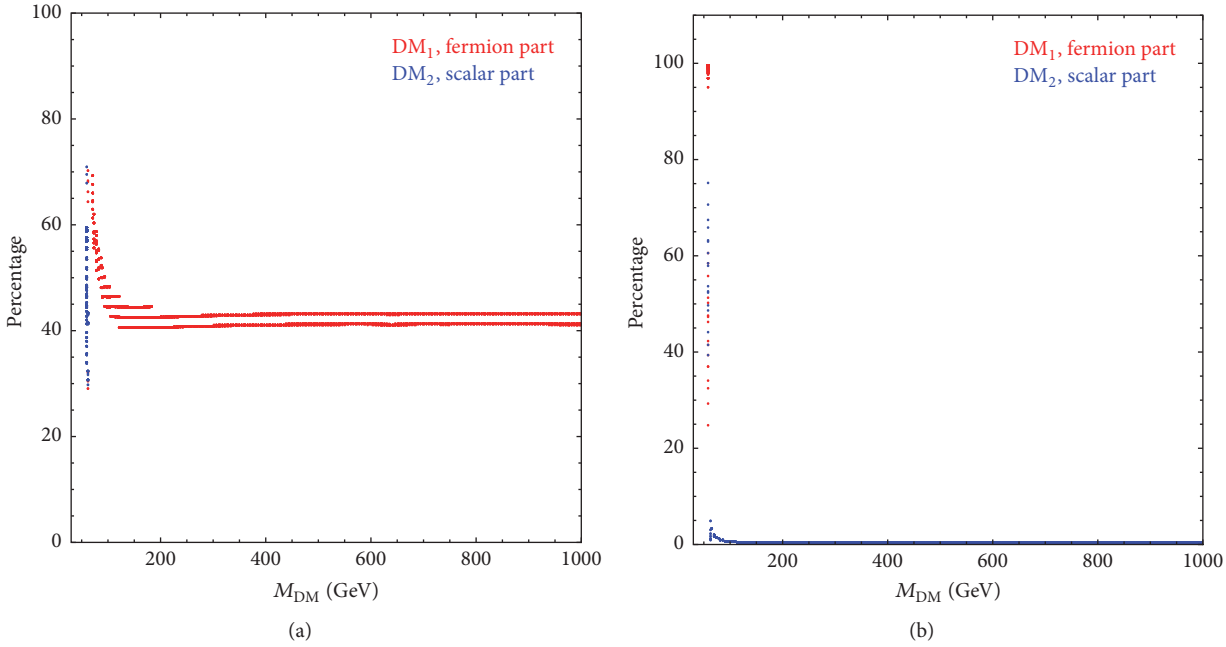

FIGURE 3: Percentage of DM contributing to the total relic density. Red points correspond to the fermionic DM contributions whereas blue points correspond to the singlet scalar.

In order to find the favored regions in the parameter space which satisfies DM relic density constraints and the recent LUX direct detection data, in Figure 2, we present two contour plots of relic density Ωh^2 in the DM-nucleon cross section versus mass plane. The red points are consistent with the relic density $\Omega h^2 = 0.1198 \pm 0.0026$ within 3σ. We vary $C_{h,3}$ from -0.7 to 0.7 and κ from 0 to 0.75 to obtain Figure 2. We also fix the coupling $C_{S,3} = 0.1$ in these plots.

In Figure 2(a), we vary the scalar DM mass between 55 GeV and 65 GeV and the fermion DM mass between 40 and 1000 GeV. In Figure 2(b), we take the variation of the fermionic DM mass between 55 GeV and 65 GeV and the scalar mass between 40 and 1000 GeV. We find that a large region in the parameter space satisfies the bound on WIMP-nucleon cross section as imposed by the recent LUX-2016 and XENON-2017 experimental data. We find that the scalar DM mass M_S~60 Gev provides the dominant contributions in the relic density. The contribution decreases with M_S. However, we need this scalar part to achieve the relic density as observed by the WMAP/Planck. In the second case, the fermionic contribution remains the same (~50%) in the region $55 \lesssim M_S \lesssim 65$ GeV. We show these variations of the DM contribution in Figure 3 with the DM mass. The red points indicate the fermionic contribution whereas blue points stand for the scalar contribution to the correct relic density ($\Omega h^2 = 0.1198 \pm 0.0026$) within 3σ.

5. Conclusion

In this paper, using two right-handed singlet fermions, we have explained the neutrino mass through type I seesaw mechanism. We have chosen three representative "benchmark points" of three different Majorana mass parameter spaces (~10^3, 10^6, and 10^{12}) and particular structure of the Yukawa couplings matrix, that is, the Dirac mass matrix to explain the neutrino mass-squared differences as observed by the neutrino experiments. We have also calculated the PMNS mixing angles and the other low-energy variables, that is, nonunitary constraints on the PMNS matrix and LFV constraints from $\mu \rightarrow e\gamma$. The combinations of the new Yukawa couplings and the heavy neutrino mass satisfied the neutrino mass and mixing angles constraints [89].

In the presence of Z_2 and Z_2' symmetries, we have also analyzed the two-component Higgs portal self-annihilating dark matter particles. The regions of mass 65–550 GeV of a Higgs portal fermionic or scalar dark matter models are excluded by the recent LUX experiment. In this model, we have shown that the regions of the parameter space with two-component dark matter particles are still allowed from direct search experiment and the WMAP/Planck data. For different fermionic Higgs portal coupling $C_{h,3}$ and fermion dark matter mass, we have obtained viable scalar dark matter mass between 50 GeV and ~300 TeV. We have also obtained the similar region of fermionic dark matter mass for different scalar Higgs portal coupling κ. The unitary bounds are violated the dark matter mass above 300 TeV [90]. Here, we do not intend to show that all the parameter spaces satisfy the experimental results. Rather, in the framework of our model, we have wanted to use the advantage of a two-component dark matter which has a large region of parameter spaces satisfying the constraint of various dark matter experiments.

The model ESSFSM is considered here to present the minimal seesaw mechanism and two-component dark matters in terms of particles content. This model can explain the observed tiny neutrino mass-squared differences and the mixing angles in oscillation experiments. The regions in the

parameter space are also consistent with the relic density of dark matter observed by the Planck, WMAP experiments, and the recent null results of the WIMPs dark matter from the direct search LUX-2016 and XENON-2017 experiments.

Conflicts of Interest

The author declares that there are no conflicts of interest regarding the publication of this paper.

Acknowledgments

The authors would like to thank Subhendu Rakshit and Vishnudath K. N. for useful discussions.

References

[1] A. Aad, T. Abajyan, and B. Abbott, "Observation of a new particle in the search for the Standard Model Higgs boson with the ATLAS detector at the LHC," *Physics Letters B*, vol. 716, no. 1, pp. 1–29, 2012.

[2] P. P. Giardino, K. Kannike, I. Masina, M. Raidal, and A. Strumia, "The universal Higgs fit," *Journal of High Energy Physics*, vol. 2014, no. 5, 2014.

[3] C. Mariotti et al., "Observation of a new boson at a mass of 125 gev with the cms experiment at the lhc," *Physics Letters B*, vol. 716, no. 1, pp. 30–61, 2012.

[4] F. Rühr, "Prospects for BSM searches at the high-luminosity LHC with the ATLAS detector," *Nuclear and Particle Physics Proceedings*, vol. 273-275, pp. 625–630, 2016.

[5] P. A. R. Ade, N. Aghanim, M. Arnaud et al., "Planck 2015 results. XIII. Cosmological parameters," *Astronomy & Astrophysics*, vol. 594, Article ID 201525830, 2016.

[6] E. Giusarma, M. Gerbino, O. Mena, S. Vagnozzi, S. Ho, and K. Freese, "Improvement of cosmological neutrino mass bounds," *Physical Review D: Particles, Fields, Gravitation and Cosmology*, vol. 94, no. 8, 2016.

[7] S. Vagnozzi, E. Giusarma, O. Mena et al., "Unveiling ν secrets with cosmological data: neutrino masses and mass hierarchy," *Physical Review D*, vol. 96, no. 12, 2017.

[8] P. Minkowski, "$\mu \rightarrow e\gamma$ at a rate of one out of 10^9 muon decays?" *Physics Letters B*, vol. 67, pp. 421–428, 1977.

[9] M. Gell-Mann, P. Ramond, and R. Slansky, "Complex spinors and unified theories," in *Proceedings of the Supergravity Workshop*, pp. 315–318, 1979.

[10] T. R. Yanagida, in *Proceedings of the Workshop on Unified Theory and Baryon Number in the Universe*, pp. 95–98, 1979.

[11] R. N. Mohapatra and G. Senjanovic, "Neutrino mass and spontaneous parity nonconservation," *Physical Review Letters*, vol. 44, p. 912, 1980.

[12] M. Mitra, G. Senjanović, and F. Vissani, "Neutrinoless double beta decay and heavy sterile neutrinos," *Nuclear Physics B*, vol. 856, no. 1, pp. 26–73, 2012.

[13] B. Karmakar and A. Sil, " Nonzero ," *Physical Review D: Particles, Fields, Gravitation and Cosmology*, vol. 91, no. 1, 2015.

[14] N. Nath, M. Ghosh, S. Goswami, and S. Gupta, "Phenomenological study of extended seesaw model for light sterile neutrino," *Journal of High Energy Physics*, vol. 3, no. 75, pp. 1–29, 2017.

[15] S. M. Boucenna, S. Morisi, and J. W. F. Valle, "The low-scale approach to neutrino masses," *Advances in High Energy Physics*, vol. 2014, Article ID 831598, 15 pages, 2014.

[16] F. F. Deppisch, P. S. B. Dev, and A. Pilaftsis, "Neutrinos and collider physics," *New Journal of Physics* , vol. 17, no. 7, Article ID 075019, 2015.

[17] S. Khan, S. Goswami, and S. Roy, "Vacuum stability constraints on the minimal singlet TeV seesaw model," *Physical Review D: Particles, Fields, Gravitation and Cosmology*, vol. 89, no. 7, 2014.

[18] J. Chakrabortty, H. Z. Devi, S. Goswami, and S. Patra, "Neutrinoless double-β decay in TeV scale left-right symmetric models," *Journal of High Energy Physics*, vol. 2012, no. 8, 2012.

[19] P. Ghosh, A. K. Saha, and A. Sil, "Study of electroweak vacuum stability from extended higgs portal of dark matter and neutrinos," *High Energy Physics-Phenomenology*, pp. 1–33, 2017.

[20] I. Garg, S. Goswami, K. Vishnudath, and N. Khan, "Electroweak vacuum stability in presence of singlet scalar dark matter in TeV scale seesaw models," *Physical Review D: Particles, Fields, Gravitation and Cosmology*, vol. 96, no. 5, 2017.

[21] S. Bhattacharya, S. Jana, and S. Nandi, "Neutrino masses and scalar singlet dark matter," *Physical Review D: Particles, Fields, Gravitation and Cosmology*, vol. 95, no. 5, 2017.

[22] N. Khan, *Exploring Extensions of the Scalar Sector of the Standard Model [Ph.D. thesis]*, Indian Institute of Technology, Indore, India, 2017.

[23] E. Aprile et al., "Dark matter results from 225 live days of XENON100 Data," *Physical Review Letters*, vol. 109, no. 18, 2012.

[24] D. S. Akerib et al., "First results from the LUX dark matter experiment at the Sanford Underground Research Facility," *Physical Review Letters*, vol. 112, no. 9, 2014.

[25] D. S. Akerib, "Results from a search for dark matter in the complete LUX exposure," *Physical Review Letters*, vol. 118, no. 2, 2017.

[26] E. Aprile et al., "First dark matter search results from the xenon1t experiment," *Physical Review Letters*, vol. 119, no. 18, 2017.

[27] M. M. Ettefaghi and R. Moazzemi, "Analyzing of singlet fermionic dark matter via the updated direct detection data," *The European Physical Journal C*, vol. 77, no. 5, 2017.

[28] P. Athron, C. Balázs, T. Bringmann et al., "Status of the scalar singlet dark matter model," *The European Physical Journal C*, vol. 77, no. 568, 2017.

[29] N. Khan and S. Rakshit, "Study of electroweak vacuum metastability with a singlet scalar dark matter," *Physical Review D: Particles, Fields, Gravitation and Cosmology*, vol. 90, no. 11, 2014.

[30] A. Dutta Banik, M. Pandey, D. Majumdar, and A. Biswas, "Two component WIMP–FImP dark matter model with singlet fermion, scalar and pseudo scalar," *The European Physical Journal C*, vol. 77, no. 10, 2017.

[31] A. Albert, B. Anderson, K. Bechtol et al., "Searching for Dark Matter Annihilation in Recently Discovered Milky Way Satellites with Fermi-LAT," *The Astrophysical Journal*, vol. 834, no. 2, 2017.

[32] D. Harvey, R. Massey, T. Kitching, A. Taylor, and E. Tittley, "The nongravitational interactions of dark matter in colliding galaxy clusters," *Science*, vol. 347, no. 6229, pp. 1462–1465, 2015.

[33] F. Kahlhoefer, K. Schmidt-Hoberg, J. Kummer, and S. Sarkar, "On the interpretation of dark matter self-interactions in Abell 3827," *Monthly Notices of the Royal Astronomical Society*, vol. 452, no. 1, pp. L54–L58, 2015.

[34] R. Campbell, S. Godfrey, H. E. Logan, A. D. Peterson, and A. Poulin, "Implications of the observation of dark matter self-interactions for singlet scalar dark matter," *Physical Review D: Particles, Fields, Gravitation and Cosmology*, vol. 92, no. 5, 2015.

[35] S. Hannestad, A. Mirizzi, G. G. Raffelt, and Y. Y. Wong, "Neutrino and axion hot dark matter bounds after WMAP-7," *Journal*

of Cosmology and Astroparticle Physics, vol. 2010, no. 08, pp. 001-001, 2010.

[36] K. J. Bae, H. Baer, and E. J. Chun, "Mixed axion/neutralino dark matter in the SUSY DFSZ axion model," *Journal of Cosmology and Astroparticle Physics*, vol. 2013, no. 12, pp. 028-028, 2013.

[37] E. Ma, "Verifiable radiative seesaw mechanism of neutrino mass and dark matter," *Physical Review D: Particles, Fields, Gravitation and Cosmology*, vol. 73, Article ID 077301, 2006.

[38] K. M. Zurek, "Multi-Component Dark Matter," *Physical Review D*, vol. 79, no. 11, Article ID 115002, 2009.

[39] B. Batell, "Dark discrete gauge symmetries," *Physical Review D: Particles, Fields, Gravitation and Cosmology*, vol. 83, no. 3, 2011.

[40] H. Fukuoka, D. Suematsu, and T. Toma, "Signals of dark matter in a supersymmetric two dark matter model," *Journal of Cosmology and Astroparticle Physics*, vol. 2011, no. 07, pp. 001-001, 2011.

[41] G. Belanger, K. Kannike, A. Pukhov, and M. Raidal, "Impact of semi-annihilations on dark matter phenomenology. An example of Z_N symmetric scalar dark matter," *Journal of Cosmology and Astroparticle Physics*, 2012.

[42] M. Aoki, M. Duerr, J. Kubo, and H. Takano, "Multicomponent dark matter systems and their observation prospects," *Physical Review D: Particles, Fields, Gravitation and Cosmology*, vol. 86, no. 7, 2012.

[43] I. P. Ivanov and V. Keus, *Physical Review D: Particles, Fields, Gravitation and Cosmology*, vol. 86, no. 1, 2012.

[44] D. Chialva, P. S. Dev, and A. Mazumdar, "Multiple dark matter scenarios from ubiquitous stringy throats," *Physical Review D: Particles, Fields, Gravitation and Cosmology*, vol. 87, no. 6, 2013.

[45] J. Heeck and H. Zhang, "Exotic charges, multicomponent dark matter and light sterile neutrinos," *Journal of High Energy Physics*, vol. 5, no. 164, 2013.

[46] K. P. Modak, D. Majumdar, and S. Rakshit, "A possible explanation of low energy γ-ray excess from galactic centre and Fermi bubble by a Dark Matter model with two real scalars," *Journal of Cosmology and Astroparticle Physics*, vol. 2015, no. 03, pp. 011-011, 2015.

[47] M. Aoki, J. Kubo, and H. Takano, " Two-loop radiative seesaw mechanism with multicomponent dark matter explaining the possible ," *Physical Review D: Particles, Fields, Gravitation and Cosmology*, vol. 87, no. 11, 2013.

[48] C. Geng, D. Huang, and L. Tsai, "Imprint of multicomponent dark matter on AMS-02," *Physical Review D: Particles, Fields, Gravitation and Cosmology*, vol. 89, no. 5, 2014.

[49] Y. Kajiyama, H. Okada, and T. Toma, "Multicomponent dark matter particles in a two-loop neutrino model," *Physical Review D: Particles, Fields, Gravitation and Cosmology*, vol. 88, no. 1, 2013.

[50] S. Bhattacharya, A. Drozd, B. Grzadkowski, and J. Wudka, "Two-component dark matter," *Journal of High Energy Physics*, vol. 2013, no. 10, 2013.

[51] A. Biswas, D. Majumdar, A. Sil, and P. Bhattacharjee, "Two component dark matter: a possible explanation of 130 GeV γ-ray line from the galactic centre," *Journal of Cosmology and Astroparticle Physics*, 2013.

[52] A. Biswas, D. Majumdar, and P. Roy, "Nonthermal two component dark matter model for Fermi-LAT γ-ray excess and 3.55 keV X-ray line," *Journal of High Energy Physics*, vol. 2015, no. 65, 2015.

[53] L. Bian, T. Li, J. Shu, and X. Wang, "Two component dark matter with multi-Higgs portals," *Journal of High Energy Physics*, vol. 2015, no. 3, 2015.

[54] S. Bhattacharya, A. Drozd, B. Grzadkowski, and J. Wudka, "Constraints on Two-component Dark Matter," *Acta Physica Polonica B*, vol. 44, no. 11, p. 2373, 2013.

[55] L. Bian, R. Ding, and B. Zhu, "Two component Higgs-portal dark matter," *Physics Letters B*, vol. 728, pp. 105–113, 2014.

[56] P. Gu, "Multi-component dark matter with magnetic moments for Fermi-LAT gamma-ray line," *Physics of the Dark Universe*, vol. 2, no. 1, pp. 35–40, 2013.

[57] A. DiFranzo and G. Mohlabeng, "Multi-component dark matter through a radiative Higgs portal," *Journal of High Energy Physics*, vol. 2017, no. 1, 2017.

[58] S. Bhattacharya, P. Ghosh, and P. Poulose, "Multipartite interacting scalar dark matter in the light of updated LUX data," *Journal of Cosmology and Astroparticle Physics*, vol. 2017, no. 04, pp. 043-043, 2017.

[59] A. Chaudhuri, N. Khan, B. Mukhopadhyaya, and S. Rakshit, "Dark matter candidate in an extended type III seesaw scenario," *Physical Review D: Particles, Fields, Gravitation and Cosmology*, vol. 91, no. 5, 2015.

[60] J. A. Casas and A. Ibarra, "Oscillating neutrinos and muon —> e, gamma," *Nuclear Physics B*, vol. 618, no. 1-2, Article ID 0103065, pp. 171–204, 2001.

[61] G. Bambhaniya, P. Bhupal Dev, S. Goswami, S. Khan, and W. Rodejohann, "Naturalness, vacuum stability, and leptogenesis in the minimal seesaw model," *Physical Review D: Particles, Fields, Gravitation and Cosmology*, vol. 95, no. 9, 2017.

[62] F. Capozzi, E. Lisi, A. Marrone, D. Montanino, and A. Palazzo, "Neutrino masses and mixings: Status of known and unknown 3 ν parameters," *Nuclear Physics B*, vol. 908, pp. 218–234, 2016.

[63] I. Esteban, M. C. Gonzalez-Garcia, M. Maltoni, I. Martinez-Soler, and T. Schwetz, "Updated fit to three neutrino mixing: exploring the accelerator-reactor complementarity," *Journal of High Energy Physics*, vol. 2017, no. 1, 2017.

[64] Z. Z. Xing and S. Zhou, "Why is the 3 x 3 neutrino mixing matrix almost unitary in realistic seesaw models?" *High Energy Physics and Nuclear Physics*, vol. 30, pp. 828–830, 2006.

[65] W. Grimus and L. Lavoura, "The seesaw mechanism at arbitrary order: disentangling the small scale from the large scale," *Journal of High Energy Physics*, vol. 11, no. 42, 2000.

[66] G. Bélanger, F. Boudjema, A. Pukhov, and A. Semenov, "MicrOMEGAs4.1: Two dark matter candidates," *Computer Physics Communications*, vol. 192, pp. 322–329, 2015.

[67] B. W. Lee, C. Quigg, and H. B. Thacker, "Weak interactions at very high energies: the role of the Higgs-boson mass," *Physical Review D: Particles, Fields, Gravitation and Cosmology*, vol. 16, no. 5, pp. 1519–1531, 1977.

[68] G. Cynolter, E. Lendvai, and G. Pocsik, "Note on unitarity constraints in a model for a singlet scalar dark matter candidate," *Acta Physica Polonica B*, vol. 36, Article ID 0410102, pp. 827–832, 2005.

[69] Y. P. Yao and C. P. Yuan, "Modification of the equivalence theorem due to loop corrections," *Physical Review D: Particles, Fields, Gravitation and Cosmology*, vol. 38, no. 7, pp. 2237–2244, 1988.

[70] H. G. J. Veltman, "The equivalence theorem," *Physical Review D: Particles, Fields, Gravitation and Cosmology*, vol. 41, no. 7, pp. 2294–2311, 1990.

[71] H. He, Y. Kuang, and X. Li, "On the precise formulation of the equivalence theorem," *Physical Review Letters*, vol. 69, no. 18, pp. 2619–2622, 1992.

[72] S. Antusch and O. Fischer, "Non-unitarity of the leptonic mixing matrix: present bounds and future sensitivities," *Journal of High Energy Physics*, vol. 2014, no. 10, article 94, 2014.

[73] S. Antusch and O. Fischer, "Probing the nonunitarity of the leptonic mixing matrix at the CEPC," *International Journal of Modern Physics A*, vol. 31, no. 33, p. 1644006, 2016.

[74] P. Achard et al., "Search for heavy isosinglet neutrino in e^+e^-annihilation at LEP," *Physics Letters B*, vol. 517, no. 1-2, Article ID 0107014, pp. 67–74, 2001.

[75] O. Adriani et al., "Search for isosinglet neutral heavy leptons in Z0 decays," *Phys. Lett*, vol. 95, pp. 371–382, 1992.

[76] P. Abreu, W. Adam, and T. Adye, "Search for neutral heavy leptons produced in Z decays," *Zeitschrift für Physik C*, vol. 74, no. 1, pp. 57–71, 1997.

[77] J. Grifols and A. Méndez, "Electromagnetic properties of the tau lepton from Z0 decay," *Physics Letters B*, vol. 255, no. 4, pp. 611-612, 1991.

[78] A. M. Baldini, Y. Bao, E. Baracchini et al., "Search for the lepton flavour violating decay $\mu^+ \rightarrow e^+\gamma$ with the full dataset of the MEG experiment," *The European Physical Journal C*, 2016.

[79] D. Tommasini, G. Barenboim, J. Bernabéu, and C. Jarlskog, "Non-decoupling of heavy neutrinos and lepton flavour violation," *Nuclear Physics B*, vol. 444, no. 3, pp. 451–467, 1995.

[80] G. Bélanger, B. Dumont, U. Ellwanger, J. F. Gunion, and S. Kraml, "Global fit to Higgs signal strengths and couplings and implications for extended Higgs sectors," *Physical Review D: Particles, Fields, Gravitation and Cosmology*, vol. 88, no. 7, 2013.

[81] G. Aad, B. Abbott, J. Abdallah et al., "Measurements of the Higgs boson production and decay rates and constraints on its couplings from a combined ATLAS and CMS analysis of the LHC pp collision data at s=7 and 8 TeV," *Journal of High Energy Physics*, vol. 8, no. 54, 2016.

[82] P. A. R. Ade, N. Aghanim, and C. Armitage-Caplan, "Planck 2013 results. XVI. Cosmological parameters," *Astronomy & Astrophysics*, vol. 571, Article ID 201321591, 2014.

[83] B. Batell, M. Pospelov, and A. Ritz, "Direct detection of multicomponent secluded WIMPs," *Physical Review D: Particles, Fields, Gravitation and Cosmology*, vol. 79, no. 11, 2009.

[84] S. Profumo, K. Sigurdson, and L. Ubaldi, "Can we discover dual-component thermal WIMP dark matter?" *Journal of Cosmology and Astroparticle Physics*, vol. 2009, no. 12, pp. 016-016, 2009.

[85] J. Herrero-Garcia, A. Scaffidi, M. White, and A. G. Williams, "On the direct detection of multi-component dark matter: sensitivity studies and parameter estimation," *Journal of Cosmology and Astroparticle Physics*, vol. 2017, no. 11, pp. 021-021, 2017.

[86] A. Alloul, N. D. Christensen, C. Degrande, C. Duhr, and B. Fuks, "FeynRules 2.0—A complete toolbox for tree-level phenomenology," *Computer Physics Communications*, vol. 185, no. 8, pp. 2250–2300, 2014.

[87] L. Covi, F. Roulet, and F. Vissani, "CP violating decays in leptogenesis scenarios," *Physics Letters B*, vol. 384, no. 1–4, pp. 169–174, 1996.

[88] J. A. Harvey and M. S. Turner, "Cosmological baryon and lepton number in the presence of electroweak fermion-number violation," *Physical Review D: Particles, Fields, Gravitation and Cosmology*, vol. 42, p. 3344, 1990.

[89] A. Halprin, P. Minkowski, H. Primakoff, and S. P. Rosen, "Double-beta decay and a massive Majorana neutrino," *Physical Review D: Particles, Fields, Gravitation and Cosmology*, vol. 13, no. 9, pp. 2567–2571, 1976.

[90] K. Griest and M. Kamionkowski, "Unitarity limits on the mass and radius of dark-matter particles," *Physical Review Letters*, vol. 64, no. 6, pp. 615–618, 1990.